Daniel I. Hembree
Brian F. Platt
Jon J. Smith *Editors*

Experimental Approaches to Understanding Fossil Organisms

Lessons from the Living

Springer

Experimental Approaches to Understanding Fossil Organisms

Topics in Geobiology

Topics in Geobiology series treats geobiology – the broad discipline that covers the history of life on Earth. The series aims for high quality, scholarly volumes of original research as well as broad reviews. Recent volumes have showcased a variety of organisms including cephalopods, corals, and rodents. They discuss the biology of these organisms-their ecology, phylogeny, and mode of life – and in addition, their fossil record – their distribution in time and space.

Other volumes are more theme based such as predator-prey relationships, skeletal mineralization, paleobiogeography, and approaches to high resolution stratigraphy, that cover a broad range of organisms. One theme that is at the heart of the series is the interplay between the history of life and the changing environment. This is treated in skeletal mineralization and how such skeletons record environmental signals and animal-sediment relationships in the marine environment.

The series editors also welcome any comments or suggestions for future volumes.

Series Editors
Neil H. Landman, landman@amnh.org
Peter J. Harries, harries@shell.cas.usf.edu

Daniel I. Hembree • Brian F. Platt • Jon J. Smith
Editors

Experimental Approaches to Understanding Fossil Organisms

Lessons from the Living

Springer

Editors
Daniel I. Hembree
Department of Geological Sciences
Ohio University
Athens
Ohio
USA

Jon J. Smith
Stratigraphic Research Section
Kansas Geological Survey
Lawrence
Kansas
USA

Brian F. Platt
Department of Geology and Geological
    Engineering
University of Mississippi
Oxford
Mississippi
USA

Printed on acid-free paper

Springer is part of Springer Science+Business Media (www.springer.com)

Preface

The study of modern organisms is invaluable for understanding ancient life, eco-systems, and environments. In most instances, the only way for paleontologists to address questions related to the life activities of extinct taxa is to investigate their closest living ancestors. Modern-analog studies allow paleontologists and sedimentary geologists to assess a range of questions regarding ancient life, from the behavioral and environmental significance of ichnofossils to the conditions responsible for different modes of fossil preservation, to the biomechanics of animal locomotion. While the application of modern observation and experimentation to assessing the past has been fundamental in the geosciences since the nineteenth century, recently developed techniques have arisen in multiple disciplines that allow new questions about the history of life to be addressed.

Experimental Approaches to Understanding Fossil Organisms is based on a topical session that we organized and held on October 11, 2011 at the Geological Society of America's Annual Meeting in Minneapolis, Minnesota. This session included 24 presentations covering a wide range of topics all focused on studying modern organisms to better understand and interpret ancient life. This was the third time we organized a session with this theme for the Geological Society of America. The first was at the 2007 Joint South-Central and North-Central Section Meeting in Lawrence, Kansas and the second was at the 2008 Annual Meeting in Houston, Texas. Given the diversity of the research presented and the size of the audiences attending these sessions, we felt that this was a topic of great interest and held relevance to the modern paleontological and sedimentary geology communities.

This volume is intended to provide professionals and students in the fields of paleontology and sedimentary geology in academia and industry with specific case studies demonstrating the variety of questions that can be asked, techniques and methodologies that can be employed, and interpretations that can be made using modern analogs to study ancient life. We hope that the work described in this volume will be useful in launching new research questions and methods which will ultimately lead to a better understanding of the history of life on our planet.

Experimental Approaches to Understanding Fossil Organisms is divided into three parts. Part I includes papers that analyze the functional morphology of ancient organisms by conducting experiments with fossil material or by studying the

morphology, physiology, and behavior of similar modern organisms. These studies include the investigation of the function of a unique type of anchor-shaped crinoid holdfasts by directly testing models of well-preserved fossils (Chap. 1), an assessment of the functional role of elongate shells in bivalves (Chap. 2), a test of the morphological features of fossil bivalves thought to suggest chemosymbiosis (Chap. 3), a comparison of the interpreted life habits of eurypterids to those known in modern horseshoe crabs and scorpions (Chap. 4), and an investigation of the feeding behaviors of Eocene whales through comparisons with skull morphologies of extant whales (Chap. 5). Part II incorporates studies of taphonomy and environmental controls on organism distribution. These studies include an investigation of microbialites through time (Chap. 6), the preservation of tropical, shallow marine mollusk assemblages (Chap. 7), the distribution of burrowing organisms on beaches (Chap. 8), the concentration of iron minerals around burrows (Chap. 9), and the preservation of phytoliths in modern, disturbed ecosystems (Chap. 10). Part III broadly covers organism-substrate interactions or neoichnology. While these studies also examine aspects of functional morphology, taphonomy, and environment, the focus is on the production of biogenic structures in the sediment or other media. These studies include the characterization of burrows produced by modern scorpions (Chap. 11), salamanders (Chap. 13), skinks (Chap. 14), and lemmings (Chap. 16) in a variety of media and environmental conditions, surface trails produced by swimming fish (Chap. 12), an array of novel surface traces produced by modern African and Asian elephants (Chap. 15), and a new means of detecting animal burrows and buried tracks and trails in various types of sediment using ground-penetrating radar (Chap. 17).

We are very grateful to our group of expert reviewers who provided insightful, helpful, and timely reviews of the papers included in this volume. Our panel of expert reviewers consisted of 26 researchers from around the world including Emese Bordy (University of Cape town), Danita Brandt (Michigan State University), Joseph Carter (University of North Carolina), Al Curran (Smith College), Shahin Dashtgard (Simon Fraser University), Jason Dunlop (Museum für Naturkunde), Murray Gingras (University of Alberta), Leslie Harbargen (SUNY Oneonta), Gary Haynes (University of Nevada),Daniel Hembree (Ohio University), Jonathan Hendricks (San Jose State), Adiël Klompmaker (Florida Museum of Natural History and University of Florida), Dirk Knaust (Statoil ASA), Matthew Kosnik (Macquarie University), Ricardo Melchor (INCITAP (UNLPam-CONICET)), Radek Mikulas (Academy of Sciences of the Czech Republic), Elizabeth Nesbitt (University of Washington), Renatta Netto (PPGeo Unisinos), Karla Parsons-Hubbard (Oberlin College), Brian Platt (University of Mississippi), Roy Plotnick (University of Illinois at Chicago), Sara Pruss (Smith College), Tami Ransom (Salisbury University), Jon Smith (Kansas Geological Survey), Nigel Trewin (University of Aberdeen), and Andrea Wetzel (University of Basel). We would also like to thank Tamara Welschot, Judith Terpos, and Sherestha Saini at Springer for all their help with putting this volume together.

The wealth and breadth of active modern-analog research featured in this volume demonstrates that the solutions to many unanswered questions may be achieved

by honoring the founding geological principle of uniformitarianism. Far from being stifled or replaced by technological advances in modeling simulations, digital resources, and statistical analyses, we anticipate that modern-analog studies will remain relevant to the geosciences and will, indeed, thrive as researchers find new creative applications for empirical, experimental approaches. As geoscientists continue to look to the world around us for perspectives on the history of life, new opportunities for interdisciplinary collaborations and the integration of new technologies promise to expand the range of paleontological problems that can be addressed through modern-analog experiments.

<div style="text-align: right">

Daniel I. Hembree
Brian F. Platt
Jon J. Smith

</div>

Contents

Part II   Taphonomy and Environment

Contributors

Laurie C. Anderson Department of Geology and Geological Engineering, Museum of Geology, South Dakota School of Mines and Technology, SD, USA

Sunil Bajpai Department of Earth Sciences, Indian Institute of Technology at Roorkee, Uttarakhand, India

Jennifer Bauer Department of Geological Sciences, Ohio University, Athens, OH, USA

Andrew P. K. Bentley Department of Earth and Environmental Science, Temple University, Philadelphia, PA, USA

Danita S. Brandt Department of Geological Sciences, Michigan State University, MI, USA

Ashley Burkett Department of Earth and Environmental Systems, Indiana State University, Terre Haute, IN, USA

David Bustos White Sands National Monument, Alamogordo, NM, USA

Ilya V. Buynevich Department of Earth and Environmental Science, Temple University, Philadelphia, PA, USA

María Cristina Cardonatto Universidad Nacional de La Pampa, La Pampa, Argentina

Angeline M. Catena Department of Geological Sciences, Ohio University, Athens, OH, USA

Lisa Noelle Cooper Department of Anatomy and Neurobiology, Northeast Ohio Medical University, Rootstown, OH, USA

H. Allen Curran Department of Geosciences, Smith College, Northampton, MA, USA

Christophe Dupraz Center for Integrative Geosciences, University of Connecticut, Storrs, CT, USA

Nicole D. Dzenowski Department of Geological Sciences, Ohio University, Athens, OH, USA

Murray K. Gingras Department of Earth and Atmospheric Sciences, University of Alberta, Edmonton, Alberta, Canada

Bosiljka Glumac Department of Geosciences, Smith College, Northampton, MA, USA

Stephen T. Hasiotis Department of Geology, University of Kansas, Lawrence, KS, USA

Daniel I. Hembree Department of Geological Sciences, Ohio University, Athens, OH, USA

Tobin L. Hieronymus Department of Anatomy and Neurobiology, Northeast Ohio Medical University, Rootstown, OH, USA

Cheryl A. Hodgson Department of Earth and Atmospheric Sciences, University of Alberta, Edmonton, Alberta, Canada

Dennis Hubbard Department of Geology, Oberlin College, Oberlin, OH, USA

Ethan G. Hyland Department of Earth and Environmental Sciences, University of Michigan, Ann Arbor, MI, USA

Sergey V. Kadurin Physical and Marine Geology, Odessa National University, Odessa, Ukraine

Dirk Knaust Statoil ASA, 4035 Stavanger, Norway

Kurt O. Konhauser Department of Earth and Atmospheric Science, University of Alberta, Edmonton, Alberta, Canada

Igor A. Losev Department of Environmental Science and Policy, George Mason University, Fairfax, VA, USA

Victoria E. McCoy Department of Geology and Geophysics, Yale University, CT, USA

Luke P. McHugh Canadian Natural Resources Limited, Calgary, Alberta, Canada

Ricardo Néstor Melchor INCITAP (UNLPam-CONICET), La Pampa, Argentina

Reed A. Myers Department of Earth and Atmospheric Sciences, University of Alberta, Edmonton, Alberta, Canada

Kristen L. Myshrall Center for Integrative Geosciences, University of Connecticut, Storrs, CT, USA

Karla Parsons-Hubbard Department of Geology, Oberlin College, Oberlin, OH, USA

Brian F. Platt Department of Geology and Geological Engineering, University of Mississippi, Oxford, MS, USA

Roy E. Plotnick Earth and Environmental Sciences, University of Illinois at Chicago, Chicago, IL, USA

Michael Savarese Coastal Watershed Institute and Department of Marine and Ecological Sciences, Florida Gulf Coast University, Fort Myers, FL, USA

Jesse A. Schoengut Canadian Natural Resources Limited, Calgary, Alberta, Canada

Christopher T. Seminack Department of Environmental Science and Policy, George Mason University, Fairfax, VA, USA

Caitlin Tems Department of Earth Sciences, University of Southern California, Los Angeles, CA, USA

J. G. M. Thewissen Department of Anatomy and Neurobiology, Northeast Ohio Medical University, Rootstown, OH, USA

Christopher J. Vinyard Department of Anatomy and Neurobiology, Northeast Ohio Medical University, Rootstown, OH, USA

Pieter T. Visscher Center for Integrative Geosciences, University of Connecticut, Storrs, CT, USA

Bryce Wetthuhn Canadian Natural Resources Limited, Calgary, Alberta, Canada

Logan A. Wiest Department of Earth and Environmental Science, Temple University, Philadelphia, PA, USA

John-Paul Zonneveld Department of Earth and Atmospheric Science, University of Alberta, Edmonton, Alberta, Canada

Part I
Functional Morphology

Chapter 1
Crinoids Aweigh: Experimental Biomechanics of *Ancyrocrinus* Holdfasts

Roy E. Plotnick and Jennifer Bauer

Contents

Abstract Immobile suspension feeders living on soft substrates, although rare in modern marine habitats, were relatively common in the Paleozoic. Numerous Paleozoic taxa have been interpreted as dwelling on soft unconsolidated sediments and possessing morphologic features that either prevented them from sinking (e.g., strophomenid brachiopods) or anchored them to the sea floor (e.g., crinoid holdfasts). The quantitative expression of the static stresses for forms living on soft, muddy bottoms developed by Thayer (1975) can be easily modified to describe the forces involved in anchoring. One of the more unusual putative anchoring structures is the "grapnel" holdfast of the Devonian crinoid *Ancyrocrinus*. This form does not match the paradigm for most typical current anchoring structures, lacking

R. E. Plotnick (✉)
Earth and Environmental Sciences, University of Illinois at Chicago,
845 W. Taylor St., Chicago, IL 60607, USA
e-mail: plotnick@uic.edu

J. Bauer
Department of Geological Sciences, Ohio University,
Athens, OH 45701, USA

recurved, pointed, and flattened lateral processes. Its form is suggestive, however, of the modern, nautical mushroom anchors deployed on muddy bottoms. Plaster casts of the *Ancyrocrinus* holdfast were used to quantify the actual forces involved in penetrating, being pulled out of, or dragged across soft substrates. The forces were measured using a digital force gauge mounted on a motorized test stand. Substrates used included fine quartz sand, pure kaolin mud, and coarse carbonate sand. The holdfasts readily penetrated soft mud, but encountered much greater resistance in fine sand. They did, however, readily penetrate the latter substrate when rocked, supporting the comparison with mushroom anchors. Holdfasts do not penetrate the sediment when dragged across it, suggesting a minimal ability to passively anchor in this way. Simple calculations of the sinking velocity of *Ancyrocrinus* suggest that when dislodged, they would have easily reimplanted in soft substrates.

Keywords Holdfasts · Crinoids · Biomechanics · Functional morphology

1.1 Introduction

A number of fossil groups have structures identified as adaptations for living on soft substrates. Of these, crinoids and other stalked echinoderms have the best fossil record and have been studied in the greatest detail, although as pointed out by Donovan et al. (2007) as well as Seilacher and MacClintock (2005), the attachment structures (holdfasts) of crinoids are relatively rare as fossils and are far less studied than crown structures. Even well-preserved crinoids often lack the distal part of the stem, the dististele.

There is great morphologic disparity among fossil crinoid holdfasts, certainly greater than that among living forms (Brett 1981; Donovan et al. 2007). One of the most distinctive holdfast morphologies is the so-called grapnel of the Devonian inadunate *Ancyrocrinus* Hall 1862 (Fig. 1.1). Specimens of *Ancyrocrinus* are one of the most common crinoid holdfasts in US museum collections, represented by hundreds of specimens. Since their original description (Hall 1862), their morphology and function have been discussed by Ehrenberg (1929), Goldring (1942), Lowenstam (1942), McIntosh and Schreiber (1971), Brett (1981), and Seilacher and MacClintock (2005). In this chapter, we will apply the methods of paleobiomechanics (Plotnick and Baumiller 2000) to test alternative hypotheses of function of these unique forms, such as whether the structure functioned as a surface drag (Ubaghs 1953) or was instead embedded in the sediment (Seilacher and MacClintock 2005).

1.1.1 *Ancyrocrinus*

The morphology, stratigraphic, environmental distribution, ontogeny, and history of the study of *Ancyrocrinus* were reviewed in detail by McIntosh and Schreiber (1971) and will be only briefly summarized here. The genus is known from a num-

Fig. 1.1 Typical example of an *Ancyrocrinus* holdfast (University of Cincinnati Mus. 26158; Middle Devonian (Givetian), Beechwood Limestone, Louisville Cement Quarry, Speed, Indiana). **a** Lateral view. **b** Top view. *Lines* show the measurements taken on specimens used as models in the experiments (Table 1.1); *a* total height of grapnel; *b* height of arms above base; *c* width at the base of radices; *d* width at the top of radices. Scale bars = 1 cm
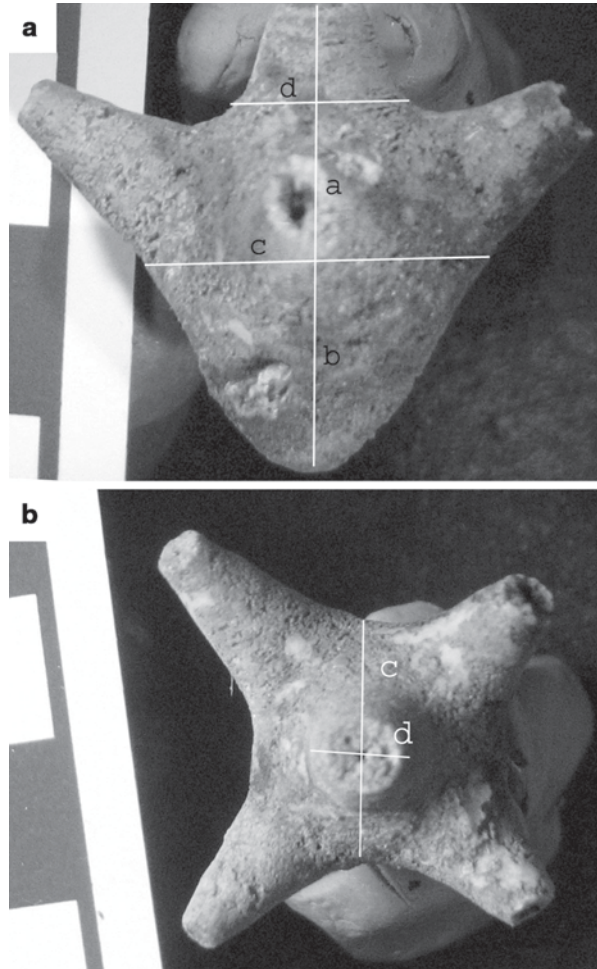
ber of localities in Hamilton Group (Middle Devonian) strata from New York, Pennsylvania, Michigan, Indiana, Ontario, and France (Le Menn and Jaouen 2003). Lithologies include both limestone and shale.

Ancyrocrinus was originally named by Hall (1862) for isolated holdfast structures and the holotype single specimen with an attached 7 in. portion of the column. The generic name derives from the anchor-like shape of the holdfast. Hall named two species, *Ancyrocrinus bulbosus* and *Ancyrocrinus spinosus,* the latter being synonymized with the former by subsequent authors. The crown was unknown until the description of several specimens by Goldring (1942), which revealed a cup not much wider than the stem, as well as a large anal tube and relatively small and sparsely pinnulate arms. This provided sufficient information to assign the genus to the inadunate family Botryocrinidae (Cladida: Dendrocrinina). Although the crown of *Ancyrocrinus* is not unusual, it is the dististele that makes it unique. First, al-

though it does occur rarely in other forms (Donovan 2006), the distal part of the stem is quadrangular. This terminates in mature forms in the "grapnel," a term used as far back as Bather (1900). Brett (1981) classified these structures as "grapnel radices." In the remainder of this chapter, we will use grapnel as a general term to refer to the holdfast structure, rather than in a functional sense.

The external form of the grapnel is quite variable (Ehrenberg 1929; Lowenstam 1942; McIntosh and Schreiber 1971). The most common form (Fig. 1.1) has a rounded bottom and a single level of four equally spaced spurs, arising just proximal to the bottom. Measurements of nine individuals show a mean angle of $60°$ ($s = 5.4°$) between the spurs and the central axis of the grapnel. Measurements were made from photographs using ImageJ (Schneider et al. 2012). The spurs are rounded in cross section and are usually rounded at the tip, although many are broken off. Interestingly, Hall (1862) illustrated the holotype specimens as having spurs ending in sharp points. This formed the basis for reconstructions in Ubaghs (1953) and Ausich et al. (1999). An illustration of this specimen by Goldring (1923) and a photo in McIntosh and Schreiber (1971, Pl. 1, Fig. 18), however, clearly show that the spurs in this specimen were broken off and showed no signs of terminating as points.

Grapnel forms show a significant variability which is apparently ecophenotypic (Ehrenberg 1929; Lowenstam 1942; McIntosh and Schreiber 1971). Variations include multiple levels of spurs, sometimes two and rarely three; fewer than four spurs in a level; an extended section distal to the spurs, so that the spurs are well above the base; longitudinally bent grapnels; and extended sections proximal to the spurs, apparently incorporating a section of the stem. Isolated spurs were labeled as "mistakes" by Seilacher and MacClintock (2005, Fig. 10). Some small individuals also possess relatively long spurs (McIntosh and Schreiber 1971) or show evidence of attachment to shell debris at the base.

The formation of the grapnel was studied by Lowenstam (1942), who examined several hundred specimens including thin sections. Additional ontogenetic data were provided by a nearly complete juvenile specimen described by McIntosh and Schreiber (1971). Juvenile organisms began life attached to shell debris, as is typical for many other crinoids. They then developed four stem radices, which grew upwards at about 60° from the stem (following Donovan (2006), we use radices in preference to cirri, since these articulate symplectially). Secretion of secondary stereom then began at the base and from the junction of the radices on the stem. Secondary stereom did not cover the entire length of the radix. At some point, the unit breaks free from the original attachment, either directly below the radices or further down the stem. In some cases, parts of the primary attachment may be retained, including shell fragments. Additional stereom then forms over the broken base. Some of the variation in grapnel form clearly comes from differences in the location of the break from the original attachment relative to that of the stem radices and the extent to which growth and secondary stereom secretion occurred prior to the break (McIntosh and Schreiber 1971). Brett (1981) classified such structures as composite holdfasts.

Lowenstam (1942) noted that well-preserved specimens showed surficial wrinkles in the stereom. He described these (p. 25) as a "wrinkled fold series arranged

peripherally around the spur bases and the proximal body portion, overlapping at the junctions of the body and spurs. Fold-like stereom masses were observed on the body and on the spurs. The folds follow each other at equal distances, the axes being vertical to that of the covered skeletal elements…. In a few specimens the folds consisted of several series of close lying tubercles." These folds were also observed by McIntosh and Schreiber (1971) and drawn by Seilacher and MacClintock (2005, Fig. 10).

1.1.2   Functional Interpretations

Hall (1862) proposed that *Ancyrocrinus* began life as attached and then became free floating, with the holdfast acting as a lower balance for the rest of the animal. This interpretation was expanded by Kirk (1911, p. 46), who suggested that the grapnel functioned "rather as a drag and ballast than as a true anchor," implying that the structure lay on the bottom rather than being buried. Kirk (1911) further suggested that the holdfast acted to maintain stability in quiet waters, but would have been dragged along the bottom by waves or currents. This interpretation was implicit in the reconstruction of *Ancyrocrinus* in Ubaghs (1953, Fig. 120), which was redrawn in Ausich et al. (1999, Fig. 20). The latter reconstruction shows drag marks on the sediment surface produced by the spurs and base. These reconstructions also show the crown in the rheophobic "tulip flower" orientation (Donovan 2011); a more realistic rheophilic orientation was favored by Breimer (1969) and McIntosh and Schreiber (1971). Breimer (1969) speculated that *Ancyrocrinus* was able to reanchor after being passively transported by currents and that this would in some way be advantageous. The idea that the holdfast rested on the sea floor was also supported by Lowenstam (1942) who suggested it was used to regain a stable resting position after detachment from the original distal root.

McIntosh and Schreiber (1971) strongly disagreed with the concept that the holdfast acted as a drag and that the organism would benefit from being moved by currents, since the chance of being relocated to a more favorable setting is low. They suggested two potential functions of the grapnel structure. First, in cases where the spurs are long, they could have prevented sinking deep into the soft muds by either becoming entangled with plants or being partially buried ("iceberg strategy" of Thayer 1975). This is similar to the suggested function of spines in some brachiopods (Leighton 2000). Second, the secretion of stereom to form the grapnel would have moved the center of mass downward away from the crown. Both of these functions were proposed to form a secure base for the crinoid (McIntosh and Schreiber 1971), so that it would have been able to maintain an upright rheophilic posture.

An alternative reconstruction was put forward by Seilacher and MacClintock (2005). Although they also showed the tulip flower crown, the holdfast was shown as being completely buried in sediment. They hypothesized that the wrinkled surface originally described by Lowenstam (1942) was produced by a tough "cuticular sock," comparable to tight clothing, that protected the underlying epidermis of the

holdfast from both chemical (from reduced pore waters) and physical attacks. The wrinkles were not functional, but a result of fabricational noise related to the presence of the tight cuticular sock. Seilacher and MacClintock (2005) suggested that burial of the *Ancyrocrinus* holdfast occurred passively as the crinoid dragged it along in currents, perhaps aided by scour on the upcurrent side. They also proposed a similar mechanism, which they termed passive implantation, for the Devonian *Aspidocrinus scutelliformis* Hall and the Ordovician *Oryctoconus lobatus* Colchen and Ubaghs.

The main alternative functional interpretation of the *Ancyrocrinus* grapnel, therefore, is that it was either a "drag" lying on the sediment surface, or that it was an "anchor" buried within the sediment. Although, technically both of these are types of anchors, we will use the terms drag and anchor to designate the two options. The paradigm method and experimental paleobiomechanics will be used to assess these alternative reconstructions (Plotnick and Baumiller 2000).

1.2 Functional Morphology of Holdfasts in Soft Sediments

1.2.1 Anchoring Structures in Modern Organisms

The most detailed studies on the biomechanics of anchoring structures have been carried out on terrestrial plants, using a combination of model and living organisms to examine the forces needed to uproot plants and/or to break them free of the anchorage. Plant roots must transfer the forces experienced by the aboveground portions of the plant (shoots) to the soil system (Ennos 1993). The nature of this force transmission depends on whether or not the stem is used to hold the plant upright. In the latter case (recumbent plants), a flexible stem transmits only tensional forces to the roots and soil. This should also be the case where there is a flexible connection between the stem and the anchoring structure. In the case of a stiff stem attached via a stiff connection to the roots, the anchoring system must also be able to resist rotational forces produced by movement of the stem due to wind. This is the case with most trees (Vogel 2003), in which most of the rotational resistance is produced by the weight of the tree.

Ennos (1993) identified three idealized plant anchoring systems. For plants with flexible stems, the roots should radiate out from the base of the stem. This produces a large surface area over which tension can be distributed. For plants with stiff stems, there can either be a stake-like extension (tap root) going deeper into the soil, stabilized by smaller roots spreading laterally, or rigid roots spreading horizontally (plate), with smaller roots spreading laterally and down (see also Vogel 2003).

Following Ennos (1993), Stokes et al. (1996) experimentally examined the resistance to uprooting on model root systems with different geometries. They constructed model root systems out of stiff steel wire. The models differed in the number,

length, and angle of "lateral roots" distributed around a central horizontal structure. They then measured the amount of tensional force required to pull the system out of a container of wet sand. Based on their results and a resulting conceptual model, they concluded that uprooting was best resisted by a design that placed more lateral roots at greater depths, with the lateral roots being perpendicular to the main axis. Similarly, Mickovski et al. (2007) compared pull-out resistance of model root systems differing in geometry and stiffness. Their results confirmed that models with deeper lateral roots were more difficult to remove and that stiffer roots had greater resistance.

The pull-out resistance of bulbs was investigated by Mickovski and Ennos (2003). They compared equal length model bulbs of different geometries (cylinders, cones, bulbous, and spheres) and orientations (apex up or down) to real bulbs (garlic and onion). The greatest resistance to uprooting was produced by a cone, with the apex pointed upward, with a model resembling an actual bulb (wider at the bottom than top) being second best. The greater resistance of the cones was attributed to their greater surface area and to the maximum diameter being most deeply buried. The latter factor increases shear resistance in sandy soils or the area of overlying material to be sheared in cohesive soils. They suggested that the bulb shape was actually superior to the cone, because it lacked sharp edges and would also allow downward movement of the bulb, being pulled by small roots at the base.

The holdfasts of marine coenocytic green algae, such as *Halimeda* and *Udotea,* were studied by Anderson et al. (2006). All of these taxa had similar holdfast morphology: a hemispherical-to-cylindrical mass formed by fine roots (rhizoids) encompassing a mass of sand. This form is thus broadly similar to the bulbs examined by Mickovski and Ennos (2003). Anderson et al. (2006) found that when these algae were subjected to upward tensile stress, they were removed whole from the substrate and did not break. This was in contrast to the forms on hard substrates which mostly break before being dislodged.

In contrast, anchoring mechanisms of modern animals in soft substrates have not been well studied. Modern pennatulacean anthozoans, such as sea pens, sea whips, and sea pansys, are anchored to the bottom by a single polyp, the peduncle. Kastendiek (1976) examined the relationship of rachis and peduncle morphology of the sea pansy *Renilla* to flow velocity. This form is common in shallow turbulent settings with sandy bottoms. The peduncle is flexible and extensible and can be used to reanchor the colony if it is uprooted. Kastendiek (1976) found that the length of the peduncle increased proportional to flow velocity. He also determined that larger colonies were more prone to uprooting.

1.2.2 Forces Acting on Anchors

As is the case with plants, the forces acting on the holdfast will be dependent on the nature of its attachment to the above substrate portion of the organism (e.g., the stem or stalk). If the connection or the above substrate structure is flexible, then the

forces will be tensional. If the structure and connection are rigid, then there will also be rotational forces. The magnitude of these forces will depend on the size and morphology of the above substrate structure and wave velocity (Denny et al. 1985), i.e., on the drag, lift, and acceleration reactions due to eddying experienced by the organism.

Thayer (1975) reviewed the morphologic adaptations of forms living on soft-muddy bottoms, in particular those that would prevent sinking into the sediments. He summarized the static stress σ exerted downward by an organism on the sediment as:

$$\sigma = (\rho_{org} - \rho_w)\frac{S_2}{nS_1}r_{org}g,$$

where p_{org} is the density of the organism; p_w is the density of the fluid; r_{org} is a characteristic linear dimension of the organism; S_1 is a shape factor that relates r_{org} to the organism's total surface area A_{org} ($A_{org} = S_1r^2$); n is the fraction of that surface area that is in contact with the surface (the bearing area); S_2 is a shape factor that relates r_{org} to the volume and thus the mass; and g is the acceleration due to gravity. As discussed by Thayer (1975), this equation predicts that an organism can reduce its downward stress by reducing its density. This can be achieved by becoming smaller or by increasing nS_1 relative to S_2; the latter occurs by either making the organism flatter ("snowshoe" strategy) or by partially burying it ("iceberg" strategy).

In case of an anchoring structure, we need to be concerned with stress acting upward, rather than downward. The formula of Thayer (1975) is still applicable, except that the concern is maximizing, rather than minimizing, downward force. In general, an attachment should thus be as dense as possible, maximize its overall size, and maximize S_2 relative to nS_1. The first two of these clearly represent a significant cost in terms of material needed. The third increases downward force per unit area and is the basic idea behind a piling, which may be a useful analog for a sediment sticker (Seilacher 1999; Dornbos 2006).

The success of a particular design and corresponding value of σ depends upon the nature of the substrate. The bearing capacity of the sediment is its ability to support the load without failure. As is the case with terrestrial soils, marine sediments are multicomponent systems of water, solids, gases, and organisms (Jumars et al. 2007). Depending on factors such as water content and particle size, physical properties including bearing capacities can vary dramatically (Bokuniewicz et al. 1974). A major control is the cohesion of the sediment; this drops strongly as water content increases and clay content decreases. Highly fluid sediments have virtually no bearing capacity.

Assuming only upward tension is acting, for an organism not to be removed from the sediment, the upward removing force F_t must be less than some downward anchoring force F_A. Conceptually, F_A should be a function of:

- The weight of the structure

- The weight of the sediment overlying the structure and thus the depth of the burial and the surface area of the structure. Increasing this factor increases downward force without a significant increase in metabolic cost of construction.
- Friction, cohesion, and adhesion between the anchor and the sediment: These will be the functions of the composition of the sediment and the geometry and surface properties of the structure, including the possible presence of biological adhesives (Vogel 2003; Parsley and Prokop 2004). For example, those forms interpreted as sediment stickers can be treated as tapered piles (Sowers and Sowers 1970), in which most of the resistance to motion is produced by skin friction.
- The friction and cohesion within the sediment: These control how the sediment will fail and how forces are distributed with the sediment. Sediments with no cohesion will provide very little resistance to uprooting. Highly cohesive sediments will come up as a relatively massive "root ball."

In the case of a stiff stalk, we will also need to factor in the relative behavior of the sediments under both compression and tension, produced as the anchoring structure is subject to rotational forces.

1.2.3 Paradigms for Anchors

There are a wide variety of nautical anchors; their use depends on such factors as the size of the moored structure, the nature of the substrate, and whether the mooring is permanent or temporary. The simplest anchor is a heavy weight. More sophisticated designs, however, are constructed to interact with the substrate to increase the anchoring force. In particular, they dig in if pulled horizontally (Taylor 2004). One of these designs is the grapnel anchor (Fig. 1.2a), from which the *Ancyrocrinus* structure gets its name. The basic parts of an anchor include the shank or stem, to which the anchor chain or rope attaches, and arms at the base of the shank which curve upward and terminate in flat, triangular flukes. The shape of the flukes allows them to penetrate the seafloor as they are being dragged. The grapnel anchor is distinguished from other types by having equally spaced arms. This allows it to set into the bottom no matter which arm is in contact; the other arms remain above the substrate. It is often also used in bottoms with rocks or coral where it can hook firmly into debris, i.e., it acts like a grappling hook. The arms of grappling hooks also recurve toward the shank so they do not become dislodged.

If we use these nautical anchors as a paradigm for the function of the *Ancyrocrinus* grapnel, sensu Rudwick (1964), then the design should include spurs that are distally flattened in cross section, end in points, and are recurved toward the stem. The observed geometry of the structure fails on all three of these criteria: The spurs are rounded, terminate bluntly, and are not curved. Similarly, if we assume that it functioned as a grappling hook to catch on debris, then the shape of the spurs does not match the predicted design.

One intriguing alternative anchor design is the mushroom anchor (Fig. 1.2b–d). Usually used for permanent anchors, it is also sometimes used in small boats for

Fig. 1.2 Modern nautical anchors. **a** Grapnel anchor—*pointed* and *flattened flukes*. **b** Mushroom anchor for small boats—*rounded bottom*. **c, d** Large mushroom-type anchor on a US Navy barge, Ketchikan, Alaska

anchoring in muddy bottoms (Hinz 1986). As the anchor oscillates on a soft seabed, it buries itself. This, in turn, greatly increases the holding power. This anchor design might thus be an appropriate paradigm for *Aspidocrinus* and *Oryctoconus,* which were reconstructed by Seilacher and MacClintock (2005) as having bowl-shaped nodal anchors. It is also possible that the rounded bottom of *Ancyrocrinus* served the same purpose.

In order to directly test the ability of the *Ancyrocrinus* grapnel to act as an anchor, we performed a series of experiments on their ability to set and hold in various bottom sediments. We measured forces needed to pull the structures vertically out of sediments, as well as those required to drag them along the sediment surface. In addition, we determined the forces necessary for the structure to penetrate sediments, assuming the holdfasts reimplanted in some manner after dislodgement. These results also led us to measure the drag coefficients of an *Ancyrocrinus* holdfast moving though water. This was also prompted by the qualitative observation that the lateral view of some grapnels closely approximated a streamlined shape. Finally, we conducted qualitative experiments on whether oscillations of the structure on the sediment surface led to deeper penetration of the grapnel.

1.3 Materials and Methods

Specimens of *Ancyrocrinus* were provided by the Cincinnati Museum Center. All specimens were collected in Speed, Indiana, from the Beechwood Member of the North Vernon Limestone (Middle Devonian, Givetian; Goldstein et al. 2009). Latex molds were made of four of the specimens and from these, plaster (Hydrocal) casts were produced (Fig. 1.1; Table 1.1). A pipe cleaner was embedded in the plaster for horizontal tension experiments and a brass rod was hot glued to the apex of the structure for vertical tension and compression studies.

Forces were measured using a Chatillon DFIS-10 digital force gauge, mounted on a Chatillon TCM-200 motorized test stand. The motorized test stand allows ten-

Table 1.1 *Ancyrocrinus* dimensions (Fig. 1.1) and experimental results. Plaster casts were made of the first four specimens (bold type), which were used in experiments. Experimental averages were based on four trials per model, except for specimen 62124a results for penetration in sand (*n*=3). Dimensions are in centimeters, mass in grams. Forces are in newtons, with negative values for compression and positive values for tension. Specimens are from the Cincinnati Museum Center, Ohio, USA

Specimen number	Total height (a)	Height of radices above base (b)	Width at base of radices (c)	Width at top of radices (d)	Mass	Average force penetration in 1 cm sand	Average force penetration in 1 cm mud	Average maximum pullout force in sand	Average maximum pullout force in mud	Average drag force in sand
62124a	2.4	0.9	1.6	0.8	10.6	−4.14	−0.04	4.83	0.20	1.31
26158	4.7	1.5	2.5	1.9	15.9	−4.28	−0.07	7.74	0.23	1.00
26158	6.4	1.8	2.5	1.8	20.4	−4.43	−0.06	7.43	0.21	0.81
26158	4.1	2.0	2.0	1.5	12.8	−5.85	0.07	4.45	0.15	
26158	2.4	1.1	1.4	1.1	3.3	–	–	–		
62124b	2.5	0.8	1.4	1.2	3.7	–	–	–		
62124c	1.9	0.7	1.7	1.2	4.6	–	–	–		
62123a	2.6	1.2	1.6	1.1	6.5	–	–	–		
62123b	3.5	1.4	2.0	1.3	9.5	–	–	–		

sion or compression to be measured over a constant range of velocities. Most runs were done at a vertical velocity of 2.54 cm/min. Data were recorded using Chatillon Nexygen DF software and uploaded into SYSTAT (version 13) for analysis. Forces were applied vertically by pulling or pushing parallel to the direction of movement of the gauge on the test stand (Fig. 1.3a). Horizontal forces were measured by attaching a length of fishing line to model, which ran horizontally to an Erector set pulley and then vertically to the moving gauge (Fig. 1.3b).

Experiments were performed with a soft-mud substrate prepared from kaolin and water or with wet, fine sand. Due to evaporation, consistent water content of the sediment between runs was difficult to maintain. As a result, we standardized among runs by measuring the forces on a brass disc at both the beginning and end of the experiments.

Forces required to penetrate the substrate were measured by attaching the model directly to the force gauge with a metal rod. The model then penetrated the sediment vertically at a constant velocity (usually 2.54 cm/min) until it completely entered the substrate. The software recorded compressive forces (recorded as negative values) experienced as a function of time; we converted time to the depth of penetration. The model was then withdrawn, and the tension (recorded as positive values) was similarly recorded. Both tension and compression measurements were repeated four times at different locations on the substrate for each of the four models.

Resistance encountered while being dragged across a fine sand surface was determined by using models attached via a pipe cleaner and fishing line to the gauge. Specimens were placed with the flanges level with the sediment surface. During the drag, forces were continuously measured and recorded; the peak tension value was
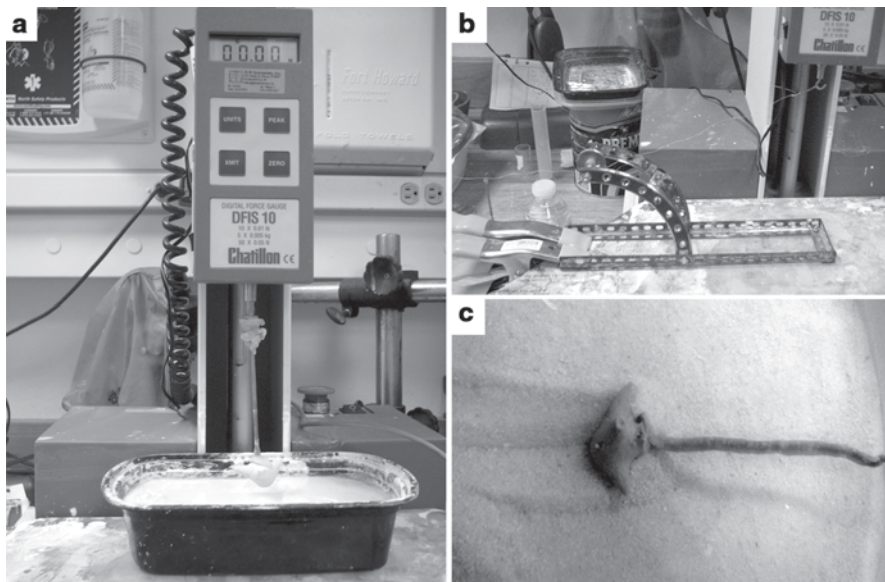
Fig. 1.3 Experimental setups. **a** Arrangement for measuring compressional and tensional forces perpendicular to the substrate surface. Models were attached to a stiff brass rod and moved vertically. **b** Arrangement for measuring forces for grapnels dragged across sediment surface. Models were attached by a pipe cleaner and fishing line around a pulley to the force gauge; **c** *Furrow* and *sand push pile* produced by dragging

recorded at the end of the run. The experiments were also repeated four times for each model. The sand was smoothed out between each run and the container was rotated after every two runs.

The drag coefficients in water of the grapnels were measured using the method described in Plotnick and Baumiller (1988) and Singer et al. (2012). Two models were placed in a recirculating flow tank with flows ranging from 0.013 to 0.255 m/s. The models were attached via a metal rod to a metal plate equipped with strain gauges, which allowed the direct measurement of drag force for each velocity. The models were oriented with the bottom of the grapnel pointing into the flow. The frontal areas of the models were measured and used with the drag measurements to calculate the dimensionless drag coefficients (C_d), using the formula:

$$C_d = \frac{2D}{U^2 A_c \rho_w},$$

where D is the measured drag force in newtons, U is the water velocity, A_c is the frontal surface area of the crinoid exposed to current, and ρ_w is the density of water (we used the approximate density value of tap water of 998 kg/m^3).

Fig. 1.4 Representative
force/distance curves for
models being pushed into
fine sand and soft kaolin mud
substrates. By convention,
compressive forces are nega-
tive. Models were pushed
into the substrate at constant
rate of 2.54 cm/min
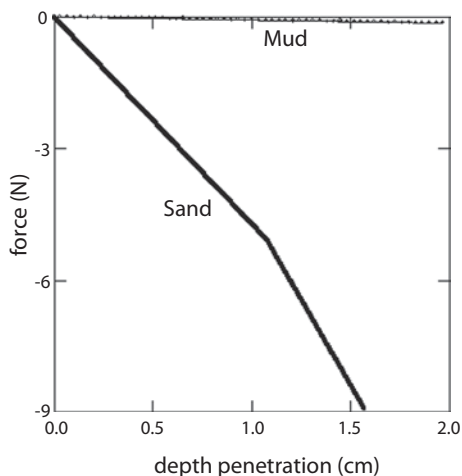
Finally, two models attached to brass rods were placed on a substrate of fine sand. These were then gently rocked by hand without pushing downward, to determine whether they buried themselves deeper in the sediment.

1.4   Results

For each holdfast design and substrate combination, 3–4 trials were performed to determine the effects of varying depth of burial and speed of vertical and horizontal pull on the maximum force for implantation (compression) and removal (tension; Table 1.1). The results for all four *Ancyrocrinus* models were very similar. Representative mud and sand force/distance curves for implantation are shown in Fig. 1.4 (by convention, compressive forces are recorded as negative values). The models penetrated soft mud with very little resistance. Resistance for fine sand was considerably greater. Of interest is the downward kink in the sand force/distance curve; this probably represents penetration to the depth of the flanges and the resulting increase in contact area. For simplicity, we compared the average force required to penetrate 0.01 m into the sediment; this is approximately the depth to the base of the flanges. For fine sand, the mean force for the four models combined was 4.7 N ($n=15$; $s=0.97$ N), whereas for mud it was 0.06 N ($n=16$; $s=0.018$).

Tensional resistance to being pulled out of sediment was measured for all four models from a depth where the flanges were completely buried. This would approximate the force available to resist removal from the sediment due to drag on the crinoid's "superstructure," i.e., the filtration fan, calyx, and stalk. In general, the forces required to remove the grapnel from the substrate were greater than the corresponding forces for implantation (Table 1.1). In case of the soft mud, forces resisting removal were about twice that necessary for implantation.
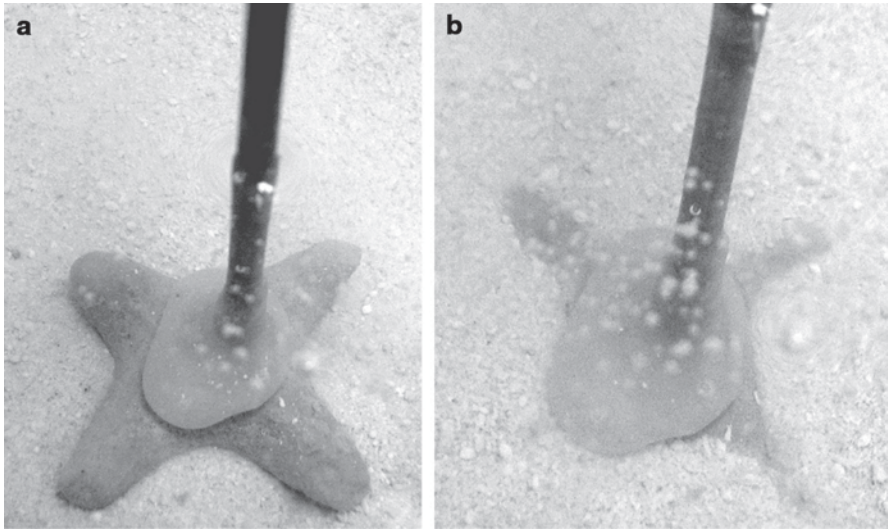
Fig. 1.5 a Plaster cast of *Ancyrocrinus* holdfast on a fine sand substrate attached to a rigid brass "stem." **b** The same grapnel after being rocked by hand in a single plane four times

Maximum resistance to being pulled across the soft-sand substrate was measured in only three models because the radicles on the fourth model were almost totally worn off (Table 1.1). When being pulled across the sand surface, the flanges created shallow furrows, but would not dig the grapnels into greater depths (Fig. 1.3b). The structures simply bulldozed sand in front of them as they were pulled, leading to a small increase in the total tension measured.

Both models rapidly buried themselves into fine sand when rocked by hand (Fig. 1.5). The result after being rocked only four times is shown in Fig. 1.5b.

Both models used to calculate the drag coefficients in water had a frontal area, A_c, of 6×10^{-4} m^2, measured from digital images. The mean coefficient of drag (C_D) measured over seven velocities was 0.75 ($s=0.17$). Drag on the second model was measured at three velocities, yielding a mean C_D of 0.71 ($s=0.07$). This can be considered the minimum estimate of C_D on the crinoid, since it does not include the drag on the stalk or arms. These estimates are not inconsistent with those obtained for motile organisms that move through air or water (Vogel 1994), albeit at the high end of the published values.

1.5 Discussion

Our results suggest that:

1. Although *Ancyrocrinus* grapnels would provide some resistance when pulled across a soft sediment surface, they would not embed themselves deeply while

being dragged. This is consistent with the interpretation based on the paradigm approach. The grapnel still may have provided a relatively stable attachment on firmer substrates, where there would have been high resistance to being pulled out.

2. The grapnels easily penetrate very soft sediments, such as fluid muds, in a manner akin to sediment penetrometers. On firmer substrates such as sand, they could have penetrated if they were rocked, comparable to modern mushroom anchors. Such rocking would have been possible if the stalk of *Ancyrocrinus* was relatively stiff (Baumiller and Ausich 1996).

3. Once buried, the grapnel would have provided significant resistance to removal. This may have been aided by the wrinkled folds on the surface, which thus may not be present due to "fabricational noise," but are actually functional (cf. Seilacher and MacClintock 2005). The overall function is similar to that observed for modern plant bulbs.

If an *Ancyrocrinus* was uprooted from the substrate, it can be assumed that it needed to reanchor as rapidly and effectively as possible. One possible way to do that would be for it to straighten its stalk and fold its arms together as close as possible. It would then fall more-or-less vertically, with the grapnel down. Simple calculations can be made of the velocity at which it would fall and the force with which it would strike the sediment.

Objects falling though fluids have three forces that are relevant (Weaver and Chamberlain 1976). The first of these is the weight (W), resulting from the acceleration due to gravity (g): $W = m_c g$, where m_c is the mass of the crinoid. This is balanced first by buoyancy (B): the density of water (ρ_w) displaced by the volume of the crinoid (V_c) or $B = \rho_w V_c g$. Assuming the crinoid is negatively buoyant, the buoyancy is less than the weight. The downward weight is also opposed by drag (D), which increases with velocity (U) and is a function of the coefficient of drag (C_D) and the frontal area (A_c) of the crinoid or $D = 0.5 C_d \rho_w U^2 A_c$.

When the crinoid starts to fall through the water, $D = 0$, so the downward force is $W - B$, it accelerates downward. As it does so, D increases proportional to the velocity squared until it equals $W - B$; the falling crinoid has now reached terminal velocity (U_T). Since, at terminal velocity $D = W - B$, we can solve for U_T:

$$U_T = \sqrt{\frac{2g(m_c - \rho_w V_c)}{C_D \rho_w A_c}}$$

For the calculation, we used $C_D = 0.8$ based on the experimental results and allowance for additional drag from the arms and the stem. The A_C used was the measured value of 6×10^{-4} m². For ρ_w, we used a sea-surface density of 1,027 kg/m³. The determination of mass and volume is more difficult. Following the method used by Baumiller (1992) for isocrinids, the animal was broken down into a set of units, each of whose volume was approximated by an ideal geometric shape. Dimensions were taken from Goldring (1923) and McIntosh and Schreiber (1971). We used an approximate density of 1,500 kg/m³, based on the values given by Baumiller (1992) and Brower (2006). A rough check on the values was obtained by measuring the

average mass of four preserved grapnels, which was 1.45×10^{-2} kg; the estimated value was 1.38×10^{-2} kg. Using these values, we obtained an estimated terminal velocity of 0.67 m/s. The distance to reach the terminal velocity is relatively short; based on the equations of movement given by Weaver and Chamberlain (1976), a sinking crinoid would reach 99% of terminal velocity in about 0.3 m. An attempt to confirm our velocity estimates was performed by Tomasz Baumiller. Working in a 2.6 m swimming pool, he dropped a model holdfast attached to a pipe cleaner and one attached to the stem and crown of a modern isocrinid through the water. The former reached a velocity of 0.70 m/s and the latter 0.54 m/s, consistent with our estimated value.

The force (F) with which the grapnel penetrates the sediment depends on its kinetic energy and the distance over which it penetrates (d_{pene}): $F = 0.5 \ mv^2/d_{pene}$. A 0.035 kg crinoid sinking at 0.65 km/s would have a kinetic energy of about 7.9×10^{-3} J. As a result, if it penetrated 0.01 m, the force would be 0.79 N; if it penetrated 0.04 m (sufficient to bury), the force would be 0.20 N. These calculations can be compared with the measured forces needed to penetrate the two sediment types. In soft mud, the downward force would be more than sufficient to penetrate and will almost certainly bury the structure. In sand, the downward force would be insufficient to penetrate more than a short distance. The structure would rest on the sediment surface and could then penetrate by rocking. Both of these results were provisionally confirmed by qualitative experiments in which we dropped model holdfasts through water onto sand and mud substrates.

1.6   Conclusions

There is a long history of interpreting the function of structures in fossil organisms by comparison with the products of human engineering. This approach is embodied in the paradigm approach of Rudwick (1964). As discussed by Plotnick and Baumiller (2000), this method is particularly valuable in developing functional hypotheses that can be tested experimentally using the methods of biomechanics (Vogel 2003).

In this study, we tested the alternative hypotheses that the unique grapnel holdfast of the crinoid *Ancyrocrinus* functioned as a drag on the sediment surface or as an anchor embedded in the substrate. Both the paradigm method and experimental studies indicate that the grapnel would have been relatively ineffective as a drag, although it may have provided some resistance to flow-induced motion of the entire animal. The same combination of approaches, however, suggests that the grapnel would have functioned well as an anchor, with a design that allows both ready penetration of the sediment for a dislodged organism and resistance to removal once the structure has been buried.

The development of functional hypotheses using recent analogs and testing these functional hypotheses experimentally can be a fruitful approach. We are currently

extending the current study to include other crinoids, such as the radicular holdfasts of *Eucalyptocrinites,* as well as other soft-substrate-dwelling organisms.

References

Anderson K, Close L, DeWreede RE, Lynch BJ, Ormond C, Walker M (2006) Biomechanical properties and holdfast morphology of coenocytic algae (Halimedales, Chlorophyta) in Bocas del Toro, Panama. J Exp Mar Biol Ecol 328(2):155–167

Ausich WI, Brett CE, Hess H, Simms MJ (1999) Crinoid form and function. In: Hess H, Ausich WI, Brett CE, Simms MJ (eds) Fossil crinoids. Cambridge University Press, Cambridge, pp 3–30

Bather FA (1900) The Crinoidea. In: Lankester RE (ed) Treatise on zoology, part III. Adam and Charles Black, London, pp 94–204

Baumiller TK (1992) Importance of hydrodynamic lift to crinoid autecology, or, could crinoids function as kites? J Paleontol 66(4):658–665

Baumiller TK, Ausich WI (1996) Crinoid stalk flexibility: theoretical predictions and fossil stalk postures. Lethaia 29(1):47–59

Bokuniewicz HJ, Gordon RB, Rhoads DC (1974) Mechanical properties of the sediment-water interface. Mar Geol 18:263–278

Breimer A (1969) A contribution to the paleoecology of Palaeozoic stalked crinoids. Proc Koninklijke Ned Akad Wet Ser B: Phys Sci 72(2):139–150

Brett CE (1981) Terminology and functional-morphology of attachment structures in pelmatozoan echinoderms. Lethaia 14(4):343–370

Brower JC (2006) Ontogeny of the food-gathering system in Ordovician crinoids. J Paleontol 80(3):430–446

Denny MW, Daniel RL, Koehl MAR (1985) Mechanical limits to size in wave-swept organisms. Ecol Monogr 55:69–102

Donovan SK (2006) Crinoid anchoring strategies for soft-bottom dwelling (comment on Seilacher and MacClintock, 2005). Palaios 21(4):397–399

Donovan SK (2011) The poorly illustrated crinoid. Lethaia 44(2):125–135.

Donovan SK, Harper DAT, Hakansson E (2007) The root of the problem: palaeoecology of distinctive crinoid attachment structures from the Silurian (Wenlock) of Gotland. Lethaia 40(4):313–320

Dornbos SQ (2006) Evolutionary palaeoecology of early epifaunal echinoderms: response to increasing bioturbation levels during the Cambrian radiation. Palaeogeog Palaeoclim Palaeoecol 237(2–4):225–239

Ehrenberg K (1929) Pelmatozoan root-forms (fixation). Bull Am Mus Nat Hist. 59(1):1–76

Ennos AR (1993) The scaling of root anchorage. J Theor Biol 161(1):61–75

Goldstein A, Greb SF, Conkin JE (2009) Stratigraphy of the Silurian and Devonian strata in the central Ohio Valley, the Falls of the Ohio, and quarries in Clark Co., Indiana. Field Guide, 9th North American Paleontological Convention, Cincinnati, Ohio, June 24, 2009

Goldring W (1923) The Devonian crinoids of the state of New York. N Y State Mus Mem 16:1–670

Goldring W (1942) Crown of *Ancyrocrinus bulbosus* Hall. Bull Buffalo Soc Nat Sci 17(3):13–18

Hall J (1862) Preliminary notice of some of the species of Crinoidea known in the Upper Helderberg and Hamilton groups of New York. N Y State Cabinet Nat Hist 15th Ann Rep 15:115–153

Hinz ER (1986) The complete book of anchoring and mooring. Cornell Maritime Press, Centreville

Jumars PA, Dorgan KM, Mayer LM, Boudreau BP, Johnson BD (2007) Material constraints on infaunal lifestyles: may the persistent and strong forces be with you. In: Miller III W (ed) Trace fossils: concepts, problems and prospects. Elsevier, Amsterdam, pp 442–457

Kastendiek J (1976) Behavior of sea pansy *Renilla kollikeri* Pfeffer (Coelenterata-Pennatulacea) and its influence on distribution and biological interactions of species. Biol Bull 151(3):518–537

Kirk E (1911) The structure and relationships of certain eleutherozoic Pelmatozoa. Proc U S Natl Mus 41:1–137

Leighton LR (2000) Environmental distribution of spinose brachiopods from the Devonian of New York: test of the soft-substrate hypothesis. Palaios 15(3):184–193

Le Menn J, Jaouen PA (2003) Nouvelles espèces d'*Ancyrocrinus* et d'*Ammonicrinus*, crinoïdes à pédoncule spécialisé du Dévonien armoricain (Brest, France). C R Palevol 2(3):205–212

Lowenstam HA (1942) The development of the crinoid root *Ancyrocrinus*. Bull Buffalo Soc Nat Sci 17(3):21–36

McIntosh GC, Schreiber RL (1971) Morphology and taxonomy of the Middle Devonian crinoid *Ancyrocrinus bulbosus* Hall 1862. Cont Mus Paleont 23(25):381–403

Mickovski SB, Ennos AR (2003) Model and whole-plant studies on the anchorage capabilities of bulbs. Plant and Soil 255(2):641–652

Mickovski SB, Bengough AG, Bransby MF, Davies MCR, Hallett PD, Sonnenberg R (2007) Material stiffness, branching pattern and soil matric potential affect the pullout resistance of model root systems. Eur J Soil Sci 58(6):1471–1481

Parsley RL, Prokop RJ (2004) Functional morphology and paleoecology of some sessile Middle Cambrian echinoderms from the Barrandian region of Bohemia. Bull Geosci 79:147–156

Plotnick RE, Baumiller TK (1988) The pterygotid telson as a biological rudder. Lethaia 21(1):13–27

Plotnick RE, Baumiller TK (2000) Invention by evolution: functional analysis in paleobiology. Paleobiol 26(4):305–323

Rudwick MJS (1964) The inference of function from structure in fossils. Br J Philos Sci 15:27–40

Schneider CA, Rasband WS, Eliceiri KW (2012) NIH Image to ImageJ: 25 years of image analysis. Nat Meth 9(7):671–675

Seilacher A (1999) Biomat-related lifestyles in the Precambrian. Palaios 14(1):86–93

Seilacher A, MacClintock C (2005) Crinoid anchoring strategies for soft-bottom dwelling. Palaios 20(3):224–240

Sowers GB, Sowers GF (1970) Introductory soil mechanics and foundations 3rd edn. Collier Macmillan Ltd, Hong Kong

Stokes A, Ball J, Fitter AH, Brain P, Coutts MP (1996) An experimental investigation of the resistance of model root systems to uprooting. Ann Bot 78(4):415–421

Taylor GI (2004) The holding power of anchors. Resonance 9(10):88–93

Thayer CW (1975) Morphologic adaptations of benthic invertebrates to soft substrata. J Mar Res 33(2):177–189

Ubaghs G (1953) Classe de Crinoides. In: Piveteau J (ed) Traite de paleontologie, vol III. Masson, Paris, pp 658–773

Vogel S (1994) Life in moving fluids: the physical biology of flow. Princeton University Press, Princeton

Vogel S (2003) Comparative biomechanics: life's physical world. Princeton University Press, Princeton

Weaver JS, Chamberlain JA Jr (1976) Equations of motion for post mortem sinking of cephalopod shells and the sinking of *Nautilus*. Paleobiol 2(1):8–18

Chapter 2
Ultra-elongate Freshwater Pearly Mussels (Unionida): Roles for Function and Constraint in Multiple Morphologic Convergences with Marine Taxa

Laurie C. Anderson

Contents

Abstract   Morphologic convergence may arise because natural selection produces an optimal solution for a given set of environmental conditions or because constructional and historical constraints limit available variation, making certain morphologies inevitable. Shell shape in bivalves typically is interpreted as functional, with emphasis placed on substrate preferences and life habits. Freshwater pearly mussels (Order Unionida) represent the most diverse freshwater bivalve clade and, although their life history and related morphologic traits are strikingly divergent from marine bivalves as well as other freshwater bivalve clades, multiple convergences in shell form within and among these groups occur. Ultra-elongate shells (length/height ratios >3.0) in both marine and unionoid taxa are one such example. At least 13 families, including 4 phylogenetically defined unionoid families, have ultra-elongate representatives. These taxa occur in substrates ranging from soft sediments to hard grounds and a variety of life habits including nonmotile semi-infaunal, active burrowers, and borers; which seems to imply weak functional/adaptive control on

L. C. Anderson (✉)
Department of Geology and Geological Engineering, Museum of Geology,
South Dakota School of Mines and Technology, Rapid City, SD 57701, USA
e-mail: Laurie.Anderson@sdsmt.edu

morphology. For many of these taxa, however, this shape may reflect functional forces related to direct substrate penetration without major anterior/posterior rotation of the shell, rather than the type of substrate penetrated. Further, shell elongation is achieved through a variety of differential growth patterns, which argues against a strong role for constructional or historical constraint. Clarifying the meaning of a modern analog or proxy is critical for evaluating paleoenvironmental and paleoecological interpretations of extinct ultra-elongate bivalve taxa as well as for informing efforts to protect and restore extinction-vulnerable extant populations.

2.1   Introduction

Function is commonly assigned to morphologic features because it is through phenotype that organisms interact with their environment. Nonetheless, evolutionary history leaves a record in the morphology of clades and, without this legacy, we could not use morphologic data alone to distinguish between homology and homoplasy, the latter arising either from parallelism (nonhomologous similarities that are the product of the same developmental genetic mechanisms) or convergence (nonhomologous similarities that are the product of different developmental genetic mechanisms) (see Wake et al. 2011). Therefore, we harness the mosaic nature of evolution to both reconstruct evolutionary relationships and understand function and adaptation. In other words, we view phenotype as resulting from the interplay of functional, constructional, and historical factors (e.g., Seilacher 1984; Savazzi 1987; Gould 2002; Cubo 2004; Schwenk and Wagner 2004; Brakefield 2006; Losos 2011).

The roles of function and history are apparent in the freshwater pearly mussels (Order Unionida). This clade represents an ancient invasion and major radiation into freshwater with members occurring on all continents except Antarctica. The Unionida includes 840 valid extant nominal species (Graf and Cummings 2007; Bogan and Roe 2008) and has a fossil record that extends to the Triassic (Watters 2001; Bogan and Roe 2008). Graf and Cummings (2006) recognized eight morphologic and/or life-history synapomorphies for the order, most of which relate to adaptations for reproduction in flowing waters, including both brooding and parasitic larval stages. The evolutionary history of unionoids, on the other hand, is readily apparent based on features such as the distinctive schizodont dentition of both this order (unless lost secondarily) and its sister taxon, the marine Trigoniida (Graf and Cummings 2006 and references therein).

Although many life history and morphologic traits in unionoids are unique to the clade, striking examples of convergence (used here to refer both to parallelism and convergence sensu stricto; see Wake et al. 2011) in shell form occur between unionoids and other bivalves. One such example is that of the freshwater "oysters" in the Etheriidae that cement their valves to hard substrates and whose shells

converge on the morphology of marine oysters (Yonge 1962; Graf and Cummings 2006). A cementing freshwater veneroid, *Posostrea anomioides* (Cyrenidae = Corbiculidae, see Bieler et al. 2010) also has been described (Bogan and Bouchet 1998).

Extremely elongate unionoid species (here defined as having length/height ratios >3.0 and referred to as ultra-elongate taxa) are another putative example of marine/freshwater convergence (Savazzi and Yao 1992; Haag 2012). In fact, several ultra-elongate unionoids have been compared, at least implicitly, to marine razor clams (Solenidae and Pharidae) through the use of scientific names that include *Solenaia, Lamproscapha ensiformis,* and *Mycetopoda soleniformis*. Some of these taxa (*Mycetopoda* spp., *Solenaia*) not only possess shells similar in shape to razor clams, but also exhibit an anteriorly directed, distally enlarged foot reminiscent of *Solen* and *Ensis*.

Ultra-elongate taxa, however, are not limited to a few clades or to a narrow range of habitats in either marine or freshwater environments. In the marine realm, ultra-elongate shells characterize razor clams, but also occur in extant genera of the Solecurtidae (*Tagelus*), Mytilidae (*Lithophaga, Adula, Mytella, Arcuatula, Adipicola,* and *Gigantidas*), Pholadidae (*Pholas*), Nuculanidae (*Poroleda, Propeleda,* and *Adrana*), Petricolidae (*Petricolaria*), Vesicomyidae (*Elenaconcha extenta*), and Arcidae (*Litharca*). Further, ultra-elongate morphologies occur in substrates ranging from soft sediment to hard grounds (rock, shell, and wood), and include active burrowers, borers, and byssally attached species.

Ultra-elongate unionoids also are represented in multiple clades, occurring in ten genera from eight subfamilies and four families (Table 2.1; Fig. 2.1) that include the Unionidae (*Arconaia, Cuneopsis, Lanceolaria, Solenaia, Elliptio*), Hyriidae (*Lortiella*), Iridinidae (*Chelidonopsis*), and Mycetopodidae (*Mycetopoda, Mycetopodella, Lamproscapha*). The ultra-elongate shape arose at least seven times within the order, based on phylogenetic placement of genera containing ultra-elongate species (Fig. 2.1; Table 2.1; also see Graf 2013).

This chapter explores functional interpretations of shell shape by summarizing available information on environmental occurrences, life habits (e.g., epifaunal/semi-infaunal, burrowing, burrow dwelling, borehole dwelling), and burrowing/boring behavior of both marine and freshwater ultra-elongate taxa, including a detailed description of the occurrence of ultra-elongate unionoids collected from three tributaries of the upper Amazon River in southeastern Peru. The various modes of differential growth that produce ultra-elongate shells are outlined, as indicated through differences in beak position, muscle scar shape, and hinge development.

A better understanding of the ecology of these unionoid bivalves can inform efforts to protect and restore their extant populations, as pearly mussels are the most critically endangered bivalve clade on a global scale (e.g., Bogan 1993; Lydeard et al. 2004). In fact, for the 499 unionoid species listed on the International Union for Conservation of Nature (IUCN) Red List 2012.2 (http://www.iucnredlist.org/), 41 % are considered threatened (175) or extinct (29), and data are insufficient to evaluate the status of an additional 94 species (18.9 %), with some ultra-elongate species threatened by habitat destruction and/or introduction of invasive species (Mansur et al. 2003; Castillo et al. 2007). In addition, a general understanding of the

Table 2.1 Unionoid genera with extant ultra-elongate species

Family (subfamily)	Genus	L/H	Environmental occurrence	Geographic distribution genus	Ultra-elongate species included in published molecular phylogeny
Unionidae (Unioninae)	*Arconaia*	4.9	*A. lanceolata*: organic-rich, anoxic lake muds (Savazzi and Yao 1992)	Asia	*A. lanceolata*: Huang et al. 2002; Zhou et al. 2007
Unionidae (Unioninae)	*Cuneopsis*	3.1	*C. celtiformis* and *C. pisciculus*: active burrowers in well oxygenated lake and river channel sediment (Savazzi and Yao 1992)	Asia	*C. celtiformis*: Zhou et al. 2007 *C. pisciculus*: Huang et al. 2002; Zhou et al. 2007
Unionidae (Unioninae)	*Lanceolaria*	4.2	*L. grayana*: active burrower in well oxygenated lake and river channel sediment (Savazzi and Yao 1992); mudbanks at mouth of streams flowing into Luc Nam River at low water (Dautzenberg and Fischer 1905)	Asia	*L. grayana*: Huang et al. 2002; Ouyang et al. 2011; *L. gladiola*: Ouyang et al. 2011
Unionidae (Ambleminae)	*Elliptio*	4.1[1]	*E. shepardiana*: along stable protected river and stream banks with fine sand and silt, behind roots and around logs and trees (University of Georgia Museum of Natural History 1996)	North America	*E. shepardiana*: Campbell and Lydeard 2012
Unionidae (Indotropical "Gonideinae")	*Solenaia*	4.2	*S. iridinea* (as *S. oleivora*): in anoxic lake muds with high methane content (Savazzi and Yao 1992) *S. soleniformis* (as *Balwantia soleniformis*): bores into firm grounds in river cutbanks (Godwin-Austen 1919)	Asia	*S. iridinea*: Huang et al. 2002; Ouyang et al. 2011 (as *S. carinatus*, *S. oleivora*, and *S. rivularis*)
Hyriidae (Velesunioninae)	*Lortiella*	3	*L. rugata*: under rocks and ledges, among roots and mud; in tube-like burrows in mudbanks (Ponder and Bayer 2004)	Australia	*L. rugata*: Graf and Cummings 2006

Table 2.1 (continued)

Family (subfamily)	Genus	L/H	Environmental occurrence	Geographic distribution genus	Ultra-elongate species included in published molecular phylogeny
Mycetopodidae (Mycetopodinae)	*Mycetopoda*	3.3	*Mycetopoda*: in permanent domichnia in firm grounds exposed in river banks and rapids (d'Orbigny 1846; Veitenheimer and Mansur 1978). *M. siliquosa*: in mud (Castillo et al. 2007) lake margins and stream channels in soft sediment (Pimpão et al. 2008; pers. obs.) *M. legumen*: in fine compacted sand in rivers (Veitenheimer and Mansur 1978) *Mycetopoda soleniformis*: in firm grounds exposed in river banks and rapids (Burmeister 1988; pers. obs.)	South America	*S. siliquosa*: Whelan et al. 2011
Mycetopodidae (Mycetopodinae)	*Mycetopodella*	4.3	*Mycetopodella falcata*: in permanent domichnia in firm grounds exposed in river banks and rapids (Burmeister 1988; pers. obs.)	South America	No
Mycetopodidae (Anodontitinae)	*Lamproscapha*	3.8	*L. ensiformis*: channels within large channel-bar complex at convergence of Rios Negro, Amazonas and Solimões (Pimpão et al. 2008)	South America	No
"Iridinidae" (Iridininae)	*Chelidonopsis*	4	*C. hirundo*: sandy and gravely river bottoms just below or above rocky barriers, Congo Basin (Pilsbry and Bequaert 1927)	Africa	No

Length/height (L/H) values are taken from figures illustrated by Haas (1969) unless otherwise indicated by a superscript. Phylogenetic placement based on Graf (2013). Higher taxa in quotations are not monophyletic as they are currently defined (see Graf and Cummings 2006; Whelan et al. 2011). Species identifications follow that of Graf and Cummings (2007) and the Mussel Project Website (http://mussel-project.uwsp.edu/index.html)
[1] From Haag (2012)

Fig. 2.1 Phylogenetic relationships among families and subfamilies of the Order Unionida, based on Graf (2013). Taxon names in quotations are paraphyletic as they are currently defined. *Superscript numbers* indicate the presence of genera with ultra-elongate species within the subfamily as follows: [1]*Arconaia, Cuneopsis,* and *Lanceolaria*; [2]*Elliptio*; [3]*Solenaia*; [4]*Lortiella*; [5]*Mycetopoda* and *Mycetopodella*; [6]*Lamproscapha*; and [7]*Chelidonopsis*. This distribution of ultra-elongate taxa indicates a conservative estimate of seven independent acquisitions of this shell morphology
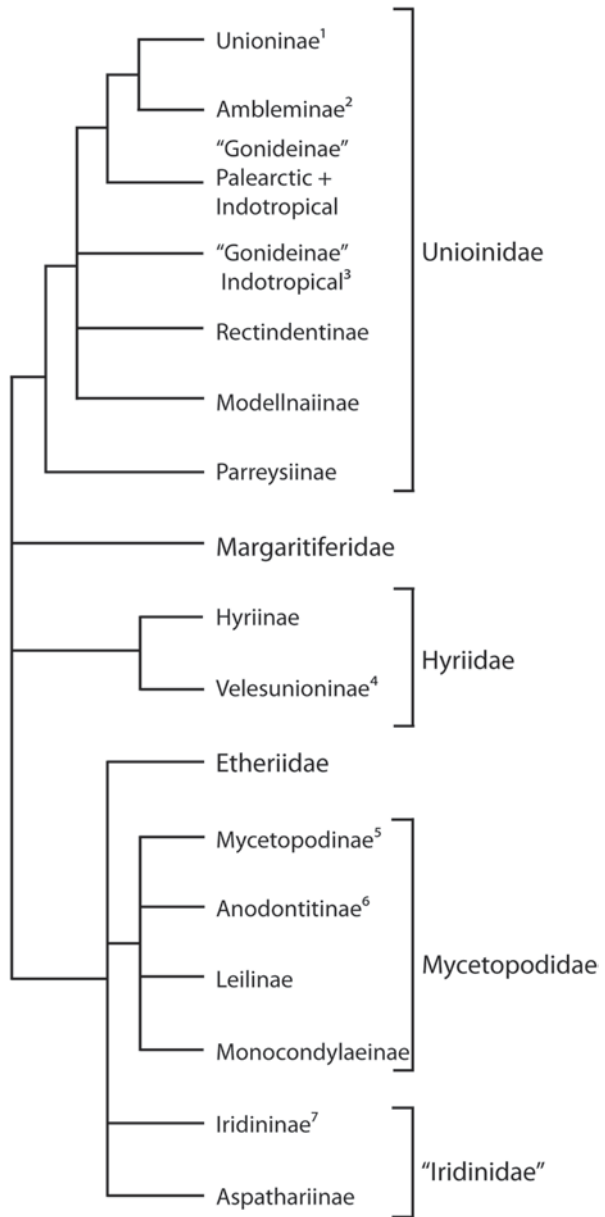
role of function and constraint in producing ultra-elongate shapes is useful in evaluating confidence in paleoenvironmental and paleoecologic interpretations of extinct ultra-elongate taxa such as species of *Prothyris* (L:H 3.0 in *P. elegans*), *Cercomya* (L:H 3.4 in *C. pinguis*), *Palaeosolen* (L:H 5.2 in *P. siliquoidea*), or *Pseudarca* (L:H 4.1 in *P. typa*).

Fig. 2.2 Examples of ultra-elongate marine taxa. Scale bars =1 cm. *Horizontal arrows* point toward the anterior of each shell. *Vertical arrows* indicate the position of the beak. **a** *Solen vagina* (Ireland). **b** *Ensis directus* (Maine). **c** *Tagelus californianus* (California). **d** *Pholas dactylus* (Spain). **e** *Petricolaria pholadiformis* (The Netherlands). **f** *Mytella speciosa* (Peru). **g** *Adula falcata* (California). **h** *Lithophaga gracilis* (Japan). **i** *Litharca lithodomus* (Ecuador). All images are of specimens in the Invertebrate Zoology collections of the California Academy of Sciences

2.2 Morphologic Features of Ultra-elongate Taxa

2.2.1 Marine Exemplars

Among extant marine bivalves, most ultra-elongate species are either razor clams or boring bivalves (Table 2.2; Fig. 2.2), and shape similarities among these taxa have previously been considered convergent (Yonge 1955; Savazzi 1999). Most members of the Solenidae and Pharidae have L:H ranging from about 3 to over 7, with parallel-sided, straight to arched dorsal and ventral margins; indistinct umbos at the shell anterior; and near-vertical anterior and posterior margins (Fig. 2.2a, b). Species of *Tagelus* (Solecurtidae; commonly called stout razor or jack-knife clams) have similar morphologies to the Solenidae and Pharidae (elongate–quadrate), although generally they are not as elongate (L:H ~3), and have the beak located at the valve midline (Fig. 2.2c). In addition, all these bivalves are distinctive in possessing

Table 2.2 Exemplar taxa for extant marine genera with ultra-elongate species

Family	Genus	L/H	Substrate occurrences and domichnia, if reported in literature
Nuculanidae	*Adrana* (11)	3.5[1]	*A. patagonica*: in muddy sand (Saavedra et al. 1999)
	Poroleda (3)	3.3	*P. spathula*: in sand (Grove 2011) *P. lanceolata*: in mud (Powell 1979)
	Propeleda (8)	3.4	*P. platessa*: in sandy mud (Nijssen-Meyer 1972)
Mytilidae	*Adipicola* (9)	4.3[1]	*A. iwaotakii*: epifaunal or infaunal byssate on wood, at whale falls and at hydrothermal vents (Owada 2007; Kyuno et al. 2009; Lorion et al. 2009)
	Adula (7)	5.4	*A. falcata*: bores into soft mudstone (Yonge 1955; Owada 2007)
	Arcuatula (11)	3.1[1]	*Arcuatula*: byssally attached semi-infaunal in mud (Grove 2011)
	Gigantidas (3)	3.4[1]	*G. sharikoshii*: semi-infaunal in sand (Hashimoto and Yamane 2005)
	Lithophaga (19)	3.1	*L. plumula*: bores into calcareous rocks (Yonge 1955)
	Mytella (4)	3.5[1]	*M. speciosa*: byssally attached semi-infaunal among mangrove roots (Riós-Jara et al. 2009; Santos et al. 2010)
Acridae	*Litharca* (1)	3.5	*L. lithodomus*: bores into sandstone (Nicol and Jones 1986)
Solecurtidae	*Tagelus*, including *Tagelus (Mesopleura)* (11)	3.3	*Tagelus*: semipermanent vertical burrows in mud (Yonge 1955) *T. plebeius*: forms Y-shaped oblique deep permanent burrows that animal can retreat into, in silty fine to very fine sand (Stanley 1970) *T. divisus*: forms Y-shaped burrows in muddy sand (Stanley 1970)
Vesicomyidae	*Elenaconcha* (1)	4.1[2]	*E. extenta* (as *Calyptogena extenta*): semi-infaunal in soft sediment at cold seeps at abyssal depths (Sibuet and Olu 1998; Decker et al. 2012)
Veneridae	*Petricolaria* (7)	3.5[1]	*P. pholadiformis*: burrows in soft sediment and bores into rocks (Savazzi 1994); bores into hard clay, mud, peat, wood, or limestone (Zenetos et al. 2009)
Pholadidae	*Pholas*, including *P. (Monothyra)* and *P. (Thovana)* (5)	3.2	*Pholas*: bore into rocks, coral, wood, and consolidated sediment (Turner 1969; Haga and Kase 2011) *P. orientalis*: deep burrowing in sandy and silty mud (Ronquillo and McKinley 2006) *Pholas campechiensis*: bores into wood, limestone or compacted silts (García-Cubas and Reguero 2007)
Solenidae	*Solen,* including *S. (Neosolen)* (67)	5.8	Solenidae: burrows rapidly in sand (Quayle and Newkirk 1989); typically in fine sand within more or less permanent vertical burrows (von Cosel 1990)
	Solena (2)	7.3	

Table 2.2 (continued)

Family	Genus	L/H	Substrate occurrences and domichnia, if reported in literature
Pharidae	*Cultellus* (11)	3.3	Pharidae: typically in fine sand within more or less permanent vertical burrows (von Cosel 1990)
	Ensiculus (4)	3.4	*Ensis*: in permanent burrows (Stanley 1970)
	Ensis (13)	5.4	*E. directus*: typically in cohesive fine sand in permanent burrows (Stanley 1970)
	Pharella (7)	4.5	
	Phaxas (3)	4.1	*Phaxas pellucidus*: deep burrower (Chambers 2008)
	Pharus (2)	5.1	

Length/height (L/H) values are taken from figures illustrated by Moore (1969) unless otherwise indicated by a superscript. Taxonomic placement is based on Carter et al. (2011). The number of species within a genus is listed in parentheses after each genus name and is based on data available in the World Registry of Marine Species (http://www.marinespecies.org/)

[1] Huber (2010)
[2] Coan and Valentich-Scott (2012)

an anterior pedal gape where the two valves do not meet when fully adducted, and through which a long and often cylindrical foot with a dilatable distal end exits the shell (Drew 1907; Yonge 1959; Trueman 1966; Stanley 1970; Bromley and Asgaard 1990; von Cosel 1990; Winter and Hosoi 2011).

Ultra-elongate boring bivalves typically have tubular to cylindrical morphologies with beaks near the valve anterior (<30% from anterior margin). Examples include *Pholas* (Pholadidae) (Fig. 2.2d), *Petricolaria* (Veneridae) (Fig. 2.2e), *Adula* (Mytilidae) (Fig. 2.2g), and *Lithophaga* (Mytilidae) (Fig. 2.2h). Differences among these taxa include the shape of the ventral margin (concave in *Adula,* convex in *Pholas,* and straight or nearly so in *Petricolaria* and *Lithophaga*), and the position of maximum shell height along the anterior–posterior axis (anterior and at the umbo in *Pholas, Petricolaria,* and *Adula*; posterior of the midline in *Lithophaga*). In contrast, *Litharca* (Arcidae) is a uniquely shaped ultra-elongate borer with a cuneiform shell and beak positioned near the posterior of the valve (Fig. 2.2i).

Ultra-elongate species that are nonmotile and epifaunal to semi-infaunal tend to have a curved tubular shell with an anterior beak, as in *Adula* (e.g., species within the mytilids *Gigantidas* or *Adipicola,* and the vesicomyid *Elenaconcha extenta*), or are modioliform (e.g., *Mytella* (Fig. 2.2f) and *Arcuatula*). The ultra-elongate nuculanids (infaunal deposit feeders), *Poroleda* and *Propeleda* retain a nuculanid shape but have greatly extended rostra and relatively low umbos. In contrast, the nuculanid *Adrana* has a nearly straight dorsal margin, anterior and posterior regions that are subequal in shape and length, and a beak located close to the midline.

2.2.2   Ultra-elongate Unionida

Ultra-elongate unionoids are distributed across several clades (Fig. 2.1; Table 2.1) and, although shell shape varies among these taxa, many are comparable to particu-
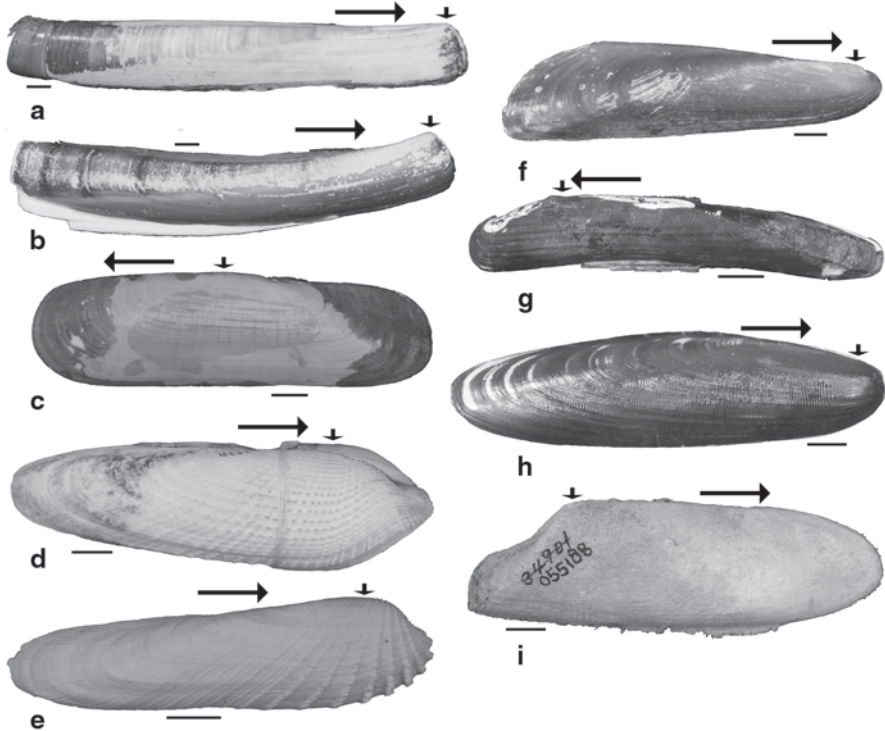
Fig. 2.3 Examples of ultra-elongate unionoids. Scale bars = 1 cm. *Horizontal arrows* point toward the anterior of each shell. *Vertical arrows* indicate the position of the beak. **a** *Mycetopoda soleniformis* (Río Juruá, Peru). **b** *Mycetopodella falcata* (Río Juruá, Peru). **c** *Elliptio shepardiana* (Altamaha River, Georgia). **d** *Lamproscapha ensiformis* (Brazil). **e** *Solenaia iridinea* (China). **f** *Chelidonopsis hirundo* (Democratic Republic of Congo). **g** *Cuneopsis celtiformis* (China). **h** *Lanceolaria grayana* (China). **i** *Lortiella rugata* (Australia). **j** *Arconaia lanceolata* (China). Images **a** and **b** are of specimens collected by the author. Image **c** is of a specimen in the Invertebrate Zoology collections of the California Academy of Sciences. Images **d–j** were provided by Daniel Graf through the MUSSEL Project (http://www.mussel-project.net/) and are of specimens in the Invertebrate Zoology collections of the Smithsonian Institution

lar ultra-elongate marine taxa. For instance, *Mycetopoda soleniformis* (Fig. 2.3a), with its soleniform shape and central beak, resembles an elongate version of *Tagelus* (Fig. 2.2c). In other species of *Mycetopoda,* the shell is more ovate than quadrate and the beak is within 25 % of the anterior margin, but is still within the range of shape variation seen in the Pharidae and Solecurtidae (see von Cosel 1990). In addition, like *Tagelus* and razor clams, species of *Mycetopoda* possess an anterior pedal gape through which a long cylindrical foot with a dilated distal end exits the shell (e.g., Fig. 2.3a; see also d'Orbigny 1846; Fischer 1890; Ortmann 1921; Veitenheimer and Mansur 1978; Pimpão and Mansur 2009).

The falcate shell with an anterior beak and concave ventral margin of *Myceto-podella* (Fig. 2.3b), and to a lesser extent *Elliptio shepardiana* (Fig. 2.3c), *Lampro-scapha* (Fig. 2.3d), and *Lanceolaria* (Fig. 2.3h), resembles that of the boring mytilid *Adula* (Fig. 2.2g). A concave ventral margin is common in mytilids and is associated with byssal attachment along the ventral margin (Stanley 1970, 1972). Unionoids with an *Adula*-like shape, like the similarly shaped vesicomyid *Elenaconcha exten-ta,* are not byssate as adults. Nonetheless, a relatively large and elongated foot that exits the shell anteroventrally may serve a similar anchoring function at least for *Elenaconcha, Mycetopodella,* and *Lamproscapha*. Similarly, the shells of *Solenaia iridinea* (Fig. 2.3e) and *Lortiella rugata* (Fig. 2.3i) resemble the semi-infaunal myt-ilid *Mytella* in shape (Fig. 2.2f) and, although not byssate, these unionoids also have a large foot that they use for anchorage (Ortmann 1921; Savazzi and Yao 1992).

Arconaia, Chelidonopsis, and *Cuneopsis* lack marine exemplars. In general out-line, *Arconaia* (Fig. 2.3j) resembles *Pholas,* although the former has a shell with a strongly twisted, nonplanar commissure (i.e., has shell torsion) and the latter is characterized by the distinctive hinge, muscle, and accessory plate features of the Pholadidae, rendering the comparison tenuous. The elongate ovate shells of *Cheli-donopsis* (Fig. 2.3f) and *Cuneopsis* (Fig. 2.3g) do not closely resemble those of ma-rine ultra-elongate taxa and other distinctive shell features such as pronounced shell torsion (in *Cuneopsis pisciculus* but not *Cuneopsis celtiformis*), or the extremely sharp posteroventral diagonal carinae and posterodorsal margin in *Chelidonopsis hirundo,* may have greater functional relevance for life habit (see Savazzi and Yao 1992).

In summary, the shape of most ultra-elongate unionoids converge on a limited number of exemplar marine taxa, namely razor clams, *Tagelus, Adula,* and *Mytella.*

2.3   Modes of Differential Shell Growth in Ultra-elongate Bivalves

Distinct modes of differential growth imply diverse developmental pathways for the production of ultra-elongate shapes. To this end, Yonge (1955) used muscle scar shape and beak position to determine patterns of differential growth in ultra-elon-gate bivalves, including razor clams, *Tagelus, Lithophaga,* and *Adula* (as *Botula*), using *Glycymeris* with its central beak and round anterior and posterior adductor scars for comparison. For example, the beak is adjacent to the anterior margin and the anterior adductor scar is elongated in most Pharidae and Solenidae, indicating posterior displacement of the area of maximum shell growth (Yonge 1955) into a region that includes the anterior adductor (Table 2.3; Fig. 2.4a).

By comparison, in *Elenaconcha extenta* (as *Calyptogena extenta*), although the beak is anterior of the midline, neither adductor scar is elongated (see Coan and Val-entich-Scott 2012, plate 176), indicating a posterior shift in the center of maximum shell growth that did not affect either adductor. In *Propeleda,* expansion primarily

Table 2.3 Beak position and shape of adductor muscle scars in extant ultra-elongate bivalves

Adductor scars	Beak ≤30% from anterior	Beak 40–50% from anterior	Beak >70% from anterior
Anterior differentially elongated	Pharidae Solenidae		
Both elongated	*Pholas* *Adula*[a, b] *Lithophaga*[a, b]	*Adrana*	
Posterior differentially elongated	*Lortiella* *Lanceolaria* *Solenaia* *Cuneopsis* *Lamproscapha* *Arconaia* *Elliptio shepardiana* *Mycetopodella*[a] *Gigantidas*[b] *Petricolaria*	*Chelidonopsis* *Tagelus*	
Neither elongate	*Elenaconcha extenta* *Propeleda* *Mycetopoda siliquosa* *Mycetopolda legumen* *Mytella*[a, b]	*Mycetopoda soleniformis*	*Litharca*
Muscle scars not observed	*Poroleda* *Adipicola* *Arcuatula*		

[a] Anterior adductor in an anteroventral position
[b] Elongation accompanied by reduced dorsoventral expansion, particularly of the posterior region of the shell

affects the rostrum posterior of the posterior adductor scar, as this genus retains a nuculanid shape (see McAlester 1969).

In contrast, the beak is central and the posterior adductor scar shows slight elongation in *Tagelus* (Table 2.3; Fig. 2.4b) indicating differential growth both anterior and posterior of the midline, but with only the posterior adductor affected. For the nuculanid *Adrana,* the beak also is central but both adductor scars are elongated (Table 2.3; Fig. 2.4c), indicating that the two growth centers were positioned more distally than in *Tagelus.*

For most ultra-elongate mytilids, elongation is accompanied by a dramatic reduction of dorsoventral height especially in the posterior part of the shell, and as a result the hinge axis has a low oblique angle relative to the anterior–posterior axis (Yonge 1955) (Fig. 2.2f–h). The effect of these proportional changes in growth on muscle scars differs among mytilid taxa. For the boring *Adula* and *Lithophaga,* the adductor scars are elongated compared to the typical heteromyarian state of mytilids, although the anterior adductor retains a characteristic anteroventral position (Fig. 2.4d; see also Yonge 1955). In the *Gigantidas,* in contrast, the posterior scar is

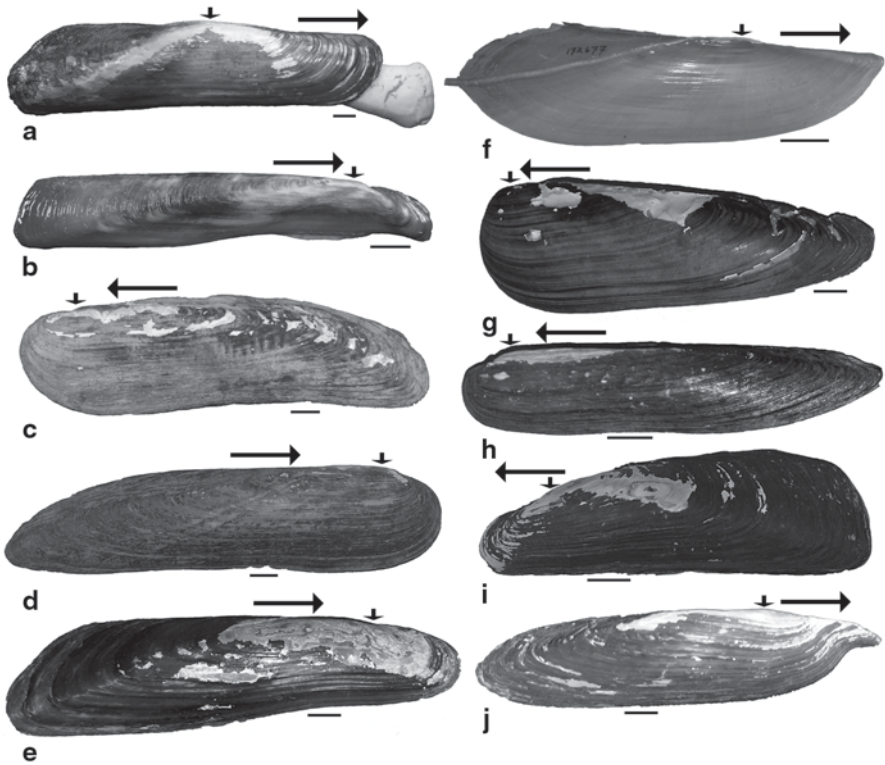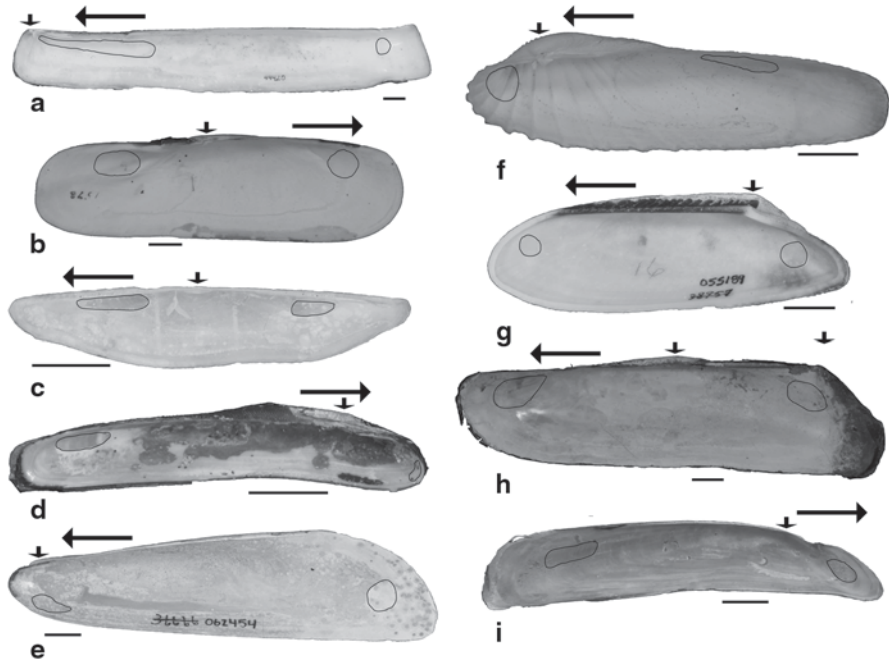**Fig. 2.4** Beak position and adductor muscle scar shape in various ultra-elongate taxa. Scale bars =1 cm. *Horizontal arrows* point toward the anterior of each shell. *Vertical arrows* indicate the position of the beak. Anterior and posterior adductor muscle scars are *outlined*. **a** *Solen vagina* (Ireland). **b** *Tagelus californianus* (California). **c** *Adrana scaphoides* (Colombia). **d** *Adula falcata* (California). **e** *Mytella speciosa* (Peru). **f** *Petricolaria pholadiformis* (the Netherlands). **g** *Litharca lithodomus* (Ecuador). **h** *Mycetopoda soleniformis* (Río Juruá, Peru). **i** *Mycetopodella falcata* (Río Juruá, Peru). Images **a–g** are of specimens in the Invertebrate Zoology collections of the California Academy of Sciences. Images **h** and **i** are of specimens collected by the author

elongated and the anterior scar is positioned more dorsally than typical in mytilids (von Cosel and Marshall 2003). *Mytella speciosa,* however, retains unelongated heteromaryian muscle scars (Fig. 2.4e).

In *Pholas* and *Petricolaria,* the beak is positioned near the shell's anterior (Fig. 2.2d, e), and in *Petricolaria* only the posterior adductor scar is elongated, indicating that the maximum area of shell expansion is in the posterior region and incorporates the posterior adductor (Table 2.3; Fig. 2.4f). In *Pholas,* both dorsal adductor scars are elongated (Turner 1969), but the extensively modified musculature and hinge features of this genus make direct comparisons to other bivalves tenuous. In *Litharca,* in contrast to all other ultra-elongate taxa, the beak is near the posterior. Further, although the adductor muscle scars are not elongated, the hinge is extended anteriorly and absent posterior to the beak, indicating anterior placement of the center of maximum shell growth (Table 2.3; Fig. 2.4g).

In most ultra-elongate unionoids, the beak is anteriorly positioned and the posterior adductor scar is elongated (Table 2.3; Fig. 2.4i), in a pattern similar to that

seen in *Petricolaria* (Fig. 2.4f) and *Gigantidas*. This configuration indicates that these ultra-elongate unionoids are posteriorly extended and the maximum area of expansion incorporates the posterior adductor. In *Chelidonopsis,* the central beak and elongated posterior adductor scar imply a pattern of shell expansion similar to *Tagelus* (Fig. 2.4b). *Mycetopoda soleniformis* (Fig. 2.4h) is an exception and has its beak near the shell midline but with neither adductor scar elongated (i.e., elongation pattern similar to *Tagelus* but without posterior adductor scar elongation). For other *Mycetopoda* species, the beak is more anteriorly positioned than in *M. soleniformis,* but like that species, the muscle scars are not elongated (i.e., pattern similar to *Elenaconcha extenta*).

In summary, there are many ways to produce an ultra-elongate shell via differential growth, although for most taxa differential posterior expansion is involved in some manner. In the unionoids, there are primarily four patterns of differential growth (Table 2.3): posterior growth that includes the posterior adductor (in most unionoids), posterior growth that affect neither adductor (in *Mycetopoda siliquosa* and *M. legumen*), both anterior and posterior growth that affects neither adductor (in *Mycetopoda soleniformis*), and both anterior and posterior growth that affects the posterior adductor (*Chelidonopsis hirundo*).

2.4 Substrate Preferences and Characteristics of Domichnia in Ultra-elongate Bivalves

Savazzi (1994) in a review of the functional morphology of boring and burrowing invertebrates makes a useful distinction among bivalves that are burrowers (motile in sediment that lacks the strength to support an open burrow), burrow dwellers (form semipermanent burrows in sediment with sufficient strength to support an open burrow), and borers (construct permanent borings in partially lithified deposits, siliciclastic or carbonate rocks, shell, and/or wood). The domichnia (trace fossils that represent dwelling structures) of burrow dwellers and borers form a continuum, with some taxa spanning this range of substrates (e.g., *Petricolaria* and *Pholas*; see Table 2.4).

2.4.1 Marine Taxa

Most ultra-elongate marine bivalves are burrow dwellers or borers, including razor clams, *Tagelus, Pholas, Petricolaria, Adula, Litharca,* and *Lithophaga* (Table 2.4). That said, several ultra-elongate species within the nuculanids likely are burrowers, based on the family's trophic role as deposit feeders. In addition, several ultra-elongate taxa are sessile epifauna and/or semi-infauna (particularly the byssate mytilids listed in Table 2.4).

Members of the Solenidae, Pharidae, and *Tagelus* are typically reported from relatively cohesive (i.e., can support an open burrow), stable fine-sand substrates

Table 2.4 Substrate and life modes of extant exemplar ultra-elongate bivalve taxa

Epifaunal to semi-infaunal nonmotile	Burrower in non-cohesive sediment	Burrow dweller in cohesive sediment	Firm ground borer	Hard ground borer
Adipicola	*Adrana*	[a]*Mycetopoda* *legumen*	*Adula*	*Litharca*
Arcuatula	[a]*Arconaia*	[a]*Mycetopoda* *siliquosa* (?)	[a]*Lortiella rugata*	*Lithophaga*
Elenaconcha	[a]*Chelidonopsis* (?)		[a]*Mycetopoda* *soleniformis*	*Petricolaria*
Gigantidas	[a]*Cuneopsis*	*Petricolaria*	[a]*Mycetopodella* *falcata*	*Pholas*
Mytella	[a]*Elliptio shepardiana* (?)	Pharidae	*Petricolaria*	
	[a]*Lamproscapha* (?)	*Pholas*	*Pholas*	
	[a]*Lanceolaria*	Solenidae	[a]*Solenaia* *soleniformis*	
	Poroleda	*Tagelus*		
	Propeleda			
	[a]*Solenaia iridinea*			

For taxa followed by a question mark (?), life habit is inferred from available literature (see Tables 2.1 and 2.2)

[a] = Unionida

(Stanley 1970; Holland and Dean 1977; Quayle and Newkirk 1989; von Cosel 1990). These bivalves are burrow dwellers, and they can quickly descend into their burrows when disturbed (Yonge 1959; Fraser 1967; Stanley 1970; Holland and Dean 1977; von Cosel 1990; also see Drew 1907). When removed from their burrows, however, *Ensis* and *Tagelus* are capable of reburial, often relatively rapidly (Stanley 1970; Winter et al. 2012), unless under physiological distress (Cadée 2000); so they may be considered primarily burrow dwellers and secondarily burrowers because they typically inhabit semipermanent burrows but can also move through soft sediment, particularly when disturbed. The domichnia of solenids and pharids are typically deep and vertical, and are either straight or curved (Yonge 1959; Stanley 1970), whereas in solecurtids burrows are Y-shaped (incurrent and excurrent siphons are unfused and occupy the two arms of the burrow's Y-shaped shafts; Stanley 1970; Holland and Dean 1977; Bromley and Asgaard 1990). The walls of these burrows may be stabilized by compaction and/or by mucus linings (Holland and Dean 1977; Savazzi 1994).

Marine ultra-elongate boring bivalves employ mechanical and/or chemical boring mechanisms. It is generally thought that mechanical boring is more common in poorly lithified siliciclastics and carbonates (here termed firm grounds), whereas chemical boring predominates in well-lithified carbonate rocks (here called hard grounds), bone, and wood. For instance, the mytilid *Adula* is a mechanical borer in mudstones (Yonge 1955; Kleemann 1990, although see Morton 1990), and *Lithophaga* species bore into carbonate rocks, shells, and coral heads by chemical means (Yonge 1955; Kleemann 1990; Morton 1990; Owada 2007), mechanical means (Fang and Shen 1988), or a combination of the two (Appukuttan 2011). Similarly, *Petricolaria* and Pholadidae include both chemical and mechanical borers (Morton 1990; Huber 2010); those taxa (i.e., *Petricolaria, Pholas*) that inhabit cohesive

sediment and firm grounds (mud, peat, clay, chalk) use mechanical means of boring (Osler 1826; Duval 1963; Ansell 1970; Haga and Kase 2011; Nederlof and Muller 2012). Boring mechanisms have not been directly investigated in *Litharca,* although Thomas (1976) used morphologic features (weak ligament, reduced anterior pedal retractors, corroded shell exterior) to infer that *Litharca* was a chemical borer, whereas Nicol and Jones (1986) argue that it is a mechanical borer because it is found in sandstones.

The domichnia of most boring bivalves are perpendicular to the bored surface (Duval 1963; Fankboner 1971; Morton 1990; Pinn et al. 2005) and are comparable to the ichnogenus *Gastrochaenolites,* a flask-shaped boring defined by a straight, narrow neck and larger ovoid chamber in firm to hard substrates (Duval 1963; Kelly and Bromley 1984; Pinn et al. 2005; Hebda 2011; Nederlof and Muller 2012). In contrast to *Gastrochaenolites,* the borings constructed by *Adula* are long and curved (Fankboner 1971). Boring bivalves are typically anchored within their domichnia by a byssus (e.g., *Lithophaga, Adula*), with a strong foot (*Pholas*), or by their siphons (*Petricolaria*), and many can retreat into the distal end of their borings and/or contract their siphons when disturbed (Yonge 1955; Nicol and Jones 1986; Savazzi 1994; Pinn et al. 2005; Owada 2007).

2.4.2 Field Observations of Mycetopodidae in the Upper Amazon Basin (Peru)

Freshwater ultra-elongate taxa also appear to be distributed across a range of substrates (Table 2.4), including fluvial firm grounds, a setting for which domichnia are minimally documented (although freshwater macroborings are reported in Pleistocene biolithites from Lake Turkana (Ekdale et al. 1989; Lamond and Tapanila 2003) and the Eocene Green River Formation (Lamond and Tapanila 2003)). In an aquatic faunal survey in southeastern Peru, occurrences of the ultra-elongate taxa *Mycetopoda soleniformis* and *Mycetopodella falcata* in fluvial firm grounds were documented (Fig. 2.5). The study area included the Ríos Las Piedras (Madre de Dios drainage), Juruá, and Purús, which drain the Fitzcarrald Arch, a structural/geomorphic feature in southeastern Peru and western Brazil. These rivers are incised, exposing Neogene sediments in some cutbanks (Dumont et al. 1990; Antoine et al. 2007). Where incision reaches well-consolidated clays, these sediments typically form the local base level and are exposed at and below the average dry-season water level in cutbanks and rapids (Campbell et al. 2010) (Fig. 2.5a).

Mycetopoda soleniformis and *Mycetopodella falcata* typically occur sympatrically below the average dry-season water level in cutbank exposures of semilithified muds and within rapids associated with similar semilithified subaqueous outcrops in the main channels of the Ríos Purús, Juruá, and Las Piedras (Fig. 2.5). Another unionoid, *Bartlettia stefanensis* (Etheriidae), also occurs but rather than boring, it wedges its posterior into crevices within these firm grounds. Burmeister (1988) reports similar cooccurrences of *Mycetopoda soleniformis, Mycetopodella falcata,*
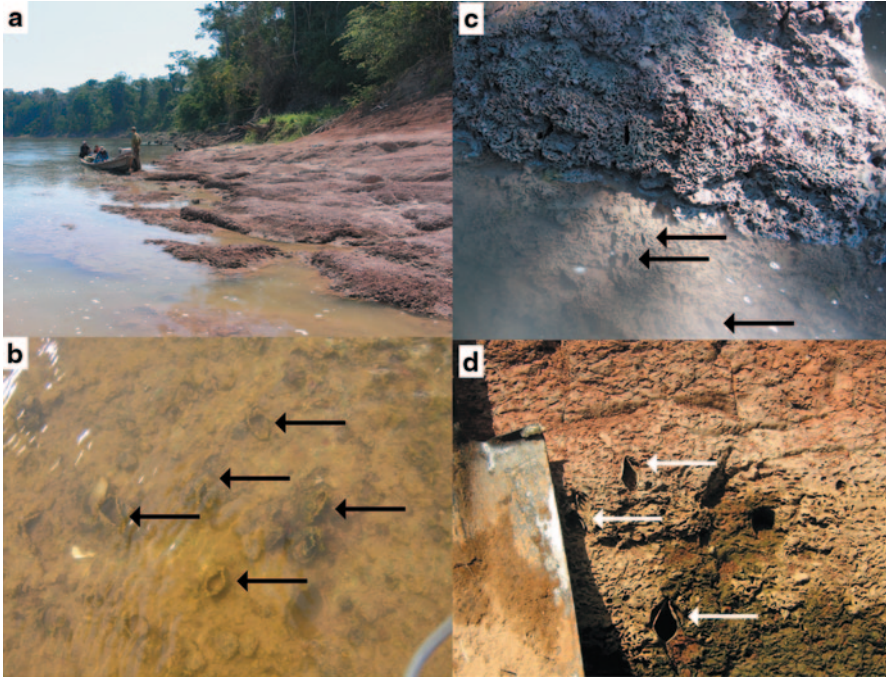
Fig. 2.5 Firm grounds in incised river channels of the Fitzcarrald Arch. Arrows indicate *Mycetopoda soleniformis* borings. **a** partially exposed firm ground at average dry season low water level in the Río Purús; **b** firm ground surface with dead *Mycetopoda soleniformis* partially exposed within their borings, Río Juruá; **c** surface of firm ground showing complex boring patterns in substrate, Río Purús; **d** partially weathered firm ground surface with dead *Mycetopoda soleniformis* within their borings, Río Juruá

and *B. stefanensis* in "hard laterites" along the banks of the Río Yuyapichis (= Yuya Pichis or Llullapichis), Peru.

The areas colonized by these unionoids possess trace assemblages similar to those in *Glossifungites* or *Trypanites* ichnofacies with much of the firm ground surface riddled with small borings made by larval insects (Fig. 2.5c, d). The borings that *M. soleniformis* and *M. falcata* excavate are roughly perpendicular to the outcrop surface below the average dry-season water line and outside of areas that experience high bedload sediment transport and deposition. *Mycetopoda soleniformis* constructs an ovate, smooth-sided boring (slightly wider and ~ 1.5 times longer than its body), into which it can retreat using rapid pedal–muscle retraction while strongly anchoring itself with the foot's bulbous end (d'Orbigny 1846; Veitenheimer and Mansur 1978; pers. obs.) (Fig. 2.5b–d). d'Orbigny (1846) compares the "manner of living" of *Mycetopoda* (as *Mycetopus*) to that of pholads boring into stone and infers that members of the genus bore by mechanical means.

Mycetopodella falcata does not have as strong an anchorable foot as *Mycetopoda,* although Marshall (1927) suggests that its falcate-shaped shell provides anchor-

age. *Mycetopodella* can be extracted from its boring with relative ease, however, because their burrows are only slightly longer than the shell's length so they cannot retreat as deeply into the substrate and their foot provides little resistance when pulled from their burrows.

For other mycetopodids, *Mycetopoda legumen* forms more or less permanent burrows in compacted sand (Veitenheimer and Mansur 1978), *M. siliquosa* occurs in muds (d'Orbigny 1846; Castillo et al. 2007; Pimpão et al. 2008) and unconsolidated sand (pers. obs.), and *Lamproscapha ensiformis* is reported from within a large channel-bar complex at the confluence of Rios Negro, Amazonas, and Solimões in Brazil (Pimpão et al. 2008). For the latter two species, it is not clear from the literature whether they are burrowers or burrow dwellers.

2.4.3   Other Ultra-elongate Unionoids

Other ultra-elongate unionoids also are firm ground dwellers. *Lortiella rugata* is reported from under rocks, among tree roots in mud, and in tube-like burrows in mudbanks in coastal rivers of northwestern Australia (Lamprell and Healy 1998; Ponder and Bayer 2004). Based on the locality description in Ponder and Bayer (2004), the "mudbanks" are likely firm grounds, and *L. rugata* excavate domichnia that they retreat into when the animals are disturbed. Similarly, *Solenaia soleniformis* (as *Balwantia*) is reported as occupying permanent burrows/borings in firm ground clays below seasonal low water in India (Annandale 1919; Godwin-Austen 1919; Prashad 1919). Annandale (1919) infers that this species is a mechanical borer, and Ortmann (1921) and Fischer (1890) note that the foot of *Solenaia* is like that of *Mycetopoda* (long with a dilated distal end), and that these bivalves retreat into their boreholes when disturbed.

Ultra-elongate unionoids are not limited to firm grounds, however. *Cuneopsis celtiformis, C. pisciculus,* and *Lanceolaria grayana,* were collected by Savazzi and Yao (1992) in well-oxygenated lake sediments and river channels. Based on subsequent aquarium observations, the authors considered these taxa active burrowers. Savazzi and Yao (1992) also reported that these taxa, as well as *Arconaia lanceolata,* are oriented subhorizontally when in life position in aquaria. Unlike *Cuneopsis* and *Lanceolaria, A. lanceolata* was collected from soft, methane-rich, anoxic lake muds with *Solenaia iridinea* (as *S. oleivora*). In fact, Savazzi and Yao (1992) infer that the latter two species may be chemosymbiotic due to their environmental occurrence and features such as a nonretractable, sulfur-yellow foot in *S. iridinea* and an anterior rostrum in *A. lanceolata*.

Chelidonopsis hirundo, which is endemic to the Congo Basin (Mandahl-Barth 1988), is reported from sandy and gravely bottoms just below or above rocky barriers (Pilsbry and Bequaert 1927). It is not clear from these descriptions whether *Chelidonopsis* is a burrower or a burrow dweller. Similarly, the North American *Elliptio shepardiana* is reported from stable protected river banks in fine sand and silt behind roots and around logs and trees (University of Georgia Museum of Natural History 1996), and it is not clear whether this species is a burrower or a burrow dweller.

2.5   Discussion

Investigations of adaptation and constraint have an important history in both pale-ontological and neontological literature, with renewed interest as mechanisms of evolutionary developmental biology have been elucidated (e.g., Shubin et al. 2009; Futuyma 2010; Losos 2011; McGhee 2011; Wake et al. 2011). In this context, mor-phologic convergence is of particular interest because it may be interpreted on a continuum from "natural selection produces an optimal solution for a given set of environmental conditions" to "constraints limit available variation so that a given morphology is inevitable" (Thomas 1978a, 1988; Wake 1999; Brakefield and Ros-kam 2006; McGhee 2011; Losos 2011). Distinguishing where on that continuum a potential modern analog falls is valuable in understanding its limits as a reliable proxy for the fossil record.

Bivalves as a whole and clades within this class have been the focus of numer-ous studies examining the roles of adaptation and constraint in morphologic evolu-tion (e.g., Stanley 1975; Thomas 1976, 1978a, b, 1988; Seilacher 1984; Savazzi 1987; Harper and Skelton 1993; Ubukata 2000; Anderson and Roopnarine 2005; Goodwin et al. 2008; Alejandrino et al. 2011). In general, traits such as gill form and function, shell microstructure, hinge features (ligament, dentition), and spiral shell growth are viewed as constrained, whereas shell shape and ornament are less refractory (Stanley 1975; Thomas 1978a, b, 1988; Seilacher 1984; Checa and Jimé-nez-Jiménez 2003; Serb et al. 2011). Interpretations of shell shape in bivalves, es-pecially marine bivalves, typically focus on functional (adaptive) inference related to substrate preferences and life habit (e.g., Stanley 1970; Seilacher 1984; Thomas 1978a, 1988; Alejandrino et al. 2011). Ultra-elongate shell shapes as convergent forms occurring in multiple clades would, therefore, seem compelling as potential environmental indicators.

Ultra-elongate morphologies, however, occur across multiple substrates and life habits (Table 2.4). In other words, these convergences do not have simple re-lationships with the factors typically thought to be important selective agents on shell shape. Even comparing bivalves with similar overall shapes (e.g., *Mytella* as a semi-infaunal byssate taxon vs. *Lortiella rugata* as a firm ground dweller) and/or similar modes of elongation (e.g., *Tagelus* as a burrow-dweller vs. *Mycetopoda soleniformis* as a firm ground borer), reveal a diversity of life modes and substrate preferences. As a consequence, ultra-elongate morphologies either are not reliable environmental proxies because shell shape is not strongly controlled by factors such as substrate type and life habit, or is indicative of a factor common across substrates and life habits.

Deeming ultra-elongate shapes as environmentally uninformative runs counter to much previous work on bivalve functional morphology. For infaunal motile bi-valves especially, the shell plays a critical role as an anchor during the burrowing cycle, but also is a resistant body part that must be pulled through the sediment, implying that functional factors strongly influence shell morphology (Stanley 1970; Seilacher 1984; Savazzi 1994). This does not mean, however, that all infaunal bi-valves have the same shape, and in fact most are not ultra-elongate. In addition,

differences in burrowing style related to differences in shell shape and ornamentation have been previously reported. For instance, clams such as *Mercenaria* incorporate an anterior/posterior rocking motion when burrowing, and rely on both shell sculpture and their prosogyrous anteriors to slice through the sediment and penetrate downward (Stanley 1975; Savazzi 1994). Some unionoids that are not ultra-elongate burrower in a similar way (Savazzi and Yao 1992).

In contrast, bivalves with ultra-elongate shells tend to burrow via direct penetration (i.e., without anterior/posterior shell rotation) and the small anterior cross-sectional area of the shell provides relatively low resistance as they move through the sediment (Stanley 1970, 1975). In fact, *Ensis directus* serves as a biological model for burrowing and retractable-anchor technologies, because of its ability to burrow efficiently (energy scales linearly with depth rather than by depth^2) and rapidly (Winter and Hosoi 2011; Winter et al. 2012). This type of burrowing has been described for Pharidae, Solenidae, *Tagelus, Petricolaria pholadiformis,* and the unionoid *Lanceolaria grayana* (Stanley 1970; von Cosel 1990; Savazzi and Yao 1992; Savazzi 1994; Winter and Hosoi 2011). The unionoid *Cuneopsis* serves as an exception to this association of direct penetration burrowing and an ultra-elongate morphology; *C. celtiformis* and *C. pisciculus* are reported to rock back and forth within the commissural plane while burrowing (Savazzi and Yao 1992). Members of this genus, however, tend to have an inflated anterior relative to other ultra-elongate taxa (Fig. 2.3g), which might explain differing burrowing behaviors.

Most boring ultra-elongate bivalves also have cylindrical forms, again providing a small cross-sectional area in the direction of penetration. In addition, for mechanical borers (pholads, *Petricolaria, Mycetopoda, Solenaia*), substrate penetration is accomplished in a similar manner to that of burrowing ultra-elongate bivalves (d'Orbigny 1846; Annandale 1919; Yonge 1955; Ansell 1970; Savazzi 1994, 1999; Haga and Kase 2011; pers. obs.), although shell ornament (ridges, teeth) in pholads and *Petricolaria* also plays a role in the boring process (Morton 1990; Savazzi 1994, 1999).

Therefore, instead of dismissing ultra-elongate morphologies as uninformative, it may be that this shape reflects the way a substrate is penetrated (i.e., direct penetration without major anterior/posterior rotation), rather than the type of substrate penetrated. In other words, the ultra-elongate shape reflects a set of behaviors rather than a particular substrate or life habit. Constructing this functional/behavioral hypothesis to explain ultra-elongate shell shapes does not rule out a role for constraint in producing these morphologies but, given that an ultra-elongate shape can be achieved through a variety of differential growth pathways (Table 2.3), it seems that its role is at most a minor one.

There are exceptions to this association between ultra-elongate shape and direct penetration of substrates. Examples include ultra-elongate epifaunal to semi-infaunal byssate mytilids, and may also include ultra-elongate unionoids that burrow in noncohesive sediments (Savazzi 1994). In these cases, an ultra-elongate shape may serve a different purpose, be an epiphenomenon, or may require additional data to be tested. For instance, in the epi- and semi-infaunal mytilids and the vesi-

comyid *Elenaconcha extenta,* an elongate shape may enhance anchorage (Stanley 1972). For the unionoids, it may be in part that substrate preferences, life habit, and burrowing behaviors are insufficiently documented to be tested. Savazzi and Yao (1992) noted, however, that in aquaria: (1) *Cuneopsis* spp. uses an anterior/posterior rocking motion during burrowing; (2) the resting position of *Cuneopsis* spp., *Lanceolaria grayana,* and *Arconaia lanceolata* is subhorizontal; and (3) unlike many marine ultra-elongates, the shells of *A. lanceolata* and *C. pisciculus* exhibit pronounced torsion. Marine bivalves with shell torsion tend to be nonsiphonate endobyssate taxa that position the posterior portion of the commissure parallel with the sediment/water interface, presumably to increase the surface area of the mantle in contact with the water column (Tevesz and Carter 1979; Seilacher 1984; Savazzi 1989; Savazzi and Yao 1992). Although unionoids are not byssate, the function of shell torsion may be similar, providing anchorage while maximizing the mantle's contact with the water column (Savazzi and Yao 1992). Similarly, *L. grayana* and *C. celtiformis,* although without torsion, show a low angle of penetration into the sediment and position themselves with their ventral margin at the sediment/water interface (Savazzi and Yao 1992). In other words, an elongate shape also may serve as a way to maximize mantle area exposure to the water column in nonsiphonate bivalves.

2.6 Conclusions

Although convergence upon an ultra-elongate shape occurs in bivalves that inhabit a range of substrates and with a variety of life habits, constraints likely are not strongly canalizing morphology, as ultra-elongate shapes are achieved through a variety of pathways of differential shell elongation. Instead, for many taxa an ultra-elongate shape primarily reflects a set of behaviors used in penetrating any substrate rather than particular types of substrate or life habits. Additional morphologic, ecologic, and behavior studies, particularly under natural conditions, for both marine and unionoid taxa could test this hypothesis. Refining modern analogs with such knowledge is useful not only in interpreting the fossil record, but also for informing efforts to protect and restore extinction-prone extant species of unionoids.

References

Alejandrino A, Puslednik L, Serb JM (2011) Convergent and parallel evolution in life habit of the scallops (Bivalvia: Pectinidae). BMC Evol Biol 11:164. doi:10.1186/1471-2148-11-164

Anderson LC, Roopnarine PD (2005) Role of constraint and selection in the morphologic evolution of *Caryocorbula* (Mollusca: Corbulidae) from the Caribbean Neogene. Palaeontol Electron 8(2):32A

Annandale N (1919) Further notes on the burrows of *Solenaia soleniformis*. Rec Indian Mus 16:205–206

Ansell AD (1970) Boring and burrowing mechanisms in *Petricola pholadiformis* Lamarck. J Exp Mar Biol Ecol 4:211–220

Antoine P-O, Salas-Gismondi RS, Baby P, Benammi M, Brusset S, de Franceschi D, Espurt N, Goillot C, Pujos F, Tejada J, Urbina M (2007) The Middle Miocene (Laventan) Fitzcarrald fauna, Amazonian Peru. In: Díaz-Martínez E, Rábano I (eds) 4th European meeting on the palaeontology and stratigraphy of Latin America. Cuadernos del Museo Geominero. Instituto Geológico y Minero de España, Madrid, pp 19–24

Appukuttan KK (2011) On *Lithophaga (Diberus) bisulcata* a mytilid borer causing damage to the commercially important gastropod shells. Indian J Fish 23:194–200

Bieler R, Carter JG, Coan EV (2010) Classification of bivalve families. In: Bouchet P, Rocroi J-P (eds) Nomenclator of bivalve families. Malacologia 52:113–184

Bogan AE (1993) Freshwater bivalve extinctions (Mollusca: Unionoida): a search for causes. Am Zool 33:599–609

Bogan A, Bouchet P (1998) Cementation in the freshwater bivalve family Corbiculidae (Mollusca: Bivalvia): a new genus and species from Lake Poso, Indonesia. Hydrobiologia 389:131–139

Bogan AE, Roe K (2008) Freshwater bivalve (Unioniformes) diversity, systematics, and evolution: status and future directions. J N Am Benthol Soc 27:349–369

Brakefield PM (2006) Evo-devo and constraints on selection. Trends Ecol Evol 21:362–368

Brakefield PM, Roskam JC (2006) Exploring evolutionary constraints is a task for an integrative evolutionary biology. Am Nat 168(Supplement):S1–S13

Bromley RG, Asgaard U (1990) *Solecurtus strigilatus*: a jet-propelled burrowing bivalve. In: Morton B (ed) The Bivalvia—proceedings of a memorial symposium in honour of Sir Charles Maurice Yonge. Hong Kong University Press, Hong Kong, pp 313–320

Burmeister E-G (1988) Beobachtungen zur Lebensweise von *Bartlettia stefanensis* (Moricand, 1856) am Rio Llullapichis (Peru) (Mollusca, Eulamellibranchia). Spixiana 11:27–36

Cadée GC (2000) Herring gulls feeding on a recent invader in the Wadden Sea, *Ensis directus*. In: Harper EM, Taylor JD, Crame JA (eds) Evolutionary biology of the Bivalvia. The Geological Society, Bath, pp 459–464

Campbell DC, Lydeard C (2012) The genera of Pleurobemini (Bivalvia: Unionidae: Ambleminae). Am Malacol Bull 30:19–38

Campbell KE Jr Prothero DR, Romero-Pittman L, Hertel F, Rivera N (2010) Amazonian magnetostratigraphy: dating the first pulse of the Great American Faunal Interchange. J S Am Earth Sci 29:619–626

Carter JG, Altaba CR, Anderson LC, Araujo R, Biakov AS, Bogan AE, Campbell DC, Campbell M, Jin-hua C, Cope JCW, Delvene G, Dijkstra HH, Zong-jie F, Gardner RN, Gavrilova VA, Goncharova IA, Harries PJ, Hartman JH, Hautmann M, Hoeh WR, Hylleberg J, Bao-yu J, Johnston P, Kirkendale L, Kleemann K, Koppka J, Kříž J, Machado D, Malchus N, Márquez-Aliaga A, Masse J-P, McRoberts CA, Middelfart PU, Mitchell S, Nevesskaja LA, Özer S, Pojeta JJ, Polubotko IV, Pons JM, Popov S, Sánchez T, Sartori AF, Scott RW, Sey II, Signorelli JH, Silantiev VV, Skelton PW, Steuber T, Waterhouse JB, Wingard GL, Yancey T (2011) A synoptical classification of the Bivalvia (Mollusca). Paleontol Contrib 4:1–47

Castillo AR, Brasil LG, Querol E, Querol MVM, Oliveira EV, Mansur MCD (2007) Moluscos bivalves da localidade de São Marcos, bacia do Médio rio Uruguai, Uruguaiana, Brasil. Biotemas 20:73–79

Chambers P (2008) Channel Island marine molluscs: an illustrated guide to the seashells of Jersey, Guernsey, Adlerney, Sark and Herm. Charonia Media

Checa AG, Jiménez-Jiménez AP (2003) Rib fabrication in Ostreoidea and Plicatuloidea (Bivalvia, Pteriomorphia) and its evolutionary significance. Zoomorphology 122:145–159

Coan EV, Valentich-Scott P (2012) Bivalve seashells of tropical Western America marine bivalve mollusks from Baja California to northern Perú. Santa Barbara Museum of Natural History, Santa Barbara

Cubo J (2004) Pattern and process in constructional morphology. Evol Dev 6:131–133

Dautzenberg P, Fischer H (1905) Liste des mollusques récoltés par M. le Capitaine de Frégate Blaise au Tonkin, et description d'espèces nouvelles. J Conch Paris 53:85–234

d'Orbigny A (1846) Voyage dans l'Amérique Méridionale (le Brésil, la République de Orientale de l'Uruguay, la République Argentine, la Patagonie, République du Chili, la République de Bolivia, la République de Pérou), exécuté pendant les années 1826, 1827, 1828, 1829, 1830, 1831, 1832 et 1833. Tome 5, Partie 3, Mollusques. Pitois-Levrault, Strasbourg

Decker C, Olu K, Cunha RL, Arnaud-Haond S (2012) Phylogeny and diversification patterns among vesicomyid bivalves. PLoS ONE 7:e33359. doi:10.1371/journal.pone.0033359

Drew GA (1907) The habits and movements of the razor-shell clam, *Ensis directus*. Biol Bull 12:127–140

Dumont JF, Lamotte S, Kahn F (1990) Wetland and upland forest ecosystems in Peruvian Amazonia: plant species diversity in the light of some geological and botanical evidence. Forest Ecol Manag 33/34:125–139

Duval DM (1963) The biology of *Petricola pholadiformis* Lamarck (Lamellibranchiata Petricolidae). Proc Malacol Soc Lond 35:89–100

Ekdale AA, Brown FH, Feibel CS (1989) Nonmarine macroborings in early Pleistocene algal biolithites (stromatolites) of the Turkana Basin, Northern Kenya. Palaios 4:389–396

Fang L-S, Shen P (1988) A living mechanical file: the burrowing mechanism of the coral-boring bivalve *Lithophaga nigra*. Mar Biol 97:349–354

Fankboner PV (1971) The ciliary currents associated with feeding, digestion, and sediment removal in *Adula (Botula) falcata* Gould 1851. Biol Bull 140:28–45

Fischer P (1890) Observations sur les genres *Mycetopus* et *Solenaia*. J Conch Paris Series 3(30):5–14

Fraser TH (1967) Contributions to the biology of *Tagelus divisus* (Tellinacea: Pelecypoda) in Biscayne Bay, Florida. B Mar Sci 17:111–132

Futuyma DJ (2010) Evolutionary constraint and ecological consequences. Evolution Int J org Evolution 64:1865–1884. doi:10.1111/j.1558-5646.2010.00960.x

García-Cubas A, Reguero M (2007) Catalogo illistrado de moluscos bivalvos del Golfo de México y Mar Caribe. UNAM, Instituuo de Ciencias del Mar y Limnología, Mexico

Godwin-Austen HH (1919) Description of a new species of *Margaritanopsis* (Unionidae) from the southern Shan States, with notes on *Solenaia soleniformis*. Rec Indian Mus 16:203–205, pl. 215

Goodwin DH, Anderson LC, Roopnarine PD (2008) Evolutionary origins of novel conchologic growth patterns in tropical American corbulid bivalves. Evol Dev 10:642–656

Gould SJ (2002) The structure of evolutionary theory. The Belknap Press of Harvard University Press, Cambridge

Graf DL (2013) Patterns of freshwater bivalve global diversity and the state of phylogenetic studies on the Unionoida, Sphaeriidae, and Cyrenidae. Am Malacol Bull 31:135–153

Graf DL, Cummings KS (2006) Palaeoheterodont diversity (Mollusca: Trigonioida + Unionoida): what we know and what we wish we knew about freshwater mussel evolution. Zool J Linn Soc-Lond 148:343–394

Graf DL, Cummings KS (2007) Review of the systematics and global diversity of freshwater mussel species (Bivalvia: Unionoida). J Mollus Stud 73:291–314

Grove SJ (2011) A guide to the seashells and other marine molluscs of Tasmania http://www.molluscsoftasmania.net. Accessed 21 Aug 2012

Haag WR (2012) North American freshwater mussels: natural history, ecology, and conservation. Cambridge University Press, Cambridge

Haas F (1969) Superfamily Unionacea Fleming, 1828. In: Moore RC (ed) Treatise on invertebrate paleontology, part N, volume 1, Mollusca 6 Bivalvia. The University of Kansas and the Geological Society of America, Inc., Boulder, pp 411–467

Haga T, Kase T (2011) *Opertochasma somaensis* n. sp. (Bivalvia: Pholadidae) from the Upper Jurassic in Japan: a perspective on pholadoidean early evolution. J Paleontol 85:478–488

Harper EM, Skelton PW (1993) The Mesozoic marine revolution and epifaunal bivalves. Scripta Geol Spec Issue 2:127–153

Hashimoto J, Yamane T (2005) A new species of *Gigantidas* (Bivalvia: Mytilidae) from a vent site on the Kaikata Seamount southwest of the Ogasawara (Bonin) Islands, Southern Japan. Venus: Jap J Malacol 64:1–10

Hebda A (2011) Information in support of a recovery potential assessment of Atlantic mud-piddock (*Barnea truncata*) in Canada. DFO Canadian Science Advisory Secretariat Research Document 2010/117:30 p

Holland AF, Dean JM (1977) The biology of the stout razor clam *Tagelus plebeius*: I. Animal-sediment relationships, feeding mechanism, and community biology. Chesap Sci 18:58–66

Huang Y, Liu H, Wu X, Ouyang S (2002) Testing the relationships of Chinese freshwater Unionidae (Bivalvia) based on analysis of partial mitochondrial 16S rRNA sequences. J Mollus Stud 68:359–363

Huber M (2010) Compendium of bivalves. ConchBooks, Hackenheim

Kelly RA, Bromley RG (1984) Ichnological nomenclature of clavate borings. Palaeontology 27:793–807

Kleemann K (1990) Evolution of chemically-boring Mytilidae (Bivalvia). In: Morton B (ed) The Bivalvia—proceedings of a memorial symposium in honour of Sir Charles Maurice Yonge. Hong Kong University Press, Hong Kong, pp 111–124

Kyuno A, Shintaku M, Fujita Y, Matsumoto H, Utsumi M, Watanabe H, Fujiwara Y, Miyazaki J-I (2009) Dispersal and differentiation of deep-sea mussels of the genus *Bathymodiolus* (Mytilidae, Bathymodiolinae). J Mar Biol 2009:1–15. doi:10/1155/2009/625672

Lamond RE, Tapanila L (2003) Embedment cavities in lacustrine stromatolites: evidence of animal interactions from Cenozoic carbonates in U.S.A. and Kenya. Palaios 18:445–453

Lamprell K, Healy J (1998) Bivalves of Australia, vol 2. Backhuys Publishers, Leiden

Lorion J, Duperron S, Gros O, Cruaud C, Samadi S (2009) Several deep-sea mussels and their associated symbionts are able to live both on wood and on whale falls. P Roy Soc B 276:177–185. doi:10.1098/rspb.2008.1101

Losos JB (2011) Convergence, adaptation, and constraint. Evolution Int J org Evolution 65:1827–1840. doi:10.1111/j.1558-5646.2011.01289.x

Lydeard C, Cowie RH, Ponder WF, Bogan AE, Bouchet P, Clark SA, Cummings KS, Frest TJ, Gargominy O, Herbert DG, Hershler R, Perez KE, Roth B, Seddon M, Strong EE, Thompson FG (2004) The global decline of nonmarine mollusks. Bioscience 54:321–330

Mandahl-Barth G (1988) Studies in African freshwater bivalves. Danish Bilharziasis Laboratory, Charrlottendlund

Mansur MCD, dos Santos CP, Darrigran G, Heydrich I, Callil CT, Cardoso FR (2003) Primeiros dados quali-quantitativos do mexilhão-dourado, *Limnoperna fortunei* (Dunker), no Delta do Jacuí, no Lago Guaíba e na Laguna dos Patos, Rio Grande do Sul, Brasil e alguns aspectos de sua invasão no novo ambiente. Rev Bras Zool 20:75–84

Marshall WB (1927) A new genus and two new species of South American fresh-water mussels. Proc US Natl Mus 71:10–12

McAlester AL (1969) Superfamily Nuculanacea H. Adams & A. Adams, 1858. In: Moore RC (ed) Treatise on invertebrate paleontology, part N, volume 1, Mollusca 6 Bivalvia. The University of Kansas and the Geological Society of America, Inc., Boulder, pp 231–235

McGhee GR Jr (2011) Convergent evolution: limited forms most beautiful. The MIT Press, Cambridge

Moore RC (1969) Treatise on invertebrate paleontology, part N, volume 1–2, Mollusca 6 Bivalvia. The University of Kansas and The Geological Society of America, Inc., Boulder

Morton B (1990) Corals and their bivalve borers—the evolution of a symbiosis. In: Morton B (ed) The Bivalvia—proceedings of a memorial symposium in honour of Sir Charles Maurice Yonge. Hong Kong University Press, Hong Kong, pp 11–45

Nederlof R, Muller M (2012) A biomechanical model of rock drilling in the piddock *Barnea candida* (Bivalvia; Mollusca). J R Soc Interface 7(76):12 p. doi:10.1098/rsif.2012.0329

Nicol D, Jones DS (1986) *Litharca lithodomus* and adaptive radiation in arcacean pelecypods. Nautilus 100:105–110

Nijssen-Meyer J (1972) *Propeleda platessa* (Dall, 1890), a nut clam new for the coastal waters of Surinam (Pelecypoda, Nuculanidae). Zool Med Leiden 47:449–456

Ortmann AE (1921) South American naiades; a contribution to the knowledge of the freshwater mussels of South America. Mem Carnegie Mus 8:451–670, pls.434–448

Osler E (1826) On burrowing and boring marine animals. Philos T R Soc Lon 116:342–371

Ouyang J, We X, Ouyang S, Li S, Zhao D (2011) Phylogenetic analysis of some Chinese freshwater Unionidae based on mitochondrial COI sequences. J Conchol 40:543–548

Owada M (2007) Functional morphology and phylogeny of the rock-boring bivalves *Leiosolenus* and *Lithophaga* (Bivalvia: Mytilidae): a third functional clade. Mar Biol 150:853–860

Pilsbry HA, Bequaert J (1927) The aquatic mollusks of the Belgian Congo. With a geographical and ecological account of Congo malacology, with field notes by the collectors, H. Land and J.P. Chapin. B Am Mus Nat Hist 53:69–602, pls. 610–677

Pimpão DM, Mansur MCD (2009) Chave pictória para identificação dos bivalves do baixo Rio Aripuanã, Amazonas, Brasil (Sphaeriidae, Hyriidae e Mycetopodidae). Biota Neotrop 9:377–384

Pimpão DM, Rocha MS, de Caastro Fettuccia D (2008) Freshwater mussels of Catalão, confluence of Solimões and Negro Rivers, State of Amazonas, Brazil. Check List 4:395–400

Pinn EH, Richardson CA, Thompson RC, Hawkins SJ (2005) Burrow morphology, biometry, age and growth of piddocks (Mollusca: Bivalvia: Pholadidae) on the south coast of England. Mar Biol 147:943–953

Ponder WF, Bayer M (2004) A new species of *Lortiella* (Mollusca: Bivalvia: Unionoidea: Hyriidae) from northern Australia. Molluscan Res 24:89–102

Powell AWB (1979) New Zealand Mollusca: marine, land and freshwater shells. Collins, Auckland

Prashad B (1919) XIX. Studies on the anatomy of Indian Mollusca. 3. The soft parts of some Indian Unionidae. Rec Indian Mus 16:289–296

Quayle DB, Newkirk GF (1989) Farming bivalve molluscs: methods for study and development. Advances in world aquaculture, vol 1. Louisiana State University, Baton Rouge

Ríos-Jara E, Navarro-Caravantes CM, Galván-Villa C-M, Lopez-Uriarte E (2009) Bivalves and gastropods of the Gulf of Tehuantepec, Mexico: a checklist of species with notes on their habitat and local distribution. J Mar Biol. 2009: 12 p. doi:10-1155/2009/176801

Ronquillo JD, McKinley RS (2006) Developmental stages and potential mariculture for coastal rehabilitation of endangered Pacific angelwing clam, *Pholas orientalis*. Aquaculture 256:180–191

Saavedra L, Dornelles LMA, Santos SB, Absalão R, Anjos SMC, Melo GV, Stanton NSG, Fonseca EM, Lima LL, Küsel ET, Ribeiro EO, Lazillota AAA, Esteves FA (1999) Caracterizaçao oceanográfica da plataforma continental interna adjacente ao Cabo Frio—RJ, no Inverno de 1995. Oecologia Aust 7:245–272

Santos HSS, Beasley CR, Tagliaro CH (2010) Changes in population characteristics of *Mytella falcata* (d'Orbigny, 1846) beds, an exploited tropical estuarine mussel. Bol Inst Pesca 36:85–97

Savazzi E (1987) Geometric and functional constraints on bivalve shell morphology. Lethaia 20:293–306

Savazzi E (1989) Shell torsion and life habit in the recent mytilid bivalve *Modiolus philippinarum*. Palaeogeogr Palaeocl 72:277–282

Savazzi E (1994) Functional morphology of boring and burrowing invertebrates. In: Donovan SK (ed) The palaeobiology of trace fossils. The Johns Hopkins University Press, Baltimore, pp 43–82

Savazzi E (1999) Boring, nestling and tube-dwelling bivalves. In: Savazzi E (ed) Functional morphology of the invertebrate skeleton. Wiley, Chinchester, pp 205–237

Savazzi E, Yao P (1992) Some morphological adaptations in freshwater bivalves. Lethaia 25:195–209

Schwenk K, Wagner GP (2004) The relativism of constraints on phenotypic evolution. In: Pigliucci M, Preston K (eds) Phenotypic integration: studying the ecology and evolution of complex phenotypes. Oxford University Press, Oxford, pp 390–408

Seilacher A (1984) Constructional morphology of bivalves: evolutionary pathways in primary versus secondary soft-bottom dwellers. Palaeontology 27:207–237

Serb JM, Alejandrino A, Otárola-Castillo E, Adams DC (2011) Morphological convergence of shell shape in distantly related scallop species (Mollusca: Pectinidae). Zool J Linn Soc-Lond 163(2):571–584. doi:10.1111/j.1096-3642.2011.00707.x

Shubin N, Tabin C, Carroll S (2009) Deep homology and the origins of evolutionary novelty. Nature 457:818–823. doi:10.1038/nature07891

Sibuet M, Olu K (1998) Biogeography, biodiversity and fluid dependence of deep-sea cold-seep communities at active and passive margins. Deep-Sea Res Pt II 45:517–567

Stanley SM (1970) Relation of shell form to life habits of the Bivalvia (Mollusca). Geo Soc Mem 125:1–296

Stanley SM (1972) Functional morphology and evolution of byssally attached bivalve mollusks. J Paleontol 46:165–212

Stanley SM (1975) Adaptive themes in the evolution of the Bivalvia (Mollusca). Annu Rev Earth Pl Sci 3:361–385

Tevesz MJS, Carter JG (1979) Form and function in *Trisidos* (Bivalvia) and a comparison with other burrowing arcoids. Malacologia 19:77–85

Thomas RDK (1976) Constraints of ligament growth, form and function on evolution in the Arcoida (Mollusca: Bivalvia). Paleobiology 2:64–83

Thomas RDK (1978a) Limits to opportunism in the evolution of the Arcoida (Bivalvia). Philos T Roy Soc B 284:335–344

Thomas RDK (1978b) Shell form and the ecological range of living and extinct Arcoida. Paleobiology 4:181–194

Thomas RDK (1988) Evolutionary convergence of bivalved shells: a comparative analysis of constructional constraints on their morphology. Am Zool 28:267–276

Trueman ER (1966) The fluid dynamics of the bivalve molluscs *Mya* and *Margaritifera*. J Exp Biol 45:369–382

Turner RD (1969) Superfamily Pholadacea Lamarck, 1809. In: Moore RC (ed) Treatise on invertebrate paleontology, part N, volume 2, Mollusca 6 Bivalvia. The University of Kansas and the Geological Society of America, Inc., Boulder, pp 702–741

Ubukata T (2000) Theoretical morphology of hinge and shell form in Bivalvia: geometric constraints derived from space conflict between umbones. Paleobiology 26:606–624

University of Georgia Museum of Natural History (1996) Altamaha River freshwater mussel species. http://amylyne.myweb.uga.edu/fwmolluscs/Altamahafwm.html#Eshep. Accessed 30 Aug 2012

Veitenheimer IL, Mansur MCD (1978) Morfologia, histologia e ecologia de *Mycetopoda legumen* (Martens, 1888)—(Bivalvia, Mycetopodidae). Iheringia 52:33–71

von Cosel R (1990) An introduction to the razor shells (Bivalvia: Solenacea). In: Morton B (ed) The Bivalvia—proceedings of a memorial symposium in honour of Sir Charles Maurice Yonge. Hong Kong University Press, Hong Kong, pp 283–311

von Cosel R, Marshall BA (2003) Two new species of large mussels (Bivalvia: Mytilidae) from active submarine volcanoes and a cold seep off the eastern North Island of New Zealand, with description of a new genus. Nautilus 117:31–46

Wake DB (1999) Homoplasy, homology and the problem of 'sameness' in biology. Novart Fdn Symp 222:24–46

Wake DB, Wake MH, Specht CD (2011) Homoplasy: from detecting pattern to determining process and mechanism of evolution. Science 331:1032–1035

Watters GT (2001) The evolution of the Unionacea in North America, and its implications for the worldwide fauna. In: Bauer G, Wächtler K (eds) Ecology and evolution of the freshwater mussels Unionoida. Springer, Berlin, pp 281–307

Whelan NV, Geneva AJ, Graf DL (2011) Molecular phylogenetic analysis of tropical freshwater mussels (Mollusca: Bivalvia: Unionoida) resolves the position of *Coelatura* and supports a monophyletic Unionidae. Mol Phylogenet Evol 61:504–514

Winter AG V, Hosoi AE (2011) Identification and evaluation of the Atlantic razor clam (*Ensis directus*) for biologically inspired subsea burrowing systems. Integr Comp Biol 51:151–157

Winter AG V, Deits RL, Hosoi AE (2012) Localized fluidization burrowing mechanics of *Ensis directus*. J Exp Biol 215:2072–2080

Yonge CM (1955) Adaptation to rock boring in *Botula* and *Lithophaga* (Lamellibranchia, Mytilidae) with a discussion of the evolution of this habit. Q J Microsc Sci 96:383–410

Yonge CM (1959) On the structure, biology and systematic position of *Pharus legumen* (L.). J Mar Biol Assoc UK 38:277–290

Yonge CM (1962) On *Etheria elliptica* LAM. and the course of evolution, including assumption of monomyarianism, in the Family Etheriidae (Bivalvia: Unionacea). Philos T Roy Soc B 244:423–458

Zenetos A, Olvalis P, Vardala-Theodorou E (2009) The American piddock *Petricola pholadiformis* Lamarck, 1818 spreading in the Mediterranean Sea. Aquat Invasions 4:385–387

Zhou C-H, Ouyang S, Wu X-P, Li M (2007) Phylogeny of the genus *Lamprotula* (Unionidae) in China based on mitochondrial DNA sequences of 16S rRNA and ND1 genes. Acta Zool Sinica 53:1024–1030

Chapter 3
Relationships of Internal Shell Features to Chemosymbiosis, Life Position, and Geometric Constraints Within the Lucinidae (Bivalvia)

Laurie C. Anderson

Contents

Abstract Lucinids are an ancient bivalve clade in which all living members examined to date possess sulfur-oxidizing bacterial endosymbionts. Although a basal synapomorphy is the most parsimonious explanation of universal chemosymbiosis, other mechanisms, including differential extinction of nonsymbiotic lineages, could produce the same character distribution. Therefore, a proxy for chemosymbiosis applicable to fossil taxa could be used to test hypotheses of endosymbiotic evolution as well as elucidate paleocommunity dynamics and biogeochemical cycling for the wide range of marine ecosystems that these bivalves inhabit. Toward that end, geometric morphometrics were used to quantify features of the anterior adductor muscle scar, an inferred basal synapomorphy for the Lucinidae that previous authors have associated with chemosymbiosis. Eight shallow-marine lucinid species were included in analyses, along with two other "lucinoid" species, one of which is chemosymbiotic. Species demonstrated significant shape differences in both a canonical variates analysis (CVA) and a series of discriminate function analyses. For all but two species, the first canonical variates (CV) axis exhibits strong positive interspecific allometry. This allometric trend describes elongation of both the anterior adductor muscle scar and inhalant channel as size increases. Comparing results to published

L. C. Anderson (✉)

Department of Geology and Geological Engineering, Museum of Geology, South Dakota School of Mines and Technology, Rapid City, SD 57701, USA
e-mail: Laurie.Anderson@sdsmt.edu

ecologic and phylogenetic data indicate that both life position within the sediment and geometric constraint control morphologic variation. In addition, although morphologic variation cannot be linked to the degree of symbiont dependence with available data, thin-plate splines (TPS) of landmark configurations may track the location of mantle gills and pallial septa, which are accessory respiratory and feeding structures thought to have evolved as lucinid ctenidia were co-opted to house bacteria.

Keywords Lucinidae · Geometric morphometrics · Chemosymbiosis · Constraint · Allometry

3.1 Introduction

In marine ecosystems, symbiotic associations between microbes and animals are widespread with at least seven phyla hosting chemosynthetic bacteria as endo- or ectosymbionts (Porifera, Platyhelminthes, Nemata (Nematoda), Mollusca, Annelidae, Arthropoda, and Echinodermata) (Ott et al. 2004; Stewart et al. 2005; Dubilier et al. 2008). Such associations are not limited to the extreme environments where they were initially documented (e.g., hydrothermal vents, hydrocarbon seeps), but also are an important component of most brackish and marine ecosystems (Dubilier et al. 2008; van der Heide et al. 2012).

Within the Bivalvia, such associations are widespread, occurring within all members of the Solemyidae, Lucinidae, and Vesicomyidae, as well as in some members of the Mytilidae, Thyasiridae, Teredinidae (Distel 1998; Duperron et al. 2012; Roeselers and Newton 2012), and Manzanellidae (Nucinellidae in Taylor and Glover 2010; Oliver and Taylor 2012). Chemosynthetic microbes housed in bivalve tissues are thiotrophic (sulfur-oxidizing) members of the Gammaproteobacteria and Epsilonproteobacteria and/or are methanotrophic members of the Gammaproteobacteria (Dubilier et al. 2008; Vrijenhoek 2010), the latter documented in some mussel species, i.e., *Bathymodiolus* and *Idas* (Petersen and Dubilier 2010); dual methane- and sulfur-oxidizing endosymbiosis also has been suggested for the thyasirid *Conchocele bisecta* (Kamenev et al. 2001). Based on the phylogeny of these hosts and the microbes they house, it is clear that chemosymbiosis evolved repeatedly within the Bivalvia.

Among chemosymbiotic bivalve clades, lucinids are the most speciose as well as the most ecologically and geographically widespread (Taylor and Glover 2010). Lucinids also represent an ancient clade, with several authors placing the Silurian species *Ilionia prisca* within the Lucinidae, noting that it possesses features characteristic of modern lucinids, such as an anterior adductor muscle scar that is detached from the pallial line (Liljedahl 1992; Taylor and Glover 2000, 2006; Kiel 2010). *Ilionia prisca* is presumed to have been chemosymbiotic, as all extant lucinids examined to date possess thiotrophic endosymbionts (Taylor and Glover 2000), and the life-position (with a horizontal anterior/posterior axis) of the species is similar to that of modern lucinids (Liljedahl 1991). Subsequently, however, Taylor et al. (2009) considered the taxonomic placement of Ilionidae as unresolved.

In spite of the inferred antiquity of the relationship between lucinids and thiotrophs, this association appears unconstrained relative to the life history of these

bivalves. For instance, molecular phylogenies of selected Lucinidae and their symbionts are incongruent, indicating no specific host/symbiont association (Brissac et al. 2010). In addition, symbionts are acquired from the environment after the larval stage, not transmitted maternally via the eggs (Gros et al. 1996a, 1998; Won et al. 2003), can be reacquired during adulthood, and may be continuously taken up by the host through its lifespan (Elisabeth et al. 2012; Gros et al. 2012). Further, lucinid species seem to vary in their reliance on external food sources, as is inferred from the presence of food in the gut of some specimens (e.g., Allen 1958; Dando et al. 1986; Le Pennec et al. 1995; Duplessis et al. 2004) and a wide range of stable carbon isotope values for soft tissues (Table 3.1). These isotopic values span a range from those typical for marine phytoplankton (-18 to $-28‰$) through those for chemoautotrophically derived carbon (-25 to $-40‰$; Fisher 1995).

A proxy for the presence of chemosymbionts and/or degree of symbiotic dependence in fossil taxa would provide more accurate data for reconstructing trophic relationships in paleocommunities and marine biogeochemical systems, as well as addressing the evolution of chemosymbiosis within clades. For example, all living lucinids are chemosymbiotic. This current character configuration could have arisen via three end-member pathways: (1) symbiosis could be a basal synapomorphy for lucinids; (2) symbiosis may have evolved multiple times, as it has in bivalves as a whole; and/or (3) nonchemosymbiotic taxa may have suffered differential extinction through the evolutionary history of lucinids. Although basal synapomorphy is the most parsimonious scenario, data from the fossil record may actually allow the various scenarios, especially differential extinction, to be tested.

Attempts have been made to calibrate geochemical proxies for lucinid chemosymbiosis, but with limited applicability for fossil taxa. For instance, although $\delta^{13}C$ and $\delta^{34}S$ values of shell conchiolin reflect the depleted values typical of lucinid soft tissues (CoBabe and Pratt 1995; Mae et al. 2007), that of shell carbonate and carbonate associated sulfate is not depleted, and their compositions primarily reflect the isotopic composition of the bicarbonate and sulfate, respectively, dissolved in porewater/seawater (e.g., Campbell 2006; Peng et al. 2007; Macdonald and Peccini 2009). Sedimentologic proxies also are of limited use because lucinids are not limited to suboxic, richly sulfidic conditions, and occupy a range of marine environments from bathyal hydrocarbon seeps to shallow subtidal seagrass beds (e.g., Schweimanns and Felbeck 1985; Mikkelsen and Bieler 2008; Duperron et al. 2012; van der Heide 2012).

As symbiont dependence appears to vary within lucinids and because lucinid soft anatomy likely reflects an evolutionary response to their gills being co-opted for housing symbionts (Taylor and Glover 2000, 2006), it is possible that shell morphology will track aspects of the chemosymbiotic relationship. For instance, Taylor and Glover (2009a) used a qualitative assessment of the anterior adductor muscle scar shape and orientation, and surface texture of the internal valve surface indicating attachment of the mantle to the shell, in Eocene *Superlucina megameris* to infer the presence and location of mantle gills (see Sect. 3.2 for a brief description of mantle gills and other internal features of lucinids).

Here, geometric morphometrics are used to explore variation in some of the traits thought to be associated with chemosymbiosis in lucinids. Although much

Table 3.1 Previously published $\delta^{13}C$ values (rounded to three significant figures) for lucinid bivalves arranged by minimum $\delta^{13}C$ value

Species	$\delta^{13}C$ (‰)	Depth (m)	Source
Jorgenia louisiana	−37.7 to −30.9	400–920	Brooks et al. 1987 (as *Pseudomiltha* sp., see Taylor and Glover 2009b)
Lucinoma atlantis	−33.0 to −31.2 Ma, F	600	Kennicutt et al. 1985
Loripes lucinalis	−32.7 Gi	Littoral	Le Pennec et al. 1995
Lucinid sp. A	−31.2 to −20.2	1400–2391	Demopoulos et al. 2010
Myrtea amorpha	−31.1 W	1950	Carlier et al. 2010
	−30.1 W	2025	
Lucinoma kazani	−30.5 Gi	507	Duperron et al. 2007
	−28.2 F		
Myrtea amorpha	−30.5 to −27.7 Gi	1706	Roy et al. 2004; Werne et al. 2004
Lucinoma asapheus	−29.8±0.4 W	358	Rodrigues et al. 2012
Loripes lucinalis	−29.7 ± 0.5 Gi	Subtidal	Johnson et al. 1994
	−27.1±0.5 F		
Lucinoma aequizonata	−29.0±0.7	490–510	Cary et al. 1989
Lucinoma borealis	−29.0 to −28.1 Gi	0–33	Spiro et al. 1986
	−25.9 to −24.1 NG		
Lucinid sp. B	−28.8±0.02	2391	Demopoulos et al. 2010
Codakia orbicularis	−28.3 to −23.9 Gi	Subtidal	Berg and Alatalo 1984
	−28.1 to −23.2 NG		
Lucinella divaricata	−28.1 Gi	Littoral	Le Pennec et al. 1995
Lucinidae	−27.2	1400–1449	Demopoulos et al. 2010
Ctena decussata	−25.2 W	5–35	Carlier et al. 2007
Codakia	−25.1±0.6	Subtidal	CoBabe and Pratt 1995
	−25.0±0.5 F		
	−24.9±0.5 Ma		
Codakia orbicularis	−24.8 F	*Subtidal*	CoBabe 1991
Myrtea spinifera	−24.2 Gi	33	Spiro et al. 1986
	−23.4 NG		
Lucina pensylvanica	−23.4 F	*Subtidal*	CoBabe 1991
Divaricella irpex	−23.1 F	Intertidal	Compton et al. 2008
Lucinisca nassula	−23.0 W	Subtidal	Berg and Alatalo 1984
Myrtea spinifera	−23.0±0.4 W	5–35	Carlier et al. 2007

Taxonomic assignments are updated where possible. Species in bold were included in morphometric analyses herein. Tissues used for analysis are abbreviated as follows: *F* foot, *Gi* gill; *Ma* mantle, *NG* body without gills, *W* whole body. If not noted, tissues used were not specified in the original publication. Water depths are as reported in original publications, except for those in italics, which are inferred from source publications

has still to be learned about the taxonomy, phylogeny, and ecology of the clade, distinguishing known environmental, phylogenetic, and ontogenetic factors associated with morphologic variation may aid in interpreting changes in morphology in the fossil record. A morphometrics approach to understanding the biology of extinct lucinid taxa is promising because critical internal shell features are readily preserved on shells and internal molds of lucinids, and are relatively resistant to diagenetic change.

3.2 Anatomical Features Associated with Chemosymbiosis in Lucinids

In addition to well-documented modifications of the labial palps, digestive tract, and gills (Allen 1958), a number of other anatomical features are associated with chemosymbiosis in lucinids. Several of these features may be recorded on lucinid shells. Of greatest potential (because of a direct association between soft anatomy and shell characteristics, and high preservation potential) is the elongation of the anterior adductor muscle and its detachment from the pallial line. These modifications create an "inhalant channel" (Allen 1958) associated with the anterior inhalant tube, a mucus-lined tube constructed by the foot that connects the infaunal animal to the overlying water column (Fig. 3.1). The inhalant channel likely serves as a major respiratory surface (especially if the mantle is thickened by a blood space or modified to form mantle gills within it) and/or an area for sorting particulate matter (i.e., feeding), as both the anterior adductor muscle and the inner mantle in this region are well ciliated (Allen 1958; Taylor and Glover 2000).

Elongation and detachment of the anterior adductor muscle neither occurs in all lucinids (the notable exception being the Fimbriinae) nor is limited to the Lucinidae (some members of the Thyasiridae show a similar detachment; Allen 1958; Taylor et al. 2007a). In fact, there may be an association between adductor muscle detachment and the possession of chemosymbionts in the Thyasiridae based on a comparison of species common to both Payne and Allen (1991) and Dufour (2005). The degree of anterior adductor muscle elongation and detachment varies as well in lucinids, although all species examined to date house thiotrophic endosymbiotic bacteria. The inhalant channel ranges from very well developed in taxa such as *Phacoides* and *Superlucina* to absent in *Fimbria* (Williams et al. 2004; Taylor and Glover 2006). Although anterior adductor muscle-scar shape, size and orientation are included in taxonomic descriptions of lucinid species and genera (e.g., Chavan 1969; Bretsky 1976; Glover et al. 2004; Garfinkle 2012), the phylogenetic significance of this character has not been tested (Taylor et al. 2011). In fact, phylogenies produced using morphologic traits traditionally thought to be of taxonomic value show low congruence with molecular phylogenies (Taylor et al. 2011).

In most lucinids, the mantle adjacent to the anterior adductor muscle is thickened by a blood space (Taylor and Glover 2006). For some lucinid species, this or other areas of the mantle are modified into mantle gills, plicated regions of the inner-mantle surface inferred to serve a respiratory function (Allen 1958; Allen and Turner 1970; Morton 1979; Taylor and Glover 2000, 2006). A "pallial septum" (a large fold of the inner mantle extending from the ventral end of the anterior adductor muscle toward the posteroventral margin and enclosing a blood space) seems to serve a similar respiratory function and may or may not be associated with mantle gills in members of the Pegophyseminae and Leucosphaerinae (Taylor and Glover 2000, 2005; Taylor et al. 2011). The location and morphology of such mantle modifications can vary greatly among species that possess them (Table 3.2).
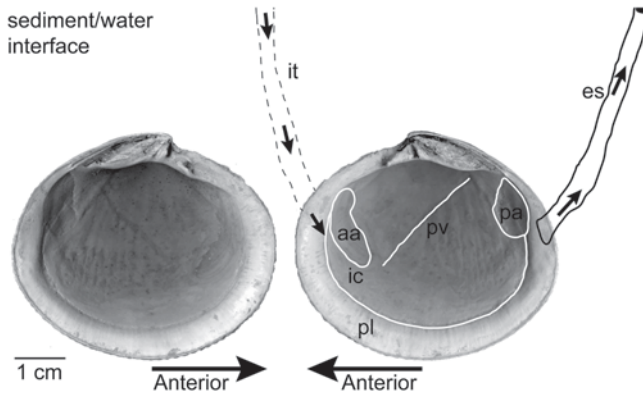
Fig. 3.1 Internal views of left and right valves from the same specimen of *Codakia orbicularis*. Morphologic features of the shell discussed in the text are highlighted and labeled on the right valve. *aa* anterior adductor muscle scar, *ic* inhalant channel, *pa* posterior adductor muscle scar, *pl* pallial line, *pv* pallial blood vessel. Approximate positions of the anterior inhalant tube (*it*) and posterior exhalant siphon (*es*) also are illustrated. Direction of water current flow is indicated by *small arrows*. Distance to sediment-water interface not to scale

Although not preserved directly on the shell, some lucinid conchologic traits have been used to indicate the possession and location of mantle gills. For instance, as mentioned above, anterior adductor muscle-scar shape and orientation, as well as a pustuler surface texture indicating close attachment of the mantle to the shell in the anterior channel, were used by Taylor and Glover (2009a) to infer the location of mantle gills in the extinct species *Superlucina megameris*.

Finally, lucinids possess a prominent pallial blood vessel that connects the heart to the mantle blood space typically located near the ventral tip of the anterior adductor muscle (and associated with mantle gills and pallial septa for those species possessing them; Taylor and Glover 2000). This blood vessel is thought to be associated with chemosymbiosis in lucinids (Taylor and Glover 2006) and can leave an impression across the inner surface of each valve (Fig. 3.1), although its degree of expression varies among species and is readily obscured by post-mortem shell alteration (either via taphonomic or diagenetic processes; pers. obs.).

3.3   Taxa Analyzed

Ten species were used in the morphometric analyses described herein (Fig. 3.2). Seven of these species are lucinids common in shallow-marine waters of the western Atlantic (Table 3.2) with specimens from personal field collections as well as lots housed at the University of Florida's Museum of Natural History (UF). Also included were UF specimens of the lucinid *Fimbria fimbriata*, a shallow-water

Table 3.2 Species used in morphometric analyses

Species	Family	Subfamily	Chemosymbiotic	Mantle gills
Anodontia alba	Lucinidae	Leucosphaerinae	Yes (Giere 1985 as *A. philippiana*)	Pallial septum without mantle gills (Taylor and Glover 2005)
Codakia orbicularis	Lucinidae	Codakiinae	Yes (Gros et al. 1998)	Yes, across inhalant channel and ventro-posteriorly from base of anterior adductor (Allen 1958)
Divalinga quadrisulcata	Lucinidae	Lucininae	Yes (Gros et al. 2000 as *Divaricella*)	No, but triangular fold of inner mantle present posterior to anterior adductor (Allen 1958 as *Divaricella*)
Lucina penyslvanica	Lucinidae	Lucininae	Yes (Gros et al. 1996b as *Linga*)	Yes, flank pallial blood vessel across body cavity (Allen 1958)
Phacoides pectinatus	Lucinidae	Lucininae	Yes (Frenkiel et al. 1996 as *Lucina pectinata*)	Yes, along inhalant channel and posteroventrally to valve midline (Narchi and Farani Assis 1980 as *Lucina pectinata*)
Lucinisca nassula	Lucinidae	Lucininae	Yes (Schweimanns and Felbeck 1985 as *Lucina*)	No (pers. obs.)
Parvilucina crenella	Lucinidae	Lucininae	Yes (Giere 1985; as *P. multilineata*)	No, but thickened blood space present (Taylor and Glover 2000 as *P. multilineata*)
Fimbria fimbriata	Lucinidae	Fimbriinae	Yes (Janssen 1992; Williams et al. 2004)	Yes, posterior of anterior adductor (Allen and Turner 1970)
Thyasira trisinuata	Thyasiridae		Yes (Dufour 2005)	No (Payne and Allen 1991)
Diplodonta sericata	Ungulinidae		No (inferred using Dando et al. 1986; Southward 1986)	No (inferred using Allen 1958)

For each, family membership, subfamily membership (based on Taylor et al. 2011), possession of chemosymbionts (and source), and presence and location of mantle gills (and source) are listed. If taxonomy is updated from source publication, the designation used in that publication is noted

Indo-Pacific taxon (Janssen 1992; Williams et al. 2004). The presence of chemosymbionts has been documented for all the lucinid species incorporated (Table 3.2), and all were part of a recent molecular phylogeny and classification of the family (Taylor et al. 2011). The taxa used fall into four phylogenetically defined subfamilies (Fig. 3.3): *Anodontia alba* from the Leucosphaerinae; *Codakia orbicularis* from the Codakiinae; *F. fimbriata* from the Fimbriinae, and *Divalinga quadrisulcata*, *Lucina pensylvanica*, *Phacoides pectinatus*, *Lucinisca nassula*, and *Parvilucina*
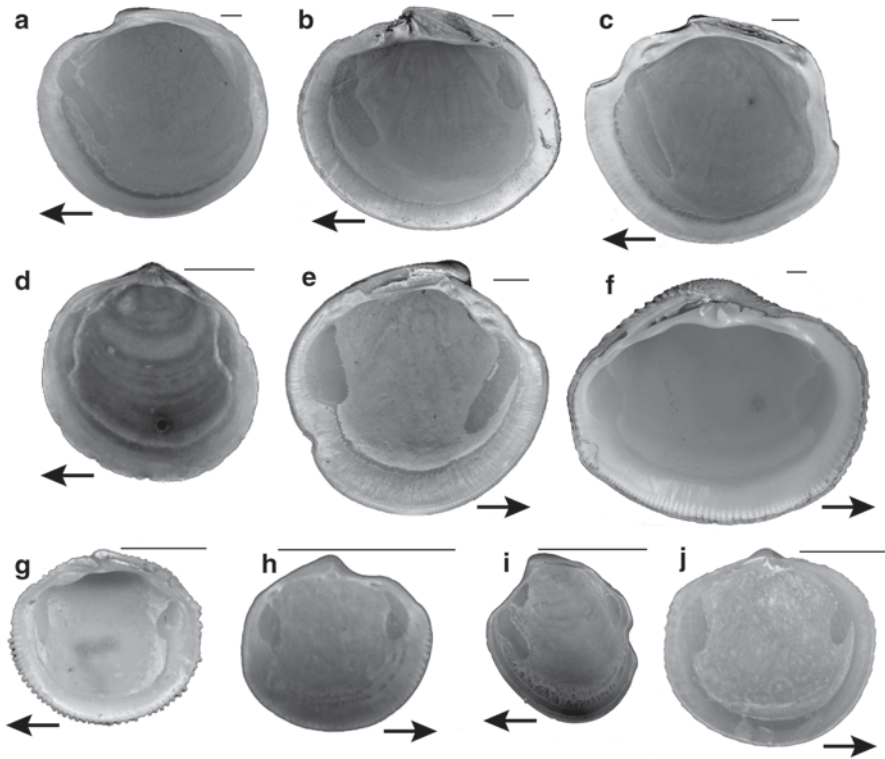
Fig. 3.2 Internal views of representative specimens of taxa used in morphometric analyses. **a** *Anodontia alba*, **b** *Codakia orbicularis*, **c** *Phacoides pectinatus*, **d** *Diplodonta sericata*, **e** *Lucina pensylvanica*, **f** *Fimbria fimbriata*, **g** *Lucinisca nassula*, **h** *Parvilucina crenella*, **i** *Thyasira trisinuata*, **j** *Divalinga quadrisultata*. Scale bars = 5 mm. *Arrows* point toward the valve anterior

crenella (= *P. multilineata* of many authors, but see Petit 2001), each from distinct unnamed subclades within the Lucininae (Taylor et al. 2011).

UF specimens of *Thyasira trisinuata* (Thyasiridae) and *Diplodonta sericata* (Ungulinidae) also were incorporated into analyses. The families these species represent were once considered part of the superfamily Lucinoidea, but are now recognized as distinct clades within the Heterodonta (Williams et al. 2004; Taylor et al. 2007a, b, 2009). Members of the Ungulinidae have a lucinoid shell shape but do not house chemosynthetic endosymbionts (although published accounts supporting the lack of chemosymbiosis are scarce; see Dando et al. 1986; Southward 1986). Thyasirids also have a lucinoid shell shape, some member species (including the taxon used here, see also Table 3.3) house chemosymbionts (Southward 1986; Dufour 2005), and in some species the anterior adductor muscle scar is detached from the pallial line (Payne and Allen 1991). Thickened blood spaces also have been documented in thyasirids (Oliver and Holmes 2007).

Out of the ten species included, four have mantle gills (Table 3.2). In *C. orbicularis*, mantle gills extend ventrally and posteriorly from the base of the anterior
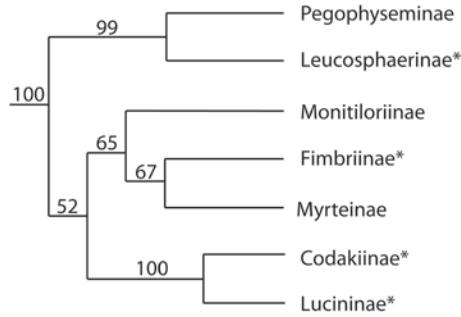
Fig. 3.3 Reconstruction of phylogenetic relationships among subfamilies of Lucinidae based on a Bayesian analysis of concatenated sequences of the nuclear 18S rRNA and 28S rRNA, and mitochondrial cytochrome *b,* genes from Taylor et al. (2011). *Numbers* at branch nodes represent Bayesian posterior probabilities (%) reported by Taylor et al. (2011). *Asterisks* indicate clade membership of taxa included in morphometric analyses: Leucosphaerinae = *Anodontia alba*; Codakiinae = *Codakia orbicularis*; Fimbriinae = *Fimbria fimbriata*; and Lucininae = *Divalinga quadrisulcata*, *Lucina pensylvanica*, *Phacoides pectinatus*, *Lucinisca nassula*, and *Parvilucina crenella*. Note that each of the Lucininae species included is from a distinct subclade of that subfamily (see Taylor et al. 2011)

adductor muscle, and fill the lower portion of the inhalant channel (Allen 1958; Taylor and Glover 2000). Mantle gills flank the pallial blood vessel that runs diagonally across the central body cavity in *Lucina pensylvanica* (Allen 1958; Taylor and Glover 2000). For *Phacoides pectinatus*, mantle gills consist of a series of small plicated ridges that are parallel to the pallial line and extend from the dorsal end of the inhalant channel to just past the midpoint of the ventral margin (Narchi and Farani Assis 1980). Mantle gills in *F. fimbriata* occur along the ventroposterior margin of the anterior adductor muscle, although they are less complexly infolded than in the species mentioned above (Allen and Turner 1970; Morton 1979).

Out of the other lucinid species used in this study, *A. alba* possesses a pallial septum but lacks mantle gills (Taylor and Glover 2005). For *Divalinga quadrisulcata*, Allen (1958) describes a triangular fold of the inner mantle posterior to the anterior adductor muscle that is associated with a blood sinus. Mantle gills are absent, although a thickened blood space within the mantle is present, in *Parvilucina* (Taylor and Glover 2000). Neither mantle gills nor a thickened blood space are observed in *Lucinisca nassula* (pers. obs.).

3.4 Methods

Landmark-based, geometric morphometric methods were used to quantify shape variation among specimens (Bookstein 1991). A simple landmark configuration was developed and focused on describing shape and orientation of the anterior

Table 3.3 Previously published $\delta^{13}C$ values (rounded to three significant figures) for thyasirid bivalves arranged by minimum $\delta^{13}C$ value

Species	$\delta^{13}C$ (‰)	Depth (m)	Source
Thyasira sarsi	−41.6 to −17.8 Gi	39–268	Dando and Spiro 1993
	−39.5 to −17.1 W		
Thyasira sarsi	−39.5 Gi	280–340	Schmaljohann et al. 1990
	−37.4 NG		
Thyasira volcolutre	−36.8±0.4 W	2200	Rodrigues et al. 2012
	−35.4±1.0 W	2175	
	−35.3±0.4 W	2199	
	−34.9±0.6 W	1321	
	−34.9±0.0 W	1320	
	−34.6±1.8 W	2200	
	−34.4±0.3 W	2200	
	−34.1±0.2 W	1562	
Thyasira sp.	−35.8±0.8 Gi	582	Duperron et al. 2012
Thyasira methanophila	−35.4 W	740–870	Sellanes et al. 2008
Thyasira sarsi	−35.1 Mu	39–340	Dando et al. 1991
	−34.7 Gu		
	−34.3 Gi		
	−33.8 to −31.4 W		
Thyasira sp.	−34.0 Gi	3040	Southward et al. 2001
Thyasira sarsi	−31.0 Gi	60	Spiro et al. 1986
	−28.2 NG		
Thyasira flexuosa	−29.3 Gi	55	Spiro et al. 1986
Thyasira striata	−28.9±1.2 W	2025	Carlier et al. 2010
Parathyasira equalis	−28.7 to −18.7 Gi	39–268	Dando and Spiro 1993
	−22 to −17.4 W		
Thyasira peregrina	−24.8 W	400	McLeod et al. 2010

Taxonomic assignments are updated where possible. Tissues used for analysis are abbreviated as follows: *Gi* gill, *Gu* gut, *Mu* muscle, *NG* body without gills, *W* whole body. Water depths are as reported in original publications

adductor muscle scar (landmarks 2–4) and its detachment from the pallial line (position of landmark 4 relative to 2 and 3) to form the inhalant channel (see Fig. 3.4 for landmark definitions). Two landmarks (4, 5) represent juxtapositions of structures (Bookstein's Type I landmarks) and four (1–3, 6) represent curvature maxima (Bookstein's Type II landmarks).

Valves were imaged on a flat-bed scanner at resolutions ranging from 300–1,200 dpi, depending on valve size. Prior to digitizing, right valves were reflected horizontally to match the orientation of left valves. Post hoc examination of results revealed no shape differences between left and right valves. Landmarks were digitized using tpsDIG2 (Rohlf 2008).

Landmark coordinate data were subject to a full Procrustes fit or superimposition to produce Procrustes coordinates (shape data) and centroid size (square root of the sum-of-squared distance of landmarks to their common centroid) using MorphoJ
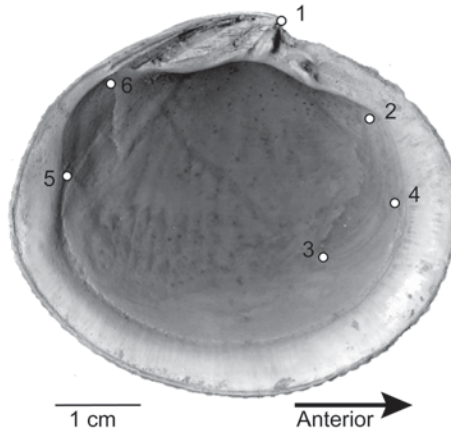
Fig. 3.4 Six-landmark configuration used for geometric morphometric analyses illustrated with a left valve of *Codakia orbicularis*. Landmarks are as follows: *1* beak, *2* maximum curvature of dorsal margin of anterior adductor muscle scar, *3* maximum curvature of ventral margin of anterior adductor muscle scar, *4* intersection of anterior adductor muscle scar and pallial line, *5* intersection of posterior adductor muscle scar and pallial line, *6* maximum curvature of dorsal margin of posterior adductor muscle scar

(Klingenberg 2011). Centroid size is the only scaling variable uncorrelated with shape in the absence of allometry (Bookstein 1991).

A covariance matrix was calculated for the Procrustes coordinates and this matrix was used in both a canonical variates analysis (CVA) and series of discriminate function analyses (DFA) with MorphoJ. For the CVA, a permutation test of pairwise distances between groups was computed using 1,000 iterations/comparison, and *p*-values for all these comparisons using both Mahalanobis and Procrustes distances were calculated. DFA were used to verify CVA permutation test results, in case the assumption of identical within-group covariance matrices was violated for this dataset. DFA results were assessed using leave-one-out cross-validation with a permutation test using both Procrustes distances and T-square values (1,000 iterations). Significance tests for correlations between CV1 and centroid size were conducted using Spearman's D statistic in PAST version 2 (Hammer et al. 2001). Correlations for each species separately, and for eight species that follow the same allometric trend combined (i.e., excluding *F. fimbriata* and *Diplodonta sericata)* were tested. Alpha values ($\alpha = 0.01$) were adjusted to account for multiple comparisons (total $= 12$; see below).

Shape differences among species were visualized using a thin-plate spline (TPS) of a landmark configuration for one specimen from each species (or in the case of *Lucina pensylvanica,* a size range within the species because the frequency distribution of individuals was right skewed over its size range) that fell close to the median value on CV1 and CV2. TPS were generated using tpsRelw (Rohlf 2007).

3.5   Results

The simple landmark configuration used herein contains significant taxonomic information, as species separate well among the first four canonical variates (CV) axes, which explain over 95 % of variation in the data (Fig. 3.5). In addition, permutation tests of all pairwise species comparisons are significantly different ($p < 0.001$) for both Mahalanobis and Procrustes distances. DFA results also are significantly different for all pairwise species comparisons ($p < 0.001$), as are cross-validation results (Tables 3.4, 3.5). In spite of clear taxonomic separation, a phylogenetic pattern is not detectable in the CV results, either within lucinids or among lucinids and the other two families incorporated.

In the CVA, each axis reflects distinct shape differences (Figs. 3.5, 3.6). CV1 explains 48.3 % of variation and describes expansion of the anterior region via elongation of the anterior adductor muscle scar and of the inhalant channel (landmarks 3 and 4; Fig. 3.6a). For high positive values, as seen in *Phacoides*, the inhalant channel is elongated via both a more dorsal placement of landmark 4 and by ventral displacement of landmark 3 (Fig. 3.7c). High negative valves, as seen in *Parvilucina* (Fig. 3.7j), represent the opposite trend. Therefore, both displacement of the detachment point between the pallial line and the anterior adductor muscle and elongation of the anterior adductor muscle play roles in extending the inhalant channel.

CV2 explains 27.8 % of variation and describes a transition from more quadrate to more anterior/posterior elongated positions of the landmarks (Fig. 3.6b, note that the landmarks define internal features of the shell and not necessarily valve outline shape). CV3 explains 10.7 % of variation and relates especially to the height of the posterior adductor scar (distance between landmarks 5 and 6) and secondarily to the depth of the inhalant channel (distance between landmarks 3 and 4) (Fig. 3.6c). CV4 explains 8.5 % of variation and describes anterior/posterior expansion of the adductor scars (particularly landmarks 2–3 and 5–6; Fig. 3.6d).

Qualitatively, TPS fall into three groups, each illustrating similar deformation patterns, especially for landmarks 2–4 (Fig. 3.7). One group, including *Codakia, Anodontia*, *Phacoides*, and large *Lucina* specimens [ln(centroid size) > 2.7], have elongated inhalant channels produced by divergence of landmarks 3 and 4 (Fig. 3.7a–d). A second group includes *Lucinisca*, *Thyasira*, and small *Lucina* [ln(centroid size) < 2.7] that have a slightly to moderately shortened anterior adductor scar (more dorsally placed landmark 3), and base of the posterior adductor scar (landmark 5) placed more anteriorly (Fig. 3.7f–h). The third group includes *Divalinga*, *Parvilucina*, *Fimbria*, and *Diplodonta*, which have a reduced distance between the base of the anterior adductor scar and the intersection of that scar with the pallial line (i.e., distance between landmarks 3 and 4), while the intersection of the posterior adductor scar and the pallial line moves posteriorly (landmark 5) (Fig. 3.7i–l).

Most taxa (excluding *Fimbria* and *Diplodonta*) follow a statistically significant allometric trend on CV1 (Fig. 3.8, Table 3.6). In addition, in spite of variability along the trend, six of ten species show a significant correlation of CV1 scores and ln(centroid size) (Table 3.6). Exceptions are *Lucinisca nassula* and *P. crenella*,
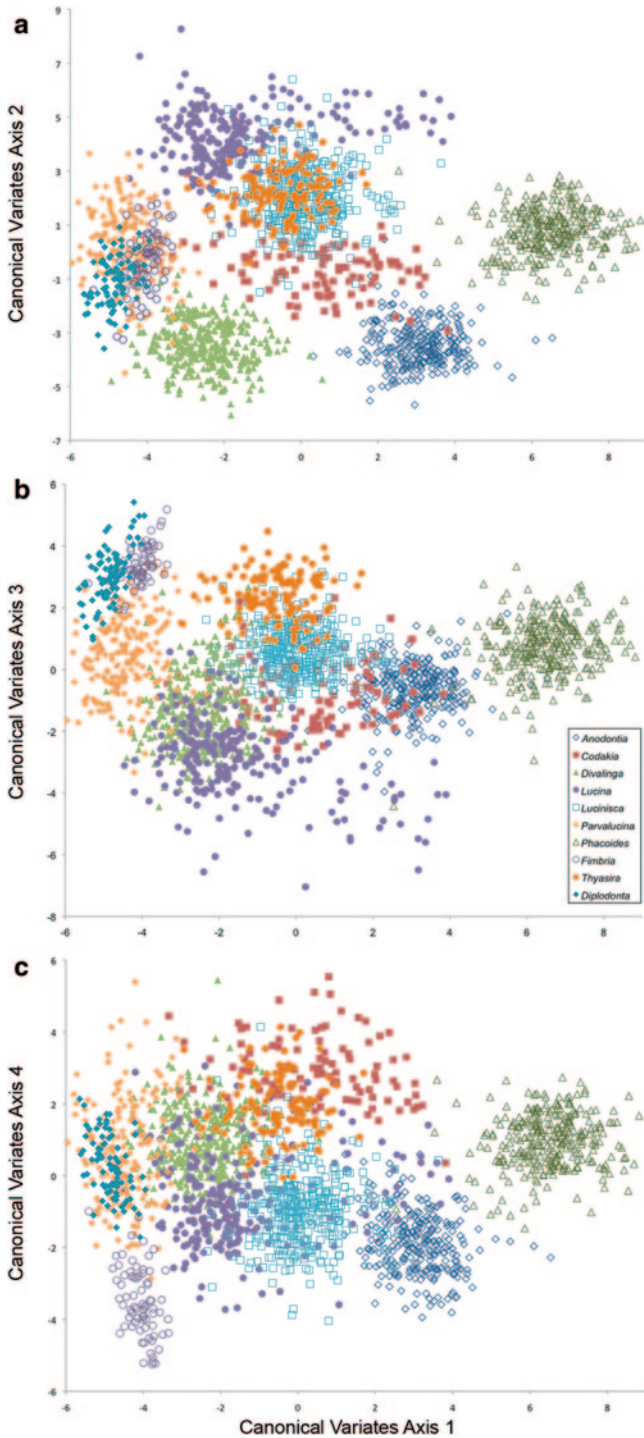
Fig. 3.5 Plots of canonical variates (*CV*) analysis scores for first four CV axes. **a** CV1 vs. CV2, **b** CV1 vs. CV3, **c** CV1 vs. CV4. Together these axes explain over 95 % of variation in the data

Table 3.4 Discriminate function analysis results for all pairwise comparisons of species

Genus	ano	cod	dip	div	fim	lis	luc	par	pha	thy
Anodontia (279)	–	100	100	100	100	100	100	100	100	100
Codakia (104)	99	–	100	100	100	100	100	98	100	100
Diplodonta (87)	100	100	–	100	100	100	100	100	100	100
Divalinga (325)	100	100	100	–	100	100	100	99.1	100	100
Fimbria (73)	100	100	100	100	–	100	100	100	100	100
Lucinisca (365)	99.7	99.2	100	99.7	100	–	99.7	99.7	100	97.5
Lucina (242)	100	99.6	100	100	100	97.9	–	100	100	99.2
Parvilucina (189)	100	98.9	96.8	96.8	100	100	99.5	–	100	100
Phacoides (284)	100	100	100	100	100	99.6	99.6	100	–	100
Thyasira (123)	100	100	100	100	100	99.2	100	100	100	–

Sample size for each species is noted with its genus name. Taxon abbreviations for columns are as follows: ano *Anodontia alba*, cod *Codakia orbicularis*, dip *Diplodonta sericata*, div *Divalinga quadrisulcata*, fim *Fimbria fimbriata*, lis *Lucinisca nassula*, luc *Lucina pensylvanica*, par *Parvilucina crenella*, pha *Phacoides pectinatus*, thy *Thyasira trisinuata*

Table 3.5 Cross-validation results for discriminate function analysis of all pairwise comparisons of species

Genus	ano	cod	dip	div	fim	lis	luc	par	pha	thy
Anodontia (279)	–	100	100	100	100	100	100	100	100	100
Codakia (104)	99	–	100	100	100	100	100	98	99	100
Diplodonta (87)	100	100	–	100	100	100	100	100	100	100
Divalinga (325)	100	100	100	–	100	100	100	99.1	100	100
Fimbria (73)	100	100	100	100	–	100	100	100	100	100
Lucinisca (365)	99.7	98.9	100	99.7	100	–	99.7	99.7	100	97.3
Lucina (242)	100	99.6	100	100	100	97.5	–	99.6	100	99.2
Parvilucina (189)	100	97.8	95.8	95.8	99.5	100	99.5	–	100	100
Phacoides (284)	100	100	100	100	100	99.6	99.6	100	–	100
Thyasira (123)	100	100	100	100	100	99.2	100	100	100	–

Sample size for each species is noted with its genus name. Taxon abbreviations for columns are as follows: ano *Anodontia alba*, cod *Codakia orbicularis*, dip *Diplodonta sericata*, div *Divalinga quadrisulcata*, fim *Fimbria fimbriata*, lis *Lucinisca nassula*, luc *Lucina pensylvanica*, par *Parvilucina crenella*, pha *Phacoides pectinatus*, thy *Thyasira trisinuata*

which nonetheless fall on the general allometric trend in Fig. 3.8, and *D. sericata*, which does not. For *F. fimbriata*, a significant correlation when all specimens are included is driven by an outlier (smallest specimen, see Fig. 3.8), so that the hypothesis of a significant correlation is rejected when this specimens is excluded (Table 3.6).

Along the allometric trend illustrated in Fig. 3.8, the lengths of both the anterior adductor scar and the inhalant channel increase, primarily via changes in the positions of landmarks 3 and 4 (Fig. 3.6a). The other CV axes did not show an allometric trend, indicating that the shape variation along these axes does not vary significantly with size.

Fig. 3.6 Thin-plate splines (*TPS*) illustrating shape variation explained by the first four *CV* axes. Each TPS depicts total deformation along the corresponding CV axis with a scale factor equal to the units of that axes (Klingenberg 2011). Vectors associated with each landmark illustrate direction and magnitude of variation for that landmark on that CV axis. **a** CV1, **b** CV2, **c** CV3, **d** CV4. Anterior is to the right for all figures
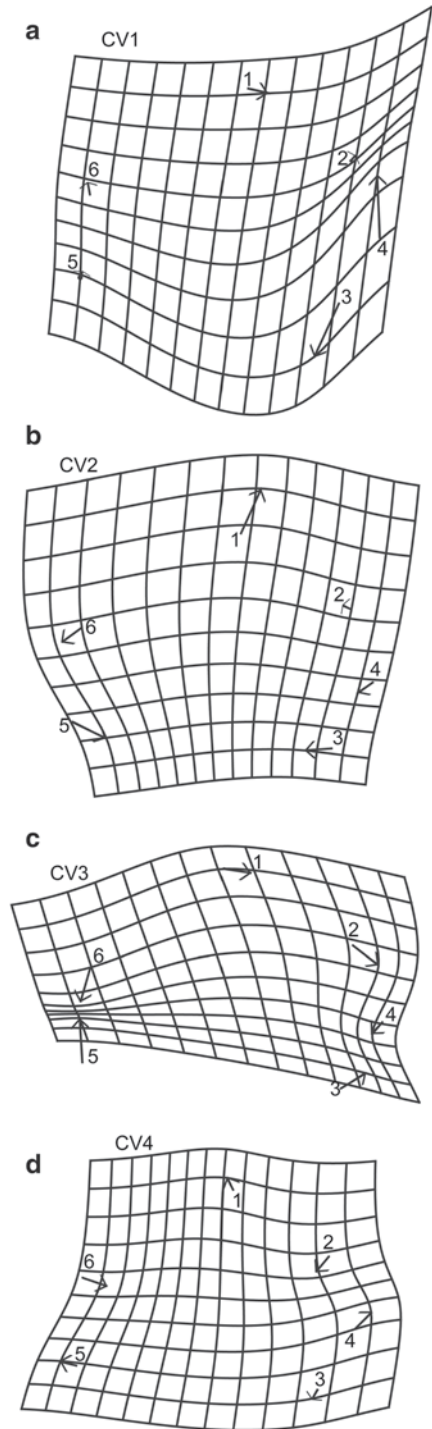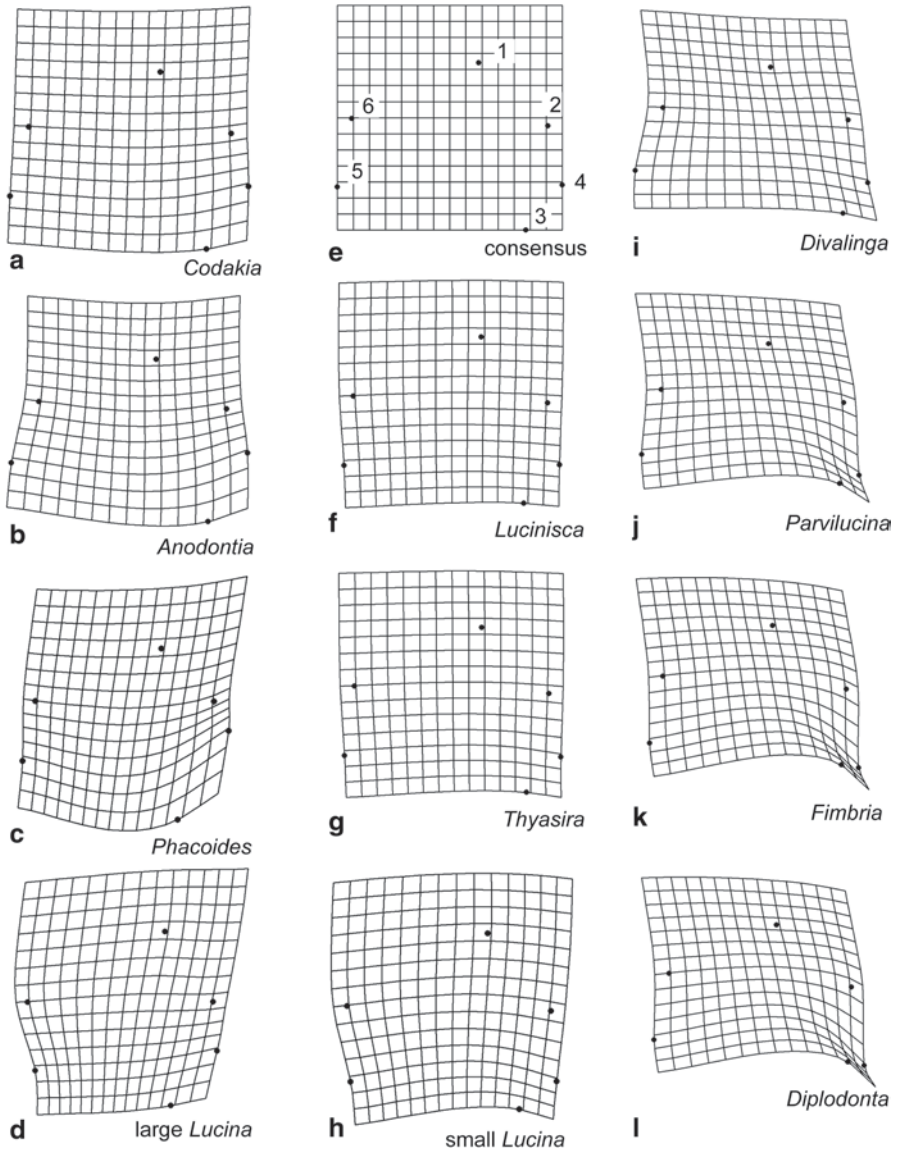
Fig. 3.7 Representative TPS illustrating deformations (shape differences) from a Procrustean distance-minimized common reference form (Rohlf 1996) for each species incorporated into the analyses. For *Lucina pensylvanica* two splines are illustrated, one for smaller valves and one for larger valves, as this species shows allometric growth and there were many more small individuals available and incorporated into the analysis. **a** *Codakia orbicularis*, **b** *Anodontia alba*, **c** *Phacoides pectinatus*, **d** large *Lucina pensylvanica* [ln(centroid size) >2.7], **e** consensus form for entire dataset, **f** *Lucinisca nassula*, **g** *Thyasira trisinuata*, **h** small *Lucina pensylvanica* [ln(centroid size) <2.7], **i** *Divalinga quadrisulcata*, **j** *Parvilucina crenella*, **k** *Fimbria fimbriata*, **l** *Diplodonta sericata*. Anterior is to the right for all figures
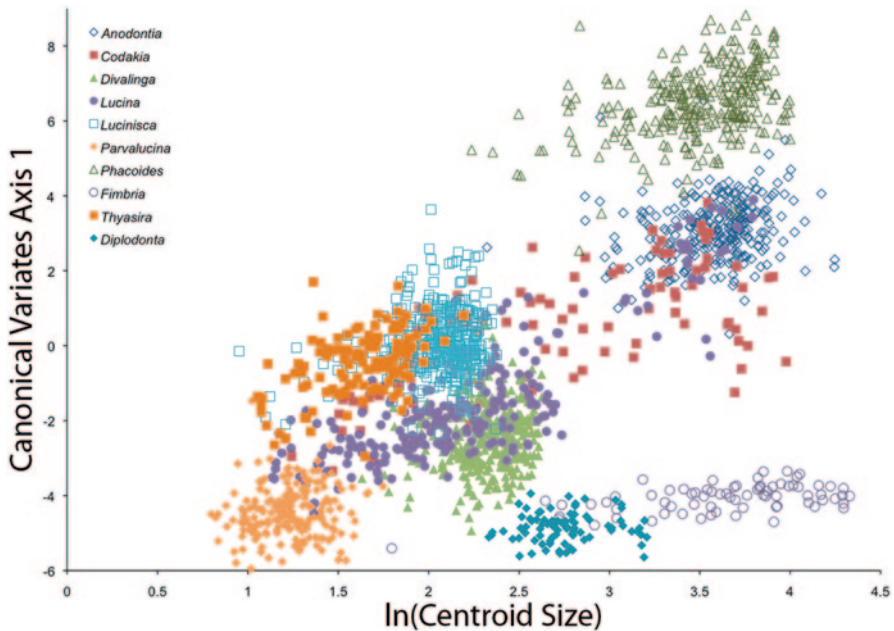
Fig. 3.8 Plot of ln(centroid size) vs. CV1 showing positive interspecific allometric trend for all taxa except *Diplodonta sericata* and *Fimbria fimbriata*. (See Table 3.6 for summary statistics for tests of significant correlation)

Table 3.6 Summary statistics for tests of significant correlation between CV1 and centroid size

Comparison	N	r	P	Significant
All taxa less *Fimbria* and *Diplodonta*	1911	0.8145	4.4×10^{-223}	Yes
Lucina	242	0.8157	5.3×10^{-29}	Yes
Codakia	104	0.6695	4.3×10^{-4}	Yes
Thyasira	123	0.4862	5.3×10^{-7}	Yes
Phacoides	284	0.3936	3.9×10^{-10}	Yes
Anodontia	279	0.2147	4.3×10^{-5}	Yes
Divalinga	325	0.2013	7.1×10^{-4}	Yes
Lucinisca	365	0.1641	0.14341	No
Parvilucina	189	0.1073	0.084	No
Fimbria all specimens	73	0.5294	7.0×10^{-4}	Yes
Fimbria less outlier	72	0.4174	1.6×10^{-3}	No
Diplodonta	87	0.0335	0.594	No

All taxa except *Fimbria* and *Diplodonta* were grouped in one test, as these eight taxa appear to follow the same allometric trend (Fig. 3.8). The significance of correlation between CV1 and centroid size also was tested for each species. *Fimbria* was tested once with and once without an outlier specimen (specimen with a centroid size of 1.80). The alpha level was adjusted to 8.0×10^{-4} to account for multiple comparisons ($n=12$)

3.6 Discussion

A goal of the morphometric analyses was to determine whether quantitative shape data could aid in inferring characteristics of chemosymbiosis in lucinid bivalves. Based on CVA results and the documented interspecific (and interclade) allometric trend, a direct morphometric signal of chemosymbiosis cannot be applied across the taxa examined. In addition, in spite of significant shape differences among species, a phylogenetic pattern is not detectable among the lucinid subfamilies or among the lucinids, *Diplodonta*, and *Thyasira*. Instead, life position and allometric growth in response to classic geometric constraints appear to be the primary factors influencing the quantified morphologic variation among species.

The interspecific allometric trend shared among seven lucinid species (all except *F. fimbriata*) and *Thyasira* appears to be related to the life position of these taxa. All of these taxa, as well as *Diplodonta* and *Fimbria*, draw in water anteriorly via apertures or through constructed tubes, as well as posteriorly via a posterior inhalant aperture (Allen 1958; Allen and Turner 1970). For the taxa that fall on the allometric trend, however, individuals generally are oriented in the sediment with their anterior/posterior axis horizontal or inclined with the anterior above the horizontal (Stanley 1970; Dando and Southward 1986; Taylor and Glover 2000; Dufour and Felbeck 2003). To draw in seawater from the overlying water column, both lucinids and thyasirids use their vermiform foot to construct an anterior inhalant tube (see Fig. 3.1) (Stanley 1970; Dufour and Felbeck 2003). Water enters the shell from the anterior and passes along the inhalant channel between the mantle and anterior adductor muscle.

The two taxa that do not follow the general allometric trend (i.e., *D. sericata* and *F. fimbriata*) have different orientations within the sediment. *Fimbria fimbriata* positions itself just below the sediment–water interface, with the anterior/posterior axis inclined and the dorsoanterior margin uppermost (Morton 1979). Similar information is not available for *D. sericata*, but its congener *D. notata* orients itself ventral side up with an anterior inhalant mucus tube connecting the animal to the sediment surface (Stanley 1970).

The shape differences observed along CV1, namely increasing length of the anterior channel caused by divergence of landmarks 3 and 4, for all taxa except *Diplodonta* and *Fimbria* may, in turn, relate to geometric constraints of mantle surface area vs. body volume with increasing size. As noted above, the inhalant channel likely serves as a major respiratory surface and/or an area for food gathering and sorting (Allen 1958; Taylor and Glover 2000). Whatever the function(s) of this area, without positive allometry, the surface area of the inhalant channel will decrease relative to body volume as size increases. To compensate for this geometric constraint, the relative length of the channel may increase with body size. At some point, however, a functional limitation must be reached because it is in the larger species where modifications to further increase surface area of the inner mantle, in the form of mantle gills and pallial septa, occur.

The allometric trend appears unrelated to depth of burial of individual lucinid species, even though a positive correlation of size and depth of burial is present within

some lucinid and thyasirid species (Stanley 1970; Dando and Southward 1986). In fact, many taxa burrow to similar depths, regardless of size. For instance, Stanley (1970) found that the larger species *A. alba* and the smaller species *Divalinga quadrisulcata* live at comparable sediment depths (10–20 cm). Other larger taxa generally inhabit shallower depths, including *Phacoides pectinatus* (5–12 cm), *C. orbicularis* (2–5 cm), and *Lucina pensylvanica* (depth not quantified but stated as between those for *Codakia* and *Phacoides*; Stanley 1970). These preferred depths overlap with those of smaller species, such as *Lucinisca nassula* and *Thyasira flexuosa* (5–10 cm and 3.5 cm, respectively; Dufour and Felbeck 2003; Reynolds et al. 2007).

Although the allometry observed is primarily a response to geometric constraint, TPS reveal possible associations of landmark configurations to the location of the mantle gills or pallial septa, with the exception of *Fimbria* (Table 3.2). For instance, the TPS of *Phacoides* is especially expanded along the anteroventral margin, the zone along which mantle gills occur, from the dorsal end of the inhalant channel to the midpoint of the ventral margin (Fig. 3.7c). For *Lucina*, especially for larger individuals, the interior area of the TPS progressively expands posterodorsally from a starting point close to the ventral tip of the anterior adductor muscle scar, i.e., in the area housing mantle gills in this species (Fig. 3.7d). In *Codakia*, the TPS shows moderate expansion of the anteroventral area, including the inhalant channel, and again, these areas correspond to the location of the mantle gills (Fig. 3.7a). Finally, although *A. alba* lacks mantle gills along its pallial septum, the ventral region along which the septum is located is expanded on its TPS plot (Fig. 3.7b).

Finally, based on available published data, an association between degree of chemosymbiont dependence and morphometric variation cannot be confirmed. Published $\delta^{13}C$ values for soft tissues are available for only three species included in the morphometric analyses: *C. orbicularis*, *L. pensylvanica,* and *Lucinisca nassula* (Table 3.1). Based on these limited data, $\delta^{13}C$ values for *Lucina* and *Lucinisca* soft tissues are similar (-23.4 and $-23\,‰$, respectively), and are heavier than those reported for *Codakia* (ranging from -28.3 to $-23.9\,‰$) (see Table 3.1). Nonetheless, all these taxa overlap along the allometric trend (Fig. 3.8), indicating that shape differences are not associated with inferred chemosymbiont dependence. Further, an examination of published $\delta^{13}C$ data indicates a stronger association between water depth and $\delta^{13}C$ than between taxon and $\delta^{13}C$ (Tables 3.1, 3.3). A larger morphometric dataset incorporating deeper-water taxa and/or additional isotopic data for shallow-water taxa may aid in better determining any link between $\delta^{13}C$ of soft tissues and morphometric variables.

3.7 Conclusions

Multivariate analyses of a simple landmark configuration that focused on describing the shape and orientation of the anterior adductor muscle scar and its detachment from the pallial line to form the inhalant channel did not indicate a direct morphometric signal of chemosymbiosis in seven common shallow-water western Atlantic

lucinids species along with three comparative taxa. A phylogenetic signal also is not apparent in the morphometric data. These analyses did, however, describe a distinctive interspecific (and interclade) allometric trend likely related to life position and to geometric constraints on morphology. Further, TPS reveal possible associations of landmark configurations to the location of the mantle gills or pallial septa.

References

Allen JA (1958) On the basic form and adaptations to habitat in the Lucinacea (Eulamellibranchia). Philos T R Soc B 684:421–484

Allen JA, Turner JF (1970) The morphology of *Fimbria fimbriata* (Linné) (Bivalia: Lucinidae). Pac Sci 24:147–154

Berg C Jr, Alatalo P (1984) Potential of chemosynthesis in molluscan mariculture. Aquaculture 39:165–179

Bookstein FL (1991) Morphometric tools for landmark data: geometry and biology. Cambridge University Press, Cambridge

Bretsky SS (1976) Evolution and classification of the Lucinidae (Mollusca; Bivalia). Palaeontogr Am 8:219–337

Brissac T, Merçot H, Gros O (2010) *Lucinidae*/sulfur-oxidizing bacteria: ancestral heritage or opportunistic association? Further insights from the Bohol Sea (the Philippines). FEMS Microbiol Ecol. doi:10.1111/j.1574-6941.2010.00989.x

Brooks JM, Kennicutt MC II, Fisher CR, Macko SA, Cole K, Childress JJ, Bidigare RR, Vetter RD (1987) Deep-sea hydrocarbon seep communities: evidence for energy and nutritional carbon sources. Science 238:1138–1142

Campbell KA (2006) Hydrocarbon seep and hydrothermal vent paleoenvironments and paleontology: past developments and future research directions. Palaeogeogr Palaeocl 232:362–407

Carlier A, Riera P, Amouroux J-M, Bodiou J-Y, Grémare A (2007) Benthic trophic network in the Bay of Banyuls-sur-Mer (northwest Mediterranean, France): an assessment based on stable carbon and nitrogen isotopes analysis. Estuar Coast Shelf S 72:1–15

Carlier A, Ritt B, Rodrigues CF, Sarrazin J, Olu K, Grall J, Clavier J (2010) Heterogeneous energetic pathways and carbon sources on deep eastern Mediterranean cold seep communities. Mar Biol 157:2545–2565. doi:10.1007/s00227-010-1518-1

Cary SC, Vetter RD, Felbeck H (1989) Habitat characterization and nutritional strategies of the endosymbiont-bearing bivalve *Lucinoma aequizonata*. Mar Ecol-Prog Ser 55:31–45

Chavan A (1969) Superfamily Lucinacea Fleming, 1828. In: Moore RC (ed) Treatise on invertebrate paleontology part N volume 2 Mollusca 6 Bivalia. The University of Kansas and the Geological Society of America, Inc., Boulder, pp 491–508

CoBabe EA (1991) Detection of chemosymbiosis in the fossil record: the use of stable isotopy on the organic matrix of lucinid bivalves. In: Dudley EC (ed) The unity of evolutionary biology. Bioscoroides Press, Portland, pp 669–673

CoBabe EA, Pratt LM (1995) Molecular and isotopic compositions of lipids in bivalve shells: a new prospect for molecular paleontology. Geochim Cosmochim Ac 59:87–95

Compton TJ, Kentie R, Storey AW, Veltheim I, Pearson GB, Piersma T (2008) Carbon isotope signatures reveal that diet is related to the relative sizes of the gills and palps in bivalves. J Exp Mar Biol Ecol 361:104–110

Dando PR, Southward AJ (1986) Chemoautotrophy in bivalve molluscs of the genus *Thyasira*. J Mar Biol Assoc UK 66:915–929

Dando PR, Spiro B (1993) Varying nutritional dependence of the thyasirid bivalves *Thyasira sarsi* and *T. equalis* on chemoautotrophic symbiotic bacteria, demonstrated by isotope ratios of tissue carbon and shell carbonate. Mar Ecol-Prog Ser 92:151–158

Dando PR, Southward AJ, Southward EC (1986) Chemoautotrophic symbionts in the gills of the bivalve mollusc *Lucinoma borealis* and the sediment chemistry of its habitat. P Roy Soc B-Biol Sci 227:227–247

Dando PR, Austen MC, Burke RA Jr, Kendall MA, Kennicutt MC II, Judd AG, Moore DC, O'Hara SCM, Schmaljohann R, Southward AJ (1991) Ecology of a North Sea pockmark with an active methane seep. Mar Ecol-Prog Ser 70:49–63

Demopoulos AWJ, Gualtieri D, Kovas K (2010) Food-web structure of seep sediment macrobenthos from the Gulf of Mexico. Deep-Sea Res Pt II 57:1972–1981

Distel DL (1998) Evolution of chemoautotrophic endosymbiosis in bivalves. Bioscience 48:277–286

Dubilier N, Bergin C, Lott C (2008) Symbiotic diversity in marine animals: the art of harnessing chemosynthesis. Nat Rev Microbiol 6:725–740

Dufour SC (2005) Gill anatomy and the evolution of symbiosis in the bivalve family Thyasiridae. Biol Bull 208:200–212

Dufour SC, Felbeck H (2003) Sulphide mining by the superextensile foot of symbiotic thyasirid bivalves. Nature 426:65–67

Duperron S, Fiala-Medioni A, Caprais J-C, Olu K, Sibuet M (2007) Evidence for chemoautotrophic symbiosis in a Mediterranean cold seep clam (Bivalvia: Lucinidae): comparative sequence analysis of bacterial 16S rRNA, APS reductase and RubisCO genes. FEMS Microbiol Ecol 59:64–70

Duperron S, Rodrigues CF, Léger N, Szafranski K, Decker C, Olu K, Gaudron SM (2012) Diversity of symbioses between chemosynthetic bacteria and metazoans at the Guiness cold seep site (Gulf of Guinea, West Africa). Microbiologyopen 1:467–480. doi:10.1002/mbo3.47

Duplessis MR, Dufour SC, Blankenship LE, Felbeck H, Yayanos AA (2004) Anatomical and experimental evidence for particular feeding in *Lucinoma aequizonata* and *Parvilucina tenuisculpta* (Bivalvia: Lucinidae) from the Santa Barbara Basin. Mar Biol 145:551–561. doi:10.1007/s00227-004-1350-6

Elisabeth NH, Gustave SDD, Gros O (2012) Cell proliferation and apoptosis in gill filaments of the lucinid *Codakia orbiculata* (Montagu, 1808) (Mollusca: Bivalvia) during bacterial decolonization and recolonization. Microsc Res Techniq 75:1136–1146

Fisher CR (1995) Toward an appreciation of hydrothermal-vent animals: their environment, physiological ecology, and tissue stable isotope values. In: Humphris SE, Zierenberg RA, Mullineaux LS, Thomson RE (eds) Seafloor hydrothermal systems: physical, chemical, biological, and geological interactions. Geoph Monog Series 91:297–316 doi:10.1029/GM091p0297

Frenkiel L, Gros O, Mouëza M (1996) Gill structure in *Lucina pectinata* (Bivalvia: Lucinidae) with reference to hemoglobin in bivalves with symbiotic sulphur-oxidizing bacteria. Mar Biol 125:511–524

Garfinkle EAR (2012) A review of North American recent *Radiolucina* (Bivalvia, Lucinidae) with the description of a new species. ZooKeys 205:19–31. doi:10.3897/zookeys.205.3120

Giere O (1985) Structure and position of bacterial endosymbionts in the gill filaments of Lucinidae from Bermuda (Mollusca, Bivalvia). Zoomorphology 105:296–301

Glover EA, Taylor JD, Rowden AA (2004) *Bathyaustriella thionipta*, a new lucinid bivalve from a hydrothermal vent on the Kermadec Ridge, New Zealand and its relationship to shallow-water taxa (Bivalvia: Lucinidae). J Mollus Stud 70:283–295

Gros O, Darrasse A, Durand P, Frenkiel L, Moueza M (1996a) Environmental transmission of a sulfur-oxidizing bacterial gill endosymbiont in the tropical lucinid bivalve *Codakia orbicularis*. Appl Environ Microb 62:2324–2330

Gros O, Frenkiel L, Mouësa M (1996b) Gill ultrastructure and symbiotic bacteria in the tropical lucinid, *Linga pensylvanica* (Linné). Symbiosis 20:259–280

Gros O, Frenkiel L, Mouëza M (1998) Gill filament differentiation and experimental colonization by symbiotic bacteria in aposymbiotic juveniles of *Codakia orbicularis* (Bivalvia: Lucinidae). Invertebr Reprod Dev 34:219–231

Gros O, Frenkiel L, Felbeck H (2000) Sulfur-oxidizing endosymbiosis in *Divaricella quadrisulcata* (Bivalvia: Lucinidae): morphological, ultrastructural, and phylogenetic analysis. Symbiosis 29:293–317

Gros O, Elisabeth NH, Gustave SDD, Caro A, Dubilier N (2012) Plasticity of symbiont acquisition throughout the life cycle of the shallow-water tropical lucinid *Codakia orbiculata* (Mollusca: Bivalvia). Environ Microbiol 14:1584–1595. doi:10.1111/j.1462-2920.2012.02748.x

Hammer Ø, Harper DAT, Ryan PD (2001) PAST: paleontological statistics software package for education and data analysis. Palaeontol Electron 4:1–9

Janssen HH (1992) Philippine bivalves and microorganisms: past research, present progress and a perspective for aquaculture. Philippine Scientist 29:5–32

Johnson M, Diouris M, Le Pennec M (1994) Endosymbiotic bacterial contribution in the carbon nutrition of *Loripes lucinalis* (Mollusca, Bivalvia). Symbiosis 17:1–13

Kamenev GM, Nadtochy VA, Kuznetsov AP (2001) *Conchocele bisecta* (Conrad, 1849) (Bivalvia: Thyasiridae) from cold-water methane-rich areas of the Sea of Okhotsk. Veliger 44:84–94

Kennicutt MC II, Brooks JM, Bidigare RR, Fay RR, Wade TL, McDonald TJ (1985) Vent-type taxa in a hydrocarbon seep region on the Louisiana Slope. Nature 317:351–353

Kiel S (2010) The fossil record of vent and seep mollusks. In: Kiel S (ed) The vent and seep biota: aspects from microbes to ecosystems. Springer, Dordrecht, pp 255–277

Klingenberg CP (2011) MorphoJ: an integrated software package for geometric morphometrics. Mol Ecol Resour 11:353–357

Le Pennec M, Beninger PG, Herry A (1995) Feeding and digestive adaptations of bivalve molluscs to sulphide-rich habitats. Comp Biochem Physiol 111A:183–189

Liljedahl L (1991) Contrasting feeding strategies in bivalves from the Silurian of Gotland. Palaeontology 34:219–235

Liljedahl L (1992) The Silurian *Ilonia prisca*, oldest known deep-burrowing suspension feeding bivalve. J Paleontol 66:206–210

Macdonald IR, Peccini MB (2009) Distinct activity phases during the recent geologic history of a Gulf of Mexico mud volcano. Mar Petrol Geol. doi:10.1016/j.marpetgeo.2008.12.005

Mae A, Yamanaka T, Shimoyama S (2007) Stable isotope evidence for identification of chemosynthesis-based fossil bivalves associated with cold-seepages. Palaeogeogr Palaeocl 245:411–420

McLeod RJ, Wing SR, Skilton JE (2010) High incidence of invertebrate-chemoautotroph symbioses in benthic communities of the New Zealand fjords. Limnol Oceanogr 55:2097–2106

Mikkelsen PM, Bieler R (2008) Seashells of southern Florida: living marine mollusks of the Florida Keys and adjacent regions: bivalves. Princeton University Press, Princeton

Morton B (1979) The biology and functional morphology of the coral-sand bivalve *Fimbria fimbriata* (Linnaeus 1758). Rec Aust Mus 32:389–420

Narchi W, Farani Assis RC (1980) Anatomia funcional de *Lucina pectinata* (Gmelin, 1791) Lucinidae-Bivalvia. Bol Zool Univ Sao Paulo 5:79–110

Oliver PG, Holmes AM (2007) A new species of *Axinus* (Bivalvia: Thyasiroidea) from the Baby Bare Seamount, Cascadia Basin, NE Pacific with a description of the anatomy. J Conchol 39:363–376

Oliver PG, Taylor JD (2012) Bacterial symbiosis in the Nucinellidae (Bivalvia: Solemyida) with descriptions of two new species. J Mollus Stud 78:81–91. doi:10.1093/mollus/eyr045

Ott J, Bright M, Bulgheresi S (2004) Marine microbial thiotrophic ectosymbioses. Oceanogr Mar Biol 42:95–118

Payne CM, Allen JA (1991) The morphology of deep-sea Thyasiridae (Mollusca: Bivalvia) from the Atlantic Ocean. Phil T R Soc B 334:481–562

Peng Y, Bao H, Anderson LC, Engel AS (2007) Carbonate-associated sulfate in lucinid (Bivalvia) shells. Eos Trans Amer Geophys Union 88:B31D–0611

Petersen JM, Dubilier N (2010) Symbiotic methane oxidizers. In: Timmis KN (ed) Handbook of hydrocarbon and lipid microbiology. Springer-Verlag, Berlin, pp 1977–1996

Petit RE (2001) A note on *Lucina multilineata* "Tuomey and Holmes" (Bivalvia: Lucinidae). Nautilus 115:35–36

Reynolds LK, Berg P, Zieman JC (2007) Lucinid clam influence on the biogeochemistry of the seagrass *Thalassia testudinum* sediments. Estuaries Coasts 30:482–490

Rodrigues CF, Hilário A, Cunha MR (2012) Chemosymbiotic species from the Gulf of Cadiz (NE Atlantic): distribution, life styles and nutritional patterns. Biogeosciences Discuss 9:17347–17376. doi:10.5194/bgd-9-17347-2012

Roeselers G, Newton ILG (2012) On the evolutionary ecology of symbioses between chemosynthetic bacteria and bivalves. Appl Microbiol Biot 94:1–10. Doi:10.1007/s00253-011-3819-9

Rohlf FJ (1996) Morphometric spaces, shape components and the effects of linear transformations. In: Marcus LF, Corti M, Loy A, Naylor GJP, Slice DE (eds) Advances in morphometrics. Plenum Press, New York, pp 117–129

Rohlf FJ (2007) tpsRelw: analysis of relative warps. Department of Ecology and Evolution, State University of New York at Stony Brook, Stony Brook

Rohlf FJ (2008) tpsDig2. Department of Ecology and Evolution, State University of New York at Stony Brook, Stony Brook

Roy KO-L, Sibuet M, Fiala-Médioni A, Gofas S, Salas C, Mariotti A, Foucher J-P, Woodside J (2004) Cold seep communities in the deep eastern Mediterranean Sea: composition, symbiosis and spatial distribution on mud volcanoes. Deep-Sea Res Pt I 51:1915–1936

Schmaljohann R, Faber E, Whiticar MJ, Dando PR (1990) Co-existence of methane- and sulphur-based endosymbioses between bacteria and invertebrates at a site in the Skagerrak. Mar Ecol-Prog Ser 61:119–124

Schweimanns M, Felbeck H (1985) Significance of the occurrence of chemoautotrophic bacterial endosymbionts in lucinid clams from Bermuda. Mar Ecol-Prog Ser 24:113–120

Sellanes J, Quiroga E, Neira C (2008) Megafauna community structure and trophic relationships at the recently discovered Concepción methane seep area, Chile, ~36°S. ICES J Mar Sci 65:1102–1111

Southward EC (1986) Gill symbionts in thyasirids and other bivalve molluscs. J Mar Biol Assoc UK 66:889–914

Southward EC, Gebruk A, Kennedy H, Southward AJ, Chevaldonné P (2001) Different energy sources for three symbiont-dependent bivalve molluscs at the Logatchev hydrothermal site (Mid-Atlantic Ridge). J Mar Biol Assoc UK 81:655–661

Spiro B, Greenwood PB, Southward AJ, Dando PR (1986) ^{13}C/^{12}C ratios in marine invertebrates from reducing sediments: confirmation of nutritional importance of chemoautotrophic endosymbiotic bacteria. Mar Ecol-Prog Ser 28:233–240

Stanley SM (1970) Relation of shell form to life habits of the Bivalvia (Mollusca). Geol Soc Am Mem 125:1–296

Stewart FJ, Newton ILG, Cavanaugh CM (2005) Chemosynthetic endosymbiosis: adaptations to oxic-anoxic interfaces. Trends Microbiol 13:439–448

Taylor JD, Glover EA (2000) Functional anatomy, chemosymbiosis and evolution of the Lucinidae. In: Harper EM, Taylor JD, Crame JA (eds) The evolutionary biology of the Bivalvia. Geological Society of London, London, pp 207–225

Taylor JD, Glover EA (2005) Cryptic diversity of chemosymbiotic bivalves: a systematic revision of worldwide *Anodontia* (Mollusca: Bivalvia: Lucinidae). Syst Biodivers 3:281–338

Taylor JD, Glover EA (2006) Lucinidae (Bivalvia)-the most diverse group of chemosymbiotic molluscs. Zool J Linn Soc-Lond 148:421–438

Taylor JD, Glover EA (2009a) A giant lucinid bivalve from the Eocene of Jamaica-systematics, life habits and chemosymbiosis (Mollusca: Bivalvia: Lucinidae). Palaeontology 52:95–109

Taylor JD, Glover EA (2009b) New lucinid bivalves from hydrocarbon seeps of the Western Atlantic (Mollusca: Bivalvia: Lucinidae). Steenstrupia 30:127–140

Taylor JD, Glover EA (2010) Chemosymbiotic bivalves. In: Kiel S (ed) The vent and seep biota: aspects from microbes to ecosystems. Springer, Dordrecht, pp 107–135

Taylor JD, Williams ST, Glover EA (2007a) Evolutionary relationships of the bivalve family Thyasiridae (Mollusca: Bivalvia), monophyly and superfamily status. J Mar Biol Assoc UK 87:565–574

Taylor JD, Williams ST, Glover EA, Dyal P (2007b) A molecular phylogeny of heterodont bivalves (Mollusca: Bivalvia: Heterodonta): new analyses of 18S and 28S rRNA genes. Zool Scr 36:587–606

Taylor JD, Glover EA, Williams ST (2009) Phylogenetic position of the bivalve family Cyrenoididae-removal from (and further dismantling of) the superfamily Lucinoidea. Nautilus 123:9–13

Taylor JD, Glover EA, Smith L, Dyal P, Williams ST (2011) Molecular phylogeny and classification of the chemosymbiotic bivalve family Lucinidae (Mollusca: Bivalvia). Zool J Linn Soc-Lond 163:15–49

van der Heide T, Govers LL, de Fouw J, Olff H, van der Geest M, van Katwijk MM, Piersma T, van de Koppel J, Silliman BR, Smolders AJP, van Gils JA (2012) A three-stage symbiosis forms the foundation of seagrass ecosystems. Science 336:1432–1434. doi:10.1126/science.1219973

Vrijenhoek RC (2010) Genetics and evolution of deep-sea chemosynthetic bacteria and their invertebrate hosts. In: Kiel S (ed) The vent and seep biota: aspects from microbes to ecosystems. Springer, Dordrecht, pp 15–49

Werne JP, Haese RR, Zitter T, Aloisi G, Bouloubassi I, Heijs S, Fiala-Médioni A, Pancost RD, Damsté JSS, de Lange G, Fomey LJ, Gottschal JC, Foucher J-P, Mascle J, Woodside J The *MEDINAUT* and *MEDINETH* Shipboard Scientific Parties (2004) Life at cold seeps: a synthesis of biogeochemical and ecological data from Kazan mud volcano, eastern Mediterranean Sea. Chem Geol 205:367–390

Williams ST, Taylor JD, Glover EA (2004) Molecular phylogeny of the Lucinoidea (Bivalvia): non-monophyly and separate acquisition of bacterial chemosynthesis. J Mollus Stud 70:187–202

Won Y-J, Hallam SJ, O'Mullan GD, Pan IL, Buck KR, Vrijenhoek RC (2003) Environmental acquisition of thiotrophic endosymbionts by deep-sea mussels of the genus *Bathymodiolus*. Appl Environ Microb 69:6785–6792

Chapter 4
Modern Analogs for the Study of Eurypterid Paleobiology

Danita S. Brandt and Victoria E. McCoy

Contents

Abstract Eurypterids are extinct, chelicerate arthropods whose life habits might be elucidated through comparison with living analogs. There are at least two potential eurypterid analogs, xiphosurans and arachnids (specifically, scorpions). Eurypterids and scorpions share striking morphologic and structural similarities despite their different habitats (aquatic vs. terrestrial); eurypterids and xiphosurans share numerous morphological characters and an aquatic habit. Despite the physiological differences inherent between aquatic and terrestrial chelicerates, the similarities in the basic body plan suggest that eurypterids and scorpions faced similar functional challenges during ecdysis, but eurypterid feeding was probably more similar to that of xiphosurans. For studies on the mechanical strength and functional morphology of the eurypterid exoskeleton, *Limulus* is the closer analog. The choice of modern analog for other aspects of eurypterid paleobiology, including reproduction and whether eurypterids were active predators, is a matter of discussion. The lack of a single, clear eurypterid analog from among extant chelicerates may reflect that eurypterids occupied an ecological niche intermediate between xiphosurans and

D. S. Brandt (✉)
Department of Geological Sciences, Michigan State University, East Lansing, MI 48824, USA
e-mail: brandt@msu.edu

V. E. McCoy
Department of Geology and Geophysics, Yale University, New Haven, CT, USA

arachnids. The search for a modern analog for eurypterids, then, is not likely to yield a single model organism.

Keywords Xiphosuran · Arachnid · Taphonomy · Molting · Ecdysis

4.1 Introduction

Extracting "lessons from the living" gains an added degree of difficulty in cases where the fossil organism under consideration is extinct. Eurypterids, the "sea scorpions" of the Paleozoic, are extinct, chelicerate arthropods with a fossil record extending from the Ordovician to the Permian, about 488–250 million years ago. The eurypterids included the largest arthropods that have ever lived; a few taxa reached lengths of 2.5 m (Braddy et al. 2007). Their size, as well as the development of the chelae into long, grasping appendages in some genera, suggests that eurypterids were predators (Størmer 1955; Sissom 1990). Eurypterids inhabited marine environments early in their geologic history, but moved into nearshore and perhaps even freshwater environments by the end of the Carboniferous period (Plotnick 1996, 1999). The fossil record of eurypterids is dominated by the numerous specimens comprising a few taxa from Silurian-aged strata of New York state (USA) (the so-called "Bertie bias," Plotnick 1999). Outside of these Lagerstätten, many eurypterid taxa are known only from incomplete specimens (Plotnick 1999). The paucity of intact eurypterid specimens is an additional complication for studies of eurypterid paleobiology.

Eurypterids are readily aligned with the other members of the Chelicerata on the basis of their chelicerae, the distinctive, pincer-bearing preoral appendages. The absence of crown group eurypterids complicates our ability to reconstruct the paleoecology and paleobiology of eurypterids. Unlike the extinct Trilobita, however, for whom no close living relative exists, a modern analog for the eurypterids may be sought among extant chelicerates. Two extant chelicerate groups, scorpions and xiphosurans, are most often employed as eurypterid analogs. In this chapter, we review the efficacy of using modern analogs in elucidating eurypterid paleobiology.

Scorpions are living chelicerate arthropods that appeared during the Silurian, about 440 million years ago. Paleozoic scorpions may have been aquatic (Selden and Jeram 1989; Jeram 1998, 2001) or not (Weygoldt 1998; Kühl et al. 2012), but were fully terrestrial by the end of the Paleozoic (Selden and Jeram 1989). Eurypterids and scorpions bear a striking resemblance in body plan (Fig. 4.1), so the use of modern scorpions as analogs for eurypterids is intuitive. But modern scorpions and eurypterids occupied significantly different habitats—terrestrial vs. marine—which are associated with different morphological, physiological, and behavioral adaptations.

Xiphosurans are aquatic chelicerates with a fossil record that extends to the Lower Ordovician (Van Roy et al. 2010). This group includes the extant horseshoe crab, *Limulus*. Eurypterids share with limulids adaptations for life in an aquatic environ-
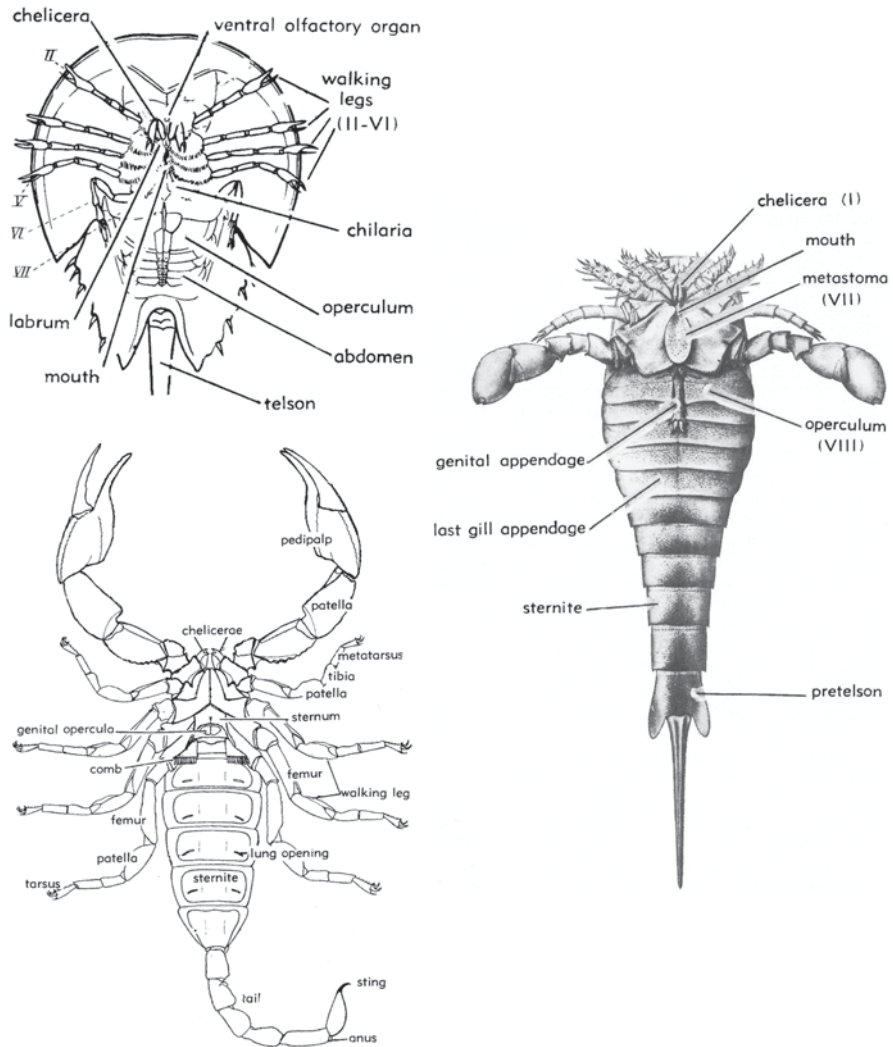
Fig. 4.1 Comparison of the ventral anatomy of xiphosurids (*upper left*), scorpions (*lower left*), and eurypterids. (From Størmer et al. 1955, used by permission)

ment, including eyes positioned on top of the head and a respiratory system that can function in water.

Phylogenetically, eurypterids have been allied with both the xiphosurans (Clarke and Ruedemann 1912; Briggs and Fortey 1989) and the arachnids/scorpions (Kjellesvig-Waering 1986; Dunlop and Braddy 1997; Braddy et al. 1999). Therefore, the choice of extant scorpions or *Limulus* as the analog for use in improving our understanding of the paleobiology and paleoecology of eurypterids requires more than a cursory examination.

4.2   Phylogenetic Considerations

Eurypterids have long been regarded as closely related to scorpions (e.g., Lank-ester 1881; Raw 1957; Sharov 1966; Bristowe 1971; Kjellesvig-Waering 1986). This interpretation has been criticized, however, as having been based on the overall similarities that might alternatively be due to convergence and symplesiomorphies rather than synapomorphies (Shultz 1990). Grasshoff (1978), for example, linked eurypterids and scorpions on the basis of overall body shape, which he interpreted as an adaptation for swimming. According to Dunlop (1997), the strongest synapo-morphy of the group Scorpiones + Eurypterida is the 5-segmented postabdomen. Other arachnids and the xiphosurans have a 3-segmented postabdomen.

Eurypterids initially were allied with the xiphosurans, particularly *Limulus* (Woodward 1865), and this interpretation still has currency (e.g., Bergström 1979; Jeram 1998; Dunlop and Braddy 2001). In still another interpretation, Dunlop (2010) placed eurypterids in a trichotomy with xiphosurans and arachnids. Other researchers cautioned that, "the paucity of informative characters and the poor or incomplete preservation of the (very) few fossils that exist make [phylogenetic] conclusions ambiguous and tentative" (Coddington et al. 2004, p. 297). Fine-scale serial sectioning of specimens combined with new digital imaging techniques, how-ever, offer unprecedented anatomical detail (e.g., Briggs et al. 2012) and informed recent conclusions of chelicerate phylogenetic relationships. In a study of the che-licerate limb, Briggs et al. (2012) placed eurypterids close to Arachnida, but not as a sister group. It is clear that chelicerate phylogeny is a subject of active discussion and continues to evolve. Therefore, we look to other lines of evidence to identify a modern analog for eurypterids.

4.3   Feeding

The large size attained by a few eurypterid genera (e.g., *Hibbertopterus*) and the presence in some eurypterids of prominent, grasping chelae are the basis for the widely held interpretation of eurypterids as "active" predators (Størmer 1955; Sis-som 1990; Selden 1984; Plotnick 1985; Plotnick and Baumiller 1988), a description that implies pursuit of mobile prey. A functional analysis of the prominent cheliceral claw of *Acutiramus*, however, led Laub et al. (2011) to conclude that, despite their imposing size and ornament, the elongated chelicerae of pterygotid eurypterids could not have been used to capture prey. Comparison with the feeding behaviors in extant analogs offers an independent line of reasoning for addressing the question of whether eurypterids were predators.

In considering their roles in ancient environments and ecosystems, xiphosurans initially may seem to be the better choice for an eurypterid analog because *Limulus* occupies a modern macrobenthic marine arthropod niche, whereas modern scor-pions are terrestrial. Eurypterids and *Limulus* would be expected to share at least

some basic morphological and physiological adaptations to the marine environment (see the subsequent discussion on cuticular structure), but some adaptations interpreted as advantageous for a predatory lifestyle are shared by aquatic and terrestrial chelicerates.

A comparison of presumed predatory features between eurypterids, *Limulus*, and scorpions yields mixed results. The presence of prominent prosomal appendages (chelae in scorpions; large chelicerae and sixth prosomal appendage in some eurypterids) distinguish both scorpions and eurypterids from the xiphosurans (Sissom 1990). *Limulus* and eurypterids, however, share a ventrally located mouth, in contrast to the anteriorly directed mouth of scorpions. Similarity in mouth position may indicate similarity in feeding strategy, thus pointing to *Limulus* as the more appropriate analog in questions of eurypterid feeding habits. Scorpions are active predators, feeding on insects, other scorpions, small lizards, and mammals (Polis 1990). In contrast, extant xiphosurans (e.g., *Limulus polyphemus* and *Tachypleus gigas*) are opportunistic foragers (Shuster et al. 2003), feeding primarily on the less-mobile thin-shelled clams and marine worms (Botton 1984; Botton and Haskin 1984; Botton and Ropes 1989; Chatterji et al. 1992). Generally, active predatory macrobenthic arthropods have anteriorly directed mouths (e.g., lobsters and crabs).

Large appendages in arthropods are known to serve functions other than predation, e.g., the enlarged claw in fiddler crabs plays a role in sexual selection (Pope 2000). Thus, the ventral position of the eurypterid mouth is the more relevant feature to consider in searching for a modern analog for eurypterid feeding habit. Therefore, *Limulus* likely is the more appropriate extant analog for eurypterid feeding. This conclusion is congruent with Laub et al.'s (2011) functional analysis of the prominent chelae in pterygotid eurypterids.

4.4   Locomotion

Trackways, trails, and burrows are the preserved record of behavior. Comparison of eurypterid tracks and trails with those of potential modern analogs might elucidate aspects of eurypterid behaviors such as whether eurypterids ventured onto land (as *Limulus* does) or whether they burrowed (as some scorpions do).

Eurypterid trails fall within the category of "generally large, Paleozoic traces showing a double row of three or four imprints" (Selden 1984, p. 43). Fossil trackways attributed to eurypterids include the ichnogenus *Palmichnium* and possibly *Nereites* (Martin and Rindsberg 2007) and are known from Silurian to Carboniferous strata (Richter 1954; Gevers et al. 1971; Hanken and Størmer 1975; Bradshaw 1981; Briggs and Rolfe 1983; Selden 1984; Draganits et al. 2001; Almond 2002; Whyte 2005; Poschmann and Braddy 2010). Several of these studies (Richter 1954; Briggs and Rolfe 1983; Whyte 2005; Poschman and Braddy 2010) described symmetrically arranged footprints on either side of a midline, indicating an "in phase" gait. There is a discussion, however, on whether this gait was typical for eurypterids

(Briggs and Rolfe 1983). Indeed, it would be unusual for eurypterids to have formed only a single type of trackway. More typical is the ichnologists' conundrum of sorting out multiple trackway types attributable to different behaviors or differences in sediment consistency or cohesiveness (e.g., Osgood 1970 on trilobites; Wang 1993 on limulids).

The tracks and trails of fossil xiphosurans are essentially the same as those of their extant descendants (Shuster et al. 2003). The ichnogenus *Kouphichnium* encompasses xiphosurid trackways (Caster 1938, 1944; Chisholm 1983), comprising "heteropodous tracks of great variability" (Häntzschel 1975, p. W75). *Kouphichnium* is characterized by a chevron-like series of four simple, oval tracks followed by a pair of digitate imprints made by the fifth, "pusher" pair of appendages. A median drag mark may or may not be present.

At least two other limulid behaviors have been interpreted from trace fossils: burrowing (*Aulichnites*) (Fenton and Fenton 1937) and "resting" (*Limulicubichnus*) (Miller 1982). Xiphosuran burrowing and resting traces both show the outline of the semicircular prosoma. There have not yet been comparable burrows or resting traces described for eurypterids.

Few fossil trackways have been attributed to scorpions (e.g., *Paleohelcura* and *Octopodichnus*), and all are from sandstones interpreted as deposited in a terrestrial environment (Brady 1947), as opposed to the eurypterid and xiphosuran trace fossils that are described from a variety of aquatic environments. Brady (1947) used neoichnological methods to document the trackway of a modern scorpion for comparison with *Paleohelcura*. He noted a range of variation in the modern scorpion trackways (e.g., presence or absence of tail drag mark, variation in the patterns of foot impression), but the basic morphological plan of symmetrically arranged *en echelon* tracks was evident in all the modern scorpion trackways and compared favorably with *Paleohelcura*. More recently, Hembree et al. (2012) characterized modern burrows of the scorpion *Hadrurus arizonensis*. The lack of known eurypterid burrows, however, precludes comparison to scorpion burrows.

Despite the difference in life habitat, scorpion trackways share basic morphological attributes with xiphosuran and eurypterid trackways. The resemblance of scorpion, xiphosuran, and eurypterid trackways reflects a similar mode of locomotion among these arthropods. The sparse eurypterid ichnological record has not yet provided the data on which to determine the more appropriate modern analog for eurypterid locomotion. The lack of fossil burrows attributed to eurypterids and the presence of fossil burrows of limulids and scorpions (both known to burrow in the modern) support the conclusion that eurypterid did not burrow.

4.5   Ecdysis

All arthropods, living and extinct, grow through a process in which the old exoskeleton is discarded to be replaced by a new one. Along with possession of an exoskeleton and paired, jointed appendages, ecdysis (molting) is a fundamental trait

of arthropods. Distinguishing between fossil molts and carcasses is important in interpreting real abundance of individuals in fossil communities, yet molting has not been systematically studied in many fossil arthropods, with the exception of trilobites (Brandt 1993, 2002), scorpions (McCoy and Brandt 2009), and in one eurypterid genus, *Eurypterus* (Tetlie et al. 2008). Most eurypterid fossils, however, are interpreted as representing molted exuvia rather than carcasses (Clarke and Ruedemann 1912; Størmer 1934; Braddy et al. 1995; Tetlie et al. 2008). Comparison with *Limulus* and scorpions may reveal differences in exuvial behavior that reflect terrestrial versus aquatic habit.

In choosing between scorpions and xiphosurans as a modern analog for eurypterid molting, scorpions are intuitively the more appealing choice as an analog because of their striking morphologic and structural similarities with eurypterids. Both the eurypterid opisthosoma and scorpion abdomen are differentiated into two portions: a broad, seven-segment anterior portion, and a narrower, five-segment posterior portion that terminates in a telson (in eurypterids) or sting (in scorpions). Moreover, the process of ecdysis is potentially constrained by the presence of morphological bottlenecks, i.e., structures that would make ecdysis more difficult due to the necessity of moving a wide body part through a narrow exoskeletal opening. Potential bottlenecks in eurypterid morphology include: enlarged, flattened paddles at the distal end of the swimming appendage; enlarged chelicerae and telson; spiniferous appendages; and an enlarged preabdomen relative to the prosoma (Tetlie et al. 2008). In this regard, eurypterids resemble scorpions more closely than they do xiphosurans. Scorpions also have enlarged appendages (the pedipalps), a preabdomen that is at least as wide as the prosoma, and constrictions between segments in the postabdomen which could cause similar problems as the enlarged telson. The similarities in basic body plan and the presence of similar potential morphological "bottlenecks" suggest that both eurypterids and scorpions faced similar functional challenges during ecdysis.

Scorpion molting can be observed directly (e.g., Gaban and Farley 2002). Eurypterid molting, on the other hand, must be inferred from recurring taphonomic patterns of dissociated tergites, recurrent patterns of dislocations along the exoskeleton, and dorsal/ventral orientation of the animal (Tetlie et al. 2008). Using taphonomic census data, Tetlie et al. (2008) constructed a molting scenario for *Eurypterus* that is very similar to the scenario known from modern scorpions (Polis 1990): The anterior carapace suture and ventral suture open, and the eurypterid crawls out through the anterior opening.

The work of Tetlie et al. (2008) on characterizing molting in the eurypterid genus *Eurypterus* and the work of McCoy and Brandt (2009) on molting in fossil and modern scorpions confirmed that eurypterids and scorpions share the basic ecdysial patterns (Fig. 4.2). Scorpion molts show a distinctive molt posture and recurring patterns of disarticulation, both of which resemble molt postures and patterns of disarticulation of eurypterids. The basic scorpion molt posture includes a curved body line, extended chelicerae, and extended, posteriorly facing pedipalps (McCoy and Brandt 2009). Many eurypterids specimens identified by Tetlie et al. (2008) as molts show similar features (Fig. 4.2). The most common patterns among disarticu-
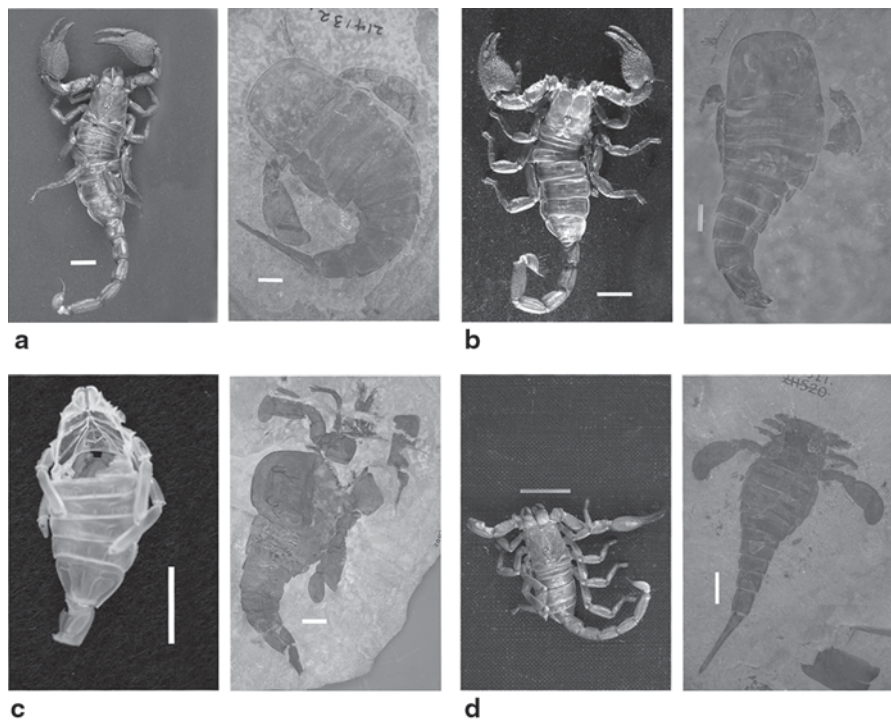
Fig. 4.2 Comparison of modern *Pandinus imperator* scorpion exuvia (*left photo* in each pair) and presumed eurypterid exuvia of *Eurypterus remipes* (*right photo* in each pair). Shared features include: **a** curved body line (YPM 214132, right); **b** telescoped segments (YPM 8349, right); **c** detached carapace (YPM 2128, right); and **d** splayed appendages (YPM 216521, right). Centimeter scale bar. (*YPM* Yale Peabody Museum, New Haven, CT)

lated elements of scorpion exuvia were the separation of the carapace and distal leg elements from the rest of the exoskeleton (McCoy and Brandt 2009). Disarticulation data for *Eurypterus* showed similar prevalence of these patterns (Tetlie et al. 2008) (Fig. 4.3).

Some arthropods seek a refuge during molting (e.g., lobsters; Herrick 1911). Modern scorpions commonly molt in burrows, presumably to avoid predation (Polis 1990), whereas *Limulus* buries itself in the muddy sediment of the offshore environment (Shuster et al. 2003). A similar self-preservation behavior has been inferred for fossil arthropods whose exuvia have been found in presumed refugia, e.g., trilobite exuvia in cephalopod shells (Davis et al. 2001). Bertie eurypterid Lagerstätten may represent molting refugia in the nearshore lagoonal environment of the Bertie Waterlime (Braddy 2001). The absence of burrows or "resting traces" (cubichnia) attributable to eurypterids suggests that eurypterids resembled neither *Limulus* nor scorpions in seeking their "normal" premolt refuge. Further, the exceptional preservation of the eurypterids suggests that the Bertie eurypterid Lagerstätten represent

Fig. 4.3 *Eurypterus remipes* showing multiple molting characteristics: curved body line, missing carapace, splayed appendages. Scale is 1.5 cm. (New York State Museum 13140)

unique and fortuitous occurrences where eurypterids had access to a restricted lagoon in which to seek refuge during molting.

Another molting behavior that potentially might be more useful to discriminate between xiphosurans and scorpions as a modern analog for eurypterids is the posture during molting. Tetlie et al. (2008) collected dorsal/ventral position data for *Eurypterus* exuvia and found no preferred orientation. There are a few reports of *Limulus* molting behavior in its natural habitat, as much of the animal's life is spent in deeper offshore environments. Lockwood (1870) and Packard (1883) observed *Limulus* molting in its natural habitat, presumably dorsal-upward, as they made no observations to the contrary. Laverock (1927), however, observed *Limulus* molt on its back in an aquarium, but he noted that the artificial laboratory setting may have affected the animal's behavior. Most scorpions molt in the prone (dorsal-up) position, but some genera molt in a supine (ventral-up) position (Auber 1963; Gaban and Farley 2002). On the basis of molt posture, then, eurypterids were more scorpion-like than limulid-like; neither show a consistent dorsal-up or dorsal-down molting position.

4.6   Reproduction

Comparisons of eurypterids with extant analogs may address questions of whether eurypterids sought refugia or congregated for the purposes of molting and/or mating. Braddy (2001) suggested that the eurypterid Lagerstätten of the Silurian "Bertie Waterlime" of New York (USA) represented an eurypterid mass-molt-mate assemblage; that is, an accumulation of multiple exuvia amassed as the result of numerous individuals congregating in an area to molt, followed by mating. Braddy (2001) invoked the behavior of modern *Limulus* as a modern analog, but incorrectly cited Rudloe (1980) as evidence for mass-molt-mate behavior in *Limulus*. Loveland (2001) reported evidence for coordinated molting among a particular size class of juvenile horseshoe crabs, as evidenced by beached exuvia of similar size, but the behavior of modern arthropods does not provide a behavioral analog for a mass-molt-mate phenomenon. Rudloe (1980) and Shuster (1982), among others, described the well-known phenomenon of *Limulus* swarming in the nearshore environment to mate, but juvenile horseshoe crabs remain offshore until they undergo a terminal molt and become sexually mature adults (Loveland 2001). Thus, molting and mating are not linked in *Limulus*. Some lobsters and crabs mate within hours of molting, but not in the aggregate (Anderton 1909; Bliss 1982). Scorpions do not congregate to mate or molt (Polis 1990) and do not contribute to an explanation for assemblages of multiple eurypterid exuvia.

A mass-molt-mate behavior may, in fact, explain assemblages of trilobites (e.g., Speyer and Brett 1985), but this behavior has not been documented in extant arthropods and thus there is no modern analog. In their study of molting in *Eurypterus*, Tetlie et al. (2008) concluded that the evidence for a mass-molt-mate behavior among the eurypterids of the Bertie Waterlime was equivocal.

On the basis of a functional morphological study of the genital appendages in the eurypterid genus *Baltoeurypterus*, Braddy and Dunlop (1997) concluded that mating in this eurypterid genus was more arachnid-like than limulid-like. Hanken and Størmer (1975), however, inferred limulid-like copulatory behavior for eurypterids from the observation of modern *Limulus* and their interpretation of a Silurian eurypterid trackway. These contradictory conclusions are consistent with Boucot's (1990) characterization of eurypterid reproductive scenarios as "fairly speculative" because the behavior is inferred from a wholly extinct taxon.

4.7   Other Considerations

4.7.1   Cuticle

An understanding of the nature of eurypterid cuticle is relevant to questions about the mechanical strength of eurypterid appendages and whether eurypterids ventured onto land. Drawing on the work of Dalingwater (1973, 1975) and Mutvei (1977),

Laub et al. (2011, p. 30) considered *Limulus* cuticle to be a "satisfactory model for the mechanical properties" of the eurypterid integument. Using a scanning electron microscopy (SEM), Mutvei (1977) had identified vertical lamellar structure in the endocuticle of *L. polyphemus*. Mutvei (1977) concluded that equivalent vertical structures could be identified in SEM images of eurypterid endocuticle from Dalingwater (1973, 1975). Further, Mutvei (1977) noted that the vertical structure was present only in the chela and leg joints of the modern scorpion *Heterometrus*. Experimental studies on the mechanical strength of the endocuticle of *Limulus* (Joffe et al. 1975) suggested that the vertical structure may have contributed to plasticity.

4.7.2 Sexual Dimorphism

Scorpions and xiphosurans exhibit sexual dimorphism and eurypterids are widely regarded as having had some sexual dimorphic traits (Selden 1984). Some eurypterids possessed ventral structures on the opisthosoma interpreted as genital appendages, although whether the long and narrow type A belonged to the male and the shorter type B to females have been a matter of contention (Selden 1984). Thus, interpretation of possible sexual dimorphic traits in eurypterids is an area that potentially could benefit from comparison to modern analogs. Scorpions and xiphosurans include taxa in which the male possesses clasping structures (Carerra et al. 2009; Rudloe 1980). Some eurypterids bore structures that have been interpreted as claspers (Selden 1984), but interpretation of these structures ranges from claspers in males to nest-digging structures in females (Selden 1984). As Laub et al. (2011) demonstrated in their functional study of the pterygotid cheliceral claw, assumptions based on morphological resemblance are not sufficient for framing functional interpretations.

4.7.3 Respiration

Understanding eurypterid respiration is a prerequisite to addressing the question of whether eurypterids were capable of leaving their aquatic habitat (Manning and Dunlop 1995). Selden and Whalley (1985) summarized the differing interpretations of the eurypterid respiratory apparatus and sought an analog for eurypterid respiration from among extant arthropods, including xiphosurans, scorpions, crustaceans, and uniramians. Selden and Whalley (1985) concluded that better preserved eurypterid specimens were needed for a detailed study to characterize the eurypterids respiratory apparatus before meaningful comparisons with possible modern analogs could be made. Manning and Dunlop (1995) recovered exceptionally preserved cuticle fragments that they interpreted as eurypterid respiratory organs. From their study of this material, Manning and Dunlop (1995) concluded that the eurypterid "Kiemenplatten" (gill tract) has no chelicerate counterpart, and that the closest arthropod analog is the brachial lung of some terrestrial crabs. This conclusion

supported the interpretation that eurypterids could have ventured onto land. The behavioral interpretation of Manning and Dunlop (1995) gained support from Scholtz and Kamenz (2006), who noted that the eurypterid respiratory lamellae shared a feature with the respiratory lamellae of the earliest putative terrestrial scorpions.

4.8   Conclusions

The search for an extant analog to elucidate aspects of the extinct eurypterids' paleobiology and paleoecology centers on xiphosurans and arachnids (scorpions). Current interpretations of chelicerate phylogeny differ in the inferred relationship between eurypterids and the xiphosurans and arachnids. Thus, phylogenetic considerations alone do not point to an unambiguous modern analog for eurypterids. Similarly, in the studies of eurypterid paleobiology, the choice of a modern eurypterid analog differs depending on the aspect of eurypterid life habit that is addressed. Eurypterid feeding was probably more *Limulus*-like than scorpion-like, but eurypterid ecdysis was probably more similar to that of scorpions. A depauperate eurypterid ichnofossil record precludes more than a general comparison with limulid and scorpion behavior, and reveals only that all three groups shared a basic arthropod mode of locomotion over the substrate. There is no modern analog for the proposed mass-mate-molt hypothesis of eurypterid reproduction; contradictory conclusions in characterizing eurypterid reproductive behavior, as xiphosuran-like in some respects and scorpion-like in others, invites further exploration of both groups as analogs for this aspect of eurypterid habit.

Eurypterids occupy an interesting place in the chelicerate fossil record, overlapping with both the marine xiphosurids and with scorpions, as the latter group transitioned from the marine environment to terrestrial niches. The observation that limulids are a closer analog for some aspects of eurypterid paleobiology and scorpions better for others may reflect that eurypterids occupied a niche intermediate between xiphosurans and arachnids. The search for a modern analog for eurypterids, then, is not likely to yield a single model organism, as the contrasting results of previous research has indicated. The exercise of seeking to identify a modern eurypterid analog, however, has proven useful in uncovering this relationship.

References

Almond JE (2002) Giant arthropod trackway Ecca Group. Geobull 45:28
Anderton T (1909) The lobster (*Homarus vulgaris*). Rep Mar Dep New Zealand 1908–1909

Auber M (1963) Reproduction et croissance de Buthus occitanus. Ann Sci Nat (Zool et Biol Anim) 5:273–286

Bergström J (1979) Morphology of fossil arthropods as a guide to phylogenetic relationships. In: Gupta AP (ed) Arthropod phylogeny. Van Nostrand Reinhold, New York, pp 3–60

Bliss DE (1982) Shrimps, lobsters and crabs. Columbia

Botton ML (1984) Diet and food preferences of the adult horseshoe crab *Limulus polyphemus* in Delaware Bay, New Jersey, USA. Mar Biol 81:193–207

Botton ML, Haskin HH (1984) Distribution and feeding of the horseshoe crab *Limulus polyphemus* on the continental shelf, New Jersey. Fish Bull USA 82:383–389

Botton ML, Ropes JW (1989) Feeding ecology of horseshoe crabs on the continental shelf, New Jersey to North Carolina. Bull Mar Sci 49:637–647

Boucot AJ (1990) Evolutionary paleobiology of behavior and coevolution. Elsevier, New York

Braddy SJ (2001) Eurypterid palaeoecology: palaeobiological, ichnological and comparative evidence for a 'mass-moult-mate' hypothesis. Palaeogeogr Palaeoclim 172:115–132

Braddy SJ, Dunlop JA (1997) The functional morphology of mating in the Silurian eurypterid, *Baltoeuryperus tetragonophthalmus* (Fischer, 1839). Zool J Linn Soc 120:435–461

Braddy SJ, Aldridge RJ, Theron JN (1995) A new eurypterid from the Late Ordovician Table Mountain Group, South Africa. Palaeontol 38:563–581

Braddy SJ, Aldridge RJ, Gabbott SE, Theron JN (1999) Lamellate bookgills in a Late Ordovician eurypterid from the Soom Shale Lagerstätte, South Africa: support for a eurypterid-scorpion clade. Lethaia 32:72–74

Braddy SJ, Poschmann M, Tetlie OE (2007) Giant claw reveals the largest ever arthropod. Biol Lett 4:106–109

Bradshaw MA (1981) Paleoenvironmental interpretations and systematics of Devonian trace fossils from the Taylor Group (Lower Beacon Supergroup), Antarctica. New Zealand J Geol Geophys 24:615–652

Brady LF (1947) Invertebrate tracks from the Coconino Sandstone of northern Arizona. J Paleont 21:466–472

Brandt DS (1993) Ecdysis in *Flexicalymene meeki* (Trilobita). J Paleontol 67:999–1005

Brandt DS (2002) Ecdysial efficiency and evolutionary efficacy among marine arthropods. Alcheringa 26:399–421

Briggs DEG, Fortey RA (1989) The early radiation and relationships of the major arthropod groups. Sci 246:241–243

Briggs DEG, Rolfe WDI (1983) A giant arthropod trackway from the Lower Mississippian of Pennsylvania. J Paleontol 57:377–390

Briggs DEG, Siveter DJ, Siveter DJ, Sutton MD, Garwood RJ, Legg D (2012) Silurian horseshoe crab illuminates the evolution of arthropod limbs. PNAS doi:10.1073/pnas.1205875109

Bristowe WS (1971) The world of spiders, 2nd edn. Collins, London

Carerra PC, Mattoni CI, Peretti AV (2009) Chelicerae as male grasping organs in scorpions: sexual dimorphism and associated behaviour. Zool 112:332–350

Caster KEC (1938) A restudy of the tracks of *Paramphibius*. J Paleont 12:3–60

Caster KEC (1944) Limuloid trails from the Upper Triassic (Chinle) of the Petrified Forest National Monument, Arizona. Am J Sci 242:74–84

Chatterji A, Mishra JK, Parulekar AH (1992) Feeding behaviour and food selection in the horseshoe crab, *Tachypleus gigas* (Müller). Hydrobiologia 246:41–48

Chisholm JI (1983) Xiphosurid burrows from the Lower Coal Measures (Westphalian A) of West Yorkshire. Palaeont 28:619–628

Clarke JM, Ruedemann R (1912) The Eurypterida of New York. Memoir of the New York state museum of natural history. New York State Education Department, New York

Coddington JA, Giribet G, Harvey MS, Prendini L, Walter DE (2004) Arachnida. In: Cracraft J, Donoghue M (eds) Assembling the tree of life. Oxford University Press, Oxford, pp 296–318

Dalingwater JE (1973) The cuticle of a eurypterid. Lethaia 6:179–186

Dalingwater JE (1975) Further observations on eurypterid cuticles. Fossils Strat 4:271–279

Davis RA, Fraaye RHB, Holland CH (2001) Trilobites within nautiloid cephalopods. Lethaia 34:37–45

Draganits E, Braddy SJ, Briggs DEG (2001) A Gondwanan coastal arthropod ichnofauna from the Muth Formation (Lower Devonian, Northern India): paleoenvironment and tracemaker behavior. Palaios 16:126–127

Dunlop JA (1997) Palaeozoic arachnids and their significance for arachnid phylogeny. In: Zabka M (ed) Proceedings of the 16th European colloquium of arachnology, Siedlce, 1996. Wyzsza Szkola Rolnicko-Pedagogiczna, Siedlce

Dunlop JA (2010) Geological history and phylogeny of Chelicerata. Arthr Struc Dev 39:124–142

Dunlop JA, Braddy SJ (1997) Slit-like structures on the prosomal appendages of the eurypterid *Baltoeurypterus*. Neues Jahrb Geol Palaontol Monatshefts 1:31–38

Dunlop JA, Braddy SJ (2001) Scorpions and their sister group relationships. In: Fet V, Selden PA (eds) Scorpions 2001, British Arachnological Society, pp 1–24

Fenton CL, Fenton MA (1937) Burrows and trails from Pennsylvanian rocks of Texas. Am Midl Nat 18:1079–1084

Gaban RD, Farley RD (2002) Ecdysis in scorpions: supine behavior and exuvial ultrastructure. Invertebr Biol 121:136–147

Gevers TW, Frakes LA, Edwards LN, Marzolf JE (1971) Trace fossils in the Lower Beacon sediments (Devonian), Darwin Mountains, Southern Victoria Land, Antarctica. J Paleont 45:81–94

Grasshoff M (1978) A model of the evolution of the main chelicerate groups. Symp Zool Soc Lond 42:273–284

Hanken NM, Størmer L (1975) The trail of a large Silurian eurypterid. Fossils Strat 4:255–270

Häntzschel W (1975) Trace fossils and problematica. Treatise on invertebrate paleontology, 2nd edn. Part W: miscellanea, supp 1. Geological Society of America and University of Kansas Press (Geol Soc Am and Univ Kansas Press), Lawrence

Hembree DI, Johnson LM, Tenwalde RW (2012) Neoichnology of the desert scorpion *Hadrurus arizonensis*: burrows to biogenic cross lamination. Palaeontol Electron 15:1–34

Herrick FH (1911) Natural history of the American lobster. U S Government Printing Office, Washington

Jeram AJ (1998) Phylogeny classification and evolution of Silurian and Devonian scorpions. In: Selden PA (ed) Proceedings of the 17th European colloquium of arachnology, Edinburgh, July 1997. British Arachnological Society, Burnham Beeches

Jeram AJ (2001) Paleontology. In: Brownell P, Polis GA (eds) Scorpion biology and research. Oxford University Press, Oxford, pp 370–392

Joffe I, Hepburn HR, Andersen SO (1975) On the mechanical properties of *Limulus* solid cuticle. J com Physio 101:147–160

Kjellesvig-Waering EN (1986) A restudy of the fossil Scorpionida of the world. Palaeontograph Am 55:1–287

Kühl G, Bergmann A, Dunlop J, Garwood RJ, Rust J (2012) Redescription and palaeobiology of *Palaeoscorpius devonicus* Lehmann, 1944 from the Lower Devonian Hunsrück Slate of Germany. Palaeon 55:775–787

Lankester ER (1881) *Limulus*, an arachnid. Q J Microsc Sci 21:504–649

Laub RS, Tollerton VP, Berkof RS (2011) The cheliceral claw of *Acutiramus* (Arthropoda: Eurypterida): functional analysis based on morphology and engineering principles. Bull Buffalo Soc Nat Sci 39:29–42

Laverock WS (1927) On the casting of the shell in *Limulus*. Trans Liverpool Biol Soc 13–16

Lockwood S (1870) The horse foot crab. Am Nat 4:257–274

Loveland RE (2001) The life history of horseshoe crabs. In: Tancredi JT (ed) *Limulus* in the limelight: a species 350 million years in the making and in peril? Kluwer Academic/Plenum, New York, pp 93–101

Manning PL, Dunlop JA (1995) The respiratory organs of eurypterids. Palaeontol 38:287–297

Martin AJ, Rindsberg AK (2007) Arthropod tracemakers of *Nereites?* Neoichnological observations of juvenile limulids and their paleoichnological applications. In: Miller WEIII (ed) Trace fossils. Elsevier, Amsterdam, pp 478–488

McCoy VE, Brandt DS (2009) Scorpion taphonomy: criteria for distinguishing fossil scorpion molts and carcasses. J Arachnol 37:312–320

Miller MF (1982) *Limulicubichnus*: a new ichnogenus of limulid resting traces. J Paleont 56:429–433

Mutvei H (1977) SEM studies on arthropod exoskeletons, 2. Horseshoe crab *Limulus polyphemus* (L.) in comparison with extinct eurypterids and recent scorpions. Zool Scripta 6:203–213

Osgood RA (1970) Trace fossils of the Cincinnati area. Palaeontogr Am VI:281–444

Packard AS (1883) Molting of the shell in *Limulus*. Am Nat 17:1075–1076

Plotnick R (1985) Lift based mechanisms for swimming in eurypterids and portunid crabs. Earth Env Sci Trans R Soc Edinburgh 76:325–337

Plotnick R (1996) The scourge of the Silurian seas. Am Paleontol 4:2–3

Plotnick R (1999) Habitat of Llandoverian-Lochkovian eurypterids. In: Boucot AJ, Lawson JD (eds) Paleocommunities: a case study from the Silurian and Lower Devonian. Cambridge University Press, Cambridge, pp 106–131

Plotnick R, Baumiller T (1988) The pterygotid telson as a biological rudder. Lethaia 21:13–27

Polis G (ed) (1990) The biology of scorpions. Stanford University Press, Stanford

Pope DS (2000) Testing function of fiddler crab claw waving by manipulating social context. Behav Ecol Sociobiol 47:432–437

Poschmann M, Braddy SJ (2010) Eurypterid trackways from Early Devonian tidal facies of Alken an der Mosel (Rheinisches Schiefergebirge, Germany). Palaeobio Palaeoenv 90:111–124

Raw F (1957) Origin of chelicerates. J Paleontol 31:139–192

Richter R (1954) Fährte eines "Riesenkrebses" im Rheinischen Schiefergebirge. Natur Volk 84:261–296

Rudloe A (1980) The breeding behavior and patterns of movement of horseshoe crabs, *Limulus polyphemus* in the vicinity of breeding beaches in Apalachee Bay, Florida. Estuaries 3:177–183

Scholtz G, Kamenz C (2006) The book lungs of Scorpiones and Tetrapulmonata (Chelicerata, Arachnida): evidence for homology and a single terrestrialisation event of a common arachnid ancestor. Zoology 109:2–13

Selden PA (1984) Autecology of Silurian eurypterids. Spec Papers Palaeontol 32:39–54

Selden PA, Jeram AJ (1989) Palaeophysiology of terrestrialisation in the Chelicerata. Trans R Soc Edinburgh. Earth Sci 80:303–310

Selden PA, Whalley P (1985) Eurypterid respiration [and discussion]. Phil Trans R Soc Lond B 309:219–226

Sharov AG (1966) Basic Arthropodan stock with special reference to insects. Pergamon Press, Oxford

Shultz JW (1990) Evolutionary morphology and phylogeny of Arachnida. Cladistics 6:1–38

Shuster CN Jr (1982) A pictorial review of the natural history and ecology of the horseshoe crab *Limulus polyphemus*, with reference to other Limulidae. In: Bonaventura J, Bonaventura C, Tesh S (eds) Physiology and biology of horseshoe crabs. Liss, New York, pp 1–52

Shuster CN Jr, Barlow RB, Brockmann HJ (2003) The American horseshoe crab. Harvard University Press, Cambridge

Sissom WD (1990) Systematics, biogeography, and paleontology. In: Polis GA (ed) The biology of scorpions. Stanford University Press, Stanford, pp 64–160

Speyer SE, Brett CE (1985) Clustered trilobite assemblages in the Middle Devonian Hamilton Group. Lethaia 18:85–103

Størmer L (1934) Merostomata from the Downtonian Sandstone of Ringerike, Norway. Skrifter utgitt av Det Norske Vidensk-Akad i Oslo I. Mat-Naturvidenskapelig Klasse 10:1–125

Størmer L (1955) Merostomata. In: Moore RC (ed) Treatise on invertebrate paleontology. Part P: Arthropoda 2: Chelicerata. Geological Society of America and University of Kansas Press, Lawrence, pp P4–P41

Størmer L, Petrunkevitch A, Hedgpeth JW (1955). Treatise on invertebrate paleontology. Part P: Arthropoda 2: Chelicerata. Geological Society of America and University of Kansas Press, Lawrence

Tetlie OE, Brandt DS, Briggs DEG (2008) Ecdysis in sea scorpions (Chelicerata: Eurypterida). Palaeogeogr Palaeoclim 265:182–194

Van Roy P, Orr PJ, Botting JP, Muir LA, Vinther J, Lefebvre B, el Hariri K, Briggs DEG (2010) Ordovician faunas of Burgess Shale type. Nature 465:215–218

Wang G (1993) Xiphosurid trace fossils from the Westbury Formation (Rhaetian) of southwest Britain. Palaeont 36:111–122

Weygoldt P (1998) Evolution and systematics of the Chelicerata. Exp App Acarol 22:63–79

Whyte M (2005) A gigantic fossil arthropod trackway. Nature 438:576

Woodward H (1865) On a new genus of Eurypterida from the Lower Ludlow rocks of Leintwardine, Shropshire. Q J Geol Soc 21:490–492

Chapter 5
New Applications for Constrained Ordination: Reconstructing Feeding Behaviors in Fossil Remingtonocetinae (Cetacea: Mammalia)

Lisa Noelle Cooper, Tobin L. Hieronymus, Christopher J. Vinyard, Sunil Bajpai and J. G. M. Thewissen

Contents

Abstract During the Eocene epoch, archaic cetaceans made the land-to-sea transition, giving rise to modern whales, dolphins, and porpoises. During this transition, the feeding apparatus of fossil remingtonocetines displayed morphologies that are distinct from other cetaceans, confounding straightforward interpretations of their feeding behaviors. This study utilized a novel combined ordination of morphology and feeding strategy, while accounting for phylogeny, in a sample of 2 remingtonocetines and 18 extant cetartiodactylans, to assess the morphological signal of feeding behaviors. Results showed that differences between prey acquisition in extant taxa were driven by a suite of mandibular characters and width of the palatal arch, providing a behaviorally constrained morphospace. Remingtonocetinae clustered

T. L. Hieronymus (✉) · L. N. Cooper · C. J. Vinyard · J. G. M. Thewissen
Department of Anatomy and Neurobiology, Northeast Ohio Medical University,
4209 State Route 44, Rootstown, OH 44272-0095, USA
e-mail: htobin@gmail.com

S. Bajpai
Department of Earth Sciences, Indian Institute of Technology at Roorkee,
Uttarakhand, India

closest to the snap-feeding river dolphins, suggesting that they too were snap feeders. The methods presented here represent a novel application for constrained ordination that links morphology with performance, and may be widely applied in the fossil record.

Keywords Archaeocetes · Feeding · Mastication · Eocene · Constrained ordination · Reconstruction

5.1   Introduction

Whales, dolphins, and porpoises (Cetacea) are a lineage of even-toed ungulates (Cetartiodactyla) that previously inhabited a terrestrial environment and during the Eocene epoch successfully invaded the seas to become obligatorily aquatic. During this aquatic invasion, dentition and feeding strategies underwent an extraordinary bloom in diversity. The morphology of the feeding apparatus also transformed from short-snouted and gracile forms into relatively long-snouted, crocodilian-like forms, with large diastema between teeth. The fossil ancestors of cetaceans displayed quadritubercular and bunodont teeth (i.e., *Indohyus*; Thewissen et al. 2007), whereas those of the earliest fossil cetaceans (archaeocetes) evolved tricuspid upper molars (e.g., pakicetids, ambulocetids, remingtonocetines, protocetids; Gingerich and Russell 1990; Cooper et al. 2009; Thewissen and Bajpai 2001; Thewissen et al. 2011) and conical upper molars bearing supernumerary cusps (i.e., basilosaurids; Kellogg 1936; Uhen 2000) (Fig. 5.1). Remingtonocetid archaeocetes, in particular, evolved an extreme combination of rostral and dental characteristics, displaying narrow, tall, and exceptionally long rostra and large, rostrocaudally elongated teeth separated by large diastemata (e.g., Sahni and Mishra 1975; Kumar and Sahni 1986; Thewissen and Hussain 2000) (Fig. 5.1). These changes in the feeding apparatus suggest shifts in the strategies used in food procurement and processing; however, little is known of the feeding strategy employed by remingtonocetines. This is unfortunate, as no extant cetartiodactylans retain a remingtonocetid-like craniofacial morphology and little is known of the events shaping the early evolution of food procurement among cetaceans. This study utilizes novel methods to reconstruct the feeding behaviors in remingtonocetines.

In contrast to the paucity of data regarding the evolution of feeding strategies within the earliest cetaceans, the morphology and feeding behaviors of extant cetaceans are comparatively well known. Dentitions of extant taxa can be grouped into three broad categories. First, toothless, or edentulous, forms are typified by baleen whales (mysticetes) in which plates of keratinized baleen extend from the roof of the mouth and function to strain small prey out of sea water. Second, most species of toothed whales (odontocetes) have a long rostrum with many single cusped teeth that are used to pierce and stabilize prey during raptorial or snap feeding where the animal pushes its mouth through the water to capture its prey, as seen in some oceanic and river dolphins (Heyning and Mead 1996; Werth 2006a, b; Johnston and Berta 2011). Extreme cases of this supernumerary and homodont dentition are seen in oceanic dolphins, which can have as many as 200 teeth
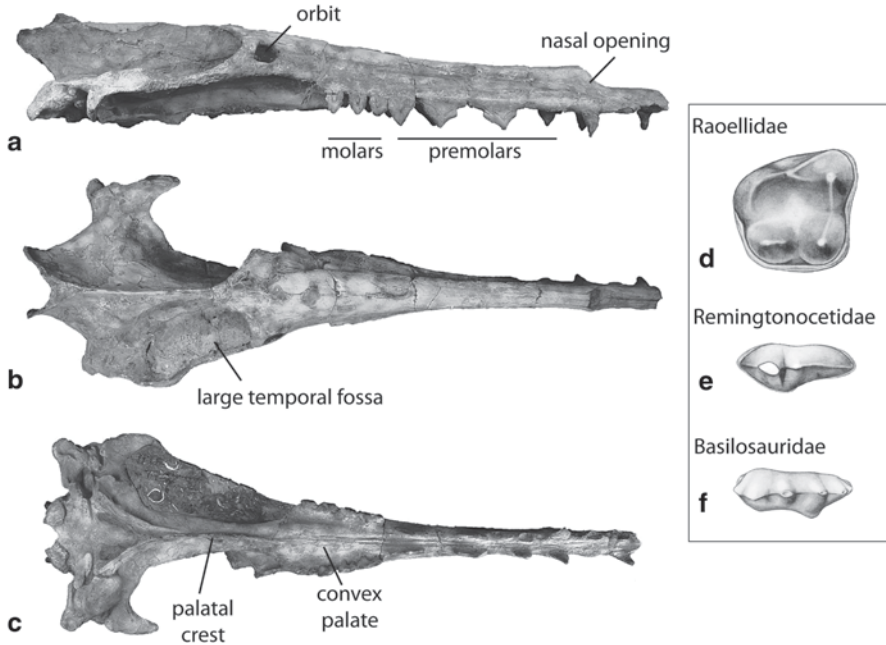
Fig. 5.1 Skull of the middle Eocene archaeocete *Remingtonocetus harudiensis*. (Sahni and Mishra 1975; IITR-SB 2770). **a** Lateral view, **b** dorsal view, **c** ventral view. Occulsal view of the upper molars of **d** Raoellidae (*Indohyus* RR-209), **e** Remingtonocetidae (*Remingtonocetus* IITR-SB 2605), and **f** Basilosauridae (*Pontogeneus* MMNS-2338). Teeth are scaled to the same craniocaudal lengths to illustrate alterations in tooth dimensions

(Leatherwood et al. 1988). Although river dolphins are almost exclusively snap feeders, most other odontocetes combine snap or ram feeding with suction, which is generated by the rapid depression and retraction of the tongue or gular structures, to swallow prey (e.g., Bloodworth and Marshall 2005; Werth 2006a, 2007; Johnston and Berta 2011). In some of these cases, however, suction alone cannot capture prey (e.g., *Tursiops*; Bloodworth and Marshall 2005). Third, some odontocetes display drastic reductions in the number of teeth. Several beaked whale taxa, for example, undergo eruptions of only one or two pairs of teeth (Heyning and Mead 1996). Most taxa with this reduced dentition have blunt rostra and rely solely on suction to capture and swallow their cephalopod prey (e.g., Clarke 1996; Heyning and Mead 1996; Bloodworth and Marshall 2005; MacLeod et al. 2006; Werth 2006a, b). Examples of suction feeders include beaked whales (e.g., Heyning and Mead 1996; Bloodworth and Marshall 2005), pilot whales (Werth 2000, 2006b), and sperm whales (Werth 2004, 2006a, b). Morphology of the feeding apparatus in these modern taxa bears little resemblance to the morphologies seen in their terrestrial artiodactyl ancestors (quadritubercular, heterodont teeth) making it difficult to reconstruct the transition between these morphological endpoints (e.g., Werth 2007; Thewissen et al. 2011). Analysis of archaeocete cetaceans is, therefore, ideal as they represent a morphological and behavioral intermediate between terrestrial and obligatorily aquatic cetartiodactylans.

5.2   Remingtonocetid Archaeocetes

Remingtonocetid archaeocetes have been collected from the middle Eocene (Lutetian) of western India and northern and central Pakistan (e.g., Sahni and Mishra 1972, 1975; Bajpai and Thewissen 1998). Fossils were recovered from mostly swamp, marsh, near shore, and lagoon deposits (e.g., Gingerich et al. 1995, 2001; Thewissen and Bajpai 2009; Bajpai et al. 2011, 2012). Stable isotopic evidence of teeth shows that most remingtonocetines ingested sea water (Thewissen et al. 1996; Roe et al. 1998), and analyses of their skeletal characteristics suggest that, while they were powerful swimmers, they were still able to walk on land (e.g., Bajpai and Thewissen 2000; Thewissen et al. 2009).

The cranial features of remingtonocetines are unique in that skulls are extremely narrow (six times longer than wide), the snout occupies roughly two-thirds of the length of the skull, and the mandibular symphyses vary between unfused to fused with the posterior extent of the joint extending up to the molars (e.g., Gingerich et al. 1998; Thewissen and Bajpai 2009; Bajpai et al. 2011, 2012). Remingtonocetines displayed tall incisor crowns and widely spaced molars (Fig. 5.1, Thewissen and Bajpai 2001; Bajpai et al. 2011). Unlike the earliest archaeocetes (i. e., pakicetids, Cooper et al. 2009), remingtonocetines lacked crushing basins on their molars. These dental characteristics support the assertion that the tall and large teeth of remingtonocetines functioned to capture and stabilize prey; however, it is currently unclear how prey were moved from the oral cavity to the oropharynx. It could be that, like crocodiles, remingtonocetines were inertial feeders, and prey were forced to the back of the throat and subsequently swallowed by throwing the head back. Alternatively, it could be that, once in the oral cavity, prey were moved to the oropharynx via gular depression as in extant suction feeding cetaceans (e.g., Werth 2006a, 2007). This study, therefore, undertakes a quantitative assessment of the feeding apparatus in extant cetartiodactylans with different feeding strategies (e.g., suction, ram/snap suction, and snap feeding) in order to reconstruct the feeding behaviors in fossil remingtonocetids.

5.3   Goals of This Study

This study had two broad objectives. First, we aimed to establish a quantitative method for reconstructing behaviors in fossil taxa based on known morphological and behavioral characteristics in modern taxa. By linking quantitative aspects of morphology and behavior, we present methods that can be applied widely to clades rich in fossil and extant taxa (e.g., chiropterans, rodents, and lizards). Second, we use remingtonocetid cetaceans as a test case for our methods as their craniofacial anatomy is unique compared to their terrestrial ancestors and modern aquatic relatives. Cetartiodactylans make an ideal group to test these methods upon, as their fossil record is rich with taxa showing progressive changes in skeletal morphology along the land-to-sea transition, and, within extant taxa, feeding morphologies and

behavior morphologies are well known. Using the methods developed in the first part of this study, we tested the hypothesis that, like modern oceanic dolphins (e.g., *Tursiops*) with long rostra and supernumerary teeth, fossil representatives of Remingtonocetinae employed a combination of snap and suction-feeding strategies to procure food.

The methods presented here are the first to utilize a phylogenetic redundancy analysis (PRDA) as a means to reconstruct unpreserved features of an extinct taxon by finding the extinct taxon's position in a functionally defined morphospace. Principal components analyses (PCA) on morphological data have seen frequent use in paleobiological studies as a means to produce a morphospace that can be related to function by identifying species groups and ecological gradients (Gingerich 2003; Andersson 2004; Egi et al. 2007). This study goes beyond those analyses by explicitly including functional information to constrain the morphospace. This study, therefore, builds on previous work in this field in two ways: first, by incorporating a phylogenetic generalized least squares (PGLS) framework, in which bias due to shared phylogenetic history is reduced, and second, relationships between morphology and function are explicitly addressed by using functional information to constrain our final morphospace.

This method, therefore, utilizes the variation in modern cetartiodactylan cranial morphology as it relates to function, and determines how different morphologies within the data set contribute to a specific behavior (snap, suction, and grazing/browsing feeding behaviors). By applying these methodologies to extant cetaceans with known feeding behaviors, our analyses identify specific cranial features that contribute to snap, suction, and browsing/grazing feeding strategies. These analyses were then used to reconstruct the feeding strategies (behaviors) employed by fossil taxa, in this case *Remingtonocetus* and *Dalanistes,* based on morphology.

5.4   Materials and Methods

Morphology of the feeding apparatus was represented in this study by a set of 14 linear measurements that capture shape and size variation in the mandible and bony components of the pharynx (Table 5.1). Morphometric analyses were conducted with linear measurements instead of landmarks (e.g., geometric morphometrics) because distortion and partial preservation in fossil cetaceans prevent the reliable application of landmark-based morphometric approaches. Measurements of the hyoid apparatus were excluded in this study because hyoid bones are not yet preserved for remingtonocetines.

Our sample included a sample of 11 extant cetaceans and 2 fossil remingtonocetines, as well as various terrestrial artiodactyl out-groups (Table 5.2). Skulls and mandibles were photographed in lateral and ventral views, and linear measurements were taken on both osteological specimens and calibrated images in ImageJ (Rasband 2006). None of the specimens of *Remingtonocetus* or *Dalanistes* available for this study preserved all of the measured features—a scaled composite mea-

Table 5.1 Linear measurements taken on the skulls and mandibles of artiodactyls, cetaceans, and the fossil taxa *Remingtonocetus* and *Dalanistes*

Measurement	Reference
Skull	
1. Basicranial length	This study
2. Medial extent of pterygoid muscle origin to middle of glenoid fossa	This study
3. Basicranial width	This study
4. Palatal arch width at anterior teeth	This study
Mandible	
5. Mandible length	Seagars 1982
6. Mandible height at right angle to greatest length measurement	Seagars 1982
7. Length of mandibular tooth row	Seagars 1982
8. Mandibular width at posterior alveolus	This study
9. Mandibular depth at the middle of tooth row	This study
10. Mandibular depth at posterior alveolus	This study
11. Length of mandibular symphysis	This study
12. Height of mandibular symphysis	This study
13. Arch width at anterior teeth (alveolus to alveolus)	This study
Skull and Mandible	
14. Masseter effort arm—distance from lateralmost surface of zygomatic arch to inferior, anteriormost masseter insertion	This study

Table 5.2 List of taxa

Taxon	Specimen ID	Feeding characters
Hexaprotodon	USNM 464982, 302054	Browser/grazer
Moschus	USNM 254799, 259383, 259385	Browser/grazer
Odocoileus	CM 40176, 40204	Browser/grazer
Phacochoerus	CM 6451	Browser/grazer
Sus scrofa	USNM 141166, 144302, 144303	Browser/grazer
Tayassu	CMNH 17908, 17909	Browser/grazer
Tragulus	USNM 123043, 123044, 123045	Browser/grazer
Phocoena spinipinnis	USNM 395379, 395380	Suction
Phocoenoides dalli	USNM 276062, 276394	Suction
Tursiops	USNM 571169, 570070, 571191	Snap
Cephalorhynchus	USNM 395374, 21167, 39375	Snap
Stenella attenuata	USNM 259311, 258641	Snap
Globicephalus	USNM 550423, 482166, 550119	Suction
Pontoporia	USNM 482708, 395674	Snap
Inia	USNM 49582, 239667, 395602	Snap
Kogia breviceps	USNM 283625	Suction
Mesoplodon densirostris	USNM 504950, 550452	Suction
Ziphius	USNM 504940, 550064, 530291	Suction
Remingtonocetus	IITR-SB-2704, 2770, RUSB 2592, VPL-1001	Unknown
Dalanistes	RUSB 2521	Unknown

CM Cleveland Museum of Natural History, *CMNH* Carnegie Museum of Natural History, *IITR-SB* Indian Institute of Technology, Roorkee, SB collection, *RUSB* Roorkee, SB collection, *USNM* US National Museum of Natural History, *VPL* Vertebrate Paleontology Lab at Panjab, Chandigarh
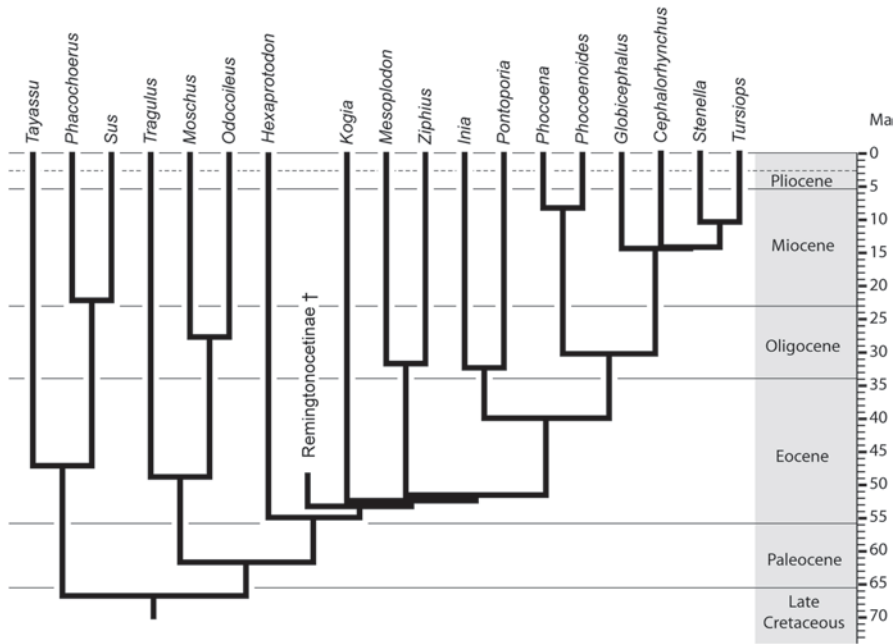
Fig. 5.2 Phylogeny of Cetartiodactyla showing the position of the Remingtonocetinae. Branch lengths scaled to standard chronostratigraphic units and absolute age in Ma

surement set for remingtonocetines was concatenated from measurements on all available specimens (Table 5.2), linearly scaled to common features.

Topology and divergence times of the clades represented in this study (Fig. 5.2) were taken from the mammalian supertree of Bininda-Emonds et al. (2007). The calibrated phylogeny was used to generate an expected phylogenetic variance/covariance matrix **C** equivalent to matrix var $[\epsilon_s]_{ij}$ of Martins and Hansen 1997) assuming Brownian motion as the evolutionary model.

Species averages for all variables were log transformed to achieve univariate normality:

$$x'_{ij} = \ln (x_{ij} + 0.5) \tag{5.1}$$

where x_{ij} is the average value of variable j for species i, and x'_{ij} is the log-transformed value. The full set of variables was then range transformed as:

$$x''_{ij} = \frac{x'_{ij}}{\max\left\{\left|x'_{j}\right|\right\}}, \tag{5.2}$$

to form **Y**, an $n \times m$ matrix of linear morphometric variables with ranges [−1, 1].

We have chosen a form of constrained ordination analysis, known as redundancy analysis (RDA; Legendre and Legendre 1998), to examine the relationships between

morphometric variables and behavioral variables. We used a PGLS approach to conduct this analysis in phylogenetic context (Simons et al. 2011). Discussion of PGLS can be found in Grafen (1989), Martins and Hansen (1997), and Garland and Ives (2000). The application of PGLS to canonical analyses is discussed in Revell and Harrison (2008) and Revell (2009). All of the subsequent analysis steps were performed in R 2.10.1 (R Development Core Team 2009) using components from the R package ape (Paradis et al. 2004); scripts are available from the authors on request.

Although RDA is based on linear regression using continuous variables, it can accommodate categorical explanatory variables dummy coded as orthogonal contrasts (Legendre and Legendre 1998; Legendre and Anderson 1999). Each categorical variable with n categories was broken into $n-1$ continuous variables, one variable each for categories 1 to $(n-1)$. Each category was scored as a positive value for its respective variable, and zero for other variables, with the exception that the nth category was scored as a negative value in all the variables as a contrast. Because sample sizes for categories were unequal, values for the positive and contrast score within each variable were adjusted to sum to zero to maintain orthogonality.

The PGLS transformation matrix $\mathbf{Z}$ (equivalent to $\mathbf{C}^{-1/2}$) was calculated by singular value decomposition of $\mathbf{C}^{-1}$, such that:

$$\mathbf{C}^{-1} = \Upsilon \Lambda \mathbf{V}' \tag{5.3}$$

where Υ and $\mathbf{V}$ are matrices of the left and right singular vectors of $\mathbf{C}^{-1}$, and Λ is a diagonal matrix of the singular values of $\mathbf{C}^{-1}$. Matrix $\mathbf{Z}$ was then calculated as:

$$\mathbf{Z} = \Upsilon(\sqrt{\Lambda})\mathbf{V}' \tag{5.4}$$

The complete set of morphometric data ($n \times m$ matrix $\mathbf{Y}$) along with range-transformed condylobasal length (CBL) and the dummy-coded orthogonal contrasts for feeding behaviors ($n \times p$ matrix $\mathbf{X}$) were concatenated into a single $n \times (m+p)$ matrix $\mathbf{W}$. A vector of ancestral character states (a) of length $m+p$ was calculated as:

$$a = [(1'\mathbf{C}^{-1}1)^{-1}1'\mathbf{C}^{-1}\mathbf{W}]; \tag{5.5}$$

where 1 is an $n \times 1$ column vector with (1) in each cell. Species data were PGLS transformed and centered on ancestral character states as:

$$\mathbf{M} = \mathbf{Z}\mathbf{W} - \mathbf{Z}1a' \tag{5.6}$$

PGLS-transformed data $\mathbf{M}$ were then separated into a matrix of dependent morphometric variables $\mathbf{D}$ and a matrix of explanatory size and feeding-related variables $\mathbf{T}$. Morphological values for remingtonocetines were included in the calculations of Eqs. 5 and 6, but this row was excluded from matrix $\mathbf{D}$ to leave complete matrices for comparison of morphology, size, and feeding in the extant taxa. As for the

standard computation of RDA, a matrix of multiple regression coefficients, $\mathbf{B}$, was calculated as:

$$\mathbf{B} = (\mathbf{T'T})^{-1}\mathbf{T'D} \tag{5.7}$$

A matrix of estimated values of $\mathbf{D}$ based on this regression, $\widehat{\mathbf{D}}$, was calculated as:

$$\widehat{\mathbf{D}} = \mathbf{TB} \tag{5.8}$$

Matrix $\widehat{\mathbf{D}}$ represents a linear combination of morphometric variables with size and feeding-related variables.

Eigenanalysis of $\widehat{\mathbf{D}}$ results in a set of eigenvalues $\mathbf{\Lambda}$ and eigenvectors $\mathbf{U}$. A set of object scores and fitted object scores in PGLS space, $\mathbf{P}$ and $\widehat{\mathbf{P}}$, respectively, can be calculated as:

$$\mathbf{P} = \mathbf{DU} \tag{5.9}$$

$$\widehat{\mathbf{P}} = \widehat{\mathbf{D}}\mathbf{U} \tag{5.10}$$

While these scores do not represent an ordination of the data in terms of real (non-PGLS transformed) units, their axis-by-axis correlation provides a measure of the strength of the relationship between morphometric and size/behavioral datasets on each ordination axis.

Points in matrix $\mathbf{U}$ provide a direct representation of the ordination space in terms of PGLS-transformed dependent variables $\mathbf{D}$. To place the PGLS-transformed explanatory variables $\mathbf{T}$ in the same context, the correlation coefficients of axis-by-axis correlations between $\mathbf{T}$ and $\widehat{\mathbf{P}}$ were scaled by $\sqrt{\lambda_i/\Sigma\Lambda}$, the square root of the proportional variance explained by that axis. Biplots of $\mathbf{U}$ and the scaled correlation coefficients of $\mathbf{T}$ and $\widehat{\mathbf{P}}$ provide a direct representation of the relationships between dependent and explanatory variables in the ordination after accounting for the effects of phylogeny.

Object scores in Euclidean (species) space can be found by substituting the untransformed species data from $\mathbf{Y}$, centered on their phylogenetic means, for $\mathbf{D}$ in Eq. 10:

$$\mathbf{S} = (\mathbf{Y} - 1a')\mathbf{U}. \tag{5.11}$$

Unlike the object scores in $\mathbf{P}$, which cannot be directly compared to one another, the taxon scores in $\mathbf{S}$ allow direct comparisons between taxon positions in constrained morphospace. Although the ordination space as defined by $\mathbf{U}$ controls for phylogenetic effects, taxon scores in $\mathbf{S}$ are not phylogenetically independent and, therefore, must still be considered in phylogenetic context. Most important in reference to the ability to use information from living animals to reconstruct extinct taxa, morphological data for remingtonocetines originally excluded from matrix $\mathbf{D}$ were included

Table 5.3 Variance explained by canonical PRDA axes

	1st axis	2nd axis	3rd axis
Proportion of variance	0.818	0.115	0.0676
Cumulative proportion of variance	0.818	0.932	0.9999

Table 5.4 Correlations *(r)* between vectors in **D** (species scores) and $\widehat{\mathbf{D}}$ (fitted species scores). Correlations represent the strength of association between the morphological variables in **D** and the head-size/feeding-behavior model of morphology in $\widehat{\mathbf{D}}$, interpreted together with the cumulative proportions of variance given in Table 5.3

	r	*p*	95 % CI for *r*
1st axis	0.959	< 0.0001[a,b]	0.891–0.985
2nd axis	0.747	0.0004[a,b]	0.431–0.900
3rd axis	0.680	0.0019[a,b]	0.312–0.870

[a] Significant correlation
[b] Significant proportion of cumulative variance

in matrix **Y**, placing the fossil taxon in a morphological ordination constrained by known functional relationships in extant taxa.

Phylogenetically non-independent variable loadings consistent with the position of species points in **S** are calculated as axis-by-axis correlations between the data in **W** and the fitted species scores **S,** scaled to the square root of the proportional variance of each canonical axis. Explanatory variable loadings can be plotted together with eigenvectors from **U** to show the relationship between dependent and explanatory variables. For ease of interpretation, the projection of loadings and object scores in **S** can be rotated, resulting in a projection that shows the greatest differences between feeding category loadings on the first two axes ($\mathbf{S}_{max}$, placing snap and suction loadings within an *x–y* plane). Taxon scores from the rotated projections were assessed for similarity in constrained morphospace using cluster analysis and neighbor-joining trees in PAST 1.99 (Hammer et al. 2001) and ancestral character state reconstruction in Mesquite 2.75 (Maddison and Maddison 2011).

5.5 Results

5.5.1 The Constrained Morphospace

Most of the variance in morphology is explained by the first three (canonical) axes (Table 5.3). The remaining noncanonical axes, which are in essence residuals of regression on size or feeding mode, explain a very small proportion of the morphological variation present in the sample. When taken together with proportional variance, the correlations between **P** and $\widehat{\mathbf{P}}$ on each axis (Table 5.4) provide complementary diagnostics of the fit of the explanatory model to the data; in this case correlations on each axis are significant.
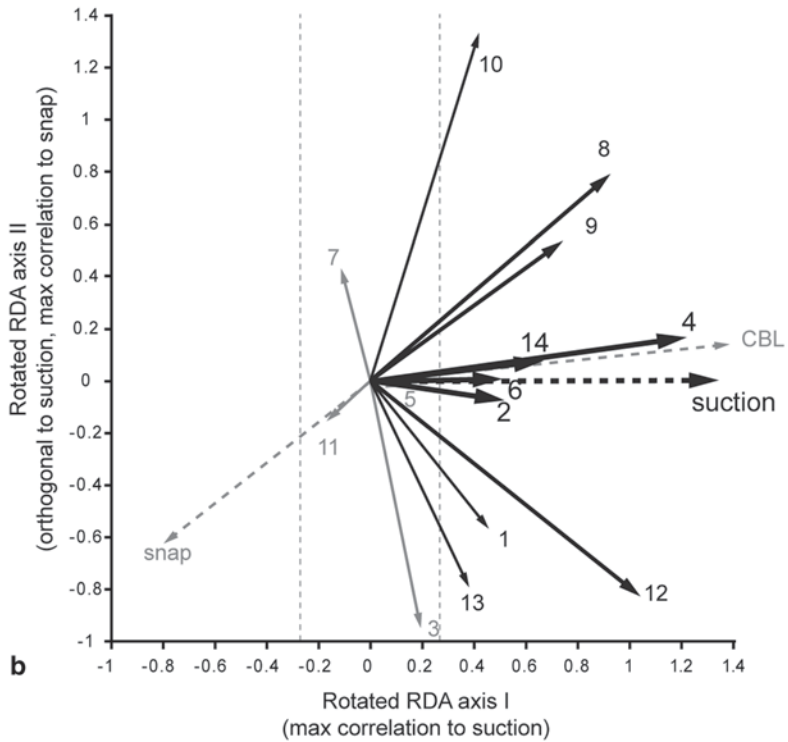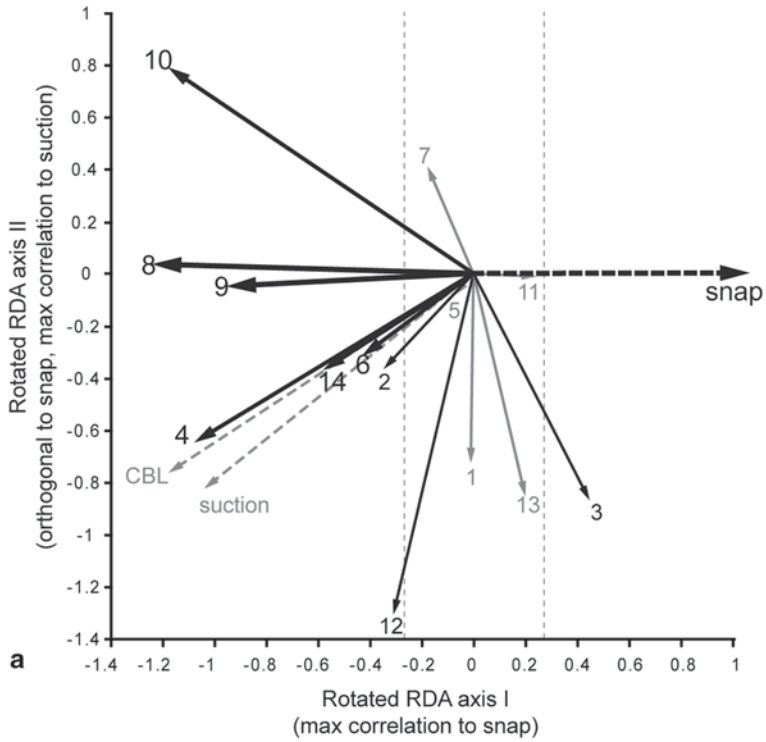
The relationships between morphological and explanatory variables in PGLS space are shown as rotated biplots (Fig. 5.3). In addition to standard variable loadings on the three canonical axes in this analysis, the loading of each morphological variable along the vectors of the explanatory variables can also be considered. For three canonical axes, as in this analysis, these relationships can be conveniently expressed as the deviation of a morphological variable from the direction of the explanatory variable's vector, together with the length of the morphological variable's vector along the explanatory variable's vector. Random relationships between morphological variables and explanatory variables would produce an expected equilibrium length (for a single axis in this analysis, expected scaled equilibrium length is 0.267).

For each explanatory feeding variable, a set of morphological variables that correlate well with that category ($\leq 30°$ deviation) and load strongly along its axis (scaled length ≥ 0.267) can be identified (Table 5.5). For snap feeding, these include mandibular depth both at the middle of the tooth row and at the posterior alveolus (8 and 9 in Fig. 5.3a). Mandibular width (10) and anterior palatal arch width (4) also load strongly, but with less tight correlation. For suction feeding, pterygoid arm (2), mandible height (6), and masseter arm (14) display tight correlation and strong loading. Anterior palatal arch width (4) loads strongly on suction feeding, but deviates from the suction-feeding axis (out-of-plane deviation in Fig. 5.3b)

5.5.2   Taxon Scores in the Constrained Morphospace

Scores for individual taxa were projected in the rotated ordination space $\mathbf{S}_{max}$ (Fig. 5.4a). All terrestrial taxa are grouped together in the morphospace, but are separate from extant aquatic taxa. Within aquatic taxa, a morphological gradient between riverine snap feeders (e.g., *Inia, Pontoporia*) and obligate suction feeders (e.g., *Globicephalus, Ziphius*) is visible in this projection. Extant taxa employing mixed feeding strategies, such as ram-suction feeding, lie in the middle of these endpoints (e.g., *Tursiops, Phocoena*). Morphological data from remingtonocetines allow them to be placed in this projection of the morphospace, nearest the ram feeders, and farthest from browsing/grazing terrestrial taxa and suction-feeding cetaceans (Fig. 5.4a). A neighbor-joining cluster analysis (Fig. 5.4b) shows the feeding-related oral morphology of remingtonocetines to be most similar to river dolphins *Inia* and *Pontoporia*.

Fig. 5.3 Rotated biplot of dependent variables and independent variable loadings in PGLS space, showing morphological variables that show strong relationships with **a** snap feeding and **b** suction feeding (*bold lines*). Morphological variables numbered as in Table 5.1. Snap feeding is tightly negatively correlated with mandibular depth at the middle of the tooth row (*8*) and at the posterior alveolus (*9*), and both of these variables, as well as anterior palatal arch width (*4*) and mandible width (*10*), show strong negative loadings on the snap feeding axis. Suction feeding is tightly positively correlated with pterygoid muscle arm (*2*), mandible height (*6*), and masseter arm (*14*) (apparent correlation with anterior palatal arch width is due to out-of-plane deviation); these three variables, as well as anterior palatal arch width (*4*), mandible depth (*8* and *9*), and mandibular symphysis height (*12*), all show strong positive loadings on the suction-feeding axis

Table 5.5 Relationships between PGLS-transformed morphological variables and independent variable loadings. Deviations are reported for symmetrical projections, with a maximum value of 90°. Small deviations from the loading axes indicate greater correlation (positive or negative) between the morphological variable and the behavioral variable. Eigenvector length provides a modified form of dependent variable loading, read along the independent variable loading axis rather than a canonical axis. Positive eigenvector lengths indicate positive correlations, and vice versa

	Deviation from snap feeding loading axis (°)	Eigenvector length on snap feeding loading axis	Deviation from suction feeding loading axis (°)	Eigenvector length on suction feeding loading axis
Basicranial length	89.3	−0.013	85.5	0.056
Pterygoid arm[b,c,d]	47.5	−0.339	15.7	0.333
Basicranial width[b]	64.5	0.436	81.1	0.109
Anterior arch width[b,d,c]	41.3	−1.04	50.6	0.519
Mandible length	64.7	−0.063	37.7	0.137
Mandible height[b,c,d]	37.2	−0.401	5.2	0.400
Mandible tooth row length	71.6	−0.176	83.6	0.048
Mandible width[a,b,d]	8.3	−1.19	38.8	0.671
Mandible depth mid[a,b,d]	8.3	−0.896	33.9	0.546
Mandible depth pos[b,d]	35.4	−1.15	73.6	0.272
Symphysis length	65.2	0.223	70.4	0.168
Symphysis height[b,d]	76.7	−0.304	31.4	0.908
Anterior mandible arch width[d]	77.2	0.194	49.2	0.470
Masseter arm[b,c,d]	32.8	−0.552	5.3	0.494

[a] Close alignment to snap axis (≤30° deviation)

[b] Eigenvector length on snap axis greater than equilibrium contribution value for single axis (≥0.267)

[c] Close alignment to suction axis (≤30° deviation)

[d] Eigenvector length on suction axis greater than equilibrium contribution value for single axis (≥0.267)

5.6 Discussion

5.6.1 Quantitative Methods in Reconstructing Behaviors

The first goal of this analysis was to establish a reliable quantitative method to reconstruct behaviors in fossil taxa. We chose RDA to address the particular research question of multivariate discrimination among groups while accounting for phylogenetic effects using PGLS. Testing categorical group membership with multivariate data is typically accomplished through canonical variate analysis (CVA), but incorporating the generalized least squares framework of PGLS led to intractable computational difficulties (but see Motani and Schmitz 2011). The solution we have settled on is very similar to the approach of variation partitioning (Desdevises et al. 2003; Cubo et al. 2005, 2008); the underlying computations are nearly identical, with the exception of how phylogenetic information is handled (as a variance/covariance matrix for generalized least squares in PRDA versus
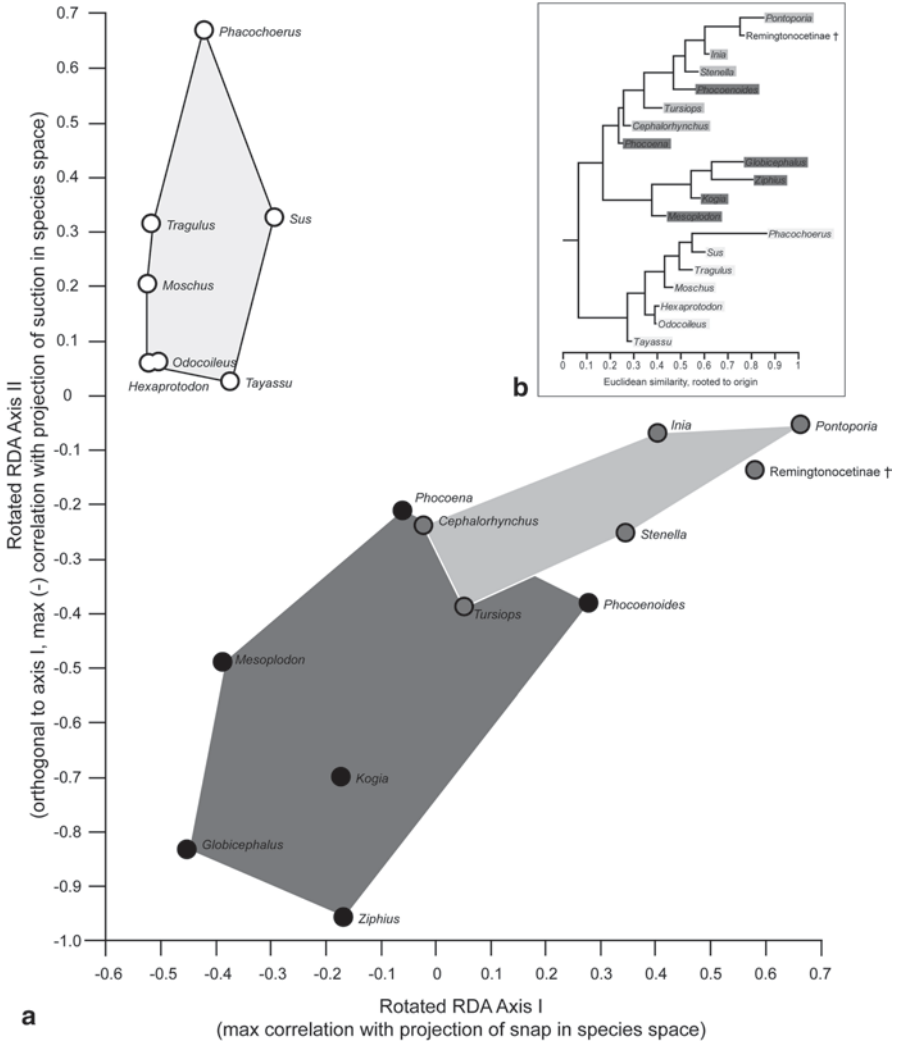
Fig. 5.4 a Taxon points in species space along the three canonical axes, rotated to align snap feeding and suction feeding loadings in the *x–y* plane (S_{max}). Convex hulls surround extant suction feeders (*dark gray*), snap feeders (*medium gray*), and terrestrial herbivores (*light gray*). Remingtonocetinae lie close to the river dolphins *Inia* and *Pontoporia* in this projection. **b** Neighbor-joining tree using the two-dimensional projection of S_{max}

employing significant principal coordinate axes of phylogenetic distance as covariates in variation partitioning). The output of the two analyses differs primarily in focus as variation partitioning compares coefficients of multiple determinations derived from regressing dependent variables on several matrices of explanatory variables to show the amount of variation explained by each set of factors. In contrast, PRDA employs the same regression procedures, but produces an ordination to graphically portray the relationships between dependent variables and explanatory

variables, and also the relationships among species' average morphologies, given the relationships between dependent and explanatory variables. This analysis is the first instance of PRDA as a means to reconstruct unpreserved features of an extinct taxon by finding the extinct taxon's position in a functionally defined morphospace.

The relationship between the numbers of regression coefficients to be estimated versus the sample size in the current study minimizes the expected difference between the constrained ordination of RDA and an unconstrained ordination (e.g., PCA). PRDA analysis provides clear distinction between function-driven variation in morphology and neutral variation in morphology when the number of extant taxa is more than double the number of regression coefficients to be estimated (i.e., $n_{extant} \geq \sim 2mp$).

Taken together, this study presents a novel suite of methods that integrated quantitative data from morphology and behavior and assumed a link through performance. These methods are amenable to multilevel comparisons that include morphology, performance, function, and other classes of covariates as they are deemed appropriate. The level of detail that can be attained in relating several sources of variation is limited only by the number of extant taxa that can be included in the analysis. Ideal groups for testing are taxon-rich extant and fossil taxa (e.g., chiropterans, rodents, and lizards).

5.6.2   Remingtonocetines as Snap Feeders

The second goal of this study was to reconstruct feeding strategies in remingtonocetid archaeocetes based on modern cetartiodactylans with varying feeding strategies (ram, combined ram/suction, obligate suction, browsing/grazing). Results showed a strong relationship between morphology and function within the extant sample. There is a morphological gradient between ram feeders (river dolphins), obligate suction feeders (beaked and pilot whales), and taxa known to use both strategies (e.g., *Phocoena* and *Cephalorhynchus*; Kastelein et al. 1997; Werth 2006a). Remingtonocetines are positioned nearest the river dolphins, suggesting that they employed very little suction, if any, during prey capture. This is consistent with the interpretation that the ancestral feeding behavior of cetaceans is snap feeding (Werth 2007).

Morphologies contributing to the snap-behavior assignment of remingtonocetines include the following characteristics: (a) long lengths of the mandible and symphysis, (b) a narrow palatal arch, (c) a long mandibular tooth row, and (d) a reduced mandibular depth along the posterior aspect of the mandible. These characteristics are also seen in extant river dolphins (Werth 2006a), specifically *Inia* and *Pontoporia*.

In addition to an elongated rostrum and modified palate, the remingtonocetid masticatory apparatus were supported by a large temporal fossa and an exceptionally large sagittal crest that extended caudally past the nuchal line (Thewissen and Bajpai 2009; Bajpai et al. 2011). These characteristics suggest that the temporalis muscle was not only massive in its cross section, but displayed a greater array of

cranio-caudally directed fibers. These could have aided in both the strength and rapidity of jaw closure, as well as resisted torsion of the skull incurred while capturing live prey. Contrary to the unusually large temporalis muscle, sites of attachment for the masseter muscle were comparatively small (Bajpai et al. 2011), potentially suggesting that lateral movements of the jaw associated with grinding prey were minimized, which is consistent with studies of tooth wear (Thewissen et al. 2011). The long mandibular symphysis, fused in andrewsiphiines and non-fused in remingtonocetines, would also have limited all jaw movements except simple adduction.

Prey capture and stabilization may have been assisted by the presence of tall incisor crowns (Thewissen and Bajpai 2001; Bajpai et al. 2011) and widely spaced premolars (Fig. 5.1). Molars of remingtonocetids lacked the crushing basins (Fig. 5.1) characteristic of some archaeocetes (e.g., pakicetids, ambulocetids, and protocetids, Cooper et al. 2009), suggesting prey received minimal crushing before swallowing and that the teeth were mainly used to shear food items. This is also consistent with dental wear in remingtonocetines (Thewissen et al. 2011). Therefore, while pakicetids, ambulocetids, and protocetids retained some crushing ability in the molars, remingtonocetids are more like basilosaurids and molar function is limited to shear. This similarity in dentition must be independently acquired, because protocetids are the sister group to the clade that includes basilosaurids, and most protocetines have both molar protocones and crushing basins.

There are pronounced differences in dental morphology in the remingtonocetines. Within remingtonocetines, shear facets are clear and well developed, and in the remingtonocetid *Dalanistes,* molar shape appears to be designed in such a way as to maximize shear surface (large, flat areas on the lingual side of the paracone and metacone). These areas are less well developed in *Remingtonocetus*. Molar morphology is less well known in the andrewsiphiine *Andrewsiphius,* but its lower molars do not show any flat shear surface, suggesting that this specific type dental function was unimportant (Thewissen et al. 2011). The andrewsiphiine *Kutchicetus* displays lower molars that are separated by diastemata, indicating a further loss of occlusal function.

Taken together, this study presents novel methods relating quantitative measures of morphology with behavior in extant taxa and applies them to fossils in order to reconstruct ancient behaviors. These methods were applied to remingtonocetid archaeocetes, and the resultant data shed light on the evolution of food procurement and masticatory behaviors along the cetacean land-to-sea transition. Future analyses may utilize these methods to reconstruct behavioral questions in other fossil taxa as these methods are only limited by the sample size of extant taxa.

References

Andersson KI (2004) Elbow-joint morphology as a guide to forearm function and foraging behaviour in mammalian carnivores. Zool J Linn Soc 142:91–104

Bajpai S, Thewissen JGM (1998) Middle Eocene cetaceans from the Harudi and Subathu formations of India. In: Thewisssen JGM (ed) The emergence of whales: evolutionary patterns in the origin of Cetacea. Plenum Press, New York, pp 213–233

Bajpai S, Thewissen JGM (2000) A new, diminutive whale from Kachchh (Gujarat, India) and its implications for locomotor evolution of cetaceans. Curr Sci (New Delhi) 79:1478–1482

Bajpai S, Thewissen JGM, Conley RW (2011) Conley anatomy of middle Eocene *Remingtonocetus* (Cetacea, Mammalia) from Kutch, India. J Paleontology 85:703–718

Bebej RM, ul-Haq M, Zalmout IS, Gingerich PD (2012) Morphology and function of the vertebral column in *Remingtonocetus domandaensis* (Mammalia, Cetacea) from the middle Eocene Domanda Formation of Pakistan. J Mamm E 19:77–104

Bininda-Emonds OR, Cardillo M, Jones KE, MacPhee RD, Beck RM, Grenyer R, Price SA, Vos RA, Gittleman JL, Purvis A (2007) The delayed rise of present-day mammals. Nature 446(7135):507–512

Bloodworth BE, Marshall CD (2005) Feeding kinematics of *Kogia* and *Tursiops* (Odontoceti: Cetacea): Characterization of suction and ram feeding. J Exp Biol 208:3721–3730

Clarke MR (1996) Cephalopods as prey. III. Cetaceans. Phil Trans R Soc Lond B 351:1053–1065

Cooper LN, Thewissen JGM, Hussain ST (2009) New Early-Middle Eocene archaeocetes (Pakicetidae and Remingtonocetidae: Cetacea) from the Kuldana Formation of Northern Pakistan. J Vertebr Paleontol 29(4):1289–1299

Cubo J, Ponton F, Laurin M, de Margerie E, Castanet J (2005) Phylogenetic signal in bone microstructure of sauropsids. Syst Biol 54(4):562–574

Cubo J, Legendre P, de Ricqlès A, Montes L, de Margerie E, Castanet J, Desdevises Y (2008) Phylogenetic, functional, and structural components of variation in bone growth rate of amniotes. Evol Dev 10(2):217–227

Desdevises Y, Legendre P, Azouzi L, Morand S (2003) Quantifying phylogenetically structured environmental variation. Evolution 57(11):2647–2652

Egi N, Nakatsukasa M, Kalmykov N, Maschenko E, Takai M (2007) Distal humerus and ulna of *Parapresbytis* (Colobinae) from the Pliocene of Russia and Mongolia: phylogenetic and ecological implications based on elbow morphology. Anthropol Sci 115:107–117

Garland T Jr, Ives AR (2000) Using the past to predict the present: confidence intervals for regression equations in phylogenetic comparative methods. Am Nat 155:346–364

Gingerich PD (2003) Land-to-sea transition in early whales: evolution of Eocene Archaeoceti (Cetacea) in relation to skeletal proportions and locomotion of living semiaquatic mammals. Paleobiology 29(3):429–454

Gingerich PD, Russell DE (1990) Dentition of Early Eocene *Pakicetus* (Mammalia, Cetacea). Contrib Mus Paleontol Univ Mich 28:1–20

Gingerich PD, Arif M, Clyde WC (1995) New archaeocetes (Mammalia, Cetacea) from the Middle Eocene Domanda Formation of the Sulaiman Range, Punjab (Pakistan). Contrib Mus Paleontol Univ Mich 29:291–330

Gingerich PD, Arif M, Bhatti MA, Clyde WC (1998) Middle Eocene stratigraphy and marine mammals (Cetacea and Sirenia) of the Sulaiman Range, Pakistan. Bull Carnegie Mus Nat Hist 34:239–259

Gingerich PD, Haq M, Khan IH, Zalmout IS (2001) Eocene stratigraphy and archaeocete whales (Mammalia, Cetacea) of Drug Lahar in the eastern Sulaiman Range, Balochistan (Pakistan). Contrib Mus Paleontol Univ Mich 30:269–319

Grafen A (1989) The phylogenetic regression. Phil Trans R Soc Lond B Biol Sci 326(1233):119–157

Hammer Ø, Harper DAT, Ryan PD (2001) PAST: paleontological statistics software package for education and data analysis. Palaeontol Electron 4(1):1–9

Heyning JE, Mead JG (1996) Suction feeding in beaked whales: morphological and observational evidence. Contrib Sci. Nat Hist Mus Los Angel Cty 464:1–12

Johnston C, Berta A (2011) Comparative anatomy and evolutionary history of suction feeding in cetaceans. Mar Mamm Sci 27(3):493–513

Kastelein RA, Staal C, Terlouw A, Muller M (1997) Pressure changes in the mouth of feeding harbor porpoise (*Phocoena phocoena*). In: Read AJ, Wiepkma PR, Nachtigall PE (eds) The biology of the harbor porpoise. De Spil Publishers, Woerden, pp 279–291

Kellogg R (1936) A review of the Archaeoceti. Carnegie Inst Wash Spec Publ 482:1–366

Kumar K, Sahni A (1986) *Remingtonocetus harudiensis*, new combination, a Middle Eocene archaeocete (Mammalia, Cetacea) from western Kutch, India. J Vert Paleontol 6(4):326–349

Leatherwood S, Reeves RR, Perrin WF, Evans WE (1988) Whales, dolphins, and porpoises of the eastern North Pacific and adjacent Arctic waters: a guide to their identification. Dover Publications, Inc., New York

Legendre P, Anderson MJ (1999) Distance-based redundancy analysis: testing multispecies responses in multifactorial ecological experiments. Ecol Monogr 69:1–24

Legendre P, Legendre L (1998) Numerical ecology. 2nd English edn. Elsevier Science BV, Amsterdam

MacLeod CD, Santos MB, Lópes A, Pierce GJ (2006) Relative prey size consumption in toothed whales: implications for prey selection and level of specialization. Mar Ecol Prog Ser 326:295–307

Maddison WP, Maddison DR (2011) Mesquite: a modular system for evolutionary analysis. Version 2.75. http://mesquiteproject.org

Martins EP, Hansen TF (1997) Phylogenies and the comparative method: a general approach to incorporating phylogenetic information into the analysis of interspecific data. Am Nat 149:646–667

Motani R, Schmitz L (2011) Phylogenetic versus functional signals in the evolution of form-function relationships in terrestrial vision. Evolution 65:2245–2257

Paradis E, Claude J, Strimmer K (2004) APE: analyses of phylogenetics and evolution in R language. Bioinformatics 20(2):289–290

R Development Core Team (2009) R: a language and environment for statistical computing. R Foundation for Statistical Computing, Vienna, Austria. http://www.R-project.org

Rasband WS (2006) Image J, U S National Institutes of Health, Bethesda, Maryland, USA. http://imagej.nih.gov/ij/

Revell LJ (2009) Size-correction and principal components for interspecific comparative studies. Evolution 63:3258–3268

Revell LJ, Harrison AS (2008) PCCA: A program for phylogenetic canonical correlation analysis. Bioinformatics 24:1018–1020

Roe LJ, Thewissen JGM, Quade J, O'Neil JR, Bajpai S, Sahni A, Hussain ST (1998) Isotopic approaches to understanding the terrestrial to marine transition of the earliest cetaceans. In: Thewissen JGM (ed) The emergence of whales, evolutionary patterns in the origin of Cetacea. Plenum Press, New York, pp 399–421

Sahni A, Mishra VP (1972) A new species of Protocetus (Cetacea) from the Middle Eocene of Kutch, western India. Palaeontology 15(3):490–495

Sahni A, Mishra VP (1975) Lower Tertiary vertebrates from western India. Monogr Palaeontol Soc India 3:1–48

Seagers DJ (1982) Jaw structure and functional mechanics of six delphinids (Cetacea: Odontoceti) Thesis, San Diego State University, pp 1–358

Simons ELR, Hieronymus TL, O'Connor PM (2011) Cross sectional geometry of the forelimb skeleton and flight mode in pelecaniform birds. J Morphol 272(8):952–971

Thewissen JGM, Bajpai S (2001) Dental morphology of the Remingtonocetidae (Cetacea, Mammalia). J Paleontol 75:463–465

Thewissen JGM, Bajpai S (2009) New skeletal material of *Andrewsiphius* and *Kutchicetus*, two Eocene cetaceans from India. J Paleontology 83(5):635–663

Thewissen JGM, Hussain ST (2000) *Attockicetus praecursor*, a new remingtonocetid cetacean from marine Eocene sediments of Pakistan. J Mamm E 7:133–146

Thewissen JGM, Roe LJ, O'Neil JR, Hussain ST, Sahni A, Bajpai S (1996) Evolution of cetacean osmoregulation. Nature 381:379–380

Thewissen JGM, Cooper LN, Clementz MT, Bajpai S, Tiwari BN (2007) Whales originated from aquatic artiodactyls in the Eocene epoch of India. Nature 450:1190–1195

Thewissen JGM, Cooper LN, George JC, Bajai S (2009) From land to water: the origin of whales, dolphins, and porpoises. Evo Edu Outreach 2:272–288

Thewissen J, Sensor J, Clementz M, Bajpai S (2011) Evolution of dental wear and diet during the origin of whales. Paleobiology 37(4):655–669

Uhen MD (2000) Replacement of deciduous first premolars and dental eruption in archaeocetes whales. J Morphol 81(1):123–133

Werth AJ (2000) A kinematic study of suction feeding and associated behavior in the long- finned pilot whale, *Globicephala melas*. Mar Mamm Sci 16:299–314

Werth AJ (2004) Functional morphology of the sperm whale tongue, with reference to suction feeding. Aquat Mamm 30:405–418

Werth AJ (2006a) Mandibular and dental variation and the evolution of suction feeding in Odontoceti. J Mamm 87:579–588

Werth AJ (2006b) Odontocete suction feeding: experimental analysis of water flow and head shape. J Morp hol 267:1415–1428

Werth AJ (2007) Adaptations of the cetacean hyolingual apparatus for aquatic feeding and thermoregulation. Anat Rec 290:546–568

Part II
Taphonomy and Environment

Chapter 6
Patterns in Microbialites Throughout Geologic Time: Is the Present Really the Key to the Past?

Kristen L. Myshrall, Christophe Dupraz and Pieter T. Visscher

Contents

Abstract Microbialites dominated the biosphere throughout the Proterozoic, becoming relatively rarer into the Phanerozoic. Microbialites are potential analogs of life on the early Earth; therefore, understanding how they form and function can provide a window to the past. Much of what we know about early life and environments derives from investigations of modern microbialites, making studies of these structures critical to interpreting the ancient fossil record. Creating a

K. L. Myshrall (✉) · C. Dupraz · P. T. Visscher
Center for Integrative Geosciences, University of Connecticut, Storrs, CT 06269, USA
e-mail: Kristen.myshrall@uconn.edu
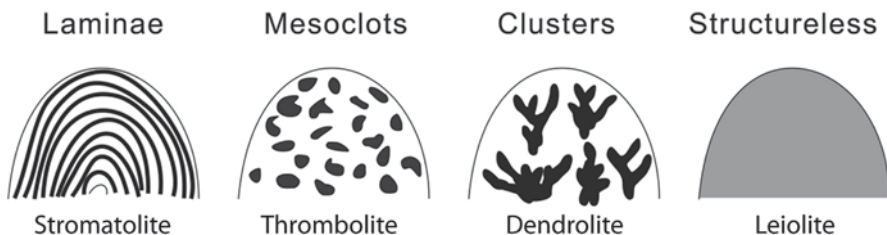
Fig. 6.1 Major defining categories of microbialites. (Modified from Shapiro 2004)

database of worldwide microbialite specimens, both modern and fossil, to be used for analyzing patterns in modern microbialite distribution, both in space and time, along with environmental characteristics and concurrence with grazing and/or boring organisms, can offer understanding into ancient microbialites, specifically the processes impacting their formation, persistence, and preservation. Additionally, analyzing the composition and structure of modern microbialites may allow for connections to patterns of the past, and also provide a clearer understanding of what is seen (or not seen) in the fossil record. A sample database of microbialites reported from the Phanerozoic was analyzed for characteristics such as distribution in time, space, and across different environments, as well as the alignment of distribution with mass extinctions, global sea level curves, and association with grazing/burrowing organisms. We find microbialite distribution is widespread worldwide and abundance fluctuates over the Phanerozoic with increases often corresponding to mass extinctions. Contrary to previous interpretations, fossil microbialites do not appear to prefer open marine environments, with data showing broad distribution in a variety of environments. Modern microbialites, however, primarily form in restricted environments. Data show that grazers/borers are commonly found in association with microbialites throughout the Phanerozoic, though it is difficult to discern if they did or did not impact microbialite formation.

Keywords Thrombolite · Stromatolites · Microbialite · Microbial · Phanerozoic

6.1   Introduction

Microbialites are organosedimentary structures that are formed by a combination of microbial, sedimentary, and mineral processes, which include lithification of a microbial mat. Microbialitic fabrics are seen in many different forms, with the most common four categories being laminated or stromatolitic, clotted or thrombolitic, branching or dendrolitic, and undifferentiated or leiolitic (Fig. 6.1). Microbialites have a very long history on the Earth, with stromatolitic fabrics found as far back as 3.4 billion years ago (Allwood et al. 2007) and thrombolitic fabrics found in rocks dating 1.92 billion years (Kah and Grotzinger 1992).

We frame our study in terms of five general statements frequently made about microbialites in the literature. These statements, which will be referred to throughout the chapter, are:

1. Modern microbialites are relatively rare, with a decline in the early-mid Paleozoic (Garrett 1970; Awramik 1971; Walter and Heys 1995; Burne and Moore 1987; Feldmann and McKenzie 1997; Awramik and Sprinkle 1999; Camoin and Gautret 2006; Riding 2006; Adachi et al. 2011).
2. Modern microbialites are forming in restricted environments. (Garrett 1970; Awramik 1971; Dill et al. 1986; Dullo et al. 1998; Awramik and Sprinkle 1999; Schmidt 2006).
3. Grazing and/or boring animals are the cause for the rarity and the restricted environmental distribution of modern microbialites. (Garrett 1970; Awramik 1971, 1991; Grotzinger 1990; Awramik and Sprinkle 1999; Pruss and Bottjer 2004; Riding and Liang 2005; Schmidt 2006).
4. In the ancient times, microbialites were mostly found in open marine environments (Awramik 1971; Hoffman 1976; Grotzinger 1986; Awramik and Sprinkle 1999; Riding 2006).
5. Microbialites are a post-extinction disaster form, rebounding in response to a clearing of an ecosystem after an extinction event (Schubert and Bottjer 1992; Rodland and Bottjer 2001; Kershaw et al. 2007; Ezaki et al. 2008; Martindale et al. 2010).

One of the key goals of understanding modern microbialites is applying that knowledge to the fossil record. Fabrics, and even potentially some of the microbes that formed the microbialites in fossilized specimens, are often visible, however, there are many features that cannot be easily seen. For example, discerning exactly how the microbial communities that created the structures functioned and interacted with the surrounding sediments is impossible. Additionally, the exact impact of grazing and boring organisms on microbialites throughout the Phanerozoic is often impossible to discern.

For these reasons, and others, modern microbialites are used as proxies for understanding ancient microbialites. However, if the assumptions listed above are true, then there are differences between modern and fossil microbialites, leading us to question whether currently growing microbialites should be used as proxies for those preserved in the fossil record.

To address this problem, three questions were asked. First, are there specific spatial or temporal patterns within the fossil microbialite record? Specifically, when the Phanerozoic is closely examined, can we find any patterns in distribution with respect to environment, geography, or other organisms? Second, are there specific patterns with respect to modern microbialites? Are they restricted geographically or environmentally, and are they being affected by the presence of other organisms? Third, are there similarities between their distribution in the modern and fossil records that permit high confidence in using the modern as a proxy for the ancient?

Based on the answers to these questions, there are five potential outcomes regarding the suitability of modern microbialites for interpreting ancient examples:

1. There is a pattern in the fossil record but not in the modern.
2. There is a pattern in the modern but not in the fossil record.
3. There is no pattern in either the modern or the fossil record.

4. There is a pattern in both the modern and the fossil record but they do not correspond.
5. There is a pattern in both the modern and the fossil record and they do correspond.

If the outcome of our analysis is one of the first four patterns, then the use of modern specimens as proxies for ancient microbialites needs to be closely examined. However, even if the patterns do not match, examining issues such as biases in the fossil record can potentially explain the disagreement. Preservational biases can obscure patterns, as can preferential analysis of specific areas of the geologic record (Patzkowsky 1999; Benton et al. 2000; Holland and Smith 2001).

Preservation biases are a constant concern when working with fossilized specimens, especially those that are composed largely of non-skeletal or non-mineralogical materials. Because microbialites are composed largely of carbonate precipitates, their preservation potential in the fossil record is much higher than structures composed primarily of organic matter.

Preferential analyses of specific periods of time, such as during periods surrounding a mass extinction, have the potential to skew results, as can sampling variability in various regions of the world.

If, however, the fifth outcome is accurate and the patterns correspond to one another, there is higher confidence in modern microbialites as proxies for their ancient counterparts.

6.2 Methods

6.2.1 Data Collection

To compare the distribution of microbialites in modern and ancient environments, we compiled a database of currently known occurrences. The accepted definition of a microbialite is an organosedimentary structure that is formed from the interactions of microbes and their surrounding sedimentary environment (Burne and Moore 1987). The literature was searched, using GeoRef, JSTOR, and Web of Science, across all years of publication, for any of the following terms: stromatolite, thrombolite, dendrolite, leiolite, microbialite, stromatolitic, thrombolitic, dendrolitic, leiolitic, and microbialitic. This particular list of search terms was used to ensure that we captured as many data points as possible. The term "microbial mat" was omitted because the presence of microbial mats in the fossil record is both rare, and those potentially preserved structures are controversial (Brasier et al. 2006; Porada and Bouougri 2007; Noffke and Paterson 2008; Noffke and Chafetz 2010).

As a preliminary study, data were collected from 203 published papers, book chapters, dissertations, and conference proceedings that contained the above terms, and a database containing characteristics about each instance was compiled (Appendix A.1). We define a specimen as one instance of a continuous buildup or nearby association of smaller heads of microbialites. If, for example, a structure had

both stromatolitic and thrombolitic features within it, it was still considered to be one specimen.

For fossil specimens, the location, time period, specific time interval, inferred paleoenvironment, and presence/absence of metazoans known to graze and/or bore (e.g., gastropods, echinoderms, etc.) in association with the microbialites, were included in our dataset. For modern specimens, the location, environment, and presence of grazing and/or boring metazoans were counted.

Databases containing microbialites already exist; however, they have several faults that warrant a fresh approach. First, they often contain extraneous specimens such as other microbial fabrics that are not true microbialites, a limited number of microbialites, or, in the case of the PaleoReef database (Kiessling et al. 1999), other reef structures are also included. The PaleoReef database was used previously by Riding (2006) to analyze stromatolite trends over the Phanerozoic with respect to metazoan abundance. This database "includes not only microbial carbonates within algal-metazoan reefs, but also microbial domes and horizons of the type referred to as Disaster Forms by Schubert and Bottjer (1992)" (Riding 2005). Disaster forms, as defined by Schubert and Bottjer (1992) are "opportunistic taxa, typically of long stratigraphic range, which normally occur in marginal and environmentally unstable settings but become abundant and environmentally widespread during times of biotic crisis." Kiessling's (2001) database only looked at reefal microbialites, ignoring all single-standing microbialite specimens.

Second, it is difficult to discern when looking at a large database how specimens were counted. We considered the presence of stromatolitic fabrics grading into thrombolitic fabrics in one "column" to be one instance of a microbialite with both stromatolites and thrombolites present. Within one locality, unless the specimens were separated by a geographic feature or by time, the overall structure was considered to be one specimen for our dataset. By creating our own database, we have control over how the microbialites were counted.

Finally, existing databases do not always contain information about the specific environment, or the presence of grazing/boring metazoans. Specimens that did not contain explicit information related to environmental conditions were omitted from the dataset used in the analyses.

6.2.2   Analysis of Distribution

The data presented in this chapter are a preliminary snapshot of approximately 300 fossil and 50 modern localities randomly selected, based on keyword relevance, from the extensive literature. We plotted the abundance of microbialites over the Phanerozoic, not including modern specimens, to compare with published distribution patterns in order to see if this initial pool of sample data sufficiently correlated.

This initial abundance plot was examined to see if any patterns could be discerned, specifically whether microbialites may or may not represent post-extinction disaster fauna, as has previously been suggested (general statement 5; Kershaw et al. 2002). The microbialite abundance pattern was then plotted to examine

correlation with global sea level trends, a correlation that has been previously suggested (Camoin et al. 2007; Ezaki et al. 2008).

6.2.3 Analysis of Environmental Preference

The database containing environmental distribution throughout the Phanerozoic and the modern was used to plot distribution across a variety of environments. This was to examine whether there was truth to the statements that ancient microbialites are mostly found in open marine environments while modern microbialites are found in restricted environments (general statements 2 and 4).

Environmental realms were divided using common terminology found in the literature database. An unprotected, normal-salinity marine location (30–35 ppt) was considered "open marine." A protected, normal-salinity marine location was considered "protected marine." Marine locations were considered "brackish" if below normal salinity or "hypersaline" if higher than normal salinity. Microbialitic fabrics present in larger reefs were considered "reefs." Any freshwater lake or lagoon was considered to be "freshwater." Microbialitic fabrics interpreted as forming on the deeper portions of a ramp or near the bottom of the photic zone were labeled "deep marine." Finally, microbialites associated with either hydrothermal vents and/or other hydrothermal waters or cold hydrocarbon seeps were combined and considered "hydrothermal/cold hydroseep."

6.2.4 Analysis of Modern Microbialite Rarity

While a term such as "rare" is subjective, for the purposes of this chapter, both the environmental distribution discussed above and the geographic distribution, were considered. If microbialites are found to only occur in a few, specific environments, or are located in only specific regions of the world, they would be considered as "rare." If, however, microbialites are found distributed across the world, on a majority of continents, and are found in a multitude of environments, they would be considered "not rare." To examine whether modern microbialites are restricted worldwide (general statement 1), data from environmental distribution were considered, along with specific location. Locations were plotted on a world map, using either GPS coordinates, if available, or site maps shown in the paper that described the microbialite, to show geographic distribution.

6.2.5 Analysis of the Role of Metazoans

Finally, to examine whether grazing and/or boring animals influence microbialite abundance (general statement 3), the percentage of microbialites during each time period that were found in association with metazoans known to bore and/or graze was plotted. The criteria for labeling a metazoan a grazer and/or burrower were as follows:
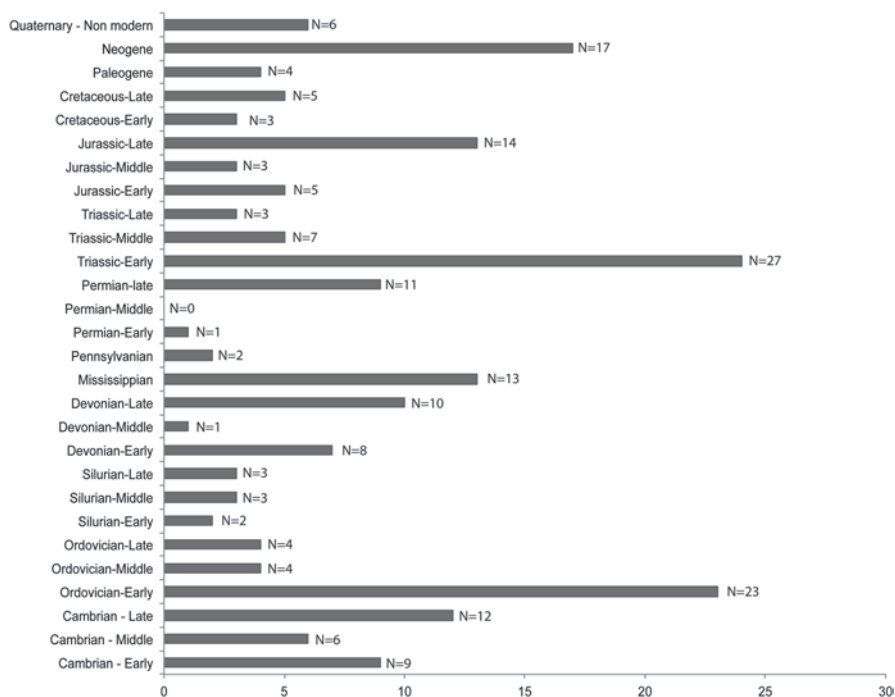
Fig. 6.2 Distribution of microbialitic fabrics throughout the Phanerozoic based on approximately 300 fossil localities as described in the literature. Number of papers used to extract data is shown for each division of time as $N=X$

Any gastropod, echinoderm, chiton, polychaete such as *Ophryotrocha*, or tri-lobite noted within, or nearby, a microbialitic fabric was considered a grazer. Any boring bivalve, boring sponge, or any mention of bioturbation or bored holes was considered to indicate the presence of a boring organism.

6.3   Results

6.3.1   Abundance Patterns in the Phanerozoic

To provide an initial look at microbialite abundance through the Phanerozoic and test general statements 1 and 5, the number of specimens found during each time period was plotted on a bar graph (Fig. 6.2).

Figure 6.2 shows that microbialites are found consistently throughout the Phanerozoic and have six peaks in abundance, most noticeably in the Late Cambrian–Early Ordovician, Early Devonian, Mid-Carboniferous, Early Triassic, Late Jurassic, and the Late Tertiary.
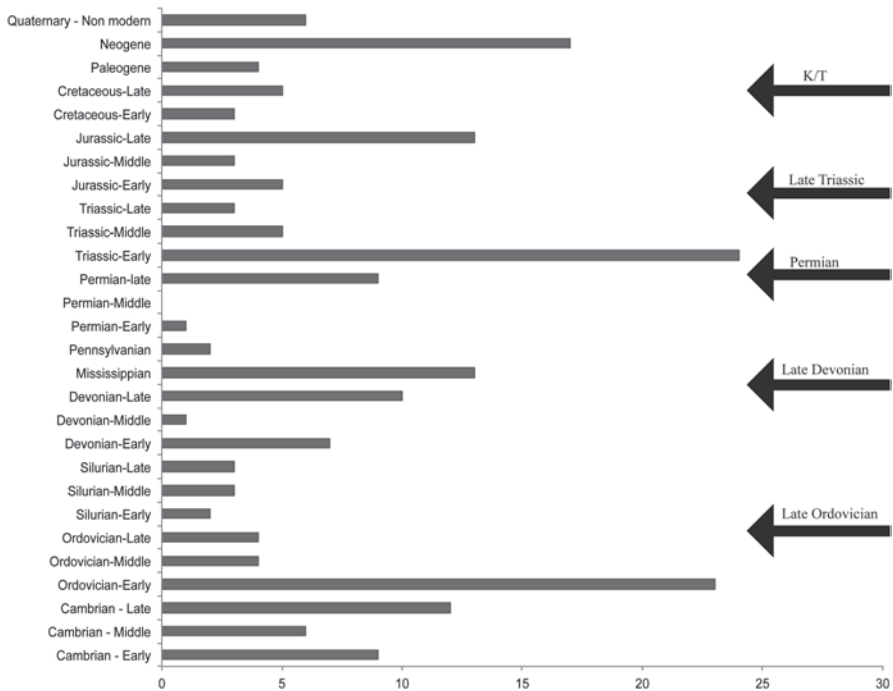
Fig. 6.3 Abundance of microbialites throughout the Phanerozoic with *arrows* showing the timing of the five major mass extinctions

This distribution partially correlates with previous analyses. Riding (1992) and Kiessling and Flügel (2002) pointed out three major abundance peaks: Cambrian–Ordovician, Late Devonian–Carboniferous, and the Late Permian–Middle Triassic.

In our dataset we do not see a peak in the Late Devonian; however, we do see additional peaks during the Late Jurassic, Early Devonian, and another during the Late Tertiary. In addition, while others have stated that microbialites decline in abundance over the Phanerozoic (Awramik and Sprinkle 1999; Riding 2006), we do not see this pattern.

The abundance curve was then analyzed for patterns between the quantities of microbialites throughout the Phanerozoic with respect to the timing of mass extinctions (Fig. 6.3).

There is a clear, immediate increase after the Permian and Devonian mass extinctions, and a delayed reaction in the Late Triassic and K/T mass extinctions. The resurgence of microbialites after the Permian extinction has been reported previously (Schubert and Bottjer 1992; Lehrmann 1998; Kershaw et al. 1999) as well as after the Devonian (Stephens and Sumner 2003; Sheehan and Harris 2004). There is an increase in the late Neogene, which may correspond with previously reported microbialite resurgence in the aftermath of the Messinian salinity crisis in the western Mediterranean (Martin and Braga 1994; Pope et al. 2000; Oliveri et al. 2010). While
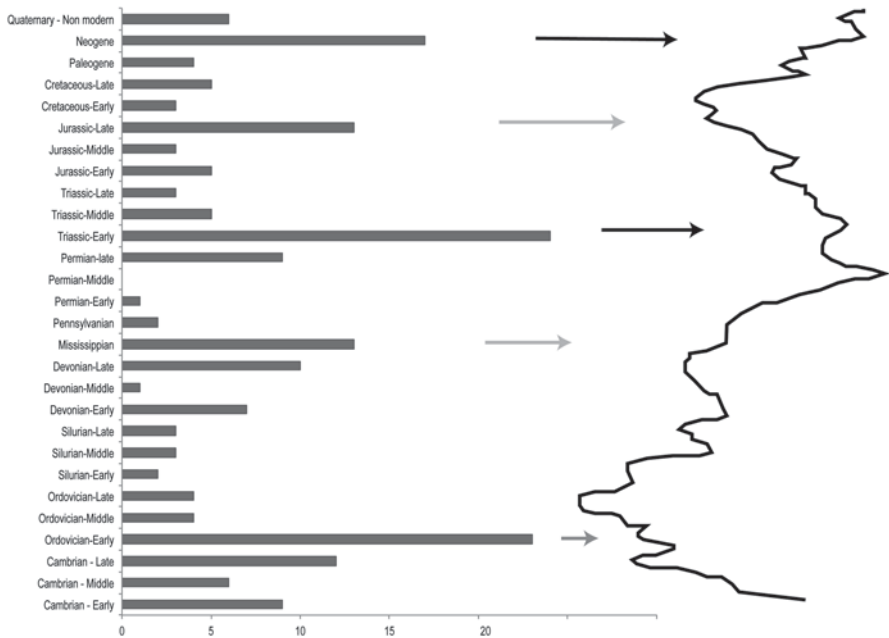
Fig. 6.4 Abundance of microbialites throughout the Phanerozoic with the global sea level curve of Miller et al. (2005). *Black arrows* show strong correlation with sea level low stands and high microbialite abundance; *dark gray arrows* show a moderate trend with high microbialite abundance; *light gray arrows* show a high correlation between sea level high stands and high microbialite abundance

we see this resurgence after some of these mass extinctions, we question the validity of general statement 5, as there is not a consistent resurgence after every event and the potential exists for abundance fluctuations to vary based on other causes.

Several authors have attributed fluctuations in microbialite abundance to sea level change (Camoin et al. 1999; Kershaw et al. 2002). The abundance chart was plotted against the global sea level curve developed by Miller et al. (2005) to examine patterns (Fig. 6.4). When microbialite abundance is compared with the sea level curve, no consistent pattern is seen. In the Early Triassic and the Neogene there are high microbialite levels during sea level low stands. In the Early Devonian, Mid-Carboniferous, and Late Jurassic there are high microbialite levels while there are moderate sea level high stands. During the Late Cambrian–Early Ordovician peak, there is a moderate, yet rising, sea level, but there are no discernable high stands.
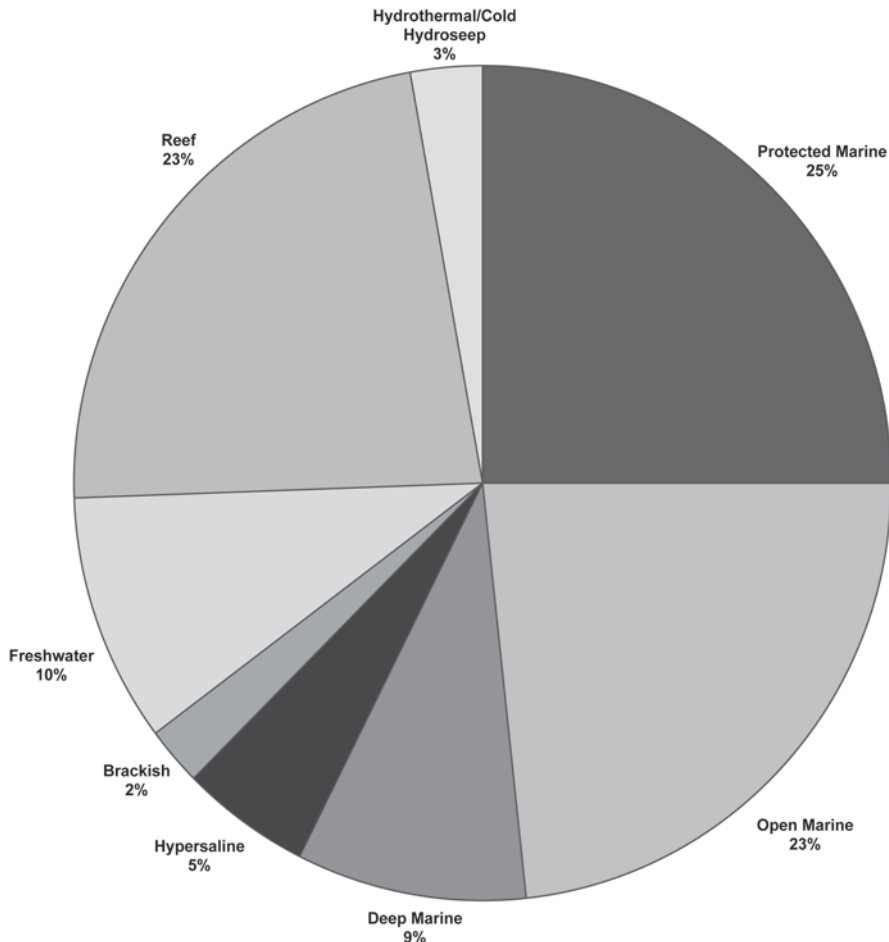
Fig. 6.5 Distribution of environments in which microbialites are interpreted to have formed during the Phanerozoic

6.3.2 Environmental Preference of Microbialites in the Phanerozoic and Modern Era

To examine environmental preferences of microbialites throughout both the fossil records of the Phanerozoic and the modern era and test general statements 2 and 4, the interpreted (in the case of fossil specimens) or current (in the case of modern specimens) environment that the structures were/are found in were plotted as pie charts (Figs. 6.5 and 6.6).

As was mentioned previously in general statement 4, it often stated that fossil microbialites were most commonly found in open marine environments (Awramik 1971; Hoffman 1976; Grotzinger 1986; Awramik and Sprinkle 1999; Riding 2006).
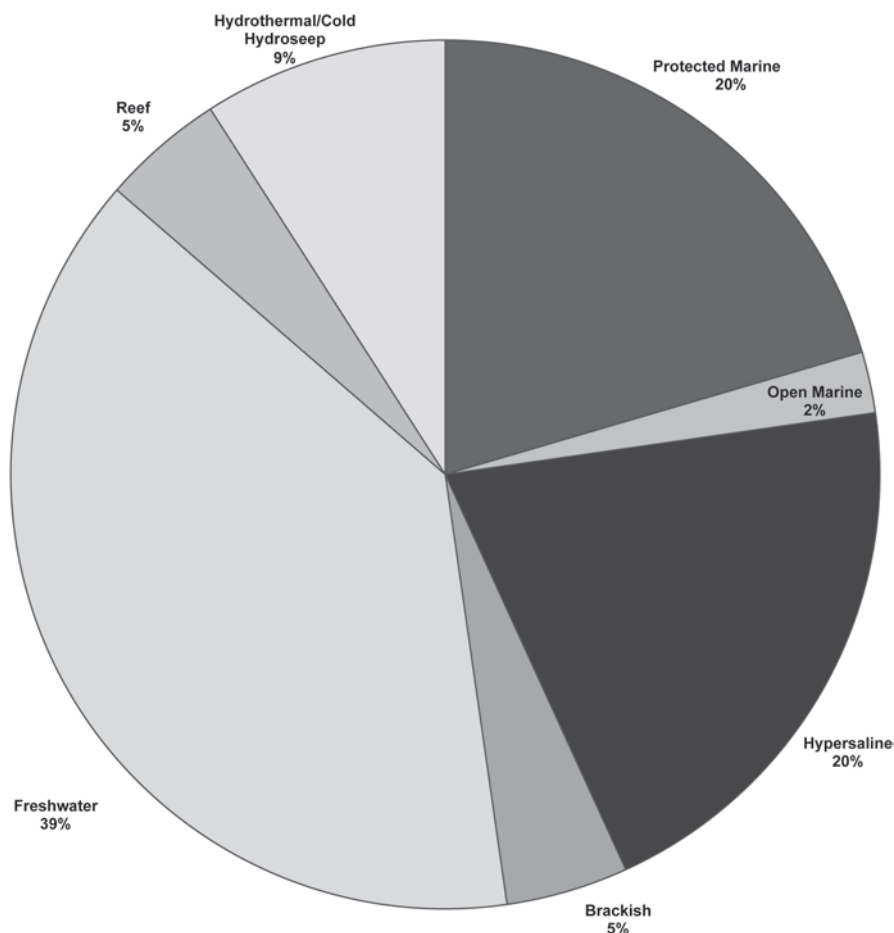
Fig. 6.6 Distribution of environments in which microbialites are currently forming today

However, as the data show, microbialites throughout the Phanerozoic were forming in a variety of environments including equal frequencies in open marine, protected marine, and as reef components (Fig. 6.5).

Another common statement (general statement 2) is that modern microbialites form in more restricted environments, including hypersaline, deep marine, and lakes (Garrett 1970; Awramik 1971; Dill et al. 1986; Dullo et al. 1998; Awramik and Sprinkle 1999; Schmidt 2006). However, the data show microbialites are still forming in a wide variety of environments. While microbialites forming in lakes and hypersaline environments account for 59 % of the dataset, nonrestrictive marine waters, both open and protected, and reefal microbialites account for 27 % of modern microbialite specimens (Fig. 6.6).

Fig. 6.7 Geographical distribution of modern, actively forming microbialites

6.3.3 Geographic Distribution of Modern Microbialites

While fossil microbialites are found in deposits around the world, modern micro-bialites are historically considered to be "rare" (general statement 1) (Garrett 1970; Awramik 1971; Walter and Heys 1995; Burne and Moore 1987; Feldmann and McK-enzie 1997; Awramik and Sprinkle 1999; Camoin and Gautret 2006; Riding 2006; Adachi et al. 2011). Figure 6.7 shows the distribution of actively growing micro-bialite fabrics worldwide. This distribution pattern indicates that microbialites are actively forming on every continent. A lack of occurrences in much of Asia may be due to the difficulty in indexing and translating many Russian and Chinese articles.

6.3.4 The Role of Grazing and/or Boring Animals with Respect to Microbialite Abundance

To analyze whether microbialites declined in abundance in the Phanerozoic, likely due to the rise of metazoans who outcompeted and fed on the microbial structures (general statements 1 and 3) (Garrett 1970; Awramik 1971, 1991; Grotzinger 1990; Awramik and Sprinkle 1999; Pruss and Bottjer 2004; Riding and Liang 2005; Schmidt 2006), the percentage of microbialites throughout the Phanerozoic that were found in association with organisms that commonly bore and/or graze was analyzed (Fig. 6.8).
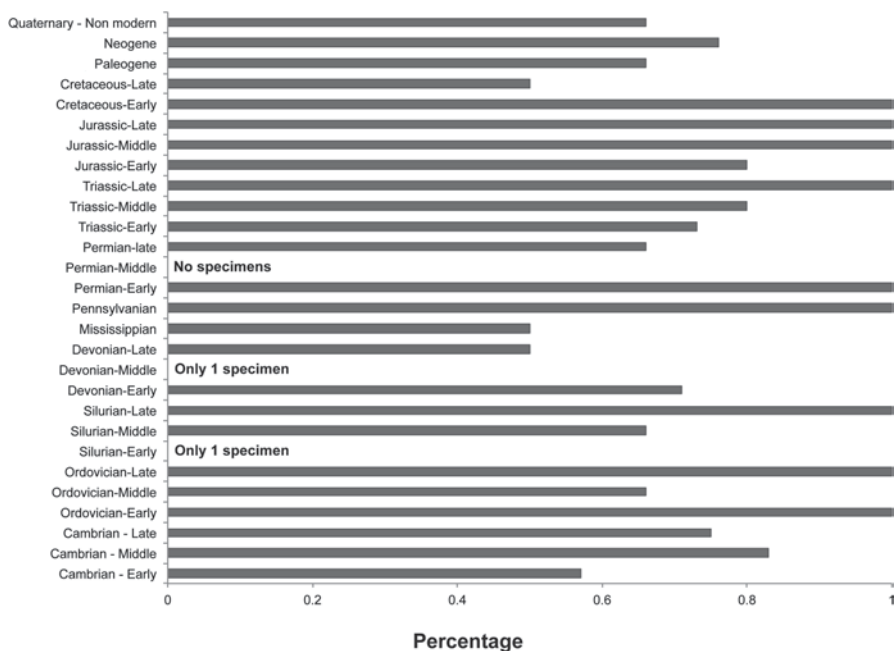
Fig. 6.8 The percentage of microbialites during each time period that were found in association with metazoans commonly known to bore and/or graze

Data presented in Fig. 6.8 show that during almost every time period throughout the Phanerozoic, grazing and/or boring organisms were present in large percentages alongside, or within microbialitic fabrics, structures, and reefs.

6.4   Discussion

6.4.1   Abundance Patterns in the Phanerozoic

While microbialite abundance fluctuates throughout the Phanerozoic, there is not a drastic decline from the Cambrian to the Quaternary. As the Proterozoic record was not examined for this study, it cannot be determined to what extent reductions in abundance occurred between the Proterozoic and the Phanerozoic. However, it is often stated that microbialites remained broadly distributed throughout the Cambrian and Ordovician before declining (general statement 1) (Garrett 1970; Awramik and Sprinkle 1999; Schmidt 2006). Specific growth forms of microbialites did decline after the Proterozoic (e.g., Conophyton) and the overall size of microbialite structures decreased as well; the reason for this is still unknown. The potential exists that competition for open space could lead to a reduction in the size of microbialites

and evolutionary changes among microorganisms forming the microbialites and/or changes in carbonate saturation levels could have changed the type of growth forms produced. Additionally, regional sea level changes that our global sea level curve does not show, or other regional environmental changes that are not seen at large scales such as in a global dataset could also have impacted microbialites.

Previous investigations on microbialites have shown a potential for resurgence after mass extinction events, specifically, the Late Devonian, Late Ordovician, and Early Triassic (general statement 5) (Riding 1992; Schubert and Bottjer 1992; Sheehan and Harris 2004). Previous data, as well as our own, show a rebound after the Permian extinction. The size of this extinction event, in which a large majority of marine species disappeared, left an abundance of open space for microbialites to colonize. A large increase in microbialite specimens is also noted after the Late Devonian mass extinction event as has been previously reported (Stephens and Sumner 2003; Sheehan and Harris 2004).

Interestingly, there is an increase in the Neogene, which has no global event association with it and therefore may be an artifact of an incomplete dataset skewed to one particular region. Specifically, this peak may correspond with a previously reported localized resurgence in the aftermath of the Messinian salinity crisis in the western Mediterranean (Oliveri et al. 2010). Based on our analyses, we question general statements 1 and 5.

6.4.2   Environmental Preference of Microbialites in the Phanerozoic and Modern

The concept that modern microbialites are environmentally restricted (general statement 2) can be dated to the 1950s. Ginsburg (1954, 1960), Rusnak (1960), Logan (1961), and Monty (1965) concluded after examining relatively few modern microbialites that the distribution is environmentally controlled and that stromatolites are essentially an intertidal phenomenon. Gebelein (1969) presented work on the first solely subtidal stromatolites from Bermuda and concluded that the environmental restrictions may not be necessary, as microbialites grow in environments beyond the intertidal. We therefore question general statement 2.

Fossil microbialites are considered to have formed primarily in open marine environments (Awramik 1971; Hoffman 1976; Grotzinger 1986; Awramik and Sprinkle 1999; Riding 2006), which, as shown in Fig. 6.5, is incorrect, leading us to reject general statement 4. Even Precambrian stromatolites were found in environments ranging from reefs to subtidal and in deeper basins (Hoffman 1976).

For both the modern and the Phanerozoic record, carbonate structures will not be found in environments that are not conducive to precipitation of calcium carbonate. However, attempts to restrict these structures based on a handful of examples should be reconsidered. Extensive data clearly show that throughout the Phanerozoic, microbialites are found in a wide variety of environments, showing little preference for any one in particular.

6.4.3   Geographic Distribution of Modern Microbialites

As can clearly be seen in Fig. 6.7, the distribution of modern microbialites is anything but rare or restricted. We find microbialitic fabrics forming in environments ranging from the open waters of the Bahamas (Reid et al. 2000; Myshrall et al. 2010) to the bottom of an ice-covered lake in Antarctica (Parker et al. 1981; Andersen et al. 2011) and from an asbestos pit in Canada (Power et al. 2011) to reef components in Tahiti (Camoin et al. 1999).

Combined with the data above that show these structures are forming in a variety of aquatic environments, we reject the geographic distribution implied by general statement 1 and hope to put to rest the notion that finding a modern microbialite is a rare event.

6.4.4   The Role of Grazing and/or Boring Animals with Respect to Microbialite Abundance

As metazoans appeared and diversified in the late Proterozoic into the early Phanerozoic, microbialites declined (general statement 3) (Fischer 1965; Awramik 1971). Garrett (1970) was the first to suggest that the decline of microbialites, specifically stromatolites, could be attributed to restriction by grazing and burrowing animals. He calculated the amount of time it would take the average number of gastropods present in an intertidal zone to consume the surface of a microbial mat and concluded that they would prevent the formation of a "cohesive algal mat" (Garrett 1970).

Garcia-Pichel et al. (2004) determined that the complex association between stromatolites and grazers is a delicate balance "between net formation and destruction." They found that in environments that are restrictive to metazoan growth, such as hypersalinity, accretion of microbialites occurs even when calcification rates are slow. In environments that are more conducive to metazoan growth, metazoan populations must be controlled for a microbialite to successfully form (Garcia-Pichel 2004).

While we agree that under conditions of extremely high levels of grazing and/or boring microbialite formation would potentially be impeded, data suggest that metazoans cannot be blamed solely for any perceived decline in microbialite abundance. We therefore disagree with general statement 3.

Throughout the Phanerozoic, metazoan abundance is high, both alongside, and within microbialites. Some of these fossil microbialites were large, successful reefs suggesting that metazoan feeding and dwelling activity did not impact their formation drastically.

As has previously been suggested by Riding and Liang (2005), geochemical changes in the environment, in conjunction with the presence of metazoans, may have influenced the success of microbialites throughout the Phanerozoic. As early as 1982, Pratt realized that post-Lower Ordovician rocks contained many more stromatolites than were previously thought. He also noted that these microbialites formed in open marine waters of normal salinity and that they were frequently

found with grazing and burrowing organisms (Pratt 1982). He concluded that the distribution and abundance of microbialites was largely controlled by sedimentology and, perhaps, competition for substrates by metazoans (Pratt 1982).

Additionally, organisms such as foraminifera may play a role in microbialite fabric disruption. Bernhard et al. (2013) found that the presence of forams within modern microbialites can disrupt laminae within stromatolites as they migrate in response to changing chemical gradients throughout the day and night. The evolution of forams is estimated to have occurred shortly before the Cambrian explosion, which corresponds with the reported decline in stromatolites. Bernhard et al. (2013) suggest that heterotrophic protists, including forams, influenced stromatolite abundance in the early Phanerozoic.

6.5   Conclusions

The goal of this initial database analysis was to test five commonly held general statements about modern and ancient microbialites. Based on our analyses, we question the validity of general statements 1, 3, and 4, and find partial, yet unconvincing, support for general statements 2 and 5.

Our compilation of microbialite structures over the Phanerozoic shows that microbialite abundance fluctuated over this eon, with several peaks corresponding to mass extinctions, though the pattern is inconsistent, leading us to question general statement 5. Both modern and fossil microbialites are found in a variety of environments and, contrary to previous interpretations, fossil microbialites are not primarily found in open marine environments as said in general statement 4. We therefore reject this statement. Modern microbialites do show a pattern of preferring more "restricted" environments including freshwater and hypersaline, providing us with an understanding of why general statement 2 is said. However, the variety of environments the microbialites are found in leads us to question the overall validity of this statement.

The idea that modern microbialites are rare throughout the Phanerozoic, as said in general statement 1, is not shown by our distribution map. They are abundant and are found worldwide with the highest concentrations reported in areas surrounding the Caribbean, South America, and Australia, based on English, Spanish, Portuguese, German, and French language publications.

The impact of grazing and/or boring metazoans on microbialites is unclear. However, the data show that grazers and borers are both found in association with microbialites throughout the entire Phanerozoic, though the abundance varies from 32 to 100 % depending on the time period, suggesting that rejection of general statement 3 is also warranted.

With regards to the five potential outcomes discussed earlier in the chapter, our data suggest that there are no discernable patterns in either the fossil or modern microbialite record with respect to environmental preference, distribution, or abundance (potential outcome 3). We do not yet understand what controls the abundance of microbialites in the fossil or modern record. This is, perhaps, due to our

limited data. However, what if we do not see any patterns even with a much larger dataset? We know that the fossil record is incomplete due to preservational issues, and does not always show every detail. The potential exists for the fossil record to obscure details that may hold patterns. In that case, all is not necessarily lost! Perhaps, instead of looking for large-scale patterns among microbialites in different environments or time periods, we should instead be focusing on specific fabrics and environmental similarities between individual specimens in both the modern and ancient times. Using individual characteristics, we can still potentially use specific modern microbialites to understand the fossil record.

For example, the stromatolites at Highborne Cay are very similar in form to many fossil stromatolites, specifically, specimens found in the Middle Devonian of New York (unpublished observations). Several stromatolites from Antarctica and New Zealand have been shown to be similar to a particular variety of Precambrian stromatolites, Conophyton or coniform (Parker et al. 1981; Jones et al. 2002). If we are selective about the microbialitic structures we use as analogs, we can still successfully extrapolate to the fossil record to attempt to understand how they formed and functioned.

Appendix

Age (Ma)	Environment	Type of microbialite	Grazers present	Reference
0.0012	H	M	X	Pedone and Dickson 2000
0.0023–0	H	S, T		Last et al. 2010
0.01–0.001	P	T		Gischler et al. 2008
0.01–0.001	R	S, T		Montaggioni and Camoin 1993
0.01–0.001	F	S, T	X	Cohen et al. 1997, 2003
0.01–0.09	F	S, T		Cabrol et al. 2004
0.1–3	F	S	X	Abell et al. 1982
0.24–06	R	S, T	X	Cabioch et al. 2006; Camoin et al. 1999, 2006
1.8–0.01	F	S		Valero-Garcés et al. 2001
2.6–0.01	F	S	X	Lamond and Tapanila 2003
5.3–2.6	R	T, M		Aguirre and Sánchez-Almazo 2004
5.3–2.6	F	S		Link et al. 1978
7.2–5.3	D	S, T	X	Braga et al. 1995
7.2–5.3	P	S, T		Castell et al. 2007
7.2–5.3	P	S, T	X	Feldmann and Mckenzie 1997
7.2–5.3	R	S, T	X	Martin et al. 1993
7.2–5.3	H	S, T		Riding and Martin 1991
7.2–5.3	O	S, T, M	X	Saint Martin et al. 1996
7.2–5.3	R	S	X	Sánchez-Almazo et al. 2007
7.2–9	O	S	X	García-García et al. 2006
7.2–9	F	M		Straccia et al. 1990
11.0–7	HD	T	X	Campbell 2006; Campbell et al. 2008
16–13	R	S, T, M	X	Saint Martin et al. 2000

Age (Ma)	Environment	Type of microbialite	Grazers present	Reference
20–26	O	S, T	X	Arenas and Pomar 2010
23–16	F	S	X	Freytet et al. 2001
28–23	R	S, T, M		Moellerhenn et al. 2007
33–23	F	S	X	Ramos et al. 2001
40–34	P	T		Khanaqa 2011
48–45	F	S, T	X	Lamond and Tapanila 2003
51–49	F	S, M		Leggitt et al. 2007
56–54	F	S	X	Davis 2006
58–55	R	S, T, M	X	Zamagni et al. 2009
70–65	D	T	X	Shapiro and Fricke 2003
70–65	D	T	X	Gotz and Mitchell. 2009
70–65	B	S, T	X	Kiessling et al. 2006
93–89	P	S	X	Krajewski et al. 2000
112–100	F	S		Nehza and Woo 2006
130–120	O	T, M		Pittet et al. 2002
136–130	D	T	X	Campbell 2006
142–139	R	S, T	X	Pawellek and Aigner 2003
145–140	R	M	X	Krajewski et al. 2011
145–140	R	S	X	Riding and Thomas 2006
148–145	P	M		Krajewski et al. 2011
150–140	D	S, T		Ellis et al. 1985
151–145	D	S, T	X	Dromart et al. 1994; Jansa and Pratt 1989
151–145	O	S	X	Kelly 1991
151–145	O	T		Krajewski et al. 2011
151–148	P	T, M	X	Krajewski et al. 2011
151–148	O	T		Krajewski et al. 2011
152–150	D	T	X	Pawellek and Aigner 2004
152–150	D	S, T	X	Pawellek and Aigner 2004
154–151	O	T		Krajewski et al. 2011
156–154	R	M	X	Olivier et al. 2007
158–154	D	M	X	Olivier et al. 2007
158–156	P	T, M	X	Krajewski et al. 2011
158–156	O	T		Krajewski et al. 2011
159–156	D	M	X	Olivier et al. 2007
159–156	R	M	X	Olivier et al. 2007
160–146	D	T		Jansa and Pratt 1989
160–152	P	T, M	X	Krajewski et al. 2011
160–156	R	S, T, M	X	Dupraz and Strasser 2002
160–156	P	S, T	X	Dupraz and Strasser 1999
160–156	R	T		Matyszkiewicz and Felisiak 1992
160–156	R	S, T, M	X	Olóriz et al. 2003
160–158	R	T	X	Bertling and Insalaco 1998
160–158	O	T	X	Carpentier et al. 2010
161–151	P	S, T, M	X	Matyszkiewicz et al. 2006
161–151	D	S, T, M	X	Ruf et al. 2005
161–156	P	T	X	Helm and Schuelke 2006

Age (Ma)	Environment	Type of microbialite	Grazers present	Reference
161–156	O	T		Mancini et al. 2004, 2008
172–166	P	T	X	Andrews 1986
172–170	D	S, T, M	X	Olivier et al. 2006
183–180	D	S	X	Campbell 2006
190–180	F	S		Eisenberg 2009
194–190	D	S, T	X	Neuweiler et al. 2001
195–193	R	S, T	X	Chafiki et al. 2004
197–190	P	S, T		Azeredo et al. 2009
200–180	P	S, T, M	X	Wilmsen and Neuweiler 2008
215–204	H	S, T, M	X	Mastandrea et al. 2006; Perri et al. 2003
235–228	R	M	X	Martindale et al. 2010
241–235	F	S	X	Clemmensen 1978
242–228	O	S		Payne et al. 2006
242–241	D	T	X	Russo et al. 2000
243–241	O	M		Senowbaridaryan and Flugel 1996
245–241	O	T	X	Baud et al. 2007
245–241	P	S, T	X	Emmerich et al. 2005
247–245	O	S		Schubert and Bottjer 1992
250–245	O	T	X	Baud et al. 2007
250–245	O	S, T	X	Baud et al. 2007
250–245	O	S, T	X	Baud et al. 2007
250–245	O	S, T	X	Baud et al. 2007
250–245	O	S		Garzanti et al. 1998
250–245	D	S, T	X	Hips and Haas 2006; Haas et al. 2006
250–245	O	T		Payne et al. 2006
250–245	R	S	X	Pruss and Bottjer 2004
250–245	R	S, T	X	Pruss et al. 2006
250–245	P	S		Sano and Nakashima 1997
250–245	P	S		Wignall and Twitchett 2002
250–249	P	S	X	Paul et al. 2011
251–245	P	M	X	Lehrmann 1998
251–250	R	S, T, M	X	Baud et al. 1997
251–250	R	S, T, M	X	Baud et al. 2002
251–250	O	S, T	X	Baud et al. 2005
251–250	O	S	X	Baud et al. 2007
251–250	O	S	X	Baud 2007
251–250	O	S		Dawes 1976
251–250	R	T		Heydari et al. 2000
251–250	O	T, O		Kershaw et al. 2007
251–250	R	T, M		Kershaw et al. 2007
251–250	R	M	X	Kershaw et al. 1999
251–250	R	S, M		Kershaw et al. 2002
251–250	P	S		Sano and Nakashima 1997
251–250	B	S		Wang et al. 2005
251–250	O	S, T, M	X	Weidlich and Bernecker 2011
251–250	P	S		Wignall and Twitchett 2002
251–254	O	T	X	Adachi et al. 2004

Age (Ma)	Environment	Type of microbialite	Grazers present	Reference
258–257	H	S	X	Becker and Bechstadt 2006
260–251	O	T	X	Ezaki et al. 2003
260–251	O	T	X	Ezaki et al. 2008
266–260	R	S, M	X	Kirkland et al. 1998
268–260	P	S	X	Alvaro et al. 2007
299–297	O	S, T		Moore 2010
299–297	P	S, T	X	Shapiro and West 1999
306–304	O	S, T	X	Busquets et al. 2005
324–320	R	T		von Blanckenburg et al. 2008
324–320	R	T		von Blanckenburg et al. 2008
326–320	HD	S, T	X	Buggisch et al. 2005
330–228	R	S, T	X	Wendt 1982
330–326	O	S	X	Alvaro et al. 2007
330–326	B	S, T		Archer 1984
330–326	P	S, T	X	Gomez-Perez 2003
335–326	P	T		Kirkham 2005
340–345	O	S, T	X	Adams 1984
345–325	R	S, T	X	Shen and Webb 2008
345–325	P	T, M		Shen and Qing 2010
359–352	R	S, T		von Blanckenburg et al. 2008
359–352	R	S, T		von Blanckenburg et al. 2008
359–352	P	S, T, M	X	Webb 2005
359–354	R	S, T	X	Webb 1998
373–374	P	S	X	Whalen et al. 2002
374–360	O	S, T		Chow and George 2004
374–360	P	S, T	X	Shen and Webb 2004
374–360	R	S, T, M	X	Stephens and Sumner 2003
374–370	R	S		Wood 2000
385–380	D	S	X	Playford and Wallace 2001
416–411	P	T	X	Adachi et al. 2006
416–411	O	S, T	X	Álvaro et al. 2007
416–411	D	T		Browne 1988
416–411	D	S	X	Buggisch and Krumm 2005
416–411	B	T		Demicco and Smith 2009
416–411	B	T		Demicco and Smith 2009
416–411	O	M		Webb 1998
418–411	R	S	X	Adachi et al. 2007
419–416	HD	S	X	Buggisch and Krumm 2005
419–416	P	S	X	Campbell 2006
421–426	P	S, T	X	Archer and Feldman 1986
427–426	R	S, M		Nose et al. 2006
428–426	O	S, T	X	Kahle 1994, 2001
470–460	O	S, T		Dix and Rodhan 2006
476–468	O	T	X	Kennard and James 1986
478–475	O	S	X	Keller and Flugel 1996
480–471	O	T	X	Hersi et al. 2003

Age (Ma)	Environment	Type of microbialite	Grazers present	Reference
480–470	O	S	X	Adachi et al. 2011
488–472	O	T	X	Bassett et al. 2007
488–471	P	T	X	Shapiro and Awramik 2006
488–478	P	T	X	Shapiro and Awramik 2006
488–478	P	T	X	Shapiro and Awramik 2006
488–479	O	T		Goldhammer and Lehmann 1993
488–479	O	T	X	Heartsill 2010
488–479	O	T	X	Heartsill 2010
488–479	O	T		Herringshaw and Raine 2007
488–479	O	T		Overstreet et al. 2003
488–479	P	S, T	X	Parcell and Warusavitharana 2010
488–480	P	S, T	X	Landing et al. 1996
488–480	P	T	X	Mazzullo and Friedman 1977
488–480	O	T		Myrow et al. 2004
490–480	O	S, T	X	Franseen 1999
492–488	R	S, T		Taylor et al. 1999
496–488	O	S, T	X	Bordonaro 2003; Buggisch et al. 2003
496–488	H	S, T		Wright 1993
496–492	P	T	X	Bordonaro 2003
496–492	P	S, T	X	Glumac 2001; Glumac and Walker 1997, 2000
498–488	P	T	X	Shapiro and Awramik 2006
498–488	P	T	X	Shapiro and Awramik 2006
500–472	P	S, T	X	Stinchcomb 1986
500–490	D	S, T		Griffin 1989
501–496	H	S	X	Bordonaro 2003
501–498	P	S, T	X	Shapiro 2004
501–507	P	T	X	Armella et al. 1996
501–507	P	S, T		Armella 1994
507–501	O	S, T		Kennard and James 1986
507–501	O	S, T, M	X	Woo et al. 2008
510–490	R	S, T	X	Demicco 1983, 1985
510–501	O	S, T	X	Sial et al. 2003
510–503	P	S	X	Heartsill 2010
513–500	P	S	X	Shapiro and Awramik 2000
513–498	P	S	x	Shapiro and Awramik 2006
517–521	O	S	X	Alvaro et al. 2006
520–510	O	S, T	X	Soudry and Weissbrod 1995
521–510	O	S, T		deWet et al. 2004
524–517	R	S, T		Hicks and Rowland 2009
524–520	P	S, T	X	Bigolski 2009
542–540	H	T	X	Amthor et al. 2003

S Stromatolite, *H* Hypersaline, *F* Freshwater, *T* Thrombolite, *O* Open marine, *D* Deep marine, *M* Other microbialite, *P* Protected marine, *HD* Hydrothermal/Hydroseep, *R* Reef

References

Abell PI, Awramik SM, Osborne RH, Tomellini S (1982) Plio-Pleistocene lacustrine stromatolites from Lake Turkana, Kenya: morphology, stratigraphy and stable isotopes. Sed Geol 32:1–26

Adachi N, Ezaki Y, Liu J (2004) The fabrics and origins of peloids immediately after the end-Permian extinction, Guizhou Province, South China. Sediment Geol 164:161–178

Adachi N, Ezaki Y, Pickett J (2006) Marked accumulation patterns characteristic of Lower Devonian stromatoporoid bindstone: palaeoecological interactions between skeletal organisms and microbes. Palaeogeogr Palaeocl 231:331–346

Adachi N, Ezaki Y, Pickett J (2007) Interrelations between framework-building and encrusting skeletal organisms and microbes: more-refined growth history of Lower Devonian bindstones. Sedimentology 54:89–105

Adachi N, Ezaki Y, Liu J (2011) Lower Ordovician stromatolites from the Anhui Province of South China: construction and geobiological significance. In. Reitner J, Quéric NV, Arp G (Eds) Advances in stromatolite geobiology, lecture notes in Earth sciences 131, Springer-Verlag Berlin Heidelberg

Adams AE (1984) Development of algal-foraminiferal-coral reefs in the Lower Carboniferous of Furness, northwest England. Lethaia 17:233–249

Aguirre J, Sánchez-Almazo IM (2004) The Messinian post-evaporitic deposits of the Gafares area (Almería-Níjar basin, SE Spain). A new view of the "Lago-Mare" facies. Sediment Geol 168:71–95

Alvaro JJ, Clausen S, El Albani A, Chellai EH (2006) Facies distribution of the Lower Cambrian cryptic microbial and epibenthic archaeocyathan-microbial communities, western Anti-Atlas, Morocco. Sedimentology 53:35–53

Alvaro JJ, Aretz M, Boulvain F, Munnecke A, Vachard D, Vennin E (2007) Fabric transitions from shell accumulations to reefs: an introduction with Palaeozoic examples. Geol Soc Lon Spec Publ 275:1–16

Allwood AC, Walter MR, Burch IW, Kamber BS (2007) 3.43 billion-year-old stromatolite reef from the Pilbara Craton of Western Australia: ecosystem-scale insights to early life on Earth. Precambrian Res 158:198–227

Amthor J, Grotzinger J, Schroder S, Bowring SA, Ramezani J, Martin MW, Matter A (2003) Extinction of *Cloudina* and *Namacalathus* at the Precambrian-Cambrian boundary in Oman. Geology 31:431–434

Andersen DT, Sumner DY, Hawes I, Webster-Brown J, McKay CP (2011) Discovery of large conical stromatolites in Lake Untersee, Antarctica. Geobiology 9:280–293

Andrews JE (1986) Microfacies and geochemistry of Middle Jurassic algal limestones from Scotland. Sedimentology 33:499–520

Archer AW (1984) Preservational control of trace-fossil assemblages: Middle Mississippian carbonates of South-Central Indiana. J Paleontol 58:285–297

Archer AW, Feldman HR (1986) Microbioherms of the Waldron Shale (Silurian, Indiana): implications for organic framework in Silurian reefs of the Great Lakes area. Palaios 1:133–140

Arenas C, Pomar L (2010) Microbial deposits in upper Miocene carbonates, Mallorca, Spain. Palaeogeogr Paleoclim 297:465–485

Armella C (1994) Thrombolitic-stromatolitic cycles of the Cambro-Ordovician boundary sequence, Precordillera Oriental Basin, Western Argentina. In: Bertrand-Sarfati J, Monty C (eds) Phanerozoic stromatolites II. Springer, Berlin, pp 421–441

Armella C, Cabaleri N, Valencio S (1996) Modelo paleoambiental de la Formacion La Flecha (Cambrico superior) en el area de Jachal, Provincia de San Juan. Rev Ass Geo Arg 51:165–176

Awramik S (1971) Precambrian columnar stromatolite diversity: reflection of metazoan appearance. Science 174:825–827

Awramik S (1991) Archaean and Proterozoic stromatolites. In: Riding R (ed) Calcareous algae and stromatolites. Springer, Berlin, pp 289–304

Awramik S, Sprinkle J (1999) Proterozoic stromatolites: the first marine evolutionary biota. Hist Biol 13:241–253

Azerêdo AC, Silva RL, Duarte LV, Cabral MC (2009) Subtidal stromatolites from the Sinemurian of the Lusitanian Basin (Portugal). Facies 56:211–230

Bassett D, Macleod KG, Miller JF, Ethington RL (2007) Oxygen isotopic composition of biogenic phosphate and the temperature of Early Ordovician seawater. Palaios 22:98–103

Baud A (2007) Lower Triassic microbialites versus skeletal carbonates, a competition on the Gondwana margin. New Mex Mus Nat Hist Sci Bull 41:23

Baud A, Cirilli S, Marcoux J (1997) Biotic response to mass extinction: the lowermost Triassic microbialites. Facies 36:238–242

Baud A, Richoz S, Cirilli S, Marcoux J (2002) Basal Triassic carbonate of the Tethys: a microbialite world. In: IAS (ed) Proceedings of the 16th international sedimentological congress. Johannesburg, pp 24–25

Baud A, Richoz S, Marcoux J (2005) Calcimicrobial cap rocks from the basal Triassic units: western Taurus occurrences (SW Turkey). Comptes Rendus Pale 4:569–582

Baud A, Richoz S, Pruss S (2007) The Lower Triassic anachronistic carbonate facies in space and time. Global Planet Change 55:81–89

Becker F, Bechstadt T (2006) Sequence stratigraphy of a carbonate-evaporite succession (Zechstein 1, Hessian Basin, Germany). Sedimentology 53:1083–1120

Benton MJ, Willis MA, Hitchin R (2000) Quality of the fossil record through time. Nature 403:534–537

Bernhard JM, Edgcomb VP, Visscher PT, McIntyre-Wressnig A, Summons RW, Bouxsein ML, Louis L, Jeglinski M (2013) Insights into foraminiferal influences on microfabrics at Highborne Cay, Bahamas. Proc Natl Acad Sci U S A 110:9830–9834

Bertling M, Insalaco E (1998) Late Jurassic coral/microbial reefs from the northern Paris Basin — facies, palaeoecology and palaeobiogeography. Palaeogeogr Palaeocl 139:139–175

Bigolski JN (2009) An inferred sea level curve from carbonate depositional facies of the Middle Cambrian Elbrook Formation, Western Maryland, USA. MS Thesis, State University of New York at Binghamton

Blanckenburg vonF, Mamberti M, Schoenberg R (2008) The iron isotope composition of microbial carbonate. Chem Geol 249:113–128

Bordonaro O (2003) Review of the Cambrian stratigraphy of the Argentine Precordillera. Geol Acta 1:11–22

Braga J, Martin J, Riding R (1995) Controls on microbial dome fabric development along a carbonate-siliciclastic shelf-basin transect, Miocene, SE Spain. Palaios 10(4):347–361

Brasier M, McLoughlin N, Green O, Wavey D (2006) A fresh look at the fossil evidence for early Archaean cellular life. Philos Trans R Soc Lond B Biol Sci 361:887–902

Browne K (1988) Thrombolites of the Lower Devonian Manlius Formation of central New York. Carbonates Evaporites 2:149–155

Buggisch W, Keller M, Lehnert O (2003) Carbon isotope record of Late Cambrian to Early Ordovician carbonates of the Argentine Precordillera. Palaeogeogr Palaeocl 195:357–373

Buggisch W, Krumm S (2005) Palaeozoic cold seep carbonates from Europe and North Africa—an integrated isotopic and geochemical approach. Facies 51:566–583

Burne R, Moore L (1987) Microbialites: organosedimentary deposits of benthic microbial communities. Palaios 2:241–254

Busquets P, Mendez-Bedia I, Colombo-Pinol F, Heredia N, Gallastegui G (2005) Upper Carboniferous carbonate shelves in the Andean Frontal Cordillera (San Juan Province, Argentina): sedimentology and tectono-sedimentary context. Proceedings of the 6th international symposium on Andean geodynamics, pp 131–134

Cabioch G, Camoin G, Webb G, Le Cornec F (2006) Contribution of microbialites to the development of coral reefs during the last deglacial period: case study from Vanuatu (South-west Pacific). Sediment Geol 185:297–318

Cabrol N, Grin E, Borics G, Fike D, Kovacs G, Hock A, Kiss K, Acs E, Sivila R, Ortega C, Chong G, Demergasso C, Zambrana J, Liberman M, Sunagua Coro M, Escudero L, Tambley C, Angel

Gaete V, Morris RL, Grigsby B, Fitzpatrick R, Hovde G (2004) Short time scale evolution of microbiolites in rapidly receding altiplanic lakes: learning how to recognize changing signatures of life. Lunar and planetary institute science conference XXXV

Camoin G, Gautret P, Montaggioni L, Cabioch G (1999) Nature and environmental significance of microbialites in Quaternary reefs: the Tahiti paradox. Sediment Geol 126:271–304

Camoin G, Gautret P (2006) Microbialites and microbial communities: biological diversity, biogeochemical functioning, diagenetic processes, tracers of environmental changes. Sediment Geol 185:127–130

Camoin G, Cabioch G, Eisenhauer A, Braga J (2006) Environmental significance of microbialites in reef environments during the last deglaciation. Sediment Geol 185:277–285

Camoin G, Iryu Y, McInroy D (2007) IODP expedition 310 reconstructs sea level, climatic, and environmental changes in the South Pacific during the last deglaciation. Sci Drill 5:4–12

Campbell K (2006) Hydrocarbon seep and hydrothermal vent paleoenvironments and paleontology: past developments and future research directions. Palaeogeo Palaeocl 232:362–407

Campbell K, Francis DA, Collins M, Gregory MR, Nelson CS, Greinert J, Aharon P (2008) Hydrocarbon seep-carbonates of a Miocene forearc (East Coast Basin) North Island, New Zealand. Sed Geol 204:83–105

Carpentier C, Lathuilière B, Ferry S (2010) Sequential and climatic framework of the growth and demise of a carbonate platform: implications for the peritidal cycles (Late Jurassic, Northeastern France). Sedimentology 57:985–1020

Chafiki D, Canérot J, Souhel A, El Hariri K, Eddine KT (2004) The Sinemurian carbonate mudmounds from central High Atlas (Morocco): stratigraphy, geometry, sedimentology and geodynamic patterns. J Afr Earth Sci 39:337–346

Chow N, George A (2004) Tepee-shaped agglutinated microbialites: an example from a Famennian carbonate platform on the Lennard Shelf, northern Canning Basin, Western Australia. Sedimentology 51:253–265

Clemmensen L (1978) Lacustrine facies and stromatolites from the Middle Triassic of East Greenland. J Sediment Petrol 48:1111–1128

Cohen A, Talbot M, Awramik S, Dettman DL, Abell P (1997) Lake level and paleoenvironmental history of Lake Tanganyika, Africa, as inferred from late Holocene and modern stromatolites. Geol Soc Am Bull 109:444

Cohen A, Talbot MR, Awramik SM, Dettman DL, Abell P (2003) Lake-level history of Lake Tanganyika, East Africa, for the past 2500 years based on ostracode-inferred water-depth reconstruction. Palaeogeogr Palaeocl 199:31–49

Cuevas Castell J, Betzler C, Rossler J, Hussner H, Peinl M (2007) Integrating outcrop data and forward computer modelling to unravel the development of a Messinian carbonate platform in SE Spain (Sorbas Basin). Sedimentology 54:423–441

Davis BS (2006) Stromatolites in the Upper Lacustrine Unit of the Paleocene Hanna Formation, Hanna Basin, South-central Wyoming. MS Thesis

Dawes PR (1976) Precambrian to Tertiary of northern Greenland. In. Escher A, Watt WS (Eds) Geology of Greenland. Geological Society of Greenland, pp 248–303

Demicco R (1983) Wavy and lenticular-bedded carbonate rocks of the Upper Cambrian Conococheague Limestone, central Appalachians. J Sed Res 52:1121–1132

Demicco R (1985) Platform and off-platform carbonates of the Upper Cambrian of western Maryland, USA. Sedimentology 32:1–22

Demicco RV, Smith J (2009) Sedimentologic observation and stratigraphic interpretation of the Lower Devonian (Lochkovian) Manlius Formation along the Mohawk River Valley in Upstate New York. J Geol 117:543–551

deWet CB, Frey HM, Gaswirth SB, Mora CI, Rahnis M, Bruno CR (2004) Origin of meter- scale submarine cavities and herringbone calcite cement in a Cambrian microbial reef, Ledger Formation (USA). J Sediment Res 74:914–923

Dill R, Shinn E, Jones A, Kelly K, Steinen RP (1986) Giant subtidal stromatolites forming in normal salinity waters. Nature 324:55–58

Dix G, Rodhan Z (2006) A new geological framework for the Middle Ordovician Carillon Formation (uppermost Beekmantown Group, Ottawa Embayment): onset of Taconic foreland deposition and tectonism within the Laurentian platform interior. Can J Earth Sci 43:1367–1387

Dromart G, Gaillard C, Jansa LF (1994) Deep-marine microbial structures in the Upper Jurassic of Western Tethys. In: Bertrand-Sarfati J, Monty C (eds) Phanerozoic stromatolites II. Springer, Heidelberg, pp 295–318

Dullo W-C, Camoin G, Blomeier D, Casanova J, Colonna M, Eisenhauer A, Faure G, Thomas BA (1998) Sediments and sea level changes of the foreslopes of Mayotte, Comoro Islands: direct observations from submersible. In: Camoin GF, Davies PJ (eds) Reefs and carbonate platforms in the Pacific and Indian oceans (SP 25) Spec Publ Int Ass Sediment 25. Wiley, pp 12–19

Dupraz C, Strasser A (1999) Microbialites and micro-encrusters in shallow coral bioherms (Middle to Late Oxfordian, Swiss Jura Mountains. Facies 40:101–130

Dupraz C, Strasser A (2002) Nutritional modes in coral-microbialite reefs (Jurassic, Oxfordian, Switzerland): evolution of trophic structure as a response to environmental change. Palaios 17:449–471

Eisenberg L (2009) Giant stromatolites and a supersurface in the Navajo Sandstone, Capitol Reef National Park, Utah. Geology 31:111–116

Ellis PM, Crevello PD, Eliuk LS (1985) Upper Jurassic and Lower Cretaceous deep-water buildups, Abenaki Formation, Nova Scotia Shelf. In: Crevello PD, Harris PM (eds) Deep-water carbonates. Core workshop notes vol 6, SEPM. Tulsa, pp 212–248

Emmerich A, Zamparelli V, Bechstädt T, Zühlke R (2005) The reefal margin and slope of a Middle Triassic carbonate platform: the Latemar (Dolomites, Italy). Facies 50:573–614

Ezaki Y, Liu J, Adachi N (2003) Earliest Triassic microbialite micro-to megastructures in the Huaying area of Sichuan Province, South China: implications for the nature of oceanic conditions after the end-Permian extinction. Palaios 18:388–402

Ezaki Y, Liu J, Nagano T, Adachi N (2008) Geobiological aspects of the earliest Triassic microbialites along the southern periphery of thetropical Yangtze Platform: initiation and cessation of a microbial regime. Palaios 23:356

Feldmann M, Mckenzie J (1997) Messinian stromatolite-thrombolite associations, Santa Pola, SE Spain: an analogue for the Palaeozoic? Sedimentology 44:893–914

Fischer A (1965) Fossils, early life, and atmospheric history. Proc Natl Acad Sci U S A 53:1205–1215

Franseen EK (1999) A review of Arbuckle Group strata in Kansas from a sedimentologic perspective. Open-file Report 49, Kansas Geological Survey, Lawrence

Freytet P, Duringer P, Koeniguer J-C, Lablanche G, Laurain M, Pons D (2001) Distribution and paleoecology of freshwater algae and stromatolites: IV, some examples from the Tertiary of the Parisian Basin and the Alsace Graben (France). Ann Paléontol 87:143–205

García-García F, Fernández J, Viseras C, Soria J (2006) High frequency cyclicity in a vertical alternation of Gilbert-type deltas and carbonate bioconstructions in the late Tortonian, Tabernas Basin, Southern Spain. Sediment Geol 192:123–139

Garcia-Pichel F, Al-Horani FA, Farmer JD, Ludwig R, Wade BD (2004) Balance between microbial calcification and metazoan bioerosion in modern stromatolitic oncolites. Geobiology 2:49–57

Garrett P (1970) Phanerozoic stromatolites: noncompetitive ecologic restriction by grazing and burrowing animals. Science 169:171

Garzanti E, Nicora A, Rettori R (1998) Permo-Triassic boundary and Lower to Middle Triassic in South Tibet. J Asian Earth Sci 16:143–157

Gebelein C (1969) Distribution, morphology, and accretion rate of recent subtidal algal stromatolites, Bermuda. J Sediment Res 39:49

Ginsburg RN (1960) Ancient analogies of recent stromatolites. XXI Int Geol Congr 22:26–35

Ginsburg RN, Isham LB, Bein SJ, Kuperberg J (1954) Laminated algal sediments of South Florida and their recognition in the fossil record. Unpublished Report, Marine Lab, Univ of Miami 54–20:1–33

Gischler E, Gibson MA, Oschmann W (2008) Giant Holocene freshwater microbialites, Laguna Bacalar, Quintana Roo, Mexico. Sedimentology 55:1293–1309

Glumac B (2001) Influence of early lithification on late diagenesis of microbialites: insights from δ^{18}O compositions of Upper Cambrian carbonate deposits from the Southern Appalachians. Palaios 16:593–600

Glumac B, Walker KR (1997) Selective dolomitization of Cambrian microbial carbonate deposits: a key to mechanisms and environments of origin. PALAIOS 12:98–110

Glumac B, Walker KR (2000) Carbonate deposition and sequence stratigraphy of the terminal Cambrian grand cycle in the Southern Appalachians, U.S.A. J Sediment Petrol 70:952–963

Goldhammer RK, Lehmann PJ (1993) The origin of high-frequency platform carbonate cycles and third-order sequences (Lower Ordovician El Paso Gp, West Texas): constraints from outcrop data and stratigraphic modeling. J Sediment Petrol 63:318–359

Gomez-Perez I (2003) An Early Jurassic deep-water stromatolitic bioherm related to possible methane seepage (Los Molles Formation, Neuquén, Argentina). Palaeogeogr Palaeocl 201:21–49

Götz S, Mitchell S (2009) The Laluziaarmini (gen. et spec. nov.) ecosystem: understanding a deeper-water rudist lithosome from the Early Maastrichtian of Mexico. Facies 55:539–551

Griffin K (1989) Microbial reefs on a carbonate ramp: a case study from western North America with a global perspective. AAPG Pacific Section Society, Palm Springs, 1989

Grotzinger J (1986) Cyclicity and paleoenvironmental dynamics, Rocknest platform, northwest Canada. Geol Soc Am Bull 97:1208–1231

Grotzinger J (1990) Geochemical model for Proterozoic stromatolite decline. Am J Sci 290(A):80–103

Haas J, Demény A, Hips K, Vennemann TW (2006) Carbon isotope excursions and microfacies changes in marine Permian-Triassic boundary sections in Hungary. Palaeogeogr Palaeocl 237:160–181

Heartsill RH (2010) Sedimentology of the Upper McKenzie Hill Formation (Ordovician), Slick Hills, southwestern Oklahoma. M.S. Thesis, Texas Christian University

Helm C, Schuelke I (2006) Patch reef development in the Florigemma-Bank Member (Oxfordian) from the Deister Mts (NW Germany): a type example for Late Jurassic coral thrombolite thickets. Facies 52:441–467

Herringshaw L, Raine R (2007) The earliest turrilepadid: a machaeridian from the Lower Ordovician of the Northern Highlands. Scot J Geol 43:97–100

Hersi O, Lavoie D, Nowlan G (2003) Reappraisal of the Beekmantown Group sedimentology and stratigraphy, Montreal area, southwestern Quebec: implications for understanding the depositional evolution of the Lower-Middle Ordovician Laurentian passive margin of eastern Canada. Can J Earth Sci 40:149–176

Heydari E, Hassandzadeh J, Wade WJ (2000) Geochemistry of central Tethyan Upper Permian and Lower Triassic strata, Abadeh region, Iran. Sed Geol 137:85–99

Hicks M, Rowland SM (2009) Early Cambrian microbial reefs, archaeocyathan inter-reef communities, and associated facies of the Yangtze Platform. Palaeogeogr Palaeocl 281:137–153

Hips K, Haas J (2006) Calcimicrobial stromatolites at the Permian–Triassic boundary in a western Tethyan section, Bükk Mountains, Hungary. Sediment Geol 185:239–253

Hoffman PF (1976) Environmental diversity of Middle Precambrian stromatolites. In: Walter MR (ed) Stromatolites. Developments in sedimentology 20. Elsevier, Amsterdam, pp 599–611

Holland SM, Patzkowsky ME (1999) Models for simulating the fossil record. Geology 27:491–494

Jansa L, Pratt B (1989) Deep water thrombolite mounds from the Upper Jurassic of offshore Nova Scotia. Reefs: Canada and adjacent areas. AAPG Memoir 13:725–735

Jones B, Renaut RW, Rosen MR, Ansdell KM (2002) Coniform stromatolites from geothermal systems, North Island, New Zealand. Palaios 17:84–103

Kahle C (1994) Facies and evolution of a Silurian coral-microbialite reef complex, Maumee, Ohio, USA. J Sed Res A6(4):711–725

Kahle C (2001) Biosedimentology of a Silurian thrombolite reef with meter-scale growth framework cavities. J Sediment Res 71:410–422

Kah LC, Grotzinger JP (1992) Early Proterozoic (1.9 Ga) thrombolites of the Rocknest Formation, Northwest Territories, Canada. Palaios 7:305–315

Keller M, Flugel E (1996) Early Ordovician reefs from Argentina: stromatoporoid vs stromatolite origin. Facies 34:177–192

Kelly SRA (1991) Antarctic stromatolites from the Late Jurassic of Alexander Island. Paleo News 12:12

Kennard JM, James NP (1986) Thrombolites and stromatolites: two distinct types of microbial structures. Palaios 1:492–503

Kershaw S, Zhang T, Lan G (1999) A ?microbialite carbonate crust at the Permian-Triassic boundary in South China, and its paleoenvironmental significance. Palaeogeogr Palaeocl 146:1–18

Kershaw S, Guo L, Swift A, Fan J (2002) ?Microbialites in the Permian-Triassic boundary interval in central China: structure, age and distribution. Facies 47:83–89

Kershaw S, Li Y, Crasquin-Soleau S, Feng Q, Mu X, Collin P-Y, Reynolds A, Guo L (2007) Earliest Triassic microbialites in the South China block and other areas: controls on their growth and distribution. Facies 53:409–425

Khanaqa PA (2011) Interpretation of new facies in the Pila Spi Formation (Middle-Late Eocene) in Sulaimaniyah, NE Iraq. Iraq Bull Geol Min 7:33–45

Kiessling W (2001) Phanerozoic reef trends based on the Paleoreef database. In: Stanley Jr GS (ed) The history and sedimentology of ancient reef systems. Kluwer Academic/Plenum Publishers, New York, pp 1–52

Kiessling W, Flügel E (2002) Paleoreefs—a database on Phanerozoic reefs. In: Kiessling W, Flügel E, Golonka J (eds) Phanerozoic reef patterns. Special Publication 72, SEPM. Tulsa, pp 77–92

Kiessling W, Flügel E, Golonka J (1999) Paleoreef maps: evaluation of a comprehensive database on Phanerozoic reefs. AAPG Bull 83:1552–1587

Kiessling W, Scasso R, Aberhan M, Ruiz L (2006) A Maastrichtian microbial reef and associated limestones in the Roca Formation of Patagonia (Neuquén Province, Argentina). Fossil Rec 9:183–197

Kirkham A (2005) Thrombolitic-Ortonella reefs and their bacterial diagenesis, Upper Visean Clifton Down Limestone, Bristol area, SW England. P Geol Assoc 116:221–234

Kirkland BI, Dickson JAD, Wood RA, Land LS (1998) Microbialite and microstratigraphy; the origin of encrustations in the Middle and Upper Capitan Formation, Guadalupe Mountains, Texas and New Mexico, USA. J Sediment Res 68:956

Krajewski K, Lesniak P, Lacka B, Zawidzki P (2000) Origin of phosphatic stromatolites in the Upper Cretaceous condensed sequence of the Polish Jura Chain. Sediment Geol 136:89–112

Krajewski M, Matyszkiewicz J, Król K, Olszewska B (2011) Facies of the Upper Jurassic-Lower Cretaceous deposits from the southern part of the Carpathian foredeep basement in the Krakow-Rzeszow area (southern Poland). Ann Soc Geol Pol 81:269–290

Lamond RE, Tapanila L (2003) Embedment cavities in lacustrine stromatolites: evidence of animal interactions from Cenozoic carbonates in U.S.A and Kenya. Palaios 18:445–453

Landing E, Westrop S, Knox L (1996) Conodonts, stratigraphy, and relative sea-level changes of the Tribes Hill Formation (Lower Ordovician, east-central New York). J Paleontol 70:656–680

Last FM, Last WM, Halden NM (2010) Carbonate microbialites and hardgrounds from Manito Lake, an alkaline, hypersaline lake in the northern Great Plains of Canada. Sediment Geol 225:34–49

Leggitt VI, Biaggi RE, Buchheim HP (2007) Palaeoenvironments associated with caddisfly-dominated microbial-carbonate mounds from the Tipton Shale Member of the Green River Formation: Eocene Lake Gosiute. Sedimentology 54:661–699

Lehrmann D (1998) Controls on facies architecture of a large Triassic carbonate platform: the Great Bank of Guizhou, Nanpanjiang Basin, South China. J Sediment Res 68:311

Lehrmann D, Wei J, Enos P (1998) Controls on facies architecture of a large Triassic carbonate platform: the Great Bank of Guizhou, Nanpanjiang Basin, South China. J Sediment Res 68:311–326

Link MH, Osborne RH, Awramik SM (1978) Lacustrine stromatolites and associated sediments of the Pliocene Ridge Route Formation, Ridge Basin, California. J Sediment Petrol 48:143–158

Logan BW (1961) Cryptozoon and associate stromatolites from the recent, Shark Bay, Western Australia. J Geol 69:517–533

Mancini E, Llinas J, Parcell W, Aurell M, Beatriz B, Leinfelder RR, Benson DJ (2004) Upper Jurassic thrombolite reservoir play, northeastern Gulf of Mexico. Am Assoc Petrol Geol Bull 88:1573–1602

Mancini E, Parcell W, Ahr W, Ramirez VO, Llinas JC, Cameron M (2008) Upper Jurassic updip stratigraphic trap and associated Smackover microbial and nearshore carbonate facies, Eastern Gulf coastal plain. Am Assoc Petrol Geol Bull 92:417

Martin J, Braga J (1994) Messinian events in the Sorbas Basin in southeastern Spain and their implications in the recent history of the Mediterranean. Sediment Geol 90:257–268

Martin J, Braga J, Riding R (1993) Siliciclastic stromatolites and thrombolites, late Miocene, SE Spain. J Sediment Res 63:131

Martindale RC, Zonneveld J-P, Bottjer DJ (2010) Microbial framework in Upper Triassic (Carnian) patch reefs from Williston Lake, British Columbia, Canada. Palaeogeogr Palaeocl 297:609–620

Mastandrea A, Perri E, Russo F, Spadafora A, Tucker M (2006) Microbial primary dolomite from a Norian carbonate platform: northern Calabria, southern Italy. Sedimentology 53:465–480

Mata SA, Bottjer DJ (2012) Microbes and mass extinctions: paleoenvironmental distribution of microbialites during times of biotic crisis. Geobiology 10:3–24

Matyszkiewicz J, Felisiak I (1992) Microfacies and diagenesis of an Upper Oxfordian carbonate buildup in Mydlniki (Cracow Area, Southern Poland). Facies 27:179–189

Matyszkiewicz J, Krajewski M, Kedzierski J (2006) Origin and evolution of an Upper Jurassic complex of carbonate buildups from Zegarowe rocks (Kraków-Wieluń Upland, Poland). Facies 52:239–263

Mazzullo SJ, Friedman GM (1977) Competitive algal colonization of peritidal flats in a schizohaline environment; the Lower Ordovician of New York. J Sediment Petrol 47:398–410

Miller KG, Kominz MA, Browning JV, Wright JD, Mountain GS, Katz ME, Sugarman PJ, Cramer BS, Christie-Black N, Pekar SF (2005) The Phanerozoic record of global sea-level change. Science 310:1293–1298

Moellerhenn S, Zamagni J, Košir A, Mutti M (2007) Thanetian coral-microbialites from the Norhtern Tethys (SW Slowenia): palaeoenvironmental interpretation. Geophys Res Ab 9:1–2

Montaggioni LF, Camoin GF (1993) Stromatolites associated with coralgal communities in Holocene high-energy reefs. Geology 21:149–152

Monty C (1965) Recent algal stromatolites in the Windward lagoon, Andros Island, Bahamas. Ann Soc Géol Bel 88:269–276

Moore KM (2010) Exploration of microbial deposits known as giant hams from the Lower Permian Laborcita Formation, Sacremento Mountains, New Mexico. MS Thesis, Mississippi State University

Myrow P, Tice L, Archuleta B, Clark B, Taylors JF, Ripperdan RL (2004) Flat-pebble conglomerate: its multiple origins and relationship to metre-scale depositional cycles. Sedimentology 51:973–996

Myshrall KL, Mobberley JM, Green SJ, Visscher PT, Havemann SA, Reid RP, Foster JS (2010) Biogeochemical cycling and microbial diversity in the thrombolitic microbialites of Highborne Cay, Bahamas. Geobiology 8:337–354

Nehza O, Woo K (2006) The effect of subaerial exposure on the morphology and microstructure of stromatolites in the Cretaceous Sinyangdong Formation, Gyeongsang Supergroup, Korea 1. Sedimentology 53:1121–1133

Neuweiler F, Mehdi M, Wilmsen M (2001) Facies of Liassic sponge mounds, Central High Atlas, Morocco. Facies 44:243–264

Noffke N, Chafetz H (2010) Microbial mats in siliciclastic depositional systems through time. Special Publication 101, SEPM. Tulsa , p.198

Noffke N, Paterson D (2008) Microbial interactions with physical sediment dynamics, and their significance for the interpretation of Earth's biological history. Geobiology 6:1–4

Nose M, Schmid D, Leinfelder R (2006) Significance of microbialites, calcimicrobes, and calcareous algae in reefal framework formation from the Silurian of Gotland, Sweden. Sediment Geol 192:243–265

Oliveri E, Neri R, Bellanca A, Riding R (2010) Carbonate stromatolites from a Messinian hypersaline setting in the Caltanissetta Basin, Sicily: petrographic evidence of microbial activity and related stable isotope and rare earth element signatures. Sedimentology 57:142–161

Olivier N, Lathuilière B, Thiry-Bastien P (2006) Growth models of Bajocian coral-microbialite reefs of Chargey-les-Port (eastern France): palaeoenvironmental interpretations. Facies 52:113

Olivier N, Pittet B, Gaillard C, Hantzpergue P (2007) High-frequency palaeoenvironmental fluctuations recorded in Jurassic coral-and sponge-microbialite bioconstructions. C R Palevol 6:21–36

Olóriz F, Reolid M, Rodríguez-Tovar F (2003) A Late Jurassic carbonate ramp colonized by sponges and benthic microbial communities (External Prebetic, Southern Spain). Palaios 18:528

Overstreet R, Oboh-Ikuenobe F, Gregg J (2003) Sequence stratigraphy and depositional facies of Lower Ordovician cyclic carbonate rocks, southern Missouri, USA. J Sediment Res 73:421–433

Parcell W, Warusavitharana CJ (2010) Stromatolite-thrombolite associations in the Lower Ordovician Cotter Dolomite at Hollister, Missouri, U.S.A. Geol Soc Am Abstr Progr 42:85

Parker B, Simmons G Jr, Love F, Wharton R Jr (1981) Modern stromatolites in Antarctic dry valley lakes. Bioscience 31:656–661

Paul J, Peryt T, Burne R (2011) Kalkowsky's stromatolites and oolites (Lower Buntsandstein, Northern Germany). In: Reitner J, Quéric NV, Arp G (eds) Advances in stromatolite geobiology. Springer, Berlin, pp 13–28

Pawellek T, Aigner T (2003) Apparently homogenous "reef-"limestones built by high-frequency cycles Upper Jurassic, SW-Germany. Sediment Geol 160:259–284

Pawellek T, Aigner T (2004) Dynamic stratigraphy as a tool in economic mineral exploration: ultra-pure limestones (Upper Jurassic, SW Germany). Mar Petrol Geol 21:499–516

Payne J, Lehrmann D, Wei J, Knoll A (2006) The pattern and timing of biotic recovery from the end-Permian extinction on the Great Bank of Guizhou, Guizhou Province, China. Palaios 21:63–85

Pedone V, Dickson J (2000) Replacement of aragonite by quasi-rhombohedral dolomite in a late Pleistocene tufa mound, Great Salt Lake, Utah, USA. J Sediment Res 70:1152

Perri E, Mastandrea A, Neri C, Russo F (2003) A micrite-dominated Norian carbonate platform from Northern Calabria (Southern Italy). Facies 49:101–118

Pittet B, Van Buchem FSP, Hillgartner H, Razin P, Grotsch J, Droste H (2002) Ecological succession, palaeoenvironmental change, and depositional sequences of Barremian-Aptian shallow-water carbonates in northern Oman. Sedimentology 49:555–581

Playford PE, Wallace MW (2001) Exhalative mineralization in Devonian reef complexes in the Canning basin, Western Australia. Econ Geol Bull Soc 96:1595–1610

Pope MC, Grotzinger JP, Schreiber BC (2000) Evaporitic subtidal stromatolites produced by *in situ* precipitation: textures, facies association, and temporal significance. J Sediment Res 70:1139–1151

Porada H, Bouougri E (2007) 'Wrinkle structures'—a critical review. In: Schieber J, Bose PK, Eriksson PG, Banerjee S, Sarkar S, Altermann W, Catuneau O (eds) Atlas of microbial mat features preserved within the clastic rock record. Elsevier, Amsterdam, pp 135–144

Power IM, Wilson SA, Dipple GM, Southam G (2011) Modern carbonate microbialites from an asbestos open pit pond, Yukon, Canada. Geobiology 9:180–195

Pratt B (1982) Stromatolite decline—a reconsideration. Geology 10:512–515

Pruss S, Bottjer D (2004) Late Early Triassic microbial reefs of the western United States: a description and model for their deposition in the aftermath of the end-Permian mass extinction. Palaeogeogr Paleocl 211:127–137

Pruss S, Bottjer D (2005) The reorganization of reef communities following the end-Permian mass extinction. C R Palevol 4:553–568

Pruss S, Bottjer D, Corsetti FA, Baud A (2006) A global marine sedimentary response to the end-Permian mass extinction: examples from southern Turkey and the western United States. Ear Sci Rev 78:193–206

Ramos E, Cabrera L, Hagemann HW, Pickel W, Zamarreno I (2001) Palaeogene lacustrine record in Mallorca (NW Mediterranean, Spain): depositional, palaeogeographic and palaeoclimatic implications for the ancient southeastern Iberian margin. Palaeogeogr Palaeocl 172:1–37

Reid RP, Visscher PT, Decho AW, Stolz JF, Bebout BM, Dupraz C, Macintyre IG, Paerl HW, Pinckney JL, Prufert-Bebout L, Steppe TF, DesMarais DJ (2000) The role of microbes in accretion, lamination and early lithification of modern marine stromatolites. Nature 406:989–992

Riding R (1992) Temporal variation in calcification in marine cyanobacteria. J Geol Soc 149:979–989

Riding R (2005) Phanerozoic reefal microbial carbonate abundance: comparisons with metazoan diversity, mass extinction events, and seawater saturations state. Rev Esp Micropal 37:23–39

Riding R (2006) Microbial carbonate abundance compared with fluctuations in metazoan diversity over geological time. Sediment Geol 185:229–238

Riding R, Liang L (2005) Geobiology of microbial carbonates: metazoan and seawater saturation state influences on secular trends during the Phanerozoic. Paleaogeogr Palaeocl 219:101–115

Riding R, Martin JM (1991) Coral-stromatolite reef framework, Upper Miocene, Almería, Spain. Sedimentology 38:799–818

Riding R, Tomas S (2006) Stromatolite reef crusts, Early Cretaceous, Spain: bacterial origin of *in situ*-precipitated peloid microspar? Sedimentology 53:23–34

Rodland DL, Bottjer DJ (2001) Biotic recovery from the end-Permian mass extinction: behavior of the inarticulate brachiopod *Lingula* as a disaster taxon. Palaios 16:95–101

Ruf M, Link E, Pross J, Aigner T (2005) A multi-proxy study of deeper-water carbonates (Upper Jurassic, southern Germany): combining sedimentology, chemostratigraphy and palynofacies. Facies 51:327–349

Rusnak GA (1960) Sediments of Laguna Madre, Texas. In: Shepard FP (ed) Recent sediments, northwest Gulf of Mexico, 1951–1958. American Petroleum Institute Project 51. AAPG, Tulsa, pp 153–196

Russo F, Mastandrea A, Stefani M, Neri C (2000) Carbonate facies dominated by syndepositional cements: a key component of Middle Triassic platforms. The Marmolada case history (Dolomites, Italy). Facies 42:211–226

Saint Martin J, Conesa G, Cornée J (1996) A new type of Messinian composite microbialitic build-up (Salemi, Sicily, Italy). Sediment Geol 106:51–63

Saint Martin J, Müller P, Moissette P, Dulai A (2000) Coral microbialite environment in a Middle Miocene reef of Hungary. Palaeogeogr Palaeocl 160:179–191

Sánchez-Almazo I, Braga J, Dinarès-Turell J, Martin JM, Spiro B (2007) Palaeoceanographic controls on reef deposition: the Messinian Cariatiz reef (Sorbas Basin, Almeria, SE Spain). Sedimentology 54:637–660

Sano H, Nakashima K (1997) Lowermost Triassic (Griesbachian) microbial bindstone-cementstone facies, southwest Japan. Facies 36:1–24

Schmidt DA (2006) Paleontology and sedimentology of calcifying microbes in the Silurian of the Ohio-Indiana region: an expanded role of carbonate-forming microbial communities. Dissertation, Ohio State University

Schubert JK, Bottjer DJ (1992) Early Triassic stromatolites as post-mass extinction disaster forms. Geology 20:883–886

Senowbaridaryan B, Flugel E (1996) A problematic fossil revealed—Pycnoporidium—Eomesoroicum Flugel, 1972 (Late Triassic, Tethys)—not an enigmatic alga but a strophomenid brachiopod (Gosaukammerella NG). Facies 34:83–99

Shapiro R (2004) Neoproterozoic-Cambrian microbialite record. In: Lipps JH, Waggoner BM (eds) Neoproterozoic-Cambrian biological revolutions. The Paleontological Society Special Papers, vol 10. Paleontological Society. Yale University Reprographics & Imaging Service, Lawrence, pp 5–15

Shapiro R, Awramik S (2000) Microbialite morphostratigraphy as a tool for correlating Late Cambrian-Early Ordovician sequences. J Geol 108:171–180

Shapiro R, Awramik S (2006) *Favosamaceria Cooperi* new group and form: a widely dispersed, time-restricted thrombolite. J Paleontol 80:411–422

Shapiro R, Fricke HC (2003) Microbial fossil record from the TePee Buttes (Upper Cretaceous, Colorado). Geol Soc Am Abstr Progr 34:381

Shapiro R, West R (1999) Late Paleozoic stromatolites: new insights from the Lower Permian of Kansas. Lethaia 32:131–139

Sheehan P, Harris M (2004) Microbialite resurgence after the Late Ordovician extinction. Nature 430:75–78

Shen JW, Webb G (2004) Famennian (Upper Devonian) stromatolite reefs at Shatang, Guilin, Guangxi, South China. Sediment Geol 170:63–84

Shen JW, Webb GE (2008) The role of microbes in reef-building communities of the Cannindah Limestone (Mississippian), Monto region, Queensland, Australia. Facies 54:89–105

Shen JW, Qing H (2010) Mississippian (Early Carboniferous) stromatolite mounds in a fore-reef slope setting, Laibin, Guangxi, South China. Int J Earth Sci 99:443–458

Sial AN, Peralta S, Ferreira VP, Toselli AJ, Acenolaza FG, Parada MA, Gaucher C, Alonso RN, Pimentel MM (2003) C-, O- and Sr- isotope chemostratigraphy of Cambrian carbonate sequences, Precordillera, Western Argentina. In: Proceedings of IV South American symposium on isotope geology, Recife, Brazil, 2003

Smith AB (2001) Large-scale heterogeneity of the fossil record: implications for Phanerozoic biodiversity studies. Philos Trans R Soc Lond B Biol Sci 356:351–369

Soudry D, Weissbrod T (1995) Morphogenesis and facies relationships of thrombolites and siliciclastic stromatolites in a Cambrian tidal sequence (Elat area, southern Israel). Palaeogeogr Palaeocl 114:339–355

Stephens N, Sumner D (2003) Famennian microbial reef facies, Napier and Oscar Ranges, Canning Basin, western Australia. Sedimentology 50:1283–1302

Stinchcomb BL (1986) New Monoplacophora (Mollusca) from Late Cambrian and Early Ordovician of Missouri. J Paleontol 60:606–626

Straccia F, Wilkinson B, Smith G (1990) Miocene lacustrine algal reefs—southwestern Snake River Plain, Idaho. Sediment Geol 67:7–23

Taylor JF, Loch JD, Perfetta PJ (1999) Trilobite faunas from Upper Cambrian microbial reefs in the Central Appalachians. J Paleontol 73:326–336

Valero-Garcés B, Arenas C, Delgado-Huertas A (2001) Depositional environments of Quaternary lacustrine travertines and stromatolites from high-altitude Andean lakes, northwestern Argentina. Can J Earth Sci 38:1263–1283

von Blanckenburg F, Mamberti M, Schonberg R, Kamber BS, Webb GE (2008) The iron isotope composition of microbial carbonates. Chem Geol 249:113–486

Walter MR, Heys GR (1995) Links between the rise of the metazoa and the decline of stromatolites. Precam Res 29:49–174

Wang W, Matsumoto R, Kakuwa Y, Mahmudy Gharaie MH, Li Y, Kano A, Matsuda N, Jansa L, Ueno K, Milroy P, Rahmati Ilkhchi M (2005) Chemostratigraphy of carbon and strontium isotopes on Permo-Triassic boundary in Zagros Mountains, Aligoudarz, Iran. Permophiles 45:31–36

Webb G (1998) Earliest known Carboniferous shallow-water reefs, Gudman Formation (Tn1b), Queensland, Australia: implications for Late Devonian reef collapse and recovery. Geology 26:951–954

Webb G (2005) Quantitative analysis and paleoecology of earliest Mississippian microbial reefs, Gudman Formation, Queensland, Australia: not just post-disaster phenomena. J Sediment Res 75:877–896

Weidlich O, Bernecker M (2011) Biotic carbonate precipitation inhibited during the Early Triassic at the rim of the Arabian Platform (Oman). Palaeogeogr Palaeocl 308:129–150

Wendt J (1982) The Cassian patch reefs (lower Carnian, southern Alps). Facies 6:185–202

Whalen MT, Day J, Eberli GP, Homewood PW (2002) Microbial carbonates as indicators of environmental change and biotic crises in carbonate systems: examples from the Late Devonian, Alberta basin, Canada. Palaeogeogr Palaeocl 181:127–151

Wignall PB, Twitchett RJ (2002) Permian-Triassic sedimentology of Jameson Land, East Greenland: incised submarine channels in an anoxic basin. J Geol Soc 159:691–703

Wilmsen M, Neuweiler F (2008) Biosedimentology of the Early Jurassic post-extinction carbonate depositional system, central High Atlas rift basin, Morocco. Sedimentology 55:773–807

Woo J, Chough S, Haz Z (2008) Chambers of *Epiphyton thalli* in microbial buildups, Zhangxia Formation (Middle Cambrian), Shandong Province, China. Palaios 23:55–64

Wood R (2000) Palaeoecology of a Late Devonian back reef: Canning Basin, Western Australia. Palaeogeogr Palaeocl 43:671–703

Wright DT (1993) Carbon isotope geochemistry of Cambrian stromatolites, N. W. Scotland. In: Studies on fossil benthic algae. Proceedings of the 5th international symposium on fossil algae, Capri, 7–12 April 1991

Zamagni J, Košir A, Mutti M (2009) The first microbialite-coral mounds in the Cenozoic (Uppermost Paleocene) from the Northern Tethys (Slovenia): environmentally-triggered phase shifts preceding the PETM? Palaeogeogr Palaeocl 274:1–17

Chapter 7
The Relationship Between Modern Mollusk Assemblages and Their Expression in Subsurface Sediment in a Carbonate Lagoon, St. Croix, US Virgin Islands

Karla Parsons-Hubbard, Dennis Hubbard, Caitlin Tems and Ashley Burkett

Contents

Abstract Much work has been done on the fidelity of a death assemblage to its present-day living community. Few studies, however, have extended this into the deeper subsurface in modern environments. This study examines the molluskan faunas accumulating at the surface in a reef/lagoon system on St. Croix, US Virgin Islands and compares those to the prefossilized assemblages in the subsurface to examine how faithfully surface assemblages are reflected in the sediment below.

K. Parsons-Hubbard (✉) · D. Hubbard
Department of Geology, Oberlin College, 52 W. Lorain St., Oberlin, OH 44074, USA
e-mail: karla.hubbard@oberlin.edu

C. Tems
Department of Earth Sciences, University of Southern California, 3651 Trousdale Pkwy, ZHS, Los Angeles, CA 90089, USA

A. Burkett
Department of Earth and Environmental Systems, Indiana State University, 200 North Seventh St., Terre Haute, IN 47809, USA

Data from 12 vibrocores through the Holocene section indicate that there is a very strong taphonomic filter in effect in the lagoon. The faunal constituents, their taphonomic signature, and the size classes represented in the surface assemblage are quite different from molluskan accumulations in deeper subsurface sediments. In fact, intense bioturbation by callianassid shrimp as deep as 3 m into the sediment has affected the entire sedimentary package resulting in a largely homogeneous section devoid of subsurface shell beds. The one exception to that pattern is a single shelly lag found at the bottom of the sediment package resting on the hard pre-Holocene surface. Most importantly, we find that the lag fauna does not resemble the modern life/death assemblage accumulating at the sediment surface. Dominant taxa in the modern life or death assemblage include small epifaunal gastropods and large bivalves. In contrast, small, thin-shelled infaunal bivalves dominate the lag along with agglutinated polychaete tubes, decapod remnants, and shell fragments. Our data suggest that the shell-rich accumulation deep within the sediment package is a time-averaged concentration of predominantly small infaunal mollusks deposited over time by deep burrowing callianassid crustaceans. Moreover, the extent of bioturbation within the lagoon suggests that some of the widely accepted live–dead paradigms may not be as robust as generally assumed.

Keywords Taphonomy · Shell beds · Live/dead fidelity · *Callianassa* · *Thalassinoides* · Reef lagoon · Bioturbation · US Virgin Islands

7.1 Introduction

Carbonate depositional environments have been the focus of experimental work on the fidelity between modern living invertebrate assemblages to their death assemblages and, by extrapolation, to the fossil record. Shell beds result from the accumulation of skeletal material over some usually unknown period of time and represent varying degrees of time averaging (Kidwell and Bosence 1991). Some beds reflect rapid burial events that capture a snapshot of a living community whereas others result from decades to millennia of slower accumulation, reworking, transport, and redeposition (Flessa et al. 1993). These end-members offer different kinds of information (see Kidwell and Flessa 1995 for a summary discussion) and it is important to understand where a particular assemblage falls along this spectrum. Despite the robust literature examining live–dead fidelity within marine shelly assemblages in modern surface sediments (Miller 1988; Kidwell and Flessa 1995; Kidwell 2001, 2002a, b; Tomasovych 2004; Tomasovych and Rothfus 2005; Lockwood and Chastant 2006; Olszewski and Kidwell 2007; Tomasovych and Kidwell 2011), there are few studies that take the critical next step and compare the surface assemblages to shell accumulations in deeper, unlithified subsurface sediment packages (but see Kosnik et al. 2007, 2009) where shells are sequestered below the taphonomically active zone (TAZ; Davies et al. 1989).

Studies suggest that faunas accumulating farther below the sediment surface may be significantly different from either the live or dead fauna found closer to

the surface and may bear only a minor resemblance to the present-day fauna. Rivadeneira (2010) found that only about one-half of extant bivalve species from the Pacific coast of South America are represented in the Quaternary fossil record of adjacent onshore outcrops. The question becomes whether this difference reflects a significant environmental shift since the Quaternary or differences in accumulation, burial, and ultimate fossilization. Without any assurance that surface death assemblages will be faithfully preserved throughout the burial process, it cannot be assumed that good live–dead fidelity within assemblages presently accumulating at the sediment surface is a good estimator for the character of the fossil record. Although the taphonomic filter acting at the levels of live community and modern death assemblage has been shown to have only a small effect, the taphonomic filter acting on shell accumulations that are below the surface may be much stronger, especially in environments affected by intense bioturbation.

Several studies have addressed the extent of faunal mixing in the subsurface by dating individual shells. Flessa et al. (1993) have shown that subsurface shelly zones (up to 50 cm deep) in Holocene deposits of Baja California contain shells with widely varying ages (767 to 3,212 calBP). More recently, Kosnik et al. (2007; 2009; 2013) used radiocarbon and amino acid racemization dating to examine stratigraphic order and mixing of the top 1.25 m of sediment in the lagoon near Rib Reef on the Australian Great Barrier Reef. Pruss et al. (2011) radiocarbon dated a suite of beach shells from San Salvador Island, Bahamas and found a mix of dates ranging from > 6,000 years before present through Recent. All of these studies show a large degree of time averaging based on both shell age and taphonomic grade within the upper meter of sediment in the lagoons. Suggested mechanisms include storm reworking and burrowing by the decapod crustacean *Callianassa* spp.

The thalassinid crustacean group that includes the callianassids influences sedimentary sequences worldwide (Dworschak 2000). Tudhope and Scoffin (1984) recognized the important role played by callianassid shrimp in influencing the potential fossil record accumulating in reef lagoons. Using dyed sediment as tracers, they documented how feeding by *Callianassa* actively sorts sediments. Grains of all sizes fall into their burrows, but only those finer than 1 or 2 mm are ejected back out of the burrow to create a mound of fine sediment that surrounds the entrance (Roberts et al. 1982; Suchanek 1983; Kosnik et al. 2009). Coarser clasts, including gravel-sized molluskan remains, were concentrated throughout the shallow subsurface, implying that the shrimp sequester the coarse fraction into side chambers of their burrow system. It has been suggested that these activities thereby create a well-sorted, gravel-free upper section overlying a coarser-grained layer that is dominated by well-preserved infaunal shell species (Tudhope and Scoffin 1984). The depth of burrowing will influence the thickness of the fine-grained surface layer and should influence the depth of the expected lag deposits.

In another study, Miller and Curran (2001) experimented with thalassinid shrimp in Mugu Lagoon, California and concluded that the shrimp are capable of moving aside large obstacles (in their experiment they used 2 × 2 cm glass plates) but can also work around dense shell beds and other impenetrable obstacles. Epoxy resin casts of burrows along with sediment coring studies have measured depths of burrowing up to 2.5 m (Tudhope and Scoffin 1984; Shinn 1968; Suchanek 1983; Felder
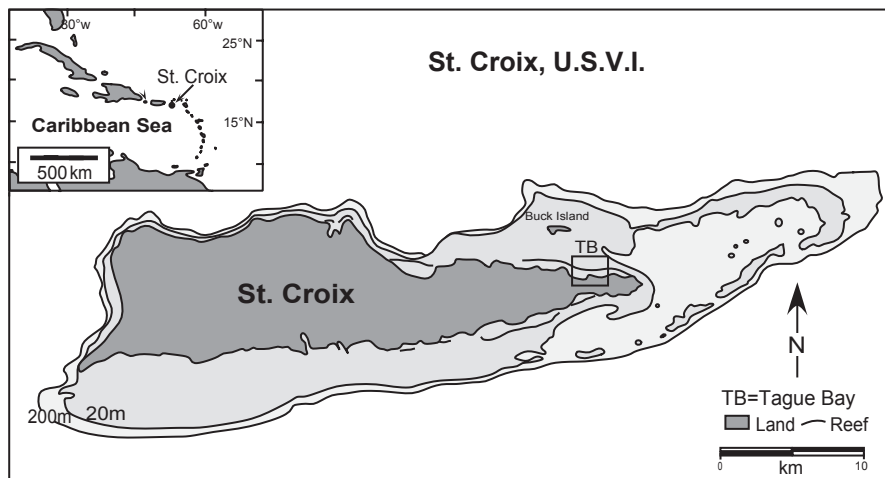
Fig. 7.1 Location map for St. Croix in the US Virgin Islands. Study area in Tague Bay Lagoon is located on the east end of the island designated by the *box labeled* TB

and Staton 1990). Therefore, the active mixing of lagoon sediments may be substantial and may obliterate stratigraphic layering to a considerable depth.

The Tague Bay system on northeastern St. Croix (US Virgin Islands; Fig. 7.1) is a locality where both near-surface living/death assemblages and the character and extent of *Callianassa* activities have been examined in detail. Miller (1988), Parsons-Hubbard (2005), Ferguson and Miller (2007), and others characterized the faunal and taphonomic makeup of surface invertebrate assemblages from the perspective of paleontology. Their primary questions included: (1) What is the faunal makeup of reef/lagoon-related surface assemblages? (2) What is the taphonomic signature of faunas within these assemblages? (3) How well does the death assemblage relate to the living community at any one point in time? (4) Does the death assemblage reflect faunal changes on a decadal scale?

After decades of study of surface environments at this site, we have cored through the Holocene sediment package to compare shell accumulations within and below the taphonomically active zone to death assemblages presently accumulating at the surface. This chapter adds an analysis of the deeper subsurface to evaluate the preservability of modern communities in a lagoon affected by deep bioturbation. In addition to the important questions above we add the following: (1) Are these modern environments ripe for preservation? (2) What are the pitfalls related to assuming that either live or dead surface communities mimic what is buried deeper in the lagoon sediments? (3) If the surface assemblages do not directly relate to assemblages at depth, do surface assemblages really have anything useful to tell us about the fossil assemblages that are preserved in analogous sedimentary environments?
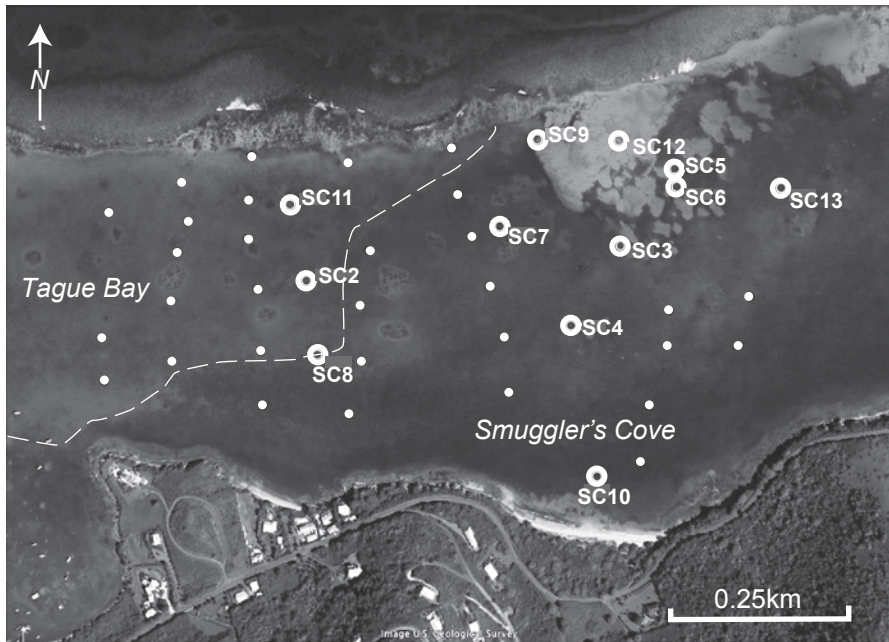
Fig. 7.2 Satellite image (Google Earth, image date 10/31/06) of Tague Bay and Knight Bay/ Smuggler's Cove. *Large open circles* indicate coring sites. Sediment depth probe sites are small *white dots*. The lagoon is floored by dense sea grass (*Thallassia*), which appears *dark* on the image; *light areas* are either open sand or areas with sparse sea grass and *Callianassa* shrimp mounds. West of the *dashed line* the lagoon floor is dominated by shrimp mounds, to the east sea grass is more typical. The reef is located along the north side of the image. The lagoon is approximately 1 km from the shore to the reef

7.2 Methods

7.2.1 Study Area

St. Croix, the largest of the US Virgin Islands (Fig. 7.1) is the easternmost island in the Greater Antilles. Unlike St. Thomas and St. John to the north, St. Croix is primarily sedimentary in origin (Whetten 1966). The eastern and western ends of the island are dominated by upturned Cretaceous volcaniclastic sediments of the Caledonia Formation. The central section of the island is dominated by carbonate deposition within a graben that formed as a result of left-lateral faulting along the Caribbean-North Atlantic boundary (Gill et al. 2002).

Tague Bay and Smuggler's Cove (also known as Knight's Bay) are located on the north shore of St. Croix, USVI (Figs. 7.1 and 7.2). The lagoon is approximately 1 km wide and is bound to the north by a fringing reef that reaches to sea level. Trade winds affect the area and seas (1–2 m) approach the reef generally from the

Fig. 7.3 Photograph of typical lagoon floor influenced by callianassid shrimp. Mounds of ejected fine sediment can reach 75 cm in height

ENE; storm waves can exceed 5 m (Lugo-Fernandez et al. 1998). The lagoon is floored by carbonate sand with sparse patch reef development. Over the past two decades, coral cover has decreased dramatically and bioerosion has reduced these to low rubble mounds. In some areas of the lagoon, sediment is stabilized by sea grass beds that increase in density to the east (Fig. 7.2). Areas with lighter sea grass cover are dotted with mounds of sand created by the burrowing ghost shrimp *Callianassa* (Fig. 7.3). Previous work on the geologic history of the reef/lagoon system includes rotary drilling of the fringing reef and back reef areas that establish the pace of reef development and the general shape of the Pleistocene precedent topography beneath, constraining the development of the reef-lagoon system (Adey 1975, 1978; Adey and Burke 1976; Burke et al. 1989).

7.2.2 Field and Laboratory Methods

Twelve locations (Fig. 7.2; Table 7.1) were sampled using a diver-operated vibrocoring device consisting of a 5 cm diameter hydraulic concrete vibrator head attached to aluminum core pipe using a custom-designed clamp with handles. The hydraulic motor was operated from a vessel anchored nearby. Cores were collected in aluminum irrigation pipe, 4.6 m long and 7.6 cm in diameter. Divers assembled the pipe and vibrating head on the bottom, moved it into a vertical position and started vibrocoring using a control mechanism on the coring unit. Coring continued until the pipe would no longer penetrate the bottom (presumably when it hit the lithified pre-Holocene subsurface) or until there was about 50 cm of pipe remaining above ground, enough to attach the extraction device. Excess pipe was removed

Table 7.1 Location, depth, and surface environment for each core. Core length is uncompacted length of sediment in core based on measurements inside and outside core pipe before extraction

Core	Location	Water depth	Core length	Environment
SC2	17.759600°N 64.597310°W	4.5 m	3.1 m	Callianassid mounds
SC3	17.760080°N 64.592770°W	4.2 m	2.8 m	Dense sea grass
SC4	17.758980°N 64.593490°W	3.6 m	3.8 m	Dense sea grass
SC5	17.761140°N 64.591990°W	4.5 m	1.75 m	Disturbed sand bottom
SC6	17.760890°N 64.591960°W	4.5 m	1.7 m	Disturbed sand bottom
SC7	17.760350°N 64.594520°W	3.7 m	3.3 m	Dense sea grass
SC8	17.758581°N 64.597156°W	5.2 m	2.2 m	Callianassid mounds
SC9	17.761550°N 64.593970°W	4.2 m	4.4 m	Dense sea grass
SC10	17.756909°N 64.593111°W	2.2 m	2.6 m	Dense sea grass
SC11	17.760650°N 64.597552°W	5.5 m	4.3 m	Callianassid mounds
SC12	17.761530°N 64.592800°W	4.6 m	3.0 m	Disturbed sand bottom
SC13	17.760880°N 64.590450°W	3.7 m	4.1 m	Dense sea grass

with a hacksaw and measured to determine the length of the remaining core pipe. Measurements to the sediment surface both inside and outside the core pipe were used to calculate the depth of penetration and the compaction during vibrocoring. The exposed pipe end was capped, extractor handles attached, and the core pipe was pulled from the bottom using a small air-filled lift bag. As soon as the bottom of the pipe was visible, another cap was placed over it to avoid loss of sediment. The pipe was kept vertical from the moment of extraction. On the surface, the uppermost section of the core tube that was still filled with water was cut off and a new cap was fixed in place, leaving only well-constrained sediment in the tube.

On shore, the core pipe was laid in a cradle and sawn in half. The core was photographed, logged, and one half of each core was sampled in alternating 8 cm and 12 cm intervals. The 8 cm sections were collected for sediment-constituent and grain-size analyses. The 12 cm intervals were sieved with a 2 phi (0.25 mm) sieve to isolate the mollusks and other coarse material. All mollusks in the 12 cm intervals were identified, counted, and assessed for taphonomic grade following the methods of Parsons-Hubbard (2005). Each shell was scored with respect to breakage, encrustation, abrasion, articulation, dissolution/microboring damage, edge rounding, and loss of color (Fig. 7.4). The average scores for each core level were combined
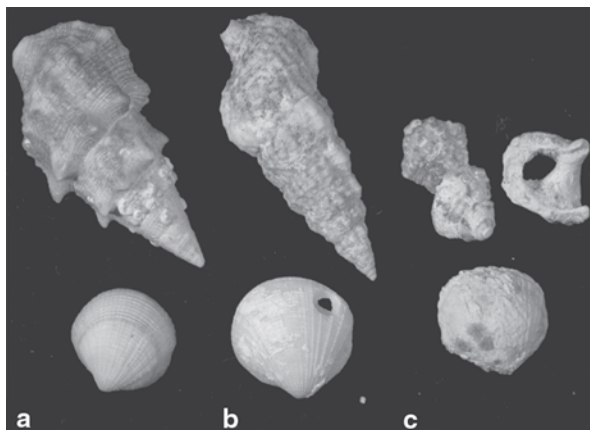
Fig. 7.4 Examples of taphonomic grade. **a** Low taphonomic grade: *Cerithium* sp. with original color, no abrasion, dissolution, and minor encrustation; bivalve, *Codakia costata,* with no encrustation, sharp ornamentation, and no dissolution. **b** Moderate taphonomic grade: Cerith with faded color, mild abrasion and some dissolution; *Codakia* with drill hole and some dissolution. **c** High taphonomic grade: fragmented, dissolved, and encrusted cerith; heavily encrusted and dissolved bivalve

to determine a general taphonomic grade. The longest axis of each mollusk was measured in the 12 cm section of three cores. The bottom 30 cm of the other half of each core was collected, sieved, and all constituents of these "lag" samples were identified.

At each coring site (Fig. 7.2; Table 7.1), two replicate samples of a 0.5 m × 0.5 m area of the surface sediments were collected using an airlift device consisting of 7.6 mm diameter PVC pipe connected to a SCUBA tank. Air entered the pipe near its lower end and rose to create suction that lifted all sediment, shell, and other debris into a 0.5 cm-mesh bag attached to the upper end. All (live and dead) mollusks collected in these airlift samples were sorted, rinsed, identified, and assessed for taphonomic grade to establish the "typical" assemblage presently accumulating in the lagoon. The initial objective was to use these to identify temporal changes in the distribution of lagoon environments over the time represented in the cores.

Additional information on the thickness of the sediment package in Tague and Knight bays was gathered using a thin (9.5 mm), 4.6 m-long steel reinforcing bar that a diver inserted into the sediment until it stopped. Multiple measurements were taken at each site and were averaged to compute the depth to the hard subsurface of the bay. Water depth at each site was determined using a digital depth gauge. Tidal range is less than 20 cm and was disregarded in water depth readings. Probing positions were located from the surface by handheld GPS.

Sediments from the 8-cm sample intervals were washed and dried. A subsection was sieved at 0.5-phi intervals to compute mean grain size and standard deviation. A smaller subsample was impregnated in epoxy, and cut parallel to the direction of

settling. Thin sections were prepared for constituent analysis. Using a polarizing microscope, transects were run at 1-mm intervals. Every grain larger than 0.25 mm was identified and recorded until 100 grains had been counted.

Three of the mollusk lags from the base of the cores were subsampled and radiocarbon dated at Beta Analytic, Inc. Isotopic analyses were used to calibrate the raw ^{14}C ages to cal BP. These ages were used to constrain the general relationship between the initial deposition of the shells and the sedimentary history of the lagoon. Uncorrected ages from previous studies of nearby reef cores were converted to cal BP using the freeware program Calib 6, which we have found to provide similar ages to those of Beta Analytic, Inc.

7.2.3 Data Analysis

Shells were identified to species level where possible. Some taxa were not identified to species, however, so data analyses using shell taxa were done at the generic level for uniformity. We used the nonmetric multidimensional scaling (NMMDS) technique to plot relatedness of each level from all cores to each other as well as to surface samples and basal lag intervals based on taxa grouped into life-habit guilds. The guilds included: (1) small infaunal bivalves, (2) larger, shallow-burrowing bivalves, (3) infaunal gastropods, (4) epifaunal gastropods, (5) epifaunal bivalves, and (6) epifaunal limpets and limpet-like gastropods. A cluster analysis was run on surface samples from three sites that were dominated by callianassid shrimp mounds and four sites where sea grass was dense and callianassid mounds were rare. This was done to test whether the surface mollusks differed between the two environments and to establish whether there is a typical sea grass mollusk "signature" that is distinct from a typical bioturbated sand assemblage. Both multivariate tests were done using Bray-Curtis dissimilarity coefficients (Bray-Curtis is a good choice when data are entered as proportion of the sample size) using the freely available statistical software PAST v.2.17c (Hammer et al. 2001).

7.3 Results

7.3.1 Life and Death Assemblages at the Sediment Surface

The two most typical surface environments in the lagoon today are sea grass environments and areas with sparse sea grass that are populated by many callianassid shrimp mounds. Cores SC4, SC10, SC13, and SC3 (Fig. 7.2) have dense sea grass at the surface and were chosen to represent that environment. Surface samples at sites SC11, SC2, and SC8 were chosen to represent shrimp-dominated environments based on density of mounds at the sediment surface. Using combined live and dead faunal data from these sites, we found that sea grass assemblages accumulating at

Fig. 7.5 Cluster analysis of samples collected from the surface at three sites dominated by callianassid shrimp mounds (2-1, 2-2, 8-1, 8-2, 11-1, 11-2) and four sites with dense sea grass at the surface (3-1, 3-2, 4-1, 4-2, 10-1, 10-2). *Stippled area* of cluster highlights sea grass samples and *shaded area* highlights shrimp mound samples
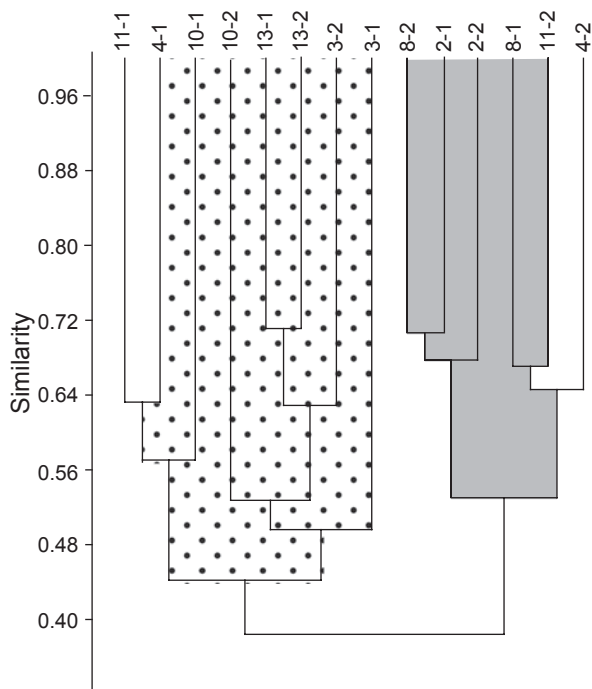
the surface differ from shrimp mound areas by having a much more diverse fauna with higher abundances within the common taxa.

Approximately nine taxa were unique to the sea grass areas including the gastropods *Columbella, Conus, Modulus,* and *Nitidella,* the epifaunal bivalves *Anadara* and *Pinna,* the limpet *Acmaea,* and the infaunal bivalves *Lucina, Strigilla*, and *Transennella*. Only one species is unique and abundant in the shrimp mound areas, the infaunal predatory gastropod *Bulla striata*. Two additional genera were more abundant in the shrimp mound areas, the epifaunal gastropod *Cerithium* and the small infaunal bivalve *Tellina*. Four genera were common to both sea grass and shrimp mound areas, but were more abundant in the sea grass environment including the gastropods *Nassarius, Tricolia,* and *Tegula*, and the large infaunal bivalve *Codakia*.

A cluster analysis of the surface faunas at these seven sites (Fig. 7.5) shows two distinct groupings of taxa that align with the two surface environments. Only two samples, one replicate from site SC11 and one from SC4, plotted with the "wrong" environmental group. For the most part, therefore, the death assemblage accumulating at the surface in shrimp mound areas is distinct from the assemblage in dense sea grass areas.
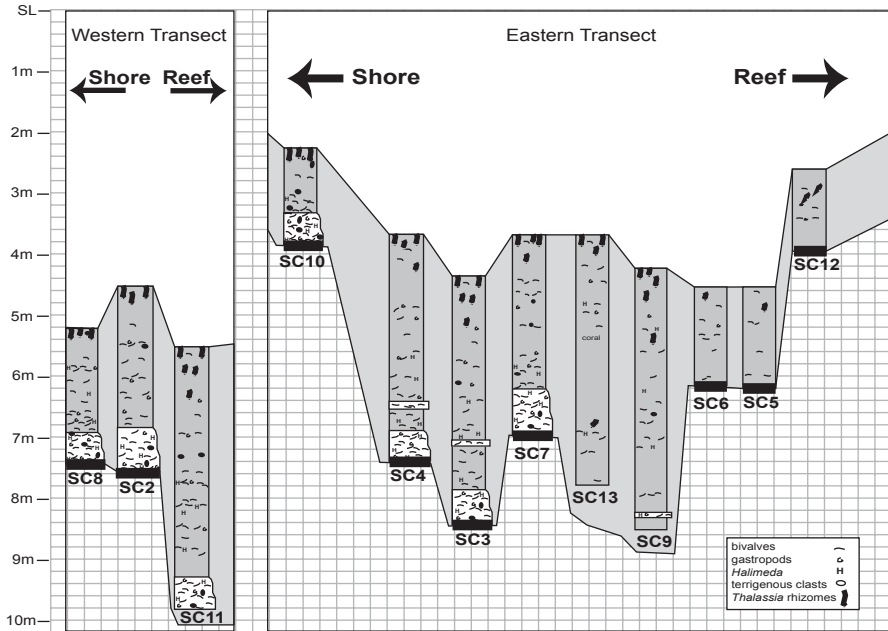
Fig. 7.6 Core diagrams arranged roughly in transects across the lagoon from shore to reef. Core heights are decompacted lengths with *black bars* across the bottom of the column for cores that reached the hard (Pleistocene) subsurface. Sea level is at the *top* of the diagram and cores are placed vertically and horizontally based on water depth and location across the lagoon, respectively. Most cores have a coarse shelly lag at their base, but have less shell content in the main body of the core

7.3.2 General Patterns Within Cores

Core length averaged 2.7 m (maximum = 4.3 m: SC11, Figs. 7.2 and 7.6). Nine of the twelve cores struck a hard surface (presumably Pleistocene; Fig. 7.6). The depth to this surface exceeded the length of our coring tubes at site SC11 where probes of the sediment confirm the thickest sediment package in the lagoon (4–5 m).

Most cores have sea grass rhizomes near the top and shells are sparse throughout with shell density increasing toward the bottom (Figs. 7.6 and 7.7). Seven of the twelve cores have a shell-rich section at the bottom ranging from 20 cm to nearly a meter in thickness. These shelly "lags" also include *Halimeda,* agglutinated tubes attributed to polychaetes, small crab fragments, and occasional terrigenous pebbles (Figs. 7.7 and 7.8). Cores 5, 6, and 12 from the bare sand patch immediately behind the reef are the shortest cores collected, contain the least mollusk material, and had no basal lag.
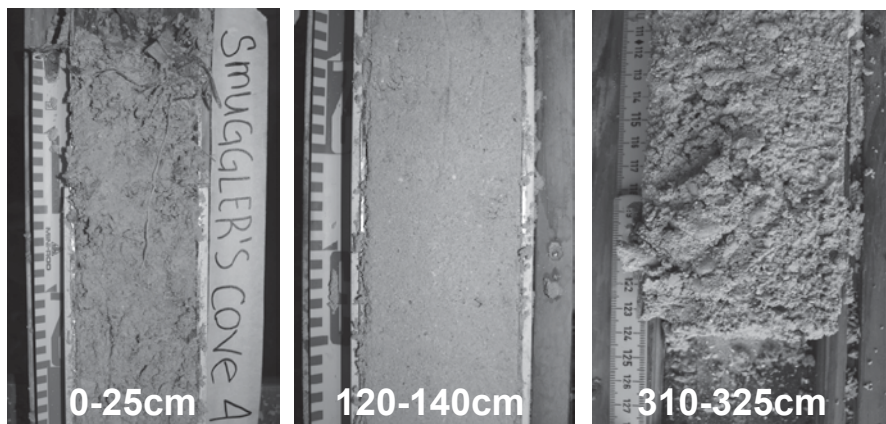
Fig. 7.7 Photographs of core segments. Photographs of *top* (*left*), *middle,* and *bottom* (*right*) of core SC4 from the center of the lagoon. Sea grass rhizomes are common near the top of the core, the middle of the core has very sparse coarse constituents, and the coarse fraction increases to a dense lag at the bottom
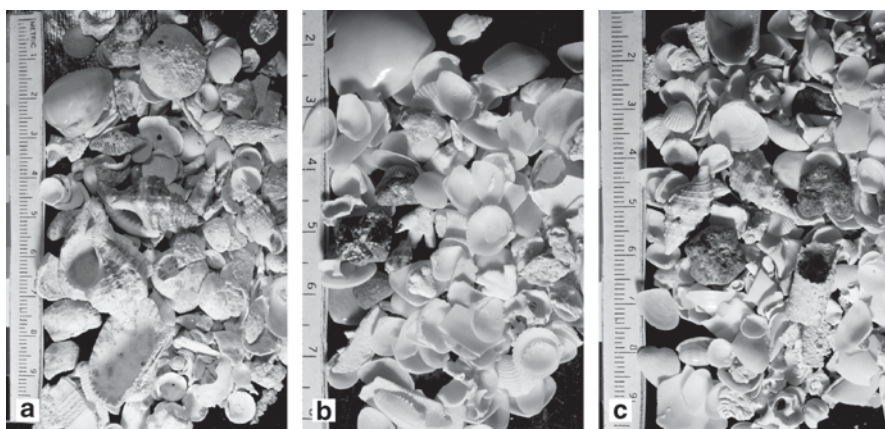
Fig. 7.8 Examples of mollusk material from 12-cm sections of core SC3. **a** The surface airlift sample contains many large epifaunal gastropods and the shells are encrusted, bored, and generally taphonomically degraded. **b** The *middle* section of the core (208–220 cm) is characterized by small infaunal bivalves in good condition. **c** The lag deposit showing a mix of small epifaunal gastropods, small infaunal bivalves, some terrigenous pebbles, and agglutinated polychaete tubes

In all cores, sediments are somewhat homogeneous with no well-formed coarse or shelly layers. In general, grain size increases down core (Fig. 7.9). The finest fraction of the lagoon sediments is dominated by coral fragments. The coarser fraction is dominated by *Halimeda* and mollusk shells and shell fragments. Intraclasts also contribute significantly to the coarse fraction of the sediment in the cores. The upper meter has a mean grain size between medium sand (1.5 phi) and fine sand
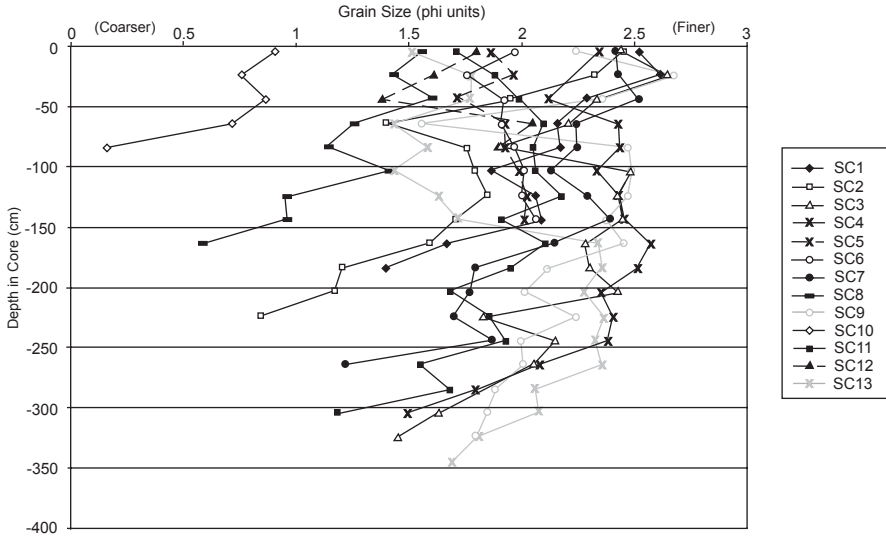
Fig. 7.9 Grain-size analysis. All cores are plotted with surface at the top. Note that most cores increase in grain size with depth in the core. Short cores from the sandy backreef zone are drawn with *dashed lines*. *Grayed lines* are cores that did not reach the hard subsurface. *Black lines* are cores that reached the hard subsurface

(2.5 phi). Below that, mean grain size increases to coarse sand. The nearshore core (SC10) was the coarsest throughout with gravel becoming a major constituent toward the bottom. Most of the coarsening in grain size below 1 m within the cores is related to greater *Halimeda* content and increasing numbers of small, disarticulated bivalves as well as agglutinated polychaete tubes and, in nearshore cores, the addition of small dark gray to black terrigenous clasts.

7.3.3   The Character of the Lag Deposits

Lag deposits sit directly on top of the pre-Holocene surface and are dominated by about 80–90 % small, infaunal bivalves. Also present are sparse (~5 %), small, epifaunal gastropods and a mix of shell fragments. In addition to the mollusk fraction, much of the coarse nature of the lag can be attributed to an abundance of *Halimeda*. Agglutinated tubes ranging in diameter from 3 to 8 mm are also common (Fig. 7.7c). These tubes are likely made by polychaetes and do not represent linings of *Callianassa* burrows (A. Curran, pers. comm.). These tubes are formed from a wide range of local sedimentary particles including coral and mollusk fragments, *Halimeda* fragments, and other constituents common to the lagoon. *Callianassa* tend to build their agglutinated burrow linings from fecal pellets giving them a more ordered appearance (Miller and Curran 2001). Additionally, the tubes found in the lags are smaller in diameter than typical *Callianassa* burrows. Also common in the lag are

small decapod crustacean claws that range from only a few millimeters to a maximum of about 1 cm in total length. If these are the remains of callianassid shrimp, they only represent juveniles based on their small size. Lastly, the lags sometimes contain terrigenous pebbles from the Caledonia Formation (a dark gray to black volcaniclastic siltstone exposed on shore), especially in cores closer to shore.

7.3.4   Molluskan Faunas Within Cores

Below the top 20 cm in each core, mollusks are sparse and diversity is generally low for the first meter (see Appendix, Fig. A.1). Diversity and abundance remain low, but increase down core, until 50–100 cm from the base, where a rapid rise in both gives way to a shelly lag deposit. The dominant mollusks within the core are small, thin-shelled bivalves including *Tellina agilis* (n.b. *caribbea*), *Americardia guppyi, Chione pygmaea, Pitar* spp., *Codakia costata,* and *Abra* spp. The infaunal gastropod *Bulla striata* is a fairly common member of the molluskan fraction in the core as well. *Nassarius albus* and *Cerithium* spp. are typical epifaunal gastropods within the cores but the ceriths are often broken and taphonomically degraded. *Nassarius,* however, tends to be in better condition than the ceriths.

In general, small infaunal bivalves are the dominant species within the core, reaching 75–100 % of individuals belonging to the guild (Fig. A.1). Surface samples tend to have a more even distribution of taxa while down core smaller, thin-shelled bivalves become increasingly dominant and move the evenness toward a value of one (severe dominance of a single taxon). In some cases there were hundreds of small bivalves with only one or two other guilds represented in a sample.

Cores SC5, SC6, and SC12 (Fig. A.1; blowout area) exhibit a different pattern. While shell content remains low overall and is still dominated by infaunal bivalves, there is no accumulation of coarse debris at their bases. These cores are short compared to most others and all three reached the hard subsurface. These cores were taken in a broad sandy area just behind a low spot in the reef that allows higher wave energy to reach the lagoon (Figs. 7.2 and 7.6).

7.3.5   Taphonomic Condition of the Molluskan Fauna

There is a marked contrast in taphonomic grade between mollusks collected by airlift (upper 20–30 cm), and those within the core and the shelly lag. Infaunal shells are consistently in better condition than their epifaunal counterparts (Fig. 7.8). Surface shells are generally in the most degraded state of all samples collected (Fig. A.1) despite the fact that the surface samples include more large and thick-shelled species and also contain live mollusks that are in excellent condition. In general, however, only the live portion of the surface sample is in good condition.

The death assemblage at the surface is encrusted, fragmented, and bored; shell carbonate appears dissolved or microbioeroded (Figs. 7.4c and 7.8). Shell material

below about 20 cm in the cores tends to be in moderate to excellent condition. The small bivalves are most often pristine whereas the gastropod portion of a sample tends to be in poorer condition (Fig. A.1). This was true for all samples, whether near the surface or at the bottom of the core. For example, a sample from 2 m deep within core SC3 shows the bivalve fraction in excellent condition compared to the epifaunal gastropods (Fig. 7.8b). The lag deposits generally follow the same taphonomic pattern. Evidence for surface dissolution of shells is most evident in the uppermost 20 cm of the core. Within the overall core and in the lag, taphonomic traits are mostly limited to fragmentation and minor dissolution and/or microbioerosion.

7.3.6 Geometry and Age of the Sediment Package

Based on probes and cores that reached the hard subsurface layer of the lagoon, the sediment package is about 1 m thick near the shoreline and reaches its thickest point in the northwest portion of the study area. The antecedent topography in the immediate back reef is irregular, and sediment thickness varies from over 4 m in the west to around 1 m in the area of cores 5, 6, and 12. This area stands out as a sandy area in the back reef behind a reef crest that does not rise all the way to sea level (Fig. 7.2). This allows storm wave energy, as well as daily swell, to come over the reef and mobilize the sandy bottom. Sea grass does not take hold here, nor does *Callianassa* occupy the sediment. It is not clear what the connection is between the low spot in the reef and the rise in antecedent topography below the sediment package in the back reef at this location. This sandy "blowout", however, has been a consistent feature of the bay back to the oldest air photos examined (1962).

Radiometric ages (^{14}C) of bulk mollusk samples in the basal lags of cores SC8, SC4, and SC7 were 3500, 3100, and 2800 cal BP, respectively. These cores were chosen because each of these lag deposits sat directly on the Pleistocene surface. Based on radiocarbon dates from corals collected in drill cores from the adjacent reef (Adey 1975, 1978; Adey and Burke 1976; Burke et al. 1989), this area of the lagoon likely flooded ~6000–7000 cal BP. Therefore, the bulk dates of shells from the lags hint at time averaging over the entire post-flooding interval.

7.3.7 Comparison of Lag Taxa to Surface Faunas and to Deeper Taxa

The lagoon in Tague Bay and Smuggler's Cove on the north shore of St. Croix is a fairly typical modern reef lagoon with sparse to dense cover by sea grass and areas of open sand with active bioturbation by thalassinid shrimp. Analyses of mollusk faunas both at the surface and in the subsurface reveal that the two communities bear little resemblance to one another. It is likely that strong bioturbation of the lagoon sediments, extending over 3 m into the subsurface, has strongly biased the subfossil record throughout and has eliminated any stratification or shell bed formation

Table 7.2 Differences between core and lag, and airlift and lag

Core site	Total genera (core + lag + surface)	% of core genera in lag	% of surface genera in lag
Back reef bare sand patch			
SC5	10	38	14
SC6	19	23	14
SC12	20	14	6
Sites with poor surface representation in lag			
SC3	34	54	39
SC4	22	63	47
SC7	31	75	59
SC8	28	92	67
SC9	21	50	33
SC11	23	53	27
SC13	29	45	28
Well-mixed core, surface, & lag			
SC10	26	89	80
SC2	23	68	89

aside from the shelly lag deposit at the base of each core atop the hard Pleistocene surface below the sediment package.

Previous work on the effect of deep bioturbation by callianassids on sediment stratigraphy (Shinn 1968; Tudhope and Scoffin 1984) suggests that the shrimp sequester coarse debris into the far end of certain burrow chambers as they move debris out of the way. According to Tudhope and Scoffin (1984) these discreet chambers should appear at all depths within the sediment package affected by burrowing. In contrast, the single thick lag deposit in Tague Bay and Smuggler's Cove may be the result of continuous bioturbation down to the Pleistocene surface over the past 7,000 years.

The taxonomic mix within the lag deposit may help to determine whether deep reworking of the infaunal debris is the source of the shelly lag or if it has a different origin. The answer will depend on whether the lag is more representative of the shell content in the main body of the core (i.e., primarily infaunal mollusks) or surface faunas (mostly epifaunal). Alternatively, it could be a mix of both or unrelated to either. To examine these possibilities, the level of similarity between the mollusk genera in the interior of each core and its corresponding shell lag was determined as well as the level of similarity between the surface airlift sample genera to the corresponding lag (Table 7.2). The results show that most cores (excluding 5, 6, and 12 that do not have lag deposits) have assemblages in the shell-rich lags that more resemble the genera present within the core than taxa typical of the surface fauna (Table 7.2). Core SC10 is located nearshore and is an exception to this pattern; SC10 is a significantly shorter core and its lag deposit is similar in faunal content to both the surface sample and the subsurface with 80% of surface species and 89% of core species occurring in the lag. Core SC2 is the only core in which surface fauna has more representation in the lag than the subsurface fauna (89% vs. 68%). Moreover, the lag fauna of SC2, SC8, and SC11 are characterized by a significant proportion of
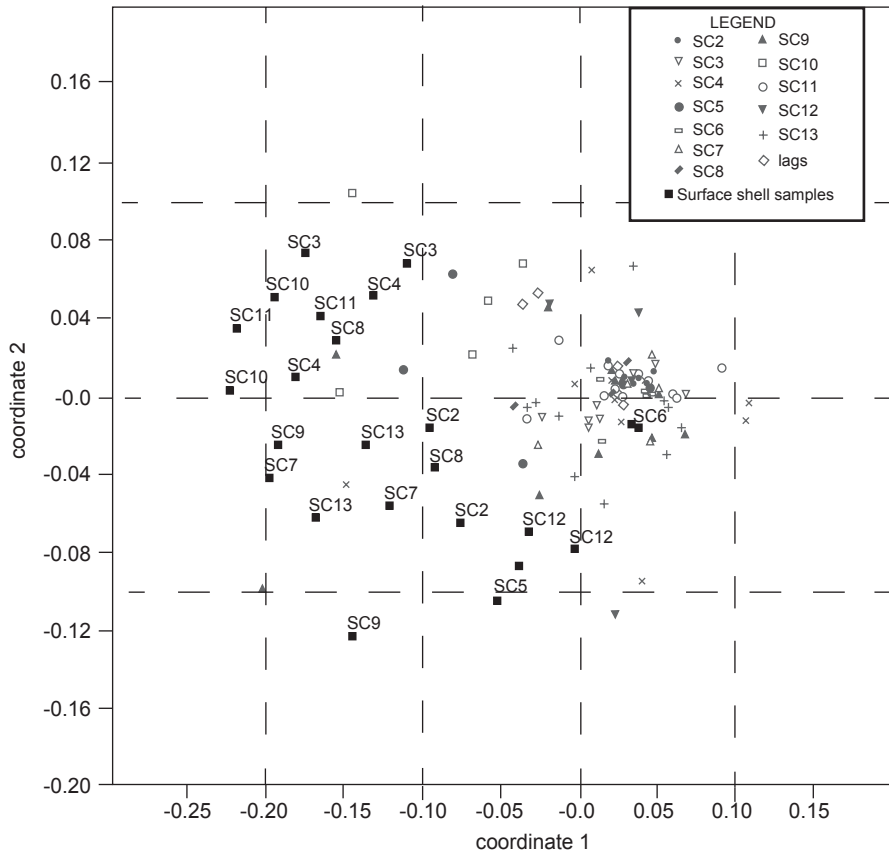
Fig. 7.10 Nonmetric, multidimensional scaling plot of coordinate 2 against coordinate 1. Each core is assigned a different *gray symbol*. Each sample interval within a core is represented by one symbol. The *black squares* are the surface airlift samples, two per core location, labeled by core location number. Data are based on guild membership of mollusks in each sample. Samples represented by only one or two mollusks were not included in this test. Note that most surface airlift samples plot away from core samples with the exception of surface sample for core location 6

unique genera. Interestingly, these cores were collected farther west than the other cores in the bay. Overall the pattern shows that lag deposits are formed from a mix of species culled from the infauna with minor contributions from epifaunal species from the surface. The few surface shells that are present in the lag are small gastropods such as ceriths and tegulids, which may have to do with the sorting abilities of the callianassids. Therefore, the majority of lag deposits reflect the taxonomic makeup of the subsurface fauna rather than the faunas presently accumulating at the sediment surface.

An examination of the faunal distribution of surface samples and samples from each level within each core support the conclusion that surface faunas are quite different from subsurface faunas (Fig. A.1). For this analysis, genera were assigned to guilds based on life habit (small infaunal bivalves, large shallow-burrowing bivalves,

infaunal predatory gastropods, epifaunal gastropods, epifaunal bivalves, and epifaunal limpet-like gastropods). A NMMDS plot of coordinate one versus coordinate two (Fig. 7.10) shows that samples collected at the surface plot well to the left (negative on coordinate 1) of most other samples. Samples from core SC10, the core closest to the shore, groups with the surface samples in the NMMDS plot. Coordinate 1 represents greater contribution from epifaunal guilds as one moves left on the *x*-axis, which would explain why the surface samples and core SC10 plot there. A few other samples plot negatively with respect to component 1 and tend to be the topmost samples from each core (the 8–20 cm segment), so overlap with surface faunas is expected. The two surface samples from core SC6 (sandy "blowout" area) both plot in the zone occupied by most of the rest of the dataset. These surface samples had very high numbers of small infaunal tellins (>400 individuals) and, therefore, resemble most core interiors rather than surface faunas. Interestingly core SC5, taken immediately adjacent to SC6, did not have the same anomalous richness of tellins in its surface sample. Regardless of these few variations, guild membership of the mollusks accumulating at the surface today does not match the patterns recorded in the cores.

Although there are recognizable differences in the generic makeup of surface assemblages presently accumulating in sea grass beds and callianassid shrimp mound areas (Fig. 7.3), no clear environmental signal (i.e., dense grass or open sand with shrimp mounds) was found in the subsurface sandy portions of cores or in the shelly lag at the base. Moreover, molluskan composition in the subsurface of all cores more closely resembles the surface faunas in present-day shrimp mound locations; that is, characterized by an abundance of small infaunal bivalves, *Bulla,* and minor *Cerithium*. This suggests that, over time, all of the lagoon sediments have been affected by the activities of the callianassids and that sea grass faunas developing at the surface remain there long enough to be taphonomically degraded and rendered unrecognizable as they become sedimentary particles.

7.4   Discussion

A major finding of this study is evidence for deep burrowing by callianassid shrimp beyond other published accounts. At the base of the deeply bioturbated sand package in Tague Bay lagoon, a lag deposit reflects complete mixing of coarse shell content throughout the period of deposition. Perhaps the most significant finding, however, is that the taxa that dominate the modern fauna of the lagoon are poorly represented in the lag deposit. Cummins et al. (1986) and Staff and Powell (1990) proposed that loss due to dissolution is concentrated among juveniles and small, thin-shelled mollusks from surface deposits in the Gulf of Mexico. In contrast, the fauna that were largely absent in the Gulf of Mexico dominate in Tague Bay, and thicker-shelled, semi-infaunal and epifaunal species from the grass beds are poorly represented in the subsurface. Moreover, evidence for dissolution and general taphonomic degradation is strongest in the thicker-shelled surface fauna and there is no indication that any of the small bivalves common in the St. Croix cores and lags are in the process of dissolving. We must conclude

that the difference in taxonomic makeup between subsurface and surface faunas is not the result of taphonomic filters that preferentially attack smaller, thin-shelled parts of an assemblage.

Ferguson and Miller (2007) demonstrate that the dominant species in the living fauna in Tague Bay changed over a 30-year period and the change was reflected in the near-surface death assemblage. If the death assemblage can vary on decadal scales, it may be naïve to expect the modern assemblage to resemble subsurface deposits accumulated over millennia. The shelly lag in Tague Bay appears to be an amalgam of countless "snapshots" over the 7,000 years of sedimentation in the lagoon. That said, although the taxonomic mix may be highly variable, the guild memberships and taphonomic grade may provide more information about the origin of the lag. The surface faunas are decidedly skewed toward epifaunal species, often larger and in poorer taphonomic condition. In contrast, the mollusks within the cores above the lag are dominated by small, well-preserved infaunal mollusks. One potential explanation is that the small, thin-shelled, infaunal mollusk community has dominated the lagoon for much of the last 7,000 years and stabilization of the lagoon by sea grass has been a recent phenomenon that introduced a new, thick-shelled, epifaunal mollusk assemblage to Tague Bay. In this scenario, the modern assemblage has had less time to be incorporated into the deep shelly lag and is, therefore, underrepresented. Alternatively, the callianassid shrimp's inability to concentrate a particular size cohort of semi-infaunal and epifaunal mollusks into the lag may have erased much of the sea grass signal from the subsurface record.

Concerns that the coring process itself influenced the distribution of larger subsurface shell material seem unwarranted since large gastropods and bivalves are rare, but not absent from the cores. If coring pushed aside larger shells, we would not have recovered large shells at all and would have observed areas of disturbed sediment within the core where shells were pushed out of the way. In addition, penetration of the sediment would have met with notable resistance if large shells were encountered. Instead, penetration was very smooth and rather rapid and no fabrics were observed that suggest shifting of larger, unrecovered shells.

The Tague Bay reef adjacent to the study area has been drilled and dated. Corals extracted via coring indicate that the reef began forming seaward of our study area approximately 6,100 years ago (Burke et al. 1989). This coincides with flooding of the bank from the east. Reef building began on a terrace that sits seaward of the highest part of what appears to have been an antecedent pre-Holocene barrier (Burke et al. 1989; Fig. 7.11). The Pleistocene subsurface dips down to the east and, as the sea level rose, the channel between St. Croix and Buck Island (Fig. 7.1) steadily filled from east to west. Lagoonal sediment began to accumulate to the present thickness of approximately 4.5 m over the past 6,100 years. Radiocarbon dates from corals in Tague Bay reef cores suggest that the reef generally accreted at the rate of sea-level rise (Hubbard et al. 2008) thereby providing a sheltered lagoon environment throughout the late Holocene.

One possible scenario for the shelly lag is that it formed early in the flooding of the lagoon and is simply a relict deposit. Radiocarbon dates do not support that hypothesis, however. The amalgam of mollusks from each of three lags dated from 3500 to 2800 cal BP and their dates are more easily explained as an average
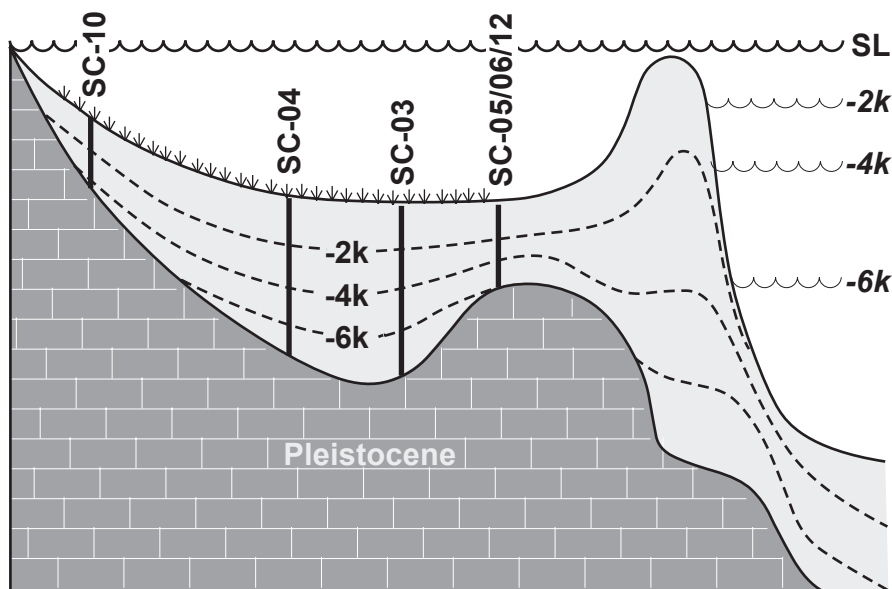
Fig. 7.11 Cross section of Tague Bay lagoon from shore to forereef showing the antecedent topography as determined using sediment probes (this study) and rotary drilling techniques (Burke et al. 1989). Dates for reef development are from radiocarbon dates of corals collected during coring (Burke et al. 1989). *Dashed lines* indicate inferred time lines for sediment filling within the lagoon based on present sediment thickness and dates from Burke et al. 1989

accumulation of shells over the past 6,000 years. This supports the conclusion that the only shell bed forming in this lagoon is a highly time-averaged accumulation deep within the sediment that has formed by the efficient and complete reworking of the entire sediment package by callianassid shrimp. Further, over the past 6,000 years there has been no burial event that captured a signature of the sea grass mollusk community that presently dominates the lagoon floor; either the sea grass community has only recently occupied the lagoon, or its preservation potential is lower. This leads us to conclude that even in a fairly well-controlled modern sedimentary system we cannot confidently address questions of faunal change, and by extension, environmental change, on short time scales if active bioturbation has occurred. Ultimately, fossil shell beds formed in sediments containing *Thalassinoides* and similar ichnogenera should be treated as highly biased representations of lagoon faunas.

Appendix

Fig. A.1 Characteristics of mollusk assemblages within the cores. Depth within core is shown on the *left* side of each diagram with the sediment-water interface at the *top*. Diversity and evenness are plotted, as well as the percentage of the sample made up of small infaunal bivalves with total
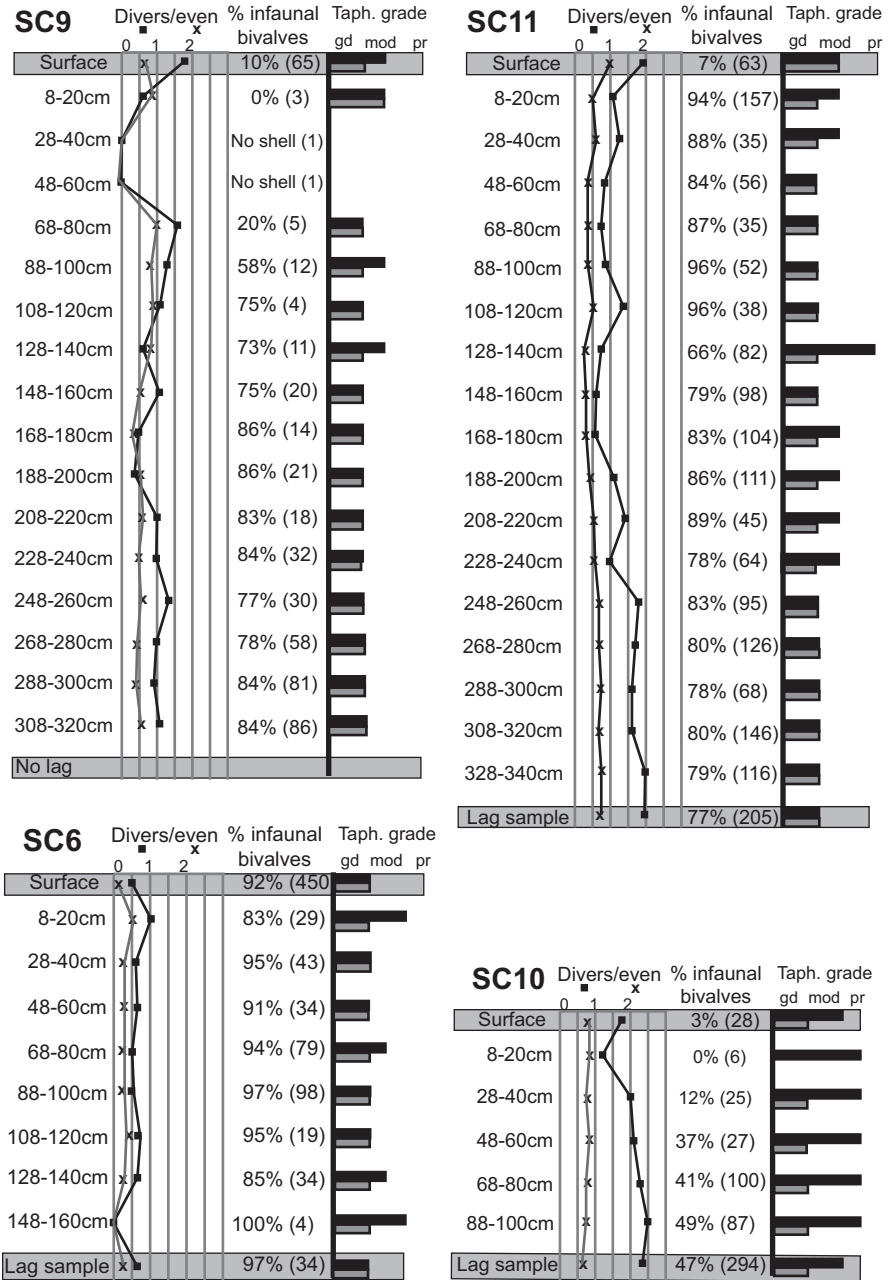
Fig. A.1 (continued) sample size in *parentheses*. The right side of each core diagram indicates taphonomic grade for epifauna (*black bars*) and infauna (*gray bars*) where *short bars* represent excellent to good condition, bars that extend midway are in moderately good condition, and *long bars* represent shells in poor condition
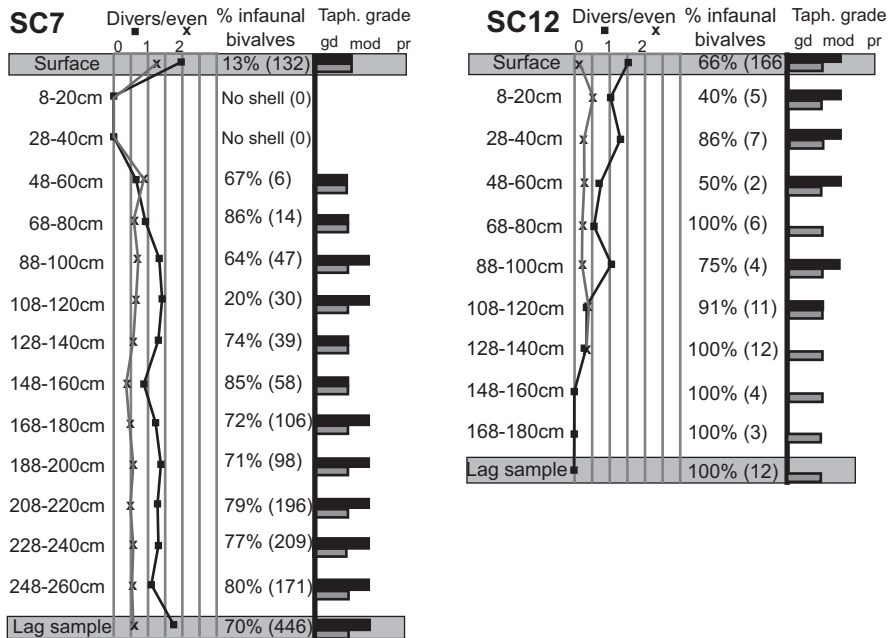
Fig. A.1 (continued)

References

Adey WH (1975) The algal ridges and coral reefs of St. Croix: their structure and Holocene development. Atoll Res Bull 187:1–67

Adey WH (1978) Algal ridges of the Caribbean Sea and West Indies. Phycolog 17:361–367

Adey WH, Burke R (1976) Holocene bioherms (algal ridges and bank barrier reefs) of the eastern Caribbean. Geol Soc Am Bull 87:95–109

Burke R, Adey HW, Macintyre IG (1989) Overview of the Holocene history, architecture, and structural components of Tague Reef and Lagoon. In: Hubbard DK (ed) Terrestrial and marine geology of St. Croix. West Indies Laboratory, Christiansted, pp 105–109. (Special publication)

Cummins H, Powell EN, Stanton RJ Jr, Staff G (1986) The rate of taphonomic loss in modern benthic habitats: how much of the potentially preservable community is preserved? Palaeogeogr Palaeocl 52:291–320

Davies DJ, Powell EN, Stanton RJ Jr (1989) Taphonomic signature as a function for environmental process: shells and shell beds in a hurricane-influenced inlet on the Texas coast. Palaeogeogr Palaeocl 72:317–356

Dworschak PC (2000) Global diversity in the Thalassinidea (Decapoda). J Crustac Biol 20:238–245

Felder DL, Staton JL (1990) Relationship of burrow morphology to population structure in the estuarine ghost shrimp *Lepidopthalmus louisianensis* (Decapoda, Thalassinoidea). Am Zool 30:137A

Ferguson CA, Miller AI (2007) A sea change in Smuggler's Cove? Detection of decadal-scale compositional transitions in the subfossil record. Palaeogeogr Palaeocl 254:418–429

Flessa CW, Cutler AH, Meldahl KH (1993) Time and taphonomy: quantitative estimates of time-averaging and stratigraphic disorder in a shallow marine habitat. Paleobiol 19:266–286

Gill IP, Hubbard DK, McLaughlin PP, Moore CH (2002) Geology of central St. Croix, U.S. Virgin Islands. In: Renkin RA, Ward WC, Gill IP, Gómez-Gómez F, Rodriguez-Martínez J (eds) Geology and hydrogeology of the Caribbean Islands aquifer system of the Commonwealth of Puerto Rico and the U.S. Virgin Islands. U.S. Geol Surv Prof Paper 1419, St. Croix, pp 79–97

Hammer O, Harper DAT, Ryan PD (2001) PAST: Paleontological statistics software package for education and data analysis. Palaeontol Electron 4:1–9

Hubbard DK, Burke RB, Gill IP, Ramirez WR, Sherman C (2008) Coral reef geology: Puerto Rico and the US Virgin Islands. In: Riegl BM, Dodge RE (eds) Coral reefs of the USA. Springer, Science + Business B.V, pp 263–302

Kidwell SM (2001) Preservation of species abundance in marine death assemblages. Science 294:1091–1094

Kidwell SM (2002a) Mesh-size effects on the ecological fidelity of death assemblages: a meta-analysis of molluscan live-dead studies. Geobios 35:107–119

Kidwell SM (2002b) Time-averaged molluscan death assemblages: palimpsests of richness, snapshots of abundance. Geol 30:803–806

Kidwell SM, Bosence DWJ (1991) Taphonomy and time-averaging of marine shelly faunas. In: Allison PA, Briggs DEG (eds) Taphonomy: releasing data locked in the fossil record. Plenum Press, New York, pp 116–209

Kidwell SM, Flessa KW (1995) The quality of the fossil record: populations, species, and communities. Annu Rev Ecol Syst 26:269–299

Kosnik MA, Hua Q, Jacobsen GE, Kaufman DS, Wust RA (2007) Sediment mixing and stratigraphic disorder revealed by the age-structure of Tellina shells in Great Barrier Reef sediment. Geol 35:811–814

Kosnik MA, Hua Q, Kaufman DS, Wüst RA (2009) Taphonomic bias and time-averaging in tropical molluscan death assemblages: differential shell half-lives in Great Barrier Reef sediment. Paleobiol 35:565–586

Kosnik MA, Kaufman DS, Hua Q (2013) Radiocarbon-calibrated multiple amino acid geochronology of Holocene molluscs from Bramble and Rib Reefs (Great Barrier Reef, Australia). Quat Geochronol 16:73–86

Lockwood R, Chastant LR (2006) Quantifying taphonomic bias of compositional fidelity, species richness, and rank abundance in molluscan death assemblages from the upper Chesapeake Bay. PALAIOS 21:376–383

Lugo-Fernandez A, Roberts HH, Wiseman, WJ Jr, Carter BL (1998) Water level and currents of tidal and infragravity periods at Tague Reef, St. Croix (USVI). Coral Reefs 17:343–349

Miller AI (1988) Spatial resolution in subfossil molluscan remains: implications for paleobiological analyses. Paleobiol 14:91–103

Miller MF, Curran HA (2001) Behavior plasticity of modern and Cenozoic burrowing thalassinidean shrimp. Palaeogeogr Palaeocl 166:219–236

Olszewski TD, Kidwell SM (2007) The preservational fidelity of evenness in molluscan death assemblages. Paleobiol 33:1–23

Parsons-Hubbard K (2005) Molluscan taphofacies in recent carbonate reef/lagoon systems and their application to sub-fossil samples from reef cores. PALAIOS 20:175–191

Pruss SB, Stevenson M, Duffey S (2011) Drilling predation and taphonomy in modern mollusk death assemblages, San Salvador Island, Bahamas. Palaeogeogr Palaeocl 311:74–81

Rivadeneira M, (2010) On the completeness and fidelity of the Quaternary bivalve record from the temperate Pacific coast of South America. PALAIOS 25:40–45

Roberts HH, Wiseman WJJ, Suchanek TH (1982) Lagoon sediment transport: the significant effect of *Callianassa* bioturbation. Proc 4th Int Coral Reef Symp 1:459–465

Shinn EA (1968) Burrowing in recent lime sediments of Florida and the Bahamas. J Paleontol 42:879–894

Suchanek TH (1983) Control of seagrass communities and sediment distribution by *Callianassa* (Crustacea, Thalassinidea) bioturbation. J Mar Res 41:281–298

Staff GM, Powell EN (1990) Taphonomic signature and the imprint of taphonomic history: discriminating between taphofacies of the inner continental shelf and a microtidal inlet. In: Miller W III (Ed) Paleocommunity temporal dynamics: the long-term development of multispecies assemblies. Paleontological Soc Spec Pub No 5:370–390

Tomasovych A (2004) Postmortem durability and population dynamics affecting the fidelity of brachiopod size-frequency distributions. PALAIOS 19:477–496

Tomasovych A, Kidwell SM (2011) Accounting for the effects of biological variability and temporal autocorrelation in assessing the preservation of species abundance. Paleobiol 37:332–354

Tomasovych A, Rothfus TA (2005) Differential taphonomy of modern brachiopods (San Juan Islands, Washington State): effect of intrinsic factors on damage and community-level abundance. LETHAIA 38:271–292

Tudhope AW, Scoffin TP (1984) The effects of *Callianassa* bioturbation on preservation of carbonate grains in Davies Lagoon, Great Barrier Reef, Australia. J Sed Pet 54:1091–1096

Whetten JT (1966) Geology of St. Croix, U.S. Virgin Islands. Geol Soc Am Mem 98:177–239

Chapter 8
Biotic Segregation in an Upper Mesotidal Dissipative Ridge and Runnel Succession, West Salish Sea, Vancouver Island, British Columbia

John-Paul Zonneveld, Murray K. Gingras, Cheryl A. Hodgson, Luke P. McHugh, Reed A. Myers, Jesse A. Schoengut and Bryce Wetthuhn

Contents

Abstract Ridge and runnel systems develop on low-gradient beaches under limited fetch conditions and moderate to high tidal ranges. The influence of beach morphology in ridge and runnel systems on biotic distribution is not well understood. This study focuses on infaunal population trends within a laterally extensive, shore parallel ridge and runnel system at Craig Bay, British Columbia, Canada. Within the study area, dense populations of *Dendraster excentricus* dominate lower intertidal runnels. These echinoids are both epifaunal and shallow infaunal. Other macroscopic infaunal organisms are absent within the runnel systems, with the exception of scattered, solitary anemones (*Anthopleura artemisia*). During low-tide intervals, *D. excentricus* in subaerially exposed runnels burrow beneath a veneer of sand and *A. artemisia* retract into their burrows. Abundant infaunal bivalves (including

J.-P. Zonneveld (✉) · M. K. Gingras · C. A. Hodgson · R. A. Myers
Department of Earth and Atmospheric Sciences, University of Alberta,
Edmonton, Alberta T6G2E3, Canada
e-mail: zonneveld@ualberta.ca

L. P. McHugh · J. A. Schoengut · B. Wetthuhn
Canadian Natural Resources Limited, 855 2nd Street SW,
Calgary, Alberta T2P4J8, Canada

Macoma nasuta, M. balthica, M. secta, Tresus capax, Clinocardium nuttallii, Protothaca staminea, and *Venerupis philippinarum*), tube-dwelling polychaetes, and threadworms characterize ridge faunas. Relatively few *D. excentricus* occur on the ridges. Carnivorous polychaetes (*Nereis* sp. and *Nephtys* sp.) occur in both ridges and runnels. Exclusion of vertical faunal components in the runnels is attributed to the feeding activities and population density of *D. excentricus,* which prefer moister sediment. Preservation of this type of ridge and runnel system in the rock record would result in a succession with zones dominated by horizontal trace fossils (e.g., *Beaconites/Scolicia*), interbedded with zones characterized by abundant vertical forms (e.g., *Siphonichnus, Skolithos,* and *Trichichnus*). The resultant trace fossil succession would have no bathymetric implications, but would reflect the influence of beach morphology on infaunal populations.

Keywords Ridge and runnel · Dissipative · Faunal exclusion · *Dendraster* · Beach morphology

8.1   Introduction

Wave-dominated beaches, which are characterized by moderate to high tidal ranges, are commonly characterized by variably complex intertidal bar systems (Hale and McCann 1982; Anthony et al. 2004; Masselink et al. 2006). These systems, commonly referred to as ridge and runnel complexes (*sensu* King and Williams 1949), are variable in aspect, ranging from low numbers of asymmetric bars with pronounced relief (>1 m) to ten or more low-relief (<0.5 m), weakly asymmetric to symmetric bars (Reichmüth and Anthony 2002; Masselink 2004; Masselink et al.).

Considerable attention has been focused on the formation and evolution of ridge and runnel beach morphology (e.g., Masselink 1993; Reichmüth and Anthony 2002; Masselink 2004; Masselink et al. 2006). Distinct morphologies have been shown to reflect specific coastal settings and hydrodynamic influences (King and Williams 1949; Owens and Frobel 1977; Orford and Wright 1978; Masselink et al. 2006). In microtidal to lower mesotidal settings with moderate to high wave energy, intertidal bars may migrate several meters per day (Owens and Frobel 1977; Masselink et al. 2006). In mesotidal to macrotidal settings under low to moderate wave influence, these bars migrate more slowly and may remain stationary for long intervals (Hale and McCann 1982; Masselink et al. 2006).

Less attention is focused on the interplay between biological and physical systems within these settings. Low-relief, dissipative intertidal beaches with well-developed intertidal bar systems provide a habitat for a moderately diverse array of marine taxa, despite the physically dynamic environments found on sandy beaches, particularly in wave-exposed settings. Various studies have emphasized the control of physical parameters (i.e., grain size, wave energy, and tidal range) on intertidal populations (e.g., McLachlan and Brown 2006; Short and Wright 1983; Brown and McLachlan
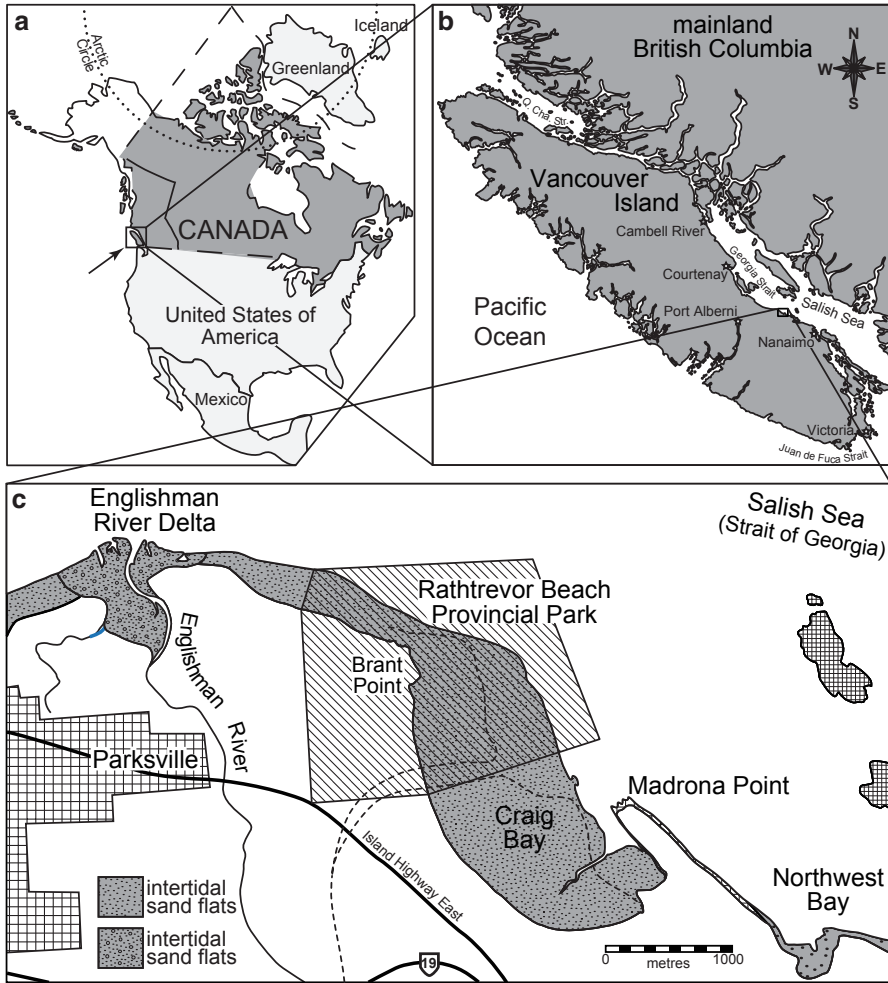
Fig. 8.1 Location map of Craig Bay. **a** Location of Vancouver Island in western British Columbia, West coast of Canada. **b** Location of the study area on the east coast of Vancouver Island, West margin of the Georgia Strait and Salish Sea. **c** Map of the Craig Bay area. The *shaded sand areas* include intertidal and deltaic sand and gravel. The *dashed lines* indicate the outline of the pre-1928 Englishman River and its outlet (British Admiralty 1928)

1990; McArdle and McLachlan 1992; McLachlan et al. 1993; Short and Hesp 1999; Hauck et al. 2008).

Ridge and runnel intertidal systems provide contrasting microhabitats where invertebrate communities can develop. Craig Bay, located on the western shore of the Salish Sea (eastern coast of Vancouver Island; Fig. 8.1), is characterized by a series of broad (50–80 m), low-relief ($<0.5°$), low amplitude (0.2–0.5 m), approximately shore-parallel ridges within an extensive ($\sim 1{,}200$ m) intertidal zone. Under

the morphological classification outlined by Masselink et al. (2006), the Craig Bay ridge and runnel system can be classified as sand waves. Restricted wave energy, a very low intertidal gradient ($\sim$0.16°), and very-fine to fine-grained sand have produced a complex system of approximately 14 intertidal bar and trough couplets (Hale and McCann 1982).

During reconnaissance fieldwork at Craig Bay, it was noted that distinct infaunal and epifaunal macrofaunal communities occupy adjacent ridge and runnel environments in lower intertidal settings. Runnel habitats are characterized by dense populations of the eccentric sand dollar (*Dendraster excentricus*), in association with abundant snails, hermit crabs, and isolated specimens of solitary anemones (*Anthopleura artemisia*). A variety of infaunal bivalves and locally abundant populations of vertical tube-dwelling polychaetes characterize ridge habitats. Semiannual observation of these communities between February 2008 and the present have established that the boundaries of these communities are well established and do not shift perceptibly, either seasonally or annually.

This chapter discusses (1) the biotic composition of the lower intertidal portion of the ridge and runnel complex at Craig Bay, (2) the possible physical and biological controls responsible for biotic segregation between the two end-member environments, and (3) the composition of the likely preserved footprint of ridge and runnel successions in the rock record. The lower intertidal portion of the Craig Bay ridge and runnel system shows clear segregation of extant biota and thus the biogenic sedimentary structures they create.

8.2   Study Area

Craig Bay is located east of the town of Parksville on the east coast of Vancouver Island, British Columbia (N 49°19'10''; W124°15'10''; Fig. 8.1a and b). It's location on the western margin of the Salish Sea (Georgia Strait coastline; Fig. 8.1b and c) results in protection from open Pacific swells and storms. Thus, Craig Bay is a relatively low wave energy depositional setting, whereby the waves are locally generated (Hale and McCann 1982). The size and severity of waves are limited by fetch and thus, even in the most severe storms, waves rarely exceed 3.0 m in wave height, with associated wave periods of less than 7.0 s (Hale and McCann 1982).

Wide sandy beaches in small embayments are common on the protected northeast coast of Vancouver Island. The beach at Craig Bay is a particularly wide example. Due to a low foreshore gradient ($<\sim$0.16°) and a moderately high tidal range (mean tidal range of 3.4 m; maximum tidal range of 5.1 m), the intertidal zone is up to 1,200 m wide in Craig Bay (McCann and Hale 1980; Hale and McCann 1982; Figs. 8.2, 8.3).

Craig Bay occurs on the eastern flank of the present-day Englishman River Delta (Fig. 8.1b). Historical evidence (British Admiralty 1928) indicates that the Englishman River flowed into Craig Bay as recently as the late 1920s (Fyles 1963; McCann and Hale 1980; Hale and McCann 1982). Mean annual discharge of the Englishman
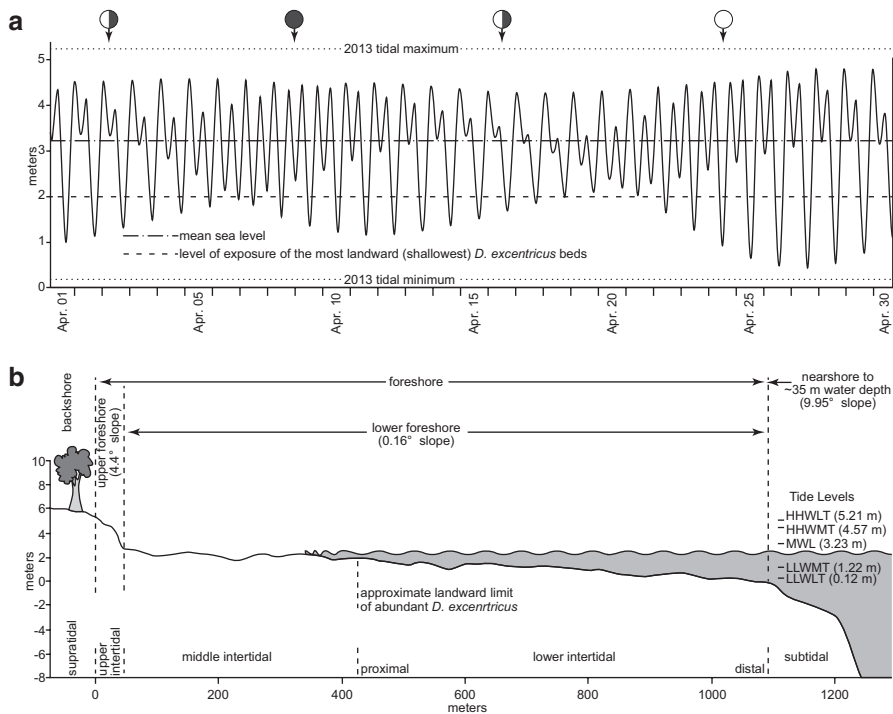
Fig. 8.2 The Craig Bay tidal regime. **a** Typical monthly tidal curve for Northwest Bay, 1 km east of Craig Bay (April, 2013). *Circles* at top indicate the lunar cycle (*solid circle* = new moon; *open circle* = full moon). The study area has an approximate 5 m tidal range between extremes. During the 2013 calendar year, the maximum high tide occurred at 5.24 m at 07:51 PST on January 14 and the mean lower low water occurred at 0.18 m on May 26, at 13:12 PDT. The 0 m datum on this graph is the mean lower low water line. **b** Generalized West–East profile through the approximate center of Craig Bay showing the morphology, typical gradients, tide levels, and environment zonation (adapted from Hale and McCann 1982). The approximate landward limit of abundant *D. excentricus* is shown

River measured periodically from 1913 to present at the Water Survey Canada hydrometric station Englishman River near Parksville (08HB002) is 13.6 M³/S. The approximate location of the former outlet occurs between transects CB-1 and CB-4 (Fig. 8.3) based on information from British Admiralty Chart 579 (1928).

The Englishman River is sourced on the eastern slopes of the Beaufort Mountain Range at Mounts Arrowsmith and Moriarty from whence it flows approximately 40 km before it debouches into the Strait of Georgia, west of the present study area (Fig. 8.1c). The short distance between source and delta results in seasonal delivery of texturally immature sediment to the coast.

Recent sediments at Craig Bay are emplaced upon slightly older sand and gravel deposits of the historical Englishman River delta (British Admiralty 1928; Fyles 1963; Hale and McCann 1982). These recent sediments consist of a thin veneer (0–1.5 m) of fine- to medium-grained sand organized into a complex ridge and run-

Fig. 8.3 Google Earth air photograph of Craig Bay showing the intricate ridge and runnel complex and the distribution of *D. excentricus* (*purple shaded area*). The *black lines* denote sediment sample transects. Also shown are ebb and flood tidal velocities from select stations (after Hale and McCann 1982). *Green stars* denote areas of grid surveys used in this study
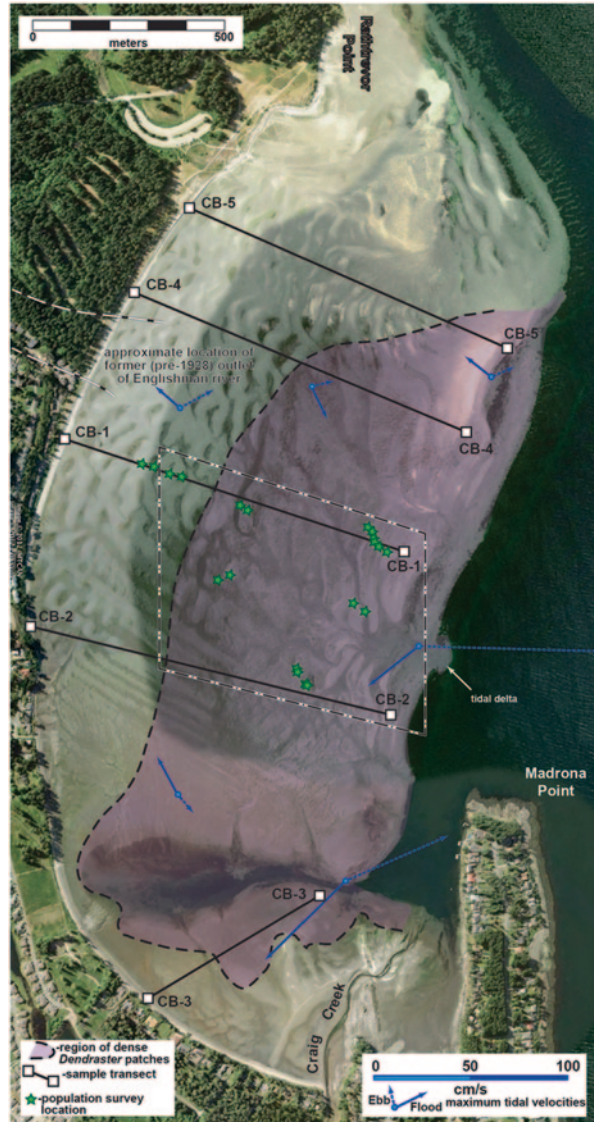
nel system consisting of approximately 14 low-amplitude/long wavelength ridges (Hale and McCann 1982).

The sand veneer becomes progressively thinner towards the north. In the northeastern part of the study area, the sand is restricted to the ridges, while coarser material, including pebbles and cobbles, occurs in the runnels. In parts of the northern portion of the bay, the sand veneer disappears entirely and is replaced by a relict substrate of pebbles and cobbles in a poorly-sorted medium-grained sand matrix. The present study is focused solely on biota and successions in the central part of

Fig. 8.4 Field photographs of the Craig Bay ridge and runnel complex. **a** Proximal lower intertidal ridge and runnels during early stages of falling tide. Photograph facing east across the Salish Sea. **b** Proximal lower intertidal zone. Runnels in this area contain dense *Dendraster* populations. Photograph facing East. **c** A ridge and runnel pair in the lower intertidal. Abundant *Dendraster* in the runnel. The tape in the foreground occurs near the seaward end of transect CB-1. Photograph facing North
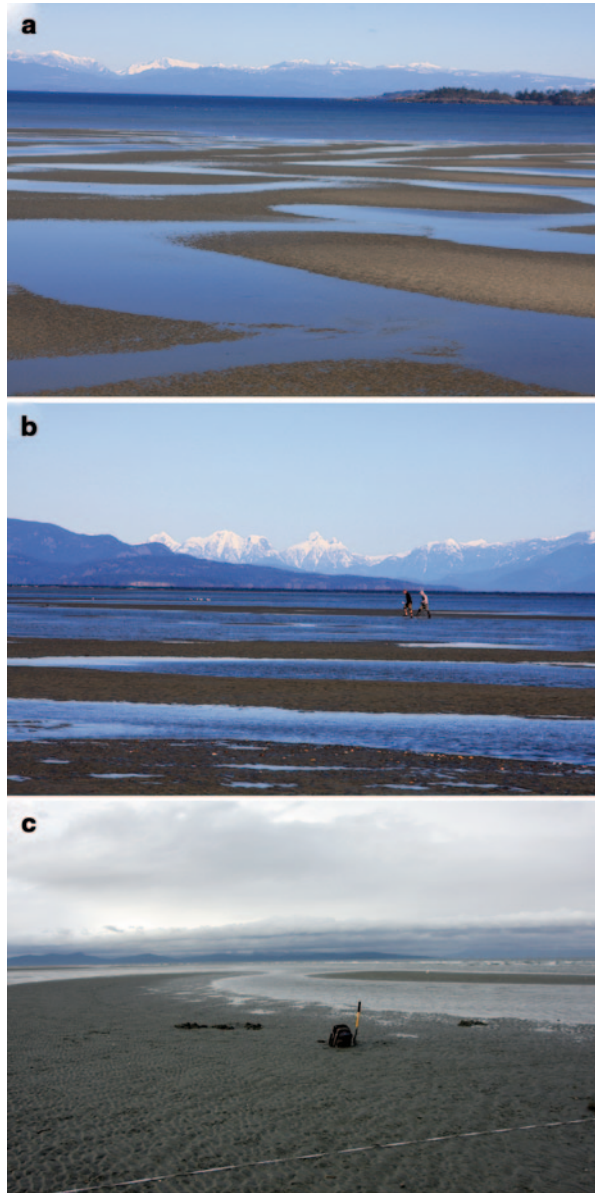
Craig Bay, in areas with a moderately thick layer of sand atop the older deltaic sediments (Fig. 8.3).

The sand waves (*sensu* Masselink et al. 2006) that comprise the Craig Bay ridge and runnel complex (Fig. 8.4) are of overall low relief (20–50 cm) above the bases of the intervening troughs with an average crest-to-crest measurement of 85 m (Hale and McCann 1982). The sand waves occur approximately parallel to the

shoreline. Many of the troughs retain water during low tide; however, some do drain completely (Fig. 8.4). The troughs drain toward the central part of the bay, where a permanent to semi-permanent tidal delta is located (Fig. 8.3). Air photos indicate that the Craig Bay ridge and runnel complex, and the location of the central tidal delta, are minimally changed since 1978, indicating that these features are indeed relatively stationary (Fig. 8.3; Hale and McCann 1982).

8.3 Material and Methods

Craig Bay is the focus of ongoing investigations by researchers from the University of Alberta. Analyses have focused on both the physical sedimentology and distribution of invertebrate macrobiota in the ridge and runnel system. Sampling has included detailed onshore–offshore-oriented transects with sediment grain-size sampling conducted every 10 m, and assessments made of both taxonomic composition and abundance for each ridge and runnel encountered via surface observations and shallow (30–60 cm deep, ~1 m wide) trenches and shallow cores (using a clam gun). Clam gun cores were used primarily to identify the makers of trace openings observed at the surface. Notes were made on all biota encountered in trenches, in clam gun core, and in surface observations.

To date, five onshore–offshore-oriented transects have been completed (Fig. 8.3). At each station, 0.2 kg samples of sediment were obtained from the surface as well as from 30 cm below the surface. All sediment samples ($n=780$) have been sieved using standard Wentworth-Udden sieve sizes to assess sorting, grain-size distribution, and mean grain size throughout the study area. Only the overall grain-size trends of Craig Bay and the grain size data pertaining to the ridge and runnel pairs analyzed for this study are discussed herein (Fig. 8.5). Taxonomic composition and abundance for the ridge and runnel pairs was assessed via detailed observation and descriptions of shallow (30–60 cm deep) trenches, in addition to using clam guns to obtain shallow sediment cores.

In order to assess faunal differences between ridge and runnel pairs, grid surveys were conducted at a number of locales in the study area (Fig. 8.3). Sampling took place primarily in 2009–2012 between mid-February and early April although some work was been completed in August. All the fieldwork was conducted during intervals in which the low tide mark reached 1.25 m above chart datum or less. Grid surveys were conducted in pairs on adjacent ridges and runnels located no further than 50 m apart from each other. All study locales were chosen near the paths of sample transects CB-1 and CB-2 (Fig. 8.3).

Grid surveys consisted of 1×1 m frames (with decimeter subdivisions demarcated by strings) placed upon the sediment surface. Each sample grid was photographed and sketched to denote the presence of surface macrobiota and siphon holes/burrow openings. The corners of the sample locality were demarcated with stakes and the upper 25 cm of each grid was excavated and sieved in the field with all macrobiota segregated by taxonomic affinity into collection containers filled
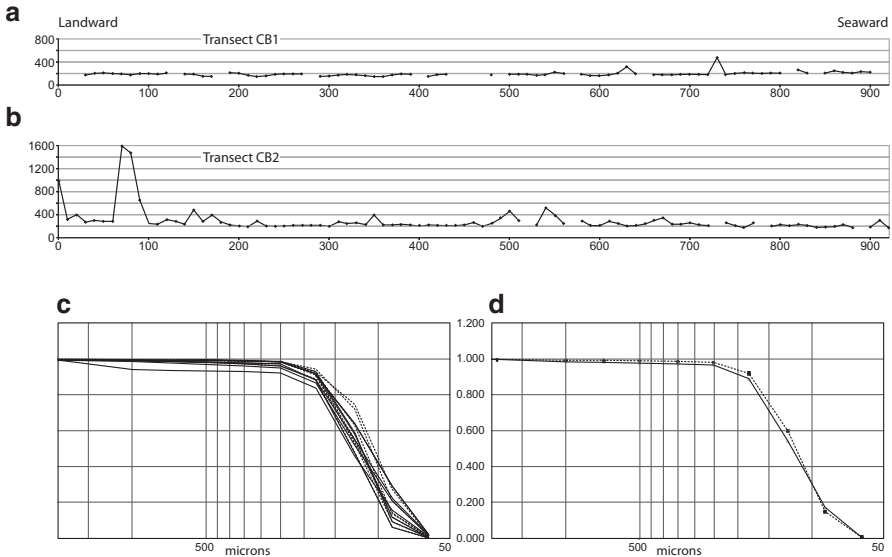
Fig. 8.5 Grain size data from Craig Bay, British Columbia. **a** Median grain size plotted in a shoreward-seaward orientation, transect CB1. **b** Median grain size plotted in a shoreward-seaward orientation, transect CB2. **c** Normalized grain size data for 10 ridge and runnel pairs. Note that all of these data plot very close to each other. **d** Normalized mean grain sizes for all ridges and runnels analyzed. The close plot of these two lines is consistent with field observations that grain size is not a controlling factor in biotic segregation in the study area

with seawater. During sampling, notes were made of the location of different taxa within the grid. When the grid was fully excavated, the collected taxa were counted and measured. The excavation was then backfilled and, where possible, the taxa emplaced as closely as possible back in their original locations. Representative samples of all taxa were collected in the field and preserved in a diluted methanol solution. After completion of grid censuses, box cores were obtained from an undisturbed location within 2 m of the grid location, from a similar morphogeographic setting (i.e., same position within a ridge or runnel). These box cores provide a record of biogenic and physical sedimentary structures in the upper ~20 cm of the sediment in each grid location.

In addition to transect sampling, sediment samples were obtained from a series of ridges and runnels to assess moisture content (Table 8.1). The samples were collected from six subaerially exposed ridges and six subaerially exposed runnels. Two water-filled runnels were also sampled (assumed to have 100% water saturation) as a control. Samples were collected in glass jars within 30 min of low tide. In the laboratory, the lids were removed and samples weighed immediately. The samples were then placed in an oven at 90 °C until all moisture was removed (24 h). Samples were then resaturated with clean seawater from Craig Bay and weighed again. The difference between field weight and 100% (laboratory) saturation weight was used as a proxy to assess substrate saturation. It is acknowledged that this method provides only a rough approximation of sediment saturation; however, these results are

Table 8.1 Sand saturation in sampled ridges and runnels

Sample ID	Original weight (g)	Dry weight (g)	Saturated weight (g)	Percent saturation
Wet runnels				
FE20-3-Ru[a]	213	177	213	100
FE21-2-Ru[a]	194	156	194	100
Dry Runnels				
FE20-1-Ru	219	178	223	91.1
FE21-3-Ru	201	167	204	91.9
FE22-02-Ru	225	192	227	94.3
MR13-02-Ru	243	196	243	100
MR14-01Ru	190	156	192	94.4
MR15-01Ru	206	168	206	100
Ridges				
FE20-1-Ri[b]	188	160	199	71.8
FE21-1-Ri	225	189	231	85.7
FE22-01-Ri	232	195	235	92.5
MR13-01-Ri	208	181	216	77.1
MR14-02Ri	211	176	215	89.7
MR15-01Ri	214	185	226	83

Saturation samples were obtained from the upper 3 cm of the sediment, were sampled within 30 min of low tide, and were sampled only during intervals in which the dropping tide interval was not coincident with rainfall. The average percent saturation in "dry" runnels was 95.3 % (range 91.1–100 %). The average percent saturation in ridges was 83.3 % (range 71.8–92.5 %) *wt.* weight
[a]*Ru* runnel
[b]*Ri* ridge

sufficient to assess the control that fluctuations in sediment saturation may have on faunal composition.

8.4   Results

8.4.1   Dominant Taxa in Ridge Settings

Within the study area, the dominant macrobiota in ridge settings consist primarily of infaunal bivalves and a variety of worms, including infaunal tube-dwelling poly-chaetes (Table 8.2). Lower intertidal ridges are dominated either by the veneroid bivalve *Macoma balthica* (Fig. 8.6a) or by patches of densely packed vertical worm tubes (Fig. 8.6f and g), made by infaunal terebellid, maldanid, or chaetopterid poly-chaetes. Also common are other *Macoma*s species, including *M. secta* and *M. na-suta*. Thin (<0.5 mm), thread-like capitellid polychaetes (likely *Heteromastus filo-brachus*) are common ridge taxa throughout the study area. The carnivorous nereid polychaete *Nephtys* sp. (Fig. 8.6e) is common in most ridge settings; however, it is absent where there are dense concentrations of vertical worm tubes. Rare examples of the naticid gastropod *Lunatia lewisii* (formerly *Polinices lewisii*) were also en-

Table 8.2 Macrofaunal taxonomic distribution in middle and lower intertidal ridges and runnels at Craig Bay

Taxon	Lower intertidal runnels		Lower intertidal ridges	
	"Dry"	"Wet"	Proximal	Distal
Dendraster excentricus	VA	VA		
Anthopleura artemesia	P	P		
Macoma balthica			A	A
Macoma nasuta			R	P
Protothaca staminea			A	
Venerupis philippinarum			A	
Tresus capax				P
Saxidomus giganteus			R	P
Clinocardium nuttallii				R
Nereis sp.	P	P		
Nephtys sp.	P		A	A
Heteromastus filobrachus			A	A
Capitella capitata			A	P
Cf. *Malddanus* sp.			A	A
Lunatia lewisii			R	R
Pagurus samuelis		A		
P. hirsutiusculus		A		
Batillaria attramentaria		VA		
Olivella biplicata		A		
Alia carinata		A		
Fusitriton oregonensis		A		
Ophiopholis aculeata		A		
Pisaster ochraceus		R		
Evasterias troschelii		R		
Hermissenda crassicornis		R		

R rare, *P* present, *A* abundant, *VA* very abundant

countered during grid surveys in ridge settings, generally 5–15 cm below the sediment surface (Fig. 8.6h).

Some taxa are clearly restricted to specific environmental ranges. In middle intertidal and proximal lower intertidal settings, the veneroid bivalves *Protothaca staminea* and *Venerupis philippinarum* (= *Tapes japonica*) are common. In distal lower intertidal settings, the large, deep-burrowing veneroid bivalve *Tresus capax*

Fig. 8.6 Key macrobiota from lower intertidal ridge and runnel systems at Craig Bay. **a** *Macoma balthica* in life position. The lines to surface extending above the clam are shafts in the sand made by the inhalant and exhalant siphons. **b** *Tresus capax* removed from its burrow. The fused siphons are fully retracted but are too large to fully disappear into the shell. The hole in the sand to the right is the siphon hole of a similar sized *T. capax*. Also visible in this photo are minute siphon holes of *M. balthica*. **c** *Anthopleura artemisia* in life position in approximately 3 cm water depth in a runnel. **d** Large (~80 cm) *Nereis* sp. collected from beneath a dense *Dendraster* bed in a lower intertidal runnel. **e** Large *Nephtys* sp. collected from a lower intertidal ridge. Note that its proboscis is extended (*arrow*). **f** Dense colony of vertical tube worms (*C. capitata*) in excavation. **g** Surface expression of dense colony of vertical tube worms (*C. capitata*). **h** *Lunatia lewesii* removed from grid excavation FE20-3. When collected, the animal retracted into its shell. When emplaced back on the sand surface, it slowly extended its foot (*shown here*) and had completely disappeared into the sediment within 5 min of release

(Fig. 8.6b) is locally abundant. This large bivalve is absent in the proximal lower intertidal zone.

Two end-member ridge faunas have been identified. Ridge faunas dominated by vertical tube-dwelling polychaetes (likely maldanids or chaetopterids) are commonly monotypic and of high population density (1,200–4,000 tubes/m^2). The agglutinated sand-mucus tubes range in thickness from 1.5–2.5 mm in diameter, and are 15–30 cm long (Fig. 8.6f and g). Other infauna are absent in areas with dense worm tubes, presumably due to the difficulties in burrowing through the tough, agglutinated sediment-mucus tubes.

Ridge faunas dominated by infaunal bivalves exhibit considerably lower population density but higher taxonomic diversity of macrobiota compared with tubeworm faunas. Grid counts ranged from 14–126 bivalves per m^2. In proximal lower intertidal areas, the dominant taxa were either the shallow infaunal taxa *P. staminea* and *V. philippinarum,* or the deep infaunal taxon *M. balthica*. *M. balthica* was also the most common bivalve in distal lower intertidal areas (Table 8.2); however, one to two specimens of the deep-burrowing veneroid bivalve *T. capax,* and the shallow burrowing veneroid *Clinocardium nuttallii,* were encountered in each distal lower intertidal grid survey. As mentioned above, present throughout the study area in ridge settings, was the carnivorous nereid polychaete *Nephtys* sp. Only a few animals were encountered on the sediment surface during ridge grid surveys— very rare gastropods and individual *D. excentricus,* which typically had lengthy, *Scolicia*-like burrows behind them. Isolated *D. excentricus* were rarely observed in ridge settings in proximal lower intertidal areas but were much more common distally at the lower intertidal limit. Box cores obtained from ridge settings were typically characterized by several vertical traces (most commonly siphon tubes) and well-preserved, cross-ripple laminae.

8.4.2   Dominant Taxa in Runnel Settings

In the lower intertidal zone at Craig Bay, runnel environments are strongly dominated by the irregular echinoid *D. excentricus* (Fig. 8.7). Every runnel grid survey in the lower intertidal area encountered these echinoids in great abundance. In runnels that did not drain fully at low tide, the sand dollars were in variable orientation, with a high proportion in a vertical to subvertical suspension feeding orientation (Fig. 8.7a, b, d, f). In runnels that drained fully at low tide, *D. excentricus* were entirely horizontal to subhorizontal, and commonly were fully to partially buried under a thin (0.25–5.0 cm) layer of sand (Fig. 8.7c and e).

Other infaunal taxa encountered in grid surveys included the solitary anemone, *A. artemisia* (Fig. 8.6c) and large (up to 80 cm in length) nereid polychaetes (*Nereis* sp.; Fig. 8.6d). Neither taxon was present in any one grid in great numbers, but they were commonly encountered in this study. Macrobiota (other than *D. excentricus*) encountered atop the sand surface in non-draining runnels included hermit crabs
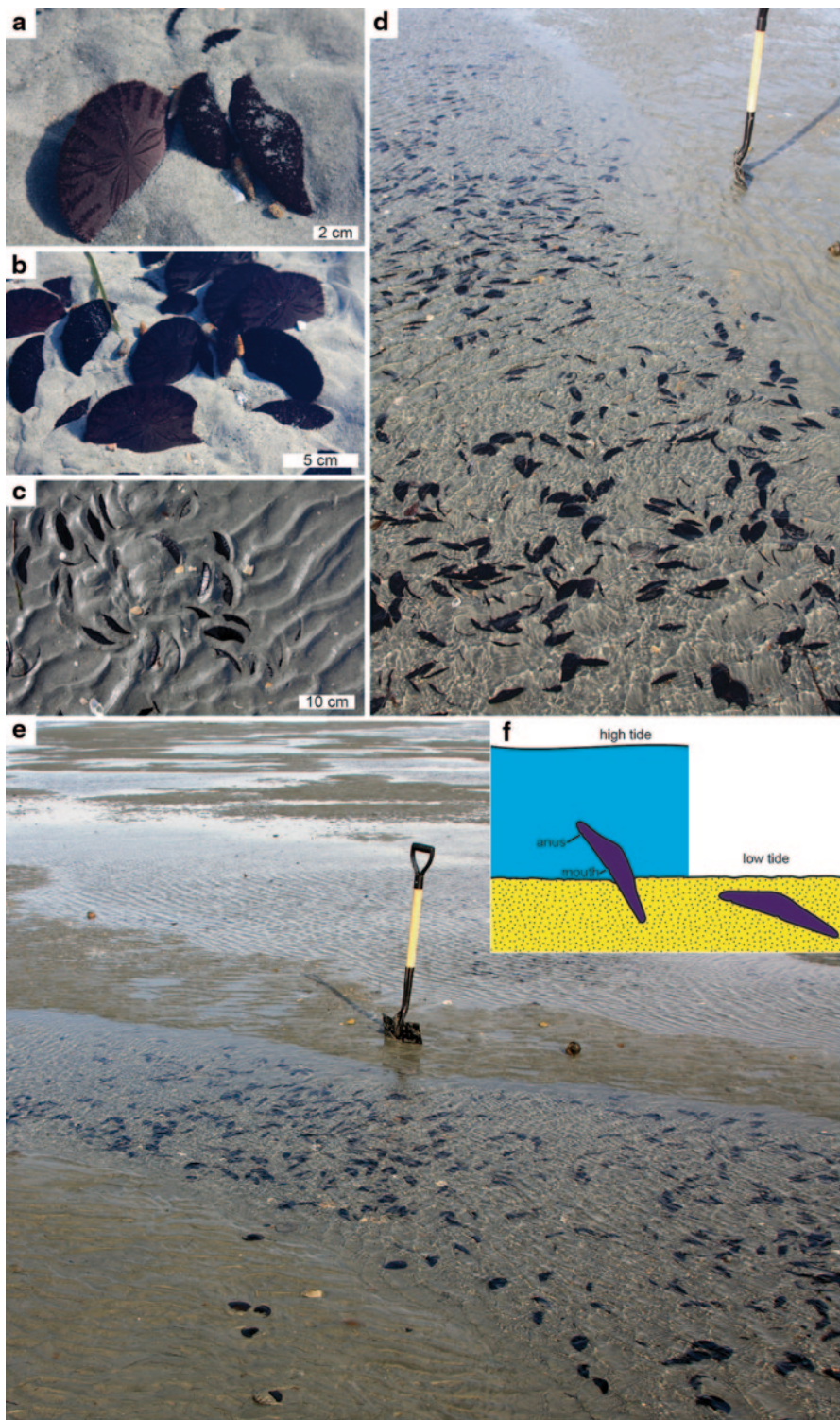
Fig. 8.7 *Dendraster excentricus* from lower intertidal ridge and runnel systems at Craig Bay.
a Close-up of *D. excentricus* in lower intertidal runnel during early stages of flood tide. The
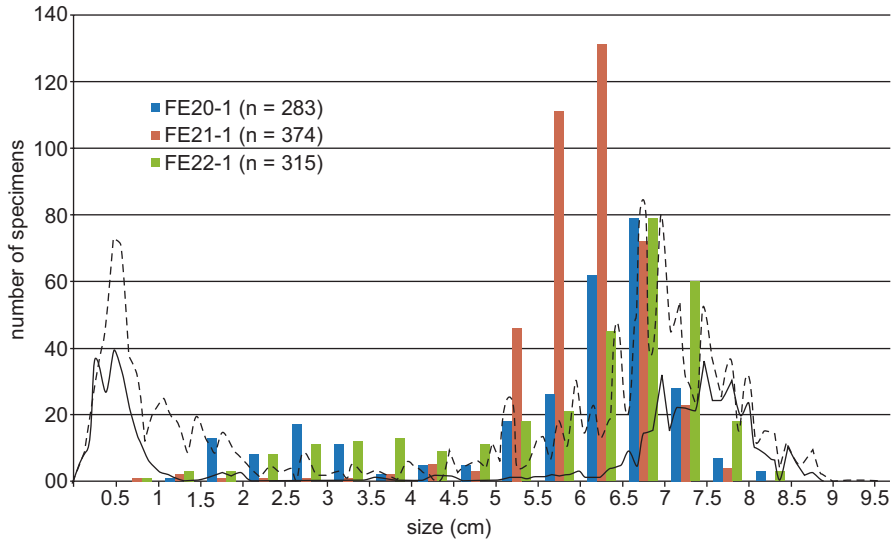
Fig. 8.8 Size distribution of live *D. excentricus*. The *colored bars* denote absolute abundances of *D. excentricus* from three of the Craig Bay sample localities (FE20-1, FE21-1, and FE22-1). The *dashed and solid lines* are provided for comparison and show size distributions for two populations of *D. excentricus* from Puget Sound, Washington (from Birkeland and Chia 1971). Note that the *colored bars* are totals within 0.5 cm size bins whereas the Puget Sound samples are binned in 0.1 cm increments. Also note that relatively few juveniles (<1.5 cm) were collected in the Craig Bay grid surveys whereas abundant juveniles were present in the Puget Sound populations

(*Pagurus samuelis* and *P. hirsutiusculus*), a variety of snails, shrimp, nudibranchs, and tide-pool sculpin.

Several hundred *D. excentricus* (between 263 and 521 specimens per m^2) were counted in each of the runnel surveys. Individual populations showed a broad range in size distribution, from individuals under 1 cm in diameter to those in excess of 8 cm in diameter (Fig. 8.8). This matches well with size distributions from Puget Sound, Washington (Fig. 8.8) (Birkeland and Chia 1971), although the Craig Bay samples contain proportionally fewer small specimens (i.e., ≤1.5 cm). The size of *D. excentricus* directly corresponds with specimen age, and thus it appears that the

---

Fig. 8.7 (continued) specimens in this photo are starting to shift into suspension feeding position. **b** Close-up photograph of *D. excentricus* from a proximal lower intertidal runnel in suspension-feeding position beneath approximately 10 cm of water. **c** Abundant *D. excentricus* on the edge of a dry proximal lower intertidal runnel during low tide. **d** The boundary of a proximal lower intertidal ridge/runnel pair. Note the sharp boundary between the runnel fauna (abundant *D. excentricus*) and the ridge area. **e** A narrow runnel in the proximal lower intertidal. Note the sharp boundary between the runnel fauna (abundant *D. excentricus*) and the ridge area. **f** Feeding behavior response of *D. excentricus* to subaqueous inundation (subvertical deposit feeding at *left*) and subaerial exposure (subhorizontal deposit feeding at *right*). (Adapted from Chia 1969)
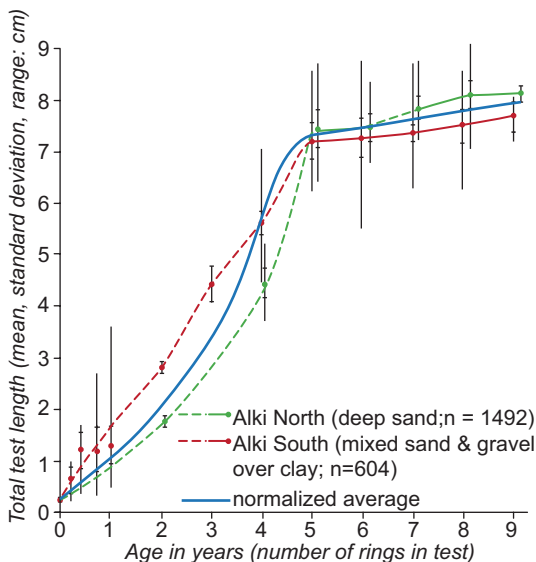
Craig Bay collections contain very few specimens less than 1 year of age (Fig. 8.9).
This is perhaps not surprising since *D. excentricus* spawn in the late spring and early
summer (Pennington et al. 1986; Strathrnann 1987) and grid counts for this project
were conducted entirely in February and March.

Box cores obtained from runnel settings commonly contained *D. excentricus*
in the upper 5–6 cm. These cores were devoid of any preserved physical sedimen-
tary structures, likely reflecting infaunal movement by *D. excentricus* and complete
reworking of the upper few centimeters of sediment.

8.4.3   Wet Runnels Versus Dry Runnels

In lower intertidal settings at Craig Bay both "wet" runnels (those that do not fully
drain through a low tide cycle) and "dry" runnels (those drained of standing water
at low tide) contained abundant populations of *D. excentricus* (Fig. 8.10). Dominant
faunal elements (*D. excentricus* and *A. artemisia*) are as common in drained runnels
as they are in non-drained runnels within similar zones.

Runnels with standing water contain a more diverse assemblage of invertebrates
than runnels that dry fully at low tide (Table 8.2). These include resident infauna (*D.
excentricus* and *A. artemisia*), mobile resident epifauna (*P. samuelis, P. hirsutius-
culus, Olivella biplicata,* and various other snails) as well as migrants (starfish and
nudibranchs). Dry runnels contain a similar resident infauna, both taxonomically
(*D. excentricus* and *A. artemisia*) as well as in terms of overall organismal abun-
dance. The main difference between the two is the absence, at low tide, of mobile
epifauna and of migrants in dry runnel settings. The presence of trackways and trails
consistent with the movement of hermit crabs and snails, however, indicates that
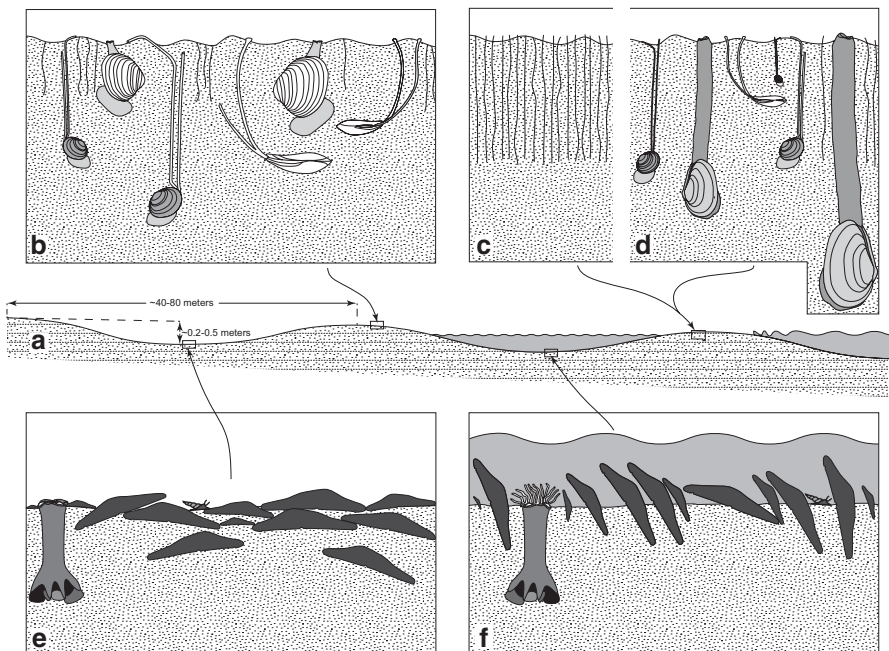
Fig. 8.10 Schematic model showing the distribution of invertebrate macrofauna in lower intertidal ridges and runnels at Craig Bay. Landward to left; seaward to right. **a** Basic morphology of Craig Bay ridge and runnel complexes. **b** Ridges in proximal areas (proximal lower intertidal) are characterized primarily by a variety of infaunal bivalves including deep infaunal forms such as *M. balthica* and less common *M. nasuta* and the shallow infaunal form *P. staminea*. **c** Patches dominated by vertical tubeworms occur on some lower intertidal ridges, increasing in abundance towards the more distal lower intertidal. **d** Ridges in the proximal and distal lower intertidal are characterized by deep infaunal forms that include the omnipresent *M. balthica,* scattered occurrences of *M. nasuta,* and *T. capax*. **e** Many runnels in lower intertidal settings are commonly drained of water during low tide cycles. Runnels are characterized by dense populations of *D. excentricus* as well as scattered anemones (*A. artemisia*) and a variety of snails and hermit crabs (*Pagurus samuelis*). During intervals of subaerial exposure, *D. excentricus* lie flat on the sand surface, or buried within the upper ~7–8 cm. **f** During high tide cycles, and in runnels that retain water during low tide cycles, *D. excentricus* occur in subvertical orientation

the lack of mobile taxa is controlled by the temporal position within the tidal cycle (i.e., mobile epifauna are common early in the exposure cycle, but vacate exposed areas later in each cycle) and does not reflect a complete absence of these forms in dry runnel settings.

8.4.4 Sediment Moisture: Ridges Versus Runnels

Sediment moisture was assessed at all sites studied. It is clear that sediment moisture content changes significantly between individual subenvironments. At low tide, wet runnels were observed to contain both still and moving water. The average

percent saturation in "dry" runnels was 95.3 % (Table 8.1), while the average percent saturation in ridge settings was 83.3 % (Table 8.1) at low tide. The data confirm that the ridges contained significantly lower water saturation than in any runnel setting tested. It is, however, acknowledged that the dataset utilized is small, and not representative of all conditions. The samples were obtained during dry, overcast conditions (nonrainfall) with moderate wind. It is expected that under sunny or windy conditions the surface sediment in ridge settings would be even drier than those described herein.

8.4.5   Grain Size

Sieve analyses of five transects have been completed in Craig Bay (locations shown in Fig. 8.3). As well, several vibracore and numerous boxcores have been obtained in Craig Bay. These are the focus of ongoing analyses; thus, the results are not discussed in detail herein, although grain size data for transects CB1 and CB2 (Fig. 8.3) are provided in Fig. 8.5 (a and b). These analyses have revealed an overall southward grain size decrease, from Brant Point to Madrona channel, with an increase in grain size in the immediate area of Craig Creek outlet. No evidence was found, however, for significant grain size or sorting differences between ridges and runnels within individual ridge and runnel pairs (Fig. 8.5c–d).

8.4.6   Middle Intertidal Versus Lower Intertidal

The focus of this project is primarily on the differences between lower intertidal ridge and runnel complexes in the central part of Craig Bay; however, several ridge and runnel sites landward of the upper limit of *D. excentricus* in the study area were also assessed. It was found that the faunas in these ridges and runnels were nondifferentiable. They consisted primarily of the deep infaunal bivalve *M. balthica,* the shallow infaunal bivalves *P. staminea* and *V. philippinarum,* and the diminutive vertical tube-dwelling polychaete *Capitella capitata*. Also present were infaunal amphipods, the nereid polychaete *Nephtys* sp. and abundant thread worms (*H. filobrachus*). No differences were noted between ridge and runnel faunas within middle intertidal settings.

8.5   Discussion and Interpretation

Over the past several decades, considerable attention has focused on the oceanographic, hydrodynamic, and sediment budget influences that result in the formation and evolution of ridge and runnel beach morphology in low-energy, dissipative shoreface settings (e.g., King and Williams 1949; Owens and Frobel 1977; Orford

and Wright 1978; Hale and McCann 1982; Masselink 1993; Reichmüth and Anthony 2002: Masselink 2004; Masselink et al. 2006). Faunal zonation in sandy beach settings has been related to a number of physical factors, including interstitial oxygen concentration, periodic (diurnal/semidiurnal) exposure and desiccation, grain size and wave stress (e.g., McLachlan and Jaramillo 1995; Gingras et al. 1999; Degraer et al. 2003; Defeo et al. 1997, 2003; Defeo and McLachlan 2005; McLachlan and Brown 2006). Most models of faunal zonation are relatively simple and consist of one to four horizontal physical zones reflecting either sediment moisture content or duration of exposure during tidal cycles (e.g., Dahl 1952; Salvat 1964; Defeo and McLachlan 2005; Moreno et al. 2006). These models possibly apply to simple beach morphologies. Low-relief ridge and runnel beaches, however, which commonly develop in low-energy mesotidal and macrotidal settings, offer microhabitats that introduce complexities that are not accounted for in simplified models (Gingold et al. 2010, 2011; Maria et al. 2013).

The Craig Bay intertidal zone is characterized by a well-developed ridge and runnel complex. As a result, in the lower intertidal zone, distinct microhabitats form in which the macrofauna are segregated (Fig. 8.10). Lower intertidal biotas that occupy the two end-member microhabitats (ridges and runnels) differ completely in their dominant forms (Fig. 8.10). Sand dollars (*D. excentricus*) are pervasive in runnels (hundreds of specimens per m^2), commonly completely covering the sediment surface area. Other taxa, such as deep and shallow infaunal bivalves and tube-dwelling polychaetes, are restricted to ridge settings in the lower intertidal. The boundary between the two end-member macrofaunas is abrupt, with population densities of *D. excentricus* dropping from ~250–500/m^2 to absent within a single decimeter, and the first bivalves or tube-dwelling polychaetes occurring within centimeters of the terminus of a *D. excentricus* bed.

The geographic restriction of these faunas is primarily a function of the environmental preference of *D. excentricus* for runnels rather than restriction of the any of the bivalve species or tube-dwelling polychaetes to ridge settings. Landward of the first *D. excentricus* beds, ridges and runnels have similar faunas consisting of deep infaunal bivalves (*M. balthica*), shallow infaunal bivalves (*P. staminea* and *V. philippinarum*) and vertical tube-dwelling polychaetes (*C. capitata*). These taxa are restricted to ridge settings only in the presence of abundant *D. excentricus*.

Dendraster excentricus occurs in high-density patches all along the west coast of North America, both in intertidal (e.g., Chia 1969; Birkeland and Chia 1971; Fodrie et al. 2007) and subtidal settings (e.g., Merrill and Hobson 1970; Morin et al. 1985; Ferraro and Cole 2007). *D. excentricus* change their position in response to population pressures and food resource distribution (Chia 1969; Birkeland and Chia 1971; Fodrie et al. 2007), and are capable of both suspension and infaunal deposit feeding (Timko 1976; Ricketts et al. 1985). While suspension feeding, they orient themselves in a stationary vertical to subvertical position at the sediment-water interface, whereas while deposit feeding they are mobile and are oriented approximately horizontal within the upper decimeter of sediment (Fig. 8.7f).

An established population of *D. excentricus* excludes colonization by other macrofauna. In many invertebrate taxa (e.g., the tube-secreting polychaete *Sabellaria*

sp.), adults may influence larval settlement and metamorphosis with settlement of larvae (Burke 1986). This has been shown to be the case with *D. excentricus*. Larval settlement is not random; rather larvae are induced to settle and metamorphose in the vicinity of adult populations by a pheromone secreted into the sand (Highsmith 1982; Burke 1984, 1986). In addition, their ability to both suspension feed and deposit feed, and their propensity to quickly develop significant biomass leads to inhibition of larval settlement and survival of other taxa.

It is unlikely that the occurrence of bivalves in the substrate has any real effect on the presence or absence of *D. excentricus*. In the distal lower intertidal, infaunal bivalves are less common at shallow depths in the sediment while intermediate and deep forms are prevalent (Fig. 8.10). These taxa are capable of retracting their siphons deep within the substrate, which they were observed to do upon any slight disturbance. *D. excentricus* occupy only the upper few centimeters (<10 cm) of sediment and thus they are not significantly affected by deep infaunal bivalves. These deep infaunal bivalves, however, are likely negatively affected by the presence of abundant *D. excentricus* in the upper decimeter of the sediment. Their siphons would be prevented from easily accessing the sediment–water interface and thus their feeding behavior would be deleteriously affected. These taxa clearly benefit from colonization of substrata that *D. excentricus* avoid. We suspect that the presence of abundant *D. excentricus* also has an exclusionary effect on the presence of vertical tube-dwelling polychaete faunas, although this relationship may be more complex. The parchment-like mucus-sediment tubes of these worms are difficult to sever and would likely prove problematic to other colonizers in the abundances observed in the study area (up to 150 tubes/dm^2; Fig. 8.6f).

The Craig Bay ridge and runnel system is presumed to have evolved shortly after avulsion of the Englishman River. British Admiralty chart 579 (1928) shows the Englishman River debouching into Craig Bay. Historical air photos dating back to 1932 exhibit the same overall patterns as air photos in Hale and McCann (1982). Comparison with recent (2013) Google Earth images indicates that the positions of the ridges and runnels have shifted somewhat over the last 35 years, although their overall number and position are not remarkably different from those observed by Hale and McCann (1982). Thus, as the two end-member faunas are restricted by microhabitat, it is feasible that the geographic boundaries between them may also be stable on a decadal scale. Repeated visits to the same ridge and runnel sets over several years between 2007 and 2013 have confirmed that the boundaries between faunas do not change significantly from year to year.

Several possible reasons exist for biotic environmental segregation at Craig Bay. These include grain size, sediment moisture content, food availability, wave stress, and duration of exposure during the low tide cycles. At this locale, grain size can be discounted as an influence on ridge and runnel biotic segregation. Although grain size does change throughout Craig Bay, no significant differences were noted between adjacent ridges and runnels. In the center of the Craig Bay foreshore, the focus area of the present study, the sand consists primarily of moderately sorted fine-grained sand with no appreciable difference between the two microhabitats.

Sediment moisture content may play a role in the separation of specific biota into microhabitats. Our analyses indicate that ridge settings are significantly drier during low tide intervals than adjacent runnels (Table 8.1). This is due, of course, to longer intervals of subaerial exposure, increased likelihood of wind-induced desiccation in ridge settings, and a drop of the water table to the mean tidal flat surface during low tide. The veneroid bivalves *P. staminea* and *V. philippinarum,* both common in intertidal ridges, are apparently tolerant of prolonged subaerial exposure. Numerous examples of these bivalves were observed in the middle and proximal lower intertidal, both at the surface and within a few centimeters of the sediment surface. Other ridge taxa either occur at a depth (~ 15 to >45 cm) or occupy lengthy vertical burrows and are capable of recoiling from the surface environment. *A. artemisia,* although not present in high abundance, were observed in almost all runnels, both wet and dry. The dominant runnel taxon, *D. excentricus,* is capable of shallow burial, but is also highly mobile and shows a strong preference for runnels. *Dendraster* clearly prefers the moister sediment within the runnels rather than the drier areas that the ridges represent.

Another significant difference between the two microhabitats is the influence of wave energy. Although Craig Bay is an overall low-energy setting, strong local winds are common and wave modification of ridge tops occurs. Obligatory infaunal ridge macrofauna are naturally protected within their burrows in this setting. Conversely, the runnels are more protected from waves and form natural conduits through which drainage occurs. Although the currents are generally insufficient to modify the sediment surface and generate ripples (Hale and McCann 1982), these settings do allow for longer intervals during which suspension feeding is possible. Additional work is necessary to gauge the distribution and quality of food resources in different parts of the Craig Bay ecosystem. Based on the principle that topographic lows in intertidal areas normally sieve organics and concentrate them, TOC may be substantially higher in these areas.

It is proposed herein that the exclusion of vertical faunal components in the runnels is a direct result of sediment disturbance due to the feeding activities and population density of *D. excentricus,* which exhibit a strong preference for the moister, possibly more organic-rich sediment within the runnel areas. The distribution of *D. excentricus* is thus governed by physical criteria in the environment, primarily wave energy and resource availability/distribution. In contrast, the distribution of infaunal bivalves and tube-dwelling polychaetes is governed by biotic exclusion due to the surficial and shallow infaunal activity of *D. excentricus*.

Habitat heterogeneity has been shown to play a crucial role in the overall diversity of meiofauna within sandy beach successions (Gingold et al. 2010, 2011; Maria et al. 2013). Structurally complex, sand-dominated beaches (barred or ridge and runnel beaches) offer microhabitat heterogeneity that is absent in homogenous beach successions (Gingold et al. 2010). Runnels and ridges (sand bars) offer microhabitats with contrasting hydrodynamic regimes (Gingold et al. 2011). Meiofaunal nematode faunas, from ridges and runnels on a dissipative beach in the upper Sea of Cortez region, Mexico, were shown to have distinct, albeit taxonomically overlapping assemblages, with more homogenous compositions on the sand bars

and comparably patchy distribution in runnel settings (Gingold et al. 2011). In addition to contrasting hydrodynamic regimes, the two microhabitats have also been shown to have contrasting availability of food resources, with consistently higher food availability in runnel settings (Gingold et al. 2010, 2011). Analysis of meiofaunal nematodes from a macrotidal ridge and runnel complex on the coast of Belgium have revealed a complex association related to the two end-member habitats. Ridge settings showed strong faunal similarity between the lower, middle, and upper beach, whereas runnel faunas showed strong differences between the three zones (Maria et al. 2013).

Macrotidal wave-dominated intertidal flats on the southwestern coast of Korea show habitat heterogeneity between sand-dominated swash bars and intervening exhumed mud-dominated swales (Yang et al. 2009). In these examples, substrate plays a dominant role controlling the macrofauna in end-member microhabitats. Short-term (a few years) shallow burial (~0.5 m) results in firm ground muds that are penetrated by incipient *Psilonichnus*- and *Thalassinoides*-like burrows (likely constructed by shrimp and crabs; Yang et al. 2009). The unconsolidated sand-dominated swash bars are dominated by a diverse assemblage of forms including crabs, lingulid brachiopods, shrimp, threadworms, and tube-dwelling polychaetes (Yang et al. 2009). Although the South Korean examples clearly differ from Craig Bay in that substrate consistency plays a dominant role in macrofaunal distribution, it does provide another example wherein habitat heterogeneity plays a seminal role in faunal composition.

Biotic segregation of macrofaunal elements has not, to our knowledge, previously been reported from ridge and runnel beach successions. Analyses of ridge and runnel successions at Craig Bay clearly show that both physical and biological controls affect beach macrofauna. Preservation in the rock record of similar ridge and runnel systems would result in a succession with horizons dominated by horizontal trace fossils (*Beaconites/Scolicia* formed by echinoids) and high ichnofabric indices, interbedded with zones characterized by abundant vertical forms (*Siphonichnus, Skolithos,* and *Trichichnus* formed by bivalves and polychaetes) and low ichnofabric indices. The resultant trace fossil succession would have no bathymetric implications but would reflect the influence of original beach morphology on infaunal populations.

A similar juxtaposition of deposit-feeding and suspension-feeding behaviors has been described from storm-influenced sedimentation (Pemberton and MacEachern 1997). These authors described proximal offshore and lower shoreface successions wherein the ambient trace-fossil assemblages comprised deposit-feeding ichnocoenoses including *Planolites, Asterosoma, Thalassinoides,* and *Helminthopsis* truncated by storm-emplaced hummocky cross-stratified (HCS) sandstone (Pemberton and MacEachern 1997). The HCS tops were recolonized first by *Skolithos* and *Arenicolites* that would grade back into strata dominated by deposit feeding or were truncated by and amalgamated with other HCS beds (Pemberton and MacEachern 1997). Preserved intertidal successions that evolved in low-energy ridge and runnel successions would preserve a similar overall fabric, differing primarily in the

nature of the individual ichnotaxa involved and the nature of the preserved physical bedforms (wave and current ripples versus HCS).

8.6   Conclusions

At Craig Bay, on the Salish Sea coast of Vancouver Island, a well-developed, permanent to semipermanent, sand-dominated ridge and runnel complex has developed. In the lower intertidal, this succession is characterized by two distinct faunas. Runnel faunas are overwhelmingly dominated by dense populations of the sand dollar *D. excentricus*. These flattened, mobile echinoids live on the sediment surface and within the upper decimeter of the sand-dominated substrate. Other macroscopic infaunal organisms are absent within runnel systems, with the exception of scattered, solitary anemones (*Anthopleura artemisia*). During high-tide intervals, *D. excentricus* arrange their bodies in a vertical to subvertical orientation with their anus and oral opening exposed. They obtain food resources by grabbing organic detritus with their tube feet, then transferring it to their oral opening. During low-tide intervals, *D. excentricus* that occupy subaerially exposed runnels, burrow beneath a veneer of sand and deposit feed, while *A. artemisia* retract their arms and retreat into burrows. *D. excentricus* are highly mobile and thoroughly bioturbate the upper decimeter of sediment in runnel settings.

Ridge settings are characterized by a macrofauna distinct in both taxonomic and ethologic character from the runnels. Abundant tube-dwelling polychaetes (*Heteromastus* sp.) and infaunal bivalves (including *Macoma nasuta, M. balthica, M. secta, T. capax, P. staminea, and V. philippinarum*) characterize ridge faunas. Shallow infaunal bivalves (*P. staminea and V. philippinarum*) are limited to middle intertidal and proximal lower intertidal ridges. Deep infaunal bivalves (*T. capax*) occur solely in distal lower intertidal ridge settings. Intermediate-depth bivalves (*M. nasuta, M. balthica,* and *M. secta*) and relatively few *D. excentricus* occur on the ridges. Carnivorous polychaetes (*Nereis* sp. and *Nephtys* sp.) occur in both ridges and runnels.

Exclusion of vertical faunal components from the runnels is attributed to the feeding activities and population density of *D. excentricus,* which prefer the moister sediment within runnels. Preservation in the rock record of this type of ridge and runnel system would result in a succession with zones dominated by horizontal trace fossils (*Beaconites/Scolicia*), interbedded with zones characterized by abundant vertical forms (*Siphonichnus, Skolithos,* and *Trichichnus*). The resultant trace fossil succession would have no bathymetric implications, but would exhibit changes in trace fossil form based on distinct infaunal populations separated by physical beach morphology.

References

Anthony EJ, Levoy F, Monfort O (2004) Morphodynamics of intertidal bars on a megatidal beach, Merlimont, Northern France. Mar Geol 208:73–100

Birkeland C, Chia F-S (1971) Recruitment risk, growth, age and predation in two populations of sand dollars, *Dendraster excentricus* (Eschscholtz). J Exp Mar Biol Ecol 6:265–278

British Admiralty (1928) Strait of Georgia—Sheet 1, between Vancouver I. & British Columbia, Fraser R. to N.E. Pt. of Texada I. including Howe Sound & Jervis Inlet, Surveyed by Capt'n H.H. Richards, R.N. British Admiralty Chart 579, 1860, updated 1928, 1 chart

Brown AC, McLachlan A (1990) The ecology of sandy shores. Elseveir, Amsterdam

Burke RD (1984) Pheromonal control of metamorphosis in the Pacific sand dollar, *Dendraster excentricus*. Science 225:442–443

Burke RD (1986) Pheromones and the gregarious settlement of marine invertebrate larvae. B Mar Sci 39:323–331

Chia F-S (1969) Some observation on the locomotion and feeding of the sand dollar *Dendraster excentricus* (Eschscholtz). J Exp Mar Biol Ecol 3:162–170

Dahl E (1952) Some aspects of the ecology and zonation of the fauna on sandy beaches. Oikos 4:1–27

Defeo O, McLachlan A (2005) Patterns, processes and regulatory mechanisms in sandy beach macrofauna: a multi-scale analysis. Mar Ecol Prog Ser 195:1–20

Defeo O, Braziero A, deAlava A, Riestra G (1997) Is sandy beach macrofauna only physically controlled? Role of substrate and completion in isopods. Estuar Coast Shelf Sci 45:453–462

Defeo O, Lercari D, Gomex J (2003) The role of morphodynamics in structuring sandy beach populations and communities: what should be expected? J Coastal Res Special Issue 35:352–362

Degraer S, Volckaert A, Vincx M (2003) Macrobenthic zonation patterns along a morphodynamical continuum of macrotidal, low bar/rip and ultradissipative sandy beaches. Estuar Coast Shelf Sci 56:459–468

Ferraro SP, Cole FA (2007) Benthic macrofauna-habitat associations in Willapa Bay, Washington, USA. Estuar Coast Shelf Sci 71:491–507

Fodrie FJ, Herzka SZ, Lucas AJ, Francisco V (2007) Intraspecific density regulates positioning and feeding mode selection of the sand dollar *Dendraster excentricus*. J Exp Mar Biol Ecol 340:169–183

Fyles JG (1963) Surficial geology of Horne Lake and Parksville map-areas, Vancouver Island, British Columbia. Geological Survey of Canada Memoir 318, 25p.

Gingold R, Nundo-Ocampo M, Holovachov O, Rocha-Olivares A (2010) The role of habitat heterogeneity in structuring the community of intertidal free-living marine nematodes. Mar Biol 157:1741–1753

Gingold R, Ibarra-Obando SE, Rocha-Olivares A (2011) Spatial aggregation patterns of free-living marine nematodes in contrasting sandy beach micro-habitats. J Mar Biol Assoc UK 91:615–622

Gingras MK, Pemberton SG, Saunders T, Clifton HE (1999) The ichnology of modern and Pleistocene brackish-water deposits at Willapa Bay, Washington: variability in estuarine settings. Palaios 14:352–374

Hale PB, McCann SB (1982) Rhythmic topography in a mesotidal, low-wave-energy environment. J Sediment Petrol 52:415–429

Hauck TE, Dashtgard SE, Gingras MK (2008) Relationships between organic carbon and Pas-cichnia morphology in intertidal deposits: Bay of Fundy, New Brunswick, Canada. PALAIOS 23:336–343

Highsmith RC (1982) Induced settlement and metamorphosis of sand dollar (*Dendraster excentricus*) larvae in predator-free sites: adult sand-dollar beds. Ecology 63:329–337

King CAM, Williams WW (1949) The formation and movement of sand bars by wave action. Geogr J 113:70–85

Maria T, Vanaverbeke J, Gingol R, Esteves AM, Vanreusel A (2013) Tidal exposure or microhabitats: what determines sandy-beach nematode zonation? A case study of a macrotidal ridge-and-runnel sandy beach in Belgium. Mar Ecol 34:207–217

Masselink G (1993) Simulating the effects of tides on beach morphodynamics. J Coastal Res Special Issue 15:180–197

Masselink G (2004) Formation and evolution of multiple intertidal bars on macrotidal beaches: application of a morphodynamic model. Coast Eng 51:713–730

Masselink G, Kroon A, Davidson-Arnott RGD (2006) Morphodynamics of intertidal bars in wave-dominated coastal settings - a review. Geomorphology 73:33–49

McArdle SB, McLachlan A (1992) Sandy beach ecology: swash features relevant to the macro-fauna. J Coast Res 8:398–407

McCann SB, Hale PB (1980) Sediment dispersal patterns and shore morphology along the Georgia Strait coastline of Vancouver Island. National Research Council of Canada, proceedings of the Canadian Coastal conference, Ottawa, 1980, pp 151–163

McLachlan A, Brown AC (2006) The ecology of sandy shores, 2nd edn. Elsevier, Amsterdam

McLachlan A, Jaramillo E (1995) Zonation of sandy beaches. Oceanogr Mar Biol 33:303–335

McLachlan A, Jaramillo E, Donn TE, Wessels F (1993) Sandy beach macrofauna communities and their control by the physical environment: a geographical comparison. J Coast Res Special Issue 15:27–38

Merrill RJ, Hobson ES (1970) Field observations of *Dendraster excentricus*, a sand dollar of western North America. Am Midl Nat 83:595–624

Moreno M, Ferraro TJ, Granelli V, Marin V, Albertelli G, Fabiano M (2006) Across shore variability and trophodynamic features of meiofauna in a microtidal beach of the NW Mediterranean. Estuar Coast Shelf Sci 66:357–367

Morin JG, Kastendiek JE, Harrington A, Davis N (1985) Organization and patterns of interactions in a subtidal community on an exposed coast. Mar Ecol Prog Ser 27:163–185

Orford JD, Wright P (1978) What's in a name? Descriptive or genetic implications of 'ridge and runnel' topography. Mar Geol 28:M1–M8

Owens EH, Frobel DH (1977) Ridge and runnel systems in the Magdalen Islands, Quebec. J Sediment Petrol 47:191–198

Pemberton SG, MacEachern JA (1997) The ichnological signature of storm deposits: the use of trace fossils in event stratigraphy. In: Brett CE, Baird GC (eds) Paleontological events: stratigraphic, ecological and evolutionary implications. Columbia University Press, New York, pp 73–109

Pennington JT, Rumrill SS, Chia FS (1986) Stage-specific predation upon embryos and larvae of the Pacific sand dollar, *Dendraster excentricus*, by 11 species of common zooplanktonic predators. B Mar Sci 39:234–240

Reichmüth B, Anthony EJ (2002) The variability of ridge and runnel beach morphology: examples from northern France. J Coastal Res Special Issue 36:612–621

Ricketts EF, Calvin J, Hedgepeth JW, Phillips DW (1985) Between Pacific tides, 5th edn. Stanford University Press, Stanford

Salvat B (1964) Les conditions hydrodynamiques interstitielles des sediment meubles intertidaux et lareparttion verticale de la jemmeendogee. CR Acad Sci Paris 259:1576–1579

Short AD, Hesp PA (1999) Beach ecology. In: Short AD (ed) Handbook of beach and shoreface morphodynamics. Wiley, New York, pp 307–333

Short AD, Wright LD (1983) Physical variability of sandy beaches. In: McLachlan A, Erasmus T (eds) Sandy beaches as ecosystems. Dr. W. Junk Publishers/Kluwer Academic, Dordrecht, pp 133–144

Strathrnann M (1987) Reproduction and development of marine invertebrates of the northern Pacific coast. University of Washington Press, Seattle

Timko PL (1976) Sand dollars as suspension feeders: a new description of feeding in *Dendraster excentricus*. Biol Bull 151:247–259

Yang B, Dalrymple RW, Gingras MK, Pemberton SG (2009) Autogenic occurrence of *Glossifungites* ichnofacies: examples from wave-dominated macrotidal flats, southwestern coast of Korea. Mar Geol 260:1–5

Chapter 9
Using X-ray Radiography to Observe Fe Distributions in Bioturbated Sediment

Murray K. Gingras, John-Paul Zonneveld and Kurt O. Konhauser

Contents

Abstract The presence of an active iron cycle in modern intertidal sediment from Willapa Bay is confirmed using X-ray radiography and X-ray diffraction (XRD) analyses. The data show that Fe minerals are present in two different redox states. The first is maghemite (Fe_2O_3), which formed on the linings of irrigated burrows. The second is pyrite (FeS_2), which formed as haloes around abandoned or filled burrows. Some pyrite halos coalesced to form nodules of pyrite around the burrow fabric. The mineral paragenesis occurred as follows: (a) detrital ferrous-rich sediment (e.g., pyroxene or organometallic complexes) is buried and progressively dissolved to Fe^{2+}; (b) the Fe^{2+} either reacts with pore-water sulfide (formed via bacterial sulfate reduction) to form pyrite in the matrix or it diffuses to the burrow margins where it is oxidized to form maghemite; (c) when the burrows become abandoned and isolated from the overlying oxic seawater, the ferric iron is biologically reduced to Fe^{2+} (via bacterial iron reduction) where it repeats Step 2. The pyrite

M. K. Gingras (✉) · J.-P. Zonneveld · K. O. Konhauser
Department of Earth and Atmospheric Science, University of Alberta, 1-26 Earth Science Building, Edmonton, Alberta, T6G 2E3, Canada
e-mail: mgingras@ualberta.ca

remains stable unless exposed again to oxidizing conditions, such as later bioturbation. The inchoate nodules appear to form in less than a decade. Interestingly, the mineral distributions observed here are reminiscent of nodules observed in several other marginal marine settings, particularly those that have an oxidized-Fe-mineral core and a pyrite rind. Although those nodules are normally taken to infer evolving pore-water compositions, perhaps they are more simply explained by the processes reported above.

Keywords Fe Nodule · Early diagenesis · Invertebrate burrows · Burrow-Facilitated cementation

9.1 Introduction

In marine settings, burrows are important loci for the precipitation and concentration of seawater-, pore water-, and sediment-derived cations. This is a result of burrows being enriched in organics, such as extra polymeric substances (EPS) in the burrow margins, and associated fecal material (see Konhauser and Gingras 2007 for a summary). These locally concentrated organics promote steep geochemical gradients from the oxygenated burrow into adjacent suboxic sediment (Aller 1980; Aller et al. 1998; Zorn et al. 2006). In instances where the burrow is active, and thus irrigated by its tenant, the burrow wall is exposed to oxidizing conditions and, in most cases, the redox conditions sharply grade to reducing conditions in the sediment. As a result, cations, including those of Fe and Mn, can be enriched on the burrow lining, but when the burrow is abandoned and becomes suboxic, those metal cations can become remobilized.

The accumulation and redistribution of cations in bioturbated sediments is important to later diagenetic processes, such as the precipitation of dolomite, ferroan cements, and in the development of nodules, as commonly the source of Fe or Mg in those processes is unknown. This chapter attempts to use X-ray radiography of modern bioturbated sediment to observe some of the ways that Fe is stored and redistributed in association with biogenic sedimentary structures. The aim is to characterize the different phases of Fe mineralization observed in, and near, the burrows to estimate the rate of Fe diffusion into the sediment, and to visualize the cycling of Fe in an example of intertidal sediment.

9.2 Background

Although the observation of metal enrichment in burrow-associated cements is routine, only a few studies have attempted to quantify the amount of metal enrichment associated with burrow-margin cementation. In one of the first quantitative studies of metal enrichment in burrow linings, Over (1990) observed that Fe, Mn, Cu, Ni, and Zn were preferentially concentrated within modern and Holocene burrow

linings. Metal enrichment occurred as oxide or oxyhydroxide coatings under oxic conditions, as sulfide or phosphate phases under reducing conditions, or as organo-metallic complexes. Several other studies associate Fe enrichment in burrows to a range of processes. Carpenter et al. (1988) showed that nodule formation in the Cretaceous Fox Hills Formation (North Dakota) resulted from incipient glauccony associated with fecal material in bioturbated media. The post-depositional pyrite-cementation of worm burrows was examined by Virtasalo et al. (2012). Zorn et al. (2006) established a paragenetic model of Fe-rich nodule formation associated with *Rosselia* in Cretaceous (Horseshoe Canyon Formation) strata from Alberta. Iron has even been shown to be stored in burrows through passive infilling with goethite spherules (Rodriguez-Tovar 2005). Enrichment of metal ions has also been considered as a mechanism to explain burrow-associated dolomite in carbonate-bearing units (Gingras et al. 2004; Rameil 2008; Corlett and Jones 2012).

Less work has been conducted on the relationship between modern burrows and their role in Fe cycling in modern sediments. Löwemark and Schäfer (2003) reported the association of pyrite framboids in recent sediments that contained waste-stowage burrows. Another example of a modern biology Fe association was provided by Ferreira et al. (2007). In a study of mangrove root- and crab burrow-associated Fe, it was shown that pyrite was more abundant in more heavily vegetated zones (Ferreira et al. 2007). Thus, it appears that more oxidizing conditions and pyrite oxidation processes promote iron oxyhydroxide precipitation (Ferreira et al. 2007). Moreover, several workers have reported the general association of Fe and bioturbation in some modern sediments (Gingras et al. 1999; Wetzel 2008), but these reports do not focus on the characterization of the Fe phase.

9.3   Study Area

All of the discussed samples come from the Palix River in the brackish and tidal zone of Willapa Bay, Washington, USA (Fig. 9.1). The samples are from the box cores taken at the lower intertidal flat adjacent to the fluvio-tidal channels. Locations of the slab images presented in Fig. 9.2 are indicated in Fig. 9.1. The sedimentology and ichnology of Willapa Bay are well studied and are summarized in Clifton (1983) and Gingras et al. (1999). Bynum (2007) showed that the river-derived sediments are clinopyroxene rich and are from the Willapa Highlands immediately east of Willapa Bay.

9.4   Material and Methods

All of the samples were collected in July, 2011. One of the samples contains a lead-shot marker bed placed in 2010 to indicate the seasonal sedimentation rate and provide a time line in the sediment.
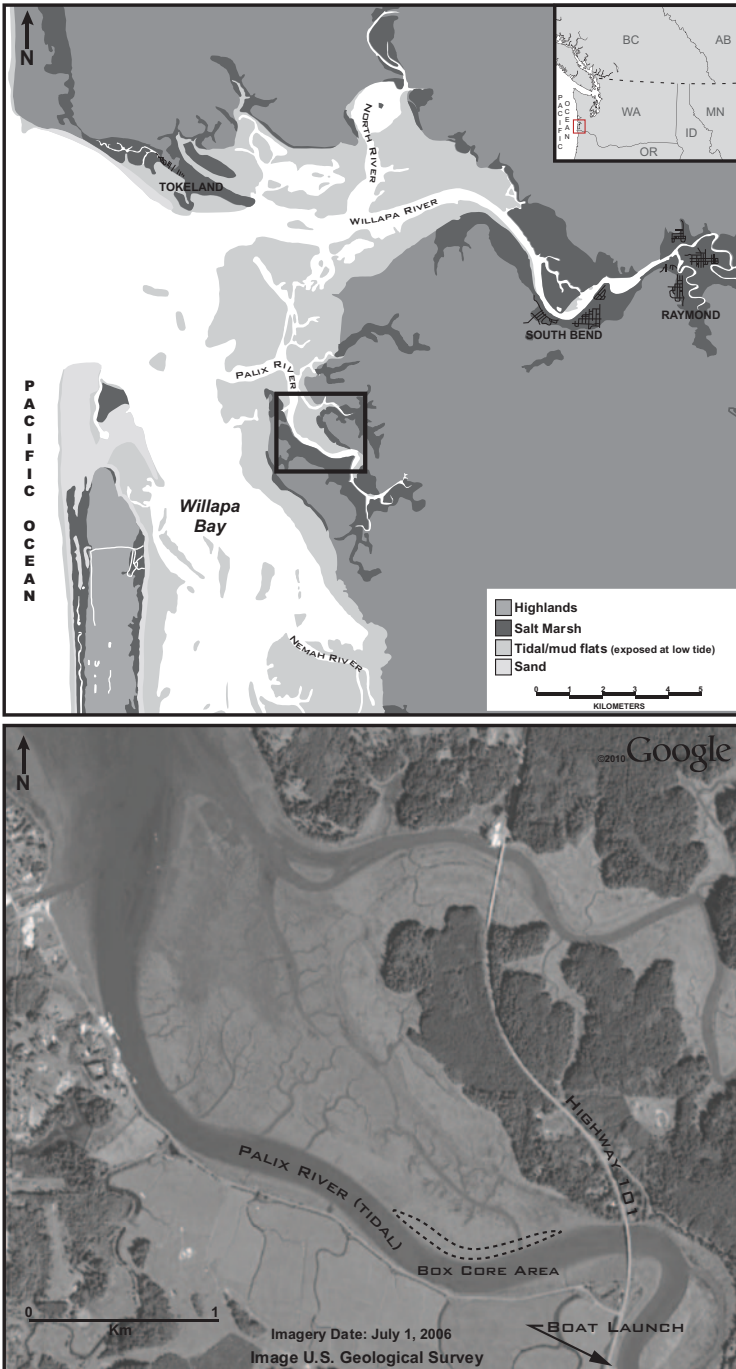
Fig. 9.1 Location map showing Willapa Bay (*top*) and the area where the box cores were retrieved (*dashed lines*). The footprint of the image in the bottom panel is shown with a heavy *black line* in the upper panel. The area is accessible with some scrambling from the HWY 101 bridge; however, safer access is to use a small watercraft from the public boat launch indicated at the *bottom right*. (Drafting courtesy of Jesse Schoengut)

Stations were chosen based on their position in the lower intertidal zone where open burrows were observed and in situ plants were absent. The stations were surveyed using a handheld Global Positioning System (GPS) with an accuracy of <10 m. Each station was sampled by collecting box core, and adjacent shovel samples were used to confirm the (macroscopic) animal content. Water was sampled from the adjacent channel.

The box cores measured 30 cm (vertical dimension) × 18 cm × 6 cm. X-rays were taken of the box cores using a Soyee portable X-ray system in plastic trays. The X-rays were collected 2 m from the source with a setting of 80 kVp/20 mA using exposure times between 1.5 and 1.7 s, depending on the mud content of the core. The X-rays provide images that reveal density contrasts. Greater densities are light colored (i.e., lower exposure of X-rays) and lesser densities are darker. In the case of the X-ray images in Fig. 9.2, void space is darkest, sand is darker than mud, and Fe minerals are lighter than the mud and sand phases (e.g., Fe-cemented burrow linings in Fig. 9.2c and d, yellow arrows). The distribution of burrows, sand, mud, and Fe cement was interpreted visually.

Mineral compositions of burrow lining and matrix were confirmed using a Rigaku Geigerflex Powder Diffractometer, equipped with a cobalt tube, graphite monochromator, and scintillation detector. The system had an online computer with analog and digital data processing capacity. Routine search/match was run on a separate computer using JADE 9.1 software and the International Centre for Diffraction Data and Inorganic Crystal Structure Database.

Water composition was determined using a Perkin Elmer Elan6000 quadrupole ICP-MS. For solution-mode analysis, a Perkin Elmer AS-91 automated sampling system was employed.

9.5   Results

Figure 9.2a shows a photograph of burrowed fresh sediment with ferric iron-stained burrow linings. The remaining images on Fig. 9.2 are X-ray plates that reveal horizontal bedding, bioturbation, iron-stained linings (see XRD results, below) (Fig. 9.2b–f), and amorphous "clouds" of Fe mineralization (Fig. 9.2e and f). Observations relating to burrow-associated Fe are separated from the description of the amorphous Fe clouds.

9.5.1   Bioturbation and Burrow Linings

Several tracemakers and their burrows are observed. U-shaped burrows (Fig. 9.2b) are made by the amphipod *Corophium volutator*. Dominantly vertical burrows with basal branches represent the domiciles of Nereid polychaetes (likely *Nereis virens*). Vertical burrows with a lower coil or loop represent the efforts of the enteropneust, *Saccoglossus kowalevskii* (Fig. 9.2c, leftmost burrow). Small-diameter burrows
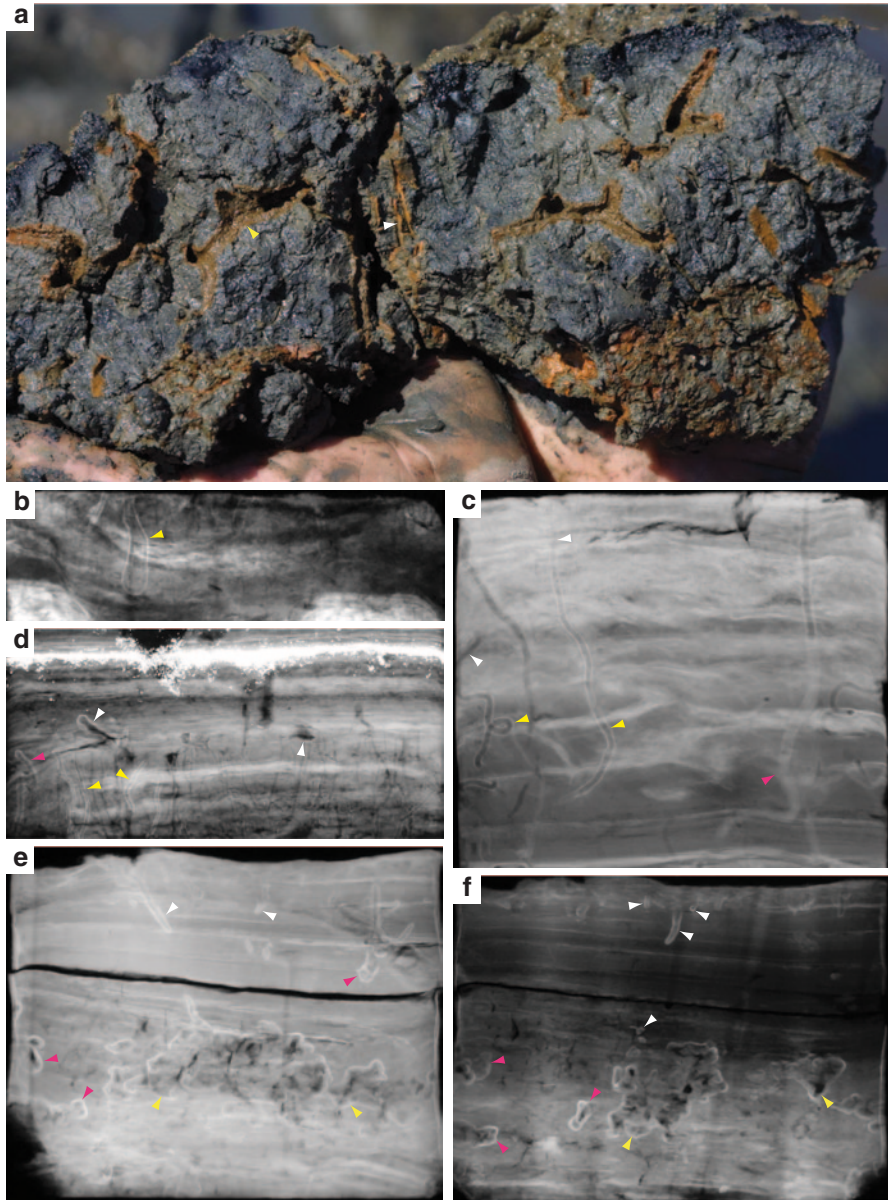
Fig. 9.2 Photograph and X-ray images of the Palix River intertidal sediments. The Fe-phase can be associated with color. Fe^{2+} is *bright orange* in color, with *deeper reds* associated with Fe^{3+}. The sulfide-bound Fe is *dark gray* to *black* (König et al. 1997). **a** Typical bioturbated intertidal sediment. The burrows are lined with amorphous Fe and/or maghemite. The darkest patches of sediment are sulfidic. This example is mixed sand and mud. Bedding is not visible, but X-rays confirm that the sediment is laminated and burrowed. Biogeochemical zones are evident as the *brown surface* and *burrow layer,* which grade into gray then black sediment. **b** *Arenicolites*-like burrow (made by *Corophium*) from the upper part of the box core. The *bright zone* is the location of

that shallowly penetrate are dominantly the work of spionid polychaetes (genus not determined). Small-diameter burrows that are observed several centimeters below the sediment–water interface are the burrows of *Heteromastus filiformis*.

Most of the open burrows show evidence of ferric iron mineralization on the burrow linings. In fresh sediment, this is observed as the orange-colored rims that contrast starkly against the dark, suboxic/anoxic sediment (Fig. 9.2a). Owing to the higher density of the ferric iron phases, they appear on all of the X-ray images as brightened linings. Burrow-associated Fe is typically <1 mm thick, is constrained to the burrow margin, and is prevalent in open burrows that have a connection to the sediment–water interface. The ferric iron lining is better developed below 2–10 cm depth, and commonly the upper part of the burrow has no observable Fe (Fig. 9.2c and d). Some burrows are partially infilled (e.g., Fig. 9.2c, pink arrow): In those examples, a ferric iron-enriched lining is not observed. Qualitatively, it appears that the locally coiled burrows of *Saccoglossus* have the best-developed ferric iron linings of the burrows observed (e.g., Fig. 9.2c) and some burrows, such as small U-shaped burrows near the sediment–water interface, have no discernible Fe-cement lining. Finally, Fig. 9.2d shows a level of burrows that have been buried by sedimentation. Although a few of these burrows still retain their ferric iron linings (yellow arrows), most of the burrows no longer possess them.

9.5.2   Reduced Iron Mineralization Zones

The other mode of iron mineralization occurs as halos around burrow fabrics. The halos are observed 2–10 mm away from, and surrounding, causative burrows (Fig. 9.2e and f, pink arrows). In extreme cases, the halos appear to coalesce into larger amorphous masses that are several centimeters across (Fig. 9.2e and f, yellow arrows). The halos are most common near burrows that have been infilled (Fig. 9.2d, pink arrow; Fig. 9.2e, white arrows) and near open burrows that have become isolated from the sediment–water interface (Fig. 9.2d, white arrows; Fig. 9.2e, yellow arrows; Fig. 9.2f, pink and yellow arrows).

Fig. 9.2 (continued) maghemite precipitation. **c** Burrows of the hemichordate *Saccoglossus* (*yellow arrows*) and *Nereis* (*pink arrow*). The *yellow arrows* also indicate areas of maghemite precipitation, whereas the *white arrows* indicate where no Fe precipitate is observable. The *pink arrow* shows an infilled part of the Nereid burrow that no longer possesses a Fe lining. **d** The burrows in the *lower part* of this image have been cut off from the sediment–water interface by previous erosion. Some burrows retain the maghemite lining (*yellow arrows*), but others do not. The *pink* and *white arrows* show areas where the Fe has diffused into the matrix and reprecipitated. The *bright zone* at the *top* of the image is a lead-shot layer emplaced for 612 months, before the sample was taken for the purpose of observing sedimentation rates. **e, f** *White arrows* indicate maghemite linings around unidentified burrows, the *pink arrows* indicate slightly remobilized Fe that is diffusing away from the burrow structures. The *yellow arrows* indicate clouds of pyrite that represent the remobilized and reprecipitated Fe. In both examples, the bedding is interpreted to represent seasonal banding resulting from mud- versus sand-dominated sedimentation in the winter and summer, respectively

9.5.3   XRD Mineralogy and Water Composition

X-ray diffraction (XRD) indicates that the burrow lining contains maghemite-C (an intermediate phase between magnetite and hematite) and typically forms via incomplete Fe(II) oxidation. The XRD signals from the analytes are weak, suggesting that some of the iron oxide is poorly crystalline. The matrix is dominated by quartz, albite and diopside, with minor pyrite. The pyrite is present as microscale framboids. XRD indicates that the pyrite is near-end-member and is neither Ni-bearing (bravoite) nor Co-bearing (cattierite). No maghemite is observed, suggesting that it is authigenically formed near burrow margins.

Inductively coupled plasma mass spectrometry (ICP-MS) analysis of the surface water collected during coring indicates a low Fe content, ~ 0.07 ppm. This is an order of magnitude higher than characteristic oceanic Fe concentrations (i.e., 0.0034 ppm; Turekian 1968).

9.6   Interpretation and Discussion

We propose that maghemite precipitates on the burrow margin where O_2 is present as a result of the animal's irrigation of the burrow. This process brings oxygenated water into the suboxic depths. Notably, O_2 does not diffuse far into the burrow lining. In a study of similar bioturbated media from the same area, Zorn et al. (2006) used an O_2 microsensor to show that O_2 diffusion into the suboxic sediment was generally limited to approximately 1 mm. The limited diffusion was ascribed to a low permeability of the sediment and a high organic content. Our observations of ferric iron present only as burrow linings, suggest a similar O_2 distribution.

Importantly, ferric iron precipitates are less common in the upper part of the burrows and are also not well developed, where the burrows have become isolated from the sediment–water interface or where the burrows are infilled. The local lack of a ferric iron precipitate near burrow apertures suggests that the Fe is primarily derived from the sediment pore water—this assertion is supported by the low concentrations of dissolved Fe measured in the depositional waters. The sediment is derived from weathering of basalt in the Willapa highlands and some Fe-rich phases, particularly clinopyroxene, are available as a source of Fe (Bynum 2007). The presence of Fe in the pore water may be explained by in situ dissolution of the detrital sediment. The Fe may also be delivered to the oceans by rivers, then bound as organometallic complexes and then deposited in association with clay minerals. Finally, Fe can also be provided through primary production. For example, many algae incorporate Fe as a trace element and some Fe may be added with the deposition of that biomass.

The Fe concentration of pore water is also a result of continuous Fe cycling in the sediment (i.e., enriched at the burrow margin, then reduced and mobilized back into the pore water). The subsequent dissolution of the ferric iron-rich linings, where

burrows are isolated from the surface or are in a state of infilling, likely occurred due to its remobilization via bacterial Fe(III) reduction. This process is driven by sediment-associated bacteria that derive their energy from the oxidation of buried organic compounds (including the burrow lining) and the concomitant reduction of ferric iron, which serves as the electron acceptor during metabolism. This process is common in marine anoxic sediments, after oxygen and Mn(IV) supplies are exhausted (see Konhauser 2007). The product of this reaction is dissolved Fe^{2+}, which then advects or diffuses away from the zone of reduction into the bulk matrix, where it is then either reoxidized (when O_2 is present) or it eventually precipitates as a ferrous-iron containing phase, such as pyrite (in saline waters) or siderite, $FeCO_3$ (in brackish waters). In our example, pyrite forms the halos and amorphous masses observed in the X-ray images.

The distribution of oxidized and reduced Fe phases in the sediment highlights the artifice of the general view of (bio)chemical zonation in marine sediments. In most of the models, the distributions of those chemical levels are portrayed as horizontal, planiform layers, also known as biogeochemical zones (seen in Fig. 9.2a as the brownish surface and burrow layer gradational to gray sediment and the black media) (König et al. 1997), that predict an orderly succession of microbial metabolites progressing from aerobic respiration, through various other metabolisms, and ultimately ending with methanogenesis at depth. Even models that account for bioturbation (Aller et al. 1998; Sandnes et al. 2000) (Fig. 9.3) have difficulties accounting for the chaotic distribution of burrows and variations in burrow distributions and depth over time. Rather, dynamic patterns of sedimentation and animal distribution for a sedimentary locale lead to the presence of burrows of variable depth, diameter, and shape, and different propensities to promote Fe mineralization. Much larger reactive surface areas contribute to greater quantities of Fe accumulating in the sediment. Fe may be reduced and precipitated as pyrite, only to be exposed to later bioturbation and thereby reoxidized (Fig. 9.3). The distributions of Fe minerals do not stabilize until the sediment passes beyond the reach of burrowing animals.

An aspect of the X-ray data is that the formation of inchoate pyrite nodules is visualized. In the provided examples, the Fe^{2+} is first concentrated within biogenic sedimentary structures, it becomes oxidized to maghemite, then subsequently reduced and redistributed as pyrite halos. Although it is not certain how long this process takes, some temporal constraints can be made from the dataset. A general observation at this location, having initiated research there in 1996, is that winter sedimentation is dominated by mud and summer sedimentation is prone to deposition of very fine sand laminae. As such, each centimeter-scale mud-sand couplet can be interpreted as a varve. Figure 9.2d, for example shows that the lower burrows are truncated approximately 3 years prior to the box-core sampling: Therein, many of the burrows have only vague ferric iron-rich linings and locally thin haloes have begun to form. The coalescent pyrite masses observed in Fig. 9.2e and f show six "annual" layers above the burrowed zone and we infer those to have been buried for 6 years before sampling: Incipient nodule formation seems to occur quite rapidly.
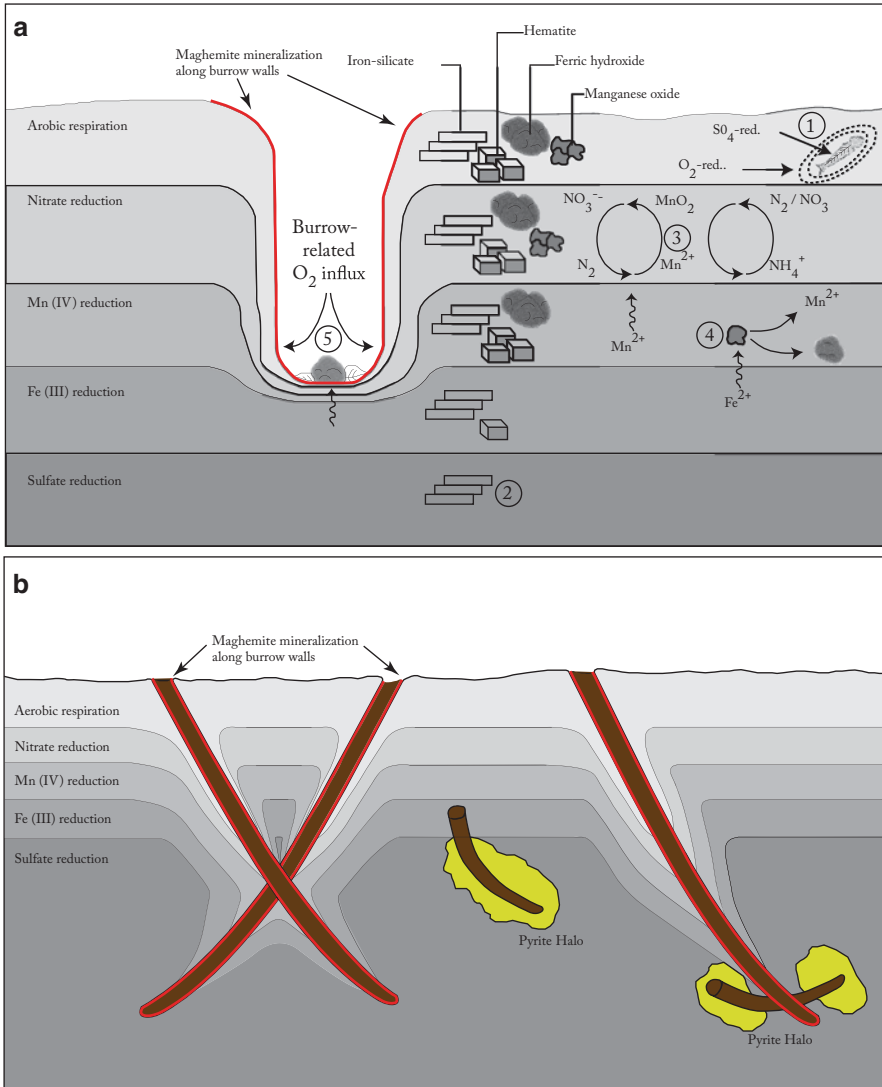
Fig. 9.3 Schematic models of geochemical levels in marine sedimentary environments. **a** Most conceptual models denote planiform chemoclines that deflect around simple burrow morphologies and may locally extend certain bacterial lifestyles deeper into the sediment (modified from Konhauser 2007). **b** Burrows generally are more complicated than the simple conceptualization and, as such, the distributions of geochemical processes are spatially complex. Also, the reactive surface area is larger. Abandoned burrows are compositionally different than the surrounding sediment and add compositional heterogeneity within geochemical zones

There are several examples of nodules that have a ferric iron core with later-stage pyrite encompassing them. These nodules are common in marginal marine strata (personal observation) and they occur in three ways: around fossil roots, in association with burrows, and as crudely spherical nodules with massive appearing

goethite at their cores. Such nodules are normally taken to indicate compositionally evolving pore water (Al-Agha et al. 1995). Another explanation is that, similar to this modern example, the minerals are essentially contemporaneous and are more closely related to the nature of Fe cementation in association with biogenic sedimentary structures.

9.7   Conclusions

Through the efficacy of X-rays for the observance of Fe mineralization in intertidal sediments, it is possible to model the distribution and cycling of Fe minerals in those deposits. In general, the source of Fe is the sediment itself, which, in this case, was derived from weathered basalts. The Fe then precipitates as maghemite on burrow linings. Following burrow abandonment or burial, the ferric iron is reduced and precipitates as pyrite haloes around the burrow fabrics. Based on the knowledge of the sedimentation rates and analysis of the sedimentary fabric, it seems likely that inchoate nodules form over the period of a few years. There are several limitations to this study: (1) Independent assessment of sedimentation rates would help interpret the temporal aspects of the Fe mineralization; (2) analysis of the fluvial sediment in the river proper might reveal the specific source of Fe; and (3) analysis of Fe-rich burrows versus burrow types that are less prone to Fe mineralization would be useful. These issues should be addressed in future research.

References

Al-Agha MR, Burley SD, Curtis CD, Esson J (1995) Complex cementation textures and authigenic mineral assemblages in recent concretions from the Lincolnshire Wash (East coast, UK) driven by Fe(0) to Fe(II) oxidation. J Geol Soc Lond 152:157–171

Aller RC (1980) Quantifying solute distributions in the bioturbated zone of marine sediments by defining an average microenvironment. Geochim Cosmochim Acta 44(12):1955–1966

Aller RC, Hall POJ, Rude PD, Aller JY (1998) Biogeochemical heterogeneity and suboxic diagenesis in hemipelagic sediments of the Panama Basin. Deep-Sea Res Part I 45(1):133–165

Bynum GL (2007) Heavy-mineral provenance in an estuarine environment, Willapa Bay, Washington, USA: palaeogeographic implications and estuarine evolution. In: Mange MA (ed) Heavy minerals in use. Developments in sedimentology, vol 58. Elsevier, Amsterdam, pp 587–605

Carpenter SJ, Erickson JM, Lohmann KC, Owen MR (1988) Diagenesis of fossiliferous concretions from the Upper Cretaceous Fox Hills Formation, North Dakota. J Sediment Petrol 58(4):706–723

Clifton HE (1983) Discrimination between subtidal and intertidal facies in Pleistocene deposits, Willapa Bay, Washington. J Sediment Petrol 53(2):353–369

Corlett HJ, Jones B (2012) Petrographic and geochemical contrasts between calcite- and dolomite-filled burrows in the Middle Devonian Lonely Bay Formation, Northwest Territories, Canada: implications for dolomite formation in Paleozoic burrows. J Sediment Res 82:648–663

Ferreira TO, Otero XL, Vidal-Torrado P, Macias F (2007) Effects of bioturbation by root and crab activity on iron and sulfur biogeochemistry in mangrove substrate. Geoderma 142(1–2):36–46

Gingras MK, Pemberton SG, Saunders T, Clifton HE (1999) The ichnology of modern and Pleistocene brackish-water deposits at Willapa Bay, Washington: variability in estuarine settings. Palaios 14(4):352–374

Gingras MK, Pemberton SG, Muehlenbachs K, Machel H (2004) Conceptual models for burrow-related, selective dolomitization with textural and isotopic evidence from the Tyndall Stone, Canada. Geobiol 2(1):21–30

Konhauser KO (2007) Introduction to geomicrobiology. Blackwell Publishing, Oxford

Konhauser KO, Gingras MK (2007) Linking geomicrobiology with ichnology in marine sediments. Palaios 22(4):339–342

König I, Drodt M, Suess E, Trautwein AX (1997) Iron reduction through the tan-green color transition in deep-sea sediments. Geochim Cosmochim Acta 61:1679–1683

Löwemark L, Schäfer P (2003) Ethological implications from a detailed X-ray radiograph and C-study of the modern deep-sea *Zoophycos*. Palaeogeogr Palaeoecol 192(14):101–121

Over DJ (1990) Trace metals in burrow walls and sediments, Georgia Bight, USA. Ichnos 1(1):31–41

Rameil N (2008) Early diagenetic dolomitization and dedolomitization of Late Jurassic and earliest Cretaceous platform carbonates: a case study from the Jura Mountains (NW Switzerland, E France). Sediment Geol 212:70–85

Rodriguez-Tovar F (2005) Fe-oxide spherules infilling *Thalassinoides* burrows at the Cretaceous-Paleogene (K-P) boundary: evidence of a near-contemporaneous macrobenthic colonization during the K-P event. Geol 33(7):585–588

Sandnes J, Forbes T, Hansen R, Sandnes B, Rygg B (2000) Bioturbation and irrigation in natural sediments, described by animal-community parameters. Mar Ecol Prog Ser 197:169–179

Turekian KK (1968) Oceans. Prentice-Hall, New Jersey

Virtasalo JJ, Whitehouse MJ, Kotilainen AT (2012) Iron isotope heterogeneity in pyrite fillings of Holocene worm burrows. Geol 41(1):39–42

Wetzel A (2008) Recent bioturbation in the deep South China Sea: a uniformitarian ichnologic approach. Palaios 23(9):601–615

Zorn ME, Lalonde SV, Gingras MK, Pemberton SG, Konhauser KO (2006) Microscale oxygen distribution in various invertebrate burrow walls. Geobiol 4:137–145

Chapter 10
Phytoliths as Tracers of Recent Environmental Change

Ethan G. Hyland

Contents

Abstract Phytoliths are more widespread, accessible, and characteristic of a local area than other terrestrial vegetation proxies. Despite work on recent soil and Cenozoic paleosol phytolith assemblages, environmental applications lag significantly behind their potential in terms of temporal resolution. Modern soil phytolith assemblages, aboveground vegetation, and soil features from Inceptisols with known vegetation and environmental histories were sampled in order to develop methods

E. G. Hyland (✉)
Department of Earth and Environmental Sciences, University of Michigan,
Ann Arbor, MI 48109 USA
e-mail: hylande@umich.edu

for describing rapid environmental change events at a high temporal resolution. Samples included agricultural fields, fluvial meanders, and wildfire sites. In each case, soil phytolith assemblages were unrepresentative of current vegetation but were characteristic of the known environmental history. As a result, rapid changes in land use or environment are identifiable in phytolith assemblages; agricultural sites can be identified by Ap horizons and grass phytoliths, fluvial meanders by weakly developed soils with channel features and spatial phytolith gradients, and wildfire sites by charcoal bodies and bimodal phytolith assemblages. These sites also provide rates of change, specific to each type of environmental change. An ecosystem experiencing wildfires changes assemblages rapidly (1–2 % per year), while change resulting from channel migration occurs slightly slower (~0.5 % per year), and that from field abandonment occurs significantly slower (<0.25 % per year). These methods can be applied to paleovegetation reconstructions, providing additional environmental information and higher-resolution vegetation interpretations. Along with more work on spatial and depth-profile sampling, these results will allow high temporal resolution for environmental and vegetation change records both in the modern and throughout the Cenozoic era.

Keywords Phytolith · Soil · Paleosol · Paleoenvironment · Paleovegetation

10.1 Introduction

10.1.1 Phytoliths

Phytoliths are an excellent tool for reconstructing vegetation assemblages of the past because they are deposited locally (primarily in situ), are taxonomically diagnostic to subfamily levels for some groups (e.g., grasses), are taphonomically resilient, and are common in most soil environments (e.g., Piperno 1988, 2006). Phytoliths are biosilica microfossils that are precipitated from unassimilated monosilicic acid that the plants uptake from groundwater (Fig. 10.1). These opaline structures form within plants, primarily in the interstices or lacunae between dermal cells and structural elements, and are believed to provide support, rigidity, and structural defenses for most plants (Piperno 1988; Jacobs et al. 1999). Due to variations in plant morphologies and in family-specific preferential silica deposition, the resulting phytoliths can have distinct morphotypes that are taxonomically diagnostic (e.g., Strömberg 2002, 2003; Piperno 2006).

Significant work by Strömberg (2002, 2003, 2005), Piperno (1988, 2006), and others have identified phytoliths from most vascular plant groups (angiosperms, conifers, ferns, etc.), and have reconstructed phytolith assemblages as far back as the Paleozoic. Modern phytolith studies have resolved many of the taphonomic and extraction-related issues surrounding phytoliths (Piperno 1988; Piperno and Pearsall 1993; Strömberg et al. 2007; Pearsall 2012; Hyland et al. 2013), and the small size (<250 μm), resistant composition (SiO_2), in situ deposition, and common occurrence throughout the lifecycle of a plant means the preservation potential
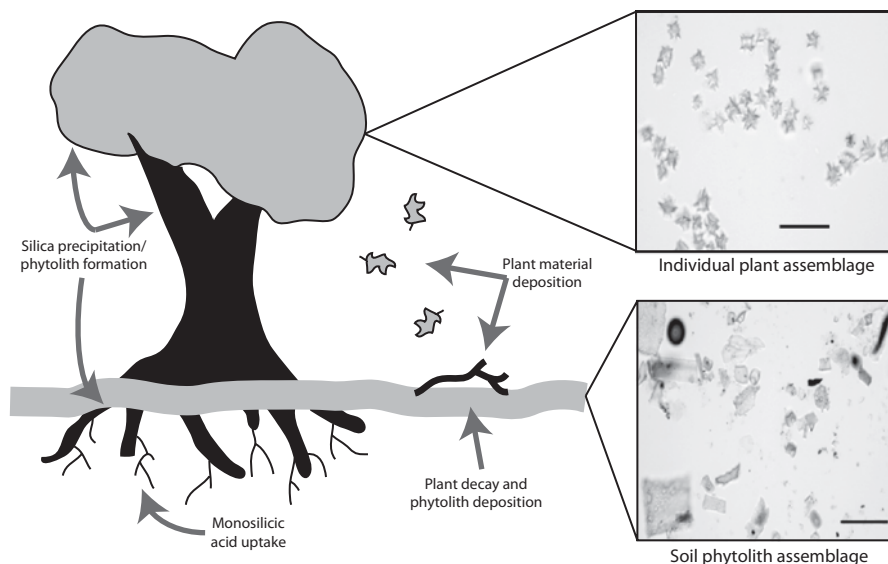
Fig. 10.1 Diagram detailing the production and deposition of phytoliths. Inset photomicrographs show examples of plant and soil phytolith assemblages. *Black bars* in images are 20 μm

for phytoliths is very high (e.g., Piperno 2006), much higher than other terrestrial records such as macrofossils or palynomorphs (e.g., Baker 1959; Hatte et al. 2008).

10.1.2   Soil Assemblages

In addition to the significant body of work on phytolith morphologies and their plant functional group affinities, phytoliths from soils, paleosols, and other sedimentary units have been used extensively to describe broad-scale ties between climate change and floral turnover throughout the Cenozoic (e.g., Strömberg 2005; Miller et al. 2012). Soils are excellent high-resolution recorders of vegetation assemblages, as they represent an integration of highly localized, temporally constrained, and relatively representative phytolith of morphologies (Fig. 10.1, e.g., Fredlund and Tieszen 1997; Piperno 2006; Hyland et al. 2013). As phytoliths occur in most soils and, therefore, most paleosols (Strömberg 2003) have identifiable environmental affinities (Borba-Roschel et al. 2006; Piperno 2006). Phytolith assemblages from soils and paleosols have been used in the interpretation of past climate and ecosystem dynamics, as well as in examining more recent phenomena such as human impacts on vegetation (e.g., Pearsall and Trimble 1984; Piperno 1985; Penny and Kealhofer 2005). Despite work on both broad-scale climate trends (e.g., Strömberg 2005) and on specific archaeological sites (e.g., Piperno 1985), however, little has been done to characterize how soil and paleosol sampling can describe how ecosystems (specifically flora) respond to environmental change on a more local or regional scale.

10.1.3   Environmental Change

Environmental or land use change is an important geological and archaeological topic, as both environmental shifts and anthropogenic influences on land surfaces can be significant drivers of ecosystem change or collapse. Most examples of past environmental change are difficult to decipher without a high-resolution vegetation record, which means that most land use studies have been conducted in stable lacustrine settings, where long-term palynological records are available (e.g., Hatte et al. 2008; Jaramillo et al. 2010). Long-term lacustrine records of pollen are not available in many locations, however, and are only representative of vegetation in certain regions (i.e., relatively proximal to large, stable lake systems). Soil is substantially more widespread and an accessible resource for vegetation records. Modern soils can record thousands of years of vegetation conditions via phytoliths (e.g., Strömberg 2005; Miller et al. 2012) and phytolith biostratigraphy has been conducted using paleosol records from many locations throughout the Cenozoic (e.g., Smith 1996; Strömberg 2005) and the Paleozoic (e.g., Carter 1999). Understanding phytolith records during times of land use change in modern ecosystems is crucial in describing natural (i.e., fires, succession, etc.) or anthropogenic drivers of environmental shifts in the past. This chapter describes phytolith records and current vegetation assemblages from modern soils that are known examples of recent environmental change. Relationships between phytoliths and vegetation are used to examine the effectiveness of such records in describing the timescale and magnitude of past change.

10.2   Methods

10.2.1   Site Selection

Each locality was chosen based on a known soil series type (Inceptisol), as described by the Natural Resources Conservation Service Soil Survey (2012), so as to minimize the potential phytolith assemblage bias (e.g., Hyland et al. 2013). Localities were also chosen to correspond with a known history of significant environmental alteration, in an attempt to examine phytolith assemblage inheritance as a function of environmental change. Each locality contained two separate sampling sites (duplicates), which were identified based on the Intensive Plot model (Barnett and Stohlgren 2003), with a larger central sampling plot (2×5 m) and four smaller sampling plots (1×1 m) located randomly within the overall site (10×20 m). Soil cores and vegetation samples were taken from each of the sampling plots, and were characterized qualitatively across the rest of the site. The three chosen localities (Fig. 10.2; Table 10.1) each had a specific history of environmental alteration: Northfield (NF) sites were subjected to widespread reseeding of tree species onto a site previously experiencing traditional farming practices (1992; ~20 years ago)
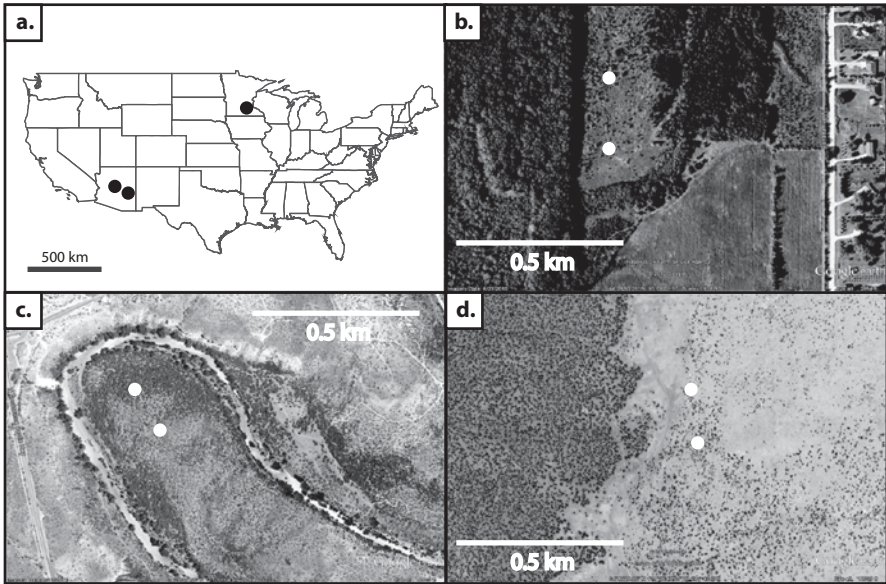
Fig. 10.2 Study areas. **a** Map of studied localities. **b** Aerial photographs of Northfield. **c** Camp Verde. **d** Knoll Lake localities. *White circles* in insets indicate the sampling sites for each locality

Table 10.1 Locality descriptions and histories

Locality	Location	Site history
Northfield, MN	44°28′52.5″N	1900?–1992 = Agricultural field
NF-1	93°8′5″W	1992 = Land fallowed, limited replanting of saplings
NF-2		1992–present = Managed forest regrowth (Bakke et al. 2010)
Camp Verde, AZ	34°36′11″N	1892–1996 = Local channel meanders migrate on average
CORN-1	111°51′14.5″W	240 m (~1–4 m year⁻¹) (Pearthree 1996; Beyer 2006)
CORN-2		
Knoll Lake, AZ	34°23′39″N	1905?–1990 = Protected forest land (Tonto National Forest)
DIS-1	111°13′48″W	1990 = "Dude" wildfire burns studied area (~28,500 acres)
DIS-2		1990–present = Unmanaged forest regrowth (Johns 2009)

(Fig. 10.2b); Camp Verde (CORN) sites are from a successional sequence on a point bar within a meander of the Verde River (Fig. 10.2c); and the Knoll Lake (DIS) sites experienced a large-scale wildfire (1990; ~22 years ago) (Fig. 10.2d). The known histories of these sites allow us to examine the effects of natural (succession, fire) and human (fallowing) impacts on vegetation over short-time scales as well as provide a model for understanding the timing and magnitude of ecosystem change in the past.

10.2.2 *Phytolith Extraction*

Modern phytolith procedures generally follow the synthetic analytical approach for Cenozoic phytolith assemblages (Strömberg 2004; Strömberg et al. 2007), which involves the study of phytoliths from all size fractions (0–250 μm), the comparison of morphotype relative frequencies over time including nondiagnostic and ecologically significant forms, and the broader generalization of correlations between phytolith assemblage composition and vegetation structure based on plant functional groups (e.g., forest vs. grassland indicators, instead of specific analogs). This approach was refined for modern applications based on a compilation of many different studies and comparison to a large modern reference collection (Strömberg 2003, 2004, 2005; Pearsall 2012; Pereira 2012; Hyland et al. 2013), and the methodology used here was modified from Strömberg et al. (2007) for the extraction of phytoliths from modern soils.

Phytolith extraction began with the systematic coring of the upper 10 cm of soil "A-horizons" without litter layers at multiple locations within each sampling plot with a 125 cm^3 push core. These samples were homogenized and subsamples of the sediment (~5 g) were processed with 10% hydrochloric acid to remove carbonates and wet oxidized in a solution of 70% nitric acid (HNO_3) and potassium chlorate ($KClO_3$) to remove organic material. Coarse material outside of the size range of phytolith morphotypes was removed with a 250 μm mesh sieve. Samples were deflocculated and rinsed by sieving through a 53 μm mesh sieve. Cleaned fractions were then recombined and material between 0 and 250 μm was gravimetrically separated via heavy liquid ($ZnBr_2$) flotation to isolate biosilica (density =2.38 g cm^{-3}). The resulting material was washed in ethanol and dried overnight before being mounted on slides in immersion oil to examine phytolith morphotypes under rotation.

Morphotypes were counted in linear, cross-slide transects and photographed through a Leica petrographic microscope (400–1000 X) on slides prepared with Cargille Meltmount 1.539. Over 400 diagnostic individuals were counted per slide and all morphotypes were identified under the classification systems of Strömberg (2003, 2005), Bozarth (1992), and Madella et al. (2005) (Table 10.2). Calculation of assemblage composition based on plant functional groups follow the designations of Strömberg (2003). Total forest indicator (FI) and grassland indicator (GI) morphotype groups follow the descriptions of Strömberg (2003), where FI total is the sum of dicotyledons, general forest indicators, conifers, non-grass plants, palms, and Zingiberales, whereas GI is the sum of all grass silica short cells (GSSCs) and diagnostic grass phytoliths (GRASS-D). While some previous authors have excluded GRASS-D morphotypes because of the possibility that their abundance is tied to the moisture availability (e.g., Bremond et al. 2002; Strömberg 2003), work in modern temperate ecosystems show little relationship between moisture and GRASS-D abundance (Hyland et al. 2013); therefore, these morphotypes were included as an important component of the total diagnostic phytolith assemblage. Error for phytolith assemblages is given at 7.7% for all phytolith groups (e.g., Strömberg 2003),

which is based on the standard deviation of multiple count experiments with morphotype classifications. For the purpose of estimating vegetation change in the most statistically appropriate manner, comparing broader-scale plant functional groups and general ecosystem types, result in a significantly smaller phytolith assemblage error of ~1.5% (Hyland et al. 2013).

10.2.3   Vegetation Cover

Within defined sampling plots, a census of major plant groups and their relative abundance was conducted and plant groups were divided into Forest Indicator (FI; closed ecosystem) and Grass Indicator (GI; open ecosystem) categories, based on their ecological affinities. For the sampled sites, ground-based estimates of relative percent cover were compared with estimates compiled from aerial photographs (e.g., Roy and Ravan 1996; Barboni et al. 2007). Aerial tree-cover data (considered FI or closed ecosystem) were derived from the Moderate Resolution Imaging Spectroradiometer (MODIS) visible bands and Normalized Difference Vegetation Index (NDVI), which provides estimates for the proportion of tree cover for any given 500×500 m sample of Earth's surface (Hansen et al. 2005). MODIS percent tree cover corresponds to the amount of skylight obstructed by tree canopies ≥ 5 m in height; values are averaged over 1 year to avoid cloud interference and phenological variation in tree cover (Hansen et al. 2003, 2005). For vegetation interpretations, soil phytolith assemblage counts were compared to ground-based and aerial percent cover estimates (e.g., Hansen et al. 2003, 2005). Although most modern studies employ some combination of percent cover and biomass estimates, many paleovegetation reconstructions simply use inferred cover estimates to determine whether a site's vegetation was open or closed, or how much of the ground surface was shaded (e.g., Strömberg 2005). This study focuses on analyzing percent cover estimates because it results in a more useful model for past environmental change, and percent cover and biomass estimates have been shown to be comparable in most temperate ecosystems (e.g., Hyland et al. 2013).

10.3   Results

10.3.1   Phytolith Assemblages

Sample material included 25 identifiable morphotypes, including 21 diagnostic phytolith groups, three nondiagnostic morphotypes, and charcoal bodies (Fig. 10.3; Table 10.2). Diagnostic morphotypes were from the general dicot (DICOT-GEN), general forest indicator (FI-GEN), conifer (CONI), general grass (GRASS-D), PACCAD clade (PACCAD-GEN), pooid grass (POOID-D), and chloridoid grass (CHLOR) plant functional groups, which were further grouped into FI and GI eco-
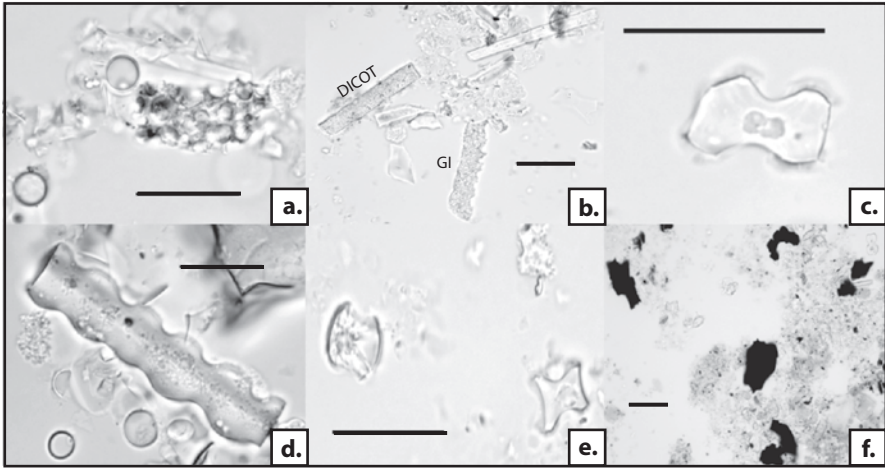
Fig. 10.3 Example phytoliths from major plant functional groups. **a** FI-GEN. **b** DICOT and GI. **c** PACCAD. **d** POOID. **e** CHLOR. **f** Charcoal fragments. *Black bar* in each image is ~10 μm

system groups for some analyses (Table 10.2). Nondiagnostic morphotypes were excluded from all analyses and charcoal bodies were recorded as additional environmental markers when present. On average, locality assemblages contained 14 morphotypes, including 5 FI groups and 6 GI groups. NF sites contained ~5.3 % FI phytoliths, CORN sites contained ~30.8 % FI phytoliths, and DIS sites contained ~65.6 % FI phytoliths.

10.3.2 Vegetation

Current vegetation at these localities is composed of 27 major plant genera which were classified as either FI or GI types based on their ecological affinities, and further categorized by plant functional groups comparable to the primary groups defined in phytolith analysis (e.g., dicot, conifer, pooid grass, chloridoid grass, etc.). Locality assemblages contained between 5 and 12 plant genera. On average NF sites contained ~43 % FI cover, CORN sites contained ~35 % FI cover, and DIS sites contained ~0 % FI cover (Table 10.3). Each locality also exhibited particular vegetation patterns based on their characteristic environmental disturbance. Vegetation at NF sites was relatively homogenous with similar plant genera and cover percentages (Fig. 10.2b). Vegetation at CORN sites was gradational with higher cover percentages and more diverse assemblages proximal to the river/riparian zone (Fig. 10.2c). Vegetation at DIS sites was patchy with standing deadwood and limited plant genera (Fig. 10.2d).

Table 10.2 Phytolith morphotype classifications with associated compound groups and total experimental counts (classifications and compounds from Strömberg 2003, 2005)

Classification	Compound	NF-1	NF-2	CORN-1	CORN-2	DIS-1	DIS-2
Knobby bodies (Kn-2)	CONI	0	0	0	0	1	2
Tracheary element (Tra-1)	FI-GEN	0	1	3	6	2	11
Mesophyll (Kn-4 or M-4)	FI-GEN	11	12	23	11	33	249
Knobbed blocks (Blo-7 or Kn-1)	FI-GEN	7	6	46	38	68	16
Ovate (Cl-1)	DICOT-GEN	4	2	10	0	33	8
Tricome (Tri-4)	DICOT-GEN	3	0	0	0	0	0
MD elongate (Elo-8 or Elo-18)	DICOT-GEN	0	0	76	52	81	39
Vertebral bodies (M-6 or M-7)	GRASS-D	3	5	15	11	0	0
Spiny elongates (Epi-11)	GRASS-D	35	36	30	28	19	18
Bulliform (Blo-10)	GRASS-D	5	4	23	18	17	4
Bilobate (Bi-6 or Bi-7)	PACCAD	36	28	8	73	15	9
Rondel (Co-2)	POOID-D	210	259	142	137	102	45
Crenate (Ce-2 or Ce-4)	POOID-D	33	27	0	0	7	0
Saddle (Sa-1 or Sa-2)	CHLOR	77	60	52	58	32	16
Elongate bodies (Elo-1 or Elo-11)	OTH	191	196	67	41	40	26
Rectangular plates (Blo-2)	OTH	87	64	3	5	8	7
Charcoal bodies	OTH	0	0	5	8	52	36
	Total	702	700	503	486	510	486
	Diagnostic	424	440	428	432	410	417

Table 10.3 Vegetation estimates from percentage cover with associated percentage FI phytolith estimates

	NF-1	NF-2	CORN-1	CORN-2	DIS-1	DIS-2
Forest cover (%)	45	40	35	50	0	0
FI phytoliths (%)	5.9	4.8	36.9	24.8	53.2	77.9

10.4   Discussion

10.4.1   Assemblages

Based on studies of modern soil phytolith assemblages and modern reference collections from similar ecosystems and climatic zones (e.g., Kerns 2001; Strömberg
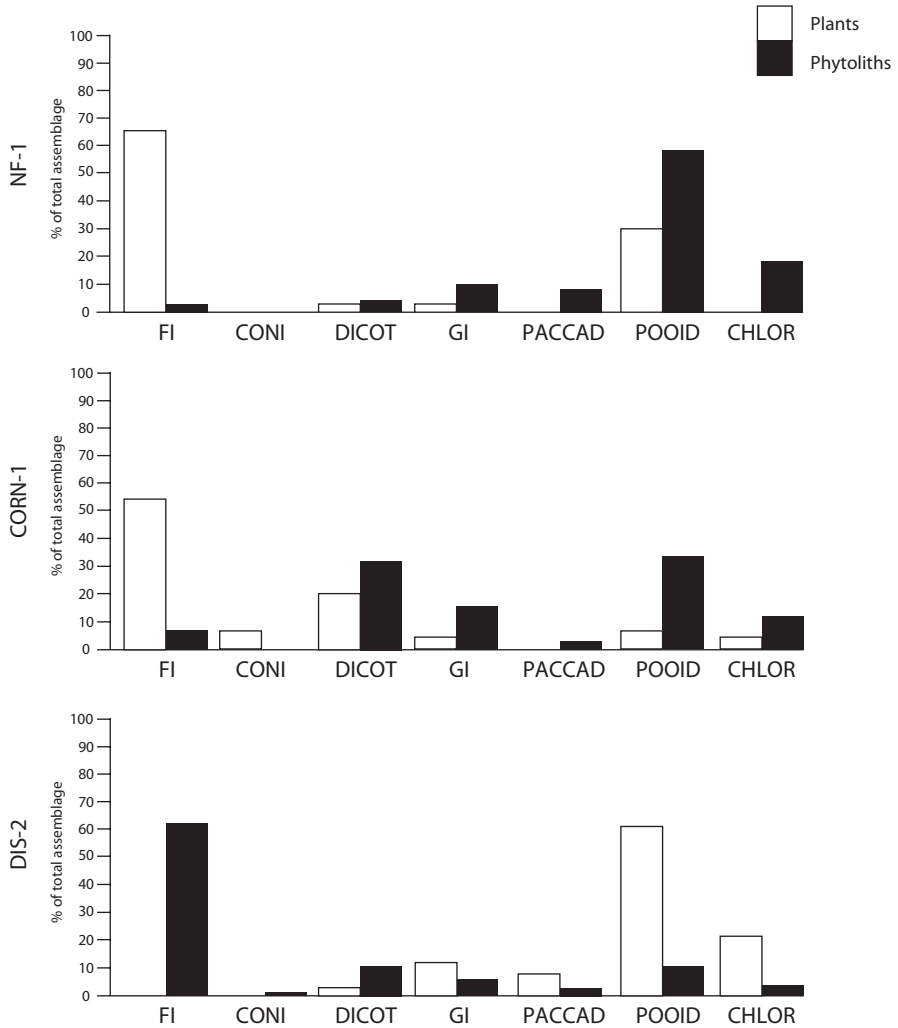
Fig. 10.4 Percent of total assemblage for each phytolith compound variable and corresponding plant category from example sites NF-1, CORN-1, and DIS-2. *White bars* indicate the percent of the total aboveground vegetation that falls into the associated plant/compound category, while *black bars* indicate the percent of the total soil phytolith assemblage for the same category (described in Table 10.2)

2002; Blinnikov 2005; Hyland et al. 2013), the significant differences between phytolith assemblages and vegetation for these sites are unexpected. Direct interpretation of soil phytolith assemblages for all the three localities (and all six sites) implies entirely different relative vegetation abundances than observed within modern sampling plots (Figs. 10.4 and 10.5). In each case, however, the vegetation assemblage inferred from soil phytolith samples is more similar to, or is only slightly modified
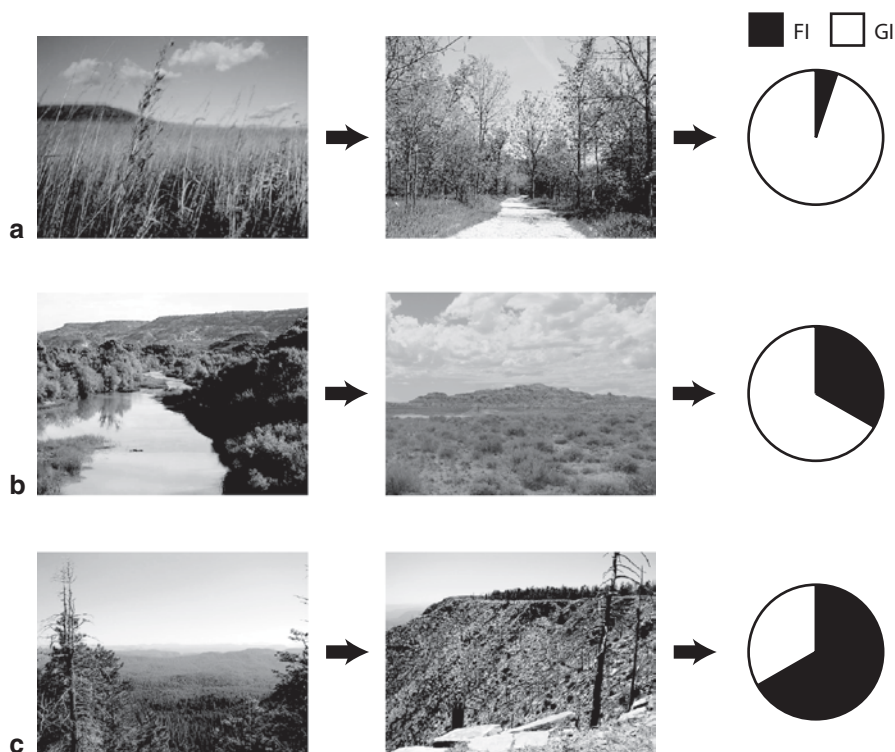
Fig. 10.5 Locality photos from. **a** Northfield (Bakke et al. 2010). **b** Camp Verde. **c** Knoll Lake (Johns 2009). *Arrows* indicate direction of change from original ecosystem (*left*) through newly established ecosystem (*center*), with the resultant soil phytolith assemblage composition (*right*)

from the known historically stable(predisturbance) ecosystem (Table 10.1). This indicates that, at least for higher-resolution sampling, local phytolith assemblages may be recording anthropogenic land use change or short-term environmental disturbances such as fluvial channel migration or wildfires within the more stable long-term ecosystem signal that is recorded by most other soil systems (e.g., Kraus 1999).

10.4.2   Environmental and Land Use Change

Due to the fact that the vegetation history for each of these localities is roughly known and that the phytolith assemblages are markedly different from modern observed vegetation assemblages (Fig. 10.5; Table 10.1), the strength of the correlation between phytolith assemblages and present vegetation can help to describe the impact of disturbances on soil phytolith assemblages and allow for the use of phytoliths as a tracer of environmental disturbance in the past. As a result of these

differences, as well as various other field observations and sample indicators, soil phytolith sampling can provide site-specific timelines for ecosystem recovery from these selected environmental disturbances and, therefore, approximate expected disturbance-specific responses for phytolith assemblages in past or unknown environments.

10.4.2.1 Agriculture

The NF locality (sites NF-1 and NF-2) has historically been a landscape characterized by human impacts, with over a century of agricultural use under traditional farming practices (Table 10.1; Bakke et al. 2010). This long history of agricultural use resulted in a disturbed soil A-horizon (Ap) due to tilling practices and, as a result of long-term grain cultivation, a characteristically grass (GI) phytolith assemblage (Bakke et al. 2010; Hyland et al. 2013). The fallowing and reforesting of the site in the summer of 1992 (Bakke et al. 2010) has resulted in a modern open forest ecosystem, with a corresponding and uncharacteristically grass-dominated (4.8–5.9 % FI) soil phytolith assemblage (Figs. 10.4 and 10.5). Given that the soil (Ap horizon) of these NF sites inherited what was likely a complete GI phytolith assemblage (~0 % FI; e.g., Hyland et al. 2013), the small percentage of FI phytoliths in the modern assemblage resulted from the past 20 years of forest growth. This suggests that changes in the A-horizon phytolith assemblage as a result of forest growth occur in the order of roughly 1 % per 4 years, as most FI groups produce phytoliths at a constant rate throughout their lifespan (e.g., Piperno 1988, 2006). The rate of FI production is overall significantly slower than the rate of GI phytolith production and explains the slow rate of change from long-term, GI-dominated agricultural assemblages to mixed-FI, open forest assemblages (e.g., Barboni et al. 2007).

  Agricultural sites have been identified in many archaeological contexts, including using phytolith assemblages (e.g., Pearsall and Trimble 1984; Piperno 1985; Piperno and Pearsall 1993) and Ap horizon soil characteristics (e.g., Retallack 2008). The combination of Ap horizon soil characteristics, such as dispersed organic carbon and unstructured or mixed organic/mineral horizons, as well as GI-dominated phytolith assemblages indicate previous agricultural usage (e.g., Piperno 1985; McDonald et al. 1990). The added characteristics of limited re-horizonation of the soil and increased FI phytolith contribution to the overall assemblage, indicate that these sites (NF-1 and NF-2) have since experienced field abandonment and subsequent forest regrowth. While many studies have identified the instances of agricultural use in the past (e.g., Piperno 1985), this locality provides evidence of land use change in the form of fallowing or field abandonment, and allows for the additional description of detailed post-agricultural site histories.

10.4.2.2 Fluvial Channel Migration

The Camp Verde locality (sites CORN-1 and CORN-2) has historically been a river valley characterized by meandering river channels and associated features, with

over a century of channel monitoring (Table 10.1; Pearthree 1996; Beyer 2006). Estimated channel migration rates based on this monitoring indicate that the studied meander (Fig. 10.2c) has moved 1–4 m year^{-1} over the past century, suggesting that the sites CORN-1 and CORN-2 were first colonized by vegetation and began forming soil roughly 100 and 50 years ago, respectively (e.g., Pearthree 1996). This successional history resulted in a weakly developed soil with fluvial features preserved in the parent material, a modern gradient of open forest (>75 % FI cover) to scrubland (<25 % FI cover) ecosystems with increasing distance from the current fluvial channel, and a mixed soil assemblage with an uncharacteristically reversed assemblage gradient containing 24.8–36.9 % FI phytoliths (Fig. 10.5; Table 10.2). Sites further from the modern fluvial channel have both been forming soil longer and were likely previously inhabited by open forest vegetation when more proximal to the channel. The increased FI phytolith composition of these distal sites (i.e., CORN-1) resulted from longer exposure to FI-dominated ecosystems as the fluvial channel migrated across the landscape. The known migration pattern of the channel and, therefore, the known length of exposure to FI-dominated ecosystems like those present in channel proximal or riparian zones suggests that changes in the soil phytolith assemblages as a result of succession occur in the order of roughly 1 % per 2 years.

Fluvial systems and the large-scale migration of channels through time have been identified in some cases through the combined use of depositional characteristics and phytolith biostratigraphy (e.g., Miller et al. 2012). Sinuous fluvial channels with fluvial parent material, characteristics of proximal soils, indicate the presence of meander systems which, in combination with a gradient of increased FI indicators in phytolith assemblages with distance from the channel, describe a full vegetation successional history of a migrating river meander at these sites (CORN-1 and CORN-2). While studies have identified and described the migration of fluvial systems in the present (e.g., Weissmann et al. 2010) and in the past (e.g., Miller et al. 2012), this locality provides the most high-resolution record available for comparison of similar paleoenvironments. Phytoliths allow for the study of vegetation responses to past fluvial systems. Spatial sampling of phytoliths provides an extremely high-resolution chronosequence (on the order of years, instead of thousands of years) unavailable in stratigraphic sampling (e.g., Miller et al. 2012).

10.4.2.3   Wildfire

The Knoll Lake locality (sites DIS-1 and DIS-2) has historically been a coniferous forest on the Mogollon Rim uplands, with over a century of ecosystem protection and monitoring within Tonto National Forest (Table 10.1; Johns 2009). The long history of protected forest ecosystem resulted in a characteristically FI phytolith assemblage and typical soil formation (e.g., Kerns 2001). In the summer of 1990, however, the locality was completely deforested during a major wildfire (Johns 2009), and has since been recolonized by only GI species, resulting in a modern grassland or scrubland (Fig. 10.5; Table 10.3). The resulting soil phytolith assem-

blage is, therefore, characteristic of neither ecosystem, with 53.2–77.9 % FI phytoliths and significant quantities of charcoal material (Table 10.2). The sites likely inherited a nearly complete FI phytolith assemblage (90–100 % FI; e.g., Kerns 2001), and after the addition of charcoal bodies and additional FI phytolith material during the fire event, have undergone the growth and deposition of GI material (~100 % GI; Table 10.3). As a result, the current mixed assemblage originates from the addition of GI phytoliths over a period of 20 years, suggesting that the soil phytolith assemblage change as a result of grass growth occurs in the order of 1–2 % per year (Fig. 10.5; Table 10.2). This significantly faster rate of change from a long-term FI-dominated forest to a GI-dominated open grass/shrubland (c.f., NF-1 and NF-2) may result from the fact that, in the case of wildfire, the original ecosystem type was completely destroyed (in the NF sites, some grass species likely remained after abandonment), and that most GI species produce phytoliths at much higher rates than the FI species (e.g., Piperno 1988; Barboni et al. 2007; Hyland et al. 2013).

Examples of wildfire and other natural disturbances from phytolith or soil records are rare, as most the studies focus on much longer time scales, although some work has been done using phytoliths to identify burned vegetation in early human sites (e.g., Albert and Marean 2012). The existence of a widespread and significant charcoal component within a soil A-horizon indicates that the locality has experienced wildfire (e.g., Albert and Marean 2012), and a contemporaneous mixed soil phytolith assemblage describes the change in ecosystem type from closed forest before the event to grassland or scrubland afterwards (Fig. 10.5). Little work has been done characterizing vegetation change due to wildfire or other abrupt disturbances in proxy records, but this locality provides an excellent high-resolution record of an abrupt ecosystem change and recovery in the past.

10.4.3   Applications of Phytolith Interpretation

Phytoliths have been used extensively to describe broad vegetation trends or identify primary ecosystem types (e.g., Strömberg 2004, 2005; Miller et al. 2012), as well as to describe vegetation use by early humans (e.g., Pearsall and Trimble 1984; Piperno 1985; Penny and Kealhofer 2005). As a result, most previous vegetation studies using phytoliths involve either broad-scale temporal sampling with thousand to million-year resolution, or spot sampling of specific archaeological sites with limited environmental applications. The modern examples discussed herein (NF, Camp Verde, and Knoll Lake localities) provide case studies detailing the uses of phytoliths as a high-resolution record of vegetation change resulting from major land use changes due to human agriculture and environmental shifts due to fluvial migration or fire disturbances.

The methods and interpretations described in these case studies can be used for investigating the full history of vegetation and land use change at archaeological sites involving agriculture, where soil phytolith assemblages change rapidly under new cultivation or the introduction of grass species (GI) to formerly forested soils

(1–2 % per year), and significantly slower where fields are abandoned to the re-growth of forest (FI) species (1 % per 4 years). These methods can also be applied to the description of recent (Pleistocene to present) environmental histories in cas-es of rapid change, such as fluvial channel migration, or even abrupt/catastrophic events, such as wildfire, where other reconstruction methods have been ineffective. In these cases, where soil phytolith assemblages are responding to drastic forces like the creation of new growth medium in the form of point bar deposition in a river, or the complete destruction of a former ecosystem by a massive wildfire, the assemblages respond more rapidly (0.5–2 % per year). After identifying an event of environmental change through the use of characteristic soil features, such as Ap horizons or substantial charcoal components, and phytolith composition, such as mixed or layered assemblages, these known rates of change can help in defining an in-depth vegetation or environmental history for a given locality (Fig. 10.5). It is important to note that in order to effectively describe the direction of environmental change for a given record, soil type and other soil properties must be appropriately characterized (e.g., Hyland et al. 2013), allowing for the distinction between the original environment (as defined by overall soil properties) and the disturbance-regime environment.

In addition to the obvious applications for modern or recent environments, these case studies have applications for high-resolution paleovegetation and paleoenvi-ronmental reconstructions as well, providing tools for further analysis of future sites as well as reanalysis of published data. As an example, Miller et al. (2012) used phytolith assemblages to describe a pattern of vegetation change in response to fluvial migration over thousands of years during the middle Eocene. This work is a spectacular example of high-resolution vegetation and environmental analysis in deeper time; however, based on the interpretations from the fluvial Camp Verde locality (CORN-1 and CORN-2), it is possible to further describe the original Eo-cene fluvial environment of Timberhills, MT (USA). The top (stratigraphically) of the Miller et al. (2012) record contains a number of Inceptisols parented on fluvial material, all of which are comparable to the depositional circumstances of the Camp Verde locality. By applying the rates of assemblage change developed above to these samples (THA09–68–69), the known soil phytolith assemblage compositions indicate that the soils at these sites, which are temporally but not spatially distinct, were roughly 20 and 150 years old, respectively (Fig. 10.6). These ages agree well with the physical attributes of the outcrop, as paleosol development indicates simi-lar ages (Miller et al. 2012) and the nearest stratigraphically comparable channel feature was roughly 10 m away from sample THA09–68 (Miller et al. 2012), im-plying that the local fluvial channel was migrating around 0.5 m year^{-1}. Such rates of channel migration are reasonable for the Timberhills site, given the similarities between the depositional environments there and at Camp Verde (e.g., Pearthree 1996; Beyer 2006; Miller et al. 2012). The addition of environmental information like soil age and fluvial migration rates can greatly improve our understanding of paleoenvironments and the details of their individual histories.
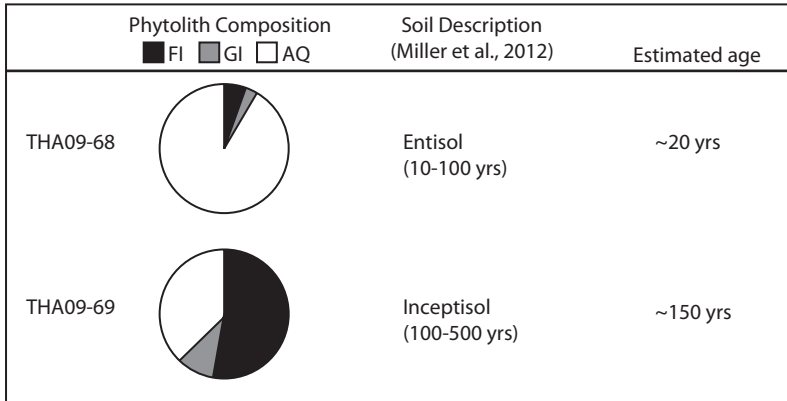
Fig. 10.6 Application of assemblage rates of change for the reconstruction of Miller et al. (2012). Estimates are based on the assumption that a time of ~0 years implies an assemblage containing 100% aquatic bodies or phytoliths characteristic of saturated soils (*AQ*), and rates of assemblage change are comparable to Camp Verde fluvial sites (*CORN-1* and *CORN-2*)

10.4.4 Further Modern Phytolith Studies

This study utilizes common sampling practices for the analysis of phytoliths, which involves the homogenization of the top 5–10 cm of a soil/paleosol A-horizon (e.g., Strömberg et al. 2007; Hyland et al. 2013). Based on the results of this study, it is clear that sampling on even the small scale at which phytolith analysis is currently performed causes some time averaging of vegetation signals (over hundreds of years). Despite the clear time averaging, studies such as this one that focus on modern materials allow for the estimation of rates of change within these assemblages, providing an even finer temporal record of vegetation shifts. Due to the fact that phytoliths are deposited via in situ decomposition of organic material (Fig. 10.1), however, it is probable that finer A-horizon sampling, perhaps on a single-centimeter scale for a given stable depth profile, would provide enough information for detailed vegetation reconstructions on a decadal or multi-year timescale. Additionally, further spatial sampling under certain circumstances where deposition is progressive (i.e., fluvial settings like sites CORN-1 and CORN-2) could provide higher resolution vegetation records by creating a detailed local chronosequence.

10.5 Conclusions

Phytoliths are useful for vegetation and environmental reconstructions, especially in cases where high-resolution records or descriptions of abrupt events are necessary. These three modern case studies provide examples of the impact of rapid environmental change on soil phytolith assemblages, which allows for the description

of both the rates of assemblage change on known timescales and the identification of characteristic assemblage features that can be used to understand the history of unknown localities. By applying these descriptors to previously published phytolith work, more detailed environmental histories can also be developed for periods in the deep past. With more work on depth profiling and spatial sampling within soils, phytolith assemblages could provide vegetation records and ecological descriptions on an extremely fine temporal scale, perhaps on the order of decades or individual years. Given these overall results, it is clear that phytoliths can provide the most direct, widely applicable, and high-resolution records of vegetation and environmental change on short-time scales.

References

Albert RM, Marean CW (2012) The exploitation of plant resources by early *Homo sapiens*: the phytolith record from Pinnacle Point 13B Cave, South Africa. Geoarchaeology 27:363–384

Baker G (1959) Opal-phytoliths in some Victorian soils and "Red Rain" residues. Aust J Bot 7:64

Bakke M, Braker N, McKone M (2010) History of the cowling arboretum. Carleton College, Northfield, MN USA. http://apps.carleton.edu/campus/arb. Accessed 1 June 2012

Barboni D, Bremond L, Bonnefille R (2007) Comparative study of modern phytolith assemblages from inter-tropical Africa. Palaeogeogr Palaeocl 246:454–470

Barnett D, Stohlgren TJ (2003) A nested-intensity design for surveying plant diversity. Biodivers Conserv 12:255–278

Beyer PJ (2006) Variability in channel form in a free-flowing dryland river. River Res Appl 22:203–217

Blinnikov M (2005) Phytoliths in plants and soils of the interior Pacific Northwest, USA. Rev Paleobot Palyno 135:71–98

Borba-Roschel M, Alexandre A, Varajao AFDC, Meunier JD, Varajao CAC, Colin F (2006) Phytoliths as indicators of pedogenesis and paleoenvironmental changes in the Brazilian cerrado. J Geochem Explor 88:172–176

Bozarth SR (1992) Classification of opal phytoliths formed in selected dicotyledons native to the Great Plains. In: Rapp G, Mulholland SC (eds) Phytolith systematics. Plenum Press, New York, pp 193–214

Bremond L, Alexandre A, Guiot J (2002) Improving vegetation models: the phytolith input. Phytolitharien 14:4–5

Carter J (1999) Late Devonian, Permian, and Triassic phytoliths from Antarctica. Micropaleontology 45:56–61

Fredlund G, Tieszen L (1997) Calibrating grass phytolith assemblages in climatic terms: application to late Pleistocene assemblages from Kansas and Nebraska. Palaeogeogr Palaeocl 136:199–211

Hansen MC, DeFries R, Townshend JRG, Carroll M, Dimiceli C, Sohlberg R (2003) Global percent tree cover at a spatial resolution of 500 meters: first results of the MODIS vegetation continuous fields algorithm. Earth Interact 7:1–15

Hansen MC, Townshend JRG, DeFries R, Carroll M (2005) Estimation of tree cover using MODIS data at global, continental, and regional/local scales. Int J Remote Sens 26:4359–4380

Hatte C, Rousseau D, Guiot J (2008) Climate reconstruction from pollen and $\delta^{13}C$ records using inverse vegetation modeling: implications for past and future climates. Clim Past 5:147–156

Hyland E, Smith SY, Sheldon ND (2013) Representational bias in phytoliths from modern soils of central North America: implications for paleovegetation reconstructions. Palaeogeogr Palaeocl 374:338–348

Jacobs B, Kingston J, Jacobs L (1999) The origin of grass-dominated ecosystems. Ann MO Bot Gard 86:590–643

Jaramillo C, Ochoa D, Contreras L, Pagani M, Carvajal-Ortiz H, Pratt LM et al (2010) Effects of rapid global warming at the Paleocene-Eocene boundary on neotropical vegetation. Science 330:957–961

Johns MA (2009) The Dude Fire. Paper presented at the 10th wildland fire safety summit, International Association of Wildland Fire, Phoenix, 30 April 2009

Kerns BK (2001) Diagnostic phytoliths for a Ponderosa pine-bunchgrass community near Flagstaff, AZ. Southwest Nat 46:957–961

Kraus MJ (1999) Paleosols in clastic sedimentary rocks: their geologic applications. Earth Sci 47:41–70

Madella M, Alexandre A, Ball T (2005) International code for phytolith nomenclature 1.0. Ann Bot-London 96:253–260

McDonald RC, Isbell RF, Speight JG, Walker J, Hopkins MS (1990) Australian soil and land survey field handbook. Inkata Press, Melbourne

Miller LA, Smith SY, Sheldon ND, Strömberg CAE (2012) Eocene vegetation and ecosystem fluctuations inferred from a high-resolution phytolith record. Geol Soc Am Bull 124:1577–1589

Natural Resources Conservation Service Soil Survey (2012) Official soil series descriptions. United States Department of Agriculture, Washington DC

Pearsall DM (2012) Phytoliths in the flora of Ecuador: University of Missouri online phytolith database. http://phytolith.missouri.edu. Accessed 1 July 2012

Pearsall DM, Trimble MK (1984) Identifying past agricultural activity through soil phytolith analysis: a case study from the Hawaiian Islands. J Archaeol Sci 11:119–133

Pearthree PA (1996) Historical geomorphology of the Verde River. Arizona Geological Survey Open-File Report 96–13. Arizona Geological Survey Press, pp 1–10

Pereira LM (2012) The Wits online phytolith database. University of Witwatersrand, Johannesburg, South Africa. http://www.wits.ac.za/Academic/Science/GeoSciences/BPI/Research. Accessed 1 August 2012

Piperno DR (1985) Phytolith taphonomy and distributions in archeological sediments from Panama. J Archaeol Sci 12:247–267

Piperno D (1988) Phytolith analysis, an archaeological and geological perspective. Academic Press, San Diego

Piperno DR (2006) Phytoliths: a comprehensive guide for archaeologists and paleoecologists. AltaMira Press, Lanham

Piperno D, Pearsall D (1993) The nature and status of phytolith analysis. In: Pearsall D, Piperno D (eds) Current research in phytolith analysis: applications in archaeology and paleoecology. (MASCA Research Papers in Science and Archaeology, University of Pennsylvania) University of Pennsylvania Press, pp 9–18

Retallack GJ (2008) Rocks, views, soils and plants at the temples of ancient Greece. Antiquity 82:640–657

Roy PS, Ravan SA (1996) Biomass estimation using satellite remote sensing data—an investigation on possible approaches for natural forest. J Bioscience 21:535–561

Smith F (1996) The evolution and paleoecology of photosynthetic pathways in grasses: estimates of the number of originations of C_4 grasses and methods for inferring photosynthetic pathways in paleocommunities using carbon isotopic signatures of fossil phytoliths. Dissertation, University of Chicago

Strömberg CAE (2002) The origin and spread of grass-dominated ecosystems in the Late Tertiary of North America: preliminary results concerning the evolution of hypsodonty. Palaeogeogr Palaeocl 177:59–75

Strömberg CAE (2003) The origin and spread of grass-dominated ecosystems during the Tertiary of North America and how it relates to the evolution of hypsodonty in equids. Dissertation, University of California Berkeley

Strömberg CAE (2004) Using phytolith assemblages to reconstruct the origin and spread of grass-dominated habitats in the Great Plains of North America during the Late Eocene/Early Miocene. Palaeogeogr Palaeocl 207:239–275

Strömberg CAE (2005) Decoupled taxonomic radiation and ecological expansion of open-habitat grasses in the Cenozoic of North America. P Natl Acad Sci USA 102:11980–11984

Strömberg CAE, Werdelin L, Friis EM, Sarac G (2007) The spread of grass-dominated habitats in Turkey and surrounding areas during the Cenozoic: phytolith evidence. Palaeogeogr Palaeocl 250:18–49

Weissmann GS, Hartley AJ, Nichols GJ, Scuderi LA, Olsen M, Buehler H, Banteah R (2010) Fluvial form in modern continental sedimentary basins: distributive fluvial systems. Geology 38:39–42

Part III
Organism-Substrate Interaction

Chapter 11
Large Complex Burrows of Terrestrial Invertebrates: Neoichnology of *Pandinus imperator* (Scorpiones: Scorpionidae)

Daniel I. Hembree

Contents

Abstract Scorpions have comprised a significant portion of the diversity of predatory arthropods since the Late Paleozoic. Many of these animals are active burrowers today and likely have a substantial, if yet unrecognized, trace fossil record. This project involved the study of the burrowing behavior and biogenic structures of the scorpion *Pandinus imperator* (Scorpiones: Scorpionidae). Individuals and groups

D. I. Hembree (✉)
Department of Geological Sciences, Ohio University, Athens, OH 45701, USA
e-mail: hembree@ohio.edu

of five animals were placed into sediment-filled terrariums for 30–50 days after which the open burrows were cast and described. Additional experiments were conducted in sediments with two different moisture contents to evaluate the response to this altered environmental condition. Specimens of *Pandinus imperator* excavated their burrows using the first three pairs of walking legs. The burrow morphologies produced consisted of subvertical ramps, helical burrows, and branching burrows. The burrow elements were elliptical in cross section (12 cm wide × 4 cm high) with concave floors and ceilings. Decreased sediment moisture reduced the complexity of the subsurface structures and reduced the likelihood of their preservation due to gravitational collapse. Burrows of *Pandinus imperator* were compared to those of the desert scorpion, *Hadrurus arizonensis,* using nonparametric statistics and found to be distinct. Data collected from these and similar neoichnological studies can be applied directly to interpret trace fossil assemblages found in continental paleoenvironments.

11.1   Introduction

The purpose of this chapter is to describe the burrowing behaviors and resulting biogenic structures of the scorpion *Pandinus imperator* (Arthropoda: Scorpiones), using basic experimental methods in a controlled laboratory setting. This chapter describes the architectural and surficial morphologies of 3D burrows produced by *Pandinus imperator* as well as surface features produced by their burrowing activity. The burrow morphologies are linked to scorpion morphology and behavior as well as environmental conditions such as sediment moisture content. The burrows of *Pandinus imperator* are then compared to burrows produced by another species of scorpion to determine if the different species produce significantly different burrows. The goal of this research is to aid in the recognition and interpretation of scorpion burrows in the fossil record for the purpose of improving our understanding of ancient terrestrial ecosystems as well as determining if specific aspects of paleoenvironments such as sediment moisture content can be evaluated using variations in burrow morphology. Finally, direct observations of the interaction of the scorpions with the sediment allow an understanding of the role of large predatory arthropods such as scorpions in the soil-forming process.

Scorpions are arthropod predators that inhabit an array of environments from rainforests to deserts around the world (Polis 1990). Scorpions (Order: Scorpiones) represent one of the oldest groups of fully terrestrial animals with a fossil record extending to the Silurian (444–416 Ma) (Petrunkevitch 1955; Kjellesvig-Waering 1986; Sissom 1990). There are currently 116 recognized fossil species of scorpions, with the majority from the Paleozoic (84), and lesser amounts from the Mesozoic (16) and Cenozoic (16) (Dunlop et al. 2013). Scorpions with morphological traits consistent

with inhabiting terrestrial environments are present by the early Devonian (410 Ma) (Kühl et al. 2012). By at least the Mississippian, scorpions were relatively common in terrestrial environments and known Carboniferous (~340 Ma) body fossils of terrestrial scorpions are morphologically similar to the extant superfamily Scorpionoidea (Petrunkevitch 1955; Kjellesvig-Waering 1986; Sissom 1990; Jeram 2001).

Trace fossils are easily preserved in many environments where body fossils are rare; therefore, the combination of both the body and trace fossil records are required to provide the best assessment of the evolutionary and biogeographic history of many taxonomic groups (Häntzschel 1975; Osgood 1975; Bromley 1996; Pemberton et al. 2001; Hasiotis 2003). Unfortunately, previously described trace fossils definitively attributed to scorpions have been limited to tracks and trails (Brady 1947; Picard 1977). This paucity of trace fossil data may simply be due to a failure of recognition, as a result of the lack of well-documented studies of the burrows produced by extant burrowing scorpions. Most descriptions of modern scorpion burrows provide only idealized diagrams or illustrations of burrow architectures (Williams 1966; Harrington 1978; Shorthouse and Marples 1980; Polis et al. 1986). Only recently have studies of scorpion burrows presented 3D burrow casts, documented the diversity of burrow morphologies produced by scorpions, described scorpion burrowing techniques, and investigated the impact of environmental conditions on burrow architecture (Hembree and Hasiotis 2006; Hembree et al. 2012).

While trace fossils are easily preserved, the interpretation of their tracemakers, the behaviors involved in their production, and the environments that influenced their production can be difficult. The study of the biogenic structures produced by modern burrowing organisms provides the data that make these interpretations possible. While experimental work with trace-making organisms has primarily involved nearshore, marine invertebrates; recently the volume of work on continental organisms has increased, especially studies involving soil invertebrates (Ahlbrandt et al. 1978; Ratcliffe and Fagerstrom 1980; Hasiotis and Mitchell 1993; O'Geen and Busacca 2001; Deocampo 2002; Tschinkel 2003; Gobetz 2005; Hembree and Hasiotis 2006, 2007; Lawfield and Pickerill 2006; Davis et al. 2007; Gingras et al. 2007; Rodríguez-Tovar 2007; Scott et al. 2007; Smith and Hasiotis 2008; Counts and Hasiotis 2009; Hembree 2009; Halfen and Hasiotis 2010; Hembree et al. 2012). In this research, the trace-making behaviors and the morphology of the resulting biogenic structures of modern continental burrowing organisms are studied in order to link specific morphologies to gross morphology, taxa, behaviors, and environmental conditions. These data are used to improve the interpretation of the paleobiological, paleoecological, and paleoenvironmental significance of continental trace fossils.

11.2 Ecology and Behavior of Burrowing Scorpions

Scorpions (Class: Arachnida) consist of almost 2,000 described extant species (Prendini 2011). Scorpions are terrestrial arthropods that have four pairs of walking legs, a pair of grasping claws or pedipalps, and a segmented tail ending in a

Fig. 11.1 *Pandinus impera-tor.* **a** Adult specimen Pedi-palp (*pd*), Chelicerae (*ce*), Telson (*te*), Walking legs (*w1–4*). **b** Side view Prosoma (*ps*), Mesosoma (*ms*), Meta-soma (*mt*)
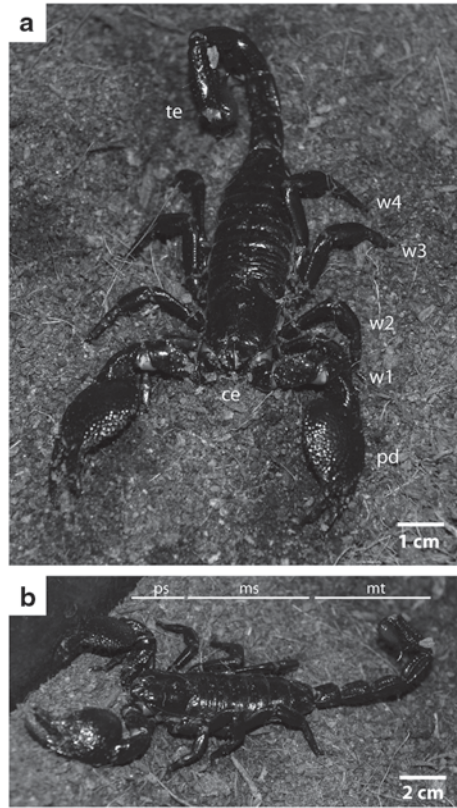
venomous telson (Fig. 11.1a) (Hjelle 1990). The body of a scorpion is divided into three parts: (1) the prosoma consisting of the carapace, eyes, chelicerae, pedipalps, and four pairs of walking legs; (2) the mesosoma consisting of seven segments each covered by a sclerotosed plate; and (3) the metasoma consisting of five seg-ments and a sixth that bears the telson (Fig. 11.1b) (Hjelle 1990). Modern scorpions have similar body plans to Paleozoic and Mesozoic scorpions and there is little difference in external morphology among modern and fossil scorpions that live in different habitats (Hjelle 1990; Sissom 1990). Scorpions inhabit a wide range of environments and climates from arid deserts to tropical rainforests on all continents except for Antarctica (Sissom 1990). Most scorpions are nocturnal and at least op-portunistically fossorial (Polis 1990). While most scorpions are solitary, some are communal and live in large groups, especially females engaged in the active care of their young (Polis and Sissom 1990). Scorpions are opportunistic predators of insects and other small arthropods as well as small reptiles and even mammals (Mc-Cormick and Polis 1990). In terms of density, diversity, and biomass, scorpions are one of the most important and successful predators in many modern habitats (Polis 1990; McCormick and Polis 1990).

Different scorpion species use a combination of chelae, chelicerae, legs, and even the tail in burrow construction (Williams 1966; Eastwood 1978; Harrington 1978; Koch 1978; Shorthouse and Marples 1980; Polis et al. 1986; Polis 1990; Rutin 1996; White 2001; Hembree et al. 2012). Burrows provide scorpions a refuge from predators and harmful environmental conditions such as extremes in temperature or humidity (Newlands 1969; Polis 1990). The burrow is an important part of almost all of the scorpion's life activities including birth, maternal care, molting, feeding, and in some species mating (Polis 1990). Burrowing scorpions spend the majority of their lives in their burrows, some only leaving for courtship, mating, and the dispersal of newborn (Williams 1966; Hadley and Williams 1968; Tourtlotte 1974; Koch 1978; Polis 1980; Bradley 1982; Shachak and Brand 1983; Warburg and Polis 1990). Burrowing scorpions that actively hunt on the surface still spend most of their time below the surface (Hadley and Williams 1968; Tourtlotte 1974; Polis 1980; Bradley 1982; Polis 1990). While on the surface, the majority of burrowing scorpions stay within 1 m of their burrow entrance (Polis 1990). These aspects of scorpion behavior highlight the importance of burrows to their ecology and evolutionary history.

Pandinus imperator, Koch 1842 (Scorpionidae), commonly referred to as the emperor scorpion, is among the largest extant species of scorpion reaching up to 20 cm in length and 65 g in mass (Sissom 1990). They are communal animals and can live in groups of up to 15–20 individuals (Mahsberg 1990, 2001). *Pandinus imperator* is a nocturnal hunter characterized by a pair of large pedipalps used in prey capture and defense (Casper 1985). Their large size allows them to feed on a variety of invertebrates including other scorpions as well as small vertebrates such as reptiles and rodents (McCormick and Polis 1990). *Pandinus imperator* inhabits forests and savannahs of West Africa with warm humid to subhumid climates and is known to be an obligate burrower (Polis 1990; Sissom 1990; Mahsberg 2001). Despite this knowledge, there has been very limited research on how these burrows are constructed or the details of their morphology.

11.3 Materials and Methods

Fifteen individuals of *Pandinus imperator* were acquired from a commercial source for use in this study. The scorpions were all mature adults (male and female) that averaged 140 mm in length (110–160 mm, SD = 14.1) from prosoma to metasoma and 25 mm in maximum width (30–40 mm, SD = 6.2) excluding the walking legs. The scorpions were allowed to acclimate in the laboratory for 1 month prior to the start of the experiments. During the acclimation period, specimens of *Pandinus imperator* were housed in groups of five individuals within 212-l terrariums filled with 20 cm of organic-rich soil and were handled as little as possible. A temperature range of 25–30 °C and humidity of 60–70 % was maintained for the enclosures and a 12-h light–dark cycle was kept in the laboratory. The scorpions were fed live crickets placed in the tank once per week; the crickets were consumed gradually over the course of the week. The environmental parameters and feeding routine were maintained during the experiments as well.

Table 11.1 Experimental parameters and resulting burrow morphologies. Sediments include organic (O), clay (C), and sand (S) components

Tank size	Specimens	Sediment composition	Sediment depth	Sediment density	Sediment moisture (%)	Burrow architecture
212	1	50-25-25% 0-C-S	55	1.1–1.4	20	None
212	1	50-25-25% 0-C-S	55	1.1–1.4	50	SR
212	1	50-25-25% 0-C-S	55	1.1–1.4	50	SR, HB
212	5	50-25-25% 0-C-S	55	1.1–1.4	20	None
212	5	50-25-25% 0-C-S	55	1.1–1.4	50	SR
212	5	50-25-25% 0-C-S	55	1.1–1.4	70	SR, HB, BB

Sediment density values are in kgf/cm^2, sediment depths are in cm, sediment moisture values are in percent total volume

SR subvertical ramp, *HB* helical burrow, *BB* branched burrow

Six different experimental set ups (Table 11.1) were designed in order to: (1) observe the burrowing methods of *Pandinus imperator* individually and in groups, (2) document the surface features produced during the occupation of the test enclosures, (3) observe the behaviors associated with the burrows, and (4) document the basic burrow morphologies by producing 3D casts once the scorpions had been removed.

Single specimens and groups of five specimens were placed in sediment-filled 212 L (76 L × 46 W × 64 H cm) terrariums. Two sets of trials were run with different numbers of scorpions to determine the effects of group behavior and solitary behavior on burrow morphology. The terrariums were filled with 55 cm of sediment. The sediment thickness provided a deep substrate for burrowing but also enough open space beneath the terrarium cover (~ 10 cm) to allow the placement of a water dish, rock, and other surface shelter as well as to prevent escape from the enclosure. The sediment used to fill the experimental enclosures had a moderate bulk density ($1.1–1.4$ kgf/cm^2) and was composed of 25% sand, 25% clay, and 50% organic matter. The density of the sediment was quantified using a Field Scout SC900 Soil Compaction Meter (Spectrum Technologies Inc.). The sediment composition was selected as the closest to the natural soil conditions inhabited by *Pandinus imperator*. The sediment components were thoroughly mixed to produce a homogenous composition and water was added to the mixture prior to adding it to the experimental enclosures. The sediment was mixed and compressed as it was added to the terrarium in order to improve homogeneity and increase density when needed. While sediment composition and density were maintained throughout the trials, the scorpions were exposed to variations in sediment moisture content. Soil moisture content was set to 20, 50, and 70%. These moisture values were obtained by adding predetermined quantities of water to the sediment mixture when the terrariums were filled. Sediment moisture was maintained during the trials by spraying the surface of the tank daily with 100, 200, and 300 mL of water to make up for evaporative water loss. The moisture content of the sediment was quantified using an Aquaterr EC-300 Multimeter. Measurements were taken vertically every 15 cm to ensure that the moisture content was homogenous.

    Each experiment commenced with the placement of the scorpions into an enclosure. The scorpions were left in the enclosures for a period of 30–50 days before removing the specimens, when they were on or near the sediment surface. The final duration of any experiment depended upon the timing of the removal of the scorpions; first attempts to remove the scorpions began after 30 days. The scorpions were observed and digitally recorded as they burrowed. Observations made during initial burrowing included the time that elapsed before the scorpion began burrowing, the burrowing techniques used, and the time required for the animal to completely burrow into the sediment. Once the burrow was completed, daily observations were conducted to document the excavation of new burrows, destruction of old burrows, and the behaviors directly associated with the burrows. If no burrows were constructed by the end of an experimental period noted, the animal was removed, and any surface features were documented. After removing the scorpions, open burrows were filled with Drystone® plaster, excavated, and described.

    The description of the 3D burrow casts included qualitative and quantitative aspects of their architectural and surficial morphology (Fig. 11.2). Architectural morphology consists of the burrow's general appearance, dimensions, cross-sectional shape of shafts and tunnels, orientation in the sediment, type and amount of branching, and degree of interconnectedness of different burrow elements. The surficial morphology includes structures (scratches, bumps, and linings) on or around the burrow walls produced during excavation and occupation of the burrow. For each burrow cast produced in these experiments, ten quantitative measurements of burrow morphology were recorded: (1) maximum depth (D), (2) total length (L), (3) tunnel or shaft width (w), (4) tunnel or shaft height (h), (5) ratio of cross-sectional width to height, (6) tunnel or shaft circumference (c), (7) angle of shafts or tunnel with respect to the horizontal (OA), (8) angle of branching (BA) if present, (9) complexity, and (10) tortuosity (Fig. 11.2). Maximum depth of a burrow was measured from the highest surface opening to the base of the deepest tunnel. The total length of the burrow is the sum of the length of all of the shafts, tunnels, and chambers. The width, height, and circumference of the tunnels and shafts were measured every 5 cm along the length of the burrow. The cross-sectional width-to-height ratio was determined from the average widths and heights of the burrow's tunnels and shafts. The angle of branching was the acute angle between intersecting burrows produced away from the walls of the enclosures. Burrow complexity and tortuosity are independent of scale and are used to compare burrow systems produced by animals of different sizes (Meadows 1991). Burrow complexity (C) is a function of: (1) the number of segments (s)—defined as non-branching lengths of a burrow, (2) the number of openings to the soil surface (e), and (3) the number of chambers (h)—defined as areas with a greater cross-sectional area than the adjacent segments (Fig. 11.2b). These measurements define an index of complexity (C) that is calculated by $C = s + h + e$, where $C \geq 1$. The tortuosity (T) of a burrow system is a measure of the deviation of the tunnels from a straight line (Fig. 11.2c). The tortuosity of an open segment is calculated by dividing the total length of the segment (u) by the straight-line distance between the ends of the segment (v). The tortuosity index of a burrow system is determined by calculating the average tortuosity of all the burrow segments.

Fig. 11.2 Burrow description models. **a** Architectural morphology was described by the angle of orientation (OA), maximum depth (D), tunnel, shaft, and chamber width (w), height (h), and circumference (c), total length (L), and branching angle (BA). **b** Complexity (C) is the sum of the number of segments (s), chambers (h), and surface openings (e) within a single burrow system. **c** Tortuosity is the average sinuosity of all of the segments within a burrow system. The tortuosity of a single segment is found by dividing the total length (u) by the straight line distance (v). (Modified from Hembree et al. (2012))
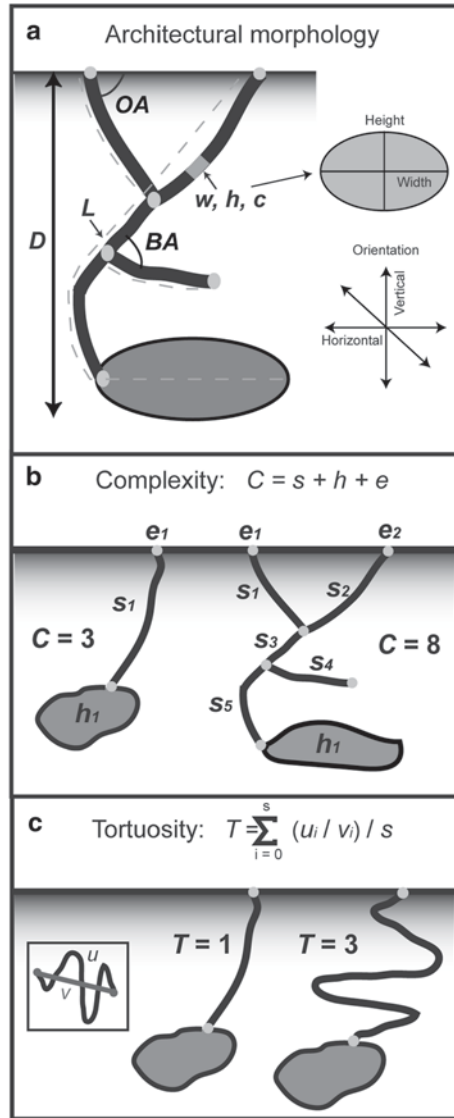
These quantitative aspects of burrow morphology were used to determine the level of similarity between the different burrows produced by specimens of *Pandinus imperator,* their level of similarity to burrows produced by another species of scorpion (*Hadrurus arizonensis*) in separate laboratory experiments (Hembree et al. 2012), and the effect of sediment moisture on burrow morphology. To determine the relative level of similarity between burrows, ten quantitative aspects of burrow morphology were used to compare the different burrow casts using a Bray–Curtis similarity test, a nonparametric statistical analysis used to determine the level of

similarity between multiple samples with multiple quantitative properties (Hammer and Harper 2006). The Bray–Curtis similarity test was ideal for this study because it analyzes all aspects of the burrow's morphology together, rather than simply comparing one feature such as diameter, length, or volume against another. This is important because the architecture of a burrow is a sum of many parts that should not be separated; while it is possible that the burrows of several different animals may have the same diameter, length, or volume, it is much less likely that all three are the same. The Bray–Curtis similarity test ranks the level of similarity from 0 to 1, 0 indicating completely different samples and 1 indicating identical samples. In this analysis, finer divisions were defined; values from 0.9–0.8 were considered to indicate a high degree of similarity, 0.7–0.6 a moderate degree of similarity, and values ≤ 0.5 dissimilarity. Mann–Whitney and Kolmogorov–Smirnov tests were used to determine the potential equality of the median and distribution of the individual properties of each burrow, respectively. These two tests were also used to compare the individual properties of the burrows of *Pandinus imperator* and *Hadrurus. arizonensis*. A *p* value of < 0.05 indicates a significant difference between two populations (Hammer and Harper 2006).

The properties of the burrows produced by *Pandinus imperator* in sediments with different moisture contents (20, 50, 70 %) were compared using Spearman's rank correlation, a nonparametric technique used to determine if two variables vary together (Hammer and Harper 2006). A correlation coefficient (Rs) of 0.90 or higher suggests a high correlation (Hammer and Harper 2006). Mann–Whitney and Kolmogorov–Smirnov tests were then used to determine the potential equality of each of the properties of the burrows produced under the different sediment moisture conditions. All statistical analyses were performed with Palaeontological Statistics (PAST ver 2.16).

11.4 Results

Specimens of *Pandinus imperator* produced temporary to permanent open burrows with three different architectural morphologies in sediment with moderate to high sediment moisture content (Table 11.1). A total of 15 complete and well-preserved burrow casts were produced from the experimental trials (Table 11.2). Some experiments resulted in incomplete burrow casts as a result of subsurface gravitational collapse or burrows that were destroyed or filled in by the scorpions before they could be preserved. In all experiments, however, the architectural morphology of the burrows *in situ* was observed and recorded.

11.4.1 Behavior

Specimens of *Pandinus imperator* started to burrow within 1–24 h of placement into the experimental enclosures. *Pandinus imperator* burrowed, by direct excavation,

Table 11.2 Architectures, measurements, and experimental parameters of 15 representative, 3D burrow casts produced by *Pandinus imperator* (ES)

	ES1	ES4	ES6	ES7	ES9	ES11	ES13	ES14	ES15	ES2	ES3	ES5	ES12	ES8	ES10
Architecture	SR	SR	SR	SR	SR	SR	SR	SR	SR	HB	HB	HB	HB	BB	BB
Surface openings	1	1	1	1	1	1	1	1	1	1	1	1	1	1	1
Maximum depth	6.5	7.5	13.0	5.0	13.0	6.0	7.0	13.0	11.0	12.5	16.0	14.0	15.0	30.0	13.0
Total length	28	12	27	18	34	29	19.5	25	14.5	34	34	29	32	80	28
Maximum width	7.6	6.8	6.2	6.3	11.6	7.1	6.3	7.1	6.4	12.0	11.3	6.4	8.3	10.6	9.9
Minimum width	6.0	4.4	4.1	3.6	3.9	3.8	4.8	5.3	4.5	7.4	5.5	4.3	4.2	4.3	3.9
Average width	6.7	6.0	4.9	5.6	8.2	6.3	5.8	6.9	5.3	9.6	8.7	5.5	6.5	6.8	6.8
Maximum height	4.4	2.9	4.8	3.6	4.2	3.8	2.7	5.8	5.4	7.1	5.4	3.4	5.9	4.4	4.9
Minimum height	2.9	1.9	2.3	2.2	1.9	1.7	1.8	4.0	1.9	3.0	3.9	2.1	2.0	2.6	2.4
Average height	3.7	2.5	3.0	2.8	2.9	2.9	2.5	5.0	3.5	3.9	4.5	2.7	4.5	3.3	3.6
Average W/H ratio	1.8	2.4	1.6	2.0	2.8	2.2	2.3	1.4	1.5	2.5	1.9	2.0	1.4	2.1	1.9
Maximum circumference	23.5	16.1	15.5	18.0	28.0	19.5	16.0	20.0	19.5	28.5	27.1	16.0	22.5	23.0	27.0
Minimum circumference	17.5	8.4	11.0	12.0	10.0	12.0	13.0	16.0	13.0	20.5	12.2	11.0	12.5	12.0	12.0
Average circumference	19.3	13.8	13.0	15.1	19.7	17.0	15.2	18.8	15.6	24.8	21.5	14.1	19.0	17.1	18.8
Maximum slope	20	40	50	20	50	20	20	35	25	30	30	50	30	40	50
Minimum slope	15	40	20	0	0	0	0	20	25	0	0	0	0	0	40
Average slope	17	40	40	13	19.3	6.7	13	27.5	25	14	24	21	18	19	47
Branching angles	NA	NA	NA	NA	NA	NA	NA	NA	NA	NA	NA	NA	NA	90	90
Complexity	3	2	3	3	3	3	2	2	2	3	3	3	3	4	4
Tortuosity	1.0	1.0	1.0	1.1	1.1	1.0	1.0	1.1	1.0	1.7	1.1	1.1	1.5	1.0	1.0
Sediment Moisture	70	50	70	50	70	70	50	50	50	70	70	70	70	70	70
Specimens	5	1	1	1	5	5	1	1	1	5	5	1	1	5	1

All measurements are in cm

NA not applicable

Fig. 11.3 Burrowing techniques used by *Pandinus imperator*. **a** Excavation of sediment using the first two to three pairs of walking legs. **b** Excavation can be accomplished even in a vertical orientation. **c** Excavated sediment is gathered and held with the first three pairs of walking legs and dragged away from the burrow opening
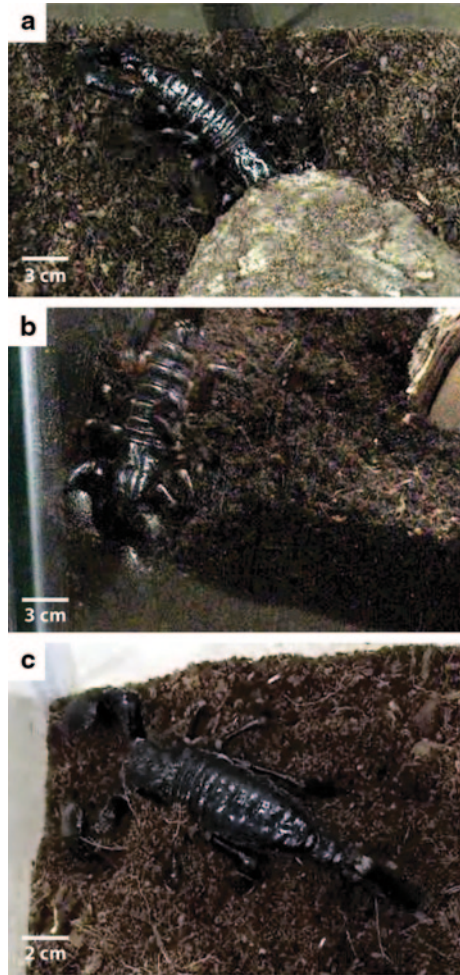
using the first two to three pairs of walking legs (Fig. 11.3). The walking legs were used to dig sediments from the sediment surface and the burrow walls. The sediment was gathered into a loose mass, held with the first two to three pairs of walking legs, and then dragged back out of the burrow and away from the burrow opening (Fig. 11.3c). The excavated sediment was deposited in a broadly distributed pile located next to and up to 20 cm away from the burrow opening that was used consistently during excavation. During some intervals of burrow expansion, sediment was deposited along the floor of preexisting tunnels. Only very rarely were entire tunnels backfilled and this occurred only before the abandonment of burrows.

Generally, at least one or two burrows were started and abandoned before construction of the final, permanent, burrow began. These temporary burrows were either never occupied or occupied for less than 24 h. These burrows tended to be very shallow, no longer than the length of the scorpion, and went underneath objects such

Fig. 11.4 *In situ* burrows. **a** Terminal chamber in a helical burrow. **b** A subvertical ramp. **c** The subhorizontal tunnel in a branched burrow
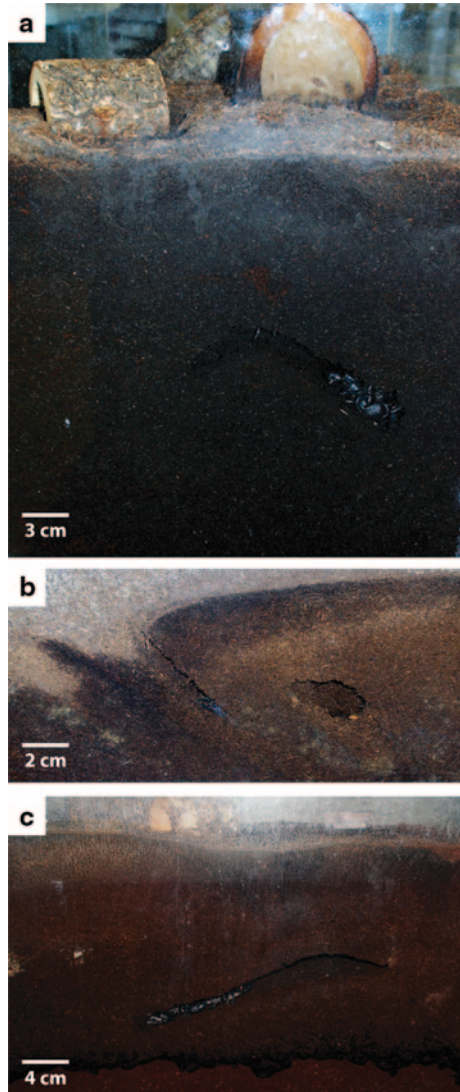
as logs, stones, or water dishes. In experiments with five individuals, each scorpion may have produced its own temporary burrow or up to three scorpions may have occupied the same shallow burrow. This involved one individual digging the burrow followed by one or two other scorpions entering the finished shelter. Construction of the final, permanent burrow occurred within 3–4 days after the scorpions were placed into the tanks. In experiments with five individuals, this burrow was typically constructed by only one or two of the scorpions. The rest simply entered the burrow after it was completed. Construction of the final burrow did not stop, however, as the structures were repaired as needed or modified to make the burrow deeper, lengthen the tunnels, widen the chambers, or construct new branches.

Some of the permanent burrows were constructed against the wall of the enclosure allowing the observation of the scorpion behavior within the burrows (Fig. 11.4). Once the permanent burrows were constructed, the scorpions moved very little within the burrow. When five individuals occupied a single burrow, the scorpions normally had little interaction with one another. There were, however, isolated occurrences of aggression between individuals and even cannibalism in these groups. The scorpions stayed within their burrows approximately 90 % of the time during the experiments coming to the surface only during active excavation or active hunting. Coming to the surface to acquire food was not necessary, however, since the prey animals (crickets) sought out and freely entered the maintained openings of the scorpion burrows. The scorpions were often positioned just inside the burrow opening and would capture and consume crickets within the burrow. This further reduced the need for the scorpions to leave their burrows.

11.4.2   Surface Morphology

The experimental tanks were set up with flat surfaces prior to the introduction of the specimens of *Pandinus imperator*. The scorpions produced an uneven surface topography as a result of their burrowing activity. The uneven surface occurred around burrow entrances and was the result of the mounding of sediment from subsurface excavation and surface collapse around unstable openings (Fig. 11.5a, b). This uneven topography was most pronounced in experiments with moderate (50 %) to low (20 %) sediment moisture. Relief of up to 6 cm was produced between the depressions and mounds.

Open burrows constructed by *Pandinus imperator* had distinct surface openings. Burrow openings occurred individually (Fig. 11.5a) or paired (Fig. 11.5b) in tanks with multiple individuals; these consisted of one main burrow and a second smaller burrow which, while in close proximity, did not intersect below the surface. Burrow entrances were typically positioned beneath a stone, log, or other flat object that concealed the opening from above (Fig. 11.5c). Scorpions positioned themselves near the burrow entrance which aided in ambush prey capture (Fig. 11.5d). Sediment piles extended away from the burrow entrance which grew as the burrow was expanded and maintained over the experimental period (Fig. 11.5e). The openings were triangular in shape and on average 5 cm wide and 4 cm high at the center of the entrance (Fig. 11.5f).

11.4.3   Burrow Morphology

Burrows constructed by *Pandinus imperator* were kept open to the surface throughout the course of the experiments. All of the burrows had a single surface opening. The burrows had sharp, irregular walls with no evidence of a constructed lining. There were three basic types of burrows produced by single and multiple

Fig. 11.5 Surface features and behaviors associated with *Pandinus imperator* burrows. **a** Burrow openings (at *arrow*) are often present beneath flat objects such as rocks or wood. **b** Multiple burrow openings (at *arrows*) may be close together. **c** Specimens of *Pandinus imperator* are typically near the burrow opening. **d** Burrow openings are used as a site of ambush predation. **e** Large piles of excavated sediment extend outward from the burrow opening. **f** Burrow openings of *Pandinus imperator* have a distinctive triangular morphology
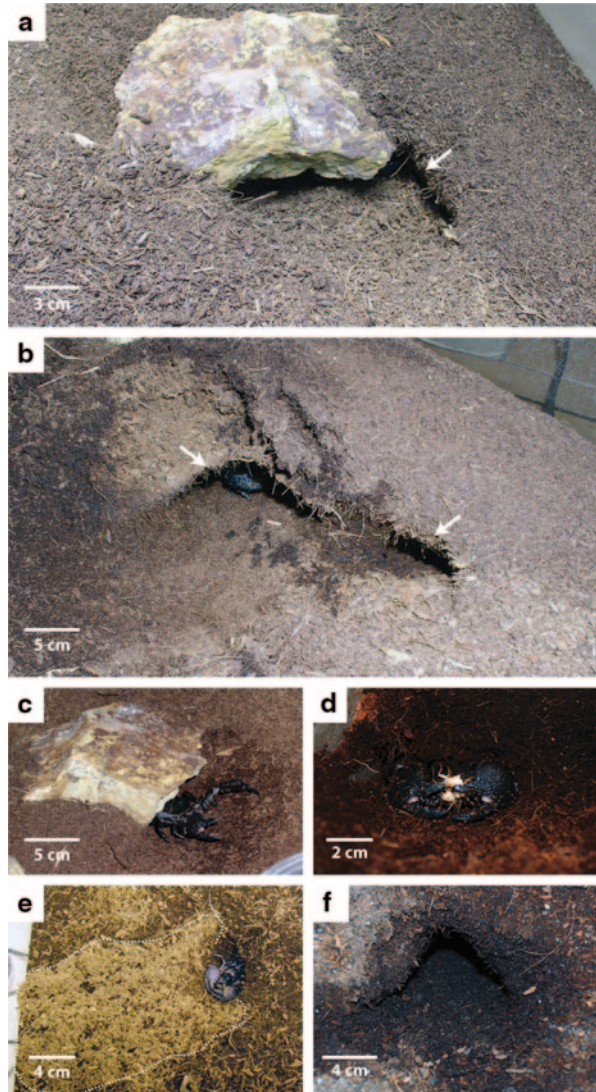
individuals of *Pandinus imperator* including subvertical ramps, helical burrows, and branched burrows (Figs. 11.6–11.8). These burrow architectures were produced regardless of the number of individuals present, but they were controlled by sediment moisture content (Table 11.1). Despite these different architectures, however, they did share several similar morphological elements and quantitative properties (Tables 11.2, 11.3). The burrows consisted of shallowly sloping (0–40°, $\bar{x}=23°$, SD$=11°$) tunnels leading to laterally expanded chambers. The tunnels and chambers were elliptical in cross section with width-to-height ratios from 1.4–2.8

Fig. 11.6 Subvertical ramps. **a** Front view of a typical subvertical ramp (ES4). **b** Side view of ES4. **c** Right oblique view of a subvertical ramp with a laterally widened terminal chamber (ES6). **d** Side view of ES6 demonstrating the difference between the top and bottom surfaces of the tunnel. **e** Top view of a gently sloping ramp with a large chamber (ES11). **f** Side view of ES11. **g** Top view of a ramp with a large laterally expanded terminal chamber (ES9). **h** Side view of ES9 showing vertical expansion of the chamber
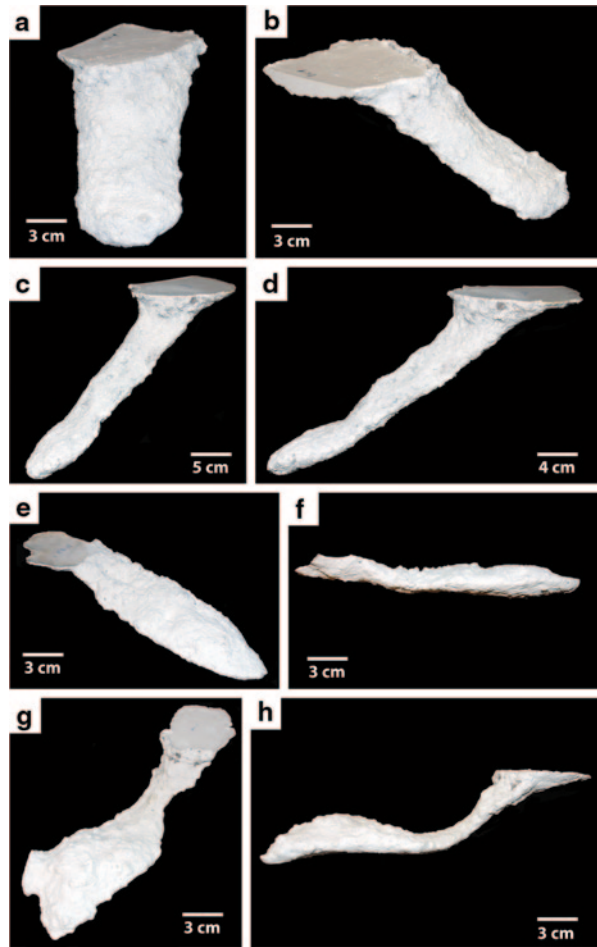
($\overline{x}$=2.0, SD=0.4). The average width of tunnels, shafts, and chambers varied only from 4.9–9.6 cm ($\overline{x}$=6.6 cm, SD=1.3 cm), the average height from 2.5–5.0 cm ($\overline{x}$=3.4 cm, SD=0.8 cm), and the average circumference from 13.0–24.8 cm ($\overline{x}$=17.5 cm, SD=3.1 cm). Each burrow was also characterized by tunnels and chambers with inconsistent widths, heights, and circumferences along their lengths as indicated by the range between the minimum and maximum values of these properties (Table 11.2) (Fig. 11.7).

The surficial features of the *Pandinus imperator* burrows were the same across the three architectures. The upper surfaces of the tunnels and chambers were arched and marked by elongate grooves and nodes (Fig. 11.9a, b). These features were irregularly placed and did not show any preferred alignment. The lower surfaces of the tunnels and chambers were consistently smooth and flat without irregular features (Fig. 11.9c).

Fig. 11.7 Helical burrow casts. **a** Oblique view of a large helical burrow with high tortuosity and a large terminal chamber (ES2). **b** Front oblique view of ES2. **c** Side oblique view of a helical burrow with low tortuosity and a small terminal chamber (ES3). **d** Front top view of ES3

3 cm

3 cm

4 cm

4 cm

11.4.3.1 Subvertical Ramps

This burrow architecture (n =9) includes a single surface opening leading to a shallowly sloping (0–50 °, $\overline{x}$=22°, SD =11°), non-branching ramp that extends 5–13 cm ($\overline{x}$=9 cm, SD=3 cm) below the sediment surface (Figs. 11.4b and 11.6). The inclination of the ramp either remains constant or may vary up to 50° along the length of the burrow. The ramps have an elliptical cross section with a width-to-height ratio of 1.4–2.8 ($\overline{x}$=2.0, SD=0.4). The ramps are 3.6–11.6 cm ($\overline{x}$=6.2 cm, SD=0.9 cm) wide and 1.7–5.8 cm ($\overline{x}$=3.2 cm, SD=0.7 cm) high with a circumference of 8.4–28.0 cm ($\overline{x}$=16.4 cm, SD=2.3 cm) and a total length of 12.0–34.0 cm ($\overline{x}$=23.0 cm, SD=6.9 cm; Tables 11.2, 11.3). Laterally expanded chambers are present in five of the subvertical ramps and are located at the end of each burrow (Fig. 11.6e, g). The subvertical ramps possess a complexity value of 2 or 3 which includes the single surface opening, a single tunnel, and a chamber if present. The tortuosity of the ramps varies from 1.0–1.1 ($\overline{x}$=1.0, SD =0.05, Table 11.2). Subvertical ramps were produced in the sediments with moderate to high moisture content (50–70 %) (Table 11.1).

11.4.3.2 Helical Burrows

This burrow architecture (n=4) includes a single surface opening leading to a shallowly sloping (0–50°, $\overline{x}$=19.3°, SD=4°), non-branching ramp that curves from 30–90° as it descends 12.5–16.0 cm ($\overline{x}$=14.4 cm, SD=1.3 cm) into the sediment (Figs. 11.4a and 11.7). The inclination of the tunnel varies up to 50° along the length

Fig. 11.8 Branched burrows.
a Side view of a large
branched burrow (ES8).
b Top view of ES8 showing
the expansion of the two
tunnels at their intersection.
c Side oblique view of ES8

Table 11.3 Average properties of the three different burrow architectures of *Pandinus imperator* (SR, HB, BB), all burrows of *Pandinus imperator* (ES), and all burrows of *Hadrurus arizonensis* (DHS)

	SR	HB	BB	ES	DHS
Surface openings	1	1	1	1	2
Maximum depth	9.1	14.4	21.5	12.2	6.6
Total length	23.0	32.3	54.0	29.6	29.5
Average width	6.2	7.6	6.8	6.6	4.6
Average height	3.2	3.9	3.5	3.4	2.0
Average W/H ratio	2.0	2.0	2.0	2.0	2.4
Average circumference	16.4	19.9	18.0	17.5	12.8
Average slope	22.4	19.3	33.0	23.0	18.9
Branching angles	NA	NA	90.0	90.0	73.0
Complexity	2.6	3.0	4.0	2.9	4.3
Tortuosity	1.0	1.4	1.0	1.1	1.9

Fig. 11.9 Surficial morphology. **a** Arched upper surface bearing elongate grooves and nodes. **b** Large central groove or ridge along the center of the arched tunnel roof. **c** Smooth and flat tunnel floor
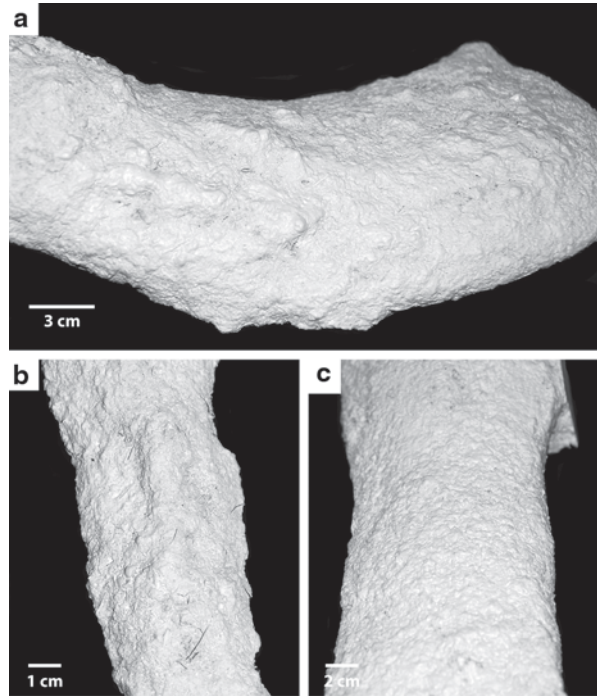
of the burrow and in all (*n*=4) examples, the tunnel terminates with a horizontally oriented, laterally expanded chamber. The helical burrows have elliptical cross sections with width-to-height ratios of 1.4–2.5 ($\overline{x}$=2.0, SD=0.4). The helical burrows are 4.2–12.0 cm ($\overline{x}$=7.6 cm, SD=1.6 cm) wide and 2.0–7.1 cm ($\overline{x}$=3.9 cm, SD=0.7 cm) high with circumferences of 11.0–28.5 cm ($\overline{x}$=19.9 cm, SD=3.9 cm) and total lengths of 29.0–34.0 cm ($\overline{x}$=32.3 cm, SD=2.0 cm; Table 11.2). The helical burrows possess a complexity value of three which includes the single surface opening, a single tunnel, and a chamber. The tortuosity of the helical burrows varies from 1.1–1.7 ($\overline{x}$=1.4, SD =0.3; Table 11.2). Helical burrows were produced only in sediments with high moisture content (70 %; Table 11.1).

11.4.3.3 Branched Burrows

This burrow architecture (*n*=2) includes a single surface opening leading to a shallowly sloping (0–50°, $\overline{x}$=33°, SD=14°) ramp that intersects a horizontally oriented tunnel at 90° (Fig. 11.8). The burrow complex extends 13–30 cm ($\overline{x}$=21.5 cm, SD=8.5 cm) below the sediment surface (Fig. 11.4c). The inclinations of the tunnels vary up to 40° along the length of the burrow. The branched burrows have elliptical cross sections with width-to-height ratios of 1.9–2.1 ($\overline{x}$=2.0, SD=0.1). The ramps are 3.9–10.6 cm ($\overline{x}$=6.8 cm, SD=0.0 cm) wide and 2.4–4.9 cm ($\overline{x}$=3.5 cm, SD=0.2 cm) high with circumferences of 12.0–27.0 cm

($\bar{x}=18.0$ cm, SD=0.9 cm) and total lengths of 28.0–80.0 cm ($\bar{x}=54.0$ cm, SD=26.0 cm, Table 11.2). Laterally expanded chambers are present in each of the branched burrows ($n=2$) and are located at the intersection of the two tunnels (Fig. 11.8b). The branched burrows possess a tortuosity value of 1.0 and a complexity value of 4.0 which includes the single surface opening, two tunnels, and a chamber (Table 11.2). Branched burrows were produced only in sediments with high moisture content (70%; Table 11.1).

11.4.4   Environmental Effects on Burrow Morphology

Specimens of *Pandinus imperator* constructed burrows in all of the experiments, despite changes in the sediment moisture content or the number of individuals in the enclosure. The sediment moisture did significantly reduce the preservation potential of the burrows and influenced the complexity of the final architecture (Table 11.1). No burrows were able to be cast from sediments with 20% moistures due to the collapse of these structures soon after completion. Burrows that were produced in these low moisture enclosures were very shallow (2–4 cm) subvertical ramps or simple depressions excavated beneath rocks, wood, or other flat objects. Overall, the greatest diversity of burrows was produced in sediment with 70% moisture, including all three architectures. Only subvertical ramps were produced in sediment with 50% moisture. The amount of time that the scorpions were within the enclosure also had some effect on the final burrow architecture. The burrows were expanded and elaborated over time, increasing their complexity and tortuosity. All burrows began as shallow subvertical ramps (10–20 days) but then were made longer and deeper as the experiments progressed (40–50 days). These ramps then began to curve as they descended into the substrate (>12 cm) to produce helical architectures or new tunnels were constructed to produce branching architectures.

   Other factors had a minimal impact on the burrow morphology of *Pandinus imperator*. There was no increase in burrow complexity with more individuals. Experiments involving a single individual and multiple individuals both resulted in helical and branched burrows, although those burrows occupied by multiple individuals tended to be larger (Tables 11.1, 11.2). The enclosures themselves did not appear to restrain the morphology of the burrows. Although some burrows did intersect the enclosure walls, both helical and branched burrows were produced without such contact. In addition, the base of the deepest of the burrows (ES8, 30 cm) was far above the maximum depth of the sediment (55 cm).

11.4.5   Analysis of Burrow Morphology

The burrows of *Pandinus imperator* were analyzed statistically to determine the similarity of the burrows to each other, the similarity of the burrows to those of another species of scorpion, and to determine the effects of sediment moisture on the burrow properties.

11.4.5.1   Comparison of Burrows of *Pandinus imperator*

The burrows of *Pandinus imperator* were found to be highly (1.0–0.8) to moderately (0.7–0.6) similar, based on 10 quantitative morphological properties used in the Bray–Curtis analysis (Table 11.4a). When compared to each other, all of the burrows, regardless of architecture, had a high average similarity ($\overline{x}=0.8$, SD$=0.09$) with a range of 1.0–0.5. A single branching burrow (ES8) was found to be dissimilar (0.5) to one subvertical ramp (ES4), but this was the only instance of dissimilarity found. The similarity was highest when comparing burrows of the same architectural morphology (Table 11.4a). These comparisons yielded mostly high similarity values (0.9–0.8) and one pair of subvertical ramps (ES7 and ES13) that were considered identical (1.0). Instances of moderate similarity (0.7) among burrows of the same architecture were the product of only one to three specimens; for example, three subvertical ramps (ES4, ES6, ES11) out of the total nine (33%) account for all of the similarity indices <0.8 within that architecture. These differences occur among the only two or three of the other subvertical ramps. Despite these minor differences, the average similarities remained high within the subvertical ramp ($\overline{x}=0.8$, SD$=0.07$) and helical burrow ($\overline{x}=0.9$, SD$=0.03$) architectures. The average similarity was only moderate ($\overline{x}=0.7$, SD$=0.00$) between the two branching burrow casts.

When comparing the different burrow architectures of *Pandinus imperator* together, there was little to no decrease in similarity as the complexity of the architecture increased (Table 11.4a). For example, comparing subvertical ramps to helical burrows resulted in the same overall similarity ($\overline{x}=0.8$, SD$=0.07$) as when comparing them to subvertical ramps. Likewise, comparing helical burrows to branching burrows resulted in a high level of similarity ($\overline{x}=0.8$, SD$=0.05$). Comparing subvertical ramps to branching burrows, however, resulted in a moderate level of similarity ($\overline{x}=0.7$, SD$=0.11$).

Using Mann–Whitney and Kolmogorov–Smirnov tests, it was found that the total length, depth, complexity, and tortuosity of the burrows were not consistent across the three architectures in terms of equality of their medians, distributions, or both (Table 11.5). The number of openings, width, height, circumference, width-to-height ratio, and slope, however, were all similar in both respects.

11.4.5.2   Comparison with Burrows of *Hadrurus arizonensis*

When compared to each other, the burrows of *Hadrurus arizonensis* had a high average similarity ($\overline{x}=0.8$, SD$=0.10$) regardless of the architecture with a range of 0.9–0.4 (Hembree et al. 2012). The two species of burrowing scorpions were found to have three common burrow architectures including subvertical ramps, helical burrows, and branched burrows or mazeworks (Fig. 11.10, Table 11.3). Burrows with these three architectures were compared using the Bray–Curtis similarity test to determine if there were easily recognized differences resulting from different tracemakers. The burrows of *Pandinus imperator* were, on average, found to be moderately similar ($\overline{x}=0.7$, SD$=0.10$) to burrows produced by *Hadrurus*

a

	ES1 (SR)	ES4 (SR)	ES6 (SR)	ES7 (SR)	ES9 (SR)	ES11 (SR)	ES13 (SR)	ES14 (SR)	ES15 (SR)	ES2 (HB)	ES3 (HB)	ES5 (HB)	ES12 (HB)	ES8 (BB)	ES10 (BB)
ES1 (SR)	1.0	0.8	0.8	0.9	0.9	0.8	0.9	0.8	0.9	0.8	0.8	0.8	0.9	0.6	0.8
ES4 (SR)	0.8	1.0	0.9	0.7	0.7	0.7	0.8	0.8	0.8	0.6	0.8	0.8	0.7	0.5	0.8
ES6 (SR)	0.8	0.9	1.0	0.7	0.8	0.7	0.8	0.9	0.8	0.8	0.8	0.9	0.8	0.6	0.9
ES7 (SR)	0.9	0.7	0.7	1.0	0.8	0.8	1.0	0.8	0.8	0.8	0.7	0.8	0.8	0.6	0.7
ES9 (SR)	0.9	0.7	0.8	0.8	1.0	0.8	0.9	0.8	0.8	0.9	0.9	0.9	0.9	0.7	0.8
ES11 (SR)	0.8	0.7	0.7	0.8	0.8	1.0	0.9	0.8	0.7	0.8	0.8	0.8	0.8	0.6	0.7
ES13 (SR)	0.9	0.8	0.8	1.0	0.8	0.9	1.0	0.8	0.8	0.8	0.7	0.8	0.8	0.6	0.7
ES14 (SR)	0.8	0.8	0.9	0.8	0.8	0.8	0.8	1.0	0.9	0.8	0.9	0.9	0.9	0.7	0.9
ES15 (SR)	0.9	0.8	0.8	0.8	0.8	0.7	0.8	0.9	1.0	0.7	0.9	0.9	0.8	0.6	0.8
ES2 (HB)	0.8	0.6	0.8	0.8	0.9	0.8	0.8	0.8	0.7	1.0	0.9	0.8	0.9	0.7	0.8
ES3 (HB)	0.8	0.7	0.8	0.7	0.9	0.8	0.7	0.9	0.9	0.9	1.0	0.9	0.9	0.7	0.8
ES5 (HB)	0.8	0.8	0.9	0.8	0.9	0.8	0.8	0.9	0.9	0.8	0.9	1.0	0.9	0.7	0.8
ES12 (HB)	0.9	0.7	0.8	0.8	0.9	0.8	0.8	0.9	0.8	0.9	0.9	0.9	1.0	0.7	0.8
ES8 (BB)	0.6	0.5	0.6	0.6	0.7	0.6	0.6	0.7	0.6	0.7	0.7	0.7	0.7	1.0	0.7
ES10 (BB)	0.8	0.8	0.9	0.7	0.8	0.7	0.7	0.9	0.8	0.8	0.8	0.8	0.8	0.7	1.0

b

	ES1 (SR)	ES4 (SR)	ES6 (SR)	ES7 (SR)	ES9 (SR)	ES11 (SR)	ES13 (SR)	ES14 (SR)	ES15 (SR)	ES2 (HB)	ES3 (HB)	ES5 (HB)	ES12 (HB)	ES8 (BB)	ES10 (BB)
DHS1 (SR)	0.8	0.8	0.8	0.8	0.7	0.7	0.8	0.7	0.8	0.6	0.7	0.8	0.7	0.5	0.6
DHS2 (SR)	0.7	0.6	0.6	0.8	0.6	0.7	0.7	0.6	0.7	0.6	0.5	0.6	0.6	0.4	0.5
DHS6 (SR)	0.8	0.7	0.6	0.8	0.6	0.6	0.8	0.6	0.7	0.6	0.6	0.7	0.6	0.5	0.6
DHS10 (SR)	0.8	0.6	0.6	0.8	0.6	0.8	0.8	0.6	0.7	0.6	0.6	0.7	0.6	0.5	0.6
DHS11 (SR)	0.8	0.8	0.7	0.8	0.7	0.7	0.8	0.7	0.8	0.6	0.7	0.8	0.7	0.5	0.6
DHS12 (SR)	0.8	0.7	0.7	0.9	0.7	0.9	0.9	0.7	0.7	0.7	0.6	0.7	0.7	0.5	0.6
DHS13 (SR)	0.8	0.7	0.7	0.9	0.7	0.8	0.9	0.7	0.7	0.7	0.7	0.8	0.7	0.5	0.6
DHS14 (SR)	0.8	0.7	0.7	0.9	0.8	0.9	0.9	0.7	0.7	0.7	0.7	0.8	0.8	0.6	0.7
DHS16 (SR)	0.8	0.6	0.7	0.8	0.8	0.9	0.8	0.7	0.7	0.8	0.8	0.8	0.8	0.7	0.7
DHS17 (SR)	0.8	0.7	0.8	0.9	0.8	0.9	0.9	0.8	0.7	0.8	0.7	0.8	0.8	0.6	0.7
DHS3 (HB)	0.8	0.7	0.8	0.8	0.8	0.8	0.9	0.8	0.8	0.8	0.8	0.9	0.8	0.6	0.7
DHS7 (HB)	0.8	0.8	0.7	0.8	0.7	0.7	0.8	0.7	0.8	0.6	0.7	0.7	0.7	0.5	0.6
DHS15 (HB)	0.7	0.5	0.6	0.6	0.7	0.7	0.6	0.7	0.6	0.7	0.7	0.7	0.8	0.9	0.6
DHS4 (MW)	0.7	0.7	0.7	0.6	0.7	0.7	0.7	0.7	0.7	0.7	0.7	0.8	0.7	0.8	0.7
DHS5 (MW)	0.7	0.8	0.8	0.6	0.7	0.7	0.7	0.7	0.7	0.7	0.7	0.8	0.7	0.7	0.8
DHS8 (MW)	0.8	0.8	0.9	0.7	0.8	0.8	0.8	0.8	0.8	0.8	0.8	0.9	0.8	0.6	0.8

Table 11.4 Bray–Curtis distance measure results based on ten quantitative burrow properties (a) Comparison matrix of all *Pandinus imperator* (*ES*) burrow casts. (b) Comparison matrix of *Pandinus imperator* and *Hadrurus arizonensis* (*DHS*) burrow casts. *SR* subvertical ramp, *HB* helical burrow, *BB* branched burrow, *MW* mazework, *blue* high similarity, *green* moderate similarity, *red* dissimilar

Fig. 11.10 Burrow
architectures produced by
Hadrurus arizonensis.
a Specimen of *Hadrurus
arizonensis.* **b** Subvertical
ramp. **c** Helical burrow.
d Mazework. (Modified
from Hembree et al. (2012))
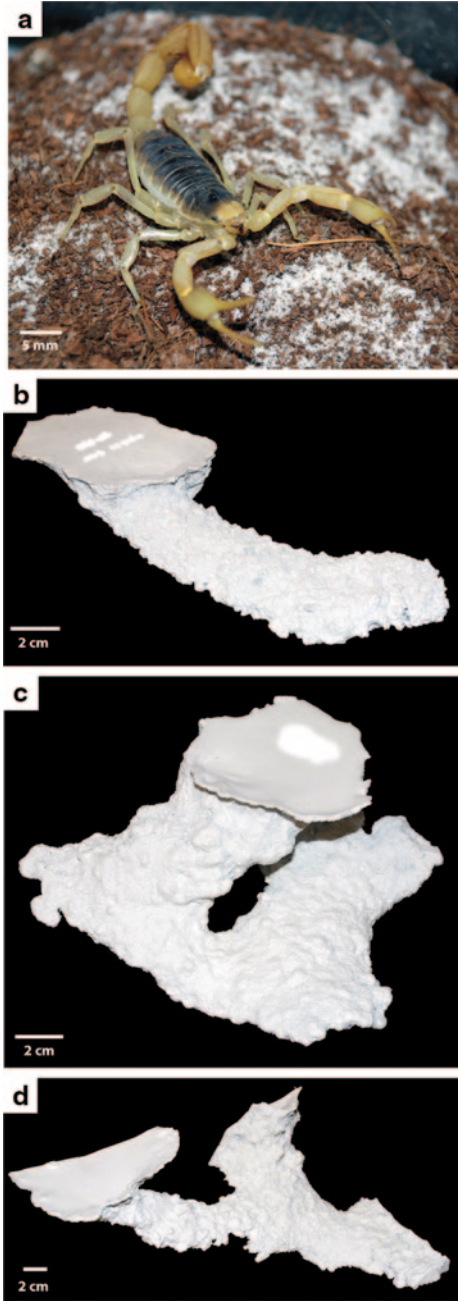
arizonensis with a range of similarity from 0.9–0.4 (Table 11.4b). The degree of similarity was found to vary little by architectural morphology. The subvertical ramps had similarity values ranging from 0.9–0.6 ($\bar{x}$=0.7, SD=0.08), the helical burrows had similarity values ranging from 0.9–0.6 ($\bar{x}$=0.7, SD=0.06), and the branching burrows had similarity values ranging from 0.8–0.7 ($\bar{x}$=0.7, SD=0.06). Similar values were obtained even when different architectures were compared (SR/HB: $\bar{x}$=0.7, SD=0.08; SR/MW: $\bar{x}$=0.7, SD=0.06; HB/MW: $\bar{x}$=0.8, SD=0.05).

Despite their different trace makers, the burrow casts of *Pandinus imperator* (*n*=15) did have a few similar quantitative properties to those of *Hadrurus arizonensis* (*n*=19) (Table 11.3). Using Mann–Whitney and Kolmogorov–Smirnov tests, it was found that the total length, average slope, and complexity of the burrows of the two species were similar (Table 11.5). The median and distribution of the depth, width, height, circumference, and tortuosity of the burrow casts were found to be different (Table 11.5). The median of the number of openings and width-to-height ratio were found to be different. On an average, the burrows of *Pandinus imperator* had fewer surface openings, were deeper, had tunnels with a greater width, height, and circumference, lower width-to-height ratio, and lower tortuosity than those of *Hadrurus arizonensis*.

11.4.5.3 Sediment Moisture and Burrow Morphology

While the architectural morphology of the burrows produced by *Pandinus imperator* was controlled by the total sediment moisture (Table 11.1), most of the quantitative aspects of burrow morphology were not significantly altered as this variable changed. Using Spearman's rank correlation, it was found that only two (length and complexity) of the nine metrics tested (depth, length, width, height, w/h ratio, circumference, slope, complexity, and tortuosity) were significantly correlated to either sediment density or moisture content (Table 11.6). The Spearman's rank correlation yielded Rs values of 0.05–0.48 (p=0.86–0.07) for seven of the properties, whereas length and complexity yielded Rs values of 0.82 (p=0.0002) and 0.79 (p=0.0005), respectively (Table 11.6). Mann–Whitney and Kolmogorov–Smirnov tests supported this result, indicating the median and distribution of the lengths and complexities of burrows produced in sediments with 50 and 70% moisture content were significantly different (Table 11.5). No other property was significantly different.

11.5 Discussion

Specimens of *Pandinus imperator* produced three different burrow architectures over the course of the experimental trials. These different architectures were not only the product of a single species, but also of individual specimens. It has been previously recognized through neoichnological research that individual species in both marine and continental settings can produce different types of biogenic

		Openings	Length	Depth	Width	Height	Circum.	W/H Ratio	Slope	Complexity	Tortuosity
Scorpion											
SR v HB	M-W	1.00	0.03	0.02	0.25	0.25	0.19	0.94	0.94	0.15	0.02
	K-S	1.00	0.03	0.04	0.36	0.12	0.30	0.99	0.51	0.51	0.10
SR v BB	M-W	1.00	0.16	0.09	0.29	0.41	0.48	0.91	0.41	0.03	0.45
	K-S	1.00	0.38	0.28	0.14	0.28	0.28	0.78	0.64	0.02	0.14
HB v BB	M-W	1.00	0.81	0.82	0.81	0.48	0.49	1.00	0.49	0.05	0.10
	K-S	1.00	0.74	0.74	0.74	0.24	0.24	0.99	0.74	0.05	0.05
ES v DHS	M-W	0.04	0.61	0.001	0.00001	0.000006	0.00002	0.02	0.25	0.20	0.0003
	K-S	0.54	0.61	0.02	0.00001	0.0000001	0.00006	0.19	0.36	0.11	0.002
Moisture											
50 v 70	M-W	1.00	0.003	0.08	0.20	0.30	0.11	0.85	0.90	0.004	0.59
	K-S	1.00	0.0006	0.11	0.11	0.27	0.11	0.86	0.54	0.003	0.86

Table 11.5 Results (p values) of Mann–Whitney (M–W) and Kolmogorov–Smirnov (K–S) tests between the quantitative properties of three burrows architectures of *Pandinus imperator* (*SR* subvertical ramp, *HB* helical burrow, *BB* branched burrow), the burrows of *Pandinus imperator* (*ES*) and *Hadrurus arizonensis* (*DHS*), and of *Pandinus imperator* burrows produced in sediment with 50 and 70% moisture content

Table 11.6 Results (Rs and *p* values) of Spearman's rank correlation between sediment moisture content and quantitative burrow properties. The number of burrow openings did not vary between burrow casts and was excluded from the analysis

	Openings	Length	Depth	Width	Height	Circum	W/H Ratio	Slope	Complexity	Tortuosity
Rs	NA	0.82	0.48	0.36	0.30	0.44	0.07	−0.05	0.79	0.16
p	NA	0.0002	0.07	0.19	0.29	0.10	0.82	0.86	0.0005	0.56

structures depending on the behavior exhibited and the environmental conditions (Bromley 1996; Pemberton et al. 2001; Hasiotis 2007).

11.5.1 Burrow Morphology and Tracemaker

Despite the different architectures of the burrows produced by *Pandinus imperator,* there was still a high level of similarity between the different burrows. The quantitative properties found to be the most similar among the three different architectures (SR, HB, BB) were the number of surface openings, average tunnel width, average tunnel height, average width-to-height ratio, average circumference, and average slope (Tables 11.3, 11.5). These properties, with the exception of the number of surface openings and slope, are directly related to the morphology of the emperor scorpions; they are an expression of the cross-sectional shape and dimensions of the animal. The tunnels are only 5–10 % larger than the largest scorpion occupying the burrow. There was a much greater deviation between the size of the scorpions and the size of the chambers. Chambers were 1–7 cm wider and 1–3 cm higher than the intersecting tunnels. The size of the chambers was a function of other variables such as the number of individuals present (1 or 5), the time of occupation, sediment moisture content, and differences in individual behavior. The surficial features preserved on the upper burrow walls (Fig. 11.9), specifically the elongate grooves, record additional evidence of organism morphology—in this case the presence of appendages on the tracemaker.

The moderate level of similarity between *Pandinus imperator* burrows and those produced by *Hadrurus arizonensis* indicates that animals with similar morphologies can produce similar burrows despite taxonomic differences. Like all scorpions, both *Pandinus imperator* and *Hadrurus arizonensis* have relatively wide, but low bodies with elliptical cross sections that are carried close to the ground (Hjelle 1990). As a result, the tunnels excavated by these animals also have elliptical cross sections and the average width-to-height ratio of the burrows was similar (Tables 11.3, 11.5). The average width, height, and circumference of the *Pandinus imperator* burrows were larger than the *Hadrurus arizonensis* burrows, but this is consistent with the larger average body size of *Pandinus imperator* (Table 11.3). Similarities and differences in other aspects of burrow morphology are likely due to differences in solitary (*Hadrurus arizonensis*) versus communal (*Pandinus imperator*) behavior, burrowing techniques, and sediment properties.

11.5.2   *Burrow Morphology and Behavior*

Burrow morphology is a direct product of behavior and the organism's interaction with the sediment (Bromley 1996). The three different architectures of *Pandinus imperator* were used for dwelling and feeding behaviors. The morphological similarities of the different architectures were most likely partially related to these simple types of behavior, despite differences in general form. The consistent burrowing technique also caused common architectural properties between the three burrow types.

Subvertical ramps were produced quickly by the emperor scorpions soon after their introduction to the experimental tanks. Later, burrows were simply modifications of this initial design. The subvertical ramps displayed a wide range of lengths (12–34 cm) and depths (5–13 cm), but all consisted of a single surface opening, a single subvertical tunnel, and, in more than half of the burrows, a laterally expanded chamber. This basic architecture was sufficient to isolate a single or even multiple individuals from the surface environment. In a natural setting, the burrow would serve to protect the scorpions from adverse environmental conditions, such as extremes in temperature or humidity and predators (Polis 1990). During the experiments, specimens of *Pandinus imperator* spent little of their time (10–15 %) outside of their burrows. This was primarily during the dark intervals when the scorpions were engaged in active hunting. Much of this time was spent within 10 cm of the burrow entrance. The laterally expanded chambers were constructed over time and were used as dwelling structures and as turn-around points for the scorpions in the subsurface, allowing the animals to reposition themselves so that they could face outward. This was particularly useful in prey ambush behaviors (Fig. 11.5d).

Some aspects of burrow morphology were affected by the communal and solitary behaviors of *Pandinus imperator*. All three architectures were produced by both solitary individuals and groups of individuals. This was likely due to the fact that final burrow construction was typically conducted by only one or two individuals; the rest simply moved into the burrow once it was complete. Differences in burrow morphology related to the number of individuals largely involved scale. While tunnels were typically the same size, chambers were larger in those burrows with multiple individuals as shown by their larger maximum values for width and circumference (Table 11.2).

The surficial structures preserved on the top of the tunnels and chambers are indicative of active excavation by *Pandinus imperator*. The elongate grooves and nodes preserved on the burrow casts record the scraping of sediment from the tunnel walls by the walking legs. The cross-sectional form of the burrows with their arched tops and flat bottoms also reflects this process. The flattened bases of the burrows are likely the result of both the compaction of the floor, by the continuous movement of the scorpions in and out of the burrow during excavation, as well as the infill of excavated sediment from deeper in the burrow along the floor.

11.5.3   Burrow Morphology and Sediment Properties

High-moisture (70 %) sediments are ideal for burrow construction by *Pandinus imperator*. This is likely due to the ability of the high moisture sediment to withstand gravitational collapse due to higher levels of sediment cohesion. The emperor scorpions produced no burrow linings to provide additional support regardless of the sediment properties as seen in other types of arthropods (Bromley 1996). There may have also been a physiological component of the preference for higher moisture sediment in these experiments since *Pandinus imperator* inhabits humid environments (Sissom 1990).

   Sediment moisture showed no impact on burrow depth, width, height, width-to-height ratio, circumference, slope, or tortuosity (Tables 11.5, 11.6). Results from the Spearman's rank correlation analysis resulted in an average Rs value of 0.25 for these properties. Burrow length (Rs=0.82, *p*=0.0002) and complexity (Rs=0.79, *p*=0.0005), however, did show a significant correlation with sediment moisture. As sediment moisture increased, burrows became longer and more complex. These two properties are primarily tied to burrow architecture. Helical burrows and branched burrows were only produced in the high moisture sediment and these two burrow architectures have consistently higher lengths and complexities than the subvertical ramps. In addition, four of the five subvertical ramps with chambers were produced in high moisture sediment giving them higher complexities. Subvertical ramps produced in high moisture sediment also had the highest total lengths (Table 11.2).

   The minimal correlation between the quantitative aspects of burrow morphology and environment is important because it suggests that the burrow morphology is primarily controlled by the organism's morphology and behavior. The burrow morphology may therefore be useful as a proxy for scorpions and the behaviors associated with terrestrial predatory arthropods.

11.6   Significance

11.6.1   Recognition in the Fossil Record

Recognizing the different architectures and surficial morphologies of burrows produced by modern animals is critical for the accurate interpretation of trace fossils. Scorpion burrows lack a significant fossil record. This is surprising, given the prevalence of burrowing behavior in modern scorpions and the long evolutionary history of the group. The absence is most likely due to a failure to recognize known fossil burrows as being the result of scorpion activity. In order to properly identify scorpion burrows in the fossil record, a set of ichnotaxobases is needed. Ichnotaxobases include the architecture of a burrow, overall shape, orientation with respect to the substrate, surficial features or bioglyphs, and internal structure such as constructed linings and active fill (Bertling et al. 2006). Detailed study of the burrows of

modern animals allows for the establishment of ichnotaxobases for different groups of animals. These groups may have similar evolutionary histories, morphologies, behaviors, or all three. While some variation in the ichnotaxobases is expected from the burrows of different families, genera, or even species of scorpions, this study of *Pandinus imperator* and others like it (Hembree et al. 2012) provide a starting set of ichnotaxobases that can be used to aid in the recognition and interpretation of scorpion burrows in the fossil record.

Architecture Scorpion burrows include subvertical ramps, helical burrows, and branched burrows. These consist of a single surface opening, subvertical to subhorizontal tunnels, and laterally expanded chambers. Branching is uncommon. Chambers occur at the base of the burrow or at branch points.

Overall Shape Tunnels are elliptical in cross section with a width-to-height ratio of approximately 2.0. The tunnel roof is curved while the floor is flattened. Chambers have the same cross-sectional characteristics as tunnels but are wider. Tunnels and chambers have variable widths and heights along their length. Tunnels may be straight or sinuous curving up to 30° along a horizontal plane.

Orientation Burrow elements vary in orientation from horizontal (0–5°) to oblique (15–50°). The orientation changes along the length of tunnels while chambers tend to be horizontal. Most burrows contain elements with both of these orientations.

Internal Structure Scorpion burrows possess no distinguishable lining. The boundary between the open burrow and the surrounding sediment is abrupt and irregular. The burrow fill may be active or passive. Active fill is generally massive in appearance and accumulates from the burrow floor upward during burrow expansion. Passive fill occurs typically as a result of gravitational collapse of upper elements of the burrow.

Surficial Features The roofs of the tunnels and chambers are irregular and possess elongate grooves and nodes. The floors are flat and featureless.

11.6.2 Paleontological and Paleoecological Significance

Continental trace fossils have a wide range of potential uses, but they are still poorly understood (Hasiotis 2007). Additionally, while modern soils are known to contain a diverse and abundant biota, most of these organisms are poorly understood both taxonomically and ecologically (Bardgett 2005). Even worse is the lack of knowledge of the burrow morphologies produced by modern burrowing animals as well as the ways in which the soil environment (soil type, temperature, soil moisture, precipitation, etc.) affects burrowing behaviors. For many taxa this information is entirely unknown. Given this lack of knowledge of modern soil ecosystems, the ability of paleontologists and sedimentary geologists to use fossil burrows to make interpretations about ancient soil ecosystems is limited. This is the knowledge that can be obtained through neoichnology.

Burrows produced by *Pandinus imperator* displayed three different types of basic architecture. These variations were largely a product of changes in burrow morphology over time as a result of burrow modification and maintenance. The potential effect of this architectural diversity is the likelihood for an overestimation of biodiversity. Trace fossil classification and interpretation relies entirely on morphology, therefore, it is possible for each burrow form to be considered indicative of a different tracemaker. There have been several studies showing that a single tracemaker can produce multiple burrow morphologies depending on the behaviors involved and the sediment properties (Bromley 1996; Pemberton et al. 2001; Hasiotis 2007). The possible diversity of forms that can be produced by a single species or even a single individual, however, is rarely fully understood. There is a similar problem with using absolute burrow size to make interpretations about potential tracemakers. Many fossil continental burrows with large (>2 cm) cross-sectional diameters are interpreted as vertebrate burrows primarily on the basis of their size (Miller et al. 2001; Hasiotis et al. 2004; Loope 2008; Storm et al. 2010; Tałanda et al. 2011). Complex branching patterns have also been considered diagnostic of vertebrate tracemakers (Miller et al. 2001; Hasiotis et al. 2004; Tałanda et al. 2011). The experiments described here and in Hembree et al. (2012) have shown that scorpions are capable of producing burrows with both large diameter tunnels and chambers, in addition to branching burrow networks.

Arthropod predators are a commonly underrepresented component of reconstructions of fossil terrestrial ecosystems (DiMichele and Hook 1992; Wing and Sues 1992). Their importance in and often dominance of ecosystems, however, is clearly demonstrated by modern studies (Dindal 1990; Polis 1990; Cloudsley-Thompson 1991; Punzo 2000a, b; Bardgett 2005; Lavelle and Spain 2005; Punzo 2007). Scorpions fill a fundamental role as the intermediate predators in many modern ecosystems feeding on a variety of prey, particularly other arthropods, and serving as prey for other large predators (McCormick and Polis 1990; Polis 1990). In semi-arid and arid environments, scorpions typically represent the dominant insectivorous predators (Marples and Shorthouse 1982; McCormick and Polis 1990). Given the obvious importance of scorpions in modern ecosystems, the recognition of fossil scorpion burrows would provide for a more complete interpretation of ancient ecosystems.

The recognition of scorpion burrows in the fossil record would also improve our understanding of the evolutionary and biogeographic history of this group of common and ecologically important animals. Scorpion body fossils are relatively common in Paleozoic strata but are rarer in Mesozoic and even Cenozoic rocks (Sissom 1990; Jeram 2001). By at least the Mesozoic if not the late Paleozoic, fossil scorpions display very modern morphologies and sizes and many have been interpreted to have used burrows as permanent shelters (Sissom 1990; Jeram 2001). Given the relative rarity of body fossils, therefore, the recognition of scorpion burrows from late Paleozoic to Cenozoic deposits may be the best way to assess the true abundance and distribution of scorpion taxa.

11.6.3   Paleopedologic and Paleoenvironmental Significance

Due to the terraphilic nature of terrestrial scorpions, the burrow architectures produced in this study would be suggestive of the upper soil profile (A/B horizon) within the vadose zone (Hasiotis 2007). The temperature, average precipitation, vegetation, and soil type could vary widely given the range of environments that modern and fossil scorpions inhabit (Polis 1990; Sissom 1990). Fossil scorpion burrows could, therefore, occur in soil types from Entisols to Oxisols. Fossil scorpion burrows would likely be found in association with trace fossils produced by other soil arthropods (arachnids, myriapods, and insects), annelids, and possibly vertebrates as well as various types of fossil root traces.

As discussed in Hembree et al. (2012), the burrowing activity of scorpions plays at least a minor role in pedogenesis. The activity of *Pandinus imperator* in the laboratory enclosures extended 30 cm into the sediment which is associated with the A and upper B horizons of soils in tropical regions. Burrows of this depth would impact soil-forming processes. Laboratory studies of other tropical genera such as *Heterometrus* have resulted in burrows up to 50 cm deep (Hembree personal observation).

Specimens of *Pandinus imperator* moved sediment from the subsurface to the surface through the excavation of their burrows. This process resulted in an undulating surface topography of loose, porous sediment distinct from the compacted surface of the original material. This modified surface facilitated the downward movement of water through the enclosure. The burrowing activity also resulted in an overall mixing of the sediment as excavated material from deeper tunnels was deposited into shallower tunnel walls during burrow expansion. The active excavation of sediment in the subsurface increased the overall porosity and permeability of the sediment along the walls of the burrow, providing additional conduits for fluid flow and gas exchange.

The permanent, open burrows of *Pandinus imperator* allowed the migration of water and oxygen through the sediment profile. Such conduits are critical in pedogenesis as they allow the dissolution of minerals, the downward transportation of water, ions, and organics, and even the upward movement of water through evapotranspiration (Schaetzl and Anderson 2009). The continual maintenance of the surface openings during the occupation of the burrows allows the constant infiltration of water, sediment, organics, and other organisms into the subsurface. Even when passively filled after being abandoned, the overall porosity and permeability of the fill is higher than the original sediment due to the disruption by the scorpion. Filled burrows, therefore, continue to serve as conduits for the downward and upward migration fluids through the soil profile. Appendages of crickets and other organic debris were found within the burrow chambers of *Pandinus imperator*. The incorporation of this organic material provides a source of nutrients for soil microbes, plants, and other soil animals (Bardgett 2005; Lavelle and Spain 2005). The potential impact of burrowing scorpions on soil formation, therefore, must be considered if fossil scorpion burrows are found within paleosols.

11.7   Conclusions

The interpretation of trace fossils is impossible without a detailed knowledge of the diversity of biogenic structures produced by modern burrowing organisms. Neoichnological studies are, therefore, critical to the interpretation of the behaviors, burrowing methods, and tracemakers represented by trace fossils as well as their paleoenvironmental significance. The architectural and surficial morphologies of the burrows of scorpions are largely unknown despite their abundance and importance in both modern and ancient ecosystems. This absence of knowledge makes the recognition of burrows, produced by scorpions and other terrestrial predatory arthropods in the fossil record, unlikely which leads to incomplete or incorrect paleoecological reconstructions.

Specimens of the burrowing scorpion *Pandinus imperator* produced burrows with three different architectures under similar environmental conditions, including subvertical ramps, helical burrows, and branched burrows. Despite their differences in architecture, there were consistent quantitative morphological properties that made the burrows similar. These properties included the number of surface openings as well as the width, height, width-to-height ratio, circumference, and slope of the tunnels and chambers. These shared properties allowed the recognition of similarity between the burrows despite the different architectures when compared using a Bray–Curtis similarity test. When compared to the burrows of another scorpion, *Hadrurus arizonensis,* the burrows of *Pandinus imperator* were found to be different from those of the other species. The burrows of *Pandinus imperator* were found to have fewer surface openings, were deeper, had tunnels with a greater width, height, and circumference, lower width-to-height ratio, and lower complexity than those of *Hadrurus arizonensis*. This suggests that even burrows produced by similar tracemakers can be distinguished when properly analyzed. These experiments effectively demonstrate that multiple burrow architectures may be produced by a single species. Individual animals produced all three of the burrow architectures observed. It is critical, to paleoecological interpretations, that each type of trace fossil does not necessarily represent a different organism. The analysis of the results of these experiments have shown that thorough descriptions of trace fossil morphology, including multiple quantitative properties, can be used to discern if distinct architectures were produced by the same or different tracemakers.

Sediment properties are considered to have an important effect, on the types of biogenic structures that can be produced and upon their final morphology, in all environmental settings (Bromley 1996; Pemberton et al 2001; Hasiotis 2007). Sediment moisture was found to affect which architectures could be produced by *Pandinus imperator*. Burrows with greater overall complexity such as helical burrows and branched burrows were only produced in sediment with high (70%) moisture content. Specimens of *Pandinus imperator* only produced simple subvertical ramps or shallow pits in sediment with lower (50%) moisture content. When sediment moisture was too low (20%), open burrows could not be maintained and collapsed. The total length and complexity of the burrows were found to be positively correlated with increasing sediment moisture.

The proper identification of large and complex burrows, produced in terrestrial ecosystems, requires knowledge of all the possible organisms that can occupy soil environments. While predatory arthropods are capable of producing large diameter, complex, branching burrow systems, fossil burrows with the size and complexity produced by the scorpions in these experiments would likely be interpreted as vertebrate burrows. A thorough understanding of these burrows and those of similar organisms such as scorpions, spiders, and centipedes will aid in revealing the hidden biodiversity of terrestrial predatory arthropods in the fossil record.

References

Ahlbrandt TS, Andrews S, Gwynne DT (1978) Bioturbation in eolian deposits. J Sed Petrol 48:839–848

Bardgett R (2005) The biology of soil: a community and ecosystem approach. Oxford University Press, Oxford

Bertling M, Braddy SJ, Bromley RG, Demathieu GR, Genise J, Mikulas R, Nielsen JK, Nielsen KS, Rindsberg AK, Schlirf M, Uchman A (2006) Names for trace fossils: a uniform approach. Lethaia 39:265–286

Bradley R (1982) Digestion time and reemergence in the desert grassland scorpion *Paruroctonus utahensis* (Williams) (Scorpionida, Vaejovidae). Oecologica 55:316–318

Brady LF (1947) Invertebrate tracks from the Coconino Sandstone of northern Arizona. J Paleontol 21:466–472

Bromley RG (1996) Trace fossils: biology, taphonomy, and applications. Chapman and Hall, London

Casper GS (1985) Prey capture and stinging behavior in the emperor scorpion, *Pandinus imperator* (Koch) (Scorpiones, Scorpionidae). J Arachnol 13:277–283

Cloudsley-Thompson JL (1991) Ecophysiology of desert arthropods and reptiles. Springer, Berlin

Counts RR, Hasiotis ST (2009) Neoichnological experiments with masked chafer beetles (Coleoptera: Scarabaeidae): implications for backfilled continental trace fossils. Palaios 24:74–91

Davis RB, Minter NJ, Braddy SJ (2007) The neoichnology of terrestrial arthropods. Palaeogeogr Palaeocl 255:284–307

Deocampo DM (2002) Sedimentary structures generated by *Hippopotamus amphibious* in a lake-margin wetland, Ngorongoro Crater, Tanzania. Palaios 17:212–217

DiMichele WA, Hook RW (1992) Paleozoic terrestrial ecosystems. In: Behrensmeyer AK, Damuth JD, DiMichele WA, Potts R, Sues HD, Wing SL (eds) Terrestrial ecosystems through time. The University of Chicago Press, Chicago

Dindal DL (1990) Soil biology guide. Wiley, New York

Dunlop JA, Penney D, Jekel D (2013) A summary list of fossil spiders and their relatives. In: Platnick NI (ed) The world spider catalog, version 13.5. American Museum of Natural History, New York

Eastwood EB (1978) Notes on the scorpion fauna of the Cape. IV, the burrowing activities of some scorpionids and buthids (Arachnida, Scorpionida). Ann S Afr Mus 74:249–255

Gingras MK, Lalond SV, Amskold L, Konhauser KO (2007) Wintering chironomids mine oxygen. Palaios 22:433–438

Gobetz KE (2005) Claw impressions in the walls of modern mole (*Scalopus aquaticus*) tunnels as a means to identify fossil burrows and interpret digging movements. Ichnos 12:227–231

Hadley NF, Williams SC (1968) Surface activities of some North American scorpions in relation to feeding. Ecology 49:726–734

Halfen AF, Hasiotis ST (2010) Neoichnological study of the traces and burrowing behaviors of the western harvester ant *Pognomyrmex occidentalis* (Insecta: Hymenoptera: Formicidea): paleopedogenic and paleoecologic implications. Palaios 25:703–720

Hammer Ø, Harper D (2006) Paleontological data analysis. Blackwell Publishing, Malden

Häntzschel W (1975) Trace fossils and problematica. In: Teichert C (ed) Treatise on invertebrate paleontology, part W. Miscellanea, supplement I. Geological Society of America and University of Kansas Press, Lawrence

Harrington A (1978) Burrowing biology of the scorpion *Cheloctonus jonesii* (Arachnida: Scorpionida: Scorpionidae). J Arachnol 5:243–249

Hasiotis ST (2003) Complex ichnofossils of solitary and social soil organisms: understanding their evolution and roles in terrestrial paleoecosystems. Palaeogeogr Palaeocl 192:259–320

Hasiotis ST, Wellner RW, Martin AJ, Demko TM (2004) Vertebrate burrows from Triassic and Jurassic continental deposits of North America and Antarctica: their paleoenvironmental and paleoecological significance. Ichnos 11:103–124

Hasiotis ST (2007) Continental ichnology: fundamental processes and controls on trace fossil distribution. In: Miller IIIW (ed) Trace fossils: concepts, problems, prospects. Elsevier, Amsterdam

Hasiotis ST, Mitchell CE (1993) A comparison of crayfish burrow morphologies: Triassic and Holocene fossil, paleo- and neo-ichnological evidence, and the identification of their burrowing signatures. Ichnos 2:291–314

Hembree DI (2009) Neoichnology of burrowing millipedes: linking modern burrow morphology, organism behavior, and sediment properties to interpret continental ichnofossils. Palaios 24:425–439

Hembree DI, Hasiotis ST (2006) The identification and interpretation of reptile ichnofossils in paleosols through modern studies. J Sed Res 76:575–588

Hembree DI, Hasiotis ST (2007) Biogenic structures produced by sand-swimming snakes: a modern analog for interpreting continental ichnofossils. J Sed Res 77:389–397

Hembree DI, Johnson LM, Tenwalde RW (2012) Neoichnology of the desert scorpion *Hadrurus arizonensis*: burrows to biogenic cross lamination. Palaeontol Electron 15:1–34

Hjelle JT (1990) Anatomy and morphology. In: Polis GA (ed) The biology of scorpions. Stanford University Press, Stanford

Jeram AJ (2001) Paleontology. In: Brownell P, Polis G (eds) Scorpion biology and research. Oxford University Press, Oxford

Kjellesvig-Waering EN (1986) A restudy of the fossil Scorpionida of the world. Palaeont Amer 55:1–287

Koch LE (1978) A comparative study of the structure, function, and adaptation to different habitats of burrows in the scorpion genus *Urodacus* (Scorpionida, Scorpionidae). Rec W Austral Mus 6:119–146

Kühl G, Bergmann A, Dunlop J, Garwood RJ, Rust J (2012) Redescription and paleobiology of *Palaeoscorpius devonicus* Lehmann, 1944 from the Lower Devonian Hünsruck Slate of Germany. Palaeontology 55:775–787

Lavelle P, Spain AV (2005) Soil ecology. Springer, Dordrecht

Lawfield AMW, Pickerill RK (2006) A novel contemporary fluvial ichnocoenose: unionid bivalves and the *Scoyenia-Mermia* ichnofacies transition. Palaios 21:391–396

Loope DB (2008) Life beneath the surfaces of active Jurassic dunes: burrows from the Entrada Sandstone of south-central Utah. Palaios 23:411–419

Mahsberg D (1990) Brood care and family cohesion in the tropical scorpion *Pandinus imperator* (Koch) (Scorpiones: Scorpionidae). Acta Zool Fennica 190:267–272

Mahsberg D (2001) Brood care and social behavior. In: Brownell P, Polis G (eds) Scorpio biology and research. Oxford University Press, Oxford

Marples TG, Shorthouse DJ (1982) An energy and water budget for a population of arid zone scorpion *Urodacus yaschenkoi* (Birula, 1903). Aust J Ecol 7:119–127

McCormick SJ, Polis GA (1990) Prey, predators, and parasites. In: Polis GA (ed) The biology of scorpions. Stanford University Press, Stanford

Meadows PS (1991) The environmental impact of burrows and burrowing animals—conclusions and a model. In: Meadows PS, Meadows A (eds) The environmental impact of burrowing animals and animal burrows. Clarendon Press, Oxford

Miller MF, Hasiotis ST, Babcock LE, Isbell JL, Collinson JW (2001) Tetrapod and large burrows of uncertain origin in Triassic high paleolatitude floodplain deposits, Antarctica. Palaios 16:218–232

Newlands G (1969) Scorpion defensive behavior. Afr Wildl 23:147–153

O'Geen AT, Busacca AJ (2001) Faunal burrows as indicators of paleo-vegetation in eastern Washington, USA. Palaeogeogr Palaeocl 169:23–37

Osgood Jr RG (1975) The paleontological significance of trace fossils. In: Frey RW (ed) The study of trace fossils: a synthesis of principles, problems, and procedures in ichnology. Springer-Verlag, New York

Pemberton SG, Spila M, Pulham AJ, Saunders T, MacEachern JA, Robbins D, Sinclair IK (2001) Ichnology and sedimentology of shallow to marginal marine systems: Ben Nevis and Avalon Reservoirs, Jeanne d'Arc Basin. Geological Association of Canada, Newfoundland

Petrunkevitch A (1955) Arachnida. In: Moore RC (ed) Treatise on invertebrate paleontology, part P, Arthropoda 2. Geological Society of America and University of Kansas Press, Lawrence

Picard MD (1977) Stratigraphic analysis of the Navajo Sandstone: a discussion. J Sed Petrol 47:475–483

Polis GA (1980) Seasonal patterns and age specific variation in the surface activity of a population of desert scorpions in relation to environmental factors. J Anim Ecol 49:1–18

Polis GA (1990) Ecology. In: Polis GA (ed) The biology of scorpions. Stanford University Press, Stanford

Polis GA, Sissom WD (1990) Life history. In: Polis GA (ed) The biology of scorpions. Stanford University Press, Stanford

Polis GA, Myers C, Quinlan M (1986) Burrowing biology and spatial distribution of desert scorpions. J Arid Environ 10:137–146

Prendini L (2011) Order Scorpiones C.L. Koch 1850. In: Zhang ZQ (ed) Animal biodiversity: an outline of higher level classification and survey of taxonomic richness. Magnolia Press, Aukland

Punzo F (2000a) Desert arthropods: life history variations. Springer, Berlin

Punzo F (2000b) Diel activity patterns and diet of the giant whipscorpion *Mastigoproctus giganteus* (Lucas) (Arachnida, Uropygi) in Big Bend National Park (Chihuahuan Desert). B Brit Arachnol Soc 11:385–387

Punzo F (2007) Microhabitat utilization, diet composition, intraguild predation, and diel periodicity in five sympatric species of desert arachnids: a wolf spider (*Hogna carolinensis*), tarantula spider (*Aphonopelma steindachneri*), giant whipscorpion (*Mastigoproctus giganteus*), and scorpion (*Diplocentrus bigbendensis*). B Brit Arachnol Soc 14:66–73

Ratcliffe BC, Fagerstrom JA (1980) Invertebrate Lebensspuren of Holocene floodplains: their morphology, origin, and paleoecological significance. J Paleontol 54:614–630

Rodríguez-Tovar FJ (2007) Substrate firmness controlling nesting behavior of *Bembix oculata* (Hymenoptera, Bembicinae). In: Bromley RG, Buatois LA, Mángano G, Genise JF, Melchor RN (eds) Sediment-organism interactions: a multifaceted ichnology. SEPM, Tulsa

Rutin J (1996) The burrowing activity of scorpions (*Scorpio maurus palmatus*) and their potential contribution to the erosion of Hamra soils in Karkur, central Israel. Geomorphology 15:159–168

Schaetzl R, Anderson S (2009) Soils: genesis and geomorphology. Cambridge University Press, Cambridge

Scott JJ, Renault RW, Owen RB (2007) Biogenic activity, trace formation, and trace taphonomy in the marginal sediments of saline, alkaline Lake Bogoria, Kenya Rift Valley. In: Bromley RG, Buatois LA, Mángano G, Genise JF, Melchor RN (eds) Sediment-organism interactions: a multifaceted ichnology. SEPM, Tulsa

Shachak M, Brand S (1983) The relationship between sit and wait foraging strategy and dispersal in the desert scorpion, *Scorpio maurus palmatus*. Oecologica 60:371–377

Shorthouse DJ, Marples TG (1980) Observations on the burrow and associated behavior of the arid-zone scorpion *Urodacus yaschenkoi* (Birula). Aust J Zool 28:581–590

Sissom WD (1990) Systematics, biogeography, and paleontology. In: Polis GA (ed) The biology of scorpions. Stanford University Press, Stanford

Smith JJ, Hasiotis ST (2008) Traces and burrowing behaviors of the cicada nymph *Cicadetta calliope*: neoichnology and paleoecological significance of extant soil-dwelling insects. Palaios 23:503–513

Storm L, Mattathias DN, Smith CJ, Fillmore DL, Szajna M, Simpson EL, Lucas SG (2010) Large vertebrate burrow from the Upper Mississippian Mauch Chunk Formation, eastern Pennsylvania, USA. Palaeogeogr Palaeocl 298:341–347

Tałanda M, Dzięcioł S, Sulej T, Niedźwiedzki G (2011) Vertebrate burrow system from the Upper Triassic of Poland. Palaios 26:99–105

Tourtlotte G (1974) Studies on the biology and ecology of the northern scorpion *Paruroctorus boreus* (Girard). Great Basin Nat 34:167–179

Tschinkel WR (2003) Subterranean ant nests: trace fossil past and future. Palaeogeogr. Palaeocl 192:321–333

Warburg MR, Polis GA (1990) Behavioral responses, rhythms, and activity patterns. In: Polis GA (ed) The biology of scorpions. Stanford University Press, Stanford

White CR (2001) The energetics of burrow excavation by the inland robust scorpion, *Urodacusyaschenkoi* (Birula, 1903). Aust J Zool 49:663–674

Williams SC (1966) Burrowing activities of the scorpion *Anuroctonus phaeodactylus* (Wood) (Scorpionida: Vaejovidae). Proc Calif Acad Sci 34:419–428

Wing SL, Sues HD (1992) Mesozoic and Early Cenozoic terrestrial ecosystems. In: Behrensmeyer AK, Damuth JD, DiMichele WA, Potts R, Sues HD, Wing SL (eds) Terrestrial ecosystems through time. The University of Chicago Press, Chicago

Chapter 12
Biomechanical Analysis of Fish Swimming Trace Fossils (*Undichna*): Preservation and Mode of Locomotion

María Cristina Cardonatto and Ricardo Néstor Melchor

Content

Abstract This chapter includes a morphological analysis of sinusoidal swimming trails of the ichnogenus *Undichna* and inferences on likely producers, mode of swimming, and preservation. A total of 166 *Undichna* specimens were measured, including selected examples from the literature and unpublished material from different basins of Argentina. These specimens belong to seven ichnospecies, including *U. bina, U. britannica, U. consulca, U. insolentia, U. quina, U. simplicitas,* and *U. unisulca.* The morphology of these ichnospecies is used in conjunction with that of the presumed producer to infer the mode of swimming of the fish. Most *Undichna* ichnospecies are interpreted as produced by a fish swimming with subcarangiform

R. N. Melchor (✉)
INCITAP (UNLPam-CONICET), Av. Uruguay 151,
6300 Santa Rosa, La Pampa, Argentina
e-mail: rmelchor@exactas.unlpam.edu.ar

M. C. Cardonatto
Universidad Nacional de La Pampa, Av. Uruguay 151,
6300 Santa Rosa, La Pampa, Argentina

locomotion. *U. insolentia, U. bina,* and some specimens of *U. britannica* are interpreted as reflecting anguilliform locomotion. The essential measurements used in this analysis are wavelength and wave amplitude. Maximum wavelength (in most cases interpreted as the trail produced by the caudal fin) is used to infer the length of the producer for each specimen by comparison with experiments using extant fishes from the literature. Estimated length of fish producing *Undichna* is in the range 24–800 mm, but most values are less than 250 mm. By estimating the Reynolds number (Re) for each specimen, it is inferred that a fish larger than 650 mm will produce a flow disturbance and bottom sediment suspension that will preclude the preservation of trails recognizable as *Undichna*. Larger fish may leave identifiable *Undichna* provided that the sediment underwent early cementation or the fish was swimming at a speed lower than maximum sustained speed.

Keywords Fish trail · Swimming mode · Preservation · Theoretical analysis

12.1   Introduction

Fish swim with two main mechanisms that may be used separately or in combination: (1) body and caudal fin propulsion, with undulations passing from the front to rear of the body; and (2) oscillation of median and/or paired fins, where the body is only slightly undulated. Other forms of nonswimming underwater locomotion are also employed by fish, including water jets and "walking" or hopping on the bottom (Lindsey 1978). Most of these locomotion mechanisms are roughly represented in the trace fossil record. Body and caudal fin propulsion is inferred for single, paired, and/or intertwined sinusoidal surface trails assigned to the ichnogenus *Undichna* Anderson, 1976. Propulsion by oscillation of pectoral and pelvic fins is represented by sets of sigmoidal ridges symmetrically arranged along a linear path recognized as the ichnogenus *Parundichna* Simon et al. 2003. The ichnogenus *Broomichnium* (Kuhn 1958), composed of two pairs of nested linear imprints, reflects nonswimming locomotion by fishes (Benner et al. 2008). There is an overall agreement that *Undichna* represents fish-produced traces formed while swimming close to the bottom (Anderson 1970, 1976; Fliri et al. 1970; Higgs 1988), an interpretation partially sustained by the observation of similar trails in modern settings (Gibert et al. 1999). In particular, ventral features including fins (both paired and medial), spiny fins, or spines are usually envisaged as interacting with the bottom sediment and producing the trails. Experiments with modern fish designed to reproduce this kind of trails are scarce. The only published report is by Stanley (1971) when comparing with some of the modern traces observed in the seafloor, along with a brief mention of unpublished experiments by Anderson (1970). After erection of the ichnogenus, it has been recorded worldwide in increasing numbers and in stratigraphic sequences ranging in age from the Devonian to recent.

Several issues on the preservation and taphonomy of *Undichna* have been raised. The paleoenvironmental distribution of the first records of *Undichna* suggested a preferential preservation in freshwater settings (Buatois and Mángano 1994);

however, subsequent findings confirmed that the trace fossil also occurs in marine settings (Melchor and Cardonatto 1998; Gibert et al. 1999; Gibert 2001). It has been suggested that the key aspects of preservation of fish trails include the absence or scarcity of infaunal burrowers (favored in oxygen-deficient settings), very fine-grained sediment, low-energy conditions, and relatively rapid burial without erosion (Gibert et al. 1999; Trewin 2000). Trewin (2000) suggested that the presence of chevron marks in some trails indicates that the sediment was slightly cohesive and capable of plastic deformation. After a revision of the occurrences of the ichnogenus, Cardonatto and Melchor (1998) argued that *Undichna* was mostly produced by small fish. In this chapter, we test the hypothesis that most *Undichna* were produced by small fish and discuss the possible biomechanical explanation of this phenomenon. For this purpose, we analyzed selected *Undichna* ichnospecies whose interpretation is straightforward. These ichnospecies are then related to a definite mode of swimming. We apply empirical relations to estimate the size of the tracemaker of the selected ichnospecies and then calculate the Reynolds numbers for every occurrence. The values of this nondimensional scaling factor along with the existing hydrodynamic theory of flow around a swimming fish are then used to assess the potential disturbance in the bottom sediment by fishes of different sizes.

12.2 Material and Methods

At least 12 *Undichna* ichnospecies have been proposed to date (Anderson 1976; Higgs 1988; Turek 1989; Lu and Chen 1998; Gibert et al. 1999; Trewin 2000; Gibert 2001; Lu et al. 2003; Wisshak et al. 2004). The recent revision of the ichnotaxonomy of *Undichna* by Minter and Braddy (2006) is mostly followed in this work, although further revision is likely necessary. For example, the ichnospecies *U. trisulcata* Morrissey et al. 2004 does not contain continuous sinusoidal waves, and thus, should not be included within the ichnogenus, even if it can be interpreted as a fish swimming trace fossil. We have selected seven *Undichna* ichnospecies (*U. bina, U. britannica, U. consulca, U. insolentia, U. quina, U. simplicitas,* and *U. unisulca*) that can be analyzed using hydrodynamic principles and scaling laws of fish swimming (e.g., Bainbridge 1958; Webb and Blake 1985; Webb 1988; Videler 1993). The database is composed of 48 unpublished specimens from Argentina and 118 selected specimens from the literature (Tables A.1–A.3). They range in age from Early Devonian to recent and have a worldwide distribution. The provenance of unpublished specimens from Argentina includes: the Upper Carboniferous Agua Escondida Formation, San Rafael Basin (Figs. 12.1a, b, e and 12.2c, e), the Permian Bajo de Véliz Formation, Paganzo Basin (Fig. 12.2d), the Permian Bonete Formation, Sauce Grande Basin (Fig. 12.1b), the Middle Triassic Ischichuca and Los Rastros formations, Ischigualasto-Villa Unión Basin (Fig. 12.2a, b), and the Upper Cretaceous Calafate Formation, Austral Basin (Fig. 12.1d). Table 12.1 contains the geographic, stratigraphic, and facies provenance of unpublished specimens. For the compilation of information from the literature, published photographs were used to measure the parameters employing Image J 1.45 (http://rsbweb.nih.gov/ij/).
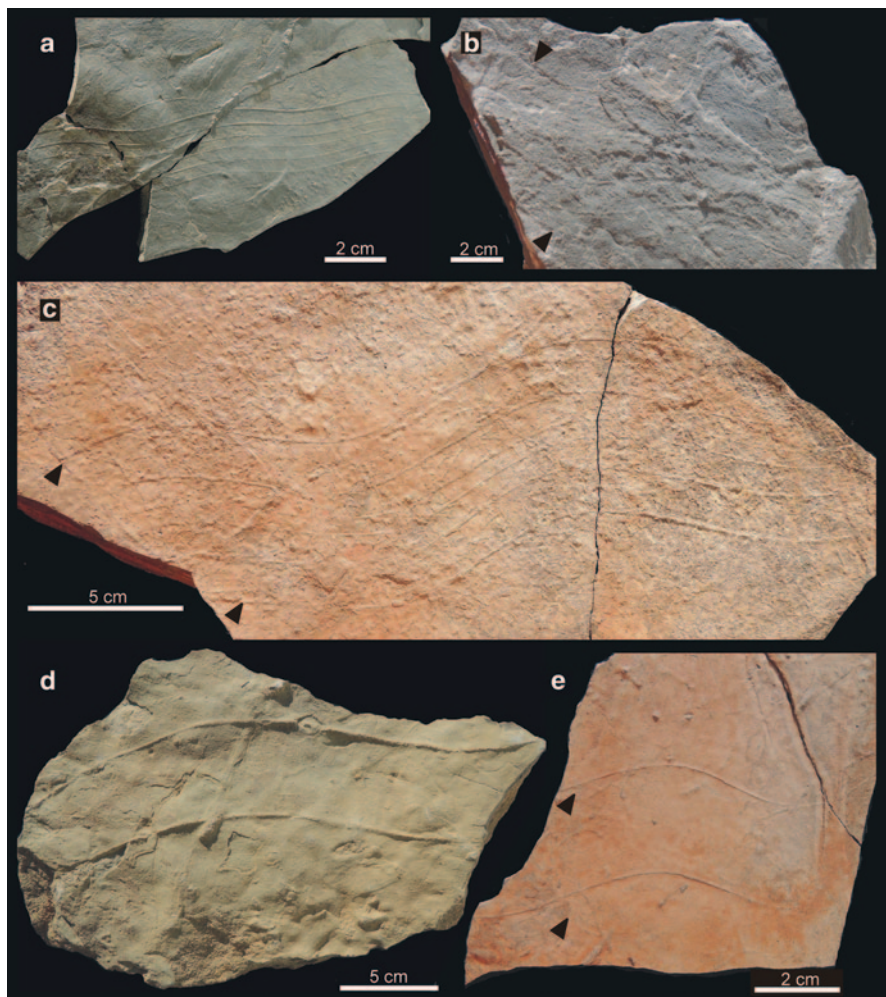
Fig. 12.1 Examples of new specimens of *U. insolentia* (**a–c**) and *U. bina* (**d** and **e**). **a** *U. insolentia,* Late Carboniferous Agua Escondida Formation (GHUNLPam 12251). **b** *U. insolentia,* Early Permian Bonete Formation (GHUNLPam 3164II). **c** *U. insolentia,* Late Carboniferous Agua Escondida Formation (GHUNLPam 12130). **d** *U. bina,* Maastrichtian Calafate Formation (GHUNLPam 3166). **e** *U. bina,* Late Carboniferous Agua Escondida Formation (GHUNLPam 12100). Black arrow points to external waves

The measured parameters for *U. bina* and *U. insolentia* are maximum wavelength (λm), maximum wave amplitude (Am), and maximum width (Wm) (Fig. 12.3). For the remaining ichnospecies, we measured the wavelength (λc) and wave amplitude (Ac) of the wave with the largest amplitude, or if crosscutting between waves is observed, those of the wave that cut the previous one. This wave is commonly interpreted as that of the caudal fin. For the purpose of this chapter, both λc and λm and Ac and Am are considered equivalent parameters because they reflect the largest
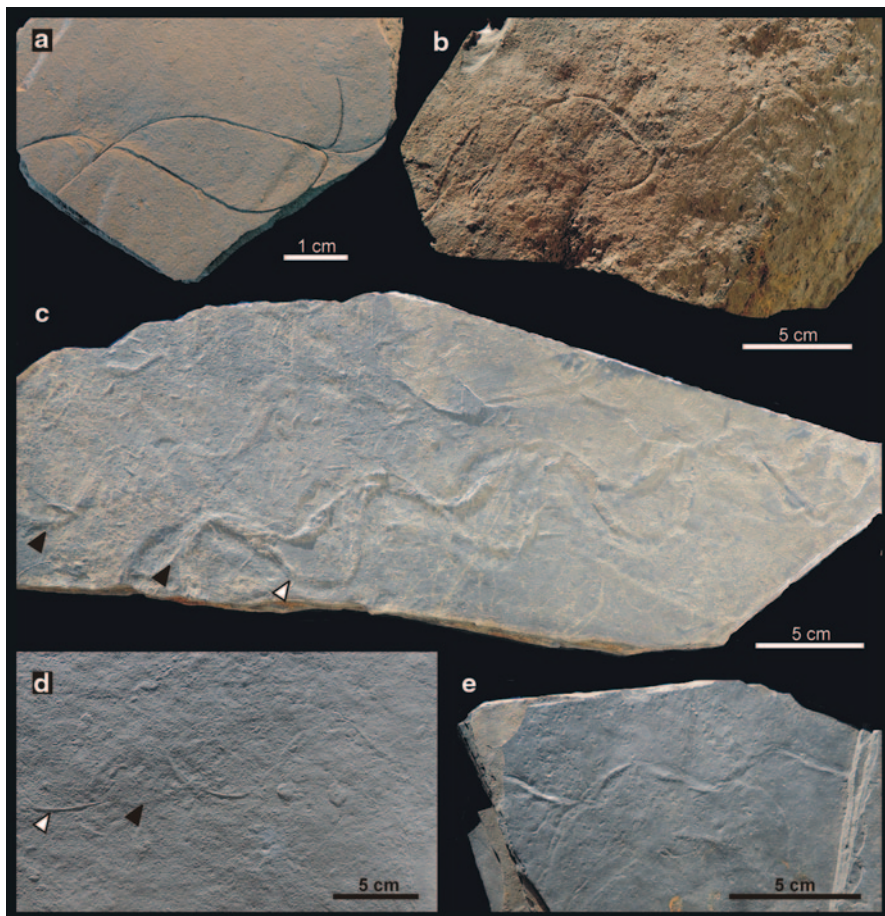
Fig. 12.2 Examples of new specimens of *U. britannica, U. quina,* and *U. unisulca* measured for this work. **a** *U. britannica,* Middle Triassic Los Rastros Formation (CRILAR-Ic 62). **b** *U. britannica,* Middle Triassic Ischichuca Formation (CRILAR-Ic 61). **c** *U. quina,* Late Carboniferous Agua Escondida Formation (GHUNLPam 12087). Black arrows point to in-phase pairs of waves, and white arrow to a single larger amplitude wave. **d** *U. britannica,* Permian Bajo de Véliz Formation (MHIN-UNSL-GEO T 663). White arrow points to the larger amplitude wave and the black arrow to the smaller amplitude wave. **e** *U. unisulca,* Late Carboniferous Agua Escondida Formation (MCNAM PI 24293)

undulations of the body of the producer. If present, the maximum wavelength (λ^*) and amplitude (A^*) of one of the waves with lower amplitude were also measured (Fig. 12.3). The lower amplitude waves have been related to anal, pelvic, or pectoral fins. For incomplete trails, the wavelength is inferred from the measured half wavelength. In order to avoid the introduction of potential errors from other measurement methods, we used our estimations of the parameters from literature-based material, except when the methodology was clearly stated and similar to the one employed here.

Fig. 12.3 Measurements on the *Undichna* ichnospecies studied for this work. *Ac* amplitude of caudal fin wave, *λc* wavelength of caudal fin wave, *Am* maximum amplitude of all waves, *λm* maximum wavelength, *Wm* maximum width of trail, *A** maximum amplitude of pectoral or pelvic fin wave, *λ** maximum wavelength of pectoral or pelvic fin wave
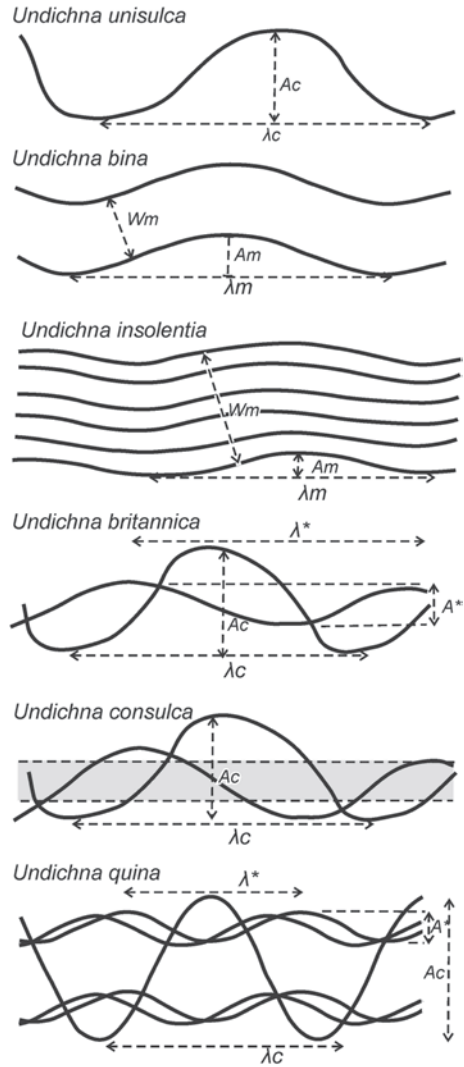
The first step in the analysis is to interpret the mode of swimming (Breder 1926; Lindsey 1978) of the probable producer of the different ichnospecies on the basis of the geometry of the trace fossil. For estimation of body length (*L*) of the producer of *Undichna*, empirical relationships between wavelength and body length of modern fish swimming at steady speeds using undulation of body and tail were used. For anguilliform locomotion, we used $\lambda = 0.60$ L (Wardle et al. 1995; Tytell and Lauder 2004), for subcarangiform or salmoniform locomotion $\lambda = 0.67$ L (Wardle et al. 1995), and for carangiform locomotion $\lambda = 1.00$ L (Videler 1993; Wardle et al. 1995).

Re, a nondimensional parameter that represents the fluid dynamics, was calculated with:

$$Re = UL/v$$

where U is the speed of the fish, L is fish length, and $v = \mu/\rho$ is the kinematic viscosity (dynamic viscosity/density) of the fluid. *Re* has a value of approximately $1.136 \times 10^{-6} m^2 \ s^{-1}$ for fresh water at a temperature of 15 °C and $1.176 \times 10^{-6} m^2 \ s^{-1}$ for seawater at 30 ‰ salinity.

In order to estimate the velocity of the fish that produced the specimens of *Undichna* analyzed, we employed empirical linear relationships for maximum sustained speed (U_{ms}) discussed by Videler (1993, p. 209–217):

$$U_{ms} = 0.15 + 2.4 \ L.$$

The newly collected specimens are stored in the following repositories: paleontological collection of the Facultad de Ciencias Exactas y Naturales, Universidad Nacional de La Pampa, Santa Rosa City, La Pampa, Argentina (GHUNLPam); collection of the Museo de Ciencias Naturales y Antropológicas "Juan Cornelio Moyano," Mendoza, Argentina (MCNAM PI); Museo de Historia Natural, Universidad Nacional de San Luis, Geología, San Luis, Argentina (MHIN-UNSL-GEO T); and the Centro Regional de Investigaciones Científicas y Transferencia Tecnológica de La Rioja, Anillaco, Argentina (CRILAR-Ic). Detailed information on the provenance of this material is found in Table 12.1.

12.3   Fish Swimming Modes and Producer of *Undichna* Ichnospecies

12.3.1   Swimming Modes

The morphology of a sinusoidal fish trail is related to the swimming mode and anatomy of the producer and is also a reflection of fish behavior. Previous inferences about the likely tracemaker of *Undichna* have varied from definite assignation to a fish species to tentative comparisons with high-rank taxa. As the main distinctive feature of *Undichna* is the presence of sinusoidal trails, its producer must have traveled with an axial undulatory mechanism, where waves are passed along body or fin propulsor (e.g., Webb and Blake 1985). Four main modes of swimming are related to propulsion by body and/or caudal fin: anguilliform, subcarangiform, carangiform, and thunniform (Breder 1926; Lindsey 1978). In these modes of swimming, the proportion of the body involved in propulsion varies. Anguilliform is a purely undulatory mode of swimming, in which most of the body participates in moderate amplitude undulations. This mode of swimming is typical of eels or eel-like fish and of juveniles of most fish (Lindsey 1978). In fishes using subcarangiform locomotion (e.g., trout) the amplitude of undulations is slight at the anterior part of the body and expands significantly only in the

Table 12.1 Provenance of new *Undichna* specimens from Argentina

Formation	Age	Locality	Trace fossil bearing facies	Ichnospecies	Specimen #
Calafate	Maastrichtian	Arroyo 25 de Mayo, Santa Cruz province (50°23′19″ S; 72°12′24″ W)	Fine-grained wave-rippled sandstones interbeded with laminated mudstone (tidal flat)	*U. bina*	GHUNLPam 3166
Los Rastros	Middle Triassic	Gualo, Talampaya National Park, La Rioja province (29°53′03″ S; 67°46′36″ W)	Thinly bedded siltstones (lacustrine delta front)	*U. britannica*	CRILAR-Ic 62–64
Ischichuca	Middle Triassic	Quebrada de Ischichuca, La Rioja province (29°37′52″ S; 68°24′12″ W)	Thinly bedded and graded siltstone (lacustrine delta front)	*U. britannica*	CRILAR-Ic 61
Bajo de Véliz	Permian	Cantera Santa Rosa, San Luis province (32°17′06″ S; 65°24′27″ W)	Gray laminated mudstones and siltstones (lacustrine)	*U. britannica*	MHIN-UNSL-GEO T 663–665
Bonete	Early Permian	Cerro Bonete, Buenos Aires province (38°09′07″ S; 61°40′59″ W)	Laminated quartz silt-stones and sandstones (marine shelf)	*U. insolentia*	GHUNLPam 3164, 3165
Agua Escondida	Late Carboniferous	Santa Cruz Mine, Mendoza province (36°02′33″ S, 68° 28′24″ W)	Black shale, laminated mudstone, wave rippled mudstone (estuary)	*U. insolentia, U. unisulca*	GHUNLPam 3159, 3404, 3434, 3450, 3466, 3470, 3485, 12125, 12174, 12175, 12176, 12185, 12186, 12187, 12188, 12189, 12197, 12198, 12251
Agua Escondida	Late Carboniferous	Lomas Piedras de Afilar, La Pampa province (36°09′30″ S, 68°16′13″ W)	Gray to red laminated mudstones (estuary)	*U. bina, U. insolentia*	GHUNLPam 12099, 12100, 12130

Table 12.1 (continued)

Formation	Age	Locality	Trace fossil bearing facies	Ichnospecies	Specimen #
Agua Escondida	Late Carboniferous	Puesto Yantén 1, Mendoza province (36°00′47″ S, 68°27′13″ W)	Gray laminated mudstones (estuary)	*U. bina, U. quina, U. unisulca*	GHUNLPam 12086, 12087; MCNAM PI 24271, 24282, 24293.

posterior half or one-third of the body. For carangiform swimming, body undulations are confined to the posterior third of the body. In thunniform locomotion, significant lateral movements are confined to the caudal fin only (Lindsey 1978). It is unlikely that *Undichna* reflects thunniform or carangiform swimming mode as they are typical of pelagic fishes specialized in swimming at high cruising speeds. In the following sections, each *Undichna* ichnospecies (Table A.1–A.3) will be analyzed, and their probable producers discussed in order to interpret, when possible, the swimming mode employed by the tracemaker.

12.3.2   U. insolentia

U. insolentia (Fig. 12.1a–c) is characterized by the presence of four or six, sinusoidal, in-phase trails. The ichnospecies is restricted to the Late Carboniferous to Late Permian strata, and has been identified both in shallow marine and lacustrine settings. Our database (Table A.1) includes specimens with two pairs of waves (Anderson 1976; Trewin 2000; Piñeiro 2006), as well as examples with three pairs of waves that are more common. Acanthodian fishes have been proposed as possible producers (Anderson 1976; Buatois and Mángano 1994; Piñeiro 2006) although paleonisciform fishes were also considered as candidates (Trewin 2000). The almost constant separation between trails of *U. insolentia* requires a producer with up to three paired ventral structures (spines or spiny fins) located from the middle to the rear of the body (Anderson 1970). The average ratio between wave amplitude and wavelength $Am/\lambda m$ is 0.11 (range 0.04–0.25, $n=38$), suggesting limited undulation of the part of the body where these structures were located. The almost constant separation between trails also suggests a relatively stiff structure or one with minimal movement during swimming. These features point to acanthodians as the more likely producers, in particular the Climatiidae, which have up to six pairs of ventral spines located in the middle third of the body, with some genera also possessing two pectoral spines (Moy-Thomas and Miles 1971; Carroll 1988). Most acanthodians were microphagous and mid- to surface water feeders which seem to contradict the benthonic mode of life required for the producer of *U. insolentia*. The almost constant spacing between pairs of trails implies, if our assumptions about the tracemaker are correct, that the fish was swimming with waves that propagated along most of the body, and it is thus compared with anguilliform propulsion.

Table 12.2 Morphometric data of putative producers of *U. britannica*

Source	Figure	Fish species	*L* (mm)	*A–c* (mm)	*L/a–c*
Agassiz (1833)	Table D.1	*Acrolepis sedgwickii*			0.30
Su (1999)	Fig. 1	*Wayaobulepis zichangensia*	700	135	0.19
Poyato-Ariza (1995)	Fig. 1	*Ichthyemidion vidali*	275	70	0.25
López-Arbarello et al. (2006)	Fig. 4	*Rastrolepis riojaensis*	450	90	0.20
López-Arbarello et al. (2010)	Text-Fig. 2	*Neochallaia telecheai*	90	23	0.25
Rusconi (1949)	Fig. 1	*Neochallaia telecheai*	148	32	0.22

12.3.3 *U. britannica* and *U. consulca*

The ichnospecies *U. britannica* (Fig. 12.2a, b, d) is recorded from the Late Mississippian (Fillmore et al. 2011) to recent (Gibert et al. 1999), and is more common in lacustrine and estuarine settings, although it has been recorded in fluvial and other shallow marine environments. The distinctive features of the ichnospecies are two intertwined trails of different amplitude that are out of phase. It is commonly interpreted as produced by the dragging of the anal (lower amplitude trail) and caudal fins (higher amplitude trail) in the bottom sediment (Higgs 1988). The proposed producers are paleonisciformes for Late Carboniferous to Late Triassic occurrences (Higgs 1988; Turek 1989; Wang et al. 2008) and teleosts for Early Cretaceous to Pleistocene examples (Fliri et al. 1971; Gibert et al. 1999; Benner et al. 2009). One exception is the example from the Late Carboniferous of Spain that was assigned to Chondrichthyes (Soler-Gijón and Moratalla 2001), although the material available is scarce and poorly preserved. Triassic fishes from Argentina were reported from the Cuyana and Ischigualasto-Villa Unión basins (López-Arbarello et al. 2006, 2010). Those that display a caudal fin with a well-developed ventral lobe, a downward projecting anal fin, and an adequate size to produce *U. britannica* include the 450 mm long chondrostean *Rastrolepis riojaensis* (López-Arbarello et al. 2006) found in the same sedimentary sequence of the fish trails (Ischigualasto-Villa Unión Basin) and the 150 mm long paleonisciform (Acrolepidae) *Neochallaia telecheai* (López-Arbarello et al. 2010).

For all examples of *U. britannica* (Table A.2), the mean ratio between the amplitude and wavelength of the caudal fin wave ($Ac/\lambda c$) is 0.36 (range 0.13–0.75, $n=49$), the mean ratio between amplitude of the caudal and anal waves (Ac/A^*) is 1.5 (range 0.9–3.7, $n=38$), and the mean ratio between the amplitude and wavelength of the anal fin wave (A^*/λ^*) is 0.28 (range 0.07–0.90, $n=29$). These relationships suggest increasing undulation of the fish body toward the caudal fin, although the amplitude of the wave produced by the anal fin was still significant. The distance between the tip of anal and lower lobe of caudal fin for the putative producers of the trace fossils (Table 12.2) is 19–30% of the total length. Consequently, more than one third of the body was employed in undulatory movements, although a marked reduction is evident toward the anal fin, thus suggesting that the producers of *U. britannica* mostly used a subcarangiform locomotion mode (Lindsey 1978).

Further subdivision of the mode of swimming is possible by comparing amplitude distribution along the body of different modern fish. For this purpose, we compared the relative wave amplitude of the path of fishes with different swimming modes from the literature (Webb 1992, Fig. 3; Tytell et al. 2010) at approximately 77% of body length starting from the nose (approximate average location of anal fin of likely producers from Table 12.2) at a sustained speed. The amplitude is expected to roughly match that of the body of swimming fish at the position of the anal fin. The ratio of amplitude of anal to caudal fin (A^*/Ac) in fish with carangiform swimming is typically less than 0.5, those of subcarangiform fish is in the range of 0.5–0.8, and with anguilliform fish it is higher than 0.8 (Webb 1992; Tytell et al. 2010). In the specimens of *U. britannica* analyzed, the amplitude ratio of anal to caudal fin is in the range of 0.27–0.95 (mean 0.63, $n = 36$). Within this set of *U. britannica,* five specimens exhibit a similar amplitude of anal and caudal fin trails (amplitude ratio greater than 0.8), and are considered transitional to anguilliform swimming mode. These specimens belong to Late Paleozoic (Anderson 1976; Archer and Maples 1984; Martin and Pyenson 2005) and Triassic strata (Middle Triassic Los Rastros Formation, reported here). Similarly there are other specimens that exhibit an A^*/Ac lower than 0.5, and are thus interpreted as representing a trend toward a carangiform locomotion. Since true carangiform fishes are pelagic, however, this inference is only tentative. The specimens are from the Late Carboniferous (Higgs 1988; Turek 1989), Late Triassic (Lu et al. 2004), and Pleistocene (Fliri et al. 1971). In consequence, although most *U. britannica* can be interpreted as having a subcarangiform swimming, some examples are more comparable with anguilliform locomotion, and others show a trend toward carangiform swimming.

U. consulca is similar to *U. britannica* except for the presence of a shallow medial furrow. Although distinctive, the morphology has been rarely documented in the literature except for the original definition. Morphotype C of *U. radnicensis* figured by Turek (1996) was compared with *U. consulca,* but we interpret this specimen as an inorganic structure (tool mark) produced in cohesive bottom sediment. Similarly, the specimen described as *U. consulca* by Netto et al. (2013) differs significantly from the original diagnosis and should be compared with another ichnospecies. *U. consulca* was interpreted as produced by a fish dragging its belly in the upper few millimeters of bottom sediment, although it is not certain if this reflects a feeding behavior or simply locomotion (Higgs 1988). Higgs (1988) found that the only suitable fish from the Bude Formation to produce *U. consulca* was the paleonisciform *Cornuboniscus budensis*. In the reconstruction figured by Higgs (1988, Fig. 9) the lowest ventral point of *C. budensis* is located in the anterior third of the body. If we assume that the anterior third of the body was nearly touching the bottom, the straight path of the central furrow indicates that the producer did not employ an anguilliform mode of swimming, which implies the presence of waves traveling from head to tail. The mean ratio between the amplitude and wavelength of the caudal fin wave ($Ac/\lambda c$) is 0.51 (range 0.29–0.75, $n = 7$) and is within the observed range for *U. britannica*. It is, therefore, inferred that the producer of *U. consulca* used a salmoniform or subcarangiform locomotion mode. The greater apparent amplitude may be related to the small number of specimens available or may be related to the increased thrust needed to push the fish body in contact with the bottom sediment (Blevins and Lauder 2013).

12.3.4 U. bina

The ichnospecies *U. bina* (Fig. 12.1d, e) is characterized by a pair of in-phase sinu-soidal waves. The ichnospecies was previously recorded from Late Carboniferous to Late Triassic strata (Minter and Braddy 2006), and new Late Carboniferous and Late Cretaceous occurrences are reported in this contribution (Table A.1). The trail was originally related to the pelvic or pectoral fins of paleonisciform fish (Anderson 1976; Higgs 1988; Trewin 2000; Minter and Braddy 2006). Flatfish were also sug-gested (Lu et al. 2004) by comparison with modern pleuronectiform traces observed by Stanley (1971). This alternative is considered unlikely because while pleuro-nectiformes employ anguilliform locomotion, they swim on their side so that the undulations are vertical. Chondrichthyes (mainly hybodont sharks) and dipnoans can be added to the list of potential producers, as they are recorded from the regions and time span where *U. bina* is recorded, including the Permian and Cretaceous of South America, Permian of South Africa (where dipnoans are absent), and Trias-sic of China (Murray 2000; Díaz Saravia 2001; López-Arbarello 2004; Apesteguía et al. 2007; Cione et al. 2010). If the pectoral fins were involved in the production of *U. bina,* then the fish used anguilliform locomotion (Trewin 2000; Minter and Braddy 2006), and if the pelvic fins dragged in the bottom, the fish could have anguilliform or subcarangiform locomotion. The mean ratio between wave ampli-tude and wavelength $Am/\lambda m$ is 0.17 (range 0.09–0.39, $n=30$), which is close to the values for *U. insolentia,* thus suggesting anguilliform mode of locomotion for this ichnospecies.

12.3.5 U. unisulca

The simple morphology of *U. unisulca* (Fig. 12.2e) is more difficult to interpret in terms of producer and swimming mode. An unpaired ventral fin (caudal or anal) is commonly envisaged as the anatomical structure responsible for the trace fossil. The examples from the Cretaceous of Spain described by Gibert et al. (1999) were assigned to the pycnodontiform teleost *Macromesodon* aff. *bernissartensis.* The au-thors argued that this was the most suitable of all known fishes from the locality and was abundant. The presumed producer was a deep-bodied fish with markedly reduced pectoral, pelvic, and caudal fins, and well-developed anal and dorsal fins. Fishes with this morphology are not capable of lateral undulations of the body and swim essentially by oscillating the dorsal and anal fins (Lindsey 1978; Webb 1984). For this reason, Gibert et al. (1999) interpreted *U. unisulca* as the path of displace-ment of the fish by dragging its anal fin. If this interpretation is correct, it is not easy to reconcile an oscillating anal fin with the production of a sharply defined trail. All the remaining occurrences of *U. unisulca* compiled in Table A.3 were interpreted as the product of the caudal fin, an interpretation that is favored here. The mean ratio of amplitude and wavelength of the caudal fin wave ($Ac/\lambda c$) for *U. unisulca* is 0.36 (range 0.12–0.90, $n=28$), which is fairly similar to those of *U. britannica,*

supporting a similar biomechanical interpretation in terms of swimming mode. The simple morphology of *U. unisulca,* however, limits a more detailed interpretation.

12.3.6   *U. quina and U. simplicitas*

This ichnospecies is represented by intertwined sinusoidal waves of smaller amplitude (probably the trail of pelvic fins) cut by a single sinusoidal wave of larger amplitude (trail of caudal fin) (Fig. 12.2c). *U. gosiutensis* was considered a subset of *U. quina* (Minter and Braddy 2006) and is only known by two specimens to date (Gibert 2001; Todesco and Avanzini 2008). Similarly, *U. tricosta* described by Lu et al. (2004) was considered comparable with *U. quina* by Minter and Braddy (2006). These ichnospecies are recorded from Late Mississippian to Callovian strata (Table A.2). Similarly, the type material of *U. simplicitas* from the Permian of South Africa (Anderson 1976) and material compared with this ichnospecies from the Late Carboniferous of the USA (Buatois et al. 1998), one Late Triassic specimen from China originally recognized under *U. tricosta* (Lu and Chen 1998) and Early Eocene trails from the USA (Martin et al. 2010) share a set of waves linked to pelvic fins and a single wave that is related to the caudal fin. Inferences about the producer of these traces range from broad assignation to paleonisciformes (Trewin 2000) to specific comparison with a paleonisciform species (Wang et al. 2008). The specimens related to U. *quina* and *U. simplicitas* display an average ratio between the amplitude and wavelength of the caudal fin wave ($Ac/\lambda c$) of 0.35 (range 0.19–0.63, $n=12$). This is very close to the average value for *U. britannica,* and it is thus assumed that forms related to *U. quina* and *U. simplicitas* represent subcarangiform mode of swimming.

   To summarize, most *Undichna* ichnospecies are interpreted as traces produced by fish swimming with a subcarangiform mode of locomotion. *U. insolentia, U. bina,* and some specimens of *U. britannica* are interpreted as reflecting anguilliform locomotion. Also, a few specimens of *U. britannica* may reflect a transition to a carangiform mode of locomotion.

12.4   **Length of Fish Producing** *Undichna*

Empirical relationships between wavelength and body length for fish swimming at maximum sustained speed (Videler 1993; Wardle et al. 1995; Tytell and Lauder 2004) allow calculating the size of the producer of *Undichna,* provided that an estimation of the swimming mode is feasible from the morphology of the trace fossil. The use of trail wavelength to estimate producer length of *Undichna* has been criticized by Trewin (2000), who found no relationship between wavelength and trace width in a sample of Permian *U. bina* from the Malvinas/Falkland Islands. This assertion, however, assumes that a single ichnospecies was produced by fishes with similar morphology, which is not always the case and cannot be used in a general study compiling

Fig. 12.4 Estimated size of *Undichna* producer. **a** Histogram of body length of fish. **b** Average (*rhomb*) and range (*arrows*) of estimated body length of fish responsible of different ichnospecies
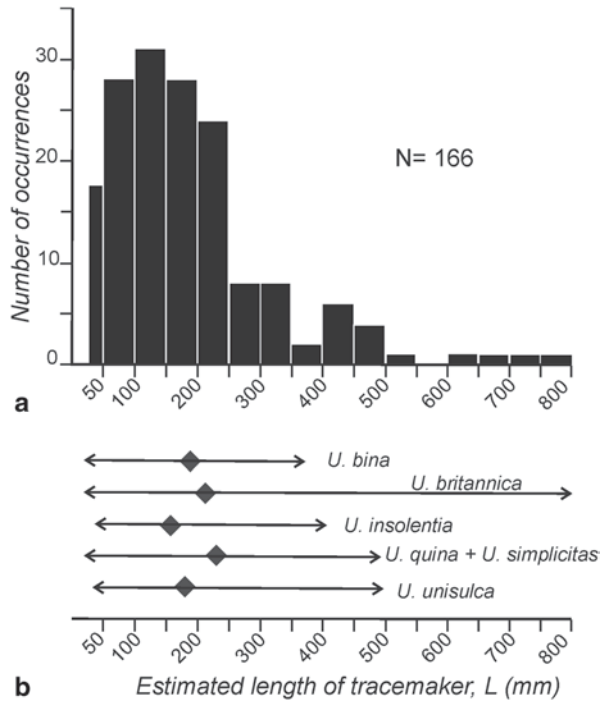
data from different ages and geographic provenance. For the 166 cases of *Undichna* measured in this study, the overall length range of the fish that produced them is 24–800 mm (Fig. 12.4a). The length of the fish producing more than three quarters of analyzed specimens is in the range 25–250 mm. The range and average size for different ichnospecies is fairly similar, although the largest fish were involved in the production of *U. britannica* (Fig. 12.4b). On the basis of these estimates of fish length, it is possible to employ empirical equations to infer the speed of the fish producing *Undichna* (Videler 1993, p. 213). Using these relationships, the maximum sustained speed ranged from 0.21–2.07 m/s (average=0.61 m/s, *n*=166; Tables A.1–A.3).

12.5 Fluid Disturbance by Swimming Fish

When fish swim with undulatory movements, the ambient fluid is modified to produce a wake whose morphology is different in carangiform and anguilliform swimmers (Müller et al. 1997; Videler et al. 1999; Müller et al. 2001). Using the estimated length and velocity of the producer of *Undichna,* it is possible to calculate the *Re* as a characterization of the fluid dynamics during production of the trace fossils. Body size and speed affect the relative importance of viscous and inertial forces. Viscous (friction) drag is restricted to the boundary layer, where flow may

Fig. 12.5 Plot of estimated body length vs. Reynolds number for the studied specimens (see data in Tables A.1–A.3). *Dashed line* indicates the intercept between the regression line at $Re = 1 \times 10^6$ (indicating turbulent separation and turbulent boundary layer) and the corresponding size of fish (about 650 mm in length)
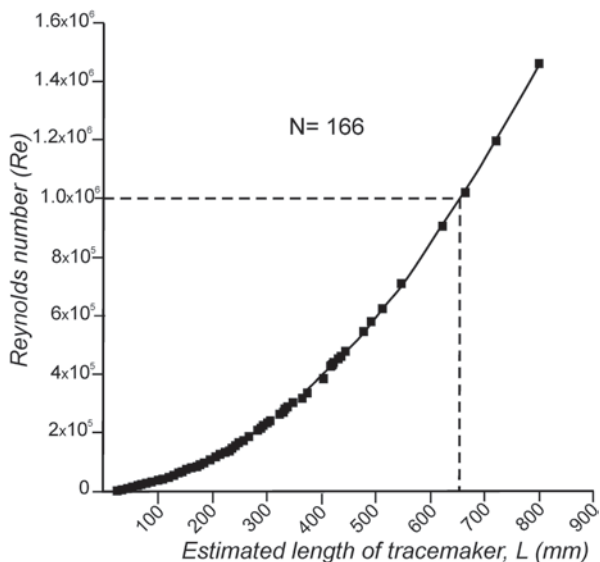
be laminar or turbulent. Transition from laminar to turbulent boundary layer flow and turbulent separation occurs at Re of 1×10^6–3.5×10^6 for well-designed bodies (Roshko 1961; Wardle 1977), whereas standard critical range for boundary layer transition are $Re = 3.5 \times 10^5$–5×10^5 (Anderson et al. 2001). Re estimated for the producer of *Undichna* ichnospecies ranged from 4,200 to nearly 1.5×10^6, assuming a maximum sustained speed during production of the trace fossil (Fig. 12.5). Most values (90 %) are in the range of subcritical Re numbers (lower than 3.5×10^5), and only three estimations (2 %) are higher than 10^6, suggesting turbulent flow and boundary layer separation. The latter examples belong to *U. britannica*.

12.6   Discussion

The biomechanical analysis of *Undichna* specimens suggests that they are essentially produced by small fish (less than 250 mm). Assuming that fish swam at maximum sustained speed, most estimates for Re are in the subcritical range, thus producing negligible disturbance in the bottom sediments. Fish larger than about 650 mm in length swimming at maximum sustained speed will induce the generation of a turbulent boundary layer and flow separation. This flow perturbation will induce resuspension of fine-grained bottom sediments, preventing preservation of a distinctive *Undichna* trail.

  The apparent anomalous presence of a few trails of fishes larger than the indicated length may be explained by either the particular composition of bottom sediments or by fish swimming at a speed lower than the maximum sustained speed observed in extant fishes. Two of the three cases belong to the Early Cretaceous

examples described by Gibert et al. (1999), where the trails are preserved in laminated limestone. Carbonate sediments are subject to early diagenetic processes, including cementation (e.g., Bathurst 1972). An important early diagenetic mechanism in lacustrine carbonates is lithification of algal mats by microbial carbonate precipitation (Armenteros 2010). A likely explanation for apparently large *Undichna* in limestone, therefore, is incipient cementation of bottom sediments that impeded erosion during passage of the fish.

Alternative explanations for the rarity or absence of trails produced by large fish may be inadequate outcrop exposure (i.e., small size of bedding planes) and/ or absence of fish larger than 650 mm in the fossil record. The first alternative may play a role in some examples, although information on the extension of bedding planes is rarely indicated. Benthic fishes larger than 650 mm are known for all the putative track makers of *Undichna*. The Late Silurian–Early Permian acanthodians were generally less than 0.2 m long, although maximum length was over 2 m (Carroll 1988; Nelson 2006). The Chondrichthyes are essentially benthonic and the dominant Paleozoic groups were the Hybodontiformes (Lower Carboniferous–Late Cretaceous) and Ctenacanthiformes (Late Devonian–Early Carboniferous). The Ctenacanthiformes were very large, including one of the largest Paleozoic fishes (*Goodrichthys*) that was about 2.5 m long. Hybodonts were the dominant Triassic and Jurassic sharks, including Jurassic forms that reached 2–3 m in length (Maisey 1987; Rees and Underwood 2008). The Neoselachii comprises very large extant and fossil sharks, including predators reaching more than 6 m in length (Miocene–recent *Carcharodon* species) (Nelson 2006; Adnet et al. 2010). The Late Devonian to Early Cretaceous Paleonisciformes included mostly small fish, although some reached lengths of up to 1 m. Among the Neopterygii, large benthonic fishes are found in Cretaceous–recent Lepisosteiformes, including Eocene representatives from the USA (*Lepisosteus*) that reached 1.7 m in length (Grande 1984). Primitive teleosts like the Middle Jurassic–Late Cretaceous Ichthyodectiformes included large predators (*Xiphactinus*) that reached lengths of more than 4 m (Nelson 2006). The Gonorynchiformes, primitive teleosts, are known since the Cretaceous, whereas Eocene specimens from the USA reach about 0.9 m in length (Grande 1984). Other teleosts like Cretaceous to recent Salmoniformes may reach a maximum length in excess of 1 m (Nelson 2006). Coelacanths are known since the Middle Devonian, while Paleozoic examples are generally small, some examples reach lengths of 1.5 m (Moy-Thomas and Miles 1971). The largest fossil coelacanth (3.5 m long) is from the Late Cretaceous of the USA (Schwimmer et al. 1994). Dipnoans are moderate-size fishes known since the Early Devonian whose maximum length in extant species is almost 2 m, whereas some Cretaceous lungfish from northern Africa were larger (Churcher et al. 2006).

A 1.5 m long Triassic coelacanth was inferred as the producer of *Parundichna*, which was interpreted as reflecting the alternating motion of pectoral and pelvic fins with minimal body undulation. This case suggests that fish swimming trace fossils whose producer exceeds the limit suggested for *Undichna* may appear, because the mechanism of swimming is different (oscillation of paired fins instead of body and caudal fin undulation).

Regarding the environmental distribution of *Undichna,* lacustrine deposits (typically deep lacustrine) yielded most specimens (more than 60 %) and successions interpreted as estuaries or fjords are also important. Specimens from shallow, normal, marine settings and floodplain lakes are rare (Appendices A.1–A.3).

In this approach, we made several assumptions on the basis of experimental work with extant fishes or inferences about the likely producer that may imply a source of error in the conclusions. These include the ventral morphology of the producer, simplifications about the swimming speed of fish, and possible changes in behavior. Although inferences about the changes in speed as reflected in *Undichna* has been discussed in the literature (Turek 1989; Martin and Pyenson 2005), no clear traces that indicate bursting behavior have been identified to date. As most of the *Undichna* specimens were recovered from flat-bedded basinal facies with no significant current action, the potential effect of currents on swimming fish are not considered in this approach. Future work on the experimental production of fish trails on aquaria under controlled conditions is desirable in order to make more precise inferences.

12.7 Conclusions

On the basis of 166 specimens of *Undichna* belonging to seven ichnospecies showing a worldwide distribution and large stratigraphic range (Early Devonian to recent), the swimming modes and preservational conditions for this trace fossil are inferred. *U. insolentia* was likely produced by Acanthodians (Climatiidae) using an anguilliform swimming mode. *U. britannica* (and the similar *U. consulca*) was produced by paleonisciformes (pre-Cretaceous examples) and teleost fishes (post-Cretaceous examples). For this ichnospecies, the ratio between the amplitude of the anal and caudal fin waves allows discrimination between fishes with an anguilliform (ratio larger than 0.8), subcarangiform (ratio between 0.8 and 0.5) and tunniform (lower than 0.5) mode of swimming. The likely producers of *U. bina* are paleonisciformes, hybodont sharks, and dipnoans. The trail is interpreted as reflecting an anguilliform mode of swimming. *U. unisulca* is a very simple trail that may have been produced by wide array of fish using subcarangiform mode of swimming. A subcarangiform swimming mode is also inferred for *U. quina* and *U. simplicitas*. The size distribution inferred for the fish producing *Undichna* is strongly biased toward small fish, mostly less than 0.25 m and up to 0.8 m. Fish larger than 0.65 m swimming with body and caudal fin propulsion at maximum sustained speed would produce a furrow instead of a recognizable *Undichna* in fine-grained siliciclastic sediments. Flow disturbance and sediment suspension produced by larger fish swimming close to the bottom explains this preferential preservation.

Appendix

Table A.1 Specimens of *U. bina* and *U. insolentia* measured for this work

Source	Age (Country)	Formation	Lithology	Specimen #	Am	λm	Wm	Environment	Tracemaker	Am/λm	L	Ums	Re
Undichna bina													
This work	Late Cretaceous (Argentina)	Calafate	Sst	GHUNLPam 3166	18.7	219[a]	39.4	Shallow marine	Hybodontiformes	0.09	365	1.02	317905
Lu et al. (2004)	Late Triassic (China)	Yanchang Group	Sst, slst	Fig. 3g	10	50	5	Lacustrine	Flat fish?	0.20	83	0.35	25675
Trewin (2000)	Late Permian (Malvinas/Falkland Is.)	Brenton Loch	Mdst, sst	Text: Fig. 5	13	77	–	Lacustrine	Paleonisciformes	0.17	128	0.46	51740
Trewin (2000)	Late Permian (Malvinas/Falkland Is.)	Brenton Loch	Mdst, sst	Text: Fig. 5	18	85	–	Lacustrine	Paleonisciformes	0.21	142	0.49	61106
Trewin (2000)	Late Permian (Malvinas/Falkland Is.)	Brenton Loch	Mdst, sst	Text: Fig. 5	18	90	–	Lacustrine	Paleonisciformes	0.20	150	0.51	67342
Trewin (2000)	Late Permian (Malvinas/Falkland Is.)	Brenton Loch	Mdst, sst	Text: Fig. 5	14	95	–	Lacustrine	Paleonisciformes	0.15	158	0.53	73870
Trewin (2000)	Late Permian (Malvinas/Falkland Is.)	Brenton Loch	Mdst, sst	Text: Fig. 5	13	103	–	Lacustrine	Paleonisciformes	0.13	172	0.56	84927
Trewin (2000)	Late Permian (Malvinas/Falkland Is.)	Brenton Loch	Mdst, sst	Text: Fig. 5	20	105	–	Lacustrine	Paleonisciformes	0.19	175	0.57	87808

Table A.1 (continued)

Source	Age (Country)	Formation	Lithology	Specimen #	Am	λm	Wm	Environment	Tracemaker	Am/λm	L	Ums	Re
Trewin (2000)	Late Permian (Malvinas/ Falkland Is.)	Brenton Loch	Mdst, sst	Text: Fig. 5	14	110	–	Lacustrine	Paleonisciformes	0.13	183	0.59	95217
Trewin (2000)	Late Permian (Malvinas/ Falkland Is.)	Brenton Loch	Mdst, sst	Text: Fig. 5	26	111	–	Lacustrine	Paleonisciformes	0.23	185	0.59	96734
Trewin (2000)	Late Permian (Malvinas/ Falkland Is.)	Brenton Loch	Mdst, sst	Text: Fig. 5	33	118	–	Lacustrine	Paleonisciformes	0.28	197	0.62	107682
Trewin (2000)	Late Permian (Malvinas/ Falkland Is.)	Brenton Loch	Mdst, sst	Text: Fig. 5	24	120	–	Lacustrine	Paleonisciformes	0.20	200	0.63	110915
Trewin (2000)	Late Permian (Malvinas/ Falkland Is.)	Brenton Loch	Mdst, sst	Text: Fig. 5	14	120	–	Lacustrine	Paleonisciformes	0.12	200	0.63	110915
Trewin (2000)	Late Permian (Malvinas/ Falkland Is.)	Brenton Loch	Mdst, sst	Text: Fig. 5	15	125	–	Lacustrine	Paleonisciformes	0.12	208	0.65	119205
Trewin (2000)	Late Permian (Malvinas/ Falkland Is.)	Brenton Loch	Mdst, sst	Text: Fig. 5	17	135	–	Lacustrine	Paleonisciformes	0.13	225	0.69	136664
Trewin (2000)	Late Permian (Malvinas/ Falkland Is.)	Brenton Loch	Mdst, sst	Text: Fig. 5	16	137	–	Lacustrine	Paleonisciformes	0.12	228	0.70	140296
Trewin (2000)	Late Permian (Malvinas/ Falkland Is.)	Brenton Loch	Mdst, sst	Text: Fig. 5	18	139	–	Lacustrine	Paleonisciformes	0.13	232	0.71	143976

Table A.1 (continued)

Source	Age (Country)	Formation	Lithology	Specimen #	Am	λm	Wm	Environment	Tracemaker	Am/λm	L	Ums	Re
Trewin (2000)	Late Permian (Malvinas/ Falkland Is.)	Brenton Loch	Mdst, sst	Text: Fig. 5	17	140	–	Lacustrine	Paleonisci- formes	0.12	233	0.71	145833
Trewin (2000)	Late Permian (Malvinas/ Falkland Is.)	Brenton Loch	Mdst, sst	Text: Fig. 5	25	140	–	Lacustrine	Paleonisci- formes	0.18	233	0.71	145833
Trewin (2000)	Late Permian (Malvinas/ Falkland Is.)	Brenton Loch	Mdst, sst	Text: Fig. 5	28	141	–	Lacustrine	Paleonisci- formes	0.20	235	0.71	147702
Trewin (2000)	Late Permian (Malvinas/ Falkland Is.)	Brenton Loch	Mdst, sst	Text: Fig. 5	20	143	–	Lacustrine	Paleonisci- formes	0.14	238	0.72	151476
Trewin (2000)	Late Permian (Malvinas/ Falkland Is.)	Brenton Loch	Mdst, sst	Text: Fig. 5	20	145	–	Lacustrine	Paleonisci- formes	0.14	242	0.73	155296
Trewin (2000)	Late Permian (Malvinas/ Falkland Is.)	Brenton Loch	Mdst, sst	Text- Fig. 5	26	150	–	Lacustrine	Paleonisci- formes	0.17	250	0.75	165053
Trewin (2000)	Late Permian (Malvinas/ Falkland Is.)	Brenton Loch	Mdst, sst	Text: Fig. 5	27	170	–	Lacustrine	Paleonisci- formes	0.16	283	0.83	207013
Trewin (2000)	Late Permian (Malvinas/ Falkland Is.)	Brenton Loch	Mdst, sst	Text: Fig. 5	26	180	–	Lacustrine	Paleonisci- formes	0.14	300	0.87	229754
Anderson (1976)	Early Perm- ian (South Africa)	Ecca	Mdst	Plate 54-2	41	105[a]	–	Lacustrine	"Classical fish"	0.39	175	0.57	87808

Table A.1 (continued)

Source	Age (Country)	Formation	Lithology	Specimen #	Am	λm	Wm	Environment	Tracemaker	$Am/\lambda m$	L	Ums	Re
Minter and Braddy (2006, 2009)	Early Permian (USA)	Robledo Mountains	Sst, slst	Text: Fig. 4	2.47	14.6	–	Estuary	Paleonisciformes	0.17	24	0.21	4464
This work	Late Carboniferous (Argentina)	Agua Escondida	Mdst	GHUNLPam 12086	13	63.3	45.6	Estuary/fjord	Unknown	0.21	106	0.40	37445
This work	Late Carboniferous (Argentina)	Agua Escondida	Mdst	GHUNLPam 12099	8.9	68[a]	26.6	Estuary/fjord	Unknown	0.13	114	0.42	40866
This work	Late Carboniferous (Argentina)	Agua Escondida	Mdst	GHUNLPam 12100	11	75	25.1	Estuary/fjord	Unknown	0.15	125	0.45	47832
Undichna insolentia													
Trewin (2000)	Late Permian (Malvinas/Falkland Is.)	Brenton Loch	Mdst, sst	Table 1	12	100	29	Lacustrine	Paleonisciformes	0.12	167	0.55	80692
Trewin (2000)	Late Permian (Malvinas/Falkland Is.)	Brenton Loch	Mdst, sst	Table 1	13	105	27	Lacustrine	Paleonisciformes	0.12	175	0.57	87808
Trewin (2000)	Late Permian (Malvinas/Falkland Is.)	Brenton Loch	Mdst, sst	Table 1	15	110	40	Lacustrine	Paleonisciformes	0.14	183	0.59	95217
Trewin (2000)	Late Permian (Malvinas/Falkland Is.)	Brenton Loch	Mdst, sst	Table 1	10	110	28	Lacustrine	Paleonisciformes	0.09	183	0.59	95217
Trewin (2000)	Late Permian (Malvinas/Falkland Is.)	Brenton Loch	Mdst, sst	Table 1	11	115	28	Lacustrine	Paleonisciformes	0.10	192	0.61	102920

Table A.1 (continued)

Source	Age (Country)	Formation	Lithology	Specimen #	Am	λm	Wm	Environment	Tracemaker	Am/λm	L	Ums	Re
Trewin (2000)	Late Permian (Malvinas/Falkland Is.)	Brenton Loch	Mdst, sst	Table 1	18	130	55	Lacustrine	Paleonisciformes	0.14	217	0.67	127788
Trewin (2000)	Late Permian (Malvinas/Falkland Is.)	Brenton Loch	Mdst, sst	Table 1	18	130	30	Lacustrine	Paleonisciformes	0.14	217	0.67	127788
Shi et al. (2010)	Late Permian (Australia)	Burngrove	Mdst	Fig. 11A	9.8	114	90	Lacustrine	Unknown	0.09	190	0.61	101356
This work	Early Permian (Argentina)	Bonete	Slst	GHUNLPam 3164	6.7	84[a]	36.3	Marine delta		0.08	140	0.48	57624
This work	Early Permian (Argentina)	Bonete	Slst	GHUNLPam 3165	8	120[a]	38.6	Marine delta		0.07	200	0.63	107143
Piñeiro (2006)	Early Permian (Uruguay)	Mangrullo	Mdst	Plate I.G	7	28	8	Estuary?	Acanthodians	0.25	47	0.26	10397
Anderson (1976)	Early Permian (South Africa)	Ecca	Sst	Plate 54:Fig. 1	14.8	84	27	Lacustrine?		0.18	140	0.49	59894
Buatois and Mángano (1994)	Late Carboniferous (Argentina)	Agua Colorada	Sst, slst	Fig. 4-2	10.3	62.5	38	Lacustrine	Acanthodians	0.16	104	0.40	36678
This work	Late Carboniferous (Argentina)	Agua Escondida	Mdst	GHUNLPam 3415	15	200[a]	56.9	Estuary/fjord	Unknown	0.08	333	0.95	269274
This work	Late Carboniferous (Argentina)	Agua Escondida	Mdst	GHUNLPam 3416	4.9	54.5[a]	19.5	Estuary/fjord	Unknown	0.09	91	0.37	28424
This work	Late Carboniferous (Argentina)	Agua Escondida	Mdst	GHUNLPam 3466	3.2	26[a]	15	Estuary/fjord	Unknown	0.12	43	0.25	9309

Table A.1 (continued)

Source	Age (Country)	Formation	Lithology	Specimen #	Am	λm	Wm	Environment	Tracemaker	Am/λm	L	Ums	Re
This work	Late Carboniferous (Argentina)	Agua Escondida	Mdst	GHUNLPam 3434	4.5	59[a]	20.6	Estuary/fjord	Unknown	0.08	98	0.39	32276
This work	Late Carboniferous (Argentina)	Agua Escondida	Mdst	GHUNLPam 3450	3.6	30[a]	13.4	Estuary/fjord	Unknown	0.12	50	0.27	11480
This work	Late Carboniferous (Argentina)	Agua Escondida	Mdst	GHUNLPam 3470	4.6	64.1	27.1	Estuary/fjord	Unknown	0.07	107	0.41	36919
This work	Late Carboniferous (Argentina)	Agua Escondida	Mdst	GHUNLPam 3400	5.6	34.2	17.8	Estuary/fjord	Unknown	0.16	57	0.29	13901
This work	Late Carboniferous (Argentina)	Agua Escondida	Mdst	GHUNLPam 3404	4.3	57.3	20.8	Estuary/fjord	Unknown	0.08	96	0.38	30794
This work	Late Carboniferous (Argentina)	Agua Escondida	Mdst	GHUNLPam 3485-II	8.5	69.2[a]	33.6	Estuary/fjord	Unknown	0.12	115	0.43	41857
This work	Late Carboniferous (Argentina)	Agua Escondida	Mdst	GHUNLPam 3485-III	4	56.4	20.2	Estuary/fjord	Unknown	0.07	94	0.37	30022
This work	Late Carboniferous (Argentina)	Agua Escondida	Mdst	GHUNLPam 3410	27	243[a]	67.7	Estuary/fjord	Unknown	0.11	405	1.12	386403
This work	Late Carboniferous (Argentina)	Agua Escondida	Slst	GHUNLPam 3159	4.7	27	16.3	Estuary/fjord	Unknown	0.17	45	0.26	9872

Table A.1 (continued)

Source	Age (Country)	Formation	Lithology	Specimen #	Am	λm	Wm	Environment	Tracemaker	Am/λm	L	Ums	Re
This work	Late Carboniferous (Argentina)	Agua Escondida	Mdst	GHUNLPam 12175	2.9	54.6[a]	29.9	Estuary/fjord	Unknown	0.05	91	0.37	28507
This work	Late Carboniferous (Argentina)	Agua Escondida	Mdst	GHUNLPam 12189	9	225[a]	51.8	Estuary/fjord	Unknown	0.04	375	1.05	334821
This work	Late Carboniferous (Argentina)	Agua Escondida	Mdst	GHUNLPam 12125 (1)	5.3	29.9	18.5	Estuary/fjord	Unknown	0.18	50	0.27	11424
This work	Late Carboniferous (Argentina)	Agua Escondida	Mdst	GHUNLPam 12125 (2)	7	61	29.4	Estuary/fjord	Unknown	0.11	102	0.39	34062
This work	Late Carboniferous (Argentina)	Agua Escondida	Mdst	GHUNLPam 12174	9.2	145.9	40.1	Estuary/fjord	Unknown	0.06	243	0.73	151690
This work	Late Carboniferous (Argentina)	Agua Escondida	Mdst	GHUNLPam 12185	5.7	56.2	35.3	Estuary/fjord	Unknown	0.10	94	0.37	29852
This work	Late Carboniferous (Argentina)	Agua Escondida	Mdst	GHUNLPam 12187	9.8	148[a]	38	Estuary/fjord	Unknown	0.07	247	0.74	155635
This work	Late Carboniferous (Argentina)	Agua Escondida	Mdst	GHUNLPam 12186	4.5	87.4[a]	36.3	Estuary/fjord	Unknown	0.05	146	0.50	61884
This work	Late Carboniferous (Argentina)	Agua Escondida	Mdst	GHUNLPam 12188	10	117.6[a]	58.9	Estuary/fjord	Unknown	0.09	196	0.62	103400

Table A.1 (continued)

Source	Age (Country)	Formation	Lithology	Specimen #	Am	λm	Wm	Environment	Tracemaker	Am/λm	L	Ums	Re
This work	Late Carboniferous (Argentina)	Agua Escondida	Mdst	GHUNLPam 12130	18.1	132.7	53.2	Estuary/fjord	Unknown	0.14	221	0.68	128036
This work	Late Carboniferous (Argentina)	Agua Escondida	Mdst	GHUNLPam 12176	7	156	35.8	Estuary/fjord	Unknown	0.04	260	0.77	171122
This work	Late Carboniferous (Argentina)	Agua Escondida	Mdst	GHUNLPam 12198	5.7	59	25.3	Estuary/fjord	Unknown	0.10	98	0.39	32276
This work	Late Carboniferous (Argentina)	Agua Escondida	Mdst	GHUNLPam 12251	4.3	47	20.6	Estuary/fjord	Unknown	0.09	78	0.34	22514
This work	Late Carboniferous (Argentina)	Agua Escondida	Mdst	MCNAM PI 24282	8	175	67	Estuary/fjord	Unknown	0.05	292	0.85	210813

Am maximum amplitude of trail (mm), *λm* maximum wavelength of trail (mm), *Wm* maximum width of trace fossil (mm), *L* body length (mm), *Ums* maximum sustained speed (m/s), *Re* Reynolds number, Mdst mudstone, Sha shale, Slst siltstone, Sst sandstone

[a] Wavelength estimated from incomplete trail

Table A.2 Specimens of *U. britannica*, *U. consulca*, *U. quina*, and *U. simplicitas* measured for this work

Source	Age (country)	Formation	Lithology	Specimen #	Ac	λc	A*	λ*	Environment	Tracemaker	Ac/λc	A*/Ac	A*/λ*	L	Ums	Re
Undichna britannica																
Gibert et al. (1999)	Recent (UK)			Text-Fig. 7	17	52	nd	nd	Estuary	Unknown	0.33	–	–	78	0.34	22193
Fliri et al. (1971)	Pleistocene (Austria)	Bänderton	Slst, mdst	Fig. 8	180	512	77	497	Lacustrine	*Esox?*	0.35	0.43	0.15	512	1.38	621431
Fliri et al. (1970)	Pleistocene (Austria)	Bänderton	Slst, mdst	Fig. 9	14	35	6	31	Lacustrine	Unknown	0.40	0.43	0.19	35	0.23	7210
Benner et al. (2009)	Pleistocene (USA)	New England varves	Sst, slst, mdst	Fig. 3A	20	40	nd	nd	Lacustrine	*Salvelinus* spp.	0.50	–	–	60	0.29	15413
Benner et al. (2009)	Pleistocene (USA)	New England varves	Sst, slst, mdst	Fig. 3B	72	298	41	279	Lacustrine	*Salvelinus* spp.	0.24	0.57	0.15	445	1.22	476671
Benner et al. (2009)	Pleistocene (USA)	New England varves	Sst, slst, mdst	Fig. 3E	102	292	51	266	Lacustrine	*Salvelinus* spp.	0.35	0.50	0.19	436	1.20	458828
Benner et al. (2009)	Pleistocene (USA)	New England varves	Sst, slst, mdst	Fig. 3G	28	62	13	68	Lacustrine	*Salvelinus* spp.	0.45	0.46	0.19	93	0.37	30310
Gibert et al. (1999)	Berrasian-Valanginian (Spain)	La Pedrera de Rúbies	Lst	Text-Fig. 3A	172	536	82	468	Lacustrine	*Ichthyemidion vidali*	0.32	0.48	0.18	800	2.07	1457746
Gibert et al. (1999)	Berrasian-Valanginian (Spain)	La Pedrera de Rúbies	Lst	Text-Fig. 3A	150	484	111	514	Lacustrine	*Ichthyemidion vidali*	0.31	0.74	0.22	722	1.88	1197874
Lu et al. (2004), Wang et al. (2008)	Late Triassic (China)	Yanchang Group	Sst, slst	Fig. 3a	143	303	61	308	Lacustrine	*Wayaobulepis zichangensia*	0.47	0.43	0.20	303	0.88	233971
Lu et al. (2004), Wang et al. (2008)	Late Triassic (China)	Yanchang Group	Sst, slst	Fig. 3b	123	367	66	336	Lacustrine	*Wayaobulepis zichangensia*	0.34	0.54	0.20	548	1.46	706220

Table A.2 (continued)

Source	Age (country)	Formation	Lithology	Specimen #	Ac	λc	A*	λ*	Environment	Tracemaker	Ac/λc	A*/Ac	A*/λ*	L	Ums	Re
Lu et al. (2004), Wang et al. (2008)	Late Triassic (China)	Yanchang Group	Sst, slst	Fig. 3c	91	284	nd	nd	Lacustrine	*Wayaobulepis zichangensia*	0.32	–	–	424	1.17	435565
Melchor et al. (2003)	Middle Triassic (Argentina)	Los Rastros	Sst	Fig. 6E	152	445	nd	nd	Lacustrine	*Rastrolepis riojaensis*	0.34			664	1.74	1019673
This work	Middle Triassic (Argentina)	Ischichuca	Slst	CRILAR-Ic 61	31.8	72.2	24.2	68.5	Lacustrine	*Rastrolepis riojaensis/ Neochallaia telecheai*	0.44	0.76	0.35	108	0.41	38762
This work	Middle Triassic (Argentina)	Ischichuca	Slst	CRILAR-Ic 61	13.3	103	10.4	100.8	Lacustrine	*Rastrolepis riojaensis/ Neochallaia telecheai*	0.13	0.78	0.10	154	0.52	70229
This work	Middle Triassic (Argentina)	Los Rastros	Slst	CRILAR-Ic 62	37	119.6	35	116.8	Lacustrine	*Rastrolepis riojaensis*	0.31	0.95	0.30	199	0.63	110265
This work	Middle Triassic (Argentina)	Los Rastros	Slst	CRILAR-Ic 63	42	168.6	–	–	Lacustrine	*Rastrolepis riojaensis*	0.25	–	–	252	0.75	167010
This work	Middle Triassic (Argentina)	Los Rastros	Slst	CRILAR-Ic 64	29.7	126.8	–	–	Lacustrine	*Rastrolepis riojaensis*	0.23	–	–	189	0.60	100659
Melchor (2004)	Middle Triassic (Argentina)	Los Rastros	Slst	Fig. 6a	74	154	59	122.2	Lacustrine	*Rastrolepis riojaensis*	0.48	0.80	0.48	182	0.59	94362
This work	Middle Triassic (Argentina)	Los Rastros	Slst	Field data	35.9	135.2	–	–	Lacustrine	*Rastrolepis riojaensis*	0.27	–	–	202	0.63	112672

Table A.2 (continued)

Source	Age (country)	Formation	Lithology	Specimen #	Ac	λc	A*	λ*	Environment	Tracemaker	Ac/λc	A*/Ac	A*/λ*	L	Ums	Re
This work	Middle Triassic (Argentina)	Los Rastros	Slst	Field data	70.6	205	–	–	Lacustrine	*Rastrolepis riojaensis*	0.34	–	–	306	0.88	238185
This work	Middle Triassic (Argentina)	Los Rastros	Slst	Field data	40	113.1	–	–	Lacustrine	*Rastrolepis riojaensis*	0.35	–	–	169	0.56	82491
This work	Middle Triassic (Argentina)	Los Rastros	Slst	Field data	50.7	172.4	–	–	Lacustrine	*Rastrolepis riojaensis*	0.29	–	–	257	0.77	173857
This work	Middle Triassic (Argentina)	Los Rastros	Slst	Field data	25	128	22	117	Lacustrine	*Rastrolepis riojaensis*	0.20	0.88	0.19	213	0.66	124319
This work	Middle Triassic (Argentina)	Los Rastros	Slst	Field data	104	330	–	–	Lacustrine	*Rastrolepis riojaensis*	0.32	–	–	493	1.33	577556
Bordy et al. (2011)	Late Permian (South Africa)	Middleton	Sst	Fig. 4D	217	418[a]	115	321	Floodplain lake	Unknown	0.52	0.53	0.36	624	1.65	904689
This work	Permian (Argentina)	Bajo de Véliz	Sha	MHIN-UNSL-GEO T 663	38	122	25	100	Lacustrine	Unknown	0.31	0.66	0.25	182	0.59	94093
This work	Permian (Argentina)	Bajo de Véliz	Sha	MHIN-UNSL-GEO T 664	41.1	120	–	–	Lacustrine	Unknown	0.34	–	–	179	0.58	91421
This work	Permian (Argentina)	Bajo de Véliz	Sha	MHIN-UNSL-GEO T 665	38.5	120	–	–	Lacustrine	Unknown	0.32	–	–	179	0.58	91421
This work	Permian (Argentina)	Bajo de Véliz	Sha	MHIN-UNSL-GEO T 665	37.8	90	–	–	Lacustrine	Unknown	0.42	–	–	134	0.47	55858
Anderson (1976)	Early Permian (South Africa)	Ecca	Mdst	Plate 54-Fig. 5	27	142	22	134	Lacustrine?	Unknown	0.19	0.81	0.16	237	0.72	149583

Table A.2 (continued)

Source	Age (country)	Formation	Lithology	Specimen #	Ac	λc	A*	λ*	Environment	Tracemaker	Ac/λc	A*/Ac	A*/λ*	L	Ums	Re
Soler-Guijón and Moratalla (2001)	Late Carboniferous (Spain)	"Emma" layer	Slst	Fig. 3	137	354	154	389	Shallow marine?	*Orthacantus*	0.39	1.12	0.40	–	–	–
This work	Late Carboniferous (Argentina)	Agua Escondida	Mdst	GHUNLPam 12087	40	74.5	25.7	73.6	Estuary	Unknown	0.54	0.64	0.35	111	0.42	39416
Turek (1989)	Late Carboniferous (Czech Republic)	Kladno	Mdst	Plate 73.2	11	38	3	42	Lacustrine	Paleonisciformes	0.29	0.27	0.07	38	0.24	8068
Higgs, 1988	Late Carboniferous (UK)	Bude	Slst	E.3841b	65	160	30	–	Lacustrine	*Acrolepis*	0.41	0.46	–	239	0.72	152015
Higgs (1988)	Late Carboniferous (UK)	Bude	Slst	E.3842a	40	130	25	–	Lacustrine	*Acrolepis*	0.31	0.63	–	194	0.62	105157
Higgs (1988)	Late Carboniferous (UK)	Bude	Slst	Text-fig 4, trail a	45	179	nd	nd	Lacustrine	*Acrolepis*	0.25	–	–	267	0.79	186073
Higgs (1988)	Late Carboniferous (UK)	Bude	Slst	Text-fig 4, trail b	28	94	16	110	Lacustrine	*Acrolepis*	0.30	0.57	0.15	140	0.49	60111
Higgs (1988)	Late Carboniferous (UK)	Bude	Slst	UR14404	30	140	20	–	Lacustrine	*Acrolepis*	0.21	0.67	–	209	0.65	119835
Higgs (1988)	Late Carboniferous (UK)	Bude	Slst	Latex peel	120	420	45	–	Lacustrine	*Acrolepis*	0.29	0.38	–	420	1.16	428134
Buatois et al. (1998)	Late Carboniferous (USA)	Tonganoxie Sandstone	Slst, mdst	Fig. 9.1	14	31	9	26	Estuary	None proposed	0.45	0.64	0.35	46	0.26	10271
Buatois et al. (1998)	Late Carboniferous (USA)	Tonganoxie Sandstone	Slst, mdst	Fig. 9.1	21	34	16	31	Estuary	None proposed	0.62	0.76	0.52	51	0.27	11728

Table A.2 (continued)

Source	Age (country)	Formation	Lithology	Specimen #	Ac	λc	A*	λ*	Environment	Tracemaker	Ac/λc	A*/Ac	A*/λ*	L	Ums	Re
Buatois and Mángano (2003)	Late Carboniferous (Argentina)	Guandacol	Mdst	Fig. 6A	29.4	50.8	15.4	47.3	Fjord	None proposed	0.58	0.52	0.33	76	0.33	21403
Archer and Maples (1984)	Pennsylvanian (USA)	Mansfield	Slst	Fig. 7E	12	84	11	62	Floodplain lake	None proposed	0.14	0.92	0.18	140	0.49	59894
Martin and Pyenson (2005)	Early Pennsylvanian (USA)	Pottsville	Sst, mdst	Fig. 1C	22	24	19	21	Estuary	None proposed	0.92	0.86	0.90	40	0.25	8367
Martin and Pyenson (2005)	Early Pennsylvanian (USA)	Pottsville	Sst, mdst	Fig. 1D	9	23	7	27	Estuary	None proposed	0.39	0.78	0.26	34	0.23	6784
Martin and Pyenson (2005)	Early Pennsylvanian (USA)	Pottsville	Sst, mdst	Fig. 8B	20	36	14	36	Estuary	None proposed	0.56	0.70	0.39	54	0.28	12745
Haubold et al. (2005)	Early Pennsylvanian (USA)	Pottsville	Sst, mdst	Plate 62A	25	81	18	81	Estuary	None proposed	0.31	0.72	0.22	121	0.44	45248
Haubold et al. (2005)	Early Pennsylvanian (USA)	Pottsville	Sst, mdst	Plate 62C	13	27	9	27	Estuary	None proposed	0.48	0.69	0.33	40	0.25	8454
Haubold et al. (2005)	Early Pennsylvanian (USA)	Pottsville	Sst, mdst	Plate 63B	12	16	6	22	Estuary	None proposed	0.75	0.50	0.27	24	0.21	4210
Fillmore et al. (2011)	Late Mississippian (USA)	Mauch Chunk	Sst	Fig. 2A	30	63	23	66	Fluvial	Unknown	0.48	0.77	0.35	94	0.38	31095

Table A.2 (continued)

Source	Age (country)	Formation	Lithology	Specimen #	Ac	λc	A^*	λ^*	Environment	Tracemaker	$Ac/\lambda c$	A^*/Ac	A^*/λ^*	L	Ums	Re
Undichna consulca																
Higgs (1988)	Late Carboniferous (UK)	Bude	Slst	E.3841c	25	45	15	–	Lacustrine	*Cornuboniscus budensis*	0.56	–	–	67	0.31	18399
Higgs (1988)	Late Carboniferous (UK)	Bude	Slst	E.3841e	20	40	15	–	Lacustrine	*Cornuboniscus budensis*	0.50	–	–	60	0.29	15413
Higgs (1988)	Late Carboniferous (UK)	Bude	Slst	E.3843	20	70	15	–	Lacustrine	*Cornuboniscus budensis*	0.29	–	–	104	0.40	36857
Higgs (1988)	Late Carboniferous (UK)	Bude	Slst	E.3838a	15	20	15	–	Lacustrine	*Cornuboniscus budensis*	0.75	–	–	30	0.22	5824
Higgs (1988)	Late Carboniferous (UK)	Bude	Slst	E.3842b	20	50	15	–	Lacustrine	*Cornuboniscus budensis*	0.40	–	–	75	0.33	21620
Higgs (1988)	Late Carboniferous (UK)	Bude	Slst	UR14403	25	40	20	–	Lacustrine	*Cornuboniscus budensis*	0.63	–	–	60	0.29	15413
Higgs (1988)	Late Carboniferous (UK)	Bude	Slst	Latex peel	25	55	nd	–	Lacustrine	*Cornuboniscus budensis*	0.45	–	–	82	0.35	25076
Undichna quina																
Gibert (2001)	Callovian (USA)	Arapien Shale	Lst	Fig. 2	15	46	–	–	Marine shelf	Unknown	0.33	–	–	69	0.31	18377
Lu et al. (2004), Wang et al. 2008	Late Triassic (China)	Yanchang Group	Slst	Fig. 3e	203	330	–	–	Lacustrine	*Saurichthys huanshenensis*	0.62	–	–	493	1.33	577556
Lu et al. (2004), Wang et al. (2008)	Late Triassic (China)	Yanchang Group	Sst, slst	Fig. 3f	7	19	–	–	Lacustrine	*Saurichthys huanshenensis*	0.37	–	–	28	0.22	5443

Table A.2 (continued)

Source	Age (country)	Formation	Lithology	Specimen #	Ac	λc	A*	λ*	Environment	Tracemaker	Ac/λc	A*/Ac	A*/λ*	L	Ums	Re
Todesco and Avanzini (2008)	Anisian (Italy)	Voltago Conglomerate	Sst, slst	Fig. 3	23	98	–	–	Fluvial	Unknown	0.23	–	–	146	0.50	64513
Trewin (2000)	Late Permian (Malvinas/Falkland Is.)	Brenton Loch	Sst	Text: fig. 4	25	131	20	122	Lacustrine	Paleonisciformes	0.19	0.80	0.16	196	0.62	106583
Fillmore et al. (2011)	Late Mississippian (USA)	Mauch Chunk	Sst	Fig. 3E	7	26	2	15	Fluvial	Unknown	0.27	0.29	0.13	39	0.24	8306
Undichna simplicitas																
Martin et al. (2010)	Early Eocene (USA)	Green River	Mdst	Fig. 2A	109	280	43	274	Lacustrine	*Notogoneus osculus*	0.39	0.39	0.16	418	1.15	424159
Martin et al. (2010)	Early Eocene (USA)	Green River	Mdst	Table 2 FOBU-11710	100	160	–	–	Lacustrine	*Notogoneus osculus*	0.63	–	–	239	0.72	152015
Martin et al. (2010)	Early Eocene (USA)	Green River	Mdst	Table 2 FOBU-11711	90	320	–	–	Lacustrine	*Notogoneus osculus*	0.28	–	–	478	1.30	544994
Lu and Chen (1998)	Late Triassic (China)	Yanchang Group	Sst, slst	Table I	80	195	–	–	Lacustrine	None proposed	0.41	–	–	291	0.85	217389
Anderson (1976)	Early Permian (South Africa)	Ecca	Mdst	Plate 54-3	42	224	–	–	Lacustrine	Unknown	0.19	–	–	334	0.95	280291
Buatois et al. (1998)	Late Carboniferous (USA)	Tonganoxie Sandstone	Slst, mdst	Fig. 9-3	20	75	–	–	Estuary	None proposed	0.27	–	–	112	0.42	39851

Ac amplitude of caudal fin trail (mm), *λc* wavelength of caudal fin trail (mm), *A** amplitude of pelvic or pectoral fin trail (mm), *λ** wavelength of pelvic or pectoral fin trail (mm), *L* body length (mm), *Ums* maximum sustained speed (m/s), *Re* Reynolds number, Mdst mudstone, Sha shale, Slst siltstone, Sst sandstone, Lst limestone, nd no data
[a] Wavelength estimated from incomplete trail

Table A.3 Specimens of *U. unisulca* measured for this work

Source	Age (country)	Formation	Lithology	Specimen #	Ac	λc	Environment	Tracemaker	Ac/λc	L	Ums	Re
Undichna unisulca												
Gibert et al. (1999)	Recent (UK)	–	–	Text: Fig. 7	65	78	Estuary	Unknown	0.83	116	0.43	42509
Fliri et al. (1970)	Pleistocene (Austria)	Bänderton	Silt, clay	Fig. 9	14	36	Lacustrine	Unknown	0.39	54	0.28	13194
Benner et al. (2009)	Pleistocene (USA)	New England glacilacus-trine varves	Sand, silt, clay	Fig. 6A	31	95	Lacustrine	*Salvelinus* spp.	0.33	142	0.49	61197
Benner et al. (2009)	Pleistocene (USA)	New England glacilacus-trine varves	Sand, silt, clay	Fig. 6C	24	58	Lacustrine	*Salvelinus* spp.	0.41	87	0.36	27263
Benner et al. (2009)	Pleistocene (USA)	New England glacilacus-trine varves	Sand, silt, clay	Fig. 6D	41	80	Lacustrine	*Salvelinus* spp.	0.51	119	0.44	45887
Benner et al. (2009)	Pleistocene (USA)	New England glacilacus-trine varves	Sand, silt, clay	Fig. 6F	46	119	Lacustrine	*Salvelinus* spp.	0.39	178	0.58	90099
Martin et al. (2010)	Early Eocene (USA)	Green River	Mdst	Table 2 FOBU-3145	70	100	Lacustrine	Teleost	0.70	149	0.51	66771
Loewen and Gibert, (1999)	Early Eocene (USA)	Green River	Lst	Poster	70	78	Lacustrine	*Diplomystus dentatus/Crossopholis magnicaudatus*	0.90	116	0.43	44005
Gibert et al. (1999)	Barremian (Spain)	La Huérguina Limestones	Lst	LH-13931-Plate 1.2	37	227	Lacustrine	*Macromesodon*	0.16	339	0.96	287250
Gibert et al. (1999)	Barremian (Spain)	La Huérguina Limestones	Lst	LH-13932-Plate 1.2	22	166	Lacustrine	*Macromesodon*	0.13	248	0.74	162403

Table A.3 (continued)

Source	Age (country)	Formation	Lithology	Specimen #	Ac	λc	Environment	Tracemaker	Ac/λc	L	Ums	Re
Gibert et al. (1999)	Barremian (Spain)	La Huérguina Limestones	Lst	LH-13850-Plate 1.3	87	218	Lacustrine	*Macromesodon*	0.40	325	0.93	266627
Gibert et al. (1999)	Barremian (Spain)	La Huérguina Limestones	Lst	LH-13851-Plate 1.3	71	197	Lacustrine	*Macromesodon*	0.36	294	0.86	221473
Gibert et al. (1999)	Barremian (Spain)	La Huérguina Limestones	Lst	LH-13926- Text: Fig 4e	72	332	Lacustrine	*Macromesodon*	0.22	496	1.34	584182
This work	Middle Triassic (Argentina)	Los Rastros	Slst	Field data	43.5	148.5	Lacustrine	*Rastrolepis riojaensis*	0.29	222	0.68	133051
This work	Middle Triassic (Argentina)	Los Rastros	Slst	Field data	47.1	233	Lacustrine	*Rastrolepis riojaensis*	0.20	348	0.98	301422
This work	Middle Triassic (Argentina)	Los Rastros	Slst	Field data	75.4	290[a]	Lacustrine	*Rastrolepis riojaensis*	0.26	433	1.19	452956
Lu et al. (2012)	Early Triassic (China)	Jialing jiang	Ca Slst	Fig. 2a Nr 1	8	26.5	Estuary	*Perleidus*	0.30	40	0.24	8238
Lu et al. (2012)	Early Triassic (China)	Jialing jiang	Ca Slst	Fig. 2a Nr 2	9	29	Estuary	*Perleidus*	0.31	43	0.25	9344
Lu et al. (2012)	Early Triassic (China)	Jialing jiang	Ca Slst	Fig. 2b	14	42	Estuary	*Perleidus*	0.33	63	0.30	16015
Soler-Guijón and Moratalla (2001)	Late Carboniferous (Spain)		Slst	Fig. 7	101	202	Shallow marine?	*Orthacantus*	0.50	301	0.87	223961
This work	Late Carboniferous (Argentina)	Agua Escondida	Sha	GHUNLPam 12197	31.9	104.9	Estuary/fjord	Unknown	0.30	157	0.53	69997

Table A.3 (continued)

Source	Age (country)	Formation	Lithology	Specimen #	Ac	λc	Environment	Tracemaker	Ac/λc	L	Ums	Re
This work	Late Carboniferous (Argentina)	Agua Escondida	Sha	GHUNLPam 12197	12.3	80.9	Estuary/fjord	Unknown	0.15	121	0.44	45156
This work	Late Carboniferous (Argentina)	Agua Escondida	Mdst	MCNAM PI 24271	38.5	155[a]	Estuary/fjord	Unknown	0.25	231	0.71	138732
This work	Late Carboniferous (Argentina)	Agua Escondida	Mdst	MCNAM PI 24293	18	59	Estuary/fjord	Unknown	0.31	88	0.36	27058
Buatois and Mángano (2003)	Late Carboniferous (Argentina)	Guandacol	Mdst	Fig. 6B	27.1	95.2	Fjord	None proposed	0.28	142	0.49	59327
Morrissey et al. (2004)	Early Devonian (UK)	Freshwater West formation	Mdst	Fig. 4-A	13	75	Floodplain lake	Cephalaspid	0.17	112	0.42	41254
Morrissey et al. (2004)	Early Devonian (UK)	Freshwater West formation	Mdst	Fig. 4-C	11	92	Floodplain lake	Cephalaspid	0.12	137	0.48	57966
Morrissey et al. (2012)	Early Devonian (UK)	Freshwater West formation	Mdst, slst	Fig. 8c	24.8	56.9	Floodplain lake	Cephalaspid	0.44	85	0.35	26451

Ac amplitude of caudal trail (mm), *λc* wavelength of caudal trail (mm), *L* body length (mm), *Ums* maximum sustained speed (m/s), *Re* Reynolds number, Mdst mudstone, Sha shale, Slst siltstone, Sst sandstone, Ca slst calcareous siltstone, Lst limestone
[a] Wavelength estimated from incomplete trail

References

Adnet S, Balbino AC, Antunes MT et al (2010) New fossil teeth of the white shark (*Carcharodon carcharias*) from the Early Pliocene of Spain. Implication for its paleoecology in the Mediterranean. Neues Jahrb Geol P-A 256(1):7–16

Agassiz L (1833) Recherches sur les poissons fossiles vol I (Atlas). Petitpierre, Neuchatel. doi:10.5962/bhl.title.4275

Anderson AM (1970) An analysis of supposed fish trails from interglacial sediments in the Dwyka Series, near Vryheid, Natal. In: Second Gondwana symposium, Pretoria, 1970. IUGS, pp 637–647

Anderson AM (1976) Fish trails from the Early Permian of South Africa. Palaeontol 19:397–409

Anderson EJ, McGillis WR, Grosenbaugh MA (2001) The boundary layer of swimming fish. J Exp Biol 204 (1):81–102

Apesteguía S, Agnolin FL, Claeson K (2007) Review of Cretaceous dipnoans from Argentina (Sarcopterygii: Dipnoi) with descriptions of new species. Rev Mus Arg Cs Nat 9 (1):27–40

Archer AW, Maples CG (1984) Trace-fossil distribution across a marine-to-nonmarine gradient in the Pennsylvanian of southwestern Indiana. J Paleontol 58(2):448–466

Armenteros I (2010) Diagenesis of carbonates in continental settings. In: Alonso-Zarza AM, Tanner LH (eds) Carbonates in continental settings: geochemistry, diagenesis and applications, Developments in sedimentology, vol 62. Elsevier, pp 61–151. doi:http://dx.doi.org/10.1016/S0070-4571(09)06202-5

Bainbridge R (1958) The speed of swimming of fish as related to size and to the frequency and amplitude of the tail beat. J Exp Biol 35(1):109–133

Bathurst RGC (1972) Carbonate sediments and their diagenesis, vol 12. Developments in sedimentology. Elsevier, Amsterdam

Benner JS, Ridge JC, Taft NK (2008) Late Pleistocene freshwater fish (Cottidae) trackways from New England (USA) glacial lakes and a reinterpretation of the ichnogenus Broomichnium Kuhn. Palaeogeogr Palaeocl 260 (3–4):375–388

Benner JS, Ridge JC, Knecht RJ (2009) Timing of post-glacial reinhabitation and ecological development of two New England, USA, drainages based on trace fossil evidence. Palaeogeogr Palaeocl 272(3–4):212–231

Blevins E, Lauder GV (2013) Swimming near the substrate: a simple robotic model of stingray locomotion. Bioinspir Biomim 8(1):016005

Bordy EM, Linkermann S, Prevec R (2011) Palaeoecological aspects of some invertebrate trace fossils from the mid- to Upper Permian Middleton Formation (Adelaide Subgroup, Beaufort Group, Karoo Supergroup), Eastern Cape, South Africa. J Afr Earth Sci 61(3):238–244

Breder CM (1926) The locomotion of fishes. Zoologica-N Y 4(5):159–297

Buatois LA, Mángano MG (1994) Pistas de peces en el Carbonífero de la Cuenca Paganzo (Argentina): su significado estratigrafico y paleoambiental. Ameghiniana 31(1):33–40

Buatois LA, Mángano MG (2003) Caracterización icnológica y paleoambiental de la localidad tipo de *Orchesteropus atavus* Frenguelli, Huerta de Huachi, provincia de San Juan, vol 40, issue 1. Ameghiniana, Argentina. pp 53–70

Buatois LA, Mángano MG, Maples CG et al (1998) Ichnology of an Upper Carboniferous fluvio-estuarine paleovalley: the Tonganoxie Sandstone, Buildex Quarry, eastern Kansas. J Paleontol 71:152–180

Cardonatto MC, Melchor RN (1998) Biomechanical analysis of fish trace fossils (*Undichna*): implications for taphonomy. In: VII Congreso Argentino de Paleontología y Bioestratigrafía, Resúmenes, Bahía Blanca, 1998. Universidad Nacional del Sur, p 106

Carroll RL (1988) Vertebrate paleontology and evolution. W. H. Freeman and Company, New York

Cione AL, Gouiric-Cavalli S, Mennucci JA et al (2010) First vertebrate body remains from the Permian of Argentina (Elasmobranchii and Actinopterygii). P Geologist Assoc 121(3):301–312

Churcher CS, De Iuliis G, Kleindienst MR (2006) A new genus for the Dipnoan species *Ceratodus tuberculatus* Tabaste, 1963. Geodiversitas 28(4):635–647

Díaz Saravia P (2001) Upper Carboniferous fish micro-remains from western Argentina. Rev Esp Micropaleont 33:123–134

Fillmore DL, Lucas SG, Simpson EL (2011) The fish swimming trace *Undichna* from the Mississippian Mauch Chunk Formation, eastern Pennsylvania. Ichnos 18(1):27–34

Fliri F, Bortenschlager S, Felber H et al (1970) Der Bänderton von Baumkirchen (Inntal, Tirol) eine neue Schlüsselstelle zur Kenntnis der Würmvereisung der Alpen. Z Gletsch Glazialgeol 6:5–35

Fliri F, Hilscher H, Markgraf V (1971) Weitere Untersuchungen zur Chronologie der alpinen Vereisung (Bänderton von Baumkirchen, Inntal, Nordtirol). Z Gletsch Glazialgeol 7(1–2):5–24

Gibert JMd (2001) *Undichna gosiutensis* isp. nov.: a new fish trace fossil from the Jurassic of Utah. Ichnos 8(1):15–22

Gibert JMd, Buatois LA, Fregenal-Martínez MA et al (1999) The fish trace fossil *Undichna* from the Cretaceous of Spain. Palaeontol 42(3):409–427

Grande L (1984) Paleontology of the Green River Formation, with a review of the fish fauna. Geol Surv Wyo Bull 63:1–333

Haubold H, Buta RJ, Rindsberg AK et al (2005) Atlas of Union Chapel Mine vertebrate trackways and swimming traces. In: Buta RJ, Rindsberg AK, Kopaska-Merkel DC (eds) Pennsylvanian footprints in the Black Warrior basin of Alabama, Alabama Paleontological Society Monograph, vol 1. pp 207–276

Higgs R (1988) Fish trails from the Upper Carboniferous of south-west England. Palaeontology 31:255–272

Kuhn O (1958) Die Fährten der vorzeitlichen Amphibien und Reptilien. Bamberg, Meisenbach

Lindsey CC (1978) Form function and locomotory habits in fish. In: Hoar WS, Randall DJ (eds) Fish physiology, vol VII. locomotion. Academic Press, New York, pp 1–100

Loewen MA, Gibert JMd (1999) The first occurrence of Cenozoic fish trails (*Undichna*) from Eocene fossil lake, Wyoming. J Vertebr Paleontol 19(SUPPL. 3):59A

López-Arbarello A (2004) The record of Mesozoic fishes from Gondwana (excluding India and Madagascar). In: Arratia G, Tintori A (eds) Mesozoic fishes 3– systematics, paleoenvironments and biodiversity. Verlag Dr. Friedich Pfeil, München, Germany, pp 597–624

López-Arbarello A, Rogers R, Puerta P (2006) Freshwater actinopterygians of the Los Rastros Formation (Triassic), Bermejo Basin, Argentina. Foss Rec 9(2):238–258. doi:10.1002/mmng.200600011

López-Arbarello A, Rauhut OWM, Cerdeño E (2010) The Triassic fish faunas of the Cuyana Basin, western Argentina. Palaeontol 53(2):249–276. doi:10.1111/j.1475–4983.2010.00931.x

Lu TQ, Wang ZL, Yang XY et al (2012) First record of Lower Triassic *Undichna* sp. fish swimming traces from Emei, Sichuan Province, China. Chinese Sci Bull 57(11):1320–1324

Lu ZS, Chen B (1998) Discovery of Late Triassic fish trails (*Undichna*) in Hengshan County, Shaanxi, China. Acta Palaeontol Sin 37(1):76–84

Lu ZS, Hao ZK, Chen B et al (2003) New evidences of Late Triassic fish swimming traces in Hengsahn County, Shaanxi Province, China. Acta Palaeontol Sin 42(2):266–276

Lu Z, Hou J, Chen B et al (2004) Genetic interpretation of fish swimming trails and calculation of fish-body length in Late Triassic Hengshan, Shaanxi Province, China. Sci China Ser D 47(3):272–279

Maisey JG (1987) Cranial anatomy of the Lower Jurassic shark *Hybodus reticulatus* (Chondrichthyes: Elasmobranchii), with comments on hybodontid systematics. Am Mus Novit 2878:1–39

Martin AJ, Pyenson ND (2005) Behavioral significance of vertebrate trace fossils from the Union Chapel site. In: Buta RJ, Rindsberg AK, Kopaska-Merkel DC (eds) Pennsylvanian footprints in the Black Warrior basin of Alabama, Alabama Paleontological Society monograph, vol 1., pp 59–73

Martin AJ, Vazquez-Prokopec GM, Page M (2010) First known feeding trace of the Eocene bottom-dwelling fish *Notogoneus osculus* and its paleontological significance. PLoS ONE 5 (5):e10420. doi:10.1371/journal.pone.0010420

Melchor RN (2004) Trace fossil distribution in lacustrine deltas: examples from the Triassic rift lakes of the Ischigualasto – Villa Unión basin, Argentina. In: McIlroy D (ed) The application

of ichnology to palaeoenvironmental and stratigraphic analysis. Geological Society Special Publication, vol 228. Geological Society, London, pp 333–352

Melchor RN, Cardonatto MC Pistas de peces (*Undichna*) (1998) Rango estratigráfico, paleoambientes y mecanismos de propulsión del productor. In: Tercera Reunión Argentina de Icnología and Primera Reunión de Icnología del Mercosur, Mar del Plata, 1998, pp 20–21

Melchor RN, Bellosi E, Genise JF (2003) Invertebrate and vertebrate trace fossils from a Triassic lacustrine delta: the Los Rastros Formation, Ischigualasto Provincial Park, San Juan, Argentina. In: Buatois LA, Mángano MG (eds) Icnología: Hacia una convergencia entre geología y biología, vol 9. Publicación Especial. Asociación Paleontológica Argentina, Buenos Aires, pp 17–33

Minter NJ, Braddy SJ (2006) The fish and amphibian swimming traces *Undichna* and *Lunichnium*, with examples from the Lower Permian of New Mexico, USA. Palaeontol 49(5):1123–1142. doi:10.1111/j.1475–4983.2006.00588.x

Minter NJ, Braddy SJ (2009) Ichnology of an Early Permian intertidal flat: the Robledo Mountains Formation of southern New Mexico, USA. Spec Pap Palaeontol 82:1–107

Morrissey LB, Braddy SJ, Bennett JP et al (2004) Fish trails from the Lower Old Red Sandstone of Tredomen Quarry, Powys, southeast Wales. Geol J 39 (3–4):337–358

Morrissey LB, Braddy S, Dodd C et al (2012) Trace fossils and palaeoenvironments of the Middle Devonian Caherbla Group, Dingle Peninsula, southwest Ireland. Geol J 47(1):1–29

Moy-Thomas JA, Miles RS (1971) Palaeozoic fishes. Chapman and Hall, London

Müller UK, van den Heuvel BLE, Stamhuis E et al (1997) Fish foot prints: morphology and energetics of the wake behind a continuously swimming mullet (*Chelon labrosus* Risso). J Exp Biol 200:2893–2906

Müller UK, Smit J, Stamhuis EJ et al (2001) How the body contributes to the wake in undulatory fish swimming: flow fields of a swimming eel (*Anguilla anguilla*). J Exp Biol 204 (16):2751–2762

Murray AM (2000) The Palaeozoic, Mesozoic and early Cenozoic fishes of Africa. Fish Fish 1(2):111–145. doi:10.1046/j.1467–2979.2000.00015.x

Nelson JS (2006) Fishes of the world, 4th edn. John Wiley & Sons, New Jersey

Netto RG, Tognoli FMW, Gandini R et al (2013) Ichnology of the Phanerozoic deposits of southern Brazil: synthetic review. In: Netto RG, Carmona NB, Tognoli FMW (eds) Ichnology of Latin America—selected papers. Monograph Sociedade Brasileira de Paleontologia, 2, Porto Alegre, pp 129–140

Piñeiro G (2006) Nuevos aportes a la paleontología del Pérmico de Uruguay. In: Veroslavsky G, Martínez S, Ubilla M (eds) Cuencas sedimentarias de Uruguay. Geología, paleontología y recursos naturales. Paleozoico. DIRAC – Facultad de Ciencias (Universidad de la República), Montevideo, pp 257–278

Poyato-Ariza FJ (1995) *Ichthyemidion*, a new genus for the elopiform fish '*Anaethalion*' *vidali*, from the Early Cretaceous of Spain: phylogenetic comments. CR Acad Sci IIA 320:133–139

Rees J, Underwood CJ (2008) Hybodont sharks of the English Bathonian and Callovian (Middle Jurassic). Palaeontology 51(1):117–147

Roshko A (1961) Experiments on the flow past a circular cylinder at very high Reynolds number. J Fluid Mech 10(3):345–356

Rusconi C (1949) Acerca del pez pérmico *Neochallaia minor* y otras especies. Rev Mus Hist Nat Mendoza 3:231–236

Schwimmer DR, Stewart JD, Williams GD (1994) Giant fossil coelacanths of the Late Cretaceous in the eastern United States. Geology 22(6):503–506

Shi GR, Waterhouse JB, McLoughlin S (2010) The Lopingian of Australasia: a review of biostratigraphy, correlations, palaeogeography and palaeobiogeography. Geol J 45(2–3):230–263. doi:10.1002/gj.1213

Simon T, Hagdorn H, Hagdorn MK et al (2003) Swimming trace of a coelacanth fish from the Lower Keuper of south-west Germany. Palaeontology 46(5):911–926. doi:10.1111/1475–4983.00326

Soler-Gijón R, Moratalla JJ (2001) Fish and tetrapod trace fossils from the Upper Carboniferous of Puertollano, Spain. Palaeogeogr Palaeocl 171(1–2):1–28

Stanley DJ (1971) Fish-produced markings on the outer continental margin east of the middle Atlantic states. J Sediment Res 41(1):159–170

Su DZ (1999) A new palaeoniscoid fish from the Upper Triassic of Zichang, northern Shaanxi. Vertebr Palasiat 37(4):257–266

Todesco R, Avanzini M (2008) First record of the fish trace fossil *Undichna* from the Middle Triassic of Italy. Stu Trentini Sci NatActa Geol 83:253–257

Trewin NH (2000) The ichnogenus *Undichna*, with examples from the Permian of the Falkland Islands. Palaeontol 43(6):979–997

Turek V (1989) Fish and amphibian trace fossils from Westphalian sediments of Bohemia. Palaeontol 32:623–643

Turek V (1996) Fish trace fossil interpreted as a food gathering swimming trail from the Upper Carboniferous (Westphalian) of Bohemia. Casopis Narodniho Muzea Rada Prirodovedna 165(1–4):5–8

Tytell ED, Lauder GV (2004) The hydrodynamics of eel swimming: I. Wake structure. J Exp Biol 207(11):1825–1841

Tytell E, Borazjani I, Sotiropoulos F et al (2010) Disentangling the functional roles of morphology and motion in the swimming of fish. Integr Comp Biol 50(6):1140–1154

Videler JJ (1993) Fish swimming. Chapman & Hall, London

Videler JJ, Müller UK, Stamhuis EJ (1999) Aquatic vertebrate locomotion: wakes from body waves. J Exp Biol 202(23):3423–3430

Wang LF, Lu ZS, Gong DH et al (2008) Restoration of Late Triassic fish trace makers in Hengshan County, Shaanxi province, China. J China Univ Geosci 33(1):12–18

Wardle CS (1977) Effect of size on swimming speeds of fish. In: Pedley J (ed) Scale effects in animal locomotion. Academic Press, New York, pp 299–313

Wardle C, Videler J, Altringham J (1995) Tuning in to fish swimming waves: body form, swimming mode and muscle function. J Exp Biol 198(8):1629–1636

Webb PW (1984) Form and function in fish swimming. Sci Am 251(1):72–82

Webb PW (1988) Simple physical principles and vertebrate aquatic locomotion. Am Zool 28(2):709–725

Webb PW (1992) Is the high cost of body/caudal fin undulatory swimming due to increased friction drag or inertial recoil? J Exp Biol 162(1):157–166

Webb PW, Blake RW (1985) Swimming. In: Hildebrand M, Bramble DM, Liem KF, Wake DB (eds) Functional vertebrate morphology. Belknap Press/Harvard University Press, Massachusetts, p 110–128

Wisshak M, Volohonsky E, Blomeier D (2004) Acanthodian fish trace fossils from the Early Devonian of Spitsbergen. Acta Palaeontol Pol 49(4):629–634

Chapter 13
The Neoichnology of Two Terrestrial Ambystomatid Salamanders: Quantifying Amphibian Burrows Using Modern Analogs

Nicole D. Dzenowski and Daniel I. Hembree

Contents

D. I. Hembree (✉) · N. D. Dzenowski
Department of Geological Sciences, Ohio University, Athens, OH 45701, USA
e-mail: hembree@ohio.edu

Abstract This experiment involved the study of two species of ambystomatid salamanders, *Ambystoma tigrinum* and *Ambystoma opacum* (Amphibia: Caudata). Individual salamanders were placed in sediment-filled terrariums and allowed to burrow for 7 to 14 days under natural environmental conditions. Salamanders were then removed and their burrows cast, excavated, and described both qualitatively and quantitatively. Quantitative measurements included the number of surface openings, width, height, width-to-height ratio, total length, maximum depth, slope, branching angle, complexity, and tortuosity. Additional experiments involved variations in soil composition and soil moisture. *Ambystoma tigrinum* burrowed through excavation and compaction techniques whereas *A. opacum* only used compaction. Burrows produced by *A. tigrinum* consisted of ramps, branched ramps, U-, W-, Y-, and J-shaped burrows. Small-scale surface mounds were also created by *A. tigrinum*. Burrows produced by *A. opacum* consisted of ramps and branched ramps. Sinuous to straight surface trails were also produced by *A. opacum*. There was no recognized change in behavior or burrow properties in response to changes in the environmental parameters.

Keywords Trace fossil · Vertebrate · Bioturbation · Continental · Paleoecology

13.1   Introduction

The purpose of this chapter is to document the burrow morphology of two species of fossorial salamanders, *Ambystoma opacum* and *Ambystoma tigrinum,* through simple experiments in a controlled, laboratory setting. The morphology of the burrows was analyzed to determine the architectural features unique to each species and to burrowing salamanders in general, as well as how the burrows' properties varied due to changes in sediment composition and soil moisture. These observations provide for a better understanding of the paleoecological, paleoenvironmental, and paleoclimatic significance of continental vertebrate trace fossils by aiding in the recognition of the behaviors represented, potential trace makers, and the associated environmental conditions.

   Fossil burrows and the organisms responsible for them are rarely found together, making the interpretation of trace makers and behaviors difficult. Study of modern analogs is necessary to accurately interpret trace makers, behaviors, and environmental conditions responsible for burrows within the fossil record (Bromley 1996). Neoichnological studies have generally been restricted to organisms found in the marine realm (Frey 1968, 1970; Frey et al. 1984; Gaillard 1991; Gingras et al. 2002, 2004; Martin 2006; Hertweck et al. 2007; Pearson et al. 2007; Seike and Nara 2007) with few studies of terrestrial invertebrates (Hasiotis and Mitchell 1993; Davis et al. 2007; Smith and Hasiotis 2008; Counts and Hasiotis 2009; Hembree 2009, 2013; Halfen and Hasiotis 2010; Hembree et al. 2012) and even fewer of terrestrial vertebrates (Brand 1996; Deocampo 2002; Hembree and Hasiotis 2006, 2007; Genise et al. 2009; Melchor et al. 2012). Marine trace fossils are well documented and,

through neoichnological studies, behaviors and environmental factors controlling their morphology have been accurately determined (Bromley 1996). While the study of continental ichnology is relatively new, the same methods used in the marine realm have been applied for understanding the behaviors and environmental factors involved in the occurrence and morphology of continental trace fossils, especially those of terrestrial arthropods (Hasiotis 2002, 2007). The majority of knowledge of terrestrial vertebrate ichnology is focused on fossilized tracks and trackways (e.g., Brand and Tang 1991; Lockley et al. 1994; Brand 1996; Genise et al. 2009). Increasingly, however, vertebrate burrows are being documented in the fossil record and correlations have been made between burrowing behaviors in vertebrates and climatic and environmental conditions (Romer and Olson 1954; Voorhies 1975; Groenewald et al. 2001; Miller et al. 2001; Hasiotis et al. 2004, 2007; Hembree and Hasiotis 2008).

No detailed accounts of fossil burrows definitively attributed to salamanders or salamander-like amphibians have been described in the literature. A potential reason for this is that relatively few studies of the burrowing behaviors exhibited by modern salamanders have been conducted (e.g., Semlitsch 1983) and none have described the morphology of the burrows produced. In particular, no previous studies have presented three-dimensional models of modern salamander burrows. Amphibians with body types similar to modern salamanders have a fossil record extending to the Devonian and there is a strong likelihood that some of these species were fossorial (Gardner 2001; Anderson et al. 2008; Maddin et al. 2011). True salamanders (Amphibia: Caudata) appeared in the Jurassic and fossils of salamander-like amphibians (Amphibia: Caudata: Karauridae) with morphologies indicative of burrowing behaviors appear as early as the Early Permian (Amphibia: Lepospondyli) (Holman 2006; Maddin et al. 2011). These morphological characteristics are similar to those of extant burrowing amphibians, implying that burrowing organisms with body plans similar to *A. tigrinum* and *A. opacum* extend at least as far as the Early Permian (Maddin et al. 2011). The lack of knowledge and understanding about the burrowing behaviors and burrows produced by salamanders and their ancestors could, therefore, have potentially led to the misinterpretation of these structures in the fossil record.

13.2 Salamander Ecology and Behavior

Salamanders are a diverse group of amphibians consisting of approximately 500 extant species (Vitt and Caldwell 2008). Most salamanders have well-developed tails, cylindrical and often elongate bodies, distinct heads with reduced and frequently cartilaginous skulls, and short, well-developed limbs (Vitt and Caldwell 2008). Salamanders inhabit every continent except Antarctica and Australia and are adapted to both aquatic and terrestrial habitats. The Ambystomatidae are a group of heavy bodied and tailed, mostly fossorial, salamanders ranging in length from 8–34 cm. To avoid desiccation, most species within the Ambystomatidae spend a
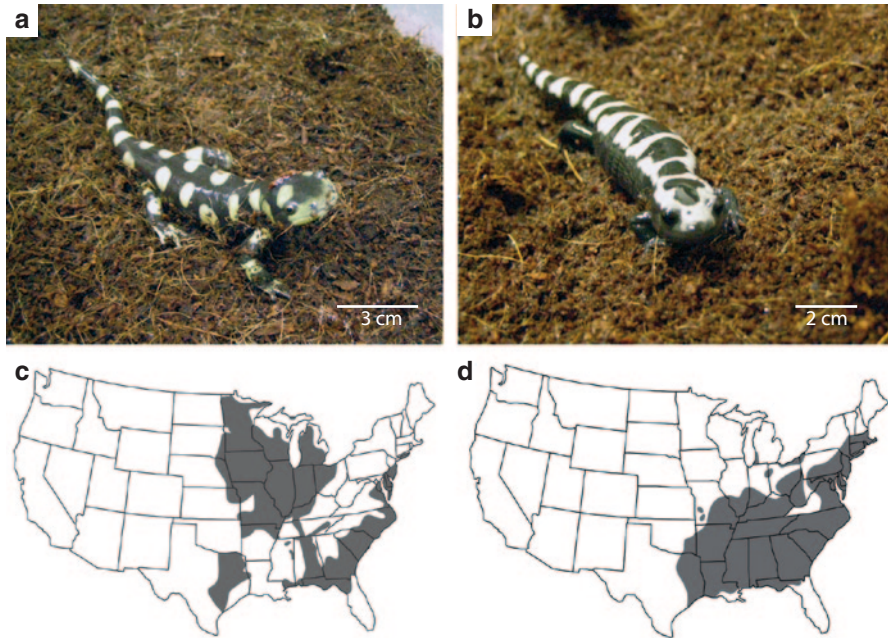
Fig. 13.1 The fossorial salamanders used in this experiment and their known geographic ranges. **a** *Ambystoma tigrinum*. **b** *Ambystoma opacum*. **c** Range of *A. tigrinum*. **d** Range of *A.opacum*

majority of their time within leaf litter or burrowed below the sediment surface (Semlitsch 1983).

Two species of salamanders from the Ambystomatidae were chosen for these experiments, *A. opacum* and *A. tigrinum* (Fig. 13.1a and b). Both species are fossorial and inhabit similar deciduous forest environments with temperatures averaging 18–20 °C within sandy loam to loamy soils with moisture levels of approximately 74 %. These are heavy bodied salamanders with short, well-developed legs and broad heads with rounded snouts. *Ambystoma tigrinum* generally has a more robust body type and adults are 5–14 cm longer than adult *A. opacum.* Both types of salamander are nocturnal, emerging from their burrow at night to hunt (Vitt and Caldwell 2008).

Ambystoma opacum (marbled salamander) has a geographic range extending from New England to Florida and as far west as eastern Texas (Anderson and Graham 1967; Fig. 13.1c). This species is the smallest of the ambystomatids, typically reaching adult sizes up to 11 cm in length. The life span of *A. opacum* is around 4 years, most of which is spent underground in burrows. Individuals mate in the fall, emerging from their burrow after a heavy rain to mate and deposit eggs. *Ambystoma opacum* burrow passively through compression by the expansion of preexisting cracks, holes, or other burrows in the sediment surface (Semlitsch 1983).

Ambystoma tigrinum (eastern tiger salamander) has a wide geographic range in eastern North America that extends from the Gulf Coastal Plains to the plains of

Table 13.1 Environmental parameters for each experiment. **a** Experiment 1. **b** Experiment 2. **c** Experiment 3

a. Basic morphology experiments			
Sediment composition	Moisture content	Enclosure size	Time
75O/25C	74%	38, 114, and 246 L	7 days
75O/25C	74%	38, 114, and 246 L	14 days
b. Variation in sediment composition			
Sediment composition	Moisture content	Enclosure size	Time
50O/50C	74%	38, 114, and 246 L	14 days
50O/25C/25S	74%	38, 114, and 246 L	14 days
c. Variation in moisture content			
Sediment composition	Moisture content	Enclosure size	Time
75O/25C	54%	38, 114, and 246 L	14 days
75O/25C	94%	38, 114, and 246 L	14 days

the Midwest, but it is mostly absent east of the Appalachians (Church et al. 2003; Fig. 13.1d). It is one of the largest salamander species within the ambystomatids, reaching total adult lengths of 15–25 cm. The life span of *A. tigrinum* is 12–15 years. Individuals mate in the spring, leaving their burrows to mate and deposit eggs within small ponds or streams. *Ambystoma tigrinum* actively excavate their burrows through the use of their snout and forelimbs using their hind limbs to move loose sediment backwards into soil piles (Semlitsch 1983; Kley and Kearney 2007).

13.3 Materials and Methods

The burrowing behavior and burrow morphology of wild-caught individuals of *A. opacum* and *A. tigrinum* (*n*=6 each) were studied over the course of these experiments. Individuals of *A. opacum* were 6.0–6.2 cm long snout to vent (SVL), 1.5–1.9 cm wide, and weighed 8–13 g. Individuals of *A. tigrinum* were 7.5–9.0 cm long SVL, 1.5–2.2 cm wide, and weighed 14–30 g. The laboratory was kept on a 12-hour light cycle and temperatures were maintained at 18–23 °C throughout the study. Prey animals (crickets) were placed in the terrarium twice per week during and in-between experiments. Three different terrarium sizes, 38 L (50×25×30 cm), 114 L (60×45×40 cm), and 246 L (91×45×61 cm), were used to account for possible variations in burrow morphology due to space constraints. The sediment depth for each terrarium remained constant: 20 cm for the 38 L, 25 cm for the 114 L, and 55 cm for the 246 L. The sediment surface was sprayed with water daily to maintain moisture levels. Sediment moisture was monitored using an Aquateer EC300 moisture meter.

Experiment 1 involved the observation of the behaviors and burrow morphologies of each salamander under ideal conditions (Table 13.1a). The composition and moisture content of the sediment used in these experiments were chosen to closely mimic the physical properties of the soils occupied by *A. tigrinum* and *A. opacum* in

the wild. Sediment compaction was kept at levels conducive to burrowing. The six individuals of both *A. tigrinum* and *A. opacum* were placed into separate terrariums containing a mixture of 75 % finely-shredded coconut fiber and 25 % clay loam soil (75O/25C; organic clay loam). Sediment moisture levels were kept at approximately 74%. The experiments were conducted over 7 and 14 days to determine if the final burrow morphologies were changed over time. Experiments 2 and 3 involved variations in either sediment composition or moisture content (Table 13.1b and c). For both species, the sediment density was either increased with the addition of 25 % more clay loam (50O/50C; clay loam) or decreased with the addition of 25 % fine-grained sand (50O/25C/25S; sandy clay loam). In experiment 3, the sediment moisture content was either increased to 94 % or decreased to 54 %. The salamanders were observed under these altered conditions for 14 days. Species of *A. tigrinum* and *A. opacum* are commonly found burrowed within organic material (Semlitsch 1983). Due to this aspect of their ecology, burrows produced by *A. tigrinum* and *A. opacum* ($n=9$ and 1, respectively) in the laboratory in 100 % organic material (i.e., coconut fiber) were also cast, excavated, and described. Terrariums filled with this sediment were primarily used as holding tanks for the salamanders between experiments. While moisture levels were not recorded with a moisture probe, they were maintained at visibly high levels (70–85 %).

During the experiments, observed burrowing activity was digitally recorded and visible changes in the sediment surface or burrow openings were recorded, measured, and photographed. At the end of each experiment, the salamanders were carefully removed from either within their burrows or from the sediment surface, as not to disturb any burrows. Open burrows were cast with quick-drying plaster, described, and measured qualitatively and quantitatively. Quantitative properties measured for each burrow cast included the number of surface openings, maximum depth, cross-sectional width, cross-sectional height, cross-sectional width-to-height ratio, total length, slope, and branching angles (Fig. 13.2a). Two additional, scale-independent, quantitative descriptions of the burrows were made: burrow complexity and tortuosity (Meadows 1991). Complexity is found by adding the total number of segments, surface openings, endpoints, and chambers of the burrow (Fig. 13.2b). Tortuosity is a measure of the deviation of a tunnel from a straight line and is found by dividing the total length of the tunnel by the straight line distance measured from end to end (Fig. 13.2c). Burrow casts were divided into different morphological types based on their qualitative and quantitative properties.

The ten quantitative measurements were then used to compare burrows of different individuals and species. The Bray–Curtis similarity test is a nonparametric statistical analysis used to determine the level of similarity between multiple samples each with multiple quantitative properties (Bray and Curtis 1957). This statistical analysis was chosen because it is capable of utilizing all ten quantitative properties together in order to quantify the similarity of each burrow cast instead of comparing each property individually. The level of similarity is ranked between 1.0–0.0, with values of 1.0 indicating burrows that are identical and 0.0 indicating burrows that are completely different (e.g., Bray and Curtis 1957). In this study, values of 0.9–0.8 indicate that the compared burrow casts have a high degree of similarity, values of
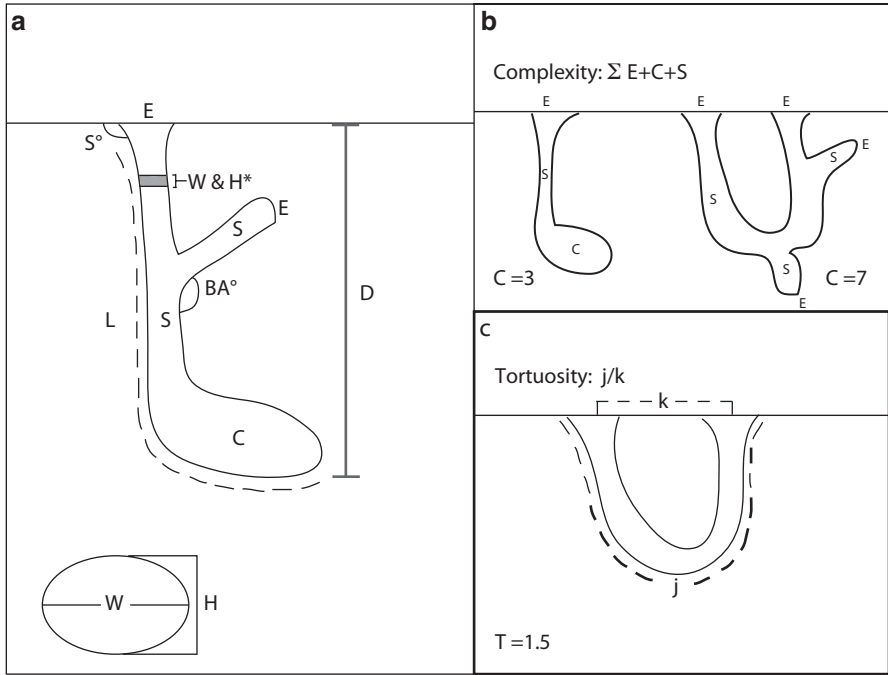
Fig. 13.2 Quantitative measurements taken for each burrow. Burrows were divided into segments (*S*), chambers (*C*), and endpoints (*E*). **a** Scale-dependent measurements include: D = maximum depth, L = total length, W = segment width, H = segment height, S = slope of burrow, and BA = branching angle. **b** Complexity. **c** Tortuosity. j = length of the burrow and k = endpoint to endpoint (*straight line*) distance. (Modified from Hembree and Hasiotis 2006)

0.7–0.6 indicate that they have a moderate level of similarity, and any values of 0.5 or less indicate that they are dissimilar following the studies of Hembree et al. (2012) and Hembree (2013).

The quantitative properties of the salamander burrows produced under different environmental conditions were analyzed using the Spearman's rank correlation test, a nonparametric statistical analysis used to determine if two variables are correlated. Sediment composition, moisture content, and enclosure size were treated as independent variables while average width, average height, average width-to-height ratio, total length, maximum depth, and slope of the burrow casts were treated as dependent variables. These analyses were performed to determine if the burrow properties were influenced by the sediment properties or habitat size. Spearman's rank correlation was also used to compare the width, height, width-to-height ratio, and length of the burrow casts to the width, height, width-to-height ratio, and length of the salamanders to determine if body size had an effect on the burrow size. Salamander body size was treated as the independent variable while burrow size was treated as the dependent variable.

Finally, two additional nonparametric analyses, the Mann–Whitney and Kolmogorov–Smirnov tests, were performed to determine if the means and distributions of the individual quantitative measurements of the burrows, excluding the number of surface openings, slope, and branching angle, produced by *A. tigrinum* and *A. opacum* were similar. All statistical analyses were conducted using PAST (Palaeontological Statistics, ver. 2.16).

13.4   Experimental Results

Both salamander species produced open burrows in all of the sediment types with little visible variation in morphology. *Ambystoma tigrinum* and *A. opacum* exhibited similar behaviors in similar sediments with occasional variation in burrowing methods unrelated to changes in the environmental parameters. Many experiments, particularly those involving *A. tigrinum,* resulted in multiple burrows being cast due to several abandoned burrows remaining open to the surface for the entire experimental period. Two experiments with *A. opacum* resulted in no burrow casts being produced. These two salamanders excavated only shallow burrows that were passively filled by gravitational collapse of the overlying sediment before the end of the experiment.

13.4.1   *A. tigrinum*

13.4.1.1   Behavior

Ambystoma tigrinum burrowed using both excavation and compaction techniques within 12 h of being placed in the terrarium. Excavation was used to start the burrow after which their method of burrowing would switch to compaction. Individuals excavated by bracing their bodies on the sediment surface with their hind limbs and then thrusting their forelimbs into the sediment; sediment was thrown and pulled back into small mounds (Fig. 13.3). Individuals pushed themselves farther below the surface by first forcing their snout into the sediment and then by moving their head both laterally and vertically. As the salamander burrowed deeper, this process compressed the sediment around the margins of the burrow. Depending on the individual, burrows were either inhabited for the entire experimental period ($n=36$) or were abandoned and new burrows were created ($n=18$). The salamanders spent approximately 80% of their time below the surface, emerging from their burrows most commonly at night either through the original burrow opening or by creating a new opening.

13.4.1.2   Burrow Morphology

Ramps These commonly produced burrows ($n=41$) consist of one elliptical surface opening, one elliptical, subhorizontal-to-subvertical tunnel or shaft, and, at

Fig. 13.3 *Ambystoma tigrinum* burrowing by excavation

the end of most ($n=27$), a laterally expanded, hemispherical chamber (Fig. 13.4a and b; Table 13.2; Table A.1). Ramps were constructed by all six salamanders in all sediment compositions and moisture conditions. The total length of the ramps is 9–26 cm ($\bar{x}=15.4$ cm, SD=3.8) and the maximum depth is 4.0–18.4 cm ($\bar{x}=9.4$ cm, SD=3.2). The tunnels and shafts enter the sediment surface at angles of 10–90° ($\bar{x}=55°$, SD=15) and have widths of 1.2–4.1 cm ($\bar{x}=2.9$ cm, SD=0.5 cm), heights of 1.5–4.2 cm ($\bar{x}=2.2$ cm, SD=0.5 cm), and width-to-height ratios of 0.6–2.1 ($\bar{x}=1.3$, SD=0.2). The terminal chambers have widths of 2.4–5.4 cm ($\bar{x}=3.7$ cm, SD=0.6), heights of 1.6–2.9 cm ($\bar{x}=2.2$ cm, SD=0.3), and width-to-height ratios of 1.2–2.9 ($\bar{x}=1.7$, SD=0.3). The heights of the chambers are, on average, the same as those of the tunnels, but the widths of the terminal chambers are typically 0.8 cm greater. Ramps have a complexity of either 2 when they consist of only one opening and a single tunnel or shaft or 3 when they also include a single chamber. The tortuosity is 1.0–1.7 ($\bar{x}=1.3$). Six ramps produced by *A. tigrinum* also possessed narrow, sinuous tunnels extending from the end of the chamber (Fig. 13.4c and d). The extensions were 1.0–2.3 cm wide, 1.2–2.6 cm high, and 2.6–5.0 cm long, dimensions which were considerably less than the rest of the burrow.

U and W-Shaped Burrows These less commonly produced burrows ($n=8$) consist of two to three, elliptical-to-circular, surface openings with two or three elliptical, subhorizontal-to-vertical tunnels or shafts connected below the surface by one or two tunnels all with similar widths and heights (Fig. 13.5; Table 13.2; Table A.1). U-shaped burrows consist of a single, continuous tunnel (Fig. 13.5a and b) whereas W-shaped burrows are composed of two intersecting U-shaped burrows (Fig. 13.5c and d). These burrows were produced in the organic clay loam and sandy clay loam sediment compositions and in soil moisture percentages of 74 and 94 %. The burrows are 12.2–34.0 cm ($\bar{x}=22.3$ cm, SD=7.7) long and extend 3.5–7.9 cm
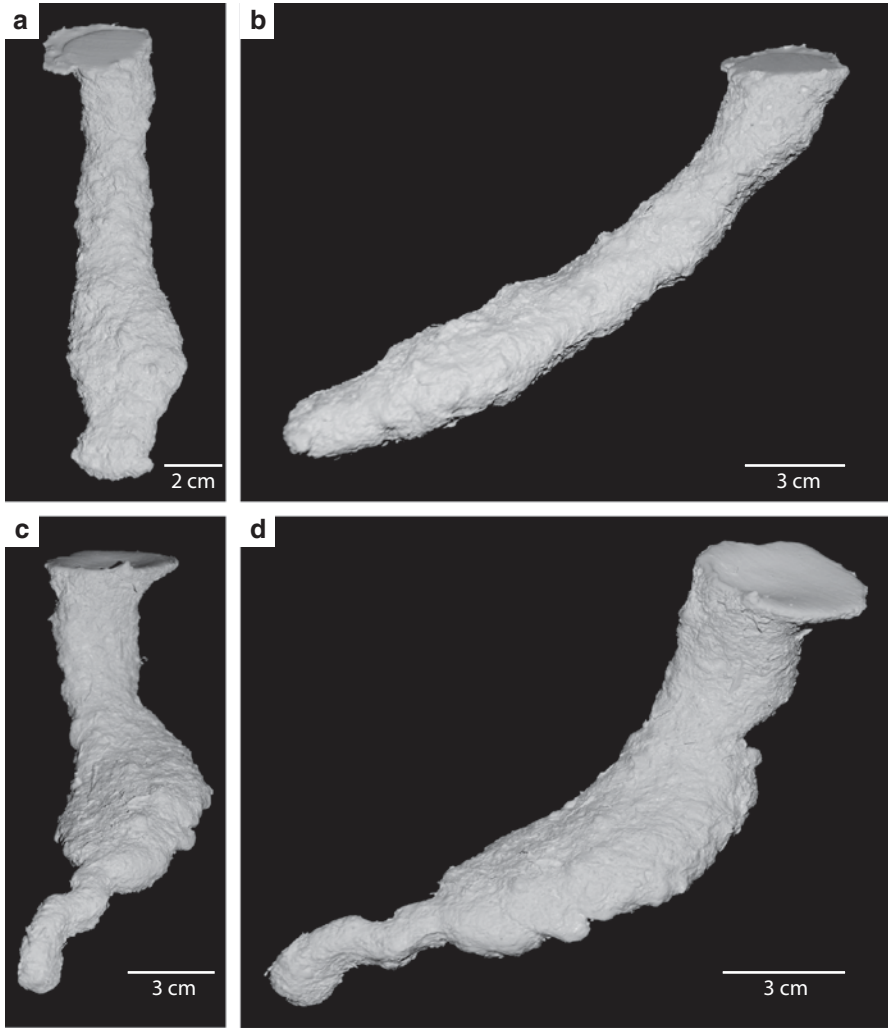
Fig. 13.4 Ramp morphologies produced by *A. tigrinum*. **a** Overhead view of a common ramp with a terminal chamber (TS2-3-1). **b** Side view of TS2-3-1. **c** Overhead view of a ramp with a narrow tunnel extending from the terminal chamber (TS6-2-2(T)). **d** Side view of TS6-2-2(T)

($\bar{x}$ =5.7 cm, SD=1.6) into the sediment at angles of 15–90° ($\bar{x}$ =53°, SD=16). The shafts and tunnels have widths of 1.5–4.8 cm ($\bar{x}$ =3.2 cm, SD=0.5), heights of 1.2–4.0 cm ($\bar{x}$ =2.3 cm, SD=0.3), and width-to-height ratios of 1.1–1.8 ($\bar{x}$ =1.4, SD=0.3). The complexity of the U-shaped burrows is 3 including two surface openings and a single continuous U-shaped tunnel. The W-shaped burrows have complexities of either 5, including three surface openings and two continuous U-shaped shafts or tunnels, or 6, including three surface openings and three curved shafts or tunnels that intersect beneath the surface. The tortuosities of the burrows are 1.1–2.8 ($\bar{x}$ =1.8, SD=0.5).

Fig. 13.5 U- and W-shaped morphologies produced by *A. tigrinum*. **a** Overhead view of a U-shaped burrow (TS3-1-1). **b** Side view of TS3-1-1. **c** Overhead view of a W-shaped burrow (TS3-1-2A). **d** Side view of TS3-1-2A
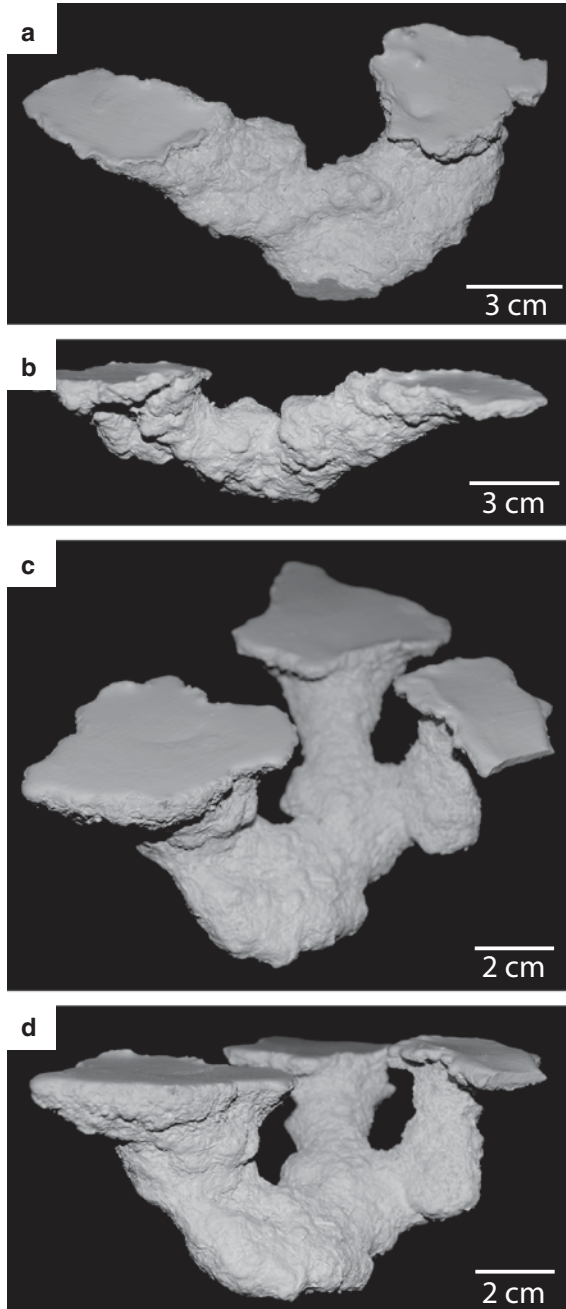
Table 13.2 Average quantitative properties of burrows produced by *A. tigrinum* and *A. opacum*

A. tigrinum

	Ramp	Branched ramp	U- and W-shaped	J-shaped	Y-shaped	Combined
Surface openings	1	1	2	1	2	1
Depth	9.4	10.1	5.7	16.7	10.7	9.0
Length	15.4	19.4	22.3	27.0	23.9	17.2
Width	3.0	2.9	3.2	2.5	2.9	3.0
Height	2.1	1.9	2.3	1.7	1.9	2.1
W/H	1.5	1.5	1.4	1.5	1.5	1.5
Slope	55.0	68.0	52.9	62.0	55.9	55.1
Branch angle	0.0	52.0	4.4	0.0	90.0	6.6
Complexity	3	5	4	2	5	3
Tortuosity	1.3	1.8	1.8	2.5	1.7	1.4

A. opacum

	Ramp	Branched ramp	Combined
Surface openings	1	1	1
Depth	7.2	5.7	7.1
Length	12.7	14.5	12.8
Width	2.9	2.9	2.9
Height	2.0	1.9	2.0
W/H	1.4	1.5	1.5
Slope	43.6	37.0	43.0
Branch angle	0.0	90.0	7.8
Complexity	2	4	2
Tortuosity	1.3	1.7	1.3

Depth, length, width, and height in cm. Combined is the average of all burrows regardless of morphology

Branched Ramp This rare burrow morphology ($n=1$) consists of an elliptical surface opening, an elliptical, subvertical tunnel, and a laterally expanded chamber with two branches (Fig. 13.6; Table 13.2; Table A.1). The branched ramp was produced in the clay loam sediment with a moisture content of 74%. The total length of the branched ramp is 19.4 cm reaching a maximum depth of 10.1 cm. The tunnel enters the sediment at an angle of 68° and has an average width of 2.7 cm, an average height of 1.9 cm, and an average width-to-height ratio of 1.5. The chamber has an average width of 3.7 cm, an average height of 2.2 cm, and an average width-to-height ratio of 1.7. The two branches extend from the chamber at angles of 52 and 70 ° leading upward and downward, respectively. The complexity of the burrow is 5 due to the single surface opening, three tunnel segments, and a single chamber. The tortuosity is 1.8.

Y-Shaped Burrows This uncommon burrow morphology ($n=3$) consists of two or three surface openings and two or three subhorizontal-to-subvertical shafts that meet under the sediment surface and terminate in one vertical shaft (Fig. 13.7a and b; Table 13.2; Table A.1). These burrows were produced in holding tanks in organic sediment. The Y-shaped burrows are 23.0–25.2 cm ($\bar{x}$ =23.9 cm, SD=1.1) in length and reach depths of 9.6–12.4 cm ($\bar{x}$ =10.7 cm, SD=1.5). The tunnels and
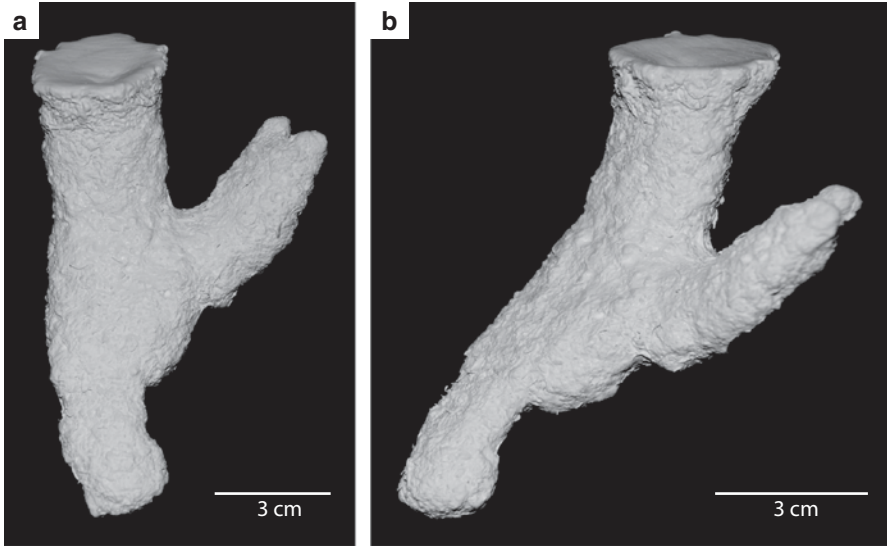
Fig. 13.6 Branched ramp morphology produced by *A. tigrinum*. **a** Overhead view of the branched ramp (TS6-2-1A). **b** Oblique view of TS6-2-1A

shafts enter the sediment at angles of 36–74° ($\bar{x}$ =56.7° cm, SD=12.9) and meet the single, terminal tunnel or shaft at angles of 36–74° ($\bar{x}$ =56.7°, SD=11.9°). The terminal tunnel or shaft begins at depths of 2.5–6.0 cm ($\bar{x}$ =4.2 cm, SD=1.8). The tunnels and shafts have widths of 1.8–3.8 cm ($\bar{x}$ =2.9 cm, SD=0.5), heights of 1.2–2.5 cm ($\bar{x}$ =1.9 cm, SD=0.2), and width-to-height ratios of 1.4–1.6 ($\bar{x}$ =1.5, SD=0.09). The complexity of the burrows is 4, 5, or 7 depending on the number of shafts (2–4) and surface openings (2–3) present. The tortuosity ranges from 1.3–2.0 ($\bar{x}$ =1.7, SD=0.3).

J-Shaped Burrow A rare morphology (n=1) consisting of one surface opening leading to an elliptical, subvertical, J-shaped shaft (Fig. 13.7c; Table 13.2; Table A.1). This burrow was produced in a holding tank in organic sediment. The length of the burrow is 27 cm reaching a maximum depth of 16.7 cm. The shaft enters the sediment at an angle of 62° and has an average width of 2.5 cm, an average height of 1.7 cm, and an average width-to-height ratio of 1.5. The complexity of the J-shaped burrow is 2 due to its single surface opening and single shaft. The tortuosity is 2.5.

Bioglyphs Bioglyphs were commonly observed on all burrows, although they were best developed on burrows produced in clay loam sediment. Most of the bioglyphs present are rounded to elongate protrusions (Fig. 13.8a and b) as well as some bilobate or heart-shaped markings (Fig. 13.8c). The burrows possess 0–11 of these structures with a variable distribution along their length.

Surface Features Mounding was present in all sediments regardless of composition or moisture content (Fig. 13.9). The mounds were directly related to the burrow-

Fig. 13.7 Y- and J-shaped burrow morphologies produced by *A. tigrinum*. **a** Side view of a Y-shaped burrow with two surface openings (TSB8). **b** Side view of a Y-shaped burrow with three surface openings (TSB6). **c** Side view of a J-shaped burrow (TSB9)

Fig. 13.8 Examples of bio-glyphs preserved on burrows produced by *A. tigrinum*. **a** Overhead view of a portion of a ramp (TS6-3-2) bearing elongate and rounded bio-glyphs. **b** Overhead view of a portion of a ramp (TS6-3-1) bearing rounded and elongate bioglyphs. **c** Side view of a branched burrow (TS6-2-1) exhibiting a bilobate or heart-shaped bioglyph on the end of the burrow's branch
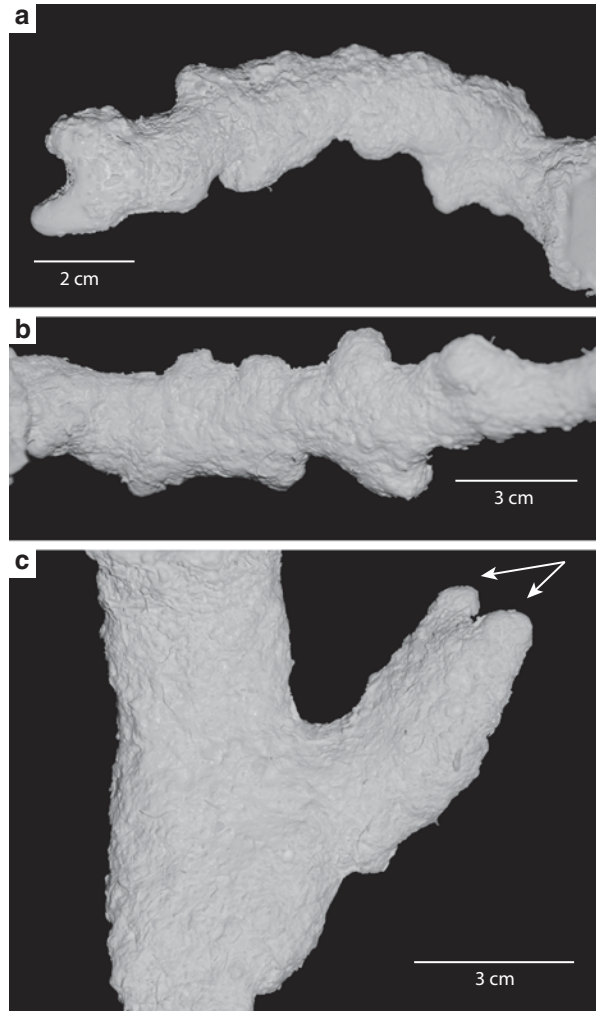
ing method employed by *A. tigrinum*. Mounds were produced as the salamanders initially excavated their burrow, using their forelimbs to pull sediment back behind them into spoil piles. Mounding was present next to the surface opening, on the side opposite the downward sloping ramp.

13.4.2   *A. opacum*

13.4.2.1   Behavior

Ambystoma opacum burrowed through compaction only, entering the sediment through cracks and holes that were already present in the surface within 24 h of
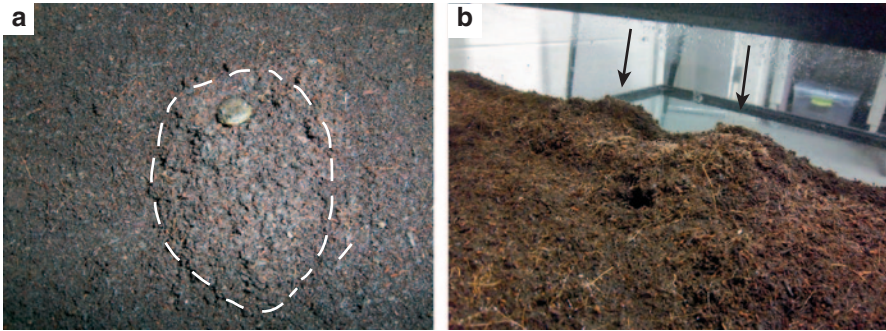
Fig. 13.9 Surface mounds produced by *A. tigrinum*. **a** Overhead view of a mound produced by an individual (TS5) in the clay loam with a moisture content of 74 %. **b** Oblique view of mounds produced by the same salamander in organic clay loam with a moisture content of 54 %

being placed in the terrariums. The salamanders first forced their snout into the sediment and then used their hind- and forelimbs to push themselves deeper. Expansion of the burrow was accomplished by moving their heads vertically and their bodies in an undulatory fashion. Once constructed, burrows commonly remained open to the surface. In 34 of the 36 experiments conducted, the burrows were inhabited for the entire length of the experiment. The salamanders spent approximately 90 % of their time in their burrow, rarely surfacing at night. When the salamanders did emerge, they did so only through their original burrow opening.

13.4.2.2 Burrow Morphology

Ramps These commonly produced burrows ($n=22$) consist of one elliptical surface opening and one elliptical-to-circular, subhorizontal-to-subvertical tunnel or shaft (Fig. 13.10a and b; Table 13.3; Table A.2). Some ramps ($n=6$) also included a laterally expanded chamber either at the end of the burrow (Fig. 13.10c and d) or just below the surface opening (Fig. 13.10e and f). Ramps were constructed in all sediment compositions and moisture conditions; those with chambers were only produced in sediments with a moisture content of 74 %. The ramps have lengths of 6.0–24.0 cm ($\bar{x} =12.2$ cm, SD=4.4) and reach depths of 3.5–14.6 cm ($\bar{x} =7.3$ cm, SD=3.0) at angles of 11–95° ($\bar{x} =46.3°$, SD=22.8). The tunnels and shafts have widths of 1.5–4.0 cm ($\bar{x} =2.9$ cm, SD=0.3), heights of 1.0–5.4 cm ($\bar{x} =2.0$ cm, SD=0.3), and width-to-height ratios of 0.8–2.6 ($\bar{x} =1.4$, SD=0.2). The chambers have similar dimensions to the adjacent tunnels except that their widths are, on average, 1.0 cm wider with a range in widths of 2.1–4.0 cm ($\bar{x} =3.2$, SD=0.5). The complexity of the ramps is either 2, including one surface opening and single tunnel or shaft or 3 when a chamber is present. Tortuosity values are 1.0–1.9 ($\bar{x} =1.3$, SD=0.3). A variation on this morphology is an L-shaped ramp which includes a subvertical to vertical shaft at the end of the burrow (Fig. 13.10g). This variation
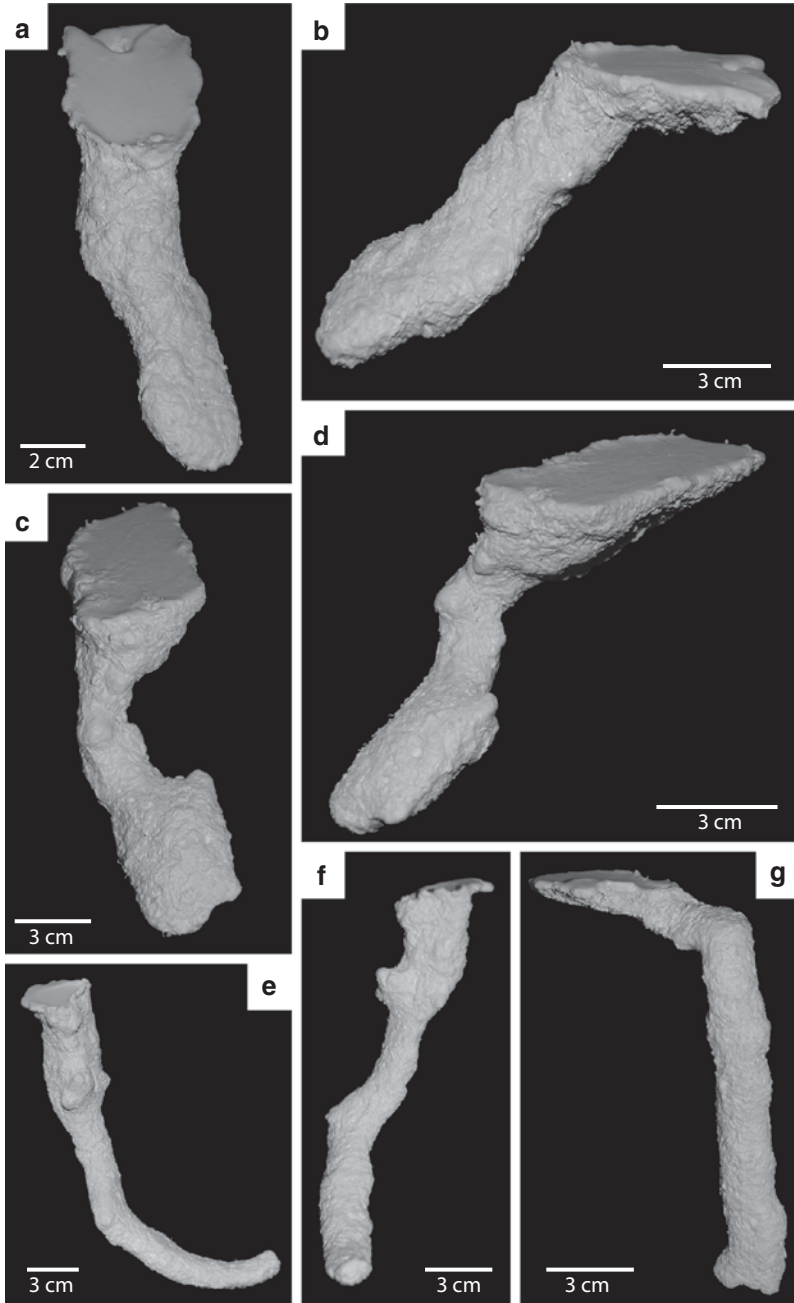
Fig. 13.10 Ramp morphologies produced by *A. opacum*. **a** Overhead view of a ramp (MS3-1-1). **b** Side view of MS3-1-1. **c** Overhead view of a ramp with a terminal chamber (MS3-2-1). **d** Side view of MS3-2-1. **e** Side view of a ramp morphology with a chamber just below the surface opening (MS4-1-1A). **f** Overhead view of MS4-1-1A. **g** Side view of an L-shaped ramp (MS4-2-2)

A. tigrinum

All	0.8
R to R	0.9
R to BR	0.7
R to UW	0.8
R to J	0.8
R to Y	0.6

UW to UW	0.8
UW to BR	0.7
UW to J	0.7
UW to Y	0.6

Y to Y	0.9
Y to BR	0.8
Y to J	0.6

A. opacum

All	0.8
R to R	0.8
R to BR	0.5

BR to BR	0.8

A. tigrinum to A. opacum

All	0.7
R to R	0.8
BR to R	0.6
UW to R	0.7
J to R	0.7
Y to R	0.5

R to BR	0.5
BR to BR	0.6
UW to BR	0.5
J to BR	0.7
Y to BR	0.9

Table 13.3 Average similarity values of the burrows produced by *A. tigrinum* and *A. opacum* compared within and between each species. R: ramp, BR: branched ramp, UW: U- and W-shaped burrow, J: J-shaped burrow, Y: Y-shaped burrow

was produced twice by the same salamander (MS4) in organic clay loam and sandy clay loam sediments with a moisture content of 74 %.

Branched Ramp A rare ramp morphology ($n=2$) produced by one individual consisting of a single, elliptical opening, an elliptical, subhorizontal tunnel, and a single elliptical, subhorizontal branch (Fig. 13.11; Table 13.3; Table A.2). Branched ramps were produced in organic clay loam sediment with moisture contents of 54 and 94 %. The branched ramps have lengths of 9.0–20.0 cm ($\bar{x} = 14.5$ cm, SD=4.4) reaching depths of 4.5–6.8 cm ($\bar{x} = 5.7$ cm, SD=1.2) at an angle of 31–43° ($\bar{x} = 37°$, SD=6). The branch extends off of the main burrow at an angle of 90°. The tunnels have widths of 1.5–3.8 cm ($\bar{x} = 2.9$ cm, SD=0.5), heights of 0.9–3.1 cm ($\bar{x} = 1.9$ cm, SD=0.2), and width-to-height ratios of 1.4–1.7 ($\bar{x} = 1.6$, SD=0.1). The complexity is 4 including the single surface opening and three tunnel segments. The tortuosity is 1.2–2.1 ($\bar{x} = 1.7$ cm, SD=0.5).

Bioglyphs Weakly formed bioglyphs were present on burrows of *A. opacum* from all experiments. Bioglyphs included bilobate or heart-shaped structures (Fig. 13.12a and b) as well as rare, round-to-elongate protrusions (Fig. 13.12c). The burrows possess 0–5 of these structures with a variable distribution along their length.

Surface Features Surface trails were common in the *A. opacum* terrariums in all experiments (Fig. 13.13). The trails were sinuous to straight, 2–3 cm wide and typically 1 cm deep. The production of surface trails was observed during the movement
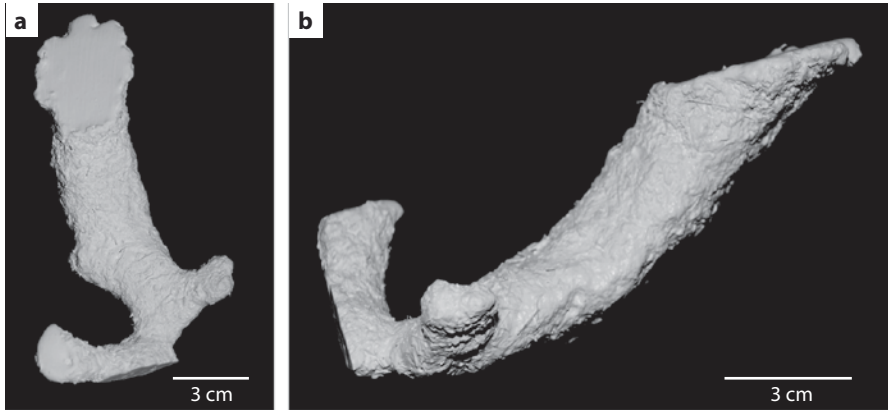
Fig. 13.11 Branched ramp produced by *A. opacum.* **a** Overhead view of branched ramp (MS2-3-1). **b** Side view of MS2-3-1

of *A. opacum* after the initiation of burrowing. Once partially burrowed, some salamanders would move laterally through the shallow sediment, pushing material aside with their snout to form the shallow trails. These trails commonly led to an open burrow.

13.5 Analysis of Burrow Morphology

13.5.1 Comparison of A. tigrinum Burrows

The burrows produced by *A. tigrinum* were found to be highly similar (1.0–0.8) to dissimilar (0.5–0.4) with an overall average similarity of 0.8 based upon the ten quantitative morphological characteristics used in the Bray–Curtis analysis (Table 13.3; Table A.3). The average level of similarity was highest (0.9–0.8) when burrows of the same morphology were compared with a range of 1.0–0.5 (Table 13.3). An exception to this was a single ramp (TS4-3-1) which was dissimilar (0.5) to three other ramps and only moderately similar (0.7–0.6) to all but one other ramp (Table A.3). This burrow had a nearly circular cross section (W/H = 1.0) and a low average slope (15°). When burrows of different morphologies were compared, the average level of similarity was lower (0.8–0.6) with a range of 1.0–0.4 (Table 13.3; Table A.3). In general, the level of similarity decreased with increasing complexity of the burrows; those burrows possessing branches (branched ramps, Y-shaped burrows) were found to be less similar to those without branches (ramps, U-, W-, J-shaped burrows). Y-shaped burrows in particular had relatively low levels of similarity (0.6) to the ramps, Y-, U-, and W-shaped burrows with several individual comparisons indicating dissimilarity (Table 13.3; Table A.3). Ramps, on the other hand, were highly similar (0.8) to U-, W-, and J-shaped burrows as were branched ramps and Y-shaped burrows (Table 13.3).
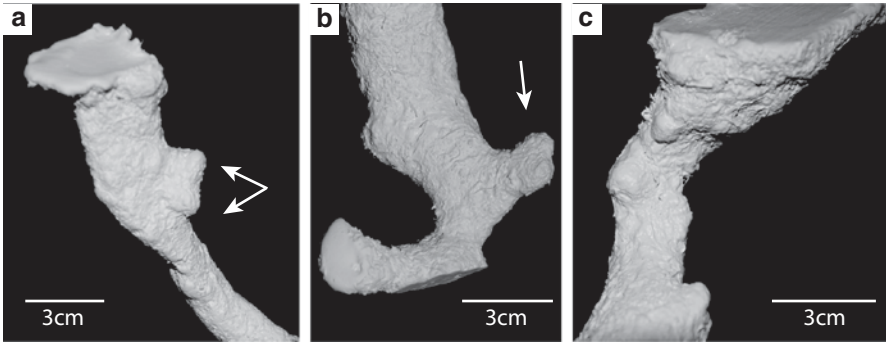
Fig. 13.12 Bioglyphs observed on burrows produced by *A. opacum*. Bilobate or heart-shaped bioglyphs exhibited on **a** the chamber of a ramp (MS4-1-1A) and **b** the shaft of the branched ramp (MS2-3-1). **c** Rounded bioglyphs on the shaft of a ramp (MS3-2-1)
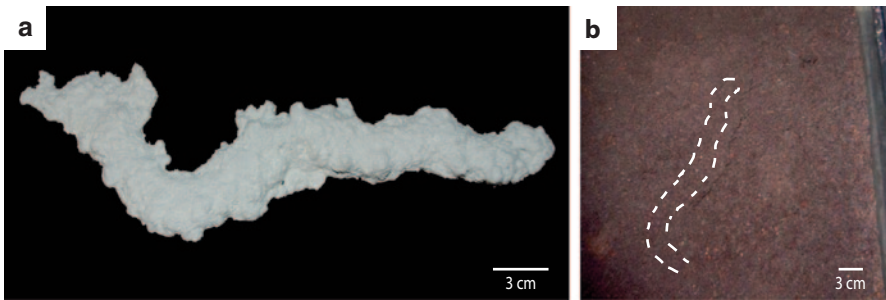
Fig. 13.13 A surface trail produced by *A. opacum.* **a** Underside of a plaster cast of a sinuous trail. **b** Trail (*outlined*) produced on the sediment surface

13.5.2 Comparison of A. opacum *Burrows*

Burrows produced by *A. opacum* were highly similar (1.0–0.8) to dissimilar (0.5–0.3) with an overall average similarity of 0.8 based upon the ten quantitative morphological characteristics used in the Bray–Curtis analysis (Table 13.3; Table A.4). The average level of similarity was highest (0.8) when burrows of the same morphology were compared with a range of 1.0–0.5 (Table 13.3). Exceptions to this included two ramps (MS4-2-2A and MS4-2-2B) which were dissimilar (0.5) to four and two other ramps, respectively (Table A.4). These two ramps had smaller average tunnel widths and heights and a lower slope than the others. Ramps and branched ramps were found to be dissimilar to each other with an average similarity of 0.5 and a range of 0.6–0.3 (Table 13.3; Table A.4). The inclusion of a branching angle and higher complexity were the primary differences.

	Width	Height	W:H Ratio	Openings	Length	Depth	Burrow Angle	Branching Angle	Tortuosity	Complexity
M-W	0.09	0.12	0.63	0.02	0.001	0.02	0.003	0.98	0.21	0.005
K-S	0.14	0.07	0.23	0.00002	0.007	0.006	0.007	0.0001	0.38	0.0001

Table 13.4 p values for the Mann–Whitney and Kolmogorov–Smirnov tests run between the quantitative burrow characteristics of *A. tigrinum* vs. *A. opacum*

13.5.3 Comparison of A. tigrinum and A. opacum Burrows

Burrows produced by *A. tigrinum* and *A. opacum* showed a wide range of similarities from high (1.0) to low (0.4) (Table A.5). On average, however, the 77 burrow casts produced by both species were found to be moderately similar (0.7) (Table 13.3). The highest levels of similarity were found between the ramp morphologies of both species (0.8) and between the Y-shaped burrows of *A. tigrinum* and the branched ramps of *A. opacum* (0.9) (Table 13.3). The ramps of *A. opacum* had the lowest levels of similarity (0.6–0.5) to the *A. tigrinum* burrows with branches (branched ramps, Y-shaped burrows). The *A. opacum* ramps were moderately similar (0.7) to the *A. tigrinum* U-, W-, and Y-shaped burrows. The branched ramps of *A. opacum* were dissimilar (0.5) to the ramps, U-, and W-shaped burrows of *A. tigrinum* and moderately similar (0.7–0.6) to the branched ramps and J-shaped burrows (Table 13.3).

While certain burrow morphologies were specific to each species, analysis of the burrow's quantitative measurements using Mann–Whitney and Kolmogorov–Smirnov tests indicated that the average width, height, width-to-height ratio, and tortuosity of all of the burrow casts of both species were similar with p values <0.05 (Table 13.4). The average values of each of these burrow properties are also similar between each species (Table 13.2). The median of the branching angles is similar between the burrows of the two species whereas the distribution is not similar (Table 13.4). Given that most (>90%) of the burrow casts of both species do not have branches, but those of *A. tigrinum* have a wider range of values, this is expected. The number of surface openings, total length, depth, average slope, and complexity of the burrow casts, however, were found to be different between the two species (Table 13.4). The average values of these burrow properties are also different between each species (Table 13.2). On average, burrows of *A. tigrinum* had more surface openings, were longer, deeper, had a greater slope, and a higher complexity than those of *A. opacum*. These differences are largely driven by the greater assortment of complex morphologies produced by *A. tigrinum*.

13.5.4 Environmental Controls on Burrow Morphology and Behavior

The quantitative properties of the burrows produced by both *A. tigrinum* and *A. opacum* were not found to have a strong correlation with variations in sediment composition, moisture content, or enclosure size (Table 13.5). The Spearman's rank

Table 13.5 Rs and associated *p* values for the Spearman's rank correlation tests run for eight of the quantitative properties of the burrows produced by *A. tigrinum* (T) and *A. opacum* (O) in comparison to: **a** Sediment composition. **b** Moisture content. **c** Enclosure size

			Width	Height	W:H ratio	Length	Depth	Burrow angle	Tortuosity	Complexity
a.	T	Rs	0.10	−0.20	0.33	0.19	0.19	0.04	0.20	0.21
		p	0.48	0.14	0.01	0.16	0.16	0.75	0.14	0.12
	O	Rs	0.07	−0.01	0.02	0.08	0.11	−0.16	−0.04	0.17
		p	0.73	0.96	0.92	0.70	0.63	0.47	0.85	0.44
b.	T	Rs	0.20	0.30	−0.03	0.19	0.10	0.06	−0.09	−0.08
		p	0.2	0.04	0.83	0.21	0.94	0.67	0.53	0.61
	O	Rs	−0.19	0.06	−0.13	−0.24	−0.37	−0.16	0.02	−0.17
		p	0.41	0.81	0.58	0.28	0.09	0.48	0.93	0.44
c.	T	Rs	−0.08	0.002	−0.19	0.09	0.10	−0.03	−0.31	−0.06
		p	0.59	0.99	0.21	0.55	0.52	0.86	0.04	0.70
	O	Rs	0.09	0.24	−0.05	0.01	0.05	−0.03	−0.15	−0.16
		p	0.68	0.28	0.81	0.96	0.81	0.88	0.52	0.48

Table 13.6 Rs and associated *p* values for the Spearman's rank correlation tests comparing burrow size to the body size of *A. tigrinum* (T) and *A. opacum* (O)

		L	W	H	W/H
T	Rs	0.33	0.29	0.21	0.07
	p	0.03	0.03	0.01	0.13
O	Rs	0.14	−0.28	−0.09	−0.03
	p	0.54	0.09	0.20	0.65

correlation yielded Rs values of −0.20–0.33 ($p=0.96$–0.01) for sediment composition, −0.37–0.30 ($p=0.94$–0.04) for sediment moisture, and −0.31–0.24 ($p=0.99$–0.04) for enclosure size (Table 13.5). None of the Rs values were near −1.0 or 1.0 indicating that there was no strong correlation between the three environmental parameters and the quantitative burrow properties.

While none of the experimental sediments prevented burrowing by either species, there were burrow morphologies only observed in sediments with specific compositions and moisture contents. Ramps produced by both *A. tigrinum* and *A. opacum* were produced in all sediment compositions and moisture levels. The Y- and J-shaped burrows of *A. tigrinum,* however, were only produced in the organic sediment. Branched ramps of both species were not produced in the sandy clay loam. The U- and W-shaped burrows of *A. tigrinum* were observed in situ in all sediment compositions and moisture levels, but were not successfully cast in the clay loam or in tanks with soil moistures of 54 %.

13.5.5   Body Size Versus Burrow Size

The widths, heights, width-to-height ratios, and lengths of the burrow casts of *A. tigrinum* and *A. opacum* were not found to have a strong correlation with these properties of the bodies of the trace-making salamanders. The Spearman's rank correlation yielded Rs values of −0.28–0.33 ($p=0.65$–0.01) for these four properties in both species (Table 13.6). None of the Rs values were near −1.0 or 1.0 indicating that there was no strong correlation between these dimensions of the burrows and the body of the tracemaker.

13.6   Discussion

13.6.1   Burrow Morphology and Tracemaker

The body plan of salamanders is, in general, not specialized for a fossorial lifestyle (Kley and Kearney 2007). Some members of the Amybstomatidae have modifications of the skull for burrowing, such as a flattening of the dorsal skull elements (Wake 1993), but other skeletal and muscular modifications have not been identified. This lack in specialized morphological adaptations has led to the general

acceptance that, while fossorial, most ambystomatid salamanders are not active bur-
rowers; they instead reside in leaf litter, in burrows of other organisms, or simply
enlarge cracks and holes that are already present in the soil (Semlitsch 1983). While
these experiments have shown that this may be true of *A. opacum,* it is not the case
for *A. tigrinum* which was observed actively excavating burrows regardless of the
presence or absence of cracks and holes on the sediment surface.

Regardless, both *A. tigrinum* and *A. opacum* produced permanent, open burrows
with similar morphologies and quantitative properties in these experiments. The
common burrow morphologies were not only produced by the same individuals, but
also by different individuals and in varying experimental conditions. Differences
in general burrow architecture are, therefore, attributed to variations in individual
behavior. While the burrow morphologies did not greatly vary between species,
the number of surface openings, lengths, depths, slopes, and complexities of the
burrows were found to be dissimilar. These dissimilar quantitative properties are re-
lated to differences in the level of architectural complexity of the burrows produced
by the two species. These differences are likely due to the different burrowing tech-
niques employed by each species as well as the behaviors exhibited while occupy-
ing the burrows. The consistency in the morphology of the burrows produced by the
different individuals and species of salamanders, however, suggests that salamander
burrows, or those of similar animals with similar behaviors, could be distinguished
from those of other tracemakers.

The results of these experiments have also reinforced that burrow size cannot
be relied upon for accurately determining the size of a tracemaker. The dimensions
of the burrows did not correlate to the dimensions of the individual tracemaker as
observed in some other burrowing animals (e.g., White 2005). The lengths, heights,
widths, and width-to-height ratios of the burrows of both species of salamanders
were consistently greater than those dimensions of the salamanders. The larger
cross-sectional diameters of the burrows are likely the result of the range of body
motion and burrowing techniques exhibited by the salamanders. Greater burrow
diameters allow for the accommodation of limb and head movements both during
initial excavation and later compaction of the burrow walls. The wider tunnels and
shafts also provide the salamanders the space needed to turn around inside their bur-
rows. Similar observations have been made with the burrows of millipedes (Hem-
bree 2009), scorpions (Hembree et al. 2012), and whip scorpions (Hembree 2013).
The width of the salamander's bodies was typically greater than their height, so the
elliptical cross-sectional shape, which was typical of the burrows produced, does
mirror the salamanders' elliptical body plan.

Well-preserved bioglyphs closely mirror the relative shape and size of the limbs
and head of the salamanders. These are best preserved in the burrows of *A. tigrinum.*
The bioglyphs were produced by the animal's head, forelimbs, and hind limbs as
it forced itself into the subsurface, compacting sediment around it along the way.
Bioglyphs observed on burrows produced by *A. opacum* are typically poorly ex-
pressed and are not similar to the size or shape of the salamander's limbs or head.
This is likely due to the weaker burrowing abilities of these salamanders. A few

well-preserved bilobate structures do, however, preserve the general size and shape of the trace-making salamander's head.

13.6.2   Burrow Morphology and Behavior

The burrows produced by both *A. tigrinum* and *A. opacum* served the same behavioral purposes. Burrowing techniques did differ between species, but this had no effect on the final behavioral purpose of the burrow or on the burrow's general architecture. Burrows of both species are commonly constructed for dwelling purposes, most importantly for protection from environmental conditions and predation (Gehlbach et al. 1969; Marangio and Anderson 1977, Semlitsch 1983). Burrows produced by both species were also observed allowing for a passive means of prey capture. Prey items typically found their way down into the burrows allowing the salamander to capture and eat the prey from the protective environment of their burrow. Burrows were typically constructed within 12 h of placing a salamander in an enclosure. Once burrows were produced, salamanders were seen only on rare occasions outside of their burrows. When the salamanders did come to the surface, it occurred during the 12-h dark period.

The simplest burrows produced by the salamanders were the ramps. These burrows are representative of typical dwelling burrows and provide the minimum protection necessary from predation and adverse environmental conditions such as extreme temperatures and dryness. Chambers present in burrows serve as both dwelling areas and as turn-around points. The burrows are typically not wide enough to allow the salamander to turn around or reorient themselves, therefore, chambers or enlarged sections are created within the burrow. Overall, burrow morphologies which terminated in a chamber occurred in terrariums in which the salamanders abandoned their burrows less often. More complex burrow morphologies seen in *A. tigrinum* such as U-, W-, and Y-shaped burrows express the same behaviors as the ramps. The extra elements of these burrows were produced over time from salamanders moving upwards through the sediment creating new tunnels, shafts, and surface openings in already existing ramps. Continued burrow modification was observed only rarely in *A. opacum* with the production of two branched ramps. More typically, once specimens of *A. opacum* completed a burrow it remained largely unchanged throughout the experiment. This difference is also a result of the weaker burrowing ability of *A. opacum.*

13.6.3   Burrow Morphology, Behavior, and Sediment Properties

Sediment composition, moisture content, and enclosure size appeared to have no effect on the quantitative properties of the burrows produced by *A. tigrinum* and *A. opacum*. Both *A. tigrinum* and *A. opacum* are generalist species which are capable of producing burrows with similar morphologies in a variety of sediment types and

soil environments. Burrows produced by both species in ideal conditions ranged from simple to complex and provided the individuals with the minimum cover necessary to protect themselves from external environmental conditions as well as predation. Lower moisture content as well as increased sand content decreased the cohesiveness of the sediment which, in turn, affected the behaviors of the salamanders expressed by a decrease in burrow complexity. Looser sediment would be expected to require more initial energy to compact and would also likely require the salamander to exert more energy throughout the habitation to keep the burrow open to the surface. As a result, only ramps were produced in these sediment types with the exception of one U-shaped burrow in sandy sediment and one branched ramp in the drier sediment.

13.7   Significance

13.7.1   Recognition of Salamander Burrows in the Fossil Record

The burrows created by *A. tigrinum* and *A. opacum* are representative of dwelling (domichnia) behaviors. In particular, the terminal chambers common in both species' burrows along with extended periods of inhabitance allow these burrows to be classified as domichnia. Surface trails observed in tanks of *A. opacum* are representative of locomotion (repichnia).

Architecture Burrow morphologies produced by *A. tigrinum* and *A. opacum* consist of vertical to subhorizontal ramps, with and without chambers and branches, as well as U-, W-, J-, and Y-shaped burrows. Burrows produced by both species consist of one, two, or three surface openings.

Overall Shape Burrow shafts, tunnels, and chambers are elliptical in cross section. Tunnels and shafts have widths that are commonly 1.5–2.0 times wider than they are high. Laterally expansive chambers may be present or absent. Chambers are approximately 1 cm wider than the associated tunnel or shaft.

Orientation Burrows range from rarely subhorizontal (11–15°), most commonly subvertical (20–70°), rarely near vertical (70–89°) to vertical (90°) with an average burrow orientation of 52°.

Internal Structure Burrows exhibit no visible lining and irregular burrow walls. Burrow fill is passive and often due to collapse of the burrow's opening that occurs during or after burrow abandonment.

Bioglyphs Burrows exhibit common, but scattered, rounded, elongate, or bilobate shaped protrusions of varying sizes extending off of the surface of the burrow.

13.7.2   *Paleontological and Paleoecological Significance*

Burrows produced by *A. tigrinum* and *A. opacum* have a moderate preservation potential. Deeper tier burrows have greater chances of preservation and the shallow nature of burrows produced by both salamander species decreases the burrows' chances of being preserved. In addition, both types of salamander produced burrows with no discernible lining. Linings are not found in all fossilized burrows and are not necessary for preservation, but they do increase the burrow's potential to be preserved and recognized. Preservation potential is increased by the fact that burrow openings were maintained by both species throughout habitation. Individuals were not observed maintaining the burrows, but the walls were continuously compacted and the burrow kept open through the animal's movements. Small-scale mounds and surface trails also have the potential to be preserved, but these would all require rapid sedimentation. Infilling of open burrows with sediment of a contrasting lithology would also aid in recognition due to the lack of a lining. This process could be common in the floodplains which salamanders typically inhabit.

Burrows of vertebrates are typically viewed as structures with large diameters (≥ 2 cm) and complex, branching networks (e.g., Miller et al. 2001; Hasiotis et al. 2004). While diameters of the burrows produced by *A. tigrinum* and *A. opacum* are commonly greater than 2 cm, small (1–2 cm) diameter burrows were produced. In addition, the majority (90 %) of the burrows produced by both species were simple ramps characterized by a single burrow opening, a single tunnel or shaft, and, in some, a single chamber. This study illustrates, therefore, that small diameter burrows with simple morphologies can be produced by vertebrates.

The body fossil record of salamanders is improving, but fossilized salamanders are poorly represented in the pre-Cenozoic record (Evans et al. 1988). Considering the abundance of extant, fossorial, salamander species, their widespread geographic range, and relatively long fossil record extending to the Jurassic (Holman 2006), fossilized salamander burrows should be moderately abundant. The ability to recognize salamander burrows from those of other tracemakers in the fossil record could aid in gaining a better understanding of the abundance and diversity of salamanders and their associated ecosystems, especially in the body fossil poor pre-Cenozoic. Salamanders are abundant, mid-level predators that play an important role in modern ecosystem processes (Davic and Welsh 2004). Salamander density in a variety of forested habitats ranging from New Hampshire to California has been estimated to be between 2,950 and 10,000 salamanders/ha (Burton and Likens 1975; Hairston 1987; Welsh and Lind 1992; Petranka et al. 1993; Stebbins and Cohen 1995). Salamanders play a critical role in these ecosystems and are often the dominant vertebrate predator (Hairston 1987). The absence of recorded salamander burrows is likely due to the inability to recognize such burrows or the misinterpretation of salamander burrows as those of other organisms. Salamander burrows would be representative of hidden biodiversity in areas generally devoid of body fossils. Uncovering such hidden biodiversity through trace fossils would allow for a more thorough interpretation of the ecology of the environment in question.

13.7.3 Paleopedological and Paleoenvironmental Significance

Burrows produced by the salamanders were restricted to the top 18 cm of the sediment, corresponding to the upper surface of most soils (A and upper B horizons); however, there are reports of individuals of both species being found at depths of a meter or more below the surface (Gruberg and Stirling 1972). It is possible that larger amphibians could create burrows at even greater depths. Observation of the salamanders' burrowing techniques and burrows in the laboratory has indicated that both species play a role in pedogenesis. Burrowing by both species has the potential to alter the soil through the destruction of sedimentary structures, the formation and destruction of peds, and through sediment mixing.

Small-scale mounds, which are evidence of sediment mixing, were observed on numerous occasions in terrariums occupied by *A. tigrinum* which utilized excavation as a burrowing method. Mixed soil is vital in the germination process of many plants whose seeds rely on bioturbated soils (Schaetzl and Anderson 2009). Excavation by *A. tigrinum* during initial burrow creation loosened sediment at and just below the surface. Compression of sediment, which was exhibited by both salamanders, increased the compaction and decreased the porosity and permeability of the sediment directly surrounding the burrows. Open and permanent burrows produced by the salamanders then serve as conduits which aid in the rapid downward movement of water and oxygen through the soil profile. As water moves downward, dissolution of minerals occurs, as well as the movement of dissolved ions and organics. The open burrows also allow for the upward movement of water through the soil profile through evapotranspiration, which is essential to plant growth (Schaetzl and Anderson 2009). Even when filled, sediment within the burrows continues to allow for the movement of fluids throughout the soil profile; the sediment which passively fills the burrows is typically looser than the surrounding sediment and has a greater porosity and permeability.

Along with downward movement of organics from the surface, alteration of the soil occurred through the direct addition of organics by the salamanders. Fecal material was rarely found at the surface of the enclosures, indicating defecation often took place within burrows. Individuals of *A. tigrinum* were directly observed excreting waste in their burrows. Remnants of prey animals were also observed within the burrows. The addition of organics to the soil provides nutrients for both soil microorganisms and plants.

Salamander burrows found in the fossil record would be indicative of a terrestrial, continental paleoenvironment. The hygrophilic nature of salamanders indicates that their burrows would be found in fairly moist soils within the vadose zone. Fossil salamander burrows are likely to be found in a wide array of soil types ranging from Entisols to, less likely, Aridisols. These burrows would be found in conjunction with traces produced by various soil invertebrates, plants, and possibly other vertebrates. Fossil root traces would likely be the most common trace found in conjunction with fossil salamander burrows.

13.8 Conclusions

Each species of salamander produced a morphologically consistent set of burrows which, despite architectural differences, were largely similar to each other. Burrows produced by *A. tigrinum* and *A. opacum* included two common morphologies, the ramp and branched ramp. Specimens of *A. tigrinum* also produced J-, U-, W-, and Y-shaped burrows. Differences in quantitative properties of the burrows produced by the two species were largely a result of the greater complexity and size of the *A. tigrinum* burrows. These dissimilarities were related to differences in burrowing techniques and behaviors associated with the burrows. The ramp morphologies of both species, however, were considered highly similar. The consistency in the morphology of the burrows produced by the two salamander species suggests that these burrow casts may be used as analogs for assessing potential tracemakers of fossil burrows.

Overall, sediment composition, moisture content, and enclosure size were found to have little effect on the properties of the burrows produced by either species. The lack of correlation between the quantifiable burrow properties and the environmental controls suggests that these properties are primarily controlled by the tracemakers morphology and behavior. This indicates that these burrow morphologies can be attributed to salamanders in a variety of environments.

The use of modern analogs is necessary in ichnology order to understand the potential burrow morphologies that different animals can produce and how that morphology can be affected by variations in environmental conditions. Having a defined set of burrow morphologies that can be attributed to specific groups of animals makes more accurate interpretations of burrowing methods, behaviors, and potential tracemakers possible. The results of this laboratory study of the burrowing behavior of *A. tigrinum* and *A. opacum* will aid in the identification of fossil burrows produced by ancient salamanders or amphibians with similar body types.

Appendix

Table A.1 Detailed measurements of burrows produced by *A. tigrinum*

ID	M	SO	MD	TL	Max W	Min W	Avg W	Max H	Min H	Avg H	W/H	Max S	Min S	Avg S	BA	C	T	TS	SC	SM	SP
TS3-2-1B	R	1	5.8	9.8	3.3	1.2	2.1	2.2	1.1	1.5	1.4	35.0	35.0	35.0	0	2	1.5	38	50O/50C	74	TS3
TS3-3-1(T)	R	1	9.3	19.5	5.0	1.6	3.5	3.1	1.6	2.4	1.5	67.0	67.0	67.0	0	2	1.3	38	75O/25C	54	TS3
TS3-3-2B	R	1	4.0	11.3	4.1	1.9	3.2	2.8	1.6	2.1	1.5	31.0	31.0	31.0	0	2	1.3	38	75O/25C	94	TS3
TS4-1-1A	R	1	7.5	9.0	2.1	0.9	1.7	1.7	1.1	1.5	1.1	64.0	64.0	64.0	0	2	1.2	38	75O/25C	74	TS4
TS4-3-1	R	1	9.7	12.0	3.3	2.3	2.7	3.3	1.9	2.6	1.0	15.0	15.0	15.0	0	2	1.3	38	75O/25C	54	TS4
TS5-1-1A	R	1	9.8	13.0	4.5	2.9	3.8	3.4	2.6	2.8	1.4	53.0	53.0	53.0	0	2	1.1	246	75O/25C	74	TS5
TS5-1-1B	R	1	12.4	15.5	3.5	2.4	2.9	2.5	1.3	1.9	1.5	65.0	65.0	65.0	0	2	1	246	75O/25C	74	TS5
TS5-2-2D	R	1	8.7	12.5	3.6	2.3	3.0	3.2	1.5	2.2	1.4	62.0	62.0	62.0	0	2	1.3	246	50O/25C/25S	74	TS5
TS6-1-1G	R	1	5.2	10.0	3.0	2.1	2.7	2.0	1.5	1.8	1.5	40.0	40.0	40.0	0	2	1.6	246	75O/25C	74	TS6
TS6-1-1H	R	1	4.2	11.3	2.5	2.0	2.2	2.6	1.6	2.0	1.1	40.0	40.0	40.0	0	2	1.3	246	75O/25C	74	TS6
TS6-3-1(T)	R	1	4.7	20.9	3.5	1.1	2.2	2.6	1.2	1.8	1.2	52.0	52.0	52.0	0	2	1.1	246	75O/25C	54	TS6
TS6-3-2	R	1	4.6	17.0	3.2	1.8	2.4	2.1	1.5	1.6	1.5	34.0	34.0	34.0	0	2	1.5	246	75O/25C	94	TS6
TS7-2-1	R	1	8.5	11.0	3.6	2.3	2.9	2.5	1.6	2.0	1.5	75.0	75.0	75.0	0	2	1.3	114	50O/50C	74	TS7
TS7-2-2	R	1	8.5	11.7	3.3	2.5	3.0	2.7	1.4	1.8	1.7	64.0	64.0	64.0	0	2	1.2	114	50O/25C/25S	74	TS7
TSB1	R	1	9.6	16.1	4.2	2.1	3.1	3.1	1.6	2.2	1.4	57.0	57.0	57.0	0	3	1.1	38	100O	80	TS1
TS2-1-2	R	1	14.0	17.5	3.9	1.6	3.0	2.2	1.2	2.0	1.5	52.0	52.0	52.0	0	3	1.5	114	75O/25C	74	TS2
TS2-2-1(T)	R	1	8.9	21.9	4.1	1.5	3.1	2.9	1.6	2.0	1.6	36.0	36.0	36.0	0	3	1.3	114	50O/50C	74	TS2
TS2-2-2	R	1	5.4	18.0	4.4	1.2	3.2	2.1	1.5	1.9	1.7	37.0	37.0	37.0	0	3	1.6	114	50O/25C/25S	74	TS2
TS2-3-1	R	1	9.0	26.0	5.3	3.1	3.9	2.8	1.7	2.4	1.6	51.0	51.0	51.0	0	3	1.4	114	75O/25C	54	TS2
TS2-3-2	R	1	12.0	16.5	4.3	2.6	3.3	3.1	1.8	2.2	1.5	63.0	63.0	63.0	0	3	1.2	114	75O/25C	94	TS2
TSB3	R	1	18.4	15.0	4.0	2.1	3.3	2.4	1.5	2.1	1.6	61.0	61.0	61.0	0	3	1.2	114	100O	80	TS2
TSB7	R	1	10.1	15.0	4.2	2.4	3.4	3.1	1.9	2.4	1.4	66.0	66.0	66.0	0	3	1.2	114	100O	80	TS2
TS3-1-2B	R	1	8.3	14.0	5.0	1.9	3.2	2.5	1.7	2.0	1.6	50.0	50.0	50.0	0	3	1.4	38	75O/25C	74	TS3
TS3-2-1A	R	1	5.2	16.0	4.9	1.5	3.8	2.6	1.4	2.1	1.8	35.0	35.0	35.0	0	3	1.7	38	50O/50C	74	TS3
TS3-3-2A	R	1	12.0	16.0	4.5	2.9	3.9	3.0	1.7	2.5	1.6	90.0	10.0	43.0	0	3	1.4	38	75O/25C	94	TS3
TSB2	R	1	7.1	15.7	5.1	2.4	3.7	3.1	1.8	2.4	1.5	45.0	45.0	45.0	0	3	1.1	38	100O	80	TS3
TS4-1-1C	R	1	9.8	14.0	4.0	1.7	3.0	2.4	1.1	2.0	1.5	65.0	65.0	65.0	0	3	1.4	38	75O/25C	74	TS4
TS4-1-2	R	1	11.2	18.0	3.4	2.0	2.8	2.4	1.4	1.9	1.5	89.0	89.0	89.0	0	3	1.2	38	75O/25C	74	TS4

Table A.1 (continued)

ID	M	SO	MD	TL	Max W	Min W	Avg W	Max H	Min H	Avg H	W/H	Max S	Min S	Avg S	BA	C	T	TS	SC	SM	SP
TS4-2-1	R	1	4.8	11.5	4.4	2.4	3.5	2.6	1.9	2.3	1.5	45.0	45.0	45.0	0	3	1.5	38	50O/50C	74	TS4
TS4-2-2(T)	R	1	14.0	15.0	3.7	1.2	2.9	2.4	1.6	1.9	1.5	85.0	85.0	85.0	0	3	1.2	38	50O/25C/25S	74	TS4
TS5-1-2(T)	R	1	11.7	15.0	4.1	1.5	3.0	2.7	1.9	2.3	1.3	55.0	55.0	55.0	0	3	1	246	75O/25C	74	TS5
TS5-2-1(T)	R	1	11.2	24.0	4.4	2.1	3.2	3.7	1.9	2.4	1.3	56.0	56.0	56.0	0	3	1.3	246	50O/50C	74	TS5
TS5-2-2C	R	1	6.1	12.0	4.0	1.9	3.1	2.6	1.6	2.1	1.5	52.0	52.0	52.0	0	3	1.3	246	50O/25C/25S	74	TS5
TS5-3-1	R	1	10.1	15.7	4.0	3.1	3.6	2.9	2.1	2.5	1.4	58.0	58.0	58.0	0	3	1.1	246	75O/25C	54	TS5
TS5-3-2	R	1	14.7	18.5	4.6	2.8	3.6	2.8	2.1	2.4	1.5	67.0	67.0	67.0	0	3	1.1	246	75O/25C	94	TS5
TS6-1-1C	R	1	10.0	13.5	3.5	2.4	3.0	2.3	1.6	2.0	1.5	66.0	66.0	66.0	0	3	1.2	246	75O/25C	74	TS6
TS6-2-1B	R	1	11.2	20.0	3.7	1.4	2.7	2.4	1.4	1.9	1.4	53.0	53.0	53.0	0	3	1.2	246	50O/50C	74	TS6
TS6-2-2	R	1	11.7	18.8	4.4	1.0	3.0	2.2	1.2	1.8	1.7	82.0	82.0	82.0	0	3	1.3	246	50O/25C/25S	74	TS6
TS7-1-1	R	1	12.4	16.1	4.2	1.0	2.7	3.4	1.1	1.9	1.4	64.0	64.0	64.0	0	3	1.1	114	75O/25C	74	TS7
TS7-1-2	R	1	10.0	12.1	3.0	2.2	2.5	2.4	1.8	2.1	1.2	65.0	65.0	65.0	0	3	1.2	114	75O/25C	74	TS7
TS7-3-1	R	1	11.9	16.5	3.8	2.3	3.0	2.9	1.5	2.1	1.4	60.0	60.0	60.0	0	3	1.2	114	75O/25C	54	TS7
TS6-2-1A	BR	1	10.1	19.4	4.0	2.2	2.9	2.7	1.3	1.9	1.5	68.0	68.0	68.0	52	5	1.8	246	50O/50C	74	TS6
TS3-1-1	U	2	6.3	19.0	4.7	3.2	4.2	2.5	1.9	2.3	1.8	35.0	30.0	32.5	0	3	1.5	38	75O/25C	74	TS3
TS3-2-2	U	2	4.1	14.2	4.1	2.6	3.5	2.1	1.2	2.0	1.8	43.0	20.0	31.5	0	3	2.8	38	50O/25C/25S	74	TS3
TS6-1-1E	U	2	4.0	16.0	4.2	2.4	3.3	3.8	2.0	3.1	1.1	60.0	15.0	37.5	0	3	1.1	246	75O/25C	74	TS6
TS6-1-2	U	2	4.9	12.2	3.4	1.8	2.9	3.3	1.7	2.2	1.3	80.0	67.0	73.5	0	3	1.7	246	75O/25C	74	TS6
TS2-1-1	W	3	7.1	30.5	3.3	1.5	2.4	3.9	1.3	2.1	1.1	90.0	45.0	65.0	0	5	1.6	114	75O/25C	74	TS2
TS4-3-2	W	3	3.5	23.0	3.9	1.7	2.6	2.7	1.5	1.9	1.4	86.0	41.0	58.0	0	5	1.7	38	75O/25C	94	TS4
TSB4	W	2	7.9	34.0	4.8	2.0	3.5	3.7	1.7	2.5	1.4	87.0	50.0	68.5	35	5	1.7	38	100O	80	TS3
TS3-1-2A	W	3	7.5	29.5	4.0	1.6	2.9	4.0	1.9	2.3	1.3	80.0	33.0	56.5	0	6	2.5	38	75O/25C	74	TS3
TSB9	J	1	16.7	27.0	3.7	1.7	2.5	2.3	1.3	1.7	1.5	62.0	62.0	62.0	0	2	2.5	114	100O	80	TS2
TSB5	Y	2	9.6	23.6	3.8	2.4	3.1	2.5	1.5	1.9	1.6	48.0	36.0	42.0	90	4	1.3	114	100O	80	TS2
TSB6	Y	3	12.4	25.2	3.4	1.8	2.6	2.1	1.2	1.8	1.4	74.0	50.0	64.7	90	7	2	114	100O	80	TS2
TSB8	Y	2	10.2	23.0	3.7	1.8	3.0	2.4	1.4	1.9	1.6	63.0	59.0	61.0	90	5	1.9	114	100O	80	TS2

BA branching angle, *C* complexity, *H* height (maximum, minimum, average), *ID* burrow cast number, *M* burrow morphology, *MD* maximum depth, *S* slope (maximum, minimum, average), *SC* sediment composition, *SM* sediment moisture, *SO* number of surface openings, *SP* salamander specimen number, *T* tortuosity, *TL* total length, *TS* tank size, *W* width (maximum, minimum, average), *W/H* width-to-height ratio

Table A.2 Detailed measurements of burrows produced by *A. opacum*

ID	M	SO	MD	TL	Max W	Min W	Avg W	Max H	Min H	Avg H	W/H	Max S	Min S	Avg S	BA	C	T	TS	SC	SM	SP
MS1-1-1	R	1	5.0	6.0	3.8	2.4	3.4	3.2	2	2.4	1.4	26	26	26	0	2	1.1	246	75O/25C	74	MS1
MS1-2-1	R	1	9.1	14.0	3.8	1.8	3.0	4.5	1.0	2.6	1.2	83	83	83	0	2	1.5	246	500/50C	74	MS1
MSB1	R	1	5.5	18.8	3.3	2.4	3.3	5.4	1.4	2.7	1.2	30	30	30	0	2	1.3	38	100O	80	MS1
MS2-1-1	R	1	7.1	10.0	3.7	2.9	3.5	2.6	2.1	2.4	1.5	37	37	37	0	2	1.3	38	75O/25C	74	MS2
MS2-1-2	R	1	5.8	16.5	3.4	2.6	3.0	2.0	1.2	1.6	1.9	55	55	55	0	2	1.5	38	75O/25C	74	MS2
MS3-1-1	R	1	7.1	10.4	3.1	2.8	3.0	2.5	1.3	1.9	1.6	45	45	45	0	2	1.1	114	75O/25C	74	MS3
MS3-1-2	R	1	10.2	16.5	3.4	2.3	2.7	2.0	1.2	1.7	1.6	40	40	40	0	2	1.1	114	75O/25C	74	MS3
MS3-3-1	R	1	5.0	13.0	3.2	2.1	2.7	2.1	1.8	1.9	1.4	20	20	20	0	2	1.4	114	75O/25C	54	MS3
MS3-3-2	R	1	3.5	10.0	2.8	2.3	2.5	2.2	1.5	1.9	1.3	22	22	22	0	2	1.3	114	75O/25C	94	MS3
MS4-1-2	R	1	4.6	13.0	2.9	1.5	2.5	2.3	1.4	1.9	1.3	41	41	41	0	2	1.9	38	75O/25C	74	MS4
MS4-2-1	R	1	5.5	10.0	3.4	2.4	3.1	1.9	1.3	1.7	1.8	30	30	30	0	2	1.0	38	500/50C	74	MS4
MS4-2-2A	R	1	14.3	17.0	2.5	1.8	2.1	1.6	1.3	1.5	1.4	11	11	11	0	2	1.1	38	500/25C/25S	74	MS4
MS4-2-2B	R	1	4.5	5.5	3.1	2.4	2.7	2.2	1.3	1.6	1.7	25	25	25	0	2	0.9	38	500/25C/25S	74	MS4
MS4-3-1	R	1	4.4	10.0	3.1	2.4	2.9	2.8	2.0	2.3	1.3	45	45	45	0	2	1.4	38	75O/25C	54	MS4
MS4-3-2	R	1	9.8	9.7	3.3	1.9	2.7	2.4	1.5	1.9	1.4	78	78	78	0	2	1.0	38	75O/25C	94	MS4
MS2-2-1	R	1	7.5	9.5	3.4	2.6	2.9	2.6	1.1	1.9	1.5	27	27	27	0	3	1.2	38	500/50C	74	MS2
MS2-2-2	R	1	5.2	12.0	4.0	2.6	3.2	2.6	1.8	2.3	1.4	48	48	48	0	3	1.3	38	500/25C/25S	74	MS2
MS3-2-1	R	1	7.7	11.0	3.5	1.8	2.5	2.2	1.5	1.7	1.5	63	63	63	0	3	1.1	114	500/50C	74	MS3
MS3-2-2	R	1	7.6	15.0	3.8	1.9	3.0	3.0	1.4	2.0	1.5	55	55	55	0	3	1.4	114	500/25C/25S	74	MS3
MS4-1-1A	R	1	14.6	24.0	3.4	1.5	2.5	3.6	1.2	1.9	1.3	90	5	51	0	3	1.3	38	75O/25C	74	MS4
MS4-1-1B	R	1	8.1	14.0	3.9	1.7	2.8	3.6	1.2	2.3	1.2	83	83	83	0	3	1.4	38	75O/25C	74	MS4
MS2-3-1	BR	1	4.5	20.0	3.4	1.5	2.4	2.7	0.9	1.7	1.4	31	31	31	90	4	2.1	38	75O/25C	54	MS2
MS2-3-2	BR	1	6.8	9.0	2.6	2.6	3.3	3.1	1.4	2.0	1.7	43	43	43	90	4	1.2	38	75O/25C	94	MS2

BA branching angle, *C* complexity, *H* height (maximum, minimum, average), *ID* burrow cast number, *M* burrow morphology, *S* slope (maximum, minimum, average), *SC* sediment composition, *SM* sediment moisture, *SO* number of surface openings, *SP* salamander specimen number, *T* tortuosity, *TL* total length, *TS* tank size, *W* width (maximum, minimum, average), *W/H* width-to-height ratio

Table A.3 Bray–Curtis similarity index tables showing relative levels of similarity of burrows of *A. tigrinum*

Table A.4 Bray–Curtis similarity index tables showing relative levels of similarity of burrows of *A. opacum*

Table A.5 Bray–Curtis similarity index tables showing relative levels of similarity between burrows of *A. tigrinum* and *A. opacum*

References

Anderson JD, Graham RE (1967) Vertical migration and stratification of larval *Ambystoma*. Copeia 1967:371–374

Anderson JS, Henrici AC, Sumida SS, Martens T, Berman DS (2008) *Georgenthalia clavinasica*, a new genus and species of dissorophoid temnospondyl from the Early Permian of Germany, and the relationships of the family Amphibamidae. J Vertebr Paleontol 28:61–75

Brand LR (1996) Variations in salamander trackways resulting from substrate differences. J Pale-
   ontol 70:1004–1010

Brand LR, Tang T (1991) Fossil vertebrate footprints in the Coconino Sandstone (Permian) of
   northern Arizona: evidence for underwater origin. Geology 19:1201–1204

Bray JR, Curtis JT (1957) An ordination of the upland forest communities of southern Wisconsin.
   Ecol Mon 27:326–349

Bromley RG (1996) Trace fossils: biology, taphonomy, and applications. Chapman and Hall, New
   York

Burton TM, Likens GE (1975) Salamander populations and biomass in the Hubbard Brook experi-
   mental forest, New Hampshire. Copeia 1975:541–546

Church SA, Kraus JM, Mitchell JC, Church DR, Taylor DR (2003) Evidence for multiple Pleisto-
   cene refugia in the postglacial expansion of the eastern tiger salamander, *Ambystoma tigrinum
   tigrinum*. Evolution Int J org Evolution 57:372–383

Counts JW, Hasiotis ST (2009) Neoichnological experiments with masked chafer beetles (Cole-
   optera: Scarabaeidae): implications for backfilled continental trace fossils. Palaios 24:74–91

Davic RD, Welsh HH Jr (2004) On the ecological role of salamanders. Annu Rev Ecol Syst
   35:405–434

Davis RB, Minter NJ, Braddy SJ (2007) The neoichnology of terrestrial arthropods. Palaeogeogr
   Palaeocl 255:284–307

Deocampo DM (2002) Sedimentary structures generated by *Hippopotamus amphibius* in a lake-
   margin wetland, Ngorongoro Crater, Tanzania. Palaios 17:212–217

Evans SE, Milner AR, Mussett F (1988) The earliest known salamanders (Amphibia, Caudata): a
   record from the Middle Jurassic of England. Geobios 21:539–552

Frey RW (1970) Environmental significance of recent marine Lebensspuren near Beaufort, North
   Carolina. J Paleontol 44:507–519

Frey RW (1968) The Lebensspuren of some common marine invertebrates near Beaufort, North
   Carolina. I. Pelecypod burrows. J Paleontol 42:570–574

Frey RW, Curran HA, Pemberton SG (1984) Tracemaking activities of crabs and their environ-
   mental significance: the ichnogenus *Psilonichnus*. J Paleontol 58:333–350

Gaillard C (1991) Recent organism traces and ichnofacies on the deep-sea floor off New Caledo-
   nia, southwestern Pacific. Palaios 6:302–315

Gardner JD (2001) Monophyly and affinities of albanerpetontid amphibians (Temnospondyli; Lis-
   samphibia). Zool J Linnean Soc 131:309–352

Gehlbach FR, Kimmel JR, Weems WA (1969) Aggregations and body water relations in tiger
   salamanders (*Ambystoma tigrinum*) from the Grand Canyon Rims, Arizona. Physiol Zool
   42:173–182

Genise JF, Ricardo N, Melchor RN, Archangelsky M, Bala LO, Straneck R, Valais S (2009) Appli-
   cation of neoichnological studies to behavioural and taphonomic interpretation of fossil bird-
   like tracks from lacustrine settings: the Late Triassic-Early Jurassic? Santo Domingo Forma-
   tion, Argentina. Palaeogeogr Palaeocl 272:143–161

Gingras MK, MacEachern JA, Pickerill RK (2004) Modern perspectives on the *Teredolites* ichno-
   facies. Observations from Willapa Bay, Washington. Palaios 19:79–88

Gingras MK, Pickerill R, Pemberton SG (2002) Resin cast of modern burrows provides analogs
   for composite trace fossils. Palaios 17:206–211

Groenewald GH, Welman J, MacEachern JA (2001) Vertebrate burrow complexes from the Early
   Triassic Cynognathus Zone (Driekoppen Formation, Beaufort Group) of the Karoo Basin,
   South Africa. Palaios 16:148–160

Gruberg ER, Stirling RV (1972) Observations on the burrowing habits of the tiger salamander
   (*Ambystoma tigrinum*). Herpetol Rev 4:85–89

Hairston NGS (1987) Community ecology and salamander guilds. Cambridge University Press,
   Cambridge

Halfen AF, Hasiotis ST (2010) Neoichnological study of the traces and burrowing behaviors of
   the western harvester ant *Pogonomyrmex occidentalis* (Insecta: Hymenoptera: Formicidae):
   paleopedogenic and paleoecological implications. Palaios 25:703–720

Hasiotis ST (2002) Continental trace fossils. Society for Sedimentary Geology, Tulsa

Hasiotis ST (2007) Continental ichnology: fundamental processes and controls on trace fossil distribution. In: Miller IIIW (ed) Trace fossils: concepts, problems, prospects. Elsevier, Amsterdam, pp 268–284

Hasiotis ST, Mitchell CE (1993) A comparison of crayfish burrow morphologies: Triassic and Holocene fossil, paleo- and neo-ichnological evidence, and the identification of their burrowing signatures. Ichnos 2:291–314

Hasiotis ST, Wellner RW, Martin AJ, Demko TM (2004) Vertebrate burrows from Triassic and Jurassic continental deposits of North America and Antarctica: their paleoenvironmental and paleoecological significance. Ichnos 11:103–124

Hasiotis ST, Platt B, Hembree DI, Everhart M, Miller W (2007) The trace-fossil record of vertebrates. In: Miller IIIW (ed) Trace fossils: concepts, problems, prospects. Elsevier, Amsterdam, pp 196–218

Hembree DI (2009) Neoichnology of burrowing millipedes: understanding the relationships between ichnofossil morphology, behavior, and sediment properties. Palaios 24:425–439

Hembree DI (2013) Neoichnology of the whip scorpion *Mastigoproctus giganteus*: complex burrows of predatory terrestrial arthropods. Palaios 28:141–162

Hembree DI, Hasiotis ST (2006) The identification and interpretation of reptile ichnofossils in paleosols through modern studies. J Sediment Res 76:575–588

Hembree DI, Hasiotis ST (2007) Biogenic structures produced by sand-swimming snakes: a modern analog for interpreting continental ichnofossils. J Sediment Res 77:389–397

Hembree DI, Hasiotis ST (2008) Miocene vertebrate and invertebrate burrows defining compound paleosols in the Pawnee Creek Formation, Colorado, U.S.A. Palaeogeogr Palaeocl 270:349–365

Hembree DI, Johnson LM, Tenwalde RW (2012) Neoichnology of the desert scorpion *Hadrurus arizonensis*: burrows to biogenic cross lamination. Palaeontol Electron 15:1–34

Hertweck G, Wehrmann A, Liebezeit G (2007) Bioturbation structures of polychaetes in modern shallow marine environments and their analogues to *Chondrites* group traces. Palaeogeogr Palaeocl 245:382–389

Holman JA (2006) Fossil salamanders of North America. Indiana University Press, Bloomington

Kley N, Kearney M (2007) Adaptation to digging and burrowing. In: Hall BK (ed) Fins into limbs. University of Chicago Press, Chicago, pp 284–309

Lockley MG, Hunt AP, Meyer C (1994) Vertebrate tracks and the ichnofacies concept: implications for paleoecology and palichnostratigraphy. In: Donovan SK (ed) The paleobiology of trace fossils. Wiley, New York, pp 241–268

Maddin HC, Olori JC, Anderson JS (2011) A redescription of *Carrolla craddocki* (Lepospondyli: Brachystelechidae) based on high-resolution CT, and the impacts of miniaturization and fossoriality on morphology. J Morphol 272:722–743

Marangio MS, Anderson JD (1977) Soil moisture preference and water relations of the marbled salamander, *Ambystoma opacum* (Amphibia, Urodela, Ambystomatidae). J Herpetol 22:169–176

Martin AJ (2006) Resting traces of *Ocypode quadrata* associated with hydration and respiration. Sapelo Island, Georgia, USA. Ichnos 13:57–67

Meadows PS (1991) The environmental impact of burrows and burrowing animals—conclusions and a model. In: Meadows PS, Meadows A (eds) The environmental impact of burrowing animals and animal burrows. Clarendon Press, Oxford, pp 327–338

Melchor RN, Genise JF, Umazano AM, Superina M (2012) Pink fairy armadillo meniscate burrows and ichnofabrics from Miocene and Holocene interdune deposits of Argentina: palaeoenvironmental and palaeoecological significance. Palaeogeogr Palaeocl 350–352:149–170

Miller MF, Hasiotis ST, Babcock LE, Isbell JL, Collinson JW (2001) Tetrapod and large burrows of uncertain origin in Triassic high paleolatitude floodplain deposits, Antarctica. Palaios 16:218–232

Pearson NJ, Gingras MK, Armitage IA, Pemberton SG (2007) Significance of Atlantic sturgeon feeding excavations, Mary's Point, Bay of Fundy, New Brunswick, Canada. Palaios 22:457–464

Petranka JW, Eldridge ME, Haley KE (1993) Effects of timber harvesting on southern Appalachian salamanders. Conserv Biol 7:363–370

Romer AS, Olson EC (1954) Aestivation in a Permian lungfish. Brevoria 30:1–8

Schaetzl R, Anderson S (2009) Soils: genesis and geomorphology. Cambridge University Press, Cambridge

Seike K, Nara M (2007) Occurrence of bioglyphs on *Ocypode* crab burrows in a modern sandy beach and its palaeoenvironmental implications. Palaeogeogr Palaeocl 252:458–463

Semlitsch RD (1983) Burrowing ability and behavior of salamanders of the genus *Ambystoma*. Can J Zool 61:616–620

Smith JJ, Hasiotis ST (2008) Traces and burrowing behaviors of the cicada nymph *Cicadetta calliope*: neoichnology and paleoecological significance of extant soil-dwelling insects. Palaios 23:503–513

Stebbins RC, Cohen N (1995) A natural history of amphibians. Princeton University Press, Princeton

Vitt LJ, Caldwell JP (2008) Herpetology: an introductory biology of amphibians and reptiles. Academic Press, San Diego

Voorhies M (1975) Vertebrate burrows. In: Frey RW (ed) The study of trace fossils. Springer-Verlag, New York, pp 325–350

Wake MH (1993) The skull as a locomotor organ. In: Hanken J, Hall BK (eds) The skull. Volume 3: functional and evolutionary mechanisms. The University of Chicago Press, Chicago, pp 197–240

Welsh HHJ, Lind AJ (1992) Population ecology of two relictual salamanders from the Klamath Mountains of northwestern California. In: McCulloch DR, Barrett RH (eds) Wildlife 2001: populations. Elsevier, London, pp 419–429

White CR (2005) The allometry of burrow geometry. J Zool 265:395–403

Chapter 14
Biogenic Structures of Burrowing Skinks: Neoichnology of *Mabuya multifaciata* (Squamata: Scincidae)

Angeline M. Catena and Daniel I. Hembree

Contents

D. I. Hembree (✉) · A. M. Catena
Department of Geological Sciences, Ohio University, Athens, OH 45701, USA
e-mail: hembree@ohio.edu

Abstract Neoichnological experiments involving a species of tropical, ground-dwelling skink, *Mabuya multifasciata,* demonstrate the diversity of biogenic structures produced by medium-sized lizards. Although the majority of skinks are ground dwellers or burrowers, little is known about the biogenic structures produced by this most diverse group of lizards. The documentation of biogenic structures produced by *M. multifasciata* will aid in the identification of trace fossils produced by skinks, help to improve the fossil record of these difficult-to-preserve animals, and allow for more complete paleoecological and paleoenvironmental reconstructions. Skinks were placed in terrariums filled with sediment of varying compositions and moisture content and were allowed to burrow. Open burrows were cast with plaster, photographed, measured, and statistically analyzed. The skinks produced seven distinct burrow morphologies including various ramps, U-, and J-shaped burrows. While there was no direct correlation between burrow properties and sediment properties, the burrows showed some variations due to the changes in sediment density and moisture content. The burrows had greater average complexities and tunnel heights when the sediment moisture was increased, whereas they had lower average widths and circumferences when the sediment density was increased. The data collected in this study can be directly applied to terrestrial trace fossil assemblages in tropical paleosols to better interpret their paleoecology and assess paleoenvironmental conditions.

Keywords Trace fossil · Bioturbation · Vertebrate · Reptile · Continental · Paleoecology · Paleopedology

14.1   Introduction

The purpose of this chapter is to document the morphology of biogenic structures produced by a species of tropical, burrowing skink, *Mabuya multifasciata* (Squamata: Scincidae), in order to improve the interpretation of continental vertebrate trace fossils. This study includes the description of the basic architecture and surficial morphologies of the burrows produced by *M. multifasciata* under both constant and varied environmental conditions. Environmental conditions, including sediment moisture, composition, and density, were altered in order to evaluate how the properties of vertebrate biogenic structures changed in response to these commonly variable factors.

Due to their *in situ* preservation, trace fossils are invaluable in paleoecological and paleoenvironmental reconstructions. Historically, marine trace fossils are well studied and have been used to interpret such paleoenvironmental conditions as turbidity, salinity, sedimentation rate, and nutrient input (e.g., Frey 1970; Rhoads 1975; Bromley 1996; Uchman and Pervesler 2006; Gingras et al. 2007). Although continental ichnology is a comparatively new field, recent ichnological studies of extinct continental organisms, along with studies of modern analogs, have shown that information pertaining to paleoenvironment and even paleoclimate can also be acquired from continental trace fossils (Retallack et al. 1984; Hasiotis 2002, 2003;

Hembree et al. 2004, 2012; Hembree and Hasiotis 2007, 2008; Smith and Hasiotis 2008; Smith et al. 2008; Melchor et al. 2010). Modern continental burrowers such as moles (Gobetz and Martin 2006), snakes (Young and Morain 2003; Hembree and Hasiotis 2007), amphisbaenians (Hembree and Hasiotis 2006), cicadas (Smith and Hasiotis 2008), chafer beetles (Counts and Hasiotis 2009), ants (Halfen and Hasiotis 2010), scorpions (Hembree et al. 2012), whip scorpions (Hembree 2013), and millipedes (Hembree 2009) have been used as analogs to help interpret trace fossils and produce more robust paleoecological reconstructions. Such modern continental trace makers are sensitive to environmental changes; accordingly, trace fossils produced by their ancient equivalents can also be used to interpret environmental factors such as soil nutrient content, sediment density, sedimentation rates, fluctuations in the water table, as well as changes in mean annual precipitation and temperature (Hasiotis 2006). For example, variations in the diversity and abundance of continental trace fossils within ichnocoenoses (i.e., faunal communities) have been used to determine the response of ecosystems to changes in soil moisture regimes, nutrient content, and soil bulk density through time (Kraus and Riggins 2007).

Although vertebrate ichnology has traditionally been limited to the study of tracks and trails (e.g., Peabody 1954; Sarjeant 1975; Currie 1983; Lockley et al. 1994; Irby and Albright 2002; Kubo and Benton 2009), vertebrate trace fossils also include complex and varied burrow structures (e.g., Martin and Bennett 1977; Smith 1987; Groenewald et al. 2001; Hembree et al. 2004; Gobetz and Martin 2006; Hembree and Hasiotis 2008) . Burrowing behavior has evolved independently in several vertebrate clades, and vertebrate burrows are well represented in the geologic record with the earliest recognized burrows dating to the Early Devonian (e.g., Romer and Olson 1954; Damiani et al. 2003; Hasiotis 2003; Hasiotis 2004; Martin 2009). Despite the early appearance and persistence of vertebrate burrows in the geologic record, few researchers have studied the biogenic structures and sediment interactions of extant continental vertebrates (Voorhies 1975; Hasiotis et al. 2007). The lack of understanding of continental vertebrate trace makers has likely led to inaccurate interpretations regarding paleoenvironment and paleoclimate as discussed by Hembree and Hasiotis (2006; 2007). Experimental studies concerning modern continental vertebrates are necessary for the accurate interpretation of trace fossils and their paleoenvironmental significance. These interpretations result directly from observations of the interactions of trace makers in response to their environment (Hembree 2009, 2013; Hembree and Hasiotis 2006, 2007; Hembree et al. 2012).

Although lizards have a large geographic range and an evolutionary history that begins in the Middle to Late Triassic (Datta and Ray 2006), their ichnology has been poorly studied. Few continental trace fossils have been attributed to lizards and only a few neoichnological experiments have involved modern traces produced by lizards (e.g., Traeholt 1995; Gupta and Sinha 2001; Young and Morain 2003; Hasiotis and Bourke 2006; Hembree and Hasiotis 2006, 2007). With over 1,200 extant species, skinks are the most diverse group of lizards and members of the second largest lizard family (Zug et al. 2001). Skinks are characterized by cylindrical bodies, shortened legs, cone-shaped heads, and tapering tails, which makes
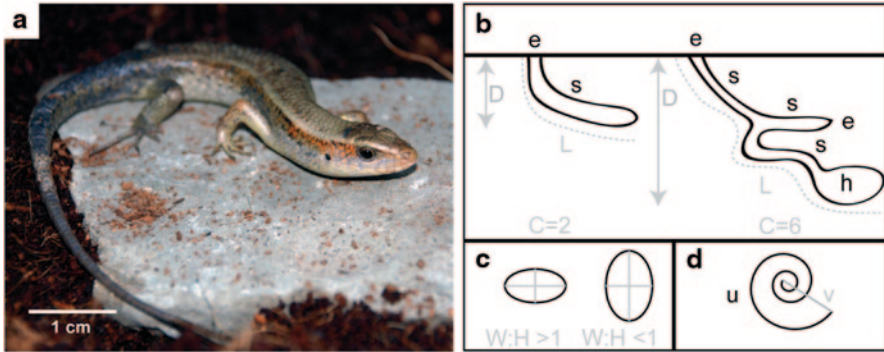
Fig. 14.1 a The many-lined sun skink *Mabuya multifasciata*. **b** Quantitative models used to describe burrows. Burrows were described in part by their maximum depth (*D*) and total length (*L*). Burrow tunnels were divided into segments (*s*) with entrances or blind endpoints (*e*), and expanded chambers (*h*). Burrow complexity (*C*) is a measure of the total number of segments, endpoints, and chambers within a single burrow: $C=s+h+e$. **c** The width-to-height ratio of two burrow tunnels. **d** The tortuosity (*T*) of a segment is calculated by dividing the total length (*u*) by the straight line distance (*v*). (Modified from Hembree and Hasiotis (2006))

them easily distinguishable from other lizards (Zug et al. 2001). Most skink species are either ground dwellers or burrowers, and are most abundant in the tropics (Zug et al. 2001). Although they have a low preservation potential due to their size and habitats, skinks are present in the fossil record as early as the Cretaceous (Estes 1969) and have been found in Paleocene, Oligocene, and Miocene sediments in North America and Australia (Estes 1969; Wellstead 1982; Martin et al. 2004). Due to their abundance, widespread habitats, and burrowing habits, skinks are excellent candidates for neoichnological investigation.

14.2   Skink Ecology and Behavior

Mabuya multifasciata, or the many-lined sun skink (Fig. 14.1a), is an exclusively tropical, medium-sized, insectivorous skink whose range extends through China, India, Malaysia, the Philippines, and New Guinea (Ji et al. 2006; Sun et al. 2009). *Mabuya multifasciata* has well developed limbs, olive gray coloration with a yellow throat, two dark brown dorsolateral lines, and numerous brown to green dorsolateral ocelli (Taylor 1963; Ji et al. 2006). Adult *Mabuya multifasciata* are known to reach a snout-to-vent (SVL) length of 117 mm (Ji et al 2006). *Mabuya multifasciata* can be distinguished from other skinks in the *Mabuya* genus by the 30–34 scale rows around the middle of the skink's body and the three to five keels on the dorsal scales (Taylor 1963). *Mabuya multifasciata* shows a preference for open, sunny spaces such as riverbeds and forest edges (Ji et al. 2006).

14.3 Materials and Methods

The burrowing behaviors of six individuals of *M. multifasciata* were observed in this study. Multiple individuals were used in order to delineate variations in biogenic structures due to differences in individual behavior. The skinks had an SVL of 9.0–9.7 cm and weighed 16.0–23.0 g.

The skinks were placed in 38 L (50 × 25 × 30 cm) and 114 L (80 × 30 × 40 cm) terrariums filled with 20 and 25 cm of sediment, respectively. Terrariums of different sizes were used to evaluate the influence of available space on the morphology of the biogenic structures. The air temperature within the terrariums was regulated with infrared, ceramic heat lamps set on a 12-h timer. A rock was placed directly underneath the heat lamp to allow for basking and a water dish was placed on the opposite side of the terrarium. A pair of UVB lights also set on a 12-h timer was also used in all of the trials. Sediments were composed of varying amounts of finely shredded coconut fiber, clay-sized soil material, fine-grained sand, and water. Sediment density was determined using a soil compaction meter (Fieldscout SC 900), and soil moisture levels were measured with a soil moisture probe (Aquaterr salinity multimeter EC−300). The surface of each terrarium was regularly sprayed with water during the experiments to maintain the desired moisture level, and the soil moisture was tested daily. Due to the temporary nature of the burrows produced by *M. multifasciata,* the trials of all the experiments were run until the skinks exited their burrows.

Experiment 1 (Exp. 1) was designed to observe and record the natural burrowing behaviors of single individuals of *M. multifasciata* under their typical sediment and moisture conditions (Table 14.1a). The sediment consisted of loose coconut fiber with an average sediment density of 0.70 kg/cm^2 and a moisture content of 40%. Trials of Exp. 1 lasted between 3 and 18 days.

Experiment 2 (Exp. 2) was designed to observe the burrowing behaviors and biogenic structures of the skinks in different types of sediment within the natural ranges of the species (Table 14.1b). The sediments consisted of a loose coconut fiber mixed with either an additional 20 wt% of clay or an additional 20 wt% of fine sand. The addition of clay to the coconut fiber increased the sediment density to an average of 1.1 kg/cm^2 whereas the addition of sand decreased the sediment density to an average of 0.35 kg/cm^2. Trials of Exp. 2 lasted between 3 and 11 days.

Experiment 3 (Exp. 3) was designed to observe the effect of sediment moisture content on skink burrowing behaviors (Table 14.1c). The sediments consisted of a loose coconut fiber with moisture content either increased to 60% or lowered to 20%. Trials of Exp. 3 lasted between 4 and 7 days.

Biogenic structures produced by the skinks were photographed daily over the test periods. Videos were also made if the skinks were actively burrowing during times of observation to document burrowing techniques. Skinks were removed from terrariums and returned to their holding tanks at the end of each test period. Removal of the skinks occurred after the animals exited their burrows to engage in feeding or basking behaviors. The open burrows were cast with Drystone™ plaster

Table 14.1 Experimental parameters

Specimen	Experiment ID	Tank size	Substrate	Temperature	Percent soil moisture	Time (days)
a. Experiment 1: Basic morphology						
MM 1	TGB1	38 L	CF	30 °C	40	7
MM 2	TGB2	38 L	CF	30 °C	40	7
MM 4	RGB1	114 L	CF	30 °C	40	7
MM 2	RGB2	114 L	CF	30 °C	40	7
MM 4	TGD1	38 L	CF	30 °C	40	14
MM 6	TGD2	38 L	CF	30 °C	40	14
b. Experiment 2: Sediment composition						
MM 4	TGL1	38 L	CFC	30 °C	40	7
MM 4	TGL2	38 L	CFC	30 °C	40	7
MM 5	RGL1	114 L	CFC	30 °C	40	7
MM 4	RGL2	114 L	CFC	30 °C	40	7
MM 2	TGN1	38 L	CFS	30 °C	40	7
MM 5	TGN2	38 L	CFS	30 °C	40	7
MM 4	RGN1	114 L	CFS	30 °C	40	7
MM 2	RGN2	114 L	CFS	30 °C	40	7
c. Experiment 3: Sediment moisture						
MM 5	TGX1	38 L	CF	30 °C	60	7
MM 5	TGX2	38 L	CF	30 °C	60	7
MM 4	RGX1	114 L	CF	30 °C	60	7
MM 2	RGX2	114 L	CF	30 °C	60	7
MM 8	TGZ1	38 L	CF	30 °C	20	7
MM 5	TGZ2	38 L	CF	30 °C	20	7
MM 4	RGZ1	114 L	CF	30 °C	20	7
MM 8	RGZ2	114 L	CF	30 °C	20	7

CF coconut fiber, *CFC* coconut fiber and 20 % clay, *CFS* coconut fiber and 20 % sand, *MM Mabuya multifasciata*

immediately after the animals were removed. The resulting casts were excavated, photographed, described, and measured using a quantitative burrow description model based on Hembree and Hasiotis (2006). The measurements in the model include maximum depth, angle of orientation, branching angles, total length, tunnel width, tunnel height, and width-to-height ratio; burrow complexity and tortuosity were then calculated for each burrow (Fig. 14.1b–d).

A nonparametric analysis was performed to test the levels of similarity among the three-dimensional burrow casts. A Bray–Curtis similarity test was performed with all burrow casts using the ten quantitative properties. The analysis produces a number between 1.0 (identical) and 0 (different) quantifying the level of similarity between the two burrows. In this study, a value of 1.0 indicates that the burrows are the same, 0.9 indicates very high similarity, 0.8 indicates high similarity, and values

of 0.7 and 0.6 indicate moderate similarity. Values less than or equal to 0.5 indicate dissimilarity.

A Spearman's rank correlation was performed to examine the potential correlation between sediment density and the properties of the skink burrows. In this analysis, each quantitative burrow property (dependent variable) was compared to the sediment density (independent variable). In Spearman's rank correlation, a correlation coefficient (Rs) above 0.90 indicates a high correlation. In addition, Mann–Whitney (M–W) and Kolmogorov–Smirnov (K–S) tests were used to determine the potential equality of the median and distribution of the properties of each burrow, respectively, under the different sediment density and moisture conditions. A ρ value of <0.05 indicates a significant difference between two samples.

14.4   Results

14.4.1   *General Bioturbation Patterns of* M. multifasciata

Mabuya multifasciata burrowed through an intrusion technique in the three different sediments. The skinks preferentially produced burrows in preexisting mounds and cracks on the sediment surface. To locate these features, the skink skimmed its cone-shaped head against the surface of the sediment. Once a mound or crack in the sediment was found, the skink used its front legs to create an open path in the sediment wide enough to force its head into the sediment while using its hind legs to compact and stabilize the sediment around the burrow entrance. As the skink forced its body into the sediment, it used lateral undulations of the head and body to compress the surrounding sediment and widen the burrow.

Active burrowing in loose, organic-rich sediments resulted in seven distinct burrow morphologies including ramps, sinuous ramps, branched ramps, U-shaped burrows, subhorizontal U-shaped burrows, branched U-shaped burrows, and J-shaped burrows. Open burrows were produced in all experiments with the exception of those with 20% sediment moisture. Each experimental trial resulted in a single burrow except for one experiment (TGL1) where the skink produced two separate burrows. One burrow type, the simple ramp, was replicated in all of the trials despite changes in terrarium size, sediment density, and sediment moisture. The open burrows had an average slope of 27° (11–49°; $\sigma=10$), average maximum depth of 5.3 cm (2.3–13.9 cm; $\sigma=3.0$), an average width of 2.8 cm (2.0–4.3 cm; $\sigma=0.6$), average height of 2.2 cm (1.4–3.6 cm; $\sigma=0.5$), an average circumference of 8.8 cm (6.7–11.9 cm; $\sigma=1.6$), average width-to-height ratio of 1.3 (0.7–1.8; $\sigma=0.3$), average total length of 19.5 cm (6.5–40.5 cm; $\sigma=9.3$), average complexity of 2.7 (2.0–5.0; $\sigma=1.0$), and an average tortuosity of 1.27 (1.02–1.56; $\sigma=0.20$; Table 14.2).

Table 14.2 Measurements of three dimensional burrow casts produced by *M. mulitfasciata* and the average and standard deviation of the ten diagnostic properties

	HT1	TGD1	TGB1	RGB1	RGN2	TGX2	TGL1B	TGD2	TGN1	TGL1A	RGL1	RGN1	RGX2	TGB2	TGN2	HT2	RGX1	TGL2	TGX1	RGB2	RGL2	Avg	Std Dev
Architecture	R	R	R	R	R	R	R	R	R	SR	SR	SR	BR	BR	BR	U	U	HU	BU	J	J		
Surface openings	1	1	1	1	1	1	1	1	1	1	1	1	1	1	1	2	2	2	2	1	1	1	0.4
Maximum depth	2.3	5.4	5.3	2.8	2.8	4.8	5.0	3.8	9.4	3.3	4.2	6.2	13.9	5.4	3.2	7.2	11.5	3.1	4.3	2.3	6.1	5.3	3.0
Total length	6.5	28.7	19.6	11.0	9.5	11.0	14.5	10.8	11.6	15.7	24.3	21.5	31.0	19.0	12.0	40.5	27.5	17.7	40.0	19.0	17.7	19.5	9.3
Maximum width	2.2	5.3	5.1	3.5	2.3	2.5	2.6	4.5	4.3	3.2	3.2	4.1	5.6	5.2	2.9	4.7	3.1	3.1	5.2	2.8	2.4		
Minimum width	1.9	2.2	1.9	2.4	2.1	2.1	1.9	2.2	2.0	1.7	1.2	2.0	1.5	3.0	2.0	2.2	2.0	1.8	2.2	1.9	1.9		
Average width	2.0	4.0	3.3	2.8	2.2	2.3	2.3	3.1	2.8	2.4	2.0	3.2	3.5	4.3	2.4	3.4	2.5	2.5	3.5	2.4	2.2	2.8	0.6
Maximum height	2.0	3.0	2.6	2.7	1.6	5.6	2.4	2.9	3.4	2.7	3.0	2.3	3.5	2.7	1.6	3.6	4.4	4.1	2.6	2.9	2.7		
Minimum height	1.3	1.9	1.5	1.6	1.2	2.4	1.4	1.4	1.5	1.3	1.2	1.7	1.6	1.9	1.5	1.9	1.4	1.8	2.0	1.6	1.4		
Average height	1.6	2.5	2.1	2.0	1.4	3.6	1.8	2.4	2.2	1.9	1.8	2.0	2.6	2.4	1.5	2.4	2.4	2.7	2.2	2.0	1.9	2.2	0.5
Average W/H ratio	1.3	1.6	1.6	1.4	1.6	0.7	1.3	1.3	1.2	1.2	1.1	1.5	1.3	1.8	1.5	1.4	1.0	0.9	1.6	1.2	1.1	1.3	0.3
Maximum circumference	7.4	13.9	12.5	9.7	6.6	14.2	8.2	11.8	14.2	9.6	11.0	10.1	17.1	13.4	7.8	14.2	16.0	13.5	13.0	9.4	8.6		
Minimum circumference	6.8	7.0	6.5	7.2	7.2	8.1	6.1	5.5	6.4	6.0	4.3	7.2	5.6	8.3	6.3	7.7	6.3	7.8	7.0	5.6	5.7		
Average circumference	7.2	11.9	9.3	8.4	6.9	10.8	6.9	8.5	9.6	7.1	6.7	8.7	10.4	11.3	7.1	10.2	9.6	10.2	9.6	7.5	7.2	8.8	1.6
Maximum slope	51	32	42	55	26	30	45	48	62	38	34	50	53	57	88	54	54	20	43	20	65		
Minimum slope	4	6	5	28	13	7	10	3	35	3	2	2	10	4	3	2	7	2	0	3	10		
Average slope	28	19	24	42	20	19	28	26	49	21	18	26	32	31	46	28	31	11	22	12	38	27	10
Branching angles	N/A	N/A	N/A	N/A	N/A	N/A	N/A	N/A	N/A	N/A	N/A	N/A	53	N/A	N/A	N/A	N/A	N/A	68	N/A	N/A		
Complexity	2	2	2	2	2	2	2	2	2	2	2	2	5	4	4	3	3	3	5	2	2	2.7	1.0
Tortuosity	1.02	1.24	1.07	1.20	1.19	1.16	1.18	1.03	1.22	1.15	1.27	1.23	1.07	1.70	1.56	1.37	1.41	1.45	1.23	1.54	1.42	1.27	0.20
Sediment density	0.70	0.70	0.70	0.70	0.35	0.70	1.1	0.70	0.35	1.1	1.1	0.35	0.70	0.70	0.35	0.70	0.70	1.1	0.70	0.70	1.1		
Sediment moisture	40	40	40	40	40	60	40	40	40	40	40	60	60	40	40	40	60	40	60	40	40		

Sediment density is in kg/cm²; all other measurements are in cm *BR* branched ramp, *BU* branched U-shaped burrow, *HU* horizontal U-shaped burrow, *J* J-shaped burrow, *N/A* not applicable, *R* ramp, *SR* sinuous ramp, *U* U-shaped burrow
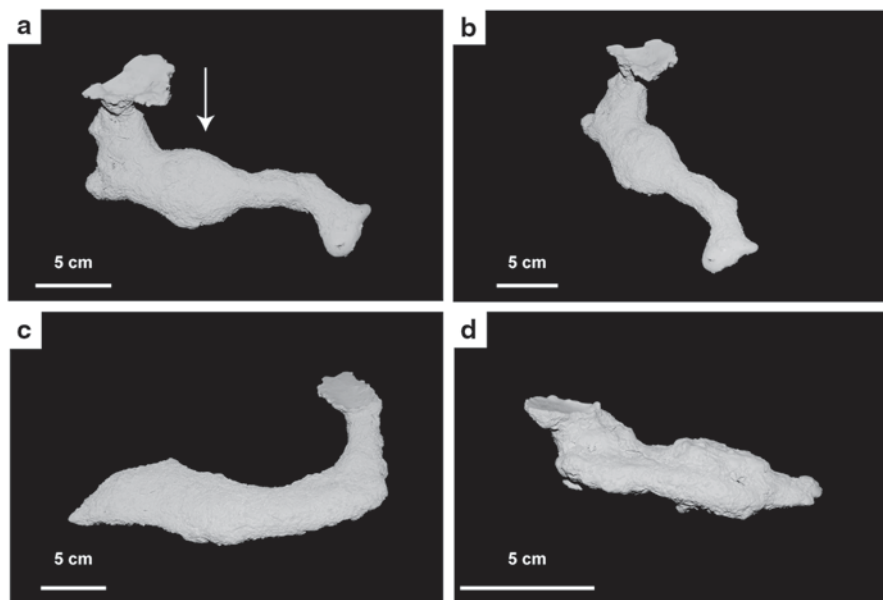
Fig. 14.2 Simple ramps. **a** Right view of a simple ramp with a laterally expanded chamber (at *arrow*; TGB1). **b** Right oblique view of a simple ramp (TGB1). **c** Left oblique view of an elongate, simple ramp (TGD1). **d** Right view of a small, simple ramp (TGD2)

14.4.2 Open Burrows and Biogenic Structures

14.4.2.1 Mounds and Depressions

These structures were simple surficial biogenic structures consisting of sediment mounds and their accompanying depressions. Mounds and depressions occurred in one experiment with 20% sediment moisture in which the skink could not produce an open burrow. The mounds and depressions had a maximum width and relief of 10.0 cm ($\bar{x}$ = 7.7 cm) and 3.9 cm ($\bar{x}$ = 2.7 cm), respectively. The observed mounds and depressions were isolated and were formed by sediment displacement during attempts at active burrowing.

14.4.2.2 Simple Ramps

Simple ramps ($n=9$) were the most common burrow morphology produced in the experiments. Simple ramps consist of a burrow with a single entrance and an elongate, sloping tunnel (Fig. 14.2). Tunnels in the simple ramp architecture have slopes of 19–49º ($\bar{x}$ = 28º, σ = 10). Ramps have an average maximum depth of 4.6 cm (2.3–9.4 cm; σ = 2.0), an average width of 2.8 cm (2.0–4.0 cm; σ = 0.6), an average height of 2.2 cm (1.4–3.6 cm; σ = 0.6), an average circumference of 8.8 cm (6.9–11.9 cm;

$\sigma=1.7$), an average width-to-height ratio of 1.3 (0.7–1.6; $\sigma=0.3$), an average length of 13.7 cm (6.5–28.7 cm; $\sigma=6.7$ cm), an average complexity of 2.1 (2.0–3.0; $\sigma=0.3$), and an average tortuosity of 1.14 (1.02–1.24; $\sigma=0.08$; Table 14.2). The cross-sectional shape of the tunnels in seven of the simple ramps is flattened elliptical, although two (TGX2, TGN1) have circular cross-sections. The simple ramp architecture does not include chambers with the exception of one burrow (TGB1) with a centrally located chamber (Fig. 14.2a). Ramps occurred in all sediment types except for those with 20% sediment moisture content (Exp. 3).

14.4.2.3 Sinuous Ramps

Sinuous ramps ($n=3$) are classified as unbranched ramps that deviate laterally at least 3.0 cm from the surface opening and have a tortuosity greater than 1.1 (Fig. 14.3). Two of the sinuous ramps are flattened elliptical in cross-section, whereas the third (RGL1) is circular. The sinuous ramps have an average slope of 22° (18–26°; $\sigma=4$), an average maximum depth of 4.6 cm (3.3–6.2 cm; $\sigma=1.5$), an average width of 2.5 cm (2.0–3.2 cm; $\sigma=0.5$), an average height of 1.9 cm (1.8–2.0 cm; $\sigma=0.1$), an average circumference of 7.5 cm (7.1–8.7 cm; $\sigma=0.9$), an average width-to-height ratio of 1.3 (1.1–1.5; $\sigma=0.2$), an average length of 20.5 cm (15.7–24.3 cm; $\sigma=4.4$), an average complexity of 2.0 (2.0; $\sigma=0.0$), and an average tortuosity of 1.21 (1.15–1.27; $\sigma=0.05$; Table 14.2). Sinuous ramps occurred in experimental sediments with 20% clay and 20% sand (Exp. 2).

14.4.2.4 Branched Ramps

Branched ramps ($n=3$) consist of a burrow with a single entrance and two intersecting, sloping tunnels (Fig. 14.4). The branched ramps have an average slope of 36° (31–46°; $\sigma=8$), an average maximum depth of 7.5 cm (3.2–13.9 cm; $\sigma=5.7$), an average width of 3.4 cm (2.4–4.3 cm; $\sigma=0.8$), an average height of 2.2 cm (1.5–2.6 cm; $\sigma=0.5$), an average circumference of 9.6 cm (7.1–11.3 cm; $\sigma=1.8$), an average width-to-height ratio of 1.6 (1.3–1.8; $\sigma=0.2$), an average total length of 20.7 cm (12.0–31.0 cm; $\sigma=9.6$), an average complexity of 4.3 (4.0–5.0 cm; $\sigma=0.5$), and an average tortuosity of 1.44 (1.07–1.70; $\sigma=0.27$; Table 14.2). Two of the branched ramps have flattened elliptical cross-sectional shapes, whereas the third (TGN2) has a flat floor and roof. One branched ramp (RGX2) possesses a terminal chamber (Fig. 14.4a and b). The branched ramps were produced in experiments with 100% coconut fiber (Exp. 1), 20% sand sediment (Exp. 2), and 60% moisture content sediment (Exp. 3).

14.4.2.5 U-shaped Burrows

U-shaped burrows ($n=2$) consist of burrows with two entrances of similar dimensions that are connected by variably sloping tunnels (Fig. 14.5a and b). The tunnels

Fig. 14.3 Sinuous ramps.
a Right oblique view of an
elongate, sinuous ramp with
a divot (at *arrow;* RGL1).
b Overhead view of a sinu-
ous ramp (RGN1). **c** Front
oblique view of a short, sinu-
ous ramp with three divots (at
arrows; TGL1A)
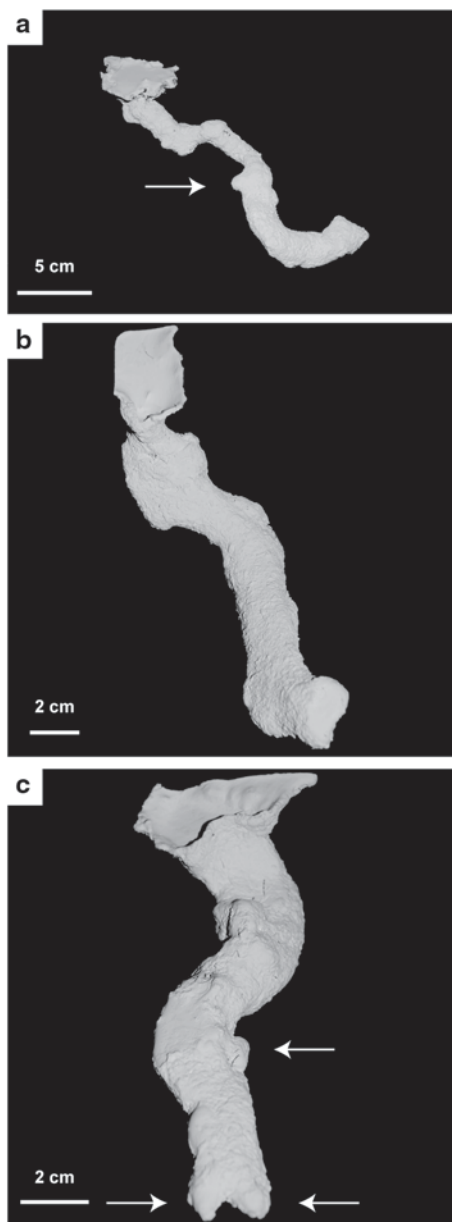
of the U-shaped burrows have an average slope of 30° (28–31°; $\sigma=2°$), an average
maximum depth of 9.4 cm (7.2–11.5 cm; $\sigma=3.0$ cm), an average width of 3.0 cm
(2.5–3.4 cm; $\sigma=0.5$), an average height of 2.4 cm (2.4 cm; $\sigma=0.01$), an average
circumference of 9.9 cm (9.6–10.2 cm; $\sigma=0.3$), an average width-to-height ratio of
1.2 (1.0–1.4; $\sigma=0.3$), an average length of 34.0 cm (27.5–40.5 cm; $\sigma=9.2$ cm), an
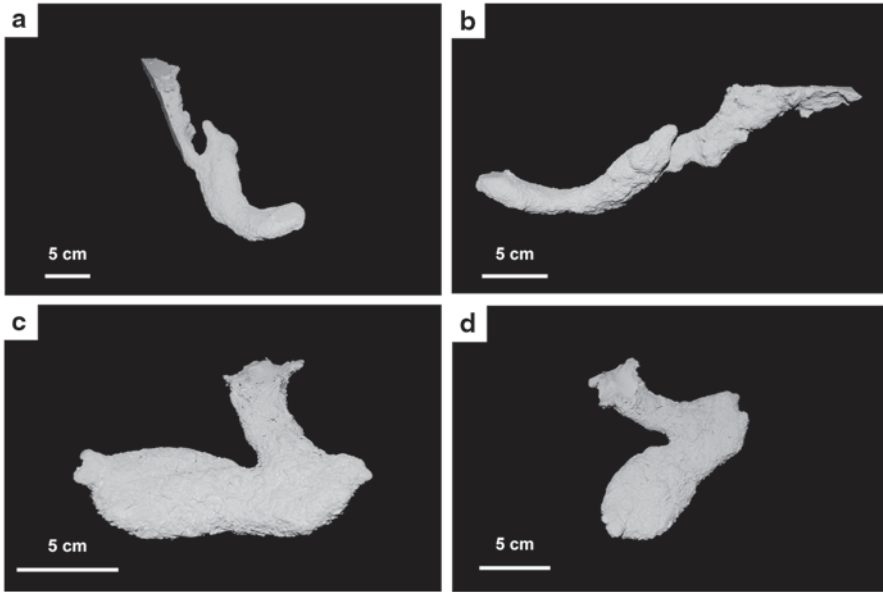
Fig. 14.4 Branched ramps. **a** Oblique view of an elongate branching ramp (RGX2). **b** Left view of an elongate branching ramp (RGX2). **c** Front view of a branched ramp with a chamber (TGB2). **d** Oblique view of a branched ramp with a chamber (TGB2)

average complexity of 3.0 (3.0; $\sigma=0.0$), and an average tortuosity of 1.39 (1.37–1.41; $\sigma=0.03$; Table 14.2). The U-shaped burrows are flattened elliptical in cross section. The paired entry tunnels either have similar slopes or slopes that may differ by up to 30°. U-shaped burrows were produced in experiments with 100% coconut fiber with 40% moisture content (Exp. 1) and 60% moisture content (Exp. 3).

14.4.2.6 Subhorizontal U-shaped Burrows

A burrow ($n=1$) consisting of two entrances of similar dimensions that are connected by a tunnel with an average slope of 15° or less (Fig. 14.5c). The entrances of the single burrow have slopes of 20° and 11°. The subhorizontal, U-shaped burrow is flattened elliptical in cross-section, with an average slope of 11°, a maximum depth of 3.1 cm, a total length of 17.7 cm, an average width of 2.5 cm, an average height of 2.7 cm, an average circumference of 10.2 cm, a width-to-height ratio of 0.9, a complexity of 3, and a tortuosity of 1.45 (Table 14.2). The subhorizontal, U-shaped burrow was produced in an experiment with 20% clay sediment (Exp. 2).

14.4.2.7 Branched U-shaped Burrows

A burrow ($n=1$) with two entrances of similar dimensions and slopes connected by a single tunnel that possesses a branch that does not connect to the surface
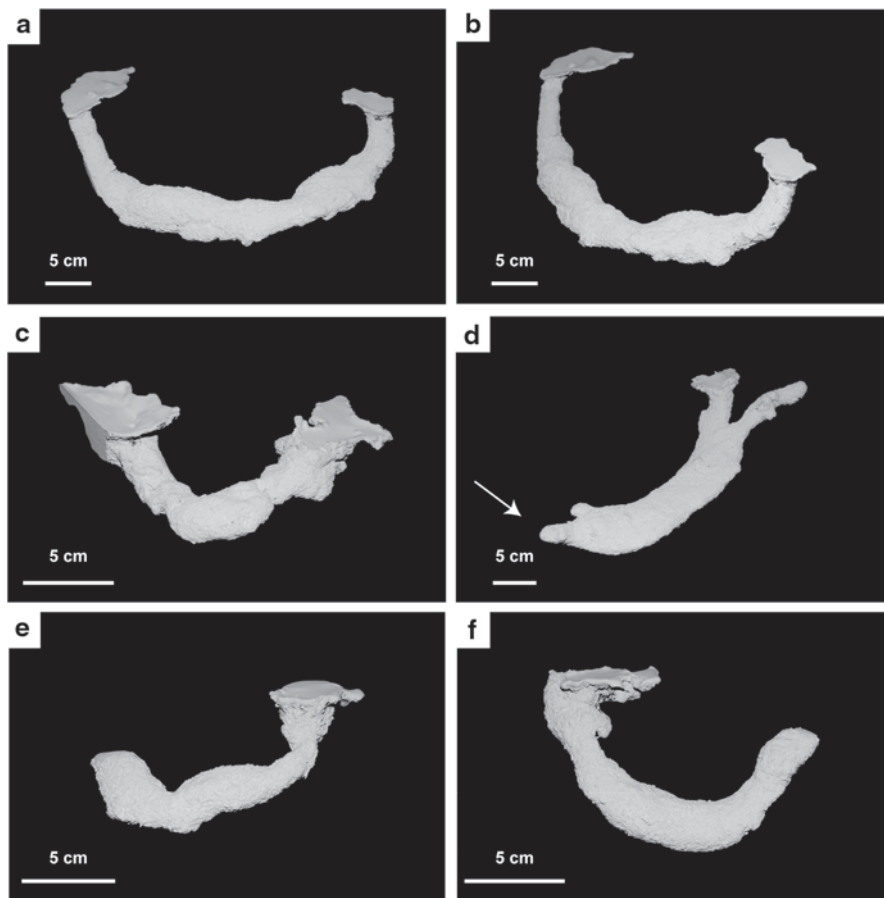
Fig. 14.5 U- and J-shaped burrows. **a** Front view of an elongate, U-shaped burrow (HT2). **b** Right oblique view of an elongate, U-shaped burrow (HT2). **c** Front view of a subhorizontal, U-shaped burrow (TGL2). **d** Left oblique view of a branched, U-shaped burrow (TGX1); second entrance not pictured (at *arrow*). **e** Left view of a J-shaped burrow (RGB2). **f** Right view of a J-shaped burrow (RGL2)

(Fig. 14.5d). The burrow has an average slope of 22°, maximum depth of 4.3 cm, an average width of 3.5 cm, an average height of 2.2 cm, an average circumference of 9.6 cm, a width-to-height ratio of 1.6, a total length of 40.0 cm, a complexity of 5, and a tortuosity of 1.23 (Table 14.2). In cross section, the branched U-shaped burrow is elliptical, but flattened on the roof and floor. The branched, U-shaped burrow was produced in an experiment with 60% sediment moisture content (Exp. 3).

14.4.2.8   J-shaped Burrows

J-shaped burrows (*n*=2) consist of a single entrance leading to a downward-to-upward sloping tunnel that terminates within 2 cm of the sediment surface

(Fig. 14.5e and f). In cross section, the J-shaped burrows are flattened elliptical. The J-shaped burrows have an average slope of 25° (12–38°; $\sigma=25$), an average maximum depth of 4.2 cm (2.3–6.1 cm; $\sigma=2.7$), an average width of 2.3 cm (2.2–2.4 cm; $\sigma=0.1$), an average height of 2.0 cm (1.9–2.0 cm; $\sigma=0.1$), an average circumference of 7.3 cm (7.2–7.5 cm; $\sigma=0.1$), an average width-to-height ratio of 1.2 (1.1–1.2; $\sigma=0.0$), an average length of 18.4 cm (17.7–19.0 cm; $\sigma=0.9$ cm), an average complexity of 2.0 (2.0; $\sigma=0.0$), and an average tortuosity of 1.48 (1.42–1.54; $\sigma=0.01$; Table 14.2). J-shaped burrows were produced in experiments with 100% coconut fiber sediment with 40% moisture content (Exp. 1) and 20% clay sediment (Exp. 2).

14.4.3 Burrow Ornamentation

With the exception of two burrow casts (HT1, RGN1), the tunnels were characterized by randomly spaced, rounded, triangular divots along the tunnel walls (Fig. 14.3a and c). A total of 75 divots were observed and measured on 19 burrow casts. The divots averaged 0.9 cm (0.4–2.6 cm; $\sigma=0.4$) in length, 1.1 cm (0.5–2.0 cm; $\sigma=0.4$) in width, and 0.8 cm (0.5–1.9 cm; $\sigma=0.3$) in height. There was no change in average divot size between experiments with different sediment properties or burrow morphology; however, the average number of divots per burrow did vary with sediment properties and with the duration of the experiments. There was an average of 3.3 divots per burrow in the 7-day experiments and 2.0 divots per burrow in 14-day experiments. The burrows produced in sediments with 20% clay averaged 4.6 divots, whereas those produced in sediments with 20% sand averaged 2.7 divots. Burrows produced in experiments with 100% coconut fiber with 60% sediment moisture content averaged 6.2 divots whereas those produced in 100% coconut fiber with 40% moisture content averaged 2.6 divots.

14.5 Analysis of Results

14.5.1 Comparison of Skink Burrow Architectures

The burrows produced by *M. multifasciata* were found to be highly to moderately similar to each other based on the ten quantitative properties used in the Bray–Curtis similarity test. The degrees of similarity between the burrows ranged from 0.9 to 0.6 with the majority (73%) of the values varying between 0.9 and 0.8 (Table 14.3). No similarity values were below 0.6, and no values of 1.0 were obtained except when comparing a burrow to itself.

The average similarity values obtained when comparing burrows with the same architecture were 0.9 or 0.8 (Table 14.3). The sinuous ramps and the U-shaped burrows had the highest ($\overline{x}=0.9$) degree of similarity, whereas simple ramps, branched ramps, and J-shaped burrows had high ($\overline{x}=0.8$) degrees of similarity. There was an

Table 14.3 Bray–Curtis similarity test results for burrow casts

		HT1	TGD1	TGB1	RGB1	RGN2	TGX2	TGL1 B	TGD2	TGN1	TGL1 A	RGL1	RGN1	RGX2	TGB2	TGN2	HT2	RGX1	TGL2	TGX1	RGB2	RGL2
		R	R	R	R	R	R	R	R	R	SR	SR	SR	BR	BR	BR	U	U	HU	BU	J	J
HT1	R	1.0	0.7	0.8	0.8	0.9	0.8	0.9	0.9	0.7	0.8	0.7	0.8	0.7	0.8	0.8	0.7	0.7	0.7	0.7	0.7	0.8
TGD1	R	0.7	1.0	0.9	0.7	0.8	0.8	0.8	0.8	0.7	0.8	0.9	0.9	0.8	0.8	0.6	0.8	0.8	0.8	0.9	0.8	0.8
TGB1	R	0.8	0.9	1.0	0.8	0.8	0.8	0.9	0.9	0.8	0.9	0.9	0.9	0.8	0.9	0.8	0.8	0.8	0.8	0.8	0.8	0.9
RGB1	R	0.8	0.7	0.8	1.0	0.8	0.8	0.8	0.9	0.9	0.8	0.7	0.8	0.7	0.8	0.9	0.7	0.8	0.7	0.7	0.7	0.9
RGN2	R	0.9	0.8	0.8	0.8	1.0	0.9	0.9	0.9	0.7	0.9	0.8	0.8	0.6	0.7	0.8	0.7	0.7	0.8	0.7	0.8	0.8
TGX2	R	0.8	0.8	0.8	0.8	0.9	1.0	0.8	0.9	0.7	0.8	0.8	0.8	0.7	0.8	0.7	0.7	0.7	0.7	0.7	0.8	0.8
TGL1 B	R	0.9	0.8	0.9	0.8	0.9	0.8	1.0	0.9	0.8	0.9	0.8	0.9	0.8	0.9	0.8	0.8	0.8	0.8	0.7	0.8	0.9
TGD2	R	0.9	0.8	0.9	0.9	0.9	0.9	1.0	1.0	0.8	0.9	0.8	0.9	0.8	0.8	0.8	0.8	0.8	0.8	0.8	0.8	0.8
TGN1	R	0.7	0.7	0.9	0.9	0.7	0.7	0.8	0.8	1.0	0.7	0.7	0.8	0.8	0.8	0.9	0.7	0.8	0.6	0.6	0.6	0.9
TGL1 A	SR	0.8	0.8	0.9	0.8	0.9	0.8	0.9	0.9	0.7	1.0	0.9	0.9	0.7	0.8	0.8	0.7	0.8	0.8	0.8	0.9	0.8
RGL1	SR	0.7	0.9	0.9	0.7	0.9	0.8	0.8	0.8	0.7	0.9	1.0	0.9	0.8	0.8	0.7	0.8	0.8	0.8	0.8	0.8	0.8
RGN1	SR	0.8	0.9	0.9	0.8	0.8	0.8	0.9	0.9	0.8	0.9	0.9	1.0	0.8	0.9	0.8	0.8	0.8	0.8	0.8	0.8	0.9
RGX2	BR	0.7	0.8	0.8	0.7	0.6	0.7	0.8	0.8	0.8	0.7	0.8	0.8	1.0	0.9	0.7	0.9	0.9	0.7	0.8	0.7	0.8
TGB2	BR	0.8	0.8	0.9	0.8	0.7	0.8	0.9	0.8	0.8	0.8	0.8	0.9	0.9	1.0	0.8	0.8	0.9	0.8	0.8	0.8	0.9
TGN2	BR	0.8	0.6	0.8	0.9	0.8	0.7	0.8	0.8	0.9	0.8	0.7	0.8	0.7	0.8	1.0	0.7	0.7	0.6	0.7	0.9	0.9
HT2	U	0.7	0.8	0.8	0.7	0.7	0.7	0.8	0.8	0.7	0.7	0.8	0.8	0.9	0.8	0.7	1.0	0.9	0.7	0.9	0.7	0.8
RGX1	U	0.7	0.8	0.8	0.8	0.7	0.7	0.8	0.8	0.8	0.8	0.8	0.8	0.9	0.9	0.7	0.9	1.0	0.7	0.8	0.7	0.8
TGL2	HU	0.7	0.8	0.8	0.7	0.8	0.8	0.8	0.8	0.6	0.8	0.8	0.8	0.7	0.8	0.6	0.7	0.7	1.0	0.7	0.9	0.7
TGX1	BU	0.7	0.9	0.8	0.7	0.7	0.7	0.7	0.7	0.6	0.8	0.8	0.8	0.8	0.8	0.7	0.9	0.8	0.7	1.0	0.7	0.7
RGB2	J	0.7	0.8	0.8	0.7	0.8	0.8	0.8	0.8	0.6	0.9	0.9	0.8	0.7	0.8	0.9	0.7	0.7	0.9	0.7	1.0	0.8
RGL2	J	0.8	0.8	0.9	0.9	0.8	0.8	0.9	0.8	0.9	0.8	0.8	0.9	0.8	0.9	0.9	0.8	0.8	0.7	0.8	0.8	1.0

BR branched ramp, *BU* branched U-shaped burrow, *HU* subhorizontal U-shaped burrow, *J* J-shaped burrow, *SR* sinuous ramp, *U* U-shaped burrow

average of one instance (0–4; $\sigma=1.1$) of moderate similarity (0.7) per burrow when comparing burrows of the same architecture. No similarity values of 0.6 or lower were obtained when comparing burrows of the same architecture, and 11 of the total 19 burrows only had very high to high similarity values.

The burrows were still found to be very highly to moderately (0.9–0.7) similar on average when burrows with different architectures were compared to each other (Table 14.3). The majority ($n=12$ of 21) of interarchitecture comparisons resulted in an average similarity value of 0.8. The comparison of the sinuous ramps and the J-shaped burrows as well as the U-shaped and branched U-shaped burrows resulted in the highest average degree of similarity (0.9). Only seven comparisons between burrow architectures resulted in moderate average similarity values (0.7) and these primarily involved the U-shaped burrows. These were between U-shaped burrows and J-shaped burrows, between the subhorizontal U-shaped burrows and the simple ramps, branched ramps, U-shaped, and branched U-shaped burrows, and between the branched U-shaped burrows and the simple ramps and J-shaped burrows. When compared to each other, however, the three types of U-shaped burrows had an average similarity of 0.8. There was an average of five instances (0–11; $\sigma=3.3$) of moderate similarity (0.7–0.6) per burrow when comparing burrows of different architectures. Values of 0.6 were only obtained six times when comparing burrows of different architectures.

There were several similar individual properties across the seven different burrow architectures. The average burrow width, height, and width-to-height ratio were similar across all of the burrow morphologies with averages of 2.8 (2.0–4.3), 2.2 (1.4–3.6), and 1.3 (0.7–1.8) and standard deviations of 0.6, 0.5, and 0.3, respectively (Table 14.2). Average maximum depth, total length, circumference, and slope varied significantly with standard deviations from 1.6–10.0 (Table 14.2).

14.5.2   Morphological Variation Due to Sediment Properties

The greatest diversity of burrows was produced in trials with 100 % coconut fiber with 40 % moisture ($n=4$; Exp. 1) and with 100 % coconut fiber with 60 % moisture ($n=4$; Exp. 3). The lowest diversity of burrows was produced in trials with 20 % sand ($n=2$; Exp. 2) and 100 % coconut fiber with 20 % moisture ($n=0$; Exp. 3).

A Spearman's rank correlation was performed with the data collected from experiments involving changes in sediment density. Correlation between the ten measured burrow properties and the three increasing sediment density values was not found to be significant (Table 14.4). The highest correlations were with width-to-height ratio and slope (Rs$=-0.48$, $\rho=0.03$; Rs$=-0.32$, $\rho=0.14$, respectively). M–W and K–S tests were used to determine if there were any statistically significant differences in the medians or distribution of burrow properties between the experiments involving changes in sediment density or moisture content

Table 14.4 Results (Rs and ρ values) of Spearman's rank correlation between sediment density and quantitative burrow properties

	Openings	Length	Depth	Width	Height	Circum.	W/H ratio	Slope	Complexity	Tortuosity
Rs	0.15	0.15	−0.09	−0.26	0.07	−0.16	−0.48	−0.33	−0.1	0.04
P	0.53	0.51	0.69	0.25	0.77	0.49	0.03	0.14	0.66	0.88

(Table 14.5). There were only two properties that were found to be significantly different in terms of both their median and distribution ($\rho < 0.05$ for both M–W and K–S) among the burrows produced in the three sediment densities. These differences were present in burrows produced in the 20 % clay sediment (1.1 kg/cm^2), which had significantly lower average widths and average circumferences than burrows produced in the 100 % coconut fiber (0.7 kg/cm^2). There were also significantly different distributions (K–S) of average height and width-to-height ratio between these sediment densities as well; the burrows produced in 100 % coconut fiber (0.7 kg/cm^2) had a higher range of values in both properties. Comparison of burrows produced in 20 % sand (0.35 kg/cm^2) sediment with those in 100 % coconut fiber (0.7 kg/cm^2) indicated that only the median (M–W) of average height was significantly different; average burrow heights were lower in the sandy sediment. Comparison of burrows produced in 20 % sand (0.35 kg/cm^2) sediment with those in 20 % clay sediment (1.1 kg/cm^2) indicated that only the median (M–W) of width-to-height ratio were significantly different; width-to-height ratio was greater in sandy sediment.

No open burrows were produced in experiments with 20 % sediment moisture. During these experiments, the skinks were observed actively burrowing by intrusion, but the sediment was not cohesive enough to form an open burrow. These experiments only resulted in the production of mounds and depressions. The comparison of burrows produced in sediment with 40 % and 60 % moisture content indicated minimal variation in burrow properties (Table 14.5). The medians (M–W) of burrow complexity and height were significantly different as was the distribution of circumference (Table 14.5); the values of all three of these properties were higher in burrow produced in sediment with 60 % moisture content than those produced in sediment with 40 % moisture content.

Experiments involving changes in terrarium size and trial duration did not appear to produce significant differences in the burrow properties. M–W and K–S tests comparing burrows produced in 38 L and 114 L terrariums yielded no significant differences (Table 14.5). The temporary nature of the burrows produced by *M. multifasciata* led to the small sample size ($n = 2$) for the 14-day experiments preventing any statistical comparison with burrows produced in 7-day experiments ($n = 19$). The properties of these two burrows, however, were not outside the normal range of those of the burrows produced in 7 days (Table 14.2).

Table 14.5 Results (ρ values) of Mann–Whitney (M–W) and Kolmogorov–Smirnov (K–S) tests between the quantitative properties of burrows produced in sediments with different densities (kg/cm^2), sediment moisture contents (%), and tank sizes (L). *Outlined values* are considered significant at $\rho < 0.05$

		Openings	Length	Depth	Width	Height	Circum.	W/H Ratio	Slope	Complexity	Tortuosity
Density											
1.1 v 0.7	**M-W**	0.89	0.49	0.63	0.03	0.12	0.02	0.06	0.40	0.23	0.52
	K-S	0.32	0.32	0.84	0.05	0.03	0.03	0.05	0.68	0.32	0.92
0.7 v 0.35	**M-W**	0.32	0.36	0.99	0.25	0.04	0.10	0.67	0.30	0.50	0.57
	K-S	0.08	0.55	0.98	0.32	0.16	0.32	0.55	0.32	0.32	0.81
1.1 v 0.35	**M-W**	0.50	0.18	0.90	0.27	0.71	0.71	0.05	0.27	0.87	0.99
	K-S	0.99	0.08	0.48	0.48	0.96	0.96	0.08	0.48	0.99	0.88
Moisture											
60 v 40	**M-W**	0.10	0.15	0.12	0.45	0.03	0.07	0.34	0.89	0.05	0.68
	K-S	0.61	0.09	0.22	0.61	0.07	0.04	0.43	0.90	0.28	0.57
Tank Size											
38 v 114	**M-W**	0.59	0.56	0.83	0.29	0.31	0.20	0.44	0.86	0.43	0.49
	K-S	0.53	0.73	0.50	0.69	0.21	0.43	0.80	0.68	0.73	0.42

14.6   Discussion

14.6.1   *Burrow Morphology and Trace Maker*

Seven burrow architectures were produced by *M. multifasciata*. Several of the burrow architectures were produced by multiple individuals and were duplicated in multiple experiments. The overall forms of the seven burrow architectures were found to be similar using nonparametric statistics and the average width, height, and width-to-height ratio were found to be similar across all of the burrow morphologies. These three burrow properties resemble the dimensions of *M. multifasciata* (average trunk width: 2.7 cm, average burrow width: 2.8 cm; average trunk height: 1.8 cm, average burrow height: 2.2 cm; average trunk width-to-height ratio: 1.7, average burrow width-to-height ratio: 1.6), and are, therefore, likely directly related to the morphology of the skinks themselves. Although the dimensions of a burrow do not always correspond exactly to those of the trace maker, they can be a good indicator of the relative size (Bromley 1996; White 2005). Similar correlations have been observed between the width and height of tunnels and trace makers in recent neoichnological studies with both vertebrates and invertebrates (e.g., Smith and Hasiotis 2008; Hembree and Hasiotis 2006; Hembree 2009, 2013; Halfen and Hasiotis 2010; Hembree et al. 2012).

The burrow shape and ornamentation also reflect the morphology of *M. multifasciata*. The burrows produced by the skinks have moderately concave roofs and floors; this is similar to the trunk morphology of the skinks (Fig. 14.1). The triangular divots present along the burrow walls were likely a result of sediment probing by the skinks' triangular-shaped head. The skinks' heads averaged 1.3 cm in length and 0.9 cm in width and height, while the burrow ornamentation averaged 0.9 cm in length, 1.1 cm in width, and 0.8 cm in height. Similar triangular impressions have also been observed along the walls of extant amphisbaenian burrows (Hembree and Hasiotis 2006).

14.6.2   *Burrow Morphology and Behavior*

The three common properties of the seven burrow architectures are also a result of *M. multifasciata's* burrowing technique and three basic behaviors: dwelling, predation, and escape. Unlike burrowing by excavation which relies heavily on subsurface limb movement and may result in burrows that are larger than the trace maker (e.g., Traeholt 1995; Begall and Gallardo 2006), burrowing by intrusion tends to produce burrows with dimensions that closely match the dimensions of the trace maker. Burrows produced by intrusion may also possess compressional linings (Bromley 1996). This relationship has been observed with other soil-burrowing animals such as millipedes (Hembree 2009) and amphisbaenians (Hembree and Hasiotis 2006). All but five of the burrows have flattened elliptical cross-sections with moderately concave roofs and floors and short, arching walls. When actively burrowing, *M. multifasciata* penetrates and probes the sediment with its cone-shaped head while

it slowly undulates its body laterally to increase the width of the burrow to accommodate its trunk. These movements produce burrows with width-to-height ratios that are, on average, greater than 1.0.

The simple ramp was the most common burrow morphology produced by the skinks. This morphology provides a basic, temporary, subsurface dwelling. Simple ramps were also produced as short-lived escape structures; during daily terrarium spraying, some of the skinks rapidly burrowed into the substrate and produced ramps (RGB1). Burrow architectures with two entrances and complexities greater than or equal to 3 may be the product of predatory behavior exhibited by *M. multifasciata*. During an experiment, one individual was observed ambushing crickets from the entrance of its burrow. The dual entrances of the three types of U-shaped burrows likely increase the skinks chances of ambushing prey. Predation behavior from burrows by fossorial skinks has also been observed in the wild by Milne et al. (2002).

14.6.3 Burrow Morphology and Sediment Properties

Observations during experiments and quantitative analyses of the *M. multifasciata* burrows indicate that sediment density and moisture had some influence on the morphology of the burrows as well as whether or not open burrows could even be constructed. Increased sediment density produced burrows with lower average widths and circumferences. The increased sediment density restricted the skinks entry into and movement beneath the sediment. The skinks' difficulty in burrowing into dense sediment was indicated by the observation that the skinks spent more time at the surface before burrow construction in tanks containing these sediments. The lower widths and circumferences of the resulting burrows were likely due to the reduced ability of the skinks to perform lateral undulations which generally widened the tunnels in less dense sediment. Sediments with higher densities typically result in burrows with dimensions that are closer approximations to those of the burrower than sediments with lower densities (Bromley 1996). Burrow architecture appeared to be unaffected by increased sediment density, however. Architectures produced in the high density sediment included simple ramps, sinuous ramps, U-shaped burrows, and J-shaped burrows. Overall, Spearman's rank correlation tests did not produce coefficients that indicated a significant correlation between any of the ten burrow properties and sediment density (Table 14.4). The lack of significant correlation coefficients suggests that the morphology and behavior of the skinks have a greater influence on burrow morphology than sediment density.

Increased sediment moisture had a minimal effect on the burrow properties including higher than average burrow complexities and heights. Of the four burrows produced in experiments with increased sediment moisture, three had complexities greater than 2 (3–5). In addition, the only two burrows with complexity values of 5 were produced in sediments with increased moisture. This difference is likely due to the increased cohesion of the sediment as a result of the high moisture content which allowed for the long-term maintenance of multiple open tunnels in addi-

tion to the low density of the sediment which allowed the skinks to move easily through the subsurface. The same effect is likely responsible for the increase in tunnel height. Conversely, the inability of the skinks to produce open burrows in sediment with 20 % moisture content is the result of little-to-no sediment cohesion. The similarity of the other burrow properties despite changes in sediment moisture content again suggests that morphology and behavior of the skinks have more influence on burrow morphology than sediment properties.

14.7 Significance

14.7.1 Recognition of Skink Burrows in the Fossil Record

In order to interpret trace makers, it is essential that we are able to recognize the architecture and surficial morphology of burrows produced by modern burrowing animals. Trace fossils are classified according to a suite of ichnotaxonomic characters known as ichnotaxobases; these include aspects of ichnofossil morphology such as overall shape, orientation with respect to the sediment surface, architecture, and surficial features (Bromley 1996; Bertling et al. 2006). An understanding of the burrows produced by modern organisms is necessary to establish a set of ichnotaxobases that can be used in the identification and interpretation of trace fossils. Although only one species of burrowing skink was studied, the burrows produced by *M. multifasciata* provide a preliminary set of ichnotaxobases that will aid in the recognition and identification of skink burrows in the fossil record.

Architecture Open burrows produced by skinks include branched and unbranched subhorizontal ramps, sinuous ramps, branched and unbranched U-shaped burrows, and J-shaped burrows. These burrows include one to two surface openings, tunnels, shafts, and laterally expanded chambers.

Overall Shape The shafts and tunnels are elliptical in cross-section, with moderately flattened concave roofs and floors, and curved walls. The shafts and tunnels are approximately 1.5 times wider than high. Side branching is uncommon, but when it does occur, the branches tend to be short and do not connect to the surface.

Orientation Burrows are often subhorizontal (11–29°), occasionally oblique (30–45°), and rarely subvertical (46–74°).

Internal Structure No lining is present. The boundary between the sediment and the burrow wall is abrupt and irregular. The burrows were passively filled as a result of gravitational collapse.

Surficial Features The surfaces of the burrows are characterized by an irregular texture resulting from the surrounding sediment; however, the tops of the tunnels and chambers tend to be smoother than the floor or sides. Triangular-shaped, irregularly spaced divots are commonly preserved along the walls of the tunnels. The

width and height of the divots are approximately 37% of the width and height of the average tunnel.

Variation from these ichnotaxobases is expected with different genera or families of skinks. For example, a burrow produced by an Australian skink (*Egernia*) is characterized by a more complex architecture consisting of multiple, interconnected, upward-branching tunnels, and a longitudinal median groove (Hasiotis and Bourke 2006). These differences in burrow morphology are likely due to the communal lifestyle and larger size of the skinks in the *Egernia* genus (Chapple 2003).

14.7.2   Paleontological and Paleoecological Significance

Burrows produced by skinks have a moderate preservation potential because they can be produced and maintained in firm and moist sediments that are resistant to collapse. The preservation of a skink burrow would require a rapid influx of sediment with a contrasting lithology. Rapid sediment influxes that could fill burrows are common along rivers and streams in Southeast Asia where storms and heavy rainfalls cause regular flooding events (Dudgeon 1999). Burrows from temperate and tropical ground-dwelling skinks such as *M. multifasciata* should, therefore, be well represented in the fossil record especially given the abundance, large geographic diversity, and long evolutionary history of skinks. The failure to recognize skink burrows has likely contributed to the scarcity of these structures in the literature. An increased awareness and recognition of skink burrows in the fossil record will allow for a more complete evolutionary and biogeographic history of this small, difficult to preserve group of animals.

Skinks are preyed upon by larger lizards, snakes, and birds (Pianka and Vitt 2006). Skinks, in turn, primarily feed on insects, but are also known to consume fruits, seeds, and vegetation (Iwamoto 1986; Grimmond et al. 1994; Attum et al. 2007; Carretero et al. 2010). Skinks are typically intermediate predators and are important components of healthy and recovering ecosystems (Iwamoto 1986; Fox 1997; Vreeland and Tietje 2000; Norbury et al. 2009). Skinks can even be the top predators in island and stressed ecosystems (Iwamoto 1986; Carretero et al. 2010) and are, therefore, vital in the maintenance of stable ecosystems as well as the further recovery of fragile ecosystems.

Due to their important roles in modern terrestrial ecosystems, the recognition of their burrows in the fossil record would allow for a better interpretation of paleoecological conditions. For example, the occurrence of skinks in a particular stratigraphic unit would suggest the presence of at least minimal vegetation for consumption, vegetative cover for thermoregulation and escape, and a stable population of arthropods. Extant lizards can typically be used to deduce the biomass of insect populations. Regressions on prey and predator weight have been used by Vezina (1985) to estimate the mean prey weight and the range of prey sizes consumed by insectivores. Sabo and Power (2002) measured the biomass of terrestrial arthropods in response to predation by the Western fence lizard (*Sceloporus occidentalis*). The

recognition of skink burrows could, therefore, be used to deduce at least the presence if not the relative abundance of other invertebrates, such as arthropods, since these food resources would be needed to support any skink population.

14.7.3 Paleopedological and Paleoenvironmental Significance

Observations made during these experiments have shown that skinks do play a role in pedogenesis. Although the burrows produced by *M. multifasciata* in the experiments did not reach a depth greater than 14.0 cm, skink burrows have been observed to reach a depth of 33.0 cm in natural settings (Hasiotis and Bourke 2006). These depths are associated with the A and B horizons of modern soils. Through the creation of burrows, mounds, and depressions, skinks mix and aerate the sediment. These processes also loosen the sediment and increase its porosity and permeability (Hole 1981; Wilkinson et al. 2009). The alteration of these sediment properties create preferred flow pathways for the migration of water and oxygen into the sediment (Schaetzl and Anderson 2005). Even when open burrows produced by *M. multifasciata* collapse, the resulting sediment is looser than the surrounding area and retains a relatively higher porosity and permeability. The creation of flow paths for water and oxygen allows for chemical processes including mineral dissolution, cementation, hydration, and oxidation to occur; these processes are essential to pedogenesis and soil maturation (Schaetzl and Anderson 2005). The skinks also directly contributed organics to the sediment in the form of fecal material and shed skin; in natural settings, these organics provide nutrients for soil microbes and plants forming the basis for soil food webs (Hole 1981; Wilkinson et al. 2009). Skinks, therefore, do affect multiple aspects of soil formation. The presence of fossil skink burrows in a paleosol would require the consideration of the influences outlined above when interpreting the soil-forming processes that produced the soil. Neoichnological work, even in laboratory settings, helps to inform on the influences of organisms on sedimentary material.

14.8 Conclusions

Neoichnological studies are necessary for the accurate interpretation of behaviors, burrowing methods, and trace makers associated with trace fossils. Because continental trace fossils are understudied with respect to their marine counterparts, traces produced in continental settings are often unrecognized, under-sampled, or excluded from study. Studies involving the neoichnology of extant continental trace makers are needed to correct this marine-based sampling bias and are crucial in the identification of continental trace makers as well as the interpretation of continental paleoenvironments and paleoecology. Since continental trace makers play a funda-

mental role in pedogenesis, continental neoichnological studies are also necessary for the interpretation of paleosols.

While engaged in dwelling, escape, and predation behaviors, the burrowing skink *M. multifasciata* produced seven distinct burrow architectures including three types of ramps (simple, sinuous, and branched), three types of U-shaped burrows (regular, subhorizontal, and branched), and J-shaped burrows. Despite the architectural differences, the burrows produced by *M. multifasciata* had similar average widths, heights, and width-to-height ratios and were found to have moderate-to-very high degrees of resemblance based on a Bray–Curtis similarity analysis (0.9–0.6). Sediment density and moisture resulted in few variations in the quantitative properties. Many of the burrows showed a conservation of form despite the changes in environmental parameters indicating that the morphology and behavior of *M. multifasciata* has a greater influence on burrow morphology than external environmental conditions.

The use of modern analogs, such as skinks, in the identification of burrows produced by reptilian continental burrowers is necessary for the accurate interpretation of the paleoecology of ancient terrestrial environments. The lack of literature concerning the burrowing behaviors and resulting structures produced by such lizards as *M. multifasciata* may result in the misidentification of lizard burrows and the exclusion of lizards from paleoecological reconstructions. Through the use of modern analogs, this study has demonstrated the range of biogenic structures produced by small, rarely preserved lizards.

This study not only allows for the potential recognition of biogenic structures produced by skinks, it also illustrates the importance of the use of modern analogs in paleontological evaluations. Biogenic structures produced by modern analogs allow for the relationships between the morphology of the trace maker, the morphology of the burrow, and environmental conditions to be directly observed. It is only through these modern observations that accurate interpretations can be made regarding trace fossils, their likely trace makers, and the surrounding environmental conditions.

References

Attum O, Eason P, Cobbs G (2007) Morphology, niche segregation, and escape tactics in a sand dune lizard community. J Arid Environ 68:564–573

Begall S, Gallardo MH (2006) *Spalacopus cyrus* (Rodentia: Octodontidae): an extremist in tunnel constructing and food storing among subterranean mammals. J Zool 251:53–60

Bertling M, Braddy SJ, Bromley RG, Demathieu GR, Genise J, Mikul R, Nielsen JK, Nielsen KSS, Rindsberg AK, Schlirf M (2006) Names for trace fossils: a uniform approach. Lethaia 39:265–286

Bromley RG (1996) Trace fossils: biology, taphonomy and applications, 2nd edn. Chapman & Hall, London

Carretero MA, Cascio PL, Corti C, Pasta S (2010) Sharing resources in a tiny Mediterranean island? Comparative diets of *Chalcides ocellatus* and *Podarcis filfolensis* in Lampione. Bonn Zool Bull 57:111–118

Chapple DG (2003) Ecology, life-history, and behavior in the Australian scincid genus *Egernia*, with comments on the evolution of complex sociality in lizards. Herpetol Monogr 17:145–180

Counts JW, Hasiotis ST (2009) Neoichnological experiments with masked chafer beetles (Coleoptera, Scarabaeidae); implications for backfilled continental trace fossils. PALAIOS 24:74–91

Currie PJ (1983) Hadrosaur trackways from the Lower Cretaceous of Canada. Acta Palaeontol Polonica 28:63–73

Damiani R, Modesto S, Yates A, Neveling J (2003) Earliest evidence of cynodont burrowing. Proc R Soc Lond Ser B: Biol Sci 270:1747

Datta P, Ray S (2006) Earliest lizard from the Late Triassic (Carnian) of India. J Vert Paleontol 26:795–800

Dudgeon D (1999) Tropical Asian streams: zoobenthos, ecology and conservation. Hong Kong University Press, Hong Kong

Estes R (1969) A scincoid lizard from the Cretaceous and Paleocene of Montana. Breviora 331:1–9

Fox BJ (1997) Fauna habitat reconstruction after mining. In: Asher CJ, Bell LC (eds) Fauna habitat reconstruction after mining. Australia Centre for Minerals Exploration and Research, Adelaide, pp 151–160

Frey RW (1970) Environmental significance of recent marine Lebensspuren near Beaufort, North Carolina. II. J Paleontol 44:507–519

Gingras MK, Bann KL, MacEachern JA, Waldron J, Pemberton SG (2007) A conceptual framework for the application of trace fossils. In: MacEachern JA, Bann KL, Gingras MK, Pemberton SG (eds) Applied ichnology. Society of Economic Paleontologists and Mineralogists Short Course Notes 52:1–25

Gobetz KE, Martin LD (2006) Burrows of a gopher-like rodent, possibly *Gregorymys* (Geomyoidea: Geomyidae: Entoptychinae), from the early Miocene Harrison Formation, Nebraska. Palaeogeogr Palaeocl 237:305–314

Grimmond NM, Preest MR, Pough FH (1994) Energetic cost of feeding on different kinds of prey for the lizard *Chalcides ocellatus*. Funct Ecol 8:17–21

Groenewald GH, Welman J, MacEachern JA (2001) Vertebrate burrow complexes from the Early Triassic *Cynognathus* Zone (Driekoppen Formation, Beaufort Group) of the Karoo Basin, South Africa. PALAIOS 16:148–160

Gupta DP, Sinha AK (2001) Notes on the burrows of *Varanus bengalensis* in and around Agra. Zoos' Print J 16:651–654

Halfen AF, Hasiotis ST (2010) Neoichnological study of the traces and burrowing behaviors of the western harvester ant *Pogonomyrmex occidentalis* (Insecta: Hymenoptera: Formicidae): paleopedogenic and paleoecological implications. PALAIOS 25:703–720

Hasiotis ST (2002) Continental trace fossils. Society for Sedimentary Geology, Tulsa

Hasiotis ST (2003) Complex ichnofossils of solitary and social soil organisms: understanding their evolution and roles in terrestrial paleoecosystems. Palaeogeogr Palaeocl 192:259–320

Hasiotis ST (2004) Reconnaissance of Upper Jurassic Morrison Formation ichnofossils, Rocky Mountain Region, USA: paleoenvironmental, stratigraphic, and paleoclimatic significance of terrestrial and freshwater ichnocoenoses. Sediment Geol 167:177–268

Hasiotis ST (2006) The application of ichnology to paleoenvironmental and stratigraphic analysis. PALAIOS 21:401–402

Hasiotis ST, Bourke MC (2006) Continental trace fossils and museum exhibits: displaying organism behaviour frozen in time. Geol Curator 8:211–226

Hasiotis ST, Platt B, Hembree DI, Everhart M, Miller W (2007) The trace-fossil record of verte-brates. In: Miller W III (ed) Trace fossils: concepts, problems, prospects. Elsevier, Amsterdam, pp 196–218

Hembree DI (2013) Neoichnology of the whip scorpion *Mastigoproctus giganteus*: complex bur-rows of predatory terrestrial arthropods. PALAIOS 28:141–162.

Hembree DI (2009) Neoichnology of burrowing millipedes: linking modern burrow morphology, organism behavior, and sediment properties to interpret continental ichnofossils. PALAIOS 24:425–439

Hembree DI, Hasiotis ST (2006) The identification and interpretation of reptile ichnofossils in paleosols through modern studies. J Sediment Res 76:575–588

Hembree DI, Hasiotis ST (2007) Biogenic structures produced by sand-swimming snakes: a mod-ern analog for interpreting continental ichnofossils. J Sediment Res 77:389–397

Hembree DI, Hasiotis ST (2008) Miocene vertebrate and invertebrate burrows defining com-pound paleosols in the Pawnee Creek Formation, Colorado, U.S.A. Palaeogeogr Palaeocl 270:349–365

Hembree DI, Martin LD, Hasiotis ST (2004) Amphibian burrows and ephemeral ponds of the Lower Permian Speiser Shale, Kansas: evidence for seasonality in the Midcontinent. Palaeo-geogr Palaeocl 203:127–152

Hembree DI, Johnson LM, Tenwalde RM (2012) Neoichnology of the desert scorpion *Hadrurus arizonensis*: burrows to biogenic cross lamination. Palaeontol Electron 15:1.10A

Hole FD (1981) Effects of animals on soil. Geoderma 25:75–112.

Irby GV, Albright III LB (2002) Tail-drag marks and dinosaur footprints from the Upper Creta-ceous Toreva Formation, northeastern Arizona. PALAIOS 17: 516–521

Iwamoto T (1986) Mammals, reptiles and crabs on the Krakatau Islands: their roles in the ecosys-tem. Ecol Res 1:249–258

Ji X, Lin LH, Lin CX, Qiu QB, Du Y (2006) Sexual dimorphism and female reproduction in the many-lined sun skink (*Mabuya multifasciata*) from China. J Herpet 40:351–357

Kraus MJ, Riggins S (2007) Transient drying during the Paleocene-Eocene thermal maxi-mum (PETM): analysis of paleosols in the Bighorn Basin, Wyoming. Palaeogeogr Palaeocl 245:444–461

Kubo T, Benton MJ (2009) Tetrapod postural shift estimated from Permian and Triassic trackways. Palaeontol 52:1029–1037

Lockley MG, Hunt AP, Meyer C (1994) Vertebrate tracks and the ichnofacies concept: implica-tions for paleoecology and palichnostratigraphy. In: Donovan SK (ed) The paleobiology of trace fossils. Wiley, New York, pp 241–268

Martin AJ (2009) Dinosaur burrows in the Otway Group (Albian) of Victoria, Australia, and their relation to Cretaceous polar environments. Cret Res 30:1223–1237

Martin LD, Bennett DK (1977) The burrows of the Miocene beaver *Palaeocastor*, western Ne-braska, USA. Palaeogeogr Palaeocl 22:173–193

Martin JE, Hutchinson MN, Meredith R, Case JA, Pledge NS (2004) The oldest genus of scin-cid lizard (Squamata) from the tertiary Etadunna Formation of South Australia. J Herpetol 38:180–187

Melchor RN, Genise JF, Farina JL, Sanchez MV, Sarzetti L, Visconti G (2010) Large striated bur-rows from fluvial deposits of the Neogene Vinchina Formation, La Rioja, Argentina: a crab origin suggested by neoichnology and sedimentology. Palaeogeogr Palaeocl 291:400–418

Milne T, Bull CM, Hutchinson MN (2002) Characteristics of litters and juvenile dispersal in the endangered Australian skink *Tiliqua adelaidensis*. J Herpetol 36:110–112

Norbury G, Heyward R, Parkes J (2009) Skink and invertebrate abundance in relation to vegeta-tion, rabbits and predators in a New Zealand dryland ecosystem. NZ J Ecol 33:24–31

Peabody FE (1954) Trackways of an ambystomid salamander from the Paleocene of Montana. J Paleontol 28:79–83

Pianka ER, Vitt LJ (2006) Lizards: windows to the evolution of diversity. University of California Press, Berkeley

Retallack GJ, Ekdale AA, Picard MD (1984) Trace fossils of burrowing beetles and bees in an Oligocene paleosol, Badlands National Park, South Dakota. J Paleontol 58:571–592

Rhoads DC (1975) The paleoecological and environmental significance of trace fossils. In: Frey RW (ed) The study of trace fossils. Springer, New York, pp 147–160

Romer AS, Olson EC (1954) Aestivation in a Permian lungfish. Brevoira 30:1–8

Sabo JL, Power ME (2002) Numerical response of lizards to aquatic insects and short-term consequences for terrestrial prey. Ecology 83:3023–3036

Sarjeant WAS (1975) Fossil tracks and impressions of vertebrates. In: Frey RW (ed) The study of trace fossils. Springer, New York, pp 283–324

Schaetzl RJ, Anderson S (2005) Soils: genesis and geomorphology. Cambridge University Press, Cambridge

Smith RMH (1987) Helical burrow casts of therapsid origin from the Beaufort Group (Permian) of South Africa. Palaeogeogr Palaeocl 60:155–169

Smith JJ, Hasiotis ST (2008) Traces and burrowing behaviors of the cicada nymph *Cicadetta calliope*; neoichnology and paleoecological significance of extant soil-dwelling insects. PALAIOS 23:503–513

Smith JJ, Hasiotis ST, Kraus MJ, Woody DT (2008) Relationship of floodplain ichnocoenoses to paleopedology, paleohydrology, and paleoclimate in the Willwood Formation, Wyoming, during the Paleocene-Eocene thermal maximum. PALAIOS 23:683–699

Sun YY, Yang J, Ji X (2009) Many-lined sun skinks (*Mabuya multifasciata*) do not compensate for the costs of tail loss by increasing feeding rate or digestive efficiency. J Exp Zool A: Ecol Genet Physiol 311:125–133

Taylor EH (1963) The lizards of Thailand. Univ Kans Sci Bull 44:687–1077

Traeholt C (1995) Notes on the burrows of the water monitor lizard, *Varanus salvator*. Malay Nat J 49:103–112

Uchman A, Pervesler P (2006) Surface Lebensspuren produced by amphipods and isopods (Crustaceans) from the Isozo delta tidal flat, Italy. PALAIOS 21:384–390

Voorhies M (1975) Vertebrate burrows. In: Frey RW (ed) The study of trace fossils. Springer, New York, pp 325–350

Vreeland JK, Tietje WD (2000) Numerical response of small vertebrates to prescribed fire in California oak woodland. In: Ford WM, Russell KR, Moorman CE (eds) The role of fire in nongame wildlife management and community restoration: traditional uses and new directions proceedings of a special workshop. USDA Forest Service, Northeastern Research Station, pp 100–110

Vezina AF (1985) Empirical relationships between predator and prey size among terrestrial vertebrate predators. Oecologia 67:555–565

Wellstead CF (1982) Lizards from the Lower Valentine Formation Miocene of northern Nebraska USA. J Herpet 16:364–375

White CR (2005) The allometry of burrow geometry. J Zool Lond 265:395–403

Wilkinson MT, Richards PJ, Humphreys GS (2009) Breaking ground: pedological, geological, and ecological implications of soil bioturbation. Earth Sci Rev 97:254–269

Young BA, Morain M (2003) Vertical burrowing in the Saharan sand vipers (Cerastes). Copeia 2003:131–137

Zug GR, Vitt LJ, Caldwell JP (2001) Herpetology: an introductory biology of amphibians and reptiles, 2nd edn. Academic Press, London

Chapter 15
Novel Neoichnology of Elephants: Nonlocomotive Interactions with Sediment, Locomotion Traces in Partially Snow-Covered Sediment, and Implications for Proboscidean Paleoichnology

Brian F. Platt and Stephen T. Hasiotis

Contents

Abstract We observed trace-making behaviors of one female African elephant (*Loxodonta africana*) and one female Asian elephant (*Elephas maximus*) in a zoo setting. Our objective was to document uncommonly studied traces, that is, traces other than dung and footprints in sediments, so that paleoichnological researchers may benefit from a broader search pattern when investigating trace fossils with potential proboscidean affinities. We observed six distinct traces: trunk-grasping traces, small pits from active and passive dispersal of water and sediment, urina-

B. F. Platt (✉)
Department of Geology and Geological Engineering, University of Mississippi, 120A Carrier Hall, Oxford, MS 38677, USA
e-mail: bfplatt@olemiss.edu

S. T. Hasiotis
Department of Geology, University of Kansas, 1475 Jayhawk Blvd., Rm. 120, Lawrence, KS, 66045, USA

tion traces, resting traces, wallowing traces, and dissected tracks created in partially snow-covered sediment. Of these traces, none attributable to proboscideans have been reported in the fossil record. The resting traces we observed, however, were created in dry sand and would likely not be preserved in the fossil record because of a high potential for disturbance before burial. Similarly, the trunk traces we observed in dry sand would likely have low preservation potential. Pits from thrown and blown sediment and water, wallowing traces, and snow-influenced tracks should have a higher probability of survival into the fossil record. Tracks representative of partially snow-covered ground are recognizable by sediment pedestals within undertracks. In such tracks, which we refer to as hanging tracks, the top surface of the pedestal is all that remains of the true track. The undertrack surrounding the pedestal(s) was created from the elephant's foot pressing snow into the underlying sediment. The snow later melted away. Pleistocene proboscideans likely encountered partially snow-covered ground, so hanging tracks may be preserved in the rock record. Recognition of these tracks would be extremely informative about paleoclimate, but further research is needed to determine if they can be easily distinguished from tracks created exclusively in sediment.

15.1 Introduction

Footprints in sedimentary media are perhaps the most often studied subjects in vertebrate ichnology and, indeed, such footprints were meant to be our focus during a recently completed elephant neoichnology project (Platt et al. 2012). During the course of our research, however, we observed a number of additional elephant traces that we consider to be of interest to the vertebrate ichnological community. The objectives of this chapter are to (1) describe surface traces made by elephants, excluding dung and footprints formed entirely in sediment, and (2) relate those traces to observed elephant behaviors. Our goal is to evaluate the potential fossil record of the observed traces and provide search patterns for future paleontological investigations of proboscidean trace fossils. Recognition of ancient examples of the traces described herein can provide important behavioral, paleoenvironmental, and even paleoclimatic information that may be otherwise overlooked.

15.2 Methods and Materials

We observed traces and behaviors of elephants during 31 visits to the Topeka Zoo, Topeka, Kansas, USA, between July 27, 2005 and November 13, 2008. Observations involved an adult female African elephant (*Loxodonta africana*) named

Fig. 15.1 Map of the elephant enclosure at the Topeka Zoo, Kansas, USA
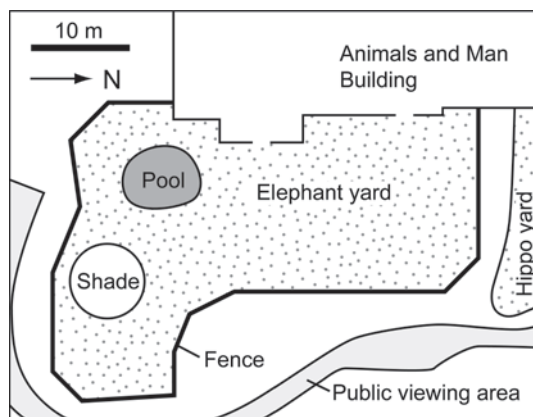
Tembo and an adult female Asian elephant (*Elephas maximus*) named Sunda. The elephants are housed in an enclosure with indoor and outdoor areas (Fig. 15.1). The outdoor area is a fenced tract of land that consists of a 22-cm-thick layer of sand derived from the Kansas River that overlies > 10 cm of dark, organic-rich clay. Surface sediment texture differs between locations within the outdoor enclosure because of differences in topography and drainage.

For safety reasons, we were separated from the elephants by protective barriers, that is, an electrified wire fence or a barred wall, for all behavioral observations. Many behaviors were recorded on a MiniDV camcorder and a digital video-capable camera. All traces were observed in the outdoor portion of the enclosure while the elephants were confined to the indoor area. Most traces could not be directly associated with a specific instance of a behavior or a specific elephant because of accessibility limitations during observations. When a trace could not be attributed to a specific behavior, an indirect association was made based on multiple observations and review of video footage.

We avoid treatment of modern dung and footprints created in sediment because we have provided documentation of those traces elsewhere (Platt et al. 2010; Platt et al. 2012). Additionally, ancient proboscidean dung and footprints are both reported in the literature, and criteria for their recognition are already well established (e.g., Mead et al. 1986; Scrivner and Bottjer 1986; Higgs et al. 2003; Roberts et al. 2008).

15.3   Results

We recognize six types of traces as a result of our observations. For each trace, we present a description followed by the observed or inferred behaviors responsible for creating the trace. Remarks about captive versus wild behaviors, preservation potential, comparative ichnofossils, and the fossil record of proboscidean traces are presented in the discussion.
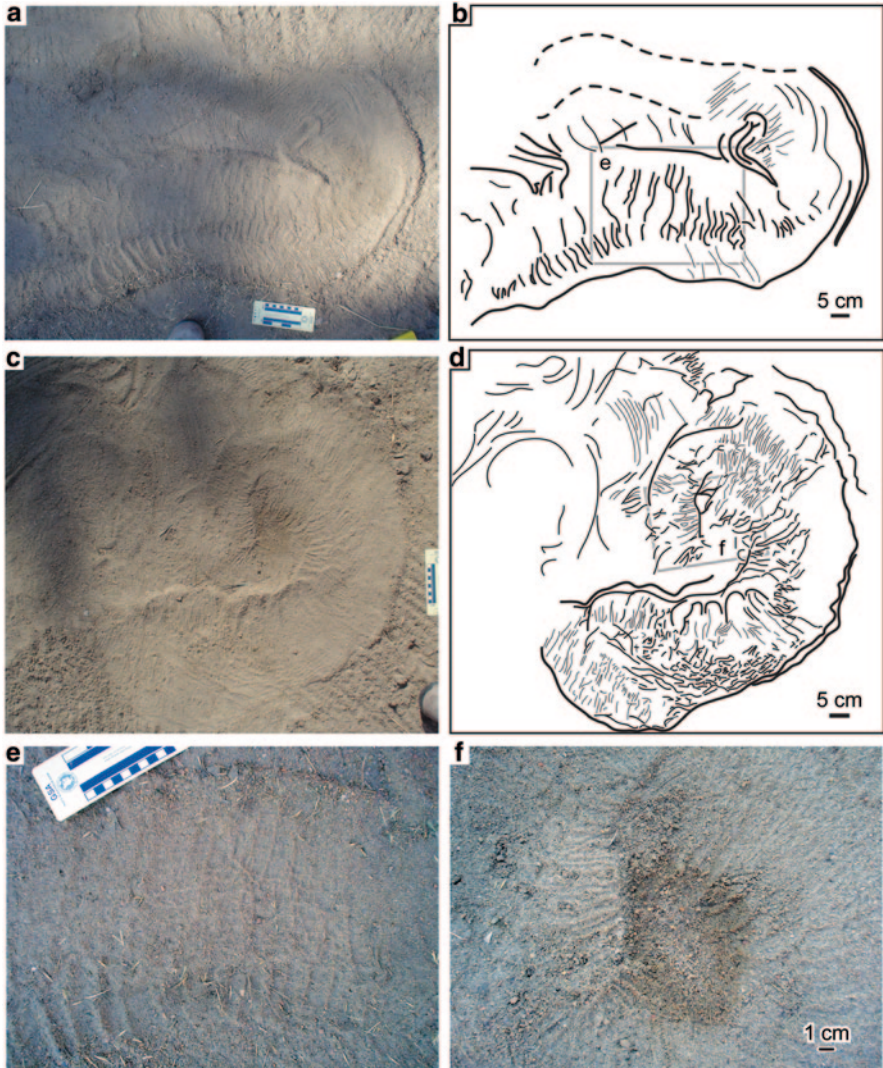
Fig. 15.2 Trunk grasping traces and behavior. **a** Surficial trunk trace in loose sand. **b** Line drawing of trace shown in (**a**). **c** Surficial trunk trace in loose sand. **d** Line drawing of trace shown in (**c**). **e** Close-up of texture in box in (**b**). **f** Close-up of texture in box in (**d**)

15.3.1 Spiral to Vermiform Surface Patterns—Trunk-Grasping Traces

Description Flat to wrinkled, elongate traces on the ground surface up to 150 cm long and 30 cm wide (Fig. 15.2). Traces are typically curved to spiraled and bordered by raised ridges. Surface features include narrow linear ridges that are per-
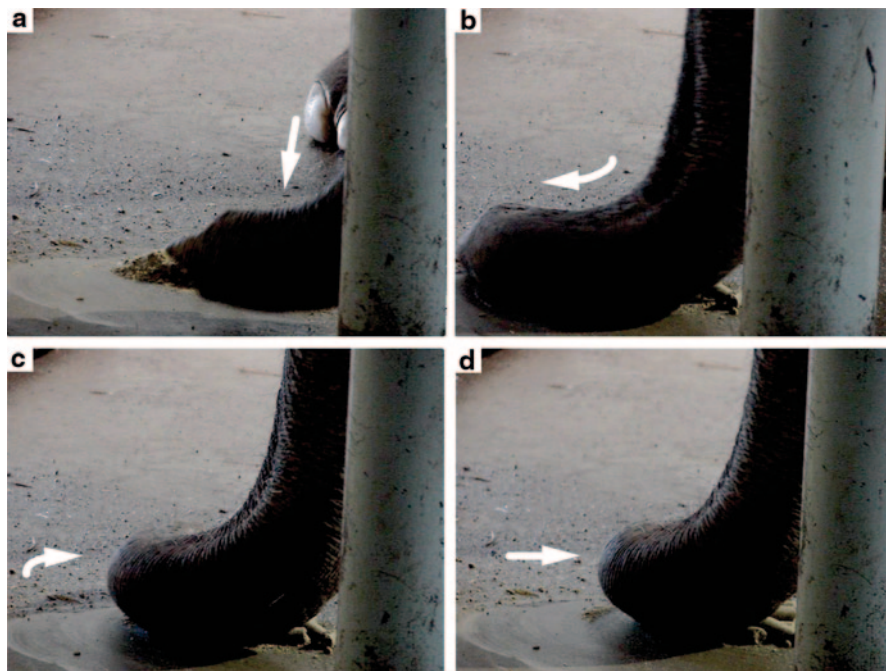
Fig. 15.3 Sequential still images captured from video showing trunk-grasping behavior. *Arrows* show approximate motion of the trunk tip prior to the capture of each still image

pendicular to the long axis of the trace and are more closely spaced in the insides of curves than in the outsides of curves. The elongate traces may also be flanked by semicircular, curved striations perpendicular to their long axes.

Behaviors These traces result from contact between the trunk and the sediment while an elephant is grasping an object or other material on the ground. The elephant curls its trunk around the object or material and lifts it off the ground (Fig. 15.3) leaving an impression of the curled trunk at its last point of contact with the ground. The sweeping motion associated with curling of the trunk leaves curved striations adjacent to the trunk impression. This behavior was observed in association with picking up food items for eating, objects of interest for inspecting, and sand for throwing.

15.3.2   Small-Diameter Pits—Traces of Blown Water, Dripped Water, and Thrown Sediment

Description Hemispherical to hemiovoid pits that range in diameter from ~0.5 to ~2 cm (Fig. 15.4a–d). A raised rim around the border of the pits is common. Some rims in moist, fine-grained sediment contain teardrop-shaped extensions radiating away
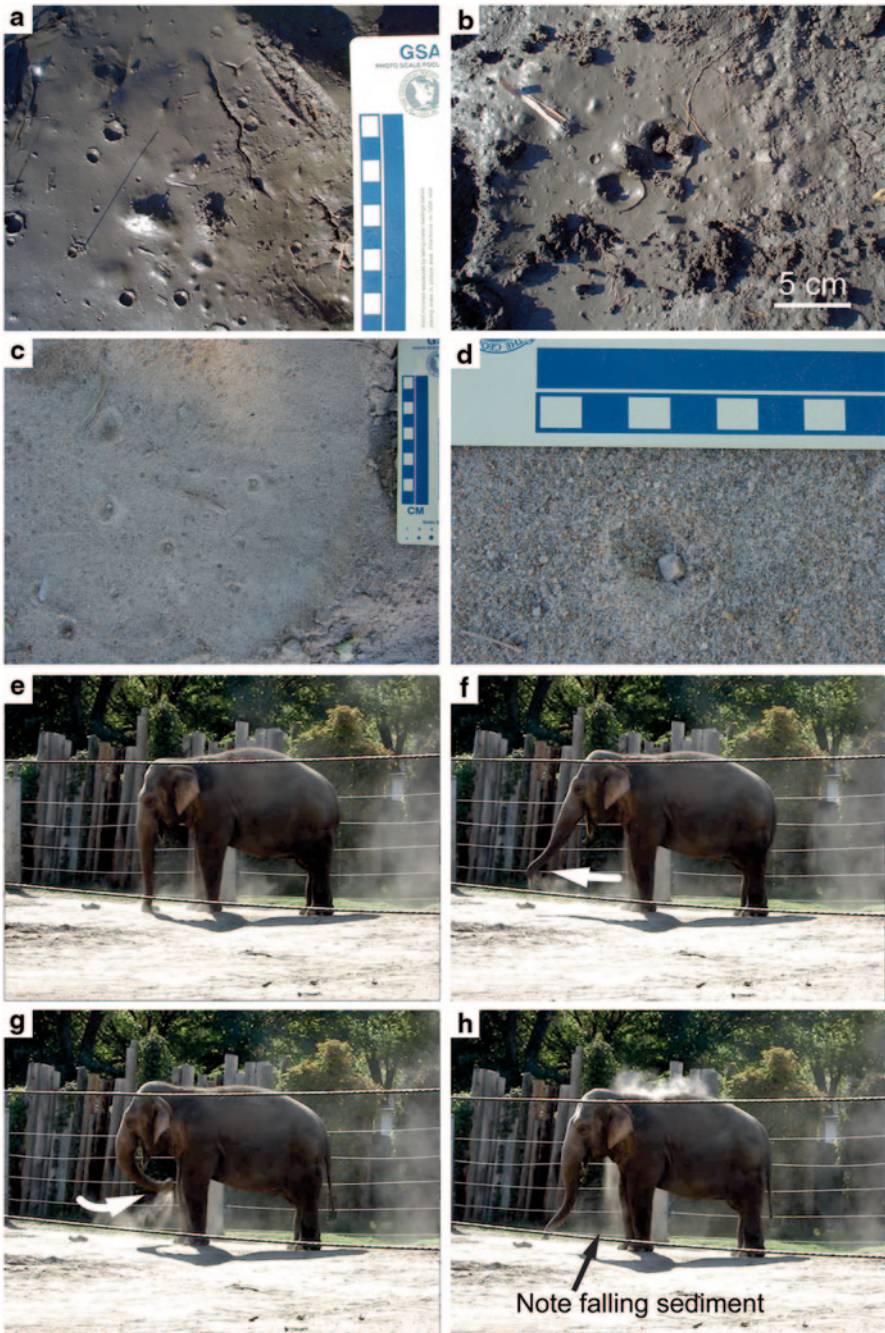
Fig. 15.4 Small pits and sediment-throwing behavior. **a** Pits in moist mud with no associated impactors, interpreted as the result of impact with water only. **b** Pits in moist mud with associated sediment clods. **c** Pits in loose sand containing single, coarse grains of sand. **d** Close-up of individual pit in loose sand with associated pebble. **e–h** Sequential still images captured from video showing sediment grasping and throwing behavior. *Arrows* show swinging trunk motion associated with throwing sediment

from the center of the pit. Lateral distribution of pits across the ground surface varies, but the density of pits we observed ranged from ~10 to ~20 per 100 cm^2. Some pits contain a pebble, very coarse sand grain, or mud clod in their centers (Fig. 15.4a–d).

Behaviors These traces represent impact pits from passive and active dispersal of water and sediment. Passive dripping of water from mouths and bodies of the elephants was observed while they were drinking and when exiting the pool in the outdoor portion of their enclosure. We also observed the elephants actively spraying water from their trunks.

We frequently observed both elephants picking up loose, dry sediment with their trunks and throwing that sediment on their backs and underneath their bodies (Fig. 15.4e–h). Pits that contain sand grains, pebbles, and mud clods appear to be the direct result of sediment-throwing behavior. The range in pit morphology from circular to elliptical represents impacts at various velocities and trajectories (e.g., Zheng et al. 2004).

15.3.3   Large-Diameter, Circular to Irregular Depressions—Urination Traces

Description Circular to irregular depressions in the sediment 8–10 cm in diameter and up to ~3 cm deep (Fig. 15.5). One single or multiple depressions may be present. Depressions are often associated with dung boluses (Fig. 15.5d–f). Depressions may have steep or gently sloped walls and may be surrounded by a raised rim from <0.5 cm to ~2 cm high. Shallow, gently sloped depressions may be present in pairs separated by up to 10 cm (Fig. 15.5e and f). Rims may contain breaks with small sediment fans radiating and fining away from the depression (Fig. 15.5c and d). The ground surface around a depression may also contain a concentric ring of coarse grains up to tens of centimeters away from the depression (Fig. 15.5a).

Behaviors These depressions are the result of urination. Unfortunately, individual depressions could not be matched up with discrete incidents of urination so we cannot be sure if there are differences in depression morphology between the elephants. Also, we cannot be sure if the elephants were completely still or were moving during urination. We suspect that elongate and double depressions may be the result of locomotion during urination. The volume of urine released also could not be measured, but presumably differences in volume may have affected the morphology of the depressions. Sediment fans and rings of coarse sediment indicate overland flow with sufficient energy to transport sand grains.

15.3.4   Body Impressions—Resting Traces

Description Large, irregular areas of the ground surface up to 3.8 m long and 1.5 m wide, with subtle relief and smooth to textured surficial morphology (Fig. 15.6). A partial raised rim at their extreme edges encloses some examples (Fig. 15.6a
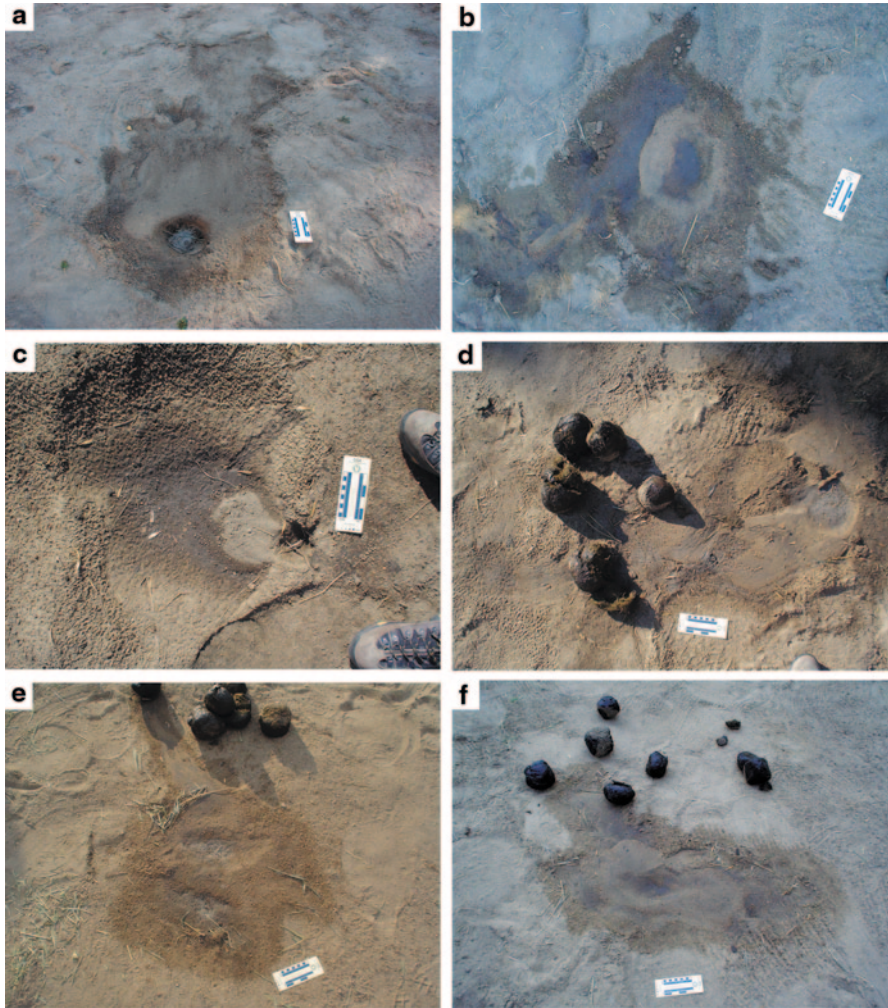
Fig. 15.5 Urination pits. **a** and **b** Circular pits. **c** and **d** Circular pits with breached walls. **e** and **f** Multiple pits. Note the general association of feces with urine pits

and b). Surface textures consist of linear, parallel (Fig. 15.6e), and/or intersecting (Fig. 15.6h), raised ridges <0.5 cm wide and <0.5 cm tall. Traces are associated with elongate grooves and footprints, with some footprints superimposed on the other traces. These traces were occasionally observed on the ground in the elephant enclosure during early morning visits to the zoo.

Behaviors We did not observe the elephants lying on the ground, but the behavior is confirmed in association with sleeping during the night (D. Olson, personal communication 2007). The raised ridges represent impressions of an elephant's skin patterns during the last period of contact with the ground before the elephant stood
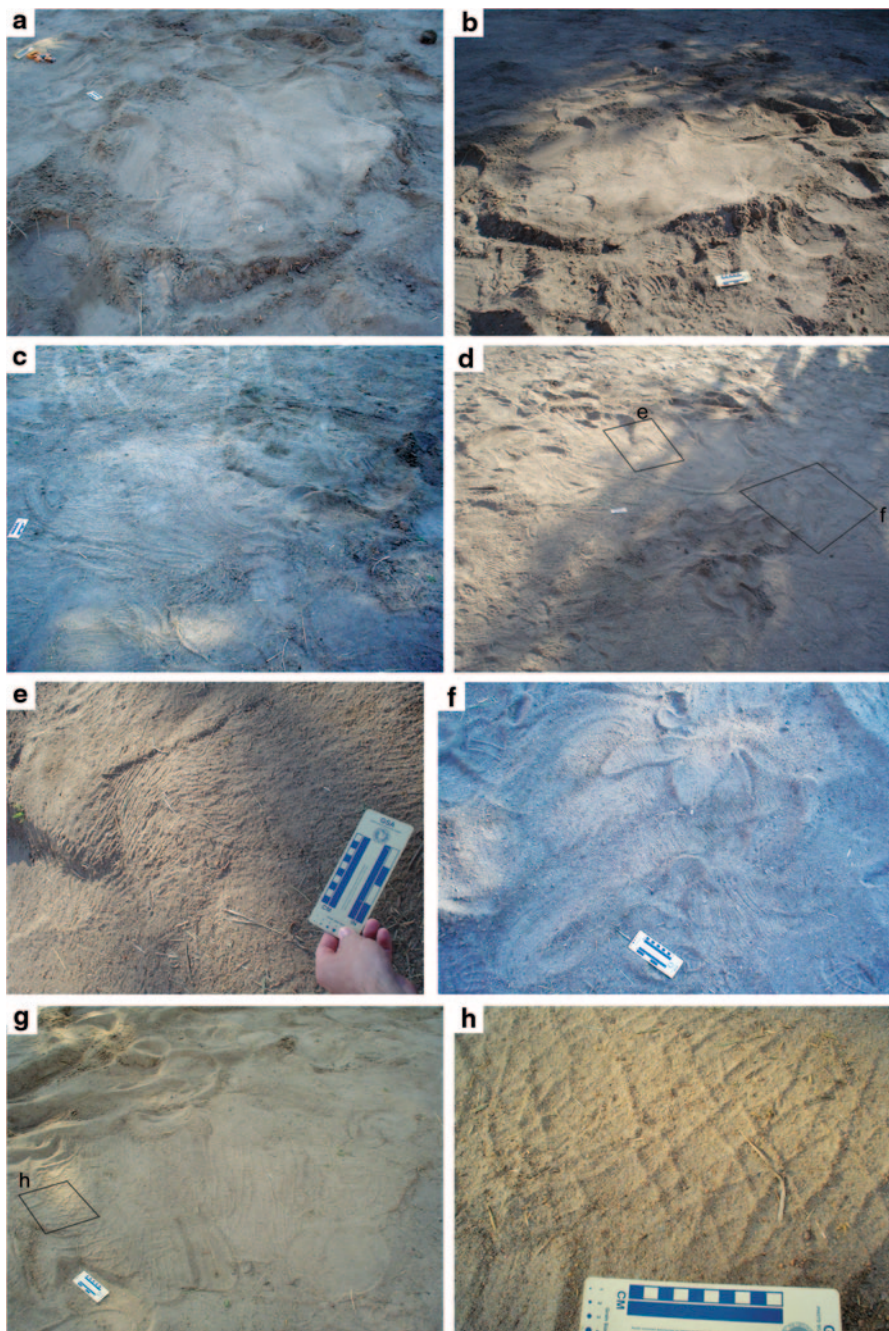
Fig. 15.6 Body impressions. **a–d** Full-body impressions, shown from oblique angles to the surface because sufficient height could not be reached to frame entire trace in perpendicular view; note that (**a**) and (**b**) show the same trace from different angles. **e** Close-up of skin texture shown in (**d**). **f** Close-up of lobate trunk? traces in (**d**). **g** Resting impression with abundant skin impressions. **h** Close-up of skin impression shown in (**g**)

up. Ridges and grooves represent sediment contact while lying down, moving while lying on the ground, or getting up. Tracks superimposed on the body impression may be associated with standing up.

15.3.5 Mega-diameter, Irregular Depressions, and Mounds—Wallowing Traces

Description Patches of ground as large as, or larger than, resting traces with irregular and scalloped borders and an extremely large semicircular depression bordered by mounded sediment (Fig. 15.7a–d). Some mounded sediment contains vertical striations. Down gradient from the main depression are several smaller depressions and sediment mounds (Fig. 15.7d and e), as well as footprints (Fig. 15.7f). Smaller depressions are linear and sinuous, some with associated sediment fans (Fig. 15.7e). Much of the sediment down gradient from the main depression has a rough, hummocky surface texture (Fig. 15.7d–f). Many raised areas of sediment and rims have smooth surfaces. Footprints are deep with vertical striations and slip marks, as well as some raised rims and slump blocks around the edges (Fig. 15.7f).

Behaviors We only witnessed one example of wallowing during our observations. That instance involved Sunda and the behavior can be tied to the resultant trace with certainty. Video review of the incident (Fig. 15.8) shows that Sunda approached a rectangular trench filled with saturated sediment so that her body was perpendicular to the long axis of the trench. She stepped in the sediment with her front feet, began sliding her front feet back and forth, and picking up sediment with her trunk and tossing it at her sides and back. After her initial contact with the sediment, she stepped with her hind legs to rotate her body to be roughly parallel with the long axis of the trench. The rotation of her body placed all four of her feet in the saturated sediment. Instead of putting down her right hind foot to conclude the rotation of her body, Sunda bent her right leg at the knee and put her knee down into the sediment. After that, she sat back with all her weight on her posterior, outstretched her front legs, and laid down on her right side. While lying down, she swung her legs forward and backward, curled her trunk, and nestled her body into the sediment. Then she rolled to her left until she was upright, tossed sediment on herself, and rolled back to the right until she was in a sprawled sitting position. She then rolled onto her left side and continued wallowing.

The final wallowing trace is the result of multiple body parts interacting with the sediment so that most parts of the trace cannot be attributed to any one specific action. The scalloped walls and raised rim are from contact with a combination of Sunda's body and feet. We interpret the hummocky surface texture as the result of sediment liquefaction (e.g., Gillette and Thomas 1985) resulting from the impact of her body with the ground. The sediment certainly was saturated, as evidenced by ponded water on tiered surfaces within the depression. Rather than infiltrating into the sand, much of this water traveled down the gradient over the surface, creating small channels and sediment fans. Footprints superimposed on the rest of the traces were the result of Sunda standing back up and walking away after wallowing (e.g., Fig. 15.7f).

Fig. 15.7 Wallowing trace. **a–d** Multiple views of wallow trace. **e** Close-up of texture of hummocky, liquefied sediment. **f** Close-up of footprint within wallow trace; note concentric slumping and mixing of dark and light sediment. Camera bag is 17 cm wide

15.3.6   Dissected Tracks—Tracks Created in Partial Snow Cover

Description Footprints with irregularly shaped, smooth-floored depressions up to 2 cm deep (Fig. 15.9). Depressions may be present throughout a large area of the track, such that adjacent portions of the track appear to be elevated as pedestals (Fig. 15.9a–d). Some edges of pedestals within tracks have low-angle slopes relative to the angles of walls of tracks created entirely in sediment (Fig. 15.9a and b). These low-angle slopes consist of coalescing sediment fans. In our field observations, these tracks were found in association with partially snow-covered ground.
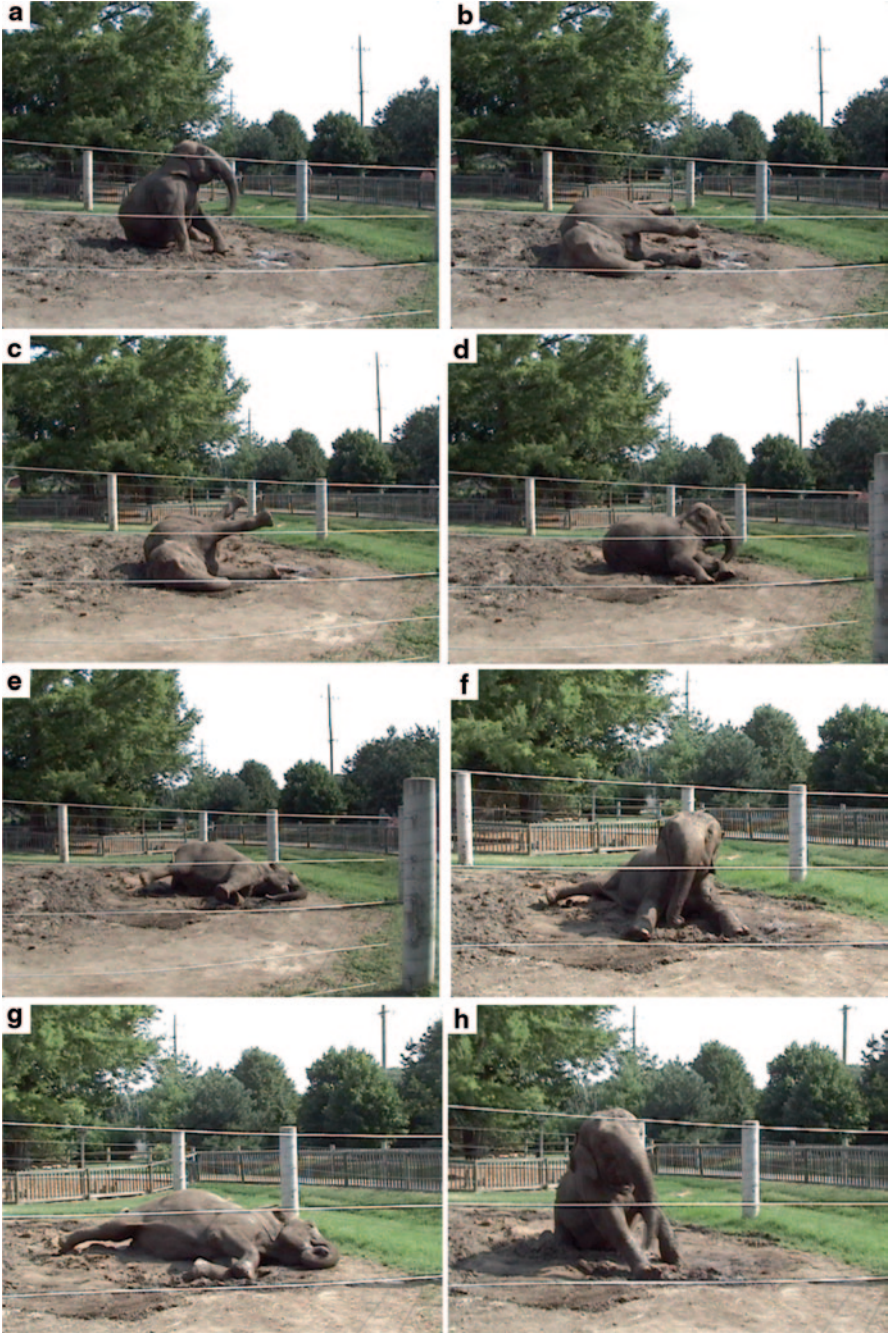
Fig. 15.8 Observed wallowing behavior. **a–h** Sequential still images captured from video of wallowing behavior
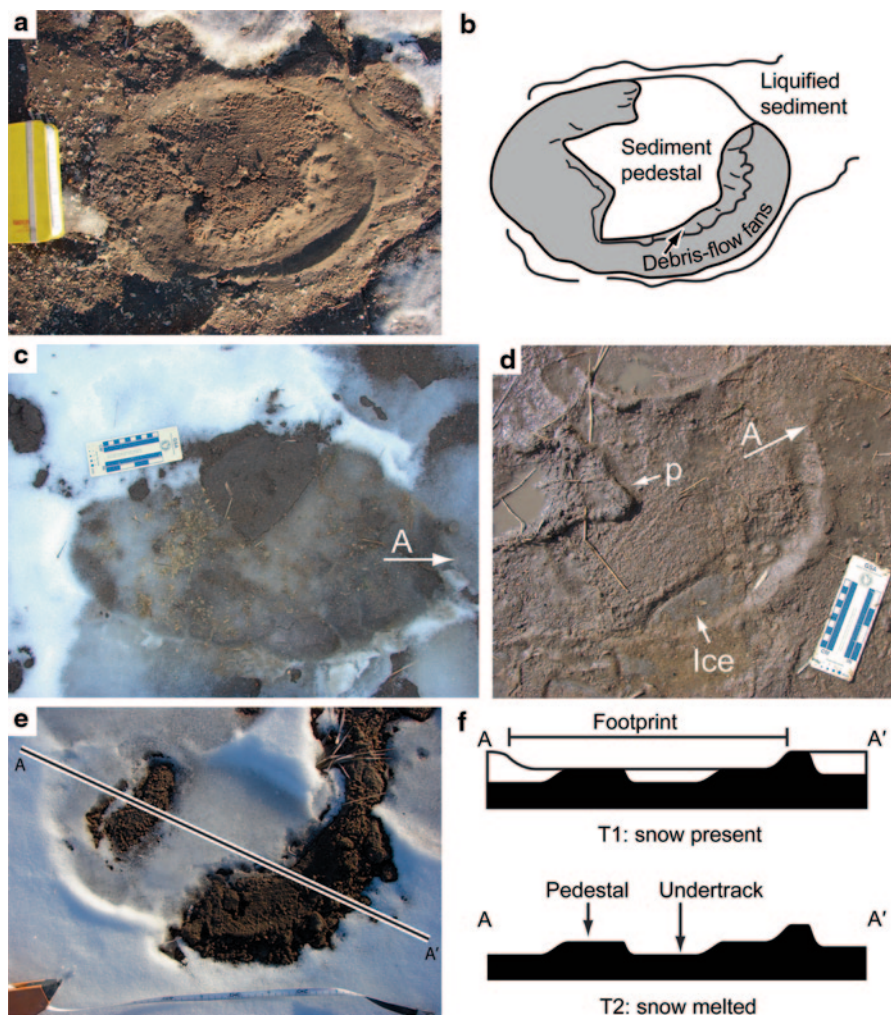
Fig. 15.9 Tracks created in partial snow cover. **a** Photograph of footprint showing sediment pedestal with eroded edges from melting snow, notebook is 17.2 cm long. **b** Line drawing of footprint in (**a**). **c** Footprint with compacted snow present; *A* represents anterior of the track. **d** Footprint from (**c**) after one day of melting; note the amount of erosion of pedestal (*p*) and remnant of ice in track. The pedestal is a remnant of the true track and the lowermost depression is an undertrack. **e** Footprint created in snow and sediment. **f** Cross-section along line *A–A′* in (**e**), showing hypothetical development of truncated or hanging footprint

Many examples of these tracks still contained ice, and inspection of many examples allowed us to piece together the effects of mixed sediment-ice surfaces on tracks.

Behaviors These traces result from normal locomotion in partially snow-covered sediment. An example of how these tracks form is shown in Fig. 15.9f. Locomotion over a surface of mixed snow and sediment creates footprints (Fig. 15.9e); com-

pacted snow becomes dense and in a short period of time turns to ice (Fig. 15.9c). As the snow melts, water collects in depressed areas of the mud. Standing water can make shaft walls (*sensu* Allen 1997) unstable, resulting in collapse and radiating, cm-scale debris flow fans (Fig. 15.9a and b). Once the snow and ice melt, and the water infiltrates into the ground or evaporates, all that remains may be several flat-topped pedestals preserving only small portions of the original footprint (Fig. 15.9f). In cases where snow trampling depressed underlying sediment, any resulting depression may be viewed as an undertrack (e.g., Fig. 15.9d–f). We refer to pedestals within undertracks as hanging tracks, as they are reminiscent of hanging valleys associated with retreating glaciers.

15.4   Discussion

15.4.1   *Behavioral Uniformity—Pervasiveness*

In using two captive elephants for neoichnological observations, we assume that their behaviors are typical of wild elephants. We must, therefore, discuss whether the behaviors we observed are known to occur in wild elephants. We will also consider whether anatomical differences between species and sexes can affect trace morphology.

Trunk Grasping We observed both Tembo and Sunda curling their trunks while in contact with the ground to pick up objects. Manipulation of objects with the trunk tip, however, may differ between African and Asian elephants because of anatomical differences. Asian elephants have a single finger-like extension on the tip of their trunks, whereas African elephants have two extensions (Shoshani 1997). Asian elephants prefer to grasp objects by curling their trunk, but African elephants are able to use the two protrusions on the tips of their trunks like fingers to grasp objects (Shoshani 1997).

Observed trunk grasping occurred in response to the introduction of a small object (e.g., a food item) into the elephants' environment. Elephants are known to use their trunks to grasp fallen fruits on the ground in the wild (Sukumar 2003); this scenario most closely approximates treat retrieval observed at the zoo. In terms of other feeding behaviors, we certainly would not expect the trunk to contact the ground during browsing. Grazing has the greatest potential for trunk-sediment contact, but ground contact may not occur at all during uprooting of grasses depending on where the plants are grasped. Short grasses offer the greatest chance for trunk-sediment contact, which has been documented during the gathering of grasses that have been dislodged by kicking (McKay 1973).

In addition to grasping, elephants use their trunks for other behaviors that may result in trunk-sediment contact. For example, elephants are known to use and modify branches for swatting flies (Hart et al. 2001). During branch modification, some elephants use their feet to hold the branch against the ground while stripping

off unnecessary parts (Hart et al. 2001). Other trunk traces on the ground surface (not reported here) may result from trunk swinging, which is a stereotypic behavior of captive elephants, and is not representative of wild behavior (Elzanowski and Sergiel 2006).

Water Spreading Passive dripping of water associated with drinking and swimming behaviors is to be expected of any elephant, regardless of species or wild or captive status. Water spraying, on the other hand, is an active behavior, and it is observed in wild elephants associated with bathing, drinking, and wallowing (Buss 1990; Owen-Smith 1994). Water spraying can also accompany sediment bathing to create a mud cover on the skin; this may be important for preventing dehydration (Lillywhite and Stein 1987).

Sediment Bathing Both African and Asian elephants sediment bathe in the wild, that is, coat their bodies in sediment (Sikes 1971; Rees 2002). This behavior may help protect the skin from the sun or flies (Sikes 1971; Shoshani 1998) and, consequently, sediment bathing is more common in elephants living in savannahs than in elephants living in forests (Sikes 1971). We have found no mentions of traces associated with sediment bathing in the literature, but we expect that both grasping traces and thrown sediment pits are associated with this behavior. Grasping traces associated with sediment bathing would likely resemble those that we observed at the zoo.

Urination Published records of urination behavior are focused largely on reproductive behaviors and the associated role of chemical signals (e.g., Hollister-Smith et al. 2008); we have seen no discussion of the resulting traces in the literature. Anatomical differences between males and females are known to affect the control and direction of urine expulsion. Bull elephants normally urinate with their penises partially erect to direct urine backward (McKay 1973), but while in the state of heightened sexual and aggressive activity known as musth, the penis remains sheathed, allowing urine to spray on the insides of the individual's hind legs (Poole 1987; Vidya and Sukumar 2005). Cows, on the other hand, normally direct their urine downward and forward (Miall and Greenwood 1878), and changes in their reproductive cycle will alter vulvar morphology (Poole et al. 1997). Whether these anatomical and physiological factors affect urine traces will require additional study.

Little information is available about typical urine volume in wild elephants, but we hypothesize that urine volume, as well as height of the individual, and movement during urination will affect urine pit morphology. Urine volume can be related to hydration (Wiedner et al. 2009), so environmental conditions should potentially influence urine pit size. Locomotion during urination is documented in wild elephants (McKay 1973), so locomotion is a valid factor to consider when interpreting urine pit morphology. We are unsure if there are differences in the urination pits produced by African and Asian elephants, but we did not notice any distinct features that we could attribute to either elephant with certainty. Observations of fecal matter near urine pits agree with other data that show elephants often urinate where they defecate (Bagley et al. 2006).

Resting Elephants are known to lie down to sleep in the wild, but they are also capable of, and may prefer, sleeping in other positions, for example, standing up (Sikes 1971; McKay 1973; Buss 1990; Katugaha 1993). Lying down also helps elephants cool off (Sikes 1971). Direct body–sediment contact while lying down, however, may be minimal in the wild because many elephants prefer to lie down in vegetated areas (Sikes 1971).

Wallowing Wallowing is a normal behavior exhibited by wild elephants and may involve individuals rolling in muddy pools or submerging their bodies in deeper water (Sikes 1971; Owen-Smith 1994). Spraying of water, mud, and dry sediment from the trunk is common during wallowing (Owen-Smith 1994). One of the main goals of these behaviors may be to coat the skin with a layer of mud to prevent dehydration (Lillywhite and Stein 1987).

Locomotion Through Partial Snow Cover Most extant elephants live in warm climates and, therefore, do not normally traverse snow-covered ground. Elephants are tolerant of low temperatures and have, on occasion, been observed encountering snow in their natural ranges. For example, an Asian elephant was documented encountering snow at an elevation of 3,419 m at Shougay La in Bhutan (Tshering 2011). African elephants have been observed at the snow line on Mount Kenya, Kenya (Spinage 1994; Rees 2004), which has an approximate modern elevation of 4,700–4,725 m (Porter 2001). The degree of interaction with snow we observed at the zoo may be representative of modern natural conditions for the observed species.

15.4.2   Preservation Potential and Ancient Records

The traces described herein are most useful to ichnologists if they have sufficient preservation potential to be recorded in ancient strata. We cannot possibly evaluate systematically the survivability of each of the traces we observed, but we can make general comments given our observations of trace frequency and longevity during the data collection period. Some traces and behaviors, beyond what we observed, have been reported in the literature from ancient settings, and we will briefly review them.

Trunk Traces All of the trunk traces we observed were preserved in mostly dry, loose sand. The traces were observed rarely and could be easily obliterated by trampling or other disturbances before burial. The traces are purely surficial and are not expected to be deep because little downward pressure was used during the observed grasping behaviors. Also, there are few natural scenarios that would require trunk–sediment contact during grasping of an object. In our opinion, grasping of sediment for throwing is the behavior most likely to produce surficial trunk traces. Hypothetically, if a trunk trace was created in muddy sediment, survivorship would be increased, but we still regard these traces as poor candidates for preservation in the fossil record. Preservation of these traces in loose sand may be facilitated by stabili-

zation from moisture supplied by fog or dew, as is hypothesized in the fossilization of surface traces in eolian environments (e.g., Hasiotis 2004, 2008; Davis et al. 2007; Schmerge et al. 2013).

We know of no reported fossil trunk traces from the literature, but this is not surprising if they have a low preservation potential, and their morphology is unknown to ichnologists. Trunk traces are also not expected to be present throughout the entire range of proboscidean evolution (Late Paleocene–recent; Gheerbrant et al. 1996) because early taxa were mostly browsers (Shoshani 1998). Evolution of an elongated proboscis likely coincided with adaptations for grazing lifestyles during radiations in the Miocene (Shoshani 1998).

Traces and trace fossils that are similar to, or may be confused with, elephant trunk traces including large annelid traces; holothurian traces; and large diameter, meniscate, vermiform ichnofossils, for example, *Scolicia* (e.g., Häntzschel 1975). Curled grasping traces may even resemble bedding-plane exposures of *Zoophycos* (e.g., Häntzschel 1975). Associated paleoenvironmental indicators can be used to determine whether proboscideans are reasonable trace makers for any given vermiform trace.

Water Spraying and Sediment Bathing We observed small sediment pits attributed to water dripping and spraying and sediment bathing in both loose sand and clay-rich mud. Such small impact craters are similar to raindrop impressions, which typically require fine grained, moist sediment for preservation (Metz 1981; Robb 1992). Given the right conditions, therefore, we expect that these features may be preserved in the rock record.

As far as we know, there are no trace fossils specifically interpreted as the result of throwing of sediment or spraying of water. As mentioned, raindrop impressions are likely the best analog for passively and actively spread water. The closest approximation of thrown sediment may be ejecta associated with footprints (Allen 1997). We expect that small pits from dispersed water and sediment are preservable in the rock record, especially since analogous sedimentary structures are known from the rock record. We suggest looking for water-and sediment-spraying traces in association with evidence of wallowing because those behaviors are often associated with wallowing.

In addition to raindrop impressions, biogenic sedimentary structures that may be confused with sediment pits from thrown objects include pit trapping traces, for example, ant lion traps, and the trace fossil *Conichnus* (e.g., Häntzschel 1975; Hasiotis et al. 2012; Lehane and Ekdale 2013). Distinguishing features of thrown-sediment pits include possible presence of a particle contained within the pit, association with other pits of the same morphology, and association with other elephant traces, especially trunk-grasping traces.

Urination Traces Since these traces are relatively large, associated with the addition of liquid to sediment, and produce distinct sedimentological features associated with scouring and fluid transport, we suspect that these features are preservable in the fossil record. We expect that these traces would be most easily recognizable on bedding surfaces, similar to footprints. Perhaps the most useful analog, albeit

on a much broader scale, is plunge-pool scouring associated with waterfalls and spillways.

The term urolite was originally applied to nonliquid urinary excrement associated with coprolites (Duvernoy 1844) and was adopted to describe sedimentary structures produced by liquid urine (Fernandes et al. 2004). Possible urine pits are reported for dinosaurs (McCarville and Bishop 2002; Fernandes et al. 2004), but none have been noted elsewhere in the fossil record. Given what we perceive is a relatively positive preservation potential, we expect that more of these traces will be recognized in the future. As elephants often urinate during locomotion (McKay 1973), fossil proboscidean urination pits should be associated with trackways.

Resting Traces The resting traces we observed were surficial traces created mostly in firm, compacted sand. As such, these traces will likely have a low preservation potential, although such traces created in muddy sediments may have a better chance of preservation, depending on depth and posttracemaking conditions. Resting traces produced in noncohesive sand, such as that found in eolian dune environments, may be preserved if the surface is stabilized by moisture from fog or dew (e.g., Hasiotis 2004, 2008; Davis et al. 2007; Schmerge et al. 2013).

Traditionally, resting traces are classified as cubichnia (Seilacher 1964), but this has been applied mainly to traces of aquatic organisms, which have favorable preservation potential. Resting traces of large vertebrates are rare in the fossil record and typically do not record an animal lying on its side. For example, there are many resting traces known from bipedal dinosaurs, which can be recognized by footprints associated with impressions of the metatarsals, ventral surface, ischial callosity, manus, and tail (e.g., Hitchcock 1865; Thulborn 1990; Platt and Hasiotis 2008; Milner et al. 2009). There are no known resting-trace fossils attributed to proboscideans.

Wallowing We witnessed only one episode of wallowing behavior during our observations. The trace that resulted from wallowing was a large surficial feature that persisted for at least 26 days. The ultimate survivorship of the trace is unknown, however, because the sand pit used for wallowing was then leveled and prepared for a footprint experiment.

We know of no trace fossils specifically attributed to proboscidean wallowing, but contorted bedding in sinkhole deposits has been attributed to mammoth wallowing (Laury 1980). Wallowing behavior is recognized as a substantial geomorphologic agent affecting modern landscapes (Butler 1995; Deocampo 2002; Haynes 2006, 2012). Elephant wallowing creates sizeable depressions, which become enlarged through repeated visits (Haynes 2006, 2012). Up to 1 m^3 of sediment can be removed from a wallow or watering hole by an individual elephant coating itself with mud (Flint and Bond 1968). Depressions attributed to wallowing by elephants and other large mammals in interdune troughs in western Zimbabwe typically hold water after a rainfall event and contain mostly fine sediment (Flint and Bond 1968). Given continued sedimentation within such structures, preservation in the rock record is probable as lenses of bioturbated sandy mudstone.

Locomotion through Partial Snow Cover   During our observations of tracks in partially covered snow, we attempted to find the same tracks during each visit to see how they evolved as the snow melted. Unfortunately, finding the same tracks was difficult because fresh trampling often obscured older tracks. Also, as snow melted, standing water in tracks allowed substantial erosion of track features (Fig. 15.9c and d). The most diagnostic features of what we have termed hanging footprints are the pedestals of sediment left behind after the melting of snow. As raised features, pedestals may have lower preservation potential than typical tracks, but we see no reason to think that they cannot be fossilized.

We know of no fossil vertebrate trackways interpreted as being influenced by the presence of snow. Such claims would be difficult to substantiate because, at this time, there are no definite criteria that can be used to differentiate hanging tracks from dissected tracks preserved on a trampled surface. Certainly, there is a possibility that such tracks attributable to proboscideans exist in the fossil record, especially since many cold-adapted proboscideans likely encountered snow and ice during Pleistocene glaciations. For example, wear marks on mammoth tusk tips have been interpreted as the result of scraping snow to clear patches of ground (Kubiak 1982).

Other Elephant Traces   There are several examples of elephant traces that have been observed in the wild that we did not witness during our research at the zoo. These traces result from interactions with nonsedimentary media and from environmental- or medium-specific behaviors. Trampling of bone, for example, is known to result in breakage patterns and parallel scratch marks similar to those produced by predation or butchering by humans (Haynes 1991, 2006, 2012; West and Hasiotis 2007). Another trace created on nonsedimentary media results from rubbing against trees or rocks, which produces smooth, polished surfaces (Haynes 2006, 2012). Possible ancient examples of rubbing sites have been described in California (Parkman 2002; Haynes 2012).

Other reported elephant traces constructed in sediments relate mostly to excavations attributable to various behaviors. Excavation may be caused by dust bathing or wallowing (Haynes 2012), but can also result from digging of holes to access water during drought periods (Sikes 1971; Haynes 2006) or mining of minerals as dietary supplements (Holdø et al. 2002). Digging by mammoths has been proposed as the source of a cylindrical pit at a Clovis archaeological site in New Mexico that has alternatively been interpreted as the result of well digging by humans (Haynes 2012). The walls of wells dug by extant elephants have the potential to contain traces from contact with the surface of the trunk during drinking (e.g., Haynes 1991).

15.5   Conclusions

The multitude of behaviors exhibited by extant elephants produces a number of traces upon interaction with sedimentary and nonsedimentary media. During observations at the Topeka Zoo, Topeka, Kansas, USA, we observed six unique traces,

in addition to commonly observed dung and tracks in sediment: trunk-grasping traces, small pits from active and passive spreading of water and sediment, urination traces, resting traces, wallowing traces, and dissected tracks created in partially snow-covered sediment. Our goal is to provide a search pattern to better inform paleoichnological studies of possible proboscidean traces. The trunk-grasping and resting traces we observed were surficial features created in compacted, noncohesive sand and would likely have the lowest preservation potential of all the observed traces. We envision dispersed water and sediment as appearing similarly to raindrop impressions if preserved in the trace fossil record. Urination pits likely have the potential to be preserved because they involve creation of depressions associated with simultaneous moistening of the sediment. Urination traces attributable to proboscideans are unknown, but depressions interpreted as dinosaur urination pits have been reported in the fossil record. Wallowing creates very large traces that have been recognized in modern landscapes and may have positive preservation potential because of their large size and influence on geomorphology. Snow-influenced tracks produce distinct features, i.e., sediment pedestals associated with undertracks; however, more studies are required to see if such tracks are distinguishable from tracks associated with standing water or other high-moisture media.

References

Allen JRL (1997) Subfossil mammalian tracks (Flandrian) in the Severn Estuary, S.W. Britain: mechanics of formation, preservation and distribution. Philos T Roy Soc B 352:481–518

Bagley KR, Goodwin TE, Rasmussen LEL, Schulte BA (2006) Male African elephants, *Loxodonta africana*, can distinguish oestrous status via urinary signals. Anim Behav 71:1439–1445

Buss IO (1990) Elephant life: fifteen years of high population density. Iowa State University Press, Ames

Butler DR (1995) Zoogeomorphology: animals as geomorphic agents. Cambridge University Press, New York

Davis RB, Minter NJ, Braddy SJ (2007) The neoichnology of terrestrial arthropods. Palaeogeogr Palaeocl 255:284–307

Deocampo DM (2002) Sedimentary structures generated by *Hippopotamus amphibius* in a lake-margin wetland, Ngorongoro Crater, Tanzania. PALAIOS 17:212–217

Duvernoy G (1844) Sur l'existence des urolithes fossiles, et sur l'utilité que la science des fossiles organiques pourra tirer de leur distinction d'avec lês coprolithes, pour la détermination de restes fossiles de Sauriens et d'Ophidiens. CR Hebd Acad Sci 19:255–260

Elzanowski A, Sergiel A (2006) Stereotypic behavior of a female Asiatic elephant (*Elephas maximus*) in a zoo. J Appl Anim Welf Sci 9:223–232

Fernandes MA, Fernandes LBDR, Souto PRDF (2004) Occurrence of urolites related to dinosaurs in the Lower Cretaceous of the Botucatu Formation, Paraná Basin, São Paulo State, Brazil. Rev Bras Paleontol 7:263–268

Flint RF, Bond G (1968) Pleistocene sand ridges and pans in western Rhodesia. Geol Soc Am Bull 79:299–314

Gheerbrant E, Sudre J, Cappetta H (1996) A Palaeocene proboscidean from Morocco. Nature 383:68–70

Gillette DD, Thomas DA (1985) Dinosaur tracks in the Dakota Formation (Aptian-Albian) at Clayton Lake State Park, Union County, New Mexico. New Mexico Geological Society Guidebook, 36th Field Conference, Santa Rosa

Häntzschel W (1975) Trace fossils and problematica, Treatise on invertebrate paleontology, part W: miscellanea, supplement 1. The Geological Society of America and the University of Kansas, Boulder

Hart BL, Hart LA, Mccoy M, Sarath CR (2001) Cognitive behavior in Asian elephants: use and modification of branches for fly switching. Anim Behav 62:839–847

Hasiotis ST (2004) Reconnaissance of Upper Jurassic Morrison Formation ichnofossils, Rocky Mountain region, USA: paleoenvironmental, stratigraphic, and paleoclimatic significance of terrestrial and freshwater ichnocoenoses. Sediment Geol 167:177–268

Hasiotis ST (2008) Reply to the comments by Bromley et al. of the paper "Reconnaissance of the Upper Jurassic Morrison Formation ichnofossils, Rocky Mountain region, USA: paleoenvironmental, stratigraphic, and paleoclimatic significance of terrestrial and freshwater ichnocoenoses" by Stephen T. Hasiotis. Sediment Geol 208:61–68

Hasiotis ST, Reilly M, Amos K, Lang S, Kennedy D, Todd J, Michel E, Platt BF (2012) Actualistic studies of the spatial and temporal distribution of terrestrial and aquatic traces in continental environments to differentiate lacustrine from fluvial, eolian, and marine environments. In: Berganz OW, Bartov Y, Bohacs K, Nummedal D (eds) Lacustrine sandstone reservoirs and hydrocarbon systems. AAPG Memoir vol 95. American Association of Petroleum Geologists, Tulsa, pp 433–489

Haynes G (1991) Mammoths, mastodonts, and elephants. Cambridge University Press, New York

Haynes G (2006) Mammoth landscapes: good country for hunter-gatherers. Quat Int 142–143: 20–29

Haynes G (2012) Elephants (and extinct relatives) as earth-movers and ecosystem engineers. Geomorphol 157–158:99–107

Higgs W, Kirkham A, Evans G, Hull D (2003) A Late Miocene proboscidean trackway from western Abu Dhabi. Tribulus 13:3–8

Hitchcock E (1865) Supplement to the ichnology of New England. Wright & Potter, Boston

Holdø RM, Dudley JP, McDowell LR (2002) Geophagy in the African elephant in relation to availability of dietary sodium. J Mammal 83:652–664

Hollister-Smith JA, Alberts SC, Rasmussen LEL (2008) Do male elephants, *Loxodonta africana*, signal musth via urine dribbling? Anim Behav 76:1892–1841

Katugaha HIE (1993) Some observations on elephants in the Ruhuna National Park, Sri Lanka. Gajah 10:26–31

Kubiak H (1982) Morphological characters of the mammoth: an adaptation to the arctic-steppe environment. In: Hopkins DM, Matthews JV, Schweger CE, Young SB (eds) Paleoecology of Beringia. Academic Press, New York, p 281–290

Laury RL (1980) Paleoenvironment of a late Quaternary mammoth-bearing sinkhole deposit, Hot Springs, South Dakota. Geol Soc Am Bull 91:465–475

Lehane JR, Ekdale AA (2013) Pitfalls, traps, and webs in ichnology: traces and trace fossils of an understudied behavioral strategy. Palaeogeogr Palaeocl 375:59–69

Lillywhite HB, Stein BR (1987) Surface sculpturing and water retention of elephant skin. J Zool Lond 211:727–734

McCarville K, Bishop GA (2002) To pee or not to pee: evidence for liquid urination in sauropod dinosaurs. J Vertebr Paleontol 22(supplement):85

McKay GM (1973) Behavior and ecology of the Asiatic elephant in southeastern Ceylon. Smithsonian Contributions to Zoology, no. 125. Smithsonian Institution Press, Washington

Mead JI, Agenbroad LD, Davis OK, Martin PS (1986) Dung of *Mammuthus* in the arid Southwest, North America. Quat Res 25:121–127

Metz RT (1981) Why not raindrop impressions? J Sediment Petrol 51:265–268

Miall LC, Greenwood F (1878) The anatomy of the Indian elephant. J Anat Physiol 13:5–84

Milner ARC, Harris JD, Lockley MG, Kirkland JI, Matthews NA (2009) Bird-like anatomy, posture, and behavior revealed by an Early Jurassic theropod dinosaur resting trace. PLoS ONE 4:1–14

Owen-Smith RN (1988) Megaherbivores: the influence of very large body size on ecology. Cambridge University Press, Cambridge

Parkman B (2002) Mammoth rocks: where Pleistocene giants got a good rub? Mammoth Trump 18:4–7, 20

Platt BF, Hasiotis ST (2008) A new system for describing and classifying tetrapod tail traces with implications for interpreting the dinosaur tail trace record. PALAIOS 23:3–13

Platt BF, Hasiotis ST, Hirmas DR (2010) Use of low-cost multistripe laser triangulation (MLT) scanning technology for three-dimensional, quantitative paleoichnological and neoichnological studies. J Sediment Res 80:590–610

Platt BF, Hasiotis ST, Hirmas DR (2012) Empirical determination of physical controls on megafaunal footprint formation through neoichnological experiments with elephants. PALAIOS 27:725–737

Poole JH (1987) Rutting behavior in African elephants: the phenomenon of musth. Behaviour 102:283–316

Poole TB, Taylor VJ, Fernando SBU, Ratnasooriya WD, Ratnayeke A, Lincoln G, McNeilly A, Manatunga AMVR (1997) Social behavior and breeding physiology of a group of Asian elephants *Elephas maximus* at the Pinnawala Elephant Orphanage, Sri Lanka. Int Zoo Yearbook 35:297–310

Porter SC (2001) Snowline depression in the tropics during the last glaciation. Quat Sci Rev 20:1067–1091

Rees PA (2002) Asian elephants (*Elephas maximus*) dust bathe in response to an increase in environmental temperature. J Therm Biol 27:353–358

Rees PA (2004) Low environmental temperature causes an increase in stereotypic behavior in captive Asian elephants (*Elephas maximus*). J Therm Biol 29:37–43

Robb III AJ (1992) Rain-impact microtopography (RIM): an experimental analogue for fossil examples from the Maroon Formation, Colorado. J Sediment Petrol 62:530–535

Roberts DL, Bateman MD, Murray-Wallace CV, Carr AS, Holmes PJ (2008) Last interglacial fossil elephant trackways dated by OSL/AAR in coastal aeolianites, Still Bay, South Africa. Palaeogeogr Palaeocl 257:261–279

Schmerge JD, Riese DJ, Hasiotis ST (2013) Vinegaroon (Arachnida: Thelyphonida: Thalyphonidae) trackway production and morphology: implications for media and moisture control on trackway morphology and a proposal for a novel system of interpreting arthropod trace fossils. PALAIOS 28:116–128

Scrivner PJ, Bottjer DJ (1986) Neogene avian and mammalian tracks from Death Valley National Monument, California: their context, classification and preservation. Palaeogeogr Palaeocl 57:285–331

Seilacher A (1964) Sedimentological classification and nomenclature of trace fossils. Sedimentology 3:253–256

Shoshani J (1997) It's a nose! It's a hand! It's an elephant's trunk! Nat Hist 106:36–42.

Shoshani J (1998) Understanding proboscidean evolution: a formidable task. Trends Ecol Evol 13:480–487

Sikes SK (1971) The natural history of the African elephant. American Elsevier, New York

Spinage C (1994) Elephants. T. and A.D. Poyser Ltd., London

Sukumar R (2003) The living elephants: evolutionary ecology, behavior, and conservation. Oxford University Press, New York

Thulborn T (1990) Dinosaur Tracks. Chapman & Hall, New York

Tshering U (2011) Height no bar for this jumbo. Renew Nat Res News 32:1–2

Vidya TNC, Sukumar R (2005) Social and reproductive behaviour in elephants. Curr Sci 89:1200–1207

West DL, Hasiotis ST (2007) Trace fossils in an archaeological context: examples from bison skeletons, Texas, USA. In: Miller III W (ed) Trace fossils: concepts, problems, prospects. Elsevier, Amsterdam, p 545–561

Wiedner E, Alleman AR, Isaza R (2009) Urinalysis in Asian elephants (*Elephas maximus*). J Zoo Wildlife Med 40:659–666

Zheng X-J, Wang Z-T, Qiu Z-G (2004) Impact craters in loose granular media. Eur Phys J E 13:321–324

Chapter 16
Burrows and Related Traces in Snow and Vegetation Produced by the Norwegian Lemming (*Lemmus lemmus*)

Dirk Knaust

Contents

Abstract Lemmings are small, fossorial rodents showing high activity day and night through summer and winter. Although their biology is the subject of many studies, their burrowing activity and burrow architecture have received little attention. In this chapter, the traces of the Norwegian lemming (*Lemmus lemmus*) produced in snow are described from two mountain sites in the tundra of southern Norway. During the long and harsh winter time, the lemmings build extensive burrow systems along the ground/snow interface and within the snow. These branching and partly anastomosing tunnel networks contain a thick lining of grass and other plant material and thus are well preserved after the snow thaw. Other burrow parts remain unlined or are scattered with fecal pellets. The tunnel networks allowed the lemmings to reach their feeding sites in the surroundings of their dwellings. The burrow systems, which are several square meters in size, contain one or two nests thickly lined with plant material. The nests may contain lemming fur and are built for breeding, nursing, and dwelling. Other parts of the burrow systems are completely filled with rounded and rod-shaped fecal pellets and serve as sites for defecation. They also contain simple rounded, nest-like burrows with the same pellet fill. Lemming burrows in snow are a good example of how those common traces can serve to understand the burrow architecture and the behavior of their producers in habitats which are otherwise difficult to investigate. Beside this neoichnological

D. Knaust (✉)
Statoil ASA, 4035 Stavanger, Norway
e-mail: dkna@statoil.com

aspect, rodent burrows in snow may also aid in the interpretation and understanding of fossil vertebrate burrows which remain poorly understood.

Keywords Neoichnology · Snow burrows · Rodents · Norwegian lemming · *Lemmus lemmus* · Norway

16.1 Introduction

Despite its enormous potential, neoichnology is much neglected in paleoichnological studies, and also hardly dealt with in zoological investigations. In the geological record, burrows are a major group of trace fossils, but only about 3 % of the named burrows are known to be produced by vertebrates (Knaust 2012), while the nomenclature of vertebrate tracks appears to have proliferated. A strict distinction of fossil invertebrate and vertebrate burrows is often impossible because relatively large burrows may be produced by both groups of animals (such as crustaceans and mammals). Therefore, neoichnological investigations have a great value for the interpretation of such trace fossils and their taxonomical treatment.

The zoological understanding of many mammals, including their behavior, is quite advanced, whereas details of burrow construction, architecture, and subterranean behavior often remain poorly understood. This fact is partly related to the difficulty in the subject itself as modern burrows of mammals require special techniques for their investigation. One way to analyze such burrows is to look for them in snow. Reichman and Smith (1990) and Kinlaw (1999) provide a good overview of burrows and burrowing behavior by extant mammals and other vertebrates and Begall et al. (2007) give an updated view on that subject. Busch et al. (2000) discuss the population ecology of subterranean rodents including a nice evaluation of various burrow systems. Well-documented examples of modern rodent burrow systems include those used for wood mice (Jennings 1975), gophers (Vleck 1981), mole rats (Šumbera et al. 2007, 2012; Škliba et al. 2012), and voles (Brügger et al. 2010).

Although, burrows in snow can reveal quite spectacular insights into the life of mammals active during winter time, the description of such phenomena is mainly neglected and only reported sporadically (Merritt 2010; Vallon and Kjeldahl-Vallon 2011). Due to their subnivean (in and underneath the snow) lifestyle, different species of lemmings are known for their ability to produce burrows in snow. One of the first descriptions of Norwegian lemming burrows is from Collet (1895). Detailed descriptions of occurrences in northern Asia are scattered in the Russian literature and are reviewed by Ognev (1963); the review includes the Norwegian lemming (*Lemmus lemmus*), the Siberian brown lemming (*Leonurus sibiricus*=*L.obensis*), and the Arctic lemming (*Dicrostonyx torquatus*). Additional information about *L. lemmus* burrows is provided by Koshkina and Khalansky (1963) and Curry-Lindahl (1980). In Alaska and Canada, the Northern collared lemming (*Dicrostonyx groenlandicus*) and the North American brown lemming (*Lemmus trimucronatus*) are known to burrow in snow (Rausch 1950; Banfield 1981). In this chapter, the traces of the Norwegian lemming (*L. lemmus*) produced in snow and vegetation are described.

16.2   Norwegian Lemming

16.2.1   Localities and Habitat

The Norwegian (or Norway) lemming (*L. lemmus*) is endemic to Norway, western and northern Sweden, northern Finland, and the Kola Peninsula in Russia. It occurs in alpine, subalpine, and subarctic habitats, where it preferably colonizes wetland areas in the tundra and in stands of willows and dwarf birch (Ognev 1963; Curry-Lindahl 1980). In years with high population densities, lemmings also colonize lower-lying habitats such as birch forests.

Norwegian lemmings used to appear in periodic population booms roughly every 3–4 years. One example of such a population boom took place in 2010 and the material described in this chapter was documented during spring and summer time of the following year in two localities. The first locality is in the vicinity of the mountain tourist cabin Øyuvsbu in the Setesdalheiene, Rogaland (936 m a.s.l., 59°01′27.80″N, 7°14′12.20″E) and was studied in May 2011 (Fig. 16.1a). The second locality is in the vicinity of the mountain tourist cabin Halne fjellstova in the Hardangervidda, Buskerud (1,250 m a.s.l., 60°25′23.80″N, 7°42′24.50″E) and was visited in August 2011.

16.2.2   Biology and Behavior

The genus *Lemmus* is the most abundant small mammal in many areas of the circumpolar tundra with an important role in arctic ecosystems (Batzli 1975). The Norwegian lemming is a small rodent (order Rodentia, family Cricetidae, subfamily Arvicolinae) with a body length of 13–15 cm (excluding tail, which is 1.5–2.0 cm long). In contrast to many other rodents, Norwegian lemmings are characteristically colored. They change their fur twice a year, the winter fur having longer hair than the summer fur. Also, the nails of the claws are longer in winter than in summer, which is related to the burrowing activity and the substrate to penetrate (soil in summer and snow in winter). The Norwegian lemming has a fossorial lifestyle, but in comparison with other lemmings (e.g., the Siberian brown lemming), it is a less advanced burrower.

Lemmings are animals active day and night. They reproduce in summer and winter, whereas breeding ceases in spring and autumn. Well known by biologists are the famous population cycles of the lemmings and the related mass migrations for seeking food and shelter. For the Norwegian lemming, quick reproduction leads to chaotic population growth in cycles of 3–4 years. The population density during such peaks in some areas is estimated to reach 100–250 individuals/ha, while minimal densities drop down to perhaps 0.1 individuals/ha (Batzli 1975). The reason for such population cycles has long been debated and is probably related to predator populations. The biology of lemmings is detailed in numerous chapters in Stenseth and Ims (1993).

Fig. 16.1 Study site 1 in the vicinity of the mountain tourist cabin Øyuvsbu in the Setesdalheiene, Rogaland (936 m a.s.l., photographs taken in May 2011). **a** Mountain habitat of the Norwegian lemming (*Lemmus lemmus*). The melting snow fields reveal well-preserved burrow networks of the lemming. **b** Thin and vegetated soil cover with numerous entrances to short burrows (ca. 3–4 cm in diameter), probably remaining from the previous summer period in 2010. **c** Extensive burrow system stuffed with grass and uncovered from the melting snow. **d** Part of a burrow system with winding and thickly grass-lined burrows together with tunnel openings cut into the grass. **e** Melting snow, faintly exposing open and branched tunnels indicated by littered fecal pellets and plant debris. **f** Dead specimen of the Norwegian lemming found close to its burrow. Note the claws with long and robust nails, which are well suited for burrowing. Burrow diameters in c–e are ca. 5 cm

In summer time, the little mammals mainly thrive above the ground and seek shelter under stones, in small soil cavities, or in shrubs. The thin, rocky soil cover is not well suited for burrowing and therefore the Norwegian lemming only excavates short and relatively simple burrows (Curry-Lindahl 1980; Fig. 16.1b).

Instead of subterranean burrow systems, Norwegian lemmings excavate a network of branched tunnels and covered paths above the ground through surface vegetation. This system closely follows micro-topography and consists of a grass-lined nest situated in the central part of the system, from which numerous runways and roofed tunnels lead in different directions. Depending on the presence and type of vegetation (grass, moss, lichen, sedge, shrub, etc.), these trails and tunnels are cut into the vegetation and may be roofed with overhanging plant parts. Sites for defecation and hiding are also part of the system. The trails and tunnels connect the central living and breeding area with the feeding sites. The lemmings feed on grasses, sedges, leaves, mosses, lichens, berries, bark, and roots, and are able to cache large quantities of plant material in their burrows. When the distance between living and feeding area becomes too large, a new nest situated closer to the feeding area is built by the lemmings (Curry-Lindahl 1980).

In many areas of its distribution, the Norwegian lemming has to deal with a thick snow cover during most of the year. It is also active through the harsh winter time, living in and underneath the snowpack from which it receives protection from predators and insulation from the elements. Extensive networks with a similar organization such as the summer networks are common, but are excavated along the snow/ground interface (Fig. 16.1c, d) and, to a lesser degree, within the snow (Fig. 16.1e). Spring and autumn are critical times for lemmings. In spring, the snow melts and the lemmings lose their protective domiciles in the snowbanks. They are forced to migrate above ground to other areas (often wetlands, bogs, etc.) and become the targets of predators. In autumn, however, the cold may appear before the snow and makes life difficult in exposed areas. Population booms, such as the one from 2010, rapidly declined after the following winter and no living animals were observed during the study period in 2011 (Fig. 16.1f).

16.2.3   Traces in Snow

The lemming traces observed in snow comprise galleries (burrows and trails), nests, and fecal pellets. The burrow systems occur in a patchy manner and are typically in the size range of few to several square meters (Fig. 16.2a). In locations with a dense occurrence of burrow systems, individual systems are hard to discern and closely spaced neighboring systems overlap or seem to be interconnected with each other. The burrow construction mainly took place along the interface between ground (soil/grass) and snow, but several burrow parts were extended into the snowpack. Due to the partly melted snow, the plant-filled burrow parts are often projected onto the ground (Fig. 16.2b) or, in cases where they are more self-sustaining, are still in their original position in the air above the ground (Fig. 16.2c). In several cases, burrow openings into the soil were preserved and probably are preexisting and abandoned dwellings from the autumn. A frequent change between connected trails and tunnels in grass and plant-stuffed burrows in snow makes it difficult to map individual systems or their parts.

The galleries are multiple branched, with T-shaped branching points which are not enlarged (Fig. 16.2d). Bifurcations too occur, but are less frequent. Crosscutting
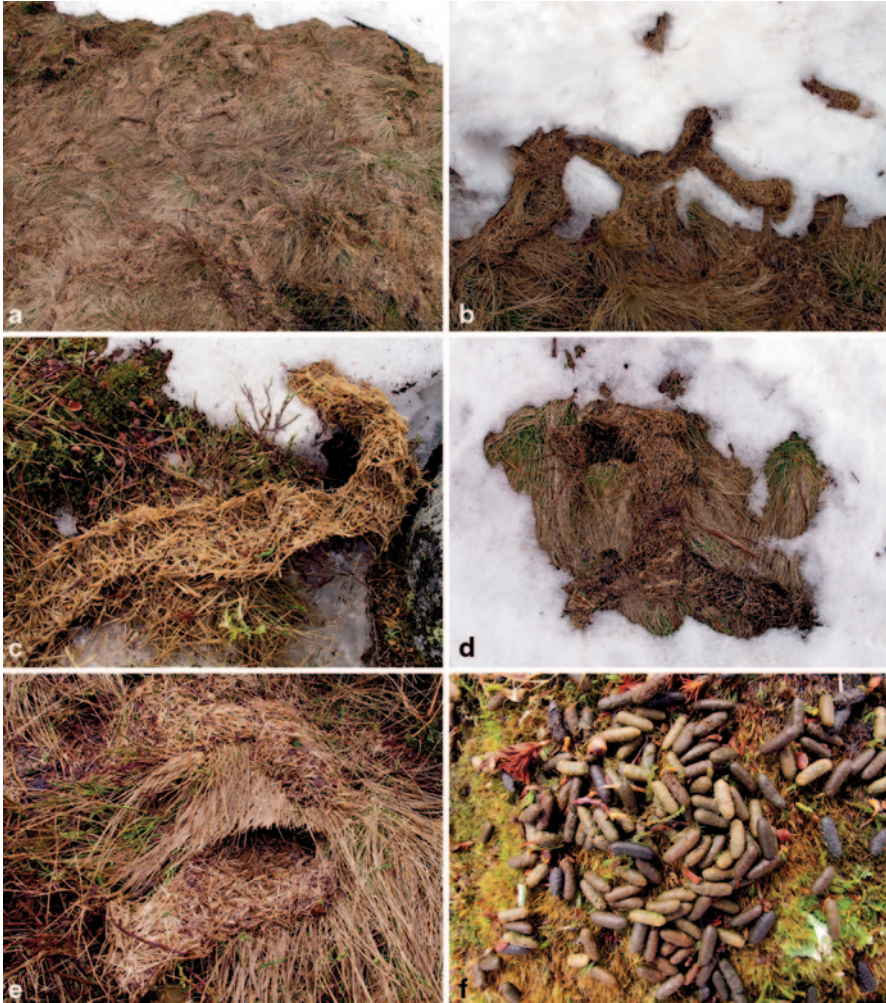
Fig. 16.2 Study site 1, burrow details and fecal pellets (photographs taken in May 2011). **a** Larger part of a tunnel system consisting of burrows thickly lined with grass which was cut into small pieces. The winding burrows are bifurcated and have short and bulbous off-branches. Other burrow parts are helical. **b** Partly exposed and partly snow-encased burrow with thick grass lining and T-shaped branching. **c** Partly grass-lined tunnel portion built within the snow and, after snowmelt, positioned above the ground. **d** Winding burrow with T-shaped branching and thick lining consisting of cut grass and leaves. **e** Tunnel cut into grass and another lined with grass and leaves above it due to projection after snowmelt. **f** Rounded cylindrical fecal pellets of varying color (ca. 6–8 mm long and 2–3 mm in diameter). Burrow diameters in a–e are ca. 5 cm

of burrows from the same or different systems is common and leads to a complication of the resulting maze after the snow melts (Fig. 16.2e). Burrow portions between the branching points are typically 5–30 cm long and have a straight, sinusoidal, or, more rarely, slightly helical course in a horizontal direction. Burrows are about 5 cm in diameter and thus slightly larger than the body size of adult lemmings.

Some burrows branch in a dendritic pattern with somewhat enlarged blind-ending terminations, while others are more anastomosing.

The composition of the burrows may vary even within a single system and partly depends on the type of plant material available in the terrain where the network is built. A common scenario is open burrows with a thick grass lining around an empty core, with individual blades of grass arranged in a random manner or more or less transverse to the burrow axis. Other burrow parts are completely filled with grass and other plant material. Open and unlined burrows in snow are by their nature hard to discern, although a faint concentration of soil suggests frequent use and helps in their identification. Easier to recognize are burrows which are lined with fecal pellets to various degrees (Fig. 16.2f).

One or more nests are important components of the burrow systems. They are typically situated in the central region of the burrow network. The nests have a subcircular outline and a diameter of about 15 (12–18) cm (Fig. 16.3a, b). Depending on the available plant material in the burrow area, they are either built with grass, moss, lichens, leaves, or a combination of these. Some better preserved specimens offer insights into nest construction, as they consist of an outer rim in the form of a burrow densely stuffed with plant material and arranged as a tight vertical spiral with one or two whorls (Fig. 16.3b). The bottom of the central depression of the nest was subsequently lined with plant material as well. Some nests have incorporated flakes of lemming fur and also contain the skeletal remains of their former inhabitants (Fig. 16.3b).

In a similar manner as the nests, defecation sites (toilets) were constructed as simple spiral loops and are densely packed with fecal pellets (Fig. 16.3c, e). They are slightly smaller than the nests and may be connected with an anastomosing network of burrows completely filled with pellets. The fecal pellets have a rounded rod shape, 6–8 mm in length and 2–3 mm in diameter. Depending on the diet of their producers, their color varies from different shades of brown, beige, to black (Figs. 16.2f and 16.3f).

Figure 16.4 contains schematic diagrams of two burrow systems to demonstrate the morphological variation.

16.3   Significance and Application of Subnivean Lemming Burrows

Given the nature of the snow substrate, the described lemming burrows present an interesting case of how surface denudation affects the morphology of 3D burrow architecture. The snow could be treated as an analog of a unit of rock that is being weathered (melted) preferentially leaving behind the burrows filled with more resistant material. This is an important problem when trying to interpret burrow systems occurring on an exposed, weathered surface. This study also demonstrates the variation in burrow morphology with changes in substrate composition over very small distances. Overall, these subnivean burrows provide a great insight into the behavior and burrow architecture of small rodents, which not only has implications for interpreting their subterranean counterparts, but also fossil burrows. However, care

Fig. 16.3 Study site 2 in the vicinity of the mountain tourist cabin Halne fjellstova in the Hardangervidda, Buskerud (1,250 m a.s.l., photographs taken in August 2011). Norwegian lemming traces produced along the soil/snow interface or within the snow and now projected onto the bare or mossy soil. **a** Nest built with grass and leaves and admixed with lemming fur (ca. 15 cm in diameter). **b** Nest built with moss and grass and admixed with lemming fur (ca. 15 cm in diameter). The nest preserves some skeletal remains of its inhabitant(s). **c** Polygonal network with anastomosing burrow parts (ca. 5 cm in diameter). All burrow parts are densely filled with fecal pellets. The nest-like feature (*arrow*) is also filled with pellets and obviously served as a defecation site (toilet). **d** Close-up view of the defecation site as highlighted in a (ca. 15 cm in diameter). **e** Runways sealed with fecal pellets along the mossy soil surface leading into small subterranean burrows which served as shelters (during the previous summer period?). The large burrow opening is ca. 9 cm wide. **f** Melting firn package including fecal pellets (ca. 6–8 mm long and 2–3 mm in diameter)

must be taken because different substrates (i.e., vegetation versus snow versus soil) may cause different characteristics of the burrows, which consequently would lead to different ichnotaxonomical treatment of resulting trace fossils in the rock record.

Fig. 16.4 Line drawings
showing the morphological
variation of two burrow sys-
tems based on photographs in
a Fig. 16.1d and **b** Fig. 16.3c
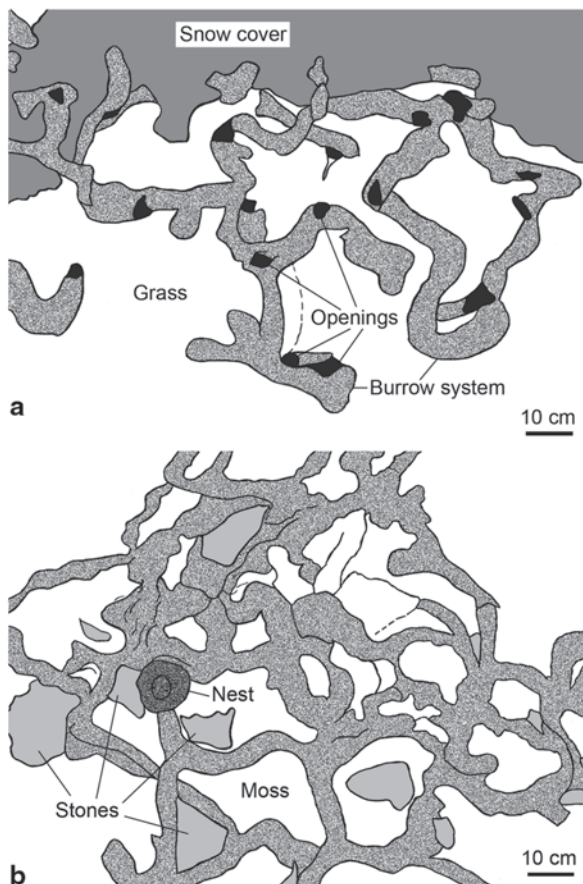
16.4   Conclusion

Burrow systems produced in snow due to the activity of the Norwegian lemming
(*L. lemmus*) become preserved after the snow thaws away in spring and summer.
These traces document the behavior of this endemic species during winter time and
under the burden of a thick snow cover. The dense burrow networks originate from
the frequent passages of their producers when visiting their feeding areas. They are
connected with nests which were used for breeding, nursing, and dwelling. Most
tunnels and the nests are thickly lined with plant material which probably helped
in isolating them against the cold and/or to cache food. Other parts of the bur-
row systems are heavily filled with large quantities of droppings (fecal pellets) and
obviously acted as defecation sites. The presented data are an example of how neo-
ichnological studies of rodent and other mammal burrows can contribute to a better
understanding of the activity and the behavior of their producers. This information
is not only relevant for zoologists but may also aid in the interpretation of mammal
burrows in the geological record. More work remains to be done in coming years to
analyze the complexity and variability of these fascinating burrow systems.

References

Banfield AWF (1981) The mammals of Canada. University of Toronto Press, Toronto

Batzli GO (1975) The role of small mammals in arctic ecosystems. In: Golley FB, Petrusewicz K, Ryszkowski L (eds) Small mammals: their productivity and population dynamics. Cambridge University Press, Cambridge, pp 243–268

Begall S, Burda CE, Schleich CE (eds) (2007) Subterranean rodents: news from underground. Springer-Verlag, Berlin

Brügger A, Nentwig W, Airoldi J-P (2010) The burrow system of the common vole (*M. arvalis*, Rodentia) in Switzerland. Mammalia 74:311–315

Busch C, Antinuchi CD, Valle JCdel, Kittlein MJ, Malizia AI, Vassallo AI, Zenuto RR (2000) Population ecology of subterranean rodents. In: Lacey E, Patton J, Cameron G (eds) Life underground: the biology of subterranean rodents. University of Chicago Press, Chicago, pp 183–226

Collet R (1895) *Muodes lemmus*: its habits and migrations in Norway. Forhandlinger Videnskabs-Selskabs Kristiana 3:1–62

Curry-Lindahl K (1980) Der Berglemming *Lemmus lemmus*. Die Neue Brehm-Bücherei 526. A. Ziemsen Verlag, Wittenberg Lutherstadt

Jennings TG (1975) Notes on the burrow systems of woodmice (*Apodemus sylvaticus*). J Zool 177:500–504

Kinlaw A (1999) A review of burrowing by semi-fossorial vertebrates in arid environments. J Arid Environ 41:127–145

Knaust D (2012) Trace-fossil systematics. In: Knaust D, Bromley RG (eds) Trace fossils as indicators of sedimentary environments. Developments in sedimentology, vol 64. Elsevier, Amsterdam, pp 79–101

Koshkina TV, Khalansky AS (1963) The dens and shelters of Norwegian lemmings. Bjull Mosk Obsčispit prirody 68:16–24 (in Russian)

Merritt JF (2010) The biology of small mammals. The Johns Hopkins University Press, Baltimore

Ognev SI (1963) Mammals of the U.S.S.R. and adjacent countries. Mammals of eastern Europe and northern Asia. Vol. VI, rodents. Israel Program for Scientific Translations, Jerusalem

Rausch R (1950) Observations on a cyclic decline of lemmings (*Lemmus*) on the arctic coast of Alaska during the spring of 1949. Faculty Publications from the Harold W. Manter Laboratory of Parasitology, Paper 501

Reichman OJ, Smith SC (1990) Burrows and burrowing behaviour by mammals. In: Genoways HH (ed) Current mammalogy. Plenum Press, New York, pp 197–244

Šklíba J, Mazoch V, Patzenhauerová H, Hrouzková E, Lövy M, Kott O, Šumbera R (2012) A maze-lover's dream: burrow architecture, natural history and habitat characteristics of Ansell's mole-rat (*Fukomys anselli*). Mamm Biol 77:420–427

Stenseth NC, Ims RA (eds) (1993) The biology of lemmings. Linnean Society Symposium Series 15. Linnean Society of London, Academic Press, Harcourt Brace & Company, London

Šumbera R, Chitaukali WN, Burda H (2007) Biology of the silvery mole-rat (*Heliophobius argenteocinereus*). Why study a neglected subterranean rodent species? In: Begall S, Burda CE, Schleich CE (eds) (2007) Subterranean rodents: news from underground. Springer-Verlag, Berlin, pp 221–236

Šumbera R, Mazoch V, Patzenhauerová H, Lövy M, Šklíba J, Bryja J, Burda H (2012) Burrow architecture, family composition and habitat characteristics of the largest social African mole-rat: the giant mole-rat constructs really giant burrow systems. Acta Theriol 57:121–130

Vallon LH, Kjeldahl-Vallon TA (2011) Ichnotaxonomical rules applied to a recent muroidean burrow produced in snow. N Jb Geol Paläont Abh 261:299–307

Vleck D (1981) Burrow structure and foraging costs in the fossorial rodent, *Thomomys bottae*. Oecologia 49:391–396

Chapter 17
Near-Surface Imaging (GPR) of Biogenic Structures in Siliciclastic, Carbonate, and Gypsum Dunes

Ilya V. Buynevich, H. Allen Curran, Logan A. Wiest, Andrew P. K. Bentley, Sergey V. Kadurin, Christopher T. Seminack, Michael Savarese, David Bustos, Bosiljka Glumac and Igor A. Losev

Contents

Abstract High-resolution geophysical methods, such as ground-penetrating radar (GPR) imaging, are increasingly applied to ichnological research. Large vertebrate and invertebrate burrows and tracks can be detected and resolved using center frequencies of >400 MHz. Geophysical images of bioturbation structures

I. V. Buynevich (✉) · L. A. Wiest · A. P. K. Bentley
Department of Earth and Environmental Science, Temple University,
Philadelphia, PA 19122, USA
e-mail: coast@temple.edu

H. A. Curran · B. Glumac
Department of Geosciences, Smith College, Northampton, MA 01063, USA

S. V. Kadurin
Physical and Marine Geology, Odessa National University, Odessa 65058, Ukraine

C. T. Seminack · I. A. Losev
Department of Environmental Science and Policy, George Mason University,
Fairfax, VA 22030, USA

M. Savarese
Coastal Watershed Institute and Department of Marine and Ecological Sciences,
Florida Gulf Coast University, Fort Myers, FL 33965, USA

D. Bustos
White Sands National Monument, Alamogordo, NM 88310, USA

in siliciclastic, carbonate, and evaporite (gypsum) dunes exhibit characteristic electromagnetic signal returns, which are associated with active burrow openings (ground–wave gap), filled burrows (hyperbolic diffraction and "pull up"), and large tracks (concave up patterns). The noninvasive imaging can be used for pseudo-3D visualization (closely spaced survey lines) and monitoring of biogenic activity (repeated surveys). Because biogenic structures induce distinct anomalies in geophysical records collected at frequencies typical of many geological investigations, caution must be taken to avoid misinterpreting them as primary sedimentary structures.

17.1   Introduction

A variety of vertebrate and invertebrate organisms are responsible for a diverse suite of biogenic structures (burrows and surface traces) in both modern and ancient aeolian settings (Ahlbrandt et al. 1978; Loope 1986; McKeever 1991; Curran and White 2001; Fornos et al. 2002; Roberts 2003; Loope 2006; Lockley et al. 2007; Milàn et al. 2007a, b; Loope 2008; Roberts 2008; Roberts et al. 2008; Buynevich et al. 2011; Kinlaw and Grasmueck 2012). Burrows are used chiefly for thermoregulation, breeding, nesting, and predator avoidance (Reichman and Smith 1990; Butler 1995). Preservation and detection of these structures, however, especially in unconsolidated dune substrates have been longstanding challenges in paleobiological and ichnological research (Loope 1986; Seilacher 2007).

In the past decades, a number of studies have demonstrated the applicability of near-surface geophysical techniques, such as ground-penetrating radar (GPR or georadar), for rapid continuous imaging of modern biogenic structures (Stott 1996; Matthews et al. 2006; Kinlaw et al. 2007; Nichol et al. 2003; Aucoin and Hasbargen 2010; Di Prinzio et al. 2010; Sensors and Software Inc. 2010; Buynevich 2011a, b; Buynevich and Hasiotis 2011; Buynevich et al. 2011; Grimes et al. 2011; Martin et al. 2011; Buynevich 2012; Kinlaw and Grasmueck 2012; Swiontek et al. 2012; Buynevich and Nyquist 2013; Pitman et al. 2013). The majority of this work emphasized ecological and conservational aspects of bioturbation, although an increasing number of workers are looking at ichnological applications of georadar in paleontological and paleoecological contexts.

The aim of this chapter is to present examples of geophysical images of animal traces produced in three aeolian lithologies: siliciclastic (quartz dominated), carbonate (oolitic), and evaporite (gypsum) from a number of geographic locations (Fig. 17.1). Though a detailed treatment of the GPR technique is beyond the scope of this chapter, the limitations of the penetration and resolution are discussed, along with specific examples of electromagnetic (EM) signal return from various parts of a biogenic structure.
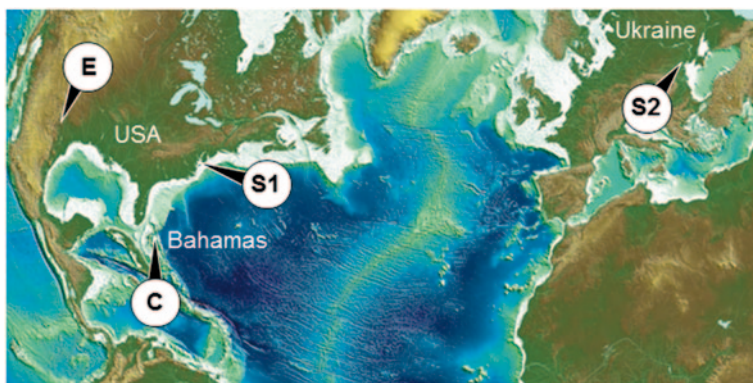
Fig. 17.1 Locations of field study sites: *S1* Siliciclastic dune site (Assateague Island, Maryland, USA); *S2* Siliciclastic dune site (Albatross Beach, Karolino-Bugaz, Odessa Region, Ukraine); *C* Carbonate substrate example (Moore Hill Beach, Little Exuma Island, Bahamas); *E* Evaporite (gypsum) dune site (White Sands National Monument, New Mexico, USA). (Source: Geoware Digital Relief Map)

17.2   Georadar Technique

GPR uses EM impulses for rapid continuous imaging of the shallow subsurface (for technical aspects of the technique, see Bristow and Jol 2003 and Di Prinzio et al. 2010). All data presented in this chapter were collected using a digital MALÅ Geoscience radar system with 500 and 800 MHz monostatic antennas. Due to the tradeoff between penetration and vertical resolution (ability to discriminate between two closely spaced objects), mid- to high-frequency antennas (>400 MHz) are most suitable for detecting and resolving biogenic structures in the shallow subsurface (Fig. 17.2).

With trade-off between GPR frequency and resolution, most biogenic structures greater than 5 cm in diameter can be both detected and resolved at center frequencies >400 MHz. The resolution (Δd) of various elements of a subsurface structure (e.g., two layers, burrow floor, and roof) is typically a quarter or higher of EM signal wavelength (λ) and is achieved when the target size exceeds the resolution in a particular substrate (Fig. 17.2; Table 17.1). At lower frequencies (200–300 MHz), larger biogenic structures (>10 cm) will produce detectable diffraction patterns.

In radargrams, buried objects exhibit a typical hyperbolic (high-amplitude point-source diffraction) signal (Fig. 17.3). The apex of the hyperbola represents the actual position of the buried target. For buried targets that exceed EM signal resolution and possess fill-matrix contrast (burrows, pipes, etc.), both the top and bottom of the object can be differentiated (Fig. 17.3). Air-filled cavities produce a characteristic "pull up" (early signal arrival) of the floor due to higher velocity of EM waves in air than in sediment (Nichol et al. 2003). Traverses directly over burrow openings would result in advanced direct signal arrival (sharp "pull up"), which will extend through a gap in ground–wave reflection.
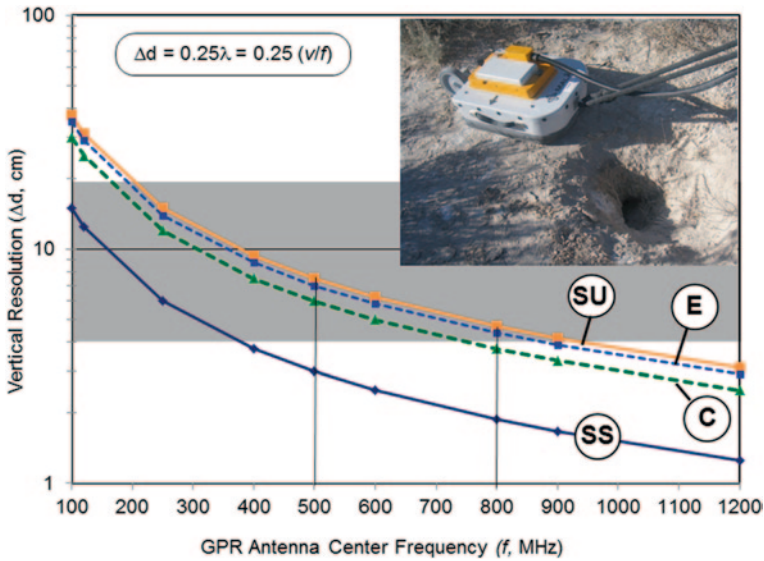
Fig. 17.2 GPR frequency versus resolution diagram shows that most large biogenic structures (>5 cm) can be both detected and resolved at center frequencies >400 MHz. The *inset* shows a 500 MHz antenna next to a burrow entrance. The resolution ($\Delta d = 0.25$) of various elements of a subsurface structure (e.g., two layers, burrow floor, and roof) is achieved when the target size exceeds the resolution (is at or above the line) for dry (unsaturated) siliciclastic (*SU*), evaporite (*E*), and carbonate (*C*) sand. At lower wave velocities, higher resolution is possible in wet (saturated) sediments (*SS*). This diagram indicates that even at lower frequencies (200–300 MHz), large biogenic structures (>10 cm) will result in detectable diffraction patterns

Table 17.1 Key physical parameters of unsaturated dune sediments investigated in this study (signal velocity based on ground truth and hyperbola fitting)

Substrate[a]	Frequency f (MHz)	Velocity v (cm/ns)	Permittivity ε_r	Resolution Δd (cm)
Siliciclastic	800	14.9	4.0	4.7
	2300[b]	14.9	4.0	1.6
Carbonate	800	12.0	6.3	3.8
Evaporite	500	14.0	4.6	7.0
	800	14.0	4.6	4.4

[a] Substrate composition: siliciclastic—quartz, minor feldspar, mica, and heavy; minerals, with higher carbonate (shell hash) fraction at site S2; carbonate—oolitic and skeletal grains; evaporite—gypsum sand

[b] Antenna frequency used in Buynevich (2011a) study referenced in this chapter

Only several live animals were observed entering or exiting their burrows during the surveys. The presence of an organism within its dwelling would produce a strong high-amplitude signal return due to dielectric contrast between fluid-filled body and largely unsaturated sand. This property is utilized in forensic applications of georadar (Hammon et al. 2000; Schultz et al. 2006).
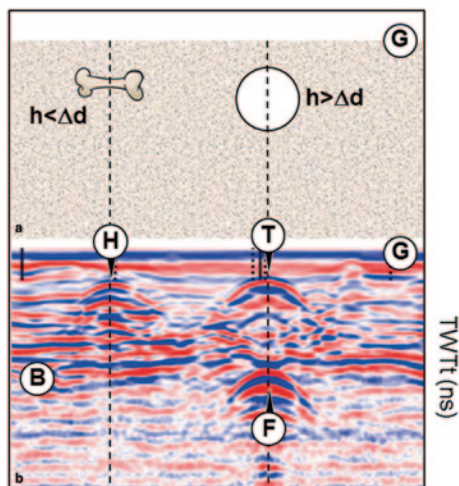
Fig. 17.3 Typical georadar reflection patterns associated with buried three-dimensional (point-source) objects. **a** Buried target (e.g., fossil bone) and an empty or filled burrow, with diameter exceeding the antenna resolution. **b** A radargram showing high-amplitude convex-upward hyperbolic diffractions related to the two targets. Note only a single hyperbola (*H*) from a small object due to its vertical dimension (*h*) being smaller than EM signal resolution. If the size of the buried target is greater than GPR resolution, both the top (*T*) and bottom (floor; *F*) of the larger structure (e.g., a burrow tunnel) can be resolved. *G* ground surface, *B* background sediment layers. The vertical axis is two-way travel time (TWTt) in nanoseconds (10^{-9} s), which can be converted to approximate depth ($\sim$d) using EM wave velocity in a particular sediment type

With sufficient dielectric contrast, fossils such as animal bones may be detected in saturated sediment or enclosing rock. Therefore, for paleontological applications, aside from mapping potential geological settings for fossil occurrence (paleo-channels, terraces, etc.), GPR is best suited for detecting skeletons or large body fossils, as well as large biogenic structures (Matthews et al. 2006; Buynevich and Hasiotis 2011).

Raw geophysical datasets were post-processed with a RadExplorer v.1.41 software package and are presented as two-dimensional images (2D radargrams). Although not presented in this study, several sites were profiled using dense survey grids for generating pseudo-3D images (true 3D for 0.25λ antenna separation) of biogenic structures (Kinlaw et al. 2007; Di Prinzio et al. 2010; Kinlaw and Grasmueck 2012). Besides 3D visualization, this tool offers depth slice and lateral views of various subsurface elements.

17.3   Siliciclastic Substrate

Two examples below show geophysical imaging of large burrows from siliciclastic coastal dune deposits. The Assateague Island National Seashore, Maryland, USA (38°03′23″ N; 75°13′38″ W; Fig. 17.1) is inhabited by several semi-fossorial
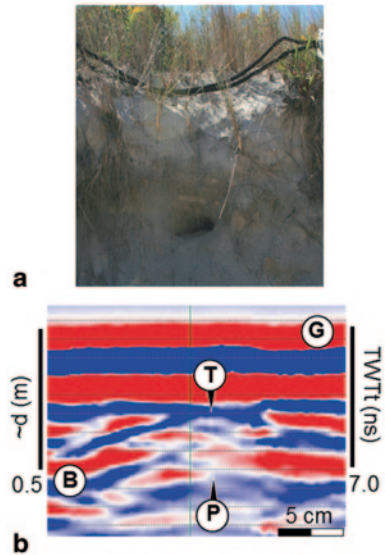
vertebrates and invertebrates, as well as cervids and feral horses (*Equus caballus*),
which produce deep tracks and affect dune vegetation (Grimes et al. 2010; Buyn-
evich et al. 2011). A red fox (*Vulpes vulpes*) is the only organism that produces
large burrows in coastal dunes on the island (Fig. 17.4). A 500 MHz radargram
collected across the top of the exposed entrance shows a characteristic hyperbolic
diffraction pattern corresponding to the top of the tunnel (Fig. 17.4b). A slight bot-
tom "pull up" is due to higher EM wave velocity in air. Nearby burrows of ghost
crabs (*Ocypode quadrata*) also resulted in slight interference patterns, although
their subvertical geometry and somewhat smaller size make their recognition more
problematic.

A diverse assemblage of mammalian and avian traces occurs in contrasting dep-
ositional settings along the coast of Odessa region, Ukraine. At Albatross strand-
plain (46°9′53.04″ N; 30°33′47.82″ E; Fig. 17.1), large fox burrows are excavated in
prograded beach-ridge complexes, especially in raised vegetated sections capped by
aeolian deposits (Fig. 17.5a). During data collection, an adult red fox was observed
traversing the ridges. Imaging with an 800 MHz GPR antenna revealed a series of
hyperbolic diffractions in a dune ridge adjacent to a 20-cm-wide den entrance. The
high-amplitude anomalies likely represent subsurface extensions of active or aban-
doned burrows (Fig. 17.5b). Although the survey line passed close to several young
trees, it is unlikely that all anomalies were related to tree roots due to changes in
bedding structure below the apex of the diffraction.

In addition to characterizing burrows, georadar has the potential for detecting
individual vertebrate tracks. In many siliciclastic aeolian settings, large tracks are
accentuated by heavy-mineral concentrations so that mineral color contrast allowed
their recognition in early field studies (Van der Lingen and Andrews 1969; Lewis
and Titheridge 1978; Buynevich 2012). Recent attempts at imaging buried mammal
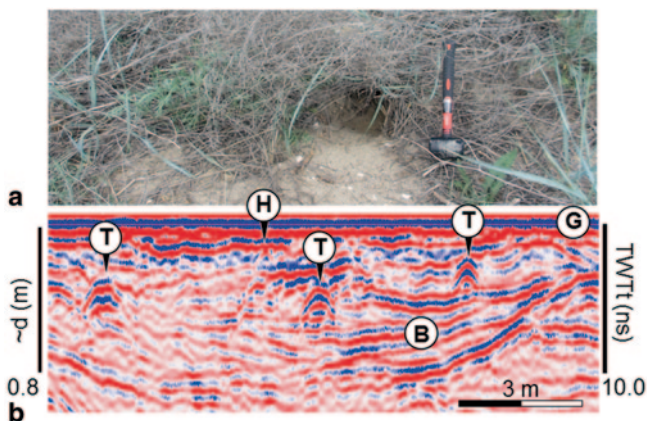
Fig. 17.5 a An entrance to a fox burrow in a dune ridge along the Black Sea coast of Ukraine. A hammer is 35 cm long. **b** An 800 MHz GPR image showing several hyperbolic signal returns likely associated with subsurface extensions of a burrow complex (*tunnel tops*). A single acute diffraction (*H*) may be the result of a shallow tree root. (See Fig. 17.3 for a list of symbols)

footprints impressed by plaster casts in the laboratory show success when using lithological anomalies (800 MHz antenna; Buynevich et al. 2011) or saturation contrast only (2.3 GHz antenna; Buynevich 2011a).

Dune migration (lateral accretion) and aggradation (vertical accretion) ensures preservation of tracks and burrows in beach and dune deposits (Loope 2008; Buynevich et al. 2011). In lower portions of coastal dunes, a rising water table (e.g., due to relative sea-level rise) may impede recognition and recovery of biogenic structures by traditional methods. The potential for their identification and mapping by georadar, however, will be improved due to increased signal resolution (~2 cm at 800 MHz; Fig. 17.2) in saturated aeolian sand.

17.4   Carbonate Substrate

An abandoned burrow of a land crab (*Gecarcinus lateralis*) was imaged at Moore Hill Beach, Little Exuma Island, Bahamas (23°26′22.91″N; 75°36′15.43″W; Fig. 17.1). The structure had a 5-cm-wide opening and was produced in very fine- to fine-grained oolitic dune sand (Fig. 17.6a). A dense grid of 800 MHz survey lines (length 1 m, spacing 0.2 m) was collected within a 1 m² box centered on the burrow entrance. A profile taken along the axis of a visibly inclined shaft shows a direct arrival produced by the opening, followed by a hyperbolic diffraction (Fig. 17.6b). A lack of the "pull up" is indicative of a partial collapse or infilling of the tunnel extension. A subsequent excavation confirmed a slightly inclined trend of the burrow, with only the outer 10 cm remaining unfilled.

To our knowledge, this is the first example of an ichnological GPR application in a carbonate setting. During the field season, a number of other structures were

Fig. 17.6 a Burrow of a land crab (*Gecarcinus lateralis*) in carbonate dune sand, Little Exuma Island, Bahamas. **b** An 800 MHz image exhibits a sharp direct arrival (*D*) from the open entrance and a subsurface expression of an inclined burrow. (See Fig. 17.3 for a list of symbols)
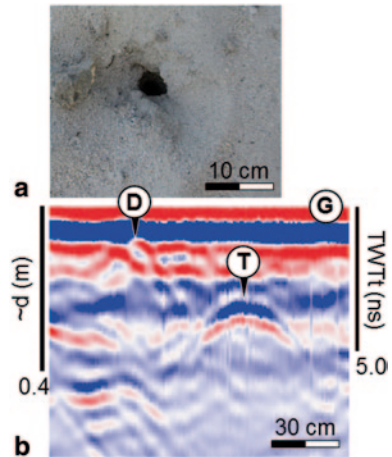
surveyed, including ghost crab (*Ocypode quadrata*) burrows, as well as buried roots and possible root traces (in aeolianites) of silver thatch palm (*Coccothrinax argentata*). This research has implications for recognizing similar structures in tropical aeolianites (Curran and White 2001) and other carbonate successions (Milàn et al. 2007a).

17.5 Evaporite (Gypsum) Substrate

White Sands National Monument, New Mexico, USA (32°47′43.09″N; 106°13′46.78″W; Fig. 17.1) provides an ideal opportunity to study both bioturbation structures and large animal tracks in a wet dunefield. The world's largest gypsum dunefield, the area is located in the Rio Grande Rift and was formed through deflation of the evaporated surface of Pluvial Lake Otero since the early Holocene (Langford 2003; Kocurek et al. 2007; Lucas et al. 2007). The northeasterly migration of 5–15 m-high gypsum dunes (barchan and parabolic forms) at times exceeds 3 m/year (Kocurek et al. 2007; Jerolmack et al. 2012). The interdunes are characterized by a relatively shallow (~1 m) water table. Various aeolian sub-environments are inhabited by semifossorial organisms, including burrowing owl (*Athene cunicularia*), desert kit fox (*Vulpes macrotis*), badger (*Taxidea taxus*), and the bannertailed kangaroo rat (*Dipodomys spectabilis*; Bugbee 1942; Reichman and Smith 1990).

GPR signal response of the near-surface parts of several burrows has been documented in various parts of the dunefield. Due to the protected nature of the field area, excavations and casting were not conducted, emphasizing the need for noninvasive visualization mapping tools. Most surveys were collected using a 500 MHz antenna, with 7–8-cm vertical resolution in unsaturated gypsum sand (signal velocity ~14 cm/ns; Fig. 17.2). Several structures were also imaged with an 800 MHz

Fig. 17.7 a A large inclined burrow in gypsum sand, White Sands National Monument, New Mexico, with a 500 MHz antenna. **b** Georadar image shows a complex "broken" direct arrival resulting from signal reverberation in a subvertical shaft and a hyperbolic return from the subsurface part of the *hollow structure*. (See Figs. 17.3 and 17.6 for a list of symbols)
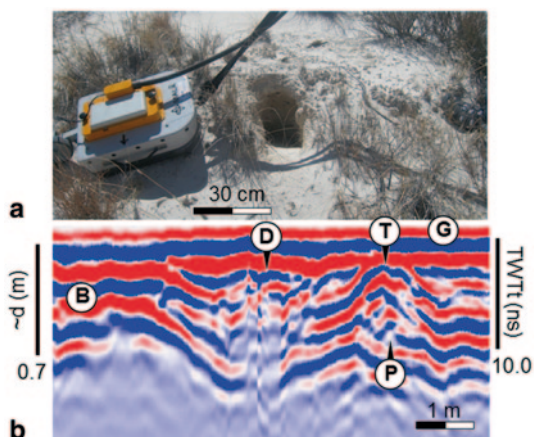
antenna, which provided higher resolution (4–5 cm). Entrance morphologies range from domed to horizontal circular openings with inclined or spiraling downward shafts, to excavations with nearly parallel sidewalls (Fig. 17.7a). Subsurface surveys of open burrows exhibit the contrasting EM signal response to surface openings and near-surface segments of shafts and tunnels. Although 2D radargrams are not sufficient for capturing the overall burrow geometry, the depth and general orientation of the tunnels can be documented. A direct arrival (sharp "pull up") or distorted signal pattern corresponds to the antenna passing over an open entrance, with a hyperbolic reflection and a slight "pull up" characteristic of its subsurface extension (Fig. 17.7b; Nichol et al. 2003).

Vertebrate track preservation in evaporite settings has been explored in a number of field studies (Laporte and Behrensmeyer 1980; Scrivner and Bottjer 1986; Cohen et al. 1991, 1993; Webb 2007; Scott et al. 2007, 2008; Lockley and Rodríguez-de la Rosa 2009; Scott et al. 2009, 2010; 2012). To date, however, no attempts have been made to assess GPR applicability to detecting buried footprints in these settings. In addition to dune settings, a suite of interdune subenvironments provided an opportunity for field experiments on taphonomy and geophysical imaging of recent tracks.

In an alkali basin adjacent to a parabolic dune front, modern human and animal trackways are lithified into a desiccated gypcrete surface (Fig. 17.8a). In a field experiment, an 8-cm-long canid track was buried with dry gypsum sand excavated from the surface of the adjacent parabolic dune (Fig. 17.8b). The fill attained a uniform horizontal surface approximately 1 cm above the tracking surface, reaching >2 cm within the track, with no visible surface expression of the footprint. In the 800 MHz radar traverse, the track was manifested as a recognizable asymmetrical depression on an otherwise horizontal subsurface reflection (Fig. 17.8d). This study has potential applications for noninvasive examination of large Pleistocene and Holocene vertebrate tracksites identified by Lucas et al. (2007) and in more recent discoveries at the *White Sands* National Monument.
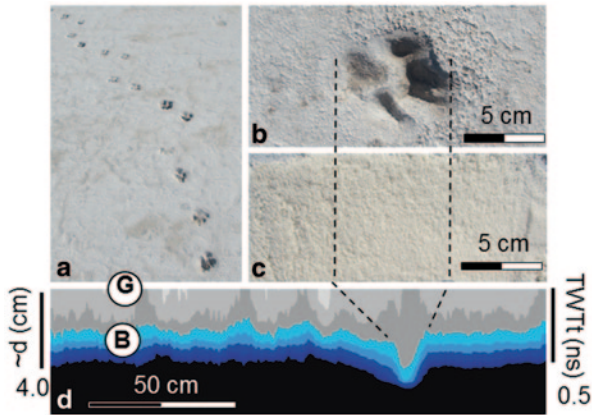
Fig. 17.8 Field experiment with modern canid tracks on alkali interdune flat, White Sands National Monument. **a** A large dog trackway preserved in gypcrete. **b** A large (8 cm) *footprint* was buried by dry gypsum sand from a nearby dune. **c** *Horizontal surface* of the gypsum cover immediately before geophysical data collection. **d** An 800 MHz GPR image shows a distinct depression associated with the buried track, which contrasts with the continuous buried track surface. (See Fig. 17.3 for a list of symbols)

17.6   Conclusion

Our findings demonstrate the viability of GPR imaging in aeolian settings and potential applicability to characterizing large burrows in ancient aeolianites and other continental ichnocoenoses (Voorhies 1975; Lea 1996; Gobetz 2006; Gobetz and Martin 2006; Jennings et al. 2006; Loope 2006; Gobetz 2007; Hasiotis et al. 2007; Hembree and Hasiotis 2008; Riese et al. 2011; Voigt et al. 2011). Because biogenic structures or large body fossils produce anomalies in geophysical records collected at frequencies typical of many geological and archaeological investigations, caution must be taken to avoid misinterpreting burrow segments as physical sedimentary structures or anthropogenic features. Whereas prospecting for buried fossils or traces with georadar is not practical for large areas, once part of a skeleton, burrow, or trackways are identified by traditional methods, geophysical surveys may aid in assessing the spatial relationships of the remaining structures (Matthews et al. 2006). Future research will involve collection of closely spaced GPR transects to produce pseudo-3D and true 3D images of biogenic structures (Grasmueck et al. 2004; Kinlaw et al. 2007; Di Prinzio et al. 2010; Kinlaw and Grasmueck 2012; Pitman et al. 2013). This will provide sequential depth slice and lateral views of tunnels and chambers, facilitating the assessment of burrow geometry and volume.

References

Ahlbrandt TS, Andrews S, Gwynne TD (1978) Bioturbation of eolian deposits. J Sediment Petrol 48:839–848

Aucoin CD, Hasbargen L (2010) Using GPR, GPS and close-range photography to map and characterize dinosaur tracks in the Connecticut River valley. GSA Abs Prog 42:276

Bristow CS, Jol HM (eds) (2003) Ground penetrating radar in sediments. Geological Society of London, Special Publication 211, London

Bugbee RE (1942) Notes on animal occurrence and activity in the White Sands National Monument, New Mexico. Trans Kans Acad Sci 45:315–321

Butler DR (1995) Zoogeomorphology: animals as geomorphic agents. Cambridge University Press, Cambridge

Buynevich IV (2011a) Buried tracks: ichnological applications of high-frequency georadar. Ichnos 18:189–191

Buynevich IV (2011b) Heavy minerals add weight to neoichnological research. Palaios 26:1–3

Buynevich IV (2012) Morphologically induced density lag formation on bedforms and biogenic structures in aeolian sands. Aeol Res 4:1–5

Buynevich IV, Hasiotis ST (2011) Georadar applications in vertebrate taphonomy and ichnology. SVP Abs Prog 71:81

Buynevich IV, Nyquist JE (2013) Scratching the subsurface: GPR characterization of bioturbation structures within a Delaware River bluff, Pennsylvania. GSA Abs Prog 45:15

Buynevich IV, Darrow JS, Grimes ZTA, Seminack CT, Griffis N (2011) Ungulate tracks in coastal sands: recognition and sedimentological significance. J Coast Res 64:334–338

Cohen AS, Lockley MG, Halfpenny J, Michel AE (1991) Modern vertebrate track taphonomy at Lake Manyara, Tanzania. Palaios 6:371–389

Cohen AS, Halfpenny J, Lockley MG, Michel AE (1993) Modern vertebrate tracks from Lake Manyara, Tanzania and their paleobiological implications. Paleobiology 19:433–458

Curran HA, White B (2001) Ichnology of Holocene carbonate eolianites of the Bahamas. In: Abegg R, Harris M, Loope D (eds) Modern and ancient carbonate eolianites: sedimentology, sequence stratigraphy, and diagenesis. SEPM Special Publication 71. SEPM, Tulsa, pp 47–56

Di Prinzio M, Bittelli M, Castellarin A, Pisa PR (2010) Application of GPR to the monitoring of river embankments. J Appl Geophys 7:53–61

Fornos JJ, Bromley RG, Clemmensen LA, Rodriguez-Perea A (2002) Tracks and trackways of *Myotragus balearicus* Bate (Artiodactyla, Caprinae) in Pleistocene aeolianites from Mallorca (Balearic Islands, Western Mediterranean). Palaeogeogr Palaeocl 180:277–313

Gobetz KE (2006) Possible burrows of mylagaulids (Rodentia: Aplodontoidea: Mylagaulidae) from the Late Miocene (Barstovian) Pawnee Creek Formation, northeastern Colorado. Palaeogeogr Palaeocl 237:119–136

Gobetz KE (2007) New considerations for interpreting fossilized mammal burrows from observations of living species. In: Lucas SG, Spielman JA, Lockley M (eds) Cenozoic vertebrate tracks and traces. New Mexico Museum of Natural History and Science Bulletin, vol 42. New Mexico Museum of Natural History and Science, Albuquerque, pp 7–9

Gobetz KE, Martin LD (2006) Burrows of a gopher-like rodent, possibly *Gregorymys* (Geomyoidea: Geomyidae: Entoptychinae) from the Early Miocene Harrison Formation, Nebraska. Palaeogeogr Palaeocl 237:305–314

Grasmueck M, Weger R, Horstmeyer H (2004) Three-dimensional ground-penetrating radar imaging of sedimentary structures, fractures, and archaeological features at submeter resolution. Geology 32:933–936

Grimes ZTA, Buynevich IV, Darrow JS, Seminack CT, Griffis N (2010) The volumetric impact of biogenic sediment reworking on the geomorphology and shallow stratigraphy of barrier islands. Paper presented at the 2010 fall meeting, AGU, San Francisco, 13–17 December 2010

Grimes ZTA, Buynevich IV, Seminack CT, Darrow JS, Stewart RM (2011) Applications of high-frequency GPR imaging to ichnological research. GSA Abs Prog 43:164

Hammon WS, McMechan GA, Zeng X (2000) Forensic GPR: finite-difference simulations of responses from buried human remains. J Appl Geophys 45:171–186

Hasiotis ST, Platt BF, Hembree DI, Everhart M (2007) The trace-fossil record of vertebrates. In: Miller WIII (ed) Trace fossils-concepts, problems, prospects. Elsevier Press, Georgia, pp 196–216

Hembree DI, Hasiotis ST (2008) Miocene vertebrate and invertebrate burrows defining compound paleosols in the Pawnee Creek Formation, Colorado, U.S.A. Palaeogeogr Palaeocl 270: 349–365

Jennings DJ, Platt BF, Hasiotis ST (2006) Distribution of vertebrate trace fossils, Upper Jurassic Morrison Formation, Bighorn Basin, Wyoming: implications for differentiating paleoecological partitioning and preservational bias. In: Foster J (ed) The Morrison Formation. New Mexico Museum of Natural History Bulletin, vol 36. New Mexico Museum of Natural History, Albuquerque, pp 183–192

Jerolmack DJ, Ewing RC, Falcini F, Martin RL, Mastellar C, Phillips C, Reitz MD, Buynevich IV (2012) Roughness controls patterns of sediment transport, vegetation and groundwater in a desert dune field. Nat Geosci 5:206–209

Kinlaw AE, Grasmueck M (2012) Evidence for and geomorphologic consequences of a reptilian ecosystem engineer: the burrowing cascade initiated by the gopher tortoise. Geomorphology 157–158:108–121

Kinlaw AE, Conyers LB, Zajac W (2007) Use of ground penetrating radar to image burrows of the gopher tortoise (*Gopherus polyphemus*). Herpetol Rev 38:50–56

Kocurek G, Mary C, Ewing R, Havholm K, Nagar Y, Singhvi A (2007) White Sands Dune Field, New Mexico: age, dune dynamics and recent accumulations. Sediment Geol 197:313–331

Langford RP (2003) The Holocene history of the White Sands dune field and influences on eolian deflation and playa lakes. Quatern Int 104:31–39

Laporte LF, Behrensmeyer AK (1980) Tracks and substrate reworking by terrestrial vertebrates in Quaternary sediments of Kenya. J Sediment Petrol 50:1337–1346

Lewis DW, Titheridge G (1978) Small scale sedimentary structures resulting from foot impressions in dune sands. J Sediment Petrol 48:835–838

Lea PD (1996) Vertebrate tracks in Pleistocene eolian sand-sheet deposits of Alaska. Quatern Res 45:226–240

Lockley MG, Culver TS, Wegweiser M (2007) An ichnofauna of hopping rodent and arthropod trackways from the Miocene of Colorado. In: Lucas SG, Spielman JA, Lockley M (eds) Cenozoic vertebrate tracks and traces. New Mexico Museum of Natural History and Science Bulletin, vol 42. New Mexico Museum of Natural History and Science, Albuquerque, pp 59–66

Lockley MG, Rodríguez-de laRRA (2009) Preservation of human tracks in arid environments. Ichnos 16:98–102

Loope DB (1986) Recognizing and utilizing vertebrate tracks in cross section, Cenozoic hoofprints from Nebraska. Palaios 1:141–151

Loope DB (2006) Burrows dug by large vertebrates into rain-moistened Middle Jurassic sand dunes. J Geol 114:753–762

Loope DB (2008) Life beneath the surfaces of active Jurassic dunes: burrows from the Entrada Sandstone of south-central Utah. Palaios 23:411–419

Lucas SG, Allen BD, Morgan GS, Myers RG, Love DW, Bustos D (2007) Mammoth footprints from the upper Pleistocene of the Tularosa Basin, Doña Ana County, New Mexico. In: Lucas SG, Spielman JA, Lockley M (eds) Cenozoic vertebrate tracks and traces. New Mexico Museum of Natural History and Science Bulletin, vol 42. New Mexico Museum of Natural History and Science, Albuquerque, pp 149–154

Martin AJ, Skaggs SA, Vance RK, Greco V (2011) Ground-penetrating radar investigation of gopher-tortoise burrows: refining the characterization of modern vertebrate burrows and associated commensal traces. GSA Abs Prog 43:381

Matthews NA, Noble TA, Breithaupt BH (2006) The application of photogrammetry, remote sensing and geographic information systems (GIS) to fossil resource management. In: Lucas SG, Spielmann JA, Hester PM, Kenworthy JP, Santucci VL (ed) America's antiquities: 100 years of

managing fossils on federal lands. New Mexico Museum of Natural History and Science Bulletin, vol 34. New Mexico Museum of Natural History and Science, Albuquerque, pp 119–131

McKeever PJ (1991) Trackway preservation in eolian sandstones from the Permian of Scotland. Geology 19:726–729

Milàn J, Bromley RG, Titschack J, Theodorou G (2007a) A diverse vertebrate ichnofauna from a Quaternary eolian oolite from Rhodes, Greece. In: Bromley R, Buatois LA (eds) Ichnology at the crossroads: a multidimensional approach to the science of organism-substrate interactions. SEPM special publication, vol 88. SEPM, Tulsa, pp 333–343

Milàn J, Clemmensen LB, Buchardt B, Noe-Nygaar N (2007b) A late Holocene tracksite in the Lodbjerg dune system, northwest Jylland, Denmark. In: Lucas SG, Spielman JA, Lockley M (eds) Cenozoic vertebrate tracks and traces. New Mexico Museum of Natural History and Science Bulletin, vol 42. New Mexico Museum of Natural History and Science, Albuquerque, pp 241–250

Nichol D, Lenham JW, Reynolds JM (2003) Application of ground-penetrating radar to investigate the effects of badger setts on slope stability at St. Asaph Bypass, North Wales. Q J Eng Geol Hydrogeol 36:143–153

Pitman L, Wiest LA, Buynevich IV, Bentley APK, Smith K, Beal I, Terry DO Jr (2013) GPR characterization of northern pine snake burrows within the Pinelands National Reserve, New Jersey. GSA Abs Prog 45:62

Reichman OJ, Smith SC (1990) Burrows and burrowing behavior by mammals. In: Genoways HH (ed) Current mammalogy. Plenum Press, New York, pp 197–244

Riese DJ, Hasiotis ST, Odier G (2011) Burrows excavated by mammals or therapsids in the Navajo Sandstone and their association with other organisms represented by trace fossils in a wet desert ecosystem. J Sediment Res 81:299–325

Roberts DL (2003) Vertebrate trackways in late Cenozoic coastal eolianites, South Africa. GSA Abs Prog 34:196

Roberts DL (2008) Last interglacial hominid and associated vertebrate fossil trackways in coastal eolianites, South Africa. Ichnos 15:190–207

Roberts DL, Bateman MD, Murray-Wallace CV, Carr AS, Holmes PJ (2008) Last interglacial fossil elephant trackways dated by OSL/AAR in coastal aeolianites, Still Bay, South Africa. Palaeogeogr Palaeocl 257:261–279

Schultz JJ, Collins ME, Falsetti AB (2006) Sequential monitoring of burials containing large pig cadavers using ground-penetrating radar. J Forensic Sci 51:607–616

Scott JJ, Renaut RW, Owen RB, Sarjeant WAS (2007) Biogenic activity, trace formation, and trace taphonomy in the marginal sediments of saline, alkaline Lake Bogoria, Kenya Rift Valley. In: Bromley R, Buatois LA (eds) Ichnology at the crossroads: a multidimensional approach to the science of organism-substrate interactions. SEPM special publication, vol 88. SEPM, Tulsa, pp 309–330

Scott JJ, Renaut RW, Owen RB (2008) Preservation and paleoenvironmental significance of a footprinted surface on the Sandai Plain, Lake Bogoria, Kenya Rift Valley. Ichnos 15:208–231

Scott JJ, Renaut RW, Buatois LA, Owen RB (2009) Biogenic structures in exhumed surfaces around saline lakes: an example from Lake Bogoria, Kenya Rift Valley. Palaeogeogr. Palaeocl 272:176–198

Scott JJ, Renaut RW, Owen RB (2010) Taphonomic controls on animal tracks at saline, alkaline Lake Bogoria, Kenya Rift Valley: impact of salt efflorescence and clay mineralogy. J Sediment Res 80:639–665

Scott JJ, Renaut RW, Owen RB (2012) Impacts of flamingos on saline lake margin and shallow lacustrine sediments in the Kenya Rift Valley. Sediment Geol 277–278:32–51

Scrivner PJ, Bottjer DJ (1986) Neogene avian and mammalian tracks from Death Valley National Monument, California: their context, classification and preservation. Palaeogeogr Palaeocl 57:285–331

Seilacher A (2007) Trace fossil analysis. Springer, Berlin

Sensors & Software Inc. (2010) Animal burrows. Subsurface views, Mississauga, Canada

Stott P (1996) Ground-penetrating radar: a technique for investigating the burrow structure of fossorial vertebrates. Wildlife Res 22:519–530

Swiontek JP, Schlosser K, Sherrod LA, Simpson EL (2012) Ground penetrating radar application to resolve burrow complexity in modern *Marmota monax* burrows: implication for the recognition of mammal burrows in the rock record. GSA Abs Prog 44:63

Van derLGJ, Andrews PB (1969) Hoof-print structures in beach sand. J Sediment Petrol 39: 350–357

Voigt S, Schneider JW, Saber H, Hminna A, Lagnaoui A, Klein H, Brosig A, Fischer J (2011) Complex tetrapod burrows from Middle Triassic red beds of the Argana Basin (Western High Atlas, Morocco). Palaios 26:555–556

Voorhies MR (1975) Vertebrate burrows. In: Frey RW (ed) The study of trace fossils. Springer, New York, pp 325–350

Webb S (2007) Further research of the Willandra Lakes fossil footprint site, southeastern Australia. J Hum Evol 52:711–715

Index